INTRAMURAL VASCULAR CELLS: KEY THERAPEUTIC TARGETS FOR VASCULAR COGNITIVE IMPAIRMENT

EDITED BY: Roxana Octavia Carare, JoAnne McLaurin and Satoshi Saito

PUBLISHED IN: Frontiers in Aging Neuroscience and Frontiers in Genetics

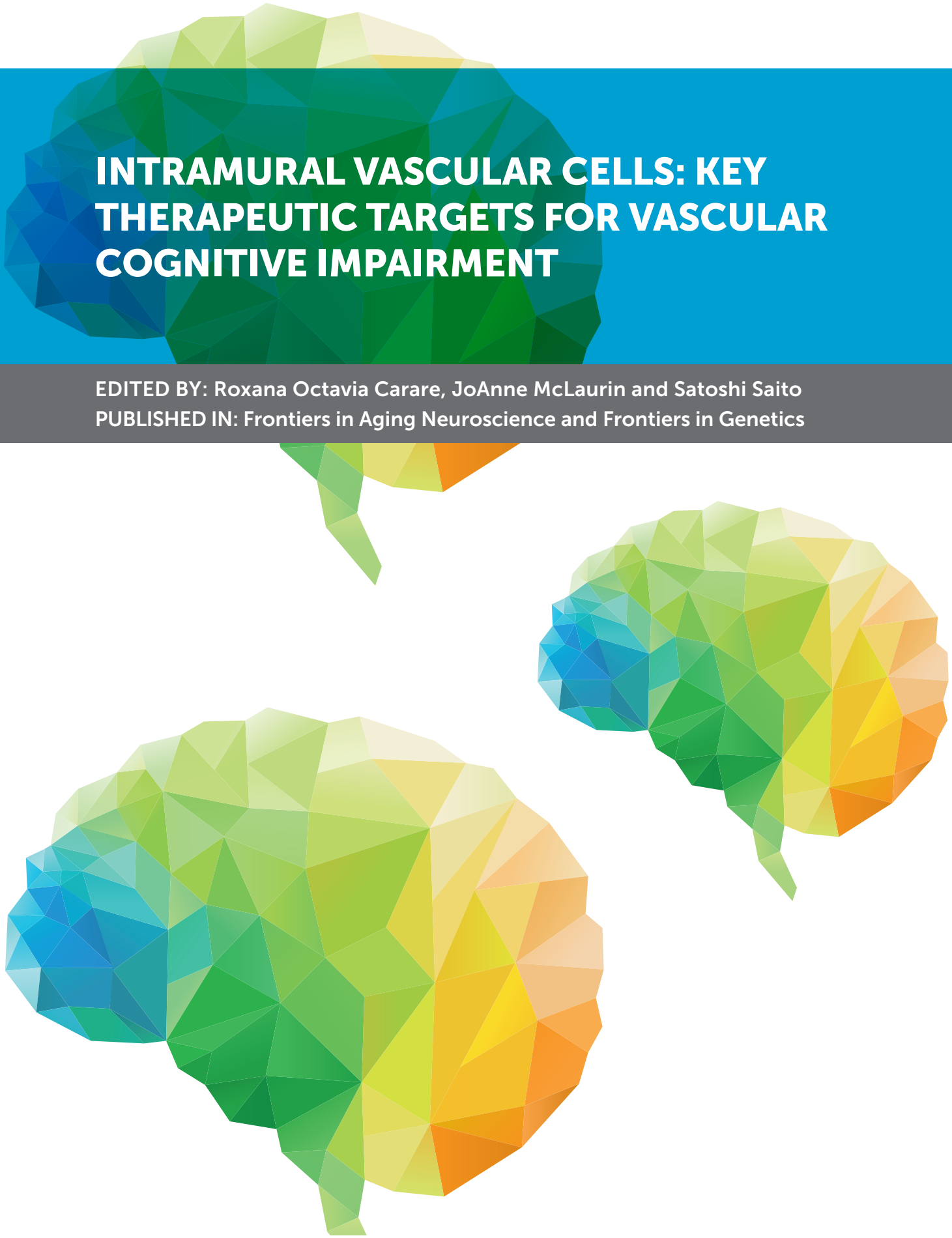

frontiers Research Topics

ISSN 1664-8714
ISBN 978-2-88966-310-1
DOI 10.3389/978-2-88966-310-1

About Frontiers

Frontiers is more than just an open-access publisher of scholarly articles: it is a pioneering approach to the world of academia, radically improving the way scholarly research is managed. The grand vision of Frontiers is a world where all people have an equal opportunity to seek, share and generate knowledge. Frontiers provides immediate and permanent online open access to all its publications, but this alone is not enough to realize our grand goals.

Frontiers Journal Series

The Frontiers Journal Series is a multi-tier and interdisciplinary set of open-access, online journals, promising a paradigm shift from the current review, selection and dissemination processes in academic publishing. All Frontiers journals are driven by researchers for researchers; therefore, they constitute a service to the scholarly community. At the same time, the Frontiers Journal Series operates on a revolutionary invention, the tiered publishing system, initially addressing specific communities of scholars, and gradually climbing up to broader public understanding, thus serving the interests of the lay society, too.

Dedication to Quality

Each Frontiers article is a landmark of the highest quality, thanks to genuinely collaborative interactions between authors and review editors, who include some of the world's best academicians. Research must be certified by peers before entering a stream of knowledge that may eventually reach the public - and shape society; therefore, Frontiers only applies the most rigorous and unbiased reviews.
Frontiers revolutionizes research publishing by freely delivering the most outstanding research, evaluated with no bias from both the academic and social point of view. By applying the most advanced information technologies, Frontiers is catapulting scholarly publishing into a new generation.

What are Frontiers Research Topics?

Frontiers Research Topics are very popular trademarks of the Frontiers Journals Series: they are collections of at least ten articles, all centered on a particular subject. With their unique mix of varied contributions from Original Research to Review Articles, Frontiers Research Topics unify the most influential researchers, the latest key findings and historical advances in a hot research area! Find out more on how to host your own Frontiers Research Topic or contribute to one as an author by contacting the Frontiers Editorial Office: researchtopics@frontiersin.org

INTRAMURAL VASCULAR CELLS: KEY THERAPEUTIC TARGETS FOR VASCULAR COGNITIVE IMPAIRMENT

Topic Editors:
Roxana Octavia Carare, University of Southampton, United Kingdom
JoAnne McLaurin, Sunnybrook Research Institute
Satoshi Saito, University of Southampton, United Kingdom

Citation: Carare, R. O., McLaurin, J., Saito, S., eds. (2021). Intramural Vascular Cells: Key Therapeutic Targets for Vascular Cognitive Impairment. Lausanne: Frontiers Media SA. doi: 10.3389/978-2-88966-310-1

Table of Contents

05 ***Editorial: Intramural Vascular Cells: Key Therapeutic Targets for Vascular Cognitive Impairment***
Satoshi Saito, JoAnne McLaurin and Roxana Octavia Carare

08 ***Solving an Old Dogma: Is it an Arteriole or a Venule?***
Matthew MacGregor Sharp, Theodore P. Criswell, Howard Dobson, Ciara Finucane, Ajay Verma and Roxana O. Carare

14 ***Vital Functions Contribute to the Spread of Extracellular Fluids in the Brain: Comparison Between Life and Death***
Alina Piotrowska, Karsten Winter, Roxana O. Carare and Ingo Bechmann

26 ***Brain Microvascular Pericytes in Vascular Cognitive Impairment and Dementia***
Maiko T. Uemura, Takakuni Maki, Masafumi Ihara, Virginia M. Y. Lee and John Q. Trojanowski

48 ***Hypertension and Pathogenic hAPP Independently Induce White Matter Astrocytosis and Cognitive Impairment in the Rat***
Alexander Levit, Sonny Cheng, Olivia Hough, Qingfan Liu, Yuksel Agca, Cansu Agca, Vladimir Hachinski and Shawn N. Whitehead

58 ***Cilostazol, a Phosphodiesterase 3 Inhibitor, Moderately Attenuates Behaviors Depending on Sex in the Ts65Dn Mouse Model of Down Syndrome***
Masahiro Tsuji, Makiko Ohshima, Yumi Yamamoto, Satoshi Saito, Yorito Hattori, Emi Tanaka, Akihiko Taguchi, Masafumi Ihara and Yuko Ogawa

70 ***Channelrhodopsin Excitation Contracts Brain Pericytes and Reduces Blood Flow in the Aging Mouse Brain*** **in vivo**
Amy R. Nelson, Meghana A. Sagare, Yaoming Wang, Kassandra Kisler, Zhen Zhao and Berislav V. Zlokovic

81 ***Clinical Features and Experimental Models of Cerebral Small Vessel Disease***
Akihiro Shindo, Hidehiro Ishikawa, Yuichiro Ii, Atsushi Niwa and Hidekazu Tomimoto

90 ***Clinical and Genetic Aspects of CADASIL***
Toshiki Mizuno, Ikuko Mizuta, Akiko Watanabe-Hosomi, Mao Mukai and Takashi Koizumi

100 ***Prevalence and Atypical Clinical Characteristics of*** **NOTCH3** ***Mutations Among Patients Admitted for Acute Lacunar Infarctions***
Takashi Okada, Kazuo Washida, Kenichi Irie, Satoshi Saito, Michio Noguchi, Tsutomu Tomita, Masatoshi Koga, Kazunori Toyoda, Shuhei Okazaki, Takashi Koizumi, Ikuko Mizuta, Toshiki Mizuno and Masafumi Ihara

110 ***Excessive Production of Transforming Growth Factor β1 Causes Mural Cell Depletion From Cerebral Small Vessels***
Taisuke Kato, Yumi Sekine, Hiroaki Nozaki, Masahiro Uemura, Shoichiro Ando, Sachiko Hirokawa and Osamu Onodera

119 ***A Nationwide Survey and Multicenter Registry-Based Database of Cerebral Autosomal Dominant Arteriopathy With Subcortical Infarcts and Leukoencephalopathy in Japan***
Akihiro Shindo, Ken-ichi Tabei, Akira Taniguchi, Hiroaki Nozaki, Osamu Onodera, Akihiko Ueda, Yukio Ando, Takao Urabe, Kazumi Kimura, Kazuo Kitagawa, Haruo Hanyu, Teruyuki Hirano, Hideaki Wakita, Hidenao Fukuyama, Tatsuo Kagimura, Yoshihiro Miyamoto, Misa Takegami, Satoshi Saito, Akiko Watanabe-Hosomi, Ikuko Mizuta, Masafumi Ihara, Toshiki Mizuno and Hidekazu Tomimoto

128 ***Altered Brain Function in Cerebral Small Vessel Disease Patients With Gait Disorders: A Resting-State Functional MRI Study***
Xia Zhou, Chao Zhang, Linlin Li, Yimei Zhang, Wei Zhang, Wenwen Yin, Xianfeng Yu, Xiaoqun Zhu, Yinfeng Qian and Zhongwu Sun

139 ***Insulin-Independent and Dependent Glucose Transporters in Brain Mural Cells in CADASIL***
Mahmod Panahi, Patricia Rodriguez Rodriguez, Seyed-Mohammad Fereshtehnejad, Donia Arafa, Nenad Bogdanovic, Bengt Winblad, Angel Cedazo-Minguez, Juha Rinne, Taher Darreh-Shori, Yoshiki Hase, Raj N. Kalaria, Matti Viitanen and Homira Behbahani

151 ***Cerebral Amyloid Angiopathy Presenting as Massive Subarachnoid Haemorrhage: A Case Study and Review of Literature***
Satoshi Saito, Yoshihiko Ikeda, Daisuke Ando, Roxana Octavia Carare, Hatsue Ishibashi-Ueda and Masafumi Ihara

frontiers in Aging Neuroscience

EDITORIAL
published: 30 October 2020
doi: 10.3389/fnagi.2020.615780

Editorial: Intramural Vascular Cells: Key Therapeutic Targets for Vascular Cognitive Impairment

Satoshi Saito[1,2]*, *JoAnne McLaurin*[3] *and Roxana Octavia Carare*[1]

[1] Faculty of Medicine, University of Southampton, Southampton, United Kingdom, [2] Department of Neurology, National Cerebral and Cardiovascular Center, Suita, Japan, [3] Biological Sciences, Sunnybrook Research Institute, Toronto, ON, Canada

Keywords: smooth muscle cells (SMCs), pericytes, Alzheimer's disease, small vessel disease, vascular cognitive impairment, mural cells

Editorial on the Research Topic

Intramural Vascular Cells: Key Therapeutic Targets for Vascular Cognitive Impairment

Alzheimer's disease is the most common type of dementia characterized by neuropathological changes such as intracellular tau tangles and extracellular deposition of β-amyloid (Aβ) as plaques and cerebral amyloid angiopathy (CAA). As the important contribution of cerebrovascular dysfunction to Alzheimer's disease has been recently uncovered, research priorities have been gradually set for basic mechanisms and clinical evidence for the role of vascular factors in the pathogenesis of dementia (Sweeney et al., 2019). The main aim of the current Research Topic was to provide a comprehensive review of cerebrovascular mural cells as a novel therapeutic target for vascular cognitive impairment.

The mural cells include pericytes within the walls of capillaries and vascular smooth muscle cells (SMCs) in the tunica media of the cerebral arterioles and leptomeningeal arteries. SMCs are observed not only in the arteries but also in the veins. The ultrastructural characteristics of the arterial and venous SMCs are described in detail by Sharp et al.. The mural cells have been known as a contributor to architectural maintenance and contraction of vessels. Recent evidence further points to their critical roles in controlling brain homeostasis such as the management of cerebral blood flow (CBF) and the clearance of waste products from the brain.

CBF is critical for the delivery of oxygen and nutrients essential for neuronal and synaptic functioning and is constantly controlled by the mural cells in response to changes in transient neuronal activity, namely neurovascular coupling. Nevertheless, whether capillary pericytes or arterial SMCs initiate the regulation is controversial. This debate mainly stems from the different definitions of the pericytes. The mural cells on the proximal branches coming off penetrating arterioles are sometimes described as pericytes, but the same cells are named as SMCs in other reports, demonstrating the heterogeneity of this cell population (Grant et al., 2019). These cells are positioned at the transition between arterioles and capillaries and have shared some characteristics with pericytes and SMCs (Uemura et al.). In this topic, Zhou et al. showed the regional and large network cerebral dysfunction in a cohort of cerebral small vessel disease with gait disturbance by using functional MRI. Considering the crucial impact of neurovascular coupling on functional MRI, the pathogenic mechanism may be represented by degenerated mural cells in small vessel disease. Nelson et al. examined contractility of brain pericytes by employing a new optogenetic model developed by crossing pericyte-specific CreER mouse line with mice expressing channelrhodopsin-2. Excitation of channelrhodopsin-2 by 488 nm light resulted in pericyte contraction followed by constriction of the capillary leading to the reduction of regional

OPEN ACCESS

Edited and reviewed by:
Thomas Wisniewski,
New York University, United States

***Correspondence:**
Satoshi Saito
saitou.satoshi.43m@kyoto-u.jp

Received: *09 October 2020*
Accepted: *12 October 2020*
Published: *30 October 2020*

Citation:
Saito S, McLaurin J and Carare RO (2020) Editorial: Intramural Vascular Cells: Key Therapeutic Targets for Vascular Cognitive Impairment. Front. Aging Neurosci. 12:615780. doi: 10.3389/fnagi.2020.615780

blood flow. These results clearly demonstrate the pivotal roles of pericytes in the regulation of capillary blood flow.

Apart from their role in cerebral perfusion mural cells also contribute to the clearance of waste products from the brain. Small molecules are internalized by pericytes through receptor-mediated endocytosis or non-specific pinocytosis. In addition, mural cells are involved in the lymphatic drainage system of the brain. The central nervous system is devoid of classical lymph vessels. Instead, waste products from neurons and glia are cleared through the intramural periarterial drainage (IPAD) (Albargothy et al., 2018). Piotrowska et al. injected a fluorescent tracer into the entorhinal cortex of living and sacrificed rats and found that the tracer accumulated in the vascular outer and inner basement membrane in living rats, while it appeared to diffuse along the ventricles and hippocampal fibre tracts in sacrificed animals. The tracer was also observed in the cervical lymph nodes in living rats, but not in sacrificed, suggesting IPAD is an active clearance system driven by vital functions.

Soluble Aβ secreted from neurons diffuse and enter IPAD pathways within the basement membranes of capillaries continuing with the basement membranes surrounding SMCs of intracerebral arteries. Accumulating lines of evidence have shown that impaired IPAD is one of the potential mechanisms for the pathogenesis of Alzheimer's disease and CAA. IPAD flow rapidly moves toward the leptomeningeal arteries where the deposition of Aβ is prominent in CAA (Keable et al., 2016). Cerebrovascular Aβ accumulation eventually induce cerebral microbleeds as well as fatal ICH as shown by Saito et al.. Interestingly, Tsuji et al. reported that cilostazol, a phosphodiesterase 3 inhibitor, improved cognitive function in the Ts65Dn mouse, a model of Down syndrome. Patients with Down syndrome exhibit Aβ plaques and CAA, which is presumably due to the triplication of genes on human chromosome 21. Increased expression of the amyloid precursor protein gene would play a major role in the pathogenesis of CAA in Down syndrome, due to the overproduction of Aβ. Considering that cilostazol can facilitate IPAD (Maki et al., 2014), promotion of IPAD can be a therapeutic approach for Down syndrome as well as Alzheimer's disease.

Cerebral autosomal dominant arteriopathy with subcortical infarcts and leukoencephalopathy (CADASIL) and cerebral autosomal recessive arteriopathy with subcortical infarcts and leukoencephalopathy (CARASIL) are two of the representative hereditary small vessel diseases accompanied by degeneration of mural cells (Uemura et al., 2020). Both CADASIL and CARASIL are characterized by lacunar infarcts, cerebral microbleeds, white matter injury, and enlarged perivascular spaces. These changes are similar to the findings in patients with sporadic small vessel disease (Shindo, Ishikawa et al.), suggesting that understanding the pathogenesis of CADASIL and CARASIL is important for analysing sporadic small vessel disease (Mizuno et al.).

Within this series of papers, Panahi et al. demonstrated that gene and protein expression of GLUT2 and GLUT4 were altered in a cellular model and post-mortem brains of CADASIL patients, which was consistent with decreased CBF and glucose uptake in CADASIL patients. CADASIL has been considered a rare disease caused by the mutation of *NOTCH3* gene. Shindo, Tabei et al. estimated the prevalence rate as 1.20 to 3.58 per 100,000 adults based on the result of a nationwide survey in Japan. Nevertheless, Okada et al. reported 3.5% of Japanese patients presenting lacunar infarction had a *NOTCH3* mutation in genetic screening. The clinical phenotype of CADASIL is diverse, ranging from asymptomatic to severe; thus, *NOTCH3* mutations would be underdiagnosed, especially in patients who are currently diagnosed with sporadic small vessel disease.

Apart from proposing several pathogenic mechanisms for small vessel disease, this topic looks to the future with several therapeutic possibilities for vascular cognitive impairment. Levit et al. described the importance of antihypertensive treatment in Alzheimer's disease. They reported that white matter perivascular astrocytes had a central role in neurological vulnerability to hypertension by using transgenic rats overexpressing a pathogenic human amyloid precursor protein. Furthermore, Kato et al. proposed that transforming growth factor β signaling is a therapeutic target for protecting mural cell degeneration, as transgenic mice overexpressing transforming growth factor β1 exhibited decreased pericyte coverage and increased diameter of the capillaries. It is becoming apparent that mural cell degeneration contributes to the pathogenic processes of dementia including Alzheimer's disease. The pericytes and SMCs have become increasingly important as a therapeutic target and thus research on this topic is likely to accelerate in the future.

AUTHOR CONTRIBUTIONS

SS, JM, and RC contributed to conceptualization and writing. All authors contributed to the article and approved the submitted version.

FUNDING

This work was supported by Grant-in-Aid for Japan Society for the Promotion of Science Fellows (SS) and the Canada Research Chair (Tier 1) in Alzheimer's Disease Therapeutics (JM).

REFERENCES

Albargothy, N. J., Johnston, D. A., MacGregor-Sharp, M., Weller, R. O., Verma, A., Hawkes, C. A., et al. (2018). Convective influx/glymphatic system: tracers injected into the CSF enter and leave the brain along separate periarterial basement membrane pathways. *Acta Neuropathol.* 136, 139–152. doi: 10.1007/s00401-018-1862-7

Grant, R. I., Hartmann, D. A., Underly, R. G., Berthiaume, A. A., Bhat, N. R., and Shih, A. Y. (2019). Organizational hierarchy and structural diversity of microvascular pericytes in adult mouse cortex. *J. Cereb. Blood Flow Metab.* 39, 411–425. doi: 10.1177/0271678X17732229

Keable, A., Fenna, K., Yuen, H. M., Johnston, D. A., Smyth, N. R., Smith, C., et al. (2016). Deposition of amyloid β in the walls of human leptomeningeal arteries in relation to perivascular drainage pathways in cerebral amyloid angiopathy.

Biochim. Biophys. Acta 1862, 1037–1046. doi: 10.1016/j.bbadis.2015.08.024

Maki, T., Okamoto, Y., Carare, R. O., Hase, Y., Hattori, Y., Hawkes, C. A., et al. (2014). Phosphodiesterase III inhibitor promotes drainage of cerebrovascular β-amyloid. *Ann. Clin. Transl. Neurol.* 1, 519–533. doi: 10.1002/acn3.79

Sweeney, M. D., Montagne, A., Sagare, A. P., Nation, D. A., Schneider, L. S., Chui, H. C., et al. (2019). Vascular dysfunction-The disregarded partner of Alzheimer's disease. *Alzheimers Dement.* 15, 158–167. doi: 10.1016/j.jalz.2018.07.222

Uemura, M., Nozaki, H., Kato, T., Koyama, A., Sakai, N., Ando, S., et al. (2020). HTRA1-Related cerebral small vessel disease: a review of the literature. *Front. Neurol.* 11:545. doi: 10.3389/fneur.2020.00545

Conflict of Interest: The authors declare that the research was conducted in the absence of any commercial or financial relationships that could be construed as a potential conflict of interest.

frontiers in Aging Neuroscience

ORIGINAL RESEARCH
published: 22 October 2019
doi: 10.3389/fnagi.2019.00289

Solving an Old Dogma: Is it an Arteriole or a Venule?

Matthew MacGregor Sharp[1], Theodore P. Criswell[1], Howard Dobson[2], Ciara Finucane[2], Ajay Verma[3] and Roxana O. Carare[1]*

[1]*Faculty of Medicine, Institute for Life Sciences, University of Southampton, Southampton, United Kingdom,* [2]*inVICRO, Boston, MA, United States,* [3]*Biogen Idec, Cambridge, MA, United States*

There are very few reliable methods in the literature to discern with certainty between cerebral arterioles and venules. Smooth muscle cells (SMC) and pericytes are present in both arterioles and venules, so immunocytochemistry for markers specific to intramural cells (IMC) is unreliable. This study employed transmission electron microscopy (TEM) and a canine brain to produce robust criteria for the correct identification of cerebral arterioles and venules based on lumen:vessel wall area, tested against the less accurate lumen diameter:vessel wall thickness. We first used morphology of IMC to identify two distinct groups of vessels; group 1 with morphology akin to venules and group 2 with morphology akin to arterioles. We then quantitatively assessed these vessels for lumen:vessel wall area ratio and lumen diameter:wall thickness ratio. After assessing 112 vessels, we show two distinct groups of vessels that can be separated using lumen:vessel wall area (group 1, 1.89 −10.96 vs. group 2, 0.27–1.57; $p < 0.001$) but not using lumen diameter:vessel wall thickness where a substantial overlap in ranges between groups occurred (group 1, 1.58–22.66 vs. group 2, 1.40–11.63). We, therefore, conclude that lumen:vessel wall area is a more sensitive and preferred method for distinguishing cerebral arterioles from venules. The significance of this study is wide, as cerebral small vessel disease is a key feature of vascular dementia and understanding the pathogenesis relies on correct identification of vessels.

Keywords: venules, arterioles, intramural cell, transmission electron microscopy, morphology

OPEN ACCESS

Edited by:
Gjumrakch Aliev,
GALLY International Biomedical Research, United States

Reviewed by:
Siu-Lung Chan,
University of Vermont, United States
Andy Shih,
Medical University of South Carolina, United States

****Correspondence:***
Matthew MacGregor Sharp
m.t.sharp@soton.ac.uk

Received: *06 August 2019*
Accepted: *07 October 2019*
Published: *22 October 2019*

Citation:
MacGregor Sharp M, Criswell TP, Dobson H, Finucane C, Verma A and Carare RO (2019) Solving an Old Dogma: Is it an Arteriole or a Venule? Front. Aging Neurosci. 11:289. doi: 10.3389/fnagi.2019.00289

INTRODUCTION

Throughout the literature on anatomical and pathological features of the cerebral circulation, there is a lack of consistent criteria for differentiating cerebral venules from arterioles. Most studies identify arterioles by ratio of lumen diameter to vessel wall thickness and/or the presence of vascular smooth muscle cells (SMC), either immunohistochemically, such as with α-smooth muscle actin stain, or microscopically by identifying a thick tunica media containing multiple SMC layers (Scharrer, 1940; Skalli et al., 1989; Albargothy et al., 2017). While this method allows for identification of larger leptomeningeal vessels that possess multiple SMC layers, its accuracy for identifying the smaller arterioles and venules found in brain

Abbreviations: SMC, smooth muscle cells; IMC, intramural cells; TEM, transmission electron microscopy.

TABLE 1 | Characteristics of the intramural cells found within the walls of intracerebral arterioles and venules, as seen in transverse sections though the vessels with transmission electron microscopy.

Ultrastructural features	Arteriole	Venule
Complete/incomplete layer around vessel	Always complete	Often incomplete
Intramural cell shape	Square/rectangular, "block like"	Flattened/spindle-like
Number of intramural cell layers	Most commonly 1, occasionally 2, rarely 3	1 Layer, occasionally cells overlap
Caveolae (flask shaped invaginations of the cell membrane)	Present	Rare
Electron dense myosin bands (part of contractile apparatus)	Present	Rare

parenchyma is questionable. These smaller vessels, derived from the neural crest of the ectoderm, both possess a form of tunica media containing a single layer of SMC and/or pericytes [both classed as intramural cells (IMC)] embedded within the same endothelial basement membrane (Rhodin, 1968; Roggendorf and Cervós-Navarro, 1983) and so could potentially have very similar ratios of lumen diameter to vessel wall thickness. Cerebral arterioles for example have been shown to be much thinner-walled than their larger counterparts (Rhodin, 1967; Dahl, 1973). Venules also traditionally have thinner walls and larger lumina, although to our knowledge, no study has provided quantification of the respective ratios for each vessel type. To confuse matters further, SMCs and pericytes both express α-smooth muscle actin and share many functional characteristics, particularly at post-capillary level (Rhodin, 1962, 1968, 1980; Krisch et al., 1984; Krisch, 1988; Skalli et al., 1989; Zhang et al., 1990; Owens et al., 2008; Díaz-Flores et al., 2009; Armulik et al., 2011). Several key differences in morphology and distribution have been observed using transmission electron microscopy (TEM) but these have been separately described and not directly compared for each vessel type (see **Table 1** for summary of key differences; Rhodin, 1962, 1967, 1968, 1980; Dahl, 1973; Motta, 1990; Armulik et al., 2011).

Currently, to correctly distinguish cerebral venules and arterioles a combination of immunohistochemistry for α-smooth muscle actin expression and ultrastructural examination by TEM (particularly for IMC morphology) is required. Several studies claiming to just use ratio of lumen diameter to vessel wall thickness fail to recognize that vessels are rarely smoothly circumscribed or fully circular and that vessel wall thickness can be dramatically altered depending on the plane of section through the tissue (Weller et al., 1998, 2009; Mendel et al., 2013). Ultimately, this has made distinguishing small venules from arterioles challenging and studies have fundamentally confused the two (Scharrer, 1940; Roggendorf et al., 1978; Roggendorf and Cervós-Navarro, 1983). This is particularly relevant to cerebral small vessel disease in which both arterioles and venules can be affected by pathological changes such as arteriolar hyalinosis (collagenosis/fibrosis), fibrinoid necrosis or venous collagenosis. Correct identification of the type of vessel involved may help to facilitate more targeted treatment strategies.

In this study, we use TEM to ascertain if the ratio of lumen to vessel wall area is more accurate than the ratio of lumen diameter to vessel wall thickness in correctly differentiating the small arterioles and venules found in brain parenchyma. We chose to use TEM as the resolution of normal light microscopy does not allow for clear identification of the vessel wall and its components. We first differentiate vessel types based on morphology and arrangement of IMCs from published literature that have utilized TEM (Rhodin, 1962, 1968, 1980; Krisch et al., 1984; Krisch, 1988; Skalli et al., 1989; Zhang et al., 1990; Owens et al., 2008; Díaz-Flores et al., 2009; Armulik et al., 2011). We then analyze these vessels for both ratio of lumen to vessel wall area and ratio of lumen diameter to vessel wall thickness. Image analysis was performed using a beagle dog brain but the TEM methods described here are easily transferrable to any mammalian tissue to produce a robust criterion to differentiate cerebral arterioles from venules.

MATERIALS AND METHODS

Animals

The 12-year-old beagle brain tissue used in this study was supplied and intracardially perfused by the Lawson Health Sciences Research Institute, London, ON, Canada. Euthanasia was performed respecting ethical governance rules at the site.

Tissue Preparation for Transmission Electron Microscopy

Under routine general anesthesia a 12-year-old Beagle dog was perfused intracardially with 0.1 M piperazine-N, N′-bis(2-ethanesulfonic acid) buffer (PIPES, PH 7.2) followed by 4% formaldehyde plus 3% glutaraldehyde in 0.1 M PIPES buffer at

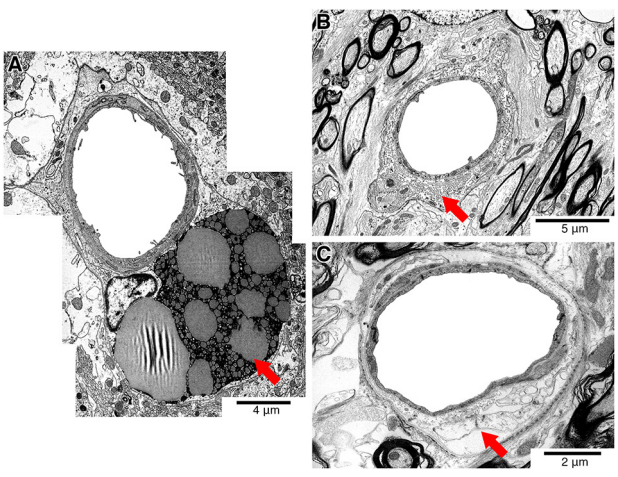

FIGURE 1 | Representative electron micrographs showing pathology that affects the vessel wall (red arrows). Vessels showing perivascular lipofuscin cuffs **(A)**, perivenous collagenosis **(B)** or dilated perivascular spaces **(C)** were excluded from the study.

PH 7.2. The brain was removed, post-fixed overnight in fresh fixative and then sectioned into 10 mm coronal slices. 60 μm coronal slices of left frontal, parietal and occipital lobes were cut using a Leica VT1000 vibratome. Representative sections of white matter and cortical gray matter were microdissected and processed for TEM according to our own optimized protocols (Sharp et al., 2017).

Tissue blocks were trimmed and 80 nm ultrathin sections cut using an Ultracut E microtome. The sections were transferred onto copper grids and counter-stained with lead citrate. Grids were examined using a Hitachi H7000 TEM operating a EMSIS MegaView III digital camera and EMSIS image capture software (formerly iTEM software, Universal TEM Imaging platform, Soft Imaging System, Münster, Germany).

Image Acquisition

Grids were examined in a sequential manner from top left to bottom right. Vessels sectioned in transverse plane were first imaged at a higher magnification for IMC analysis and then lower magnification for lumen:wall ratio analysis. We identified vessels to be in transverse plane if all components of the vessel wall could be clearly resolved.

To avoid imaging capillaries and post-capillary venules, we excluded vessels with a surface area of less than 70 μm^2. We also did not include vessels that showed artifact or vessel altering pathology such as dilated perivascular spaces, extensive perivascular lipofuscin cuffs or perivenous collagenosis which would often exceed the entire vessel surface area (Black, 2011) (**Figure 1**).

Image Analysis

Higher power images of each vessel were used to qualitatively asses the morphology of IMC based on the ultrastructural features listed in **Table 1**. Low power images of the same vessels were then used to calculate both vessel lumen:wall ratio and ratio of lumen diameter to vessel wall thickness. Briefly, the vessel lumen and vessel wall were outlined in Adobe Photoshop CS6 using two distinct colors, exported as a TIFF file and then imported into ImageJ (National Institutes of Health developed imaging processing program). Image size metrics and an ImageJ threshold function was used to measure both the surface area and width of each demarcated feature to create either a lumen:wall or lumen diameter:wall thickness ratio (**Figure 2**). Statistical analysis was performed using SPSS and a Mann–Whitney *U*-test (significance set at $P < 0.05$).

RESULTS

In total, 112 vessels were analyzed. We first assessed the vessels for the morphology and arrangement of IMCs. We found that the vessels could be separated into two distinct groups that we have labeled group 1 (81 vessels) and group 2 (31 vessels). Group

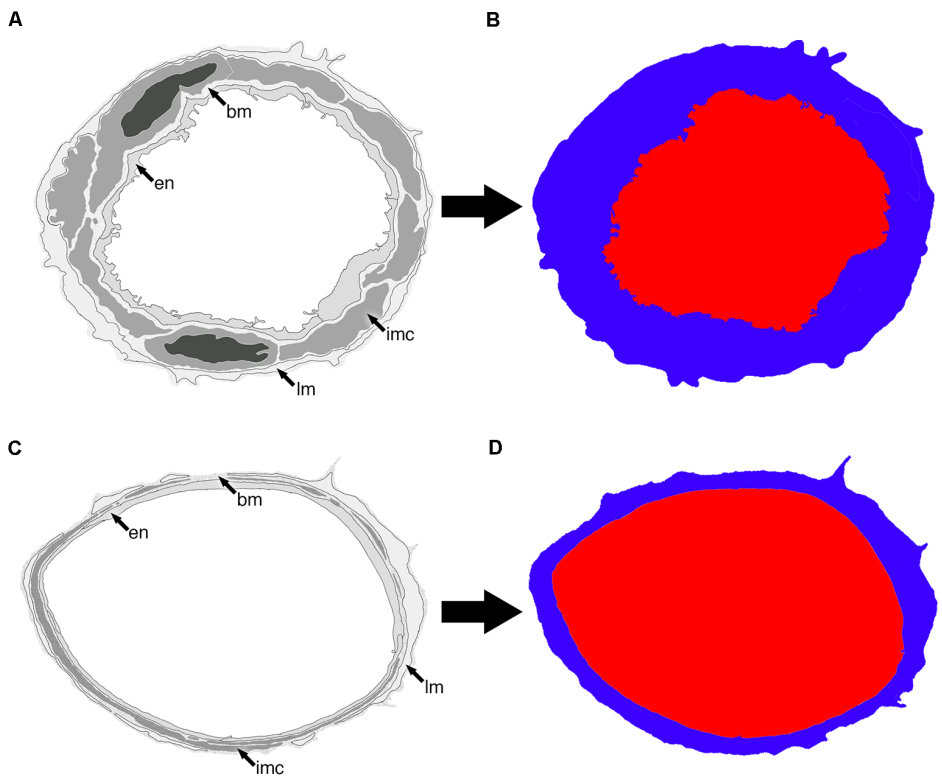

FIGURE 2 | Representative diagram of two vessels **(A,C)** and how they appear once segmented into lumen (red) and vessel wall (blue; **B,D**). The endothelium (en), basement membrane (bm), intramural cells (IMC; sm) and leptomeninges (lm) are all included as part of the vessel wall.

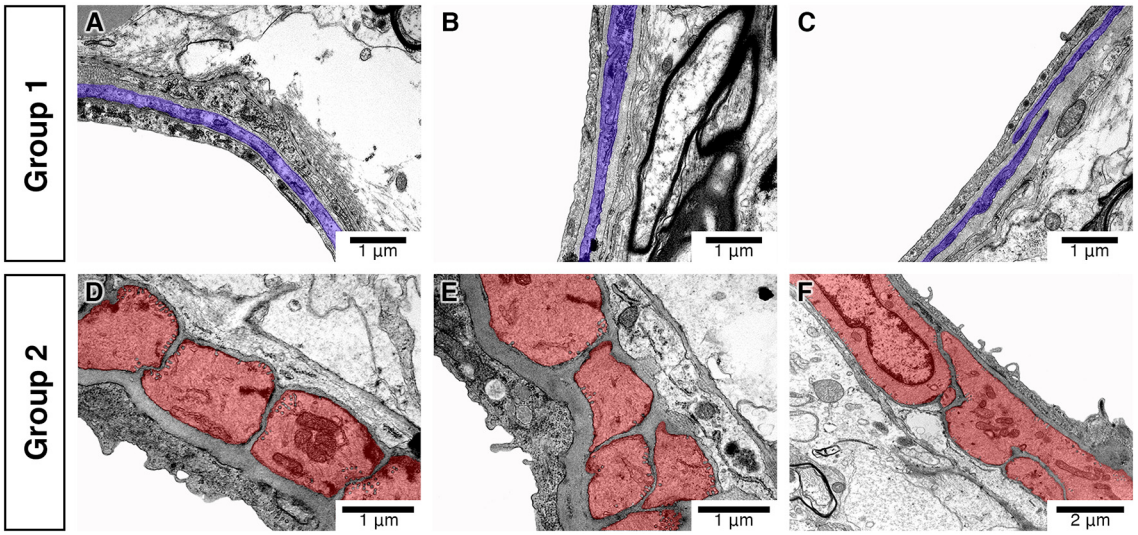

FIGURE 3 | Differences in the morphology and distribution of IMC. Vessels classified into group 1 **(A–C)** have spindle-like IMC (purple) with few caveolae and electron-dense myosin bands. Vessels classified into group 2 **(D–F)** have block-like IMC (red) with multiple caveolae and electron-dense myosin bands.

1 vessels consisted of IMCs that formed a discontinuous layer and appeared spindle-like with few caveolae and electron-dense myosin bands. Group 2 vessels formed a continuous single layer and appeared block-like with multiple caveolae and electron-dense myosin bands (**Figure 3**). These results agree with previous findings (**Table 1**).

In group 1 vessels, the area of the lumen was on average 3.9489 times bigger than that of the vessel wall (range 1.89–10.96). The diameter of the lumen was on average 7.3199 times bigger than the thickness of the vessel wall (range 1.58–22.66). The large range of group 1 vessels was partly due to an exponential increase in ratio with the largest vessels analyzed. In group 2 vessels, the area of the lumen was on average 0.9317 times smaller than that of the vessel wall (range 0.27–1.57) but the diameter of the lumen was on average 4.348 times bigger than the thickness of the vessel wall (range 1.40–11.63).

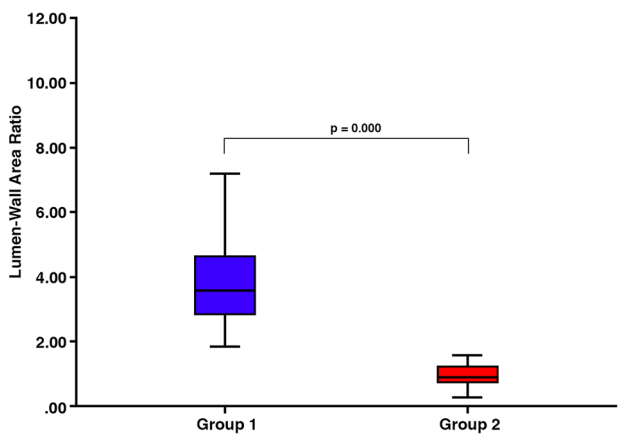

FIGURE 4 | There are significant differences in the lumen:wall area ratio between vessels classified into group 1 and those classified into group 2 ($p = 0.000$).

There was a significant difference in lumen:wall area ratio between group 1 and group 2 vessels (Mann–Whitney test, $p = 0.000$) with no overlap in the range of lumen:wall area ratio (**Figure 4**). There was also a significant difference in the lumen diameter:wall thickness ratio between group 1 and group 2 vessels (Mann–Whitney test, $p = 0.000$; **Figure 5A**). However, we found a substantial overlap in ranges between groups and were unable to distinguish between any vessels below the average lumen diameter:wall thickness ratio seen in group 2 vessels (4.97, Mann–Whitney test, $p = 0.817$; **Figure 5B**).

DISCUSSION

Early research into the ultrastructure of intracerebral blood vessels was hindered by issues with the correct identification of vessel types (Pfeiffer, 1930; Scharrer, 1940; Roggendorf et al., 1978; Roggendorf and Cervós-Navarro, 1983). These studies were based on a classification system established using dermal veins in rabbits (Rhodin, 1968). However, the ultrastructure of venules differs considerably across different organs and thus a criterion based on dermal veins cannot be used as a means of classification in the brain (Rhodin, 1968; Duvernoy et al., 1981; Roggendorf and Cervós-Navarro, 1983). Duvernoy et al. (1981) used resin casts to trace the pathway of intracortical vessels to the large surface pial vessels which were easier to identify. Even this seminal study was not able to clearly differentiate between intraparenchymal vessels concluding that this was difficult using a single plane of section (Duvernoy et al., 1981). Here, we describe a method that utilizes TEM to produce a robust criterion to differentiate parenchymal vessels based on lumen:wall area ratio. It is possible that this criterion may then be applied to other

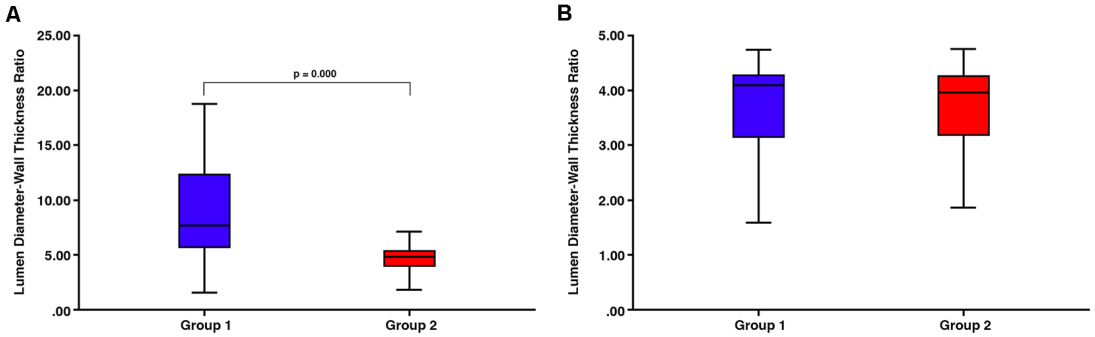

FIGURE 5 | (A) There is a substantial overlap in ranges between group 1 and group 2 vessels despite the overall significant difference in the lumen diameter:wall thickness ratio ($p = 0.000$). **(B)** There is no significant difference between any vessels below the average lumen diameter:wall thickness ratio seen in group 2 vessels (4.97, Mann–Whitney test, $p = 0.817$).

imaging techniques such as standard light microscopy but further work would be required to confirm this.

In the brain of a large mammal (beagle dog), we were able to differentiate parenchymal vessels into two groups based on the widely accepted criteria related to intramural cell morphology and distribution (Rhodin, 1962, 1967, 1968, 1980; Dahl, 1973; Motta, 1990; Armulik et al., 2011). We found that these two groups could be separated by differences in lumen:wall area ratio far more effectively than by using lumen diameter:vessel wall thickness which did not allow for the differentiation of venules that were a similar size to arterioles. As far as we are aware, combining intramural cell morphology with lumen:wall area ratio has not been done before. We found that vessels with a lumen:wall area ratio from 1.89 to 10.96 have discontinuous spindle-like IMC that in the literature have been applicable to venules. However, the larger range of lumen:wall area ratio in these vessels suggests that some ascending venules may have been included. Conversely, we found that vessels with a lumen:wall area ratio from 0.27 to 1.57 have continuous block-like IMC that also in the literature have been applicable to arterioles. We, therefore, conclude that the vessels that we have classified into group 1 are venules and group 2 are arterioles.

Emerging studies have highlighted the previously unrecognized role of venules (Moody et al., 1995, 1997; Brown et al., 2002; Pantoni, 2010; Joutel and Faraci, 2014; Kalaria, 2016) in vascular pathology such as small vessel disease. This has exposed the absence of robust criteria for accurately differentiating between small intracerebral arterioles and venules. In this study, we have shown that intracerebral venules can be successfully differentiated from intracerebral arterioles by simple vessel lumen:wall area ratios. The significance of this is wide and one application is to better understand the types of vessels affected in small vessel disease. The major pathological features of small vessel disease are the changes in small arteries and arterioles in white and gray matter that include arteriolar hyalinosis (collagenosis/fibrosis), fibrinoid necrosis and venous collagenosis. Such changes result in loss of elasticity in the vessel walls and disruption of vessel functions. A reliable system for differentiating between the types of vessels forms the basis for improving the understanding of the pathogenesis and identifying suitable therapeutic targets.

This study was limited to one beagle dog brain and only included vessels that were in transverse section. However, the methods described here could possibly be used to incorporate vessels in obliques section, assuming that all parts of the vessel wall and the lumen are affected by the same degree of distortion caused by oblique sectioning. Similarly, further work is required to ascertain if our method can be utilized in other species.

DATA AVAILABILITY STATEMENT

The datasets generated for this study are available on request to the corresponding author.

ETHICS STATEMENT

The animal study was reviewed and approved by the local Animal Care Committee and the work was carried out at a facility licensed under the Ontario Animals for Research Act and accredited with the Canadian Council on Animal Care.

AUTHOR CONTRIBUTIONS

Electron microscopy and image analysis was performed by MM and TC. HD, CF and AV provided perfused tissue. RC designed the project. All authors contributed equally to the preparation of the manuscript.

FUNDING

This project was funded by the Jean Shanks Foundation and Biogen Idec whose financial contributions are gratefully acknowledged.

ACKNOWLEDGMENTS

We gratefully acknowledge funding from Biogen for this study.

REFERENCES

Albargothy, N. J., MacGregor Sharp, M., Gatherer, M., Morris, A., Weller, R. O., Hawkes, C., et al. (2017). "Investigating the lymphatic drainage of the brain: essential skills and tools," in *Inflammation: Methods and Protocols*, eds B. E. Clausen, and J. D. Laman (New York, NY: Humana Press), 343–365. doi: 10.1007/978-1-4939-6786-5_24.

Armulik, A., Genové, G., and Betsholtz, C. (2011). Pericytes: developmental, physiological, and pathological perspectives, problems and promises. *Dev. Cell* 21, 193–215. doi: 10.1016/j.devcel.2011.07.001

Black, S. E. (2011). Vascular cognitive impairment: epidemiology, subtypes, diagnosis and management. *J. R. Coll. Physicians Edinb.* 41, 49–56. doi: 10.4997/jrcpe.2011.121

Brown, W. R., Moody, D. M., Challa, V. R., Thore, C. R., and Anstrom, J. A. (2002). Venous collagenosis and arteriolar tortuosity in leukoaraiosis. *J. Neurol. Sci.* 203–204, 159–163. doi: 10.1016/s0022-510x(02)00283-6

Dahl, E. (1973). The fine structure of intracerebral vessels. *Z. Zellforsch. Mikrosk. Anat.* 145, 577–586. doi: 10.1007/bf00306725

Díaz-Flores, L., Gutiérrez, R., Madrid, J. F., Varela, H., Valladares, F., Acosta, E., et al. (2009). Pericytes. Morphofunction, interactions and pathology in a quiescent and activated mesenchymal cell niche. *Histol. Histopathol.* 24, 909–969. doi: 10.14670/HH-24.909

Duvernoy, H. M., Delon, S., and Vannson, J. L. (1981). Cortical blood vessels of the human brain. *Brain Res. Bull.* 7, 519–579. doi: 10.1016/0361-9230(81)90007-1

Joutel, A., and Faraci, F. M. (2014). Cerebral small vessel disease: insights and opportunities from mouse models of collagen IV-related small vessel disease and cerebral autosomal dominant arteriopathy with subcortical infarcts and leukoencephalopathy. *Stroke* 45, 1215–1221. doi: 10.1161/STROKEAHA.113.002878

Kalaria, R. N. (2016). Neuropathological diagnosis of vascular cognitive impairment and vascular dementia with implications for Alzheimer's disease. *Acta Neuropathol.* 131, 659–685. doi: 10.1007/s00401-016-1571-z

Krisch, B. (1988). Ultrastructure of the meninges at the site of penetration of veins through the dura mater, with particular reference to Pacchionian granulations. Investigations in the rat and two species of New-World monkeys (*Cebus apella, Callitrix jacchus*). *Cell Tissue Res.* 251, 621–631. doi: 10.1007/bf00214011

Krisch, B., Leonhardt, H., and Oksche, A. (1984). Compartments and perivascular arrangement of the meninges covering the cerebral cortex of the rat. *Cell Tissue Res.* 238, 459–474. doi: 10.1007/bf00219861

Mendel, T., Wierzba-Bobrowicz, T., Stepien, T., and Szpak, G. M. (2013). β-amyloid deposits in veins in patients with cerebral amyloid angiopathy and intracerebral haemorrhage. *Folia Neuropathol.* 51, 120–126. doi: 10.5114/fn.2013.35954

Moody, D. M., Brown, W. R., Challa, V. R., and Anderson, R. L. (1995). Periventricular venous collagenosis: association with leukoaraiosis. *Radiology* 194, 469–476. doi: 10.1097/00005072-199505000-00227

Moody, D. M., Brown, W. R., Challa, V. R., Ghazi-Birry, H. S., and Reboussin, D. M. (1997). Cerebral microvascular alterations in aging, leukoaraiosis, and Alzheimer's disease. *Ann. N Y Acad. Sci.* 826, 103–116. doi: 10.1111/j.1749-6632.1997.tb48464.x

Motta, P. (1990). *Ultrastructure of Smooth Muscle.* Boston, MA: Kluwer Academic Publishers.

Owens, T., Bechmann, I., and Engelhardt, B. (2008). Perivascular spaces and the two steps to neuroinflammation. *J. Neuropathol. Exp. Neurol.* 67, 1113–1121. doi: 10.1097/nen.0b013e31818f9ca8

Pantoni, L. (2010). Cerebral small vessel disease: from pathogenesis and clinical characteristics to therapeutic challenges. *Lancet Neurol.* 9, 689–701. doi: 10.1016/s1474-4422(10)70104-6

Pfeiffer, R. A. (1930). *Grundlegende Untersuchungen Für die Angioarchitektonik des Menschlichen Gehirns.* Berlin: Verlag von Julius Springer.

Rhodin, J. A. G. (1962). Fine structure of vascular walls in mammals with special reference to smooth muscle component. *Physiol. Rev. Suppl.* 5, 48–87.

Rhodin, J. A. G. (1967). The ultrastructure of mammalian arterioles and precapillary sphincters. *J. Ultrastruct. Res.* 18, 181–223. doi: 10.1016/s0022-5320(67)80239-9

Rhodin, J. A. G. (1968). Ultrastructure of mammalian venous capillaries, venules, and small collecting veins. *J. Ultrastruct. Res.* 25, 452–500. doi: 10.1016/s0022-5320(68)80098-x

Rhodin, J. A. G. (1980). "Architecture of the vessel wall," in *Comprehensive Physiology*, ed. R. Terjung (Hoboken, NJ: John Wiley & Sons, Inc), 1–31.

Roggendorf, W., and Cervós-Navarro, J. (1983). "Ultrastructure of venules in human and cat brain," in *The Cerebral Veins: An Experimental and Clinical Update*, eds L. M. Auer and F. Loew (Vienna: Springer Vienna), 39–46.

Roggendorf, W., Cervós-Navarro, J., and Lazaro-Lacalle, M. D. (1978). Ultrastructure of venules in the cat brain. *Cell Tissue Res.* 192, 461–474. doi: 10.1007/bf00212326

Scharrer, E. (1940). Arteries and veins in the mammalian brain. *Anat. Rec.* 78, 173–196. doi: 10.1002/ar.1090780204

Sharp, M. M., Page, A., Morris, A., Weller, R. O., and Carare, R. O. (2017). Quantitative assessment of cerebral basement membranes using electron microscopy. *Methods Mol. Biol.* 1559, 367–375. doi: 10.1007/978-1-4939-6786-5_25

Skalli, O., Pelte, M. F., Peclet, M. C., Gabbiani, G., Gugliotta, P., Bussolati, G., et al. (1989). α-smooth muscle actin, a differentiation marker of smooth muscle cells, is present in microfilamentous bundles of pericytes. *J. Histochem. Cytochem.* 37, 315–321. doi: 10.1177/37.3.2918221

Weller, R. O., Boche, D., and Nicoll, J. A. R. (2009). Microvasculature changes and cerebral amyloid angiopathy in Alzheimer's disease and their potential impact on therapy. *Acta Neuropathol.* 118, 87–102. doi: 10.1007/s00401-009-0498-z

Weller, R. O., Massey, A., Newman, T. A., Hutchings, M., Kuo, Y. M., and Roher, A. E. (1998). Cerebral amyloid angiopathy: amyloid-β accumulates in putative interstitial fluid drainage pathways in Alzheimer's disease. *Am. J. Pathol.* 153, 725–733. doi: 10.1016/s0002-9440(10)65616-7

Zhang, E. T., Inman, C. B., and Weller, R. O. (1990). Interrelationships of the pia mater and the perivascular (Virchow-Robin) spaces in the human cerebrum. *J. Anat.* 170, 111–123.

Conflict of Interest: The authors declare that the research was conducted in the absence of any commercial or financial relationships that could be construed as a potential conflict of interest.

frontiers in Aging Neuroscience

ORIGINAL RESEARCH
published: 11 February 2020
doi: 10.3389/fnagi.2020.00015

Vital Functions Contribute to the Spread of Extracellular Fluids in the Brain: Comparison Between Life and Death

Alina Piotrowska[1], Karsten Winter[1], Roxana O. Carare[2] and Ingo Bechmann[1]**

[1] *Institute of Anatomy, Leipzig University, Leipzig, Germany,* [2] *Faculty of Medicine, University of Southampton, Southampton, United Kingdom*

Vascular pulsations, contractions of vascular smooth muscle cells and breathing have been reported to foster movement and clearance of interstitial and cerebrospinal fluids from the brain. The aim of this study was to estimate the contribution of these vital functions. We compared the spread of an injected hydrophilic tracer (Fluoro-Emerald, a 10 kDa fluorescein-coupled dextran amine) in the brains of live anesthetized and sacrificed rats at 30 and 90 min after injection. To determine the overall pattern of distribution of tracers, we created 3D-reconstructions of the horizontal transections of the whole brain. Immunofluorescence staining with laminin and collagen IV was performed to determine the pattern of distribution of tracer in relation to the cerebrovascular basement membranes. We found that diffusion was widely restricted to the periventricular region in sacrificed rats with no spread to the contralateral hemisphere, while the bulk flow occurred along the vasculature and reached the surface and the contralateral hemisphere as soon as 30 min after injection in live anesthetized animals. The tracer appeared to be localized along the vascular basement membranes and along fiber tracts as reported previously. Thus, our data indicate that vital functions are essential for the remote movement of extracellular fluids within the cerebral parenchyma.

Keywords: clearance of the brain, blood-brain-barrier, cervical lymph nodes, Virchow-Robin space, glymphatic system

OPEN ACCESS

Edited by:
Silvia Fossati,
Temple University, United States

Reviewed by:
Yorito Hattori,
Cornell University, United States
Miguel A. Gama Sosa,
James J. Peters VA Medical Center, United States

****Correspondence:***
Alina Piotrowska
Alina.b.piotrowska@gmail.com
Ingo Bechmann
Ingo.Bechmann@medizin.uni-leipzig.de

Received: *21 June 2019*
Accepted: *16 January 2020*
Published: *11 February 2020*

Citation:
Piotrowska A, Winter K, Carare RO and Bechmann I (2020) Vital Functions Contribute to the Spread of Extracellular Fluids in the Brain: Comparison Between Life and Death. Front. Aging Neurosci. 12:15. doi: 10.3389/fnagi.2020.00015

INTRODUCTION

The immune responses of the brain are restricted by the presence of a blood-brain barrier and the lack of traditional lymphatic vessels (Bechmann et al., 2007; Galea et al., 2007; Abbott et al., 2018), but homeostasis of extracellular fluids is crucial for synaptic transmission (Ivens et al., 2007).

Abbreviations: °C, degree Celsius; µl, microliter; µm, micrometer; 3D, three-dimensional; AQP4, aquaporin 4; CSF, cerebrospinal fluid; DAPI, 4′,6-Diamidin-2-phenylindol; DCLN, deep cervical lymph nodes; DKS, donkey serum; GAD, glutaraldehyde; ICP, intracranial pressure; IgG, immunoglobulin G; ILN, inguinal lymph nodes; IPAD, intramural periarterial drainage; ISF, interstitial fluid; kDa, kilodalton; min, minute; mm, millimeter; mM, millimolar; ms, millisecond; NaCl, sodium chloride; PBS, phosphate buffered saline; PFA, paraformaldehyde; PI, post injection; PVS, perivascular space; SCLN, superficial cervical lymph nodes.

While it is clear that IFS and soluble antigens drain into cervical lymph nodes (Schwalbe, 1869; el-Gindi et al., 1973; Rosenberg et al., 1980; Cserr and Knopf, 1992; Kida et al., 1993; de Vos et al., 2002; Koh et al., 2005; Goldmann et al., 2006; Kaminski et al., 2012; Locatelli et al., 2012; Ma et al., 2017, 2019), the driving forces for extracellular movements and the respective pathways have only been identified and are still under debate (Cserr et al., 1977; Rosenberg et al., 1980; Abbott et al., 2018; Gakuba et al., 2018; Plog and Nedergaard, 2018; Ma et al., 2019). One highly discussed pathway is the "glymphatic system" consisting of a convective influx system of the CSF into the brain (Iliff et al., 2012; Abbott et al., 2018). According to the "glymphatic" hypothesis CSF and ISF exchange takes place from the subarachnoid space via periarterial Robin-Virchow spaces, through the brain parenchyma toward perivenous spaces (Iliff and Nedergaard, 2013; Iliff et al., 2013; Nedergaard, 2013). Tracers in the CSF are thought to enter the parenchyma as convective flow along Virchow-Robin spaces of arteries, where AQP4 expressed on astrocytic endfeet of the *glia limitans* perivascularis is supposed to play a major role (Iliff et al., 2012), and return to the CSF via the walls of veins but this process has been extensively debated (Hladky and Barrand, 2014; Asgari et al., 2016; Bakker et al., 2016; Holter et al., 2017; Abbott et al., 2018; Faghih and Sharp, 2018; Gakuba et al., 2018; Ma et al., 2019). The anatomical route of entry of the CSF into the brain is along the basement membranes of the cerebral arterioles (pial-glial basement membranes) and the efflux of ISF is along the basement membranes surrounding arterial smooth muscle cells, the IPAD pathway (Albargothy et al., 2018). The convective influx/glymphatic network can be seen as a low resistance network and is believed to play a major role in spreading of large molecules such as 150 kDa IgG (Pizzo et al., 2018) and smaller molecules such as 40kDa peroxidase (Cserr and Ostrach, 1974; Cserr et al., 1977). CSF including different waste products experimentally tested using intracisternally injected tracers drain to cervical lymph nodes via several pathways along cranial nerves as well as spinal cord roots (Bradbury et al., 1981; McComb, 1983; Kida et al., 1993; Koh et al., 2005; Ma et al., 2017). Direct drainage to the blood via arachnoid villi has been postulated for a long time, but its contribution to CSF outflow is currently under discussion (Ma et al., 2017). As driving forces, vascular pulsations (Harrison et al., 2018) have been shown to contribute to perivascular movement within the perivascular channel system, as unilateral ligation of one carotid artery reduced vascular pulsatility and spread of a tracer (Iliff et al., 2013; Asgari et al., 2016). Moreover, sleep (Di Rocco et al., 1975; Nilsson et al., 1992; Xie et al., 2013), breathing (Dreha-Kulaczewski et al., 2015), anesthesia and death (Ma et al., 2019) have also been accounted for the movement and clearance of intrathecal fluids, but direct visualization of the latter is still missing. Commonly used imaging techniques such as MRI (Harrison et al., 2018) and CT (Murtha et al., 2014) scans offer a low resolution compared to microscopic studies whereas most microscopic approach lack a 3D view with a satisfactory depth. The aim of this study was to visualize the net effect of vital functions on the movement and distribution of extracellular fluids within the brain after intraparenchymal injections. To this end, we monitored bulk flow of soluble Fluoro-Emerald of 10.000 molecular weight at 30 and 90 min after intraparenchymal injection in living compared to sacrificed rats.

MATERIALS AND METHODS

Animals

Twenty-four, 3-month-old Sprague Dawley rats were used in this study. Animal husbandry was performed in the animal facilities of the Faculty of Medicine, University of Leipzig according to European (Council Directive 86/609/EEC) and German ("Tierschutzgesetz") guidelines for the welfare of experimental animals and approved by the local authorities (Landesdirektion Sachsen; TV03/13). Rats were housed in the central breeding facility of the Medical Faculty of the University of Leipzig under standard conditions with food and water *ad libitum*.

Stereotactic Tracer Application

Figure 1 shows the experimental setup. Animals were split into two groups. The first group was euthanized with an overdose of isoflurane, before stereotactic surgery. Consequently a 15% concentration of isoflurane was infused in a cylindrical glass box. The animal was placed in the box until it stopped breathing. Isoflurane exposure continued for one more minute subsequently. Death was verified manually by missing cardiac pulsation and missing blood flow during the following surgery. The injection was performed 20 min (±2 min) after death depending on the quickness of the surgical procedure described below. Animals of the second group were anesthetized with 100 mg/kg ketamine and 10 mg/kg xylazine diluted 50% in NaCl 0.9% injected intraperitoneally. All animals were put into a stereotactic frame (Narishige – Type ST-7 No106002, Tokyo, Japan) and received an injection of 3 µl of 10 mM FlouroEmerald using a 26 gauge Hamilton syringe (SYR 10 µL, #701, ga26s/51mm/pst2, P/N: 80300/00, WO 1002554, Hamilton company, Reno, Nevada). The surgery was performed as reported previously (Bechmann and Nitsch, 1997). Briefly, eyes were protected and after exposing the skull, a burr hole was drilled at antero-posterior (AP) 1, 3 mm, lateral (L) 4.5 mm from Lambda, and the syringe inserted vertically (V) for 5.5 mm, aiming for the entorhinal cortex. The tracer was applied over 5 min at a rate of 0.6 µl/min, the needle was then removed after 1 min to prevent backflow. Injection rate and volume were chosen accordingly to prevent raise in ICP (Yang et al., 2013). After the injection, the hole was sealed using bone wax (Ethicon, Johnson and Johnson International) to avert artifacts from ICP loss. In both groups, body temperature was measured using a rectal probe and adjusted to 37°C using a heat pad (TR-200, FST) on which the animals were placed. Animals of the second group were sacrificed with an overdose of isoflurane at 30 and 90 min after tracer injection.

Tissue Preparation

The rats were dissected either 30 or 90 min after the injection, the brain was immersion fixed in 4% PFA and 1% GAD, since transcardial perfusion was impossible to perform due to coagulation in the sacrificed animals. $N = 4$ animals received

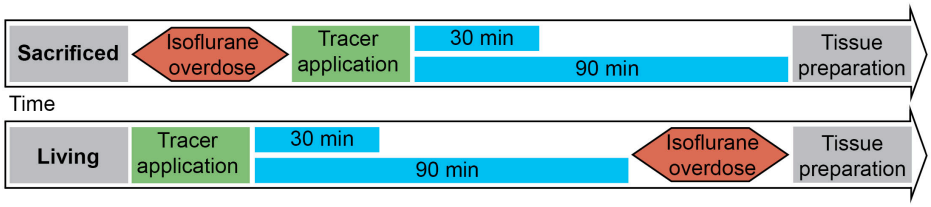

FIGURE 1 | Experimental setup: 3 μl of tracer was injected into the entorhinal cortex of sacrificed and living rats over 5 min. Body temperature was constantly monitored and kept steady until brains and lymph nodes were removed after 30 or 90 min. (n = 7 for 30 min per group, n = 3 for 90 min per group).

transcardial perfusion and were therefore excluded from the final analysis. Lymph nodes were dissected and divided into four groups according to Takahashi and Patrick (1987): right and left DCLN, SCLN, and ILN, and also immersion fixed in 4% PFA. After 24 h the brains of n = 20 animals were cut horizontally into 70 μm thick slices using a vibratome (Leica VT1200). The slices were stored in 0.09% sodium azide until they were washed and stained with DAPI for 5 min. Consecutive slices of the whole brain were prepared for n = 10 animals: n = 6 for 90 min PI (n = 3 for sacrificed (S90) and n = 3 for living (L90) animals) as well as n = 4 for 30 min PI (n = 2 for sacrificed (S30) and n = 2 for living (L30) animals). For n = 10 animals at time point 30 min (n = 5 sacrificed and n = 5 living) several slices were stored in the same well and the brains could therefore not be used for the complete 3D reconstruction. Lymph nodes were frozen in Tissue-Tek O.C.T. Compound™ at −80°C, cut into 16 μm thick slices using a cryostat (Leica CM3050 S) and stored at −80°C until they were washed, stained with DAPI for 5 min and covered with mounting medium.

3D Reconstruction

Each slice was put on a separate microscope slide and covered using (Dako Fluorescence Mounting Medium, Code S3023) mounting medium and a cover glass. The slides were then fully digitized using a digital slide scanner (Pannoramic Scan II, 3D HISTECH Ltd., Budapest, Hungary) at 20× magnification (pixel dimensions: 0.325 μm) and automatically stitched. The scanner is equipped with a quad band (DAPI/FITC/TRITC/Cy5) filter set, two filters (DAPI: nuclei for brain morphology, blue, 40 ms exposure time; FITC: fluorescent marker, green, 20 ms exposure time) were used for image acquisition. Due to the thickness of the slides they were digitized in extended focus mode with 30 focus layers and an axial layer distance of 2 μm.

Images containing whole brain slices were exported from slide scanner data sets (Pannoramic Viewer, Version 1.15.4, 3D HISTECH Ldt., Budapest, Hungary) as PNG images with pixel dimensions of 10.4 μm. Subsequently, all images were coarsely cropped and aligned by hand (Adobe Photoshop CS6, Adobe Systems Inc., San Jose, CA, United States). The cerebellum was excluded due to massive artifacts from slide mounting. Slice images of each brain were converted to image stacks and underwent rigid registration using the "StackReg" plugin for ImageJ (Version 1.51n[1]). Only rigid registration was performed since results of elastic registration were heavily influenced by occurring tissue deformations/overlaps and missing or severed tissue portions. Further image analysis was performed with Mathematica (Version 11.1, Wolfram Research, Inc., Champaign, IL, United States). Registered image stacks were transformed into volumetric data sets and maximum projections along coronal, sagittal and horizontal axes were generated (**Figure 2**). Injection site was identified and marked within these projections, a separation line between the two hemispheres was also drawn (Adobe Photoshop CS6). Subsequently, all volumetric data sets were split into blue and green channels. Image slices of the blue channels were adjusted for brightness to retain consistent morphology. The green channel was binarized to detect tracer positive voxels. Binarized green channels were subsequently submitted to distance analysis. For this purpose, the distance of every non-positive voxel within the brains to the closest positive voxel was calculated with an average of 3450 voxel per brain. Distance values of individual brains were summarized according to the groups L30, L90, S30, and S90 (**Figure 3**). Shorter distances equal higher tracer spread. Distance values of all 10 3D reconstructed brains were shown as boxplots (**Figure 3A**). Based on the manually drawn separation lines the volumetric data sets of the green channels were split into ipsi- and contralateral hemispheres and all positive voxels were counted and plotted in a point chart (**Figure 3B**). Statistical analysis was performed using Mathematica. Shapiro Wilk test for normal distribution and Wilcoxon Signed Rank test for paired data were used to test data from the segmented voxel count analysis. Kolmogorov Smirnov test for normal distribution and Kruskal Wallis test for unpaired data were applied to test data from distance analysis. Dunn-Bonferroni *post hoc* correction after multiple pair comparisons was performed. P-values less than 0.05 were regarded as statistically significant. Volumetric data sets were visualized and animated (**Supplementary Movies S1–S4**) using Vaa3d (3D Visualization-Assisted Analysis, Version 3.20[2]). Injection site was interpolated and highlighted in the red image channel based on the marked position, and transparency of all three-color channels was adapted for best viewing experience.

Lymph node slides were also fully digitized using a digital slide scanner at 20× magnification following the procedure mentioned above except for an additional red channel to detect autofluorescent material. Exposure times were 100 ms for DAPI (lymph node morphology, blue), 150 ms for FITC (fluorescent

[1]http://imagej.nih.gov/ij

[2]http://vaa3d.org

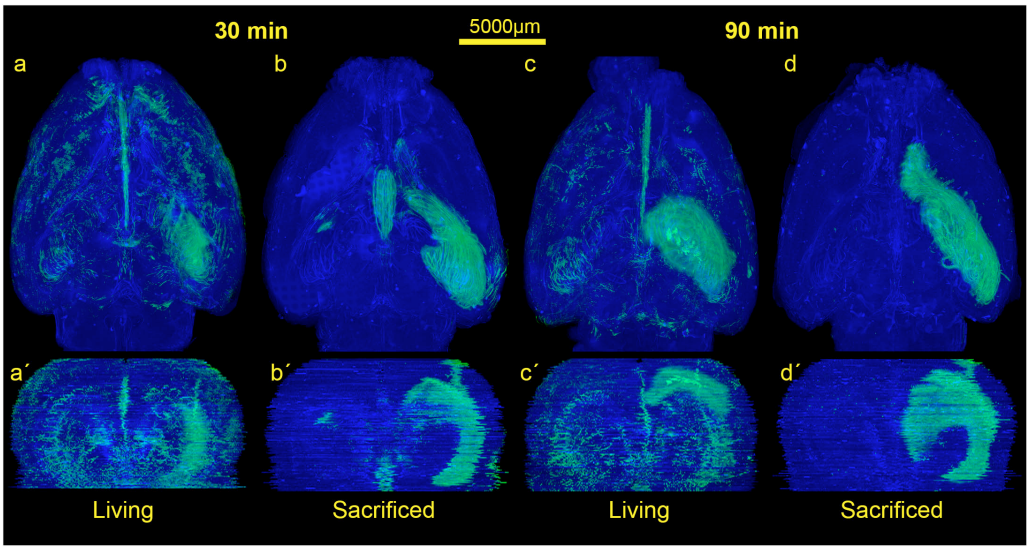

FIGURE 2 | Comparison of the spread of the injected tracer in living and sacrificed rats at 30 min and 90 min after tracer injection. Images show maximum projections of horizontal sections **(a–d)** which were reconstructed coronally **(a'–d')** of one animal per group. Evidently, the tracer reaches the contralateral hemisphere, spreads along the vasculature, fiber tracts and disseminates further within both hemispheres in living animals, while it diffuses mostly along ipsilateral hippocampal fiber tracts surrounding the ventricles in non-vital brains.

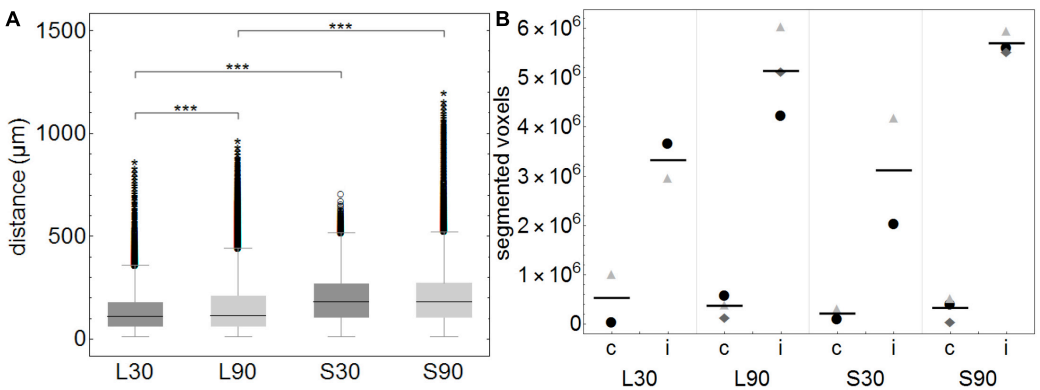

FIGURE 3 | (A) Boxplots of calculated distances of every none-positive voxel within the brains to the closest positive voxel. Distance values of all 3D reconstructed individual brains (approximately 3450 voxels per brain) were summarized according to the groups L30 = living animals, 30 min PI, $n = 2$; L90 = living animals 90 min PI, $n = 3$; S30 = sacrificed animals 30 min PI, $n = 2$; S90 = sacrificed 90 min PI, $n = 3$. Shorter distances equal higher tracer spread. When comparing living to sacrificed groups tracer spread is significantly higher in living animals at both time points (***$p \leq 0.001$). Tracer spread is significantly higher 30 min PI compared to 90 min PI in living animals, while there is statistically significant difference in sacrificed animals over time. **(B)** This subfigure shows the total number of segmented voxels per hemisphere. Within each group, identical symbols represent the corresponding hemispheres of one brain. A line is depicting the mean value. "c" the contralateral and "i" indicates the ipsilateral hemisphere of the injection site. Due to the very small group sizes a reliable statistical analysis could not be performed. Nevertheless, a trend of higher spread to the contralateral hemisphere in living animals is visible.

marker, green) and 70 ms for TRITC (autofluorescent material, red). Images containing lymph nodes were exported from slide scanner data sets (Pannoramic Viewer, Version 1.15.4, 3D HISTECH Ldt., Budapest, Hungary) as PNG images with pixel dimensions of 0.65 µm.

Image analysis was performed with Mathematica. Fluorescence images were imported and split into separate color channels. After brightness equalization the red (autofluorescent material) channel was subtracted from the green (marker) channel to obtain autofluorescence corrected images. The remaining green channel was subsequently binarized using Otsu's (cluster variance maximization) thresholding method (Otsu, 1979) and the number of segmented pixels representing detected fluorescence marker were counted. Statistical analysis was performed using Mathematica and boxplots were generated. Kolmogorov Smirnov test was applied to test data for normal distribution and Kruskal Wallis test with subsequent Dunn-Bonferroni *post hoc* correction after multiple pair comparisons was performed. *P*-values less than 0.05 were regarded as statistically significant.

Immunofluorescent Stainings

After performing the 3D scanning for the 3D reconstruction, 20 representative brain sections were selected, uncovered and blocked in 3% DKS, 0.8% Triton, and 96.2% PBS. After washing with PBS, slides were covered with rabbit anti laminin antibody (Polyclonal rabbit Anti laminin; LOT: 00051761; ON: Z0097 Dako) diluted 1:200 and goat anti collagen IV (GtX Collagen Type IV; LOT: 2716603; ON: AB 769 Millipore) diluted 1:100 in 0.8% Triton, 0.5% DKS and 97.2% PBS overnight. The next day the slides were stained for 1 h with Alexa 647 donkey anti rabbit (Alexa Fluor 647 donkey anti rabbit; LOT: 1786284; ON: A31573 life technologies) (1:1 in Glycerol) and Alexa 568 donkey anti goat (Alexa Fluor 568 donkey anti goat IgG; LOT: 1235787; ON: A11057 life technologies) (1:1 in Glycerol) each diluted 1:250 in 0.08% Triton, 0.5% DKS and 97.1% PBS. Before covering the slides with mounting medium, they were stained for 5 min in DAPI.

Images of vessels and surrounding tissue close to as well as distant from the injection site were taken using Olympus microscope (Olympus BX 40) with a digital camera (Olympus XM10) At higher magnifications focus stacking of maximum 2 z-stacks per slide was used for better viewing experience. Images were manually masked (vessels, surrounding tissue, artifacts) using Photoshop. Subsequently, original images and manually generated masks were imported into Mathematica and intensity values for vessels and surrounding tissue regions were extracted. Total intensity for the two regions was added up and normalized by dividing the total intensity value by the area of the respective regions. Statistical analysis was performed using Mathematica and box plots were generated. Shapiro Wilk was applied to test data for normal distribution and *T*-test for paired data was used for group comparisons. *P*-values less than 0.05 were regarded as statistically significant.

RESULTS

In order to visualize the contribution of vital functions to the intraparenchymal spread of fluids, we injected 3 μl of a saturated solution of the fluorescein-coupled dextran amine Fluoro-Emerald into the entorhinal cortex of living and sacrificed rats and removed the brains 30 and 90 min afterward (n = 7 for 30 min per group and n = 3 for 90 min per group). The experimental setup is shown in **Figure 1**. Images of consecutive whole horizontal sections were taken at 20 times magnification and reconstructed three-dimensionally. Evidently, the tracer was transported along the vasculature and fiber tracts to remote areas including the contralateral hemisphere in living rats, while it appeared to diffuse along the ventricles and hippocampal fiber tracts in sacrificed animals, both at 30 and 90 min after injection (**Figure 2** and **Supplementary Movies S1–S4**).

This is highlighted in the calculated 3D reconstructions where fluorescent voxels can be seen throughout both hemispheres. For each volumetric data set distance values of every non-positive voxel to the next positive voxel were calculated and summarized according to the groups L30, L90, S30, and S90 (**Figure 3A**). Shorter distances equal higher tracer spread. Kolmogorov Smirnov test revealed non-normal distribution of data from distance analysis. Kruskal Wallis test shows a highly significant increased tracer spread in living compared to sacrificed animals ($p \leq 0.001$; with approximately 3450 voxels per brain) (**Figure 3A**). Furthermore, there is a significantly higher spread in living animals compared to sacrificed at 30 (110 vs. 181 μm) and 90 min (114 vs. 180 μm) PI ($p \leq 0.001$). There is also a slightly higher spread in living animals 30 min (110 μm) PI compared to 90 min (114 μm) PI ($p \leq 0.001$) (**Figure 3A**).

Quantification of the tracer distribution shows a notable spread to the contralateral hemispheres of the injection site in all animals (**Figure 3B**). In living animals spread to the contralateral hemisphere seems higher compared to sacrificed ones. No statistically significant difference was found when comparing this rough division using a relatively small number of animals (**Figure 3B**).

The rotating volumetric reconstructions exhibit the strong difference in tracer spread in both hemispheres between living and sacrificed brains for both time points. The 3D reconstructions make it more apparent that the tracer largely remains close to the injection site in the sacrificed brain. In contrast, the tracer in the living brain spreads along the fiber tracts such as the hippocampal fimbria/fornix complex (**Supplementary Figure S1**) and the vasculature to remote areas further away from the injection site. For better orientation the approximate injection site has been marked (**Supplementary Movies S1–S4**).

We then used antibodies against collagen type IV and laminin to label the basement membranes of the neurovascular unit (Sixt et al., 2001; Bechmann et al., 2007; Engelhardt et al., 2016) and investigated the localization of the tracer within the vascular wall in sections counterstained with DAPI. Except for the immediate injection site where tissue was damaged, the tracer did not spread into the surrounding parenchyma (**Figures 4m–r**). In sacrificed animals the tracer was mainly located around the injection site. It spread within the closest ventricles as well as near fiber tracts, mainly remaining in the parenchyma, and reached the abluminal/external side of the vascular wall (**Figures 4r–y**). Shapiro Wilk test shows normal distribution. The *T*-test for paired data was performed and showed a highly significant difference for L90 ($p \leq 0.001$) and significant difference for S90 ($p = 0.003$). The tracer amount outside of vessels in living animals is highly significant lower compared to sacrificed ones ($p \leq 0.001$). Mean differences between intensity inside and outside of vessels was higher for living animals (L90 = 0.251) than for sacrificed animals (S90 = 0.114) (**Figure 4y**). In living animals, the tracer was found in the vascular outer and inner basement membrane (**Figure 5**). Tracer is also found along capillaries in the hemisphere contralateral to the injection site in living animals (**Figure 6**).

At 30 and 90 min, we also studied right and left deep cervical, superficial cervical and ILN, and searched for the tracer within them. In sacrificed rats, no tracer could be detected. However, at 90 min after tracer injection into living animals, ipsilateral deep cervical and SCLN nodes exhibited tracer signals in cells at the marginal and intermediate sinus (**Figure 7a**). Mann-Whitney test for paired data shows

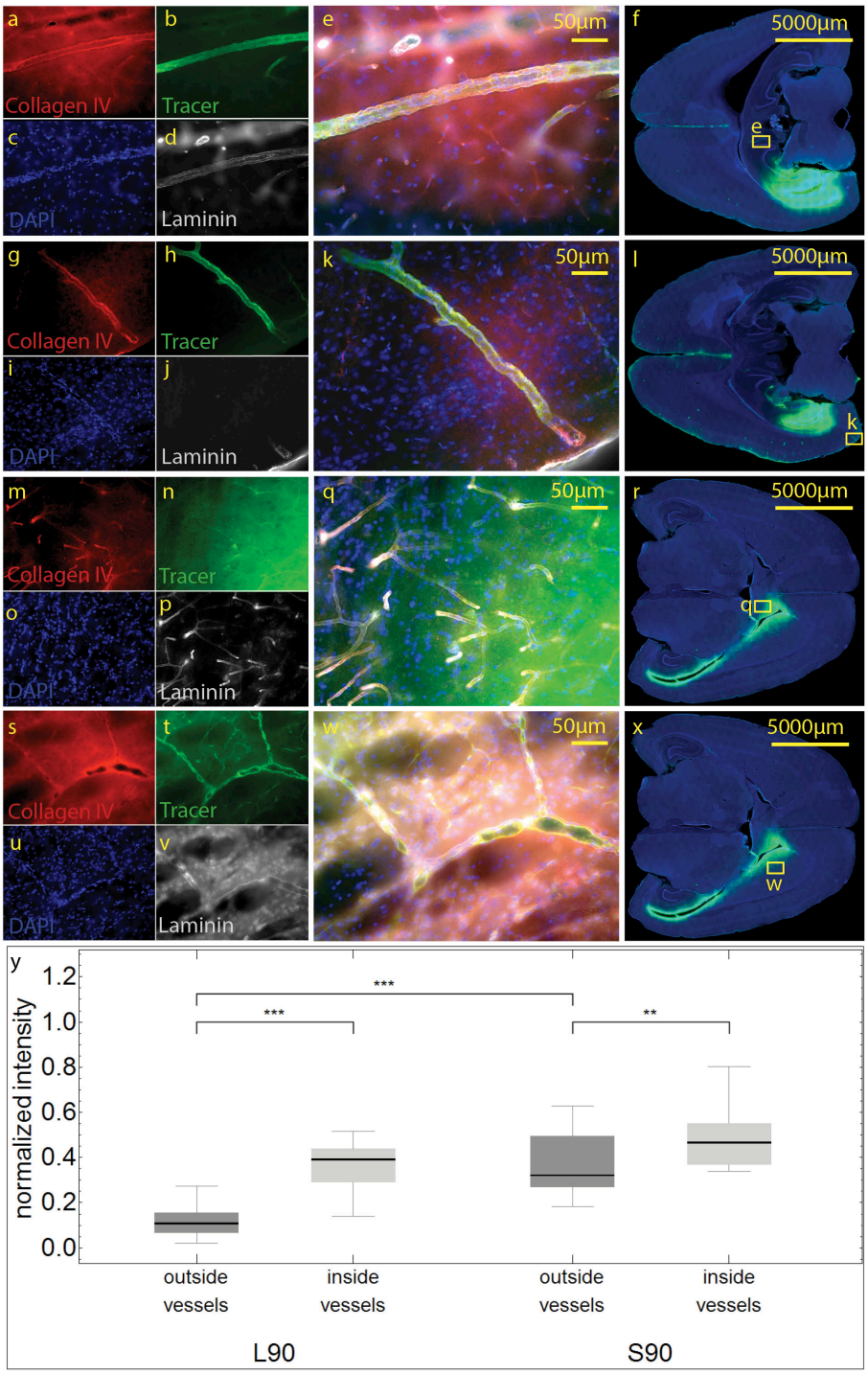

FIGURE 4 | Stained sections of living **(a–l)** rats and a sacrificed rat **(m–x)** 90 min post injection. Representative sections were stained with antibodies against collagen IV **(a,g,m,s)**, laminin **(d,j,p,v)**, DAPI **(c,l,o,u)**, tracer **(b,h,n,t)**, magnification 20× **(a–e,g–k, m–q,s–w)**. The corresponding scanned horizontal section at magnification 0.2× provides the exact location of the taken pictures **(f,l,r,w)**. In living animals the tracer is clearly transported along the vascular wall not diffusing through the outer lamina. These vessels can be identified as arterioles by their size and the orientation of the two layers of nuclei. In sacrificed animals some of the tracer spreads along the vascular wall, but also provides a background staining of the neuropil **(m–q)**. The tracer accumulates in the parenchyma surrounding vessels/the perivascular space. **(s–w)**. Subfigure **(y)** shows normalized tracer intensity inside and outside of vessels. There is a highly significant difference for L90 (***$p \leq 0.001$) and significant difference for S90 (**$p = 0.003$). The tracer amount outside of vessels in living animals is highly significant lower compared to sacrificed ones.

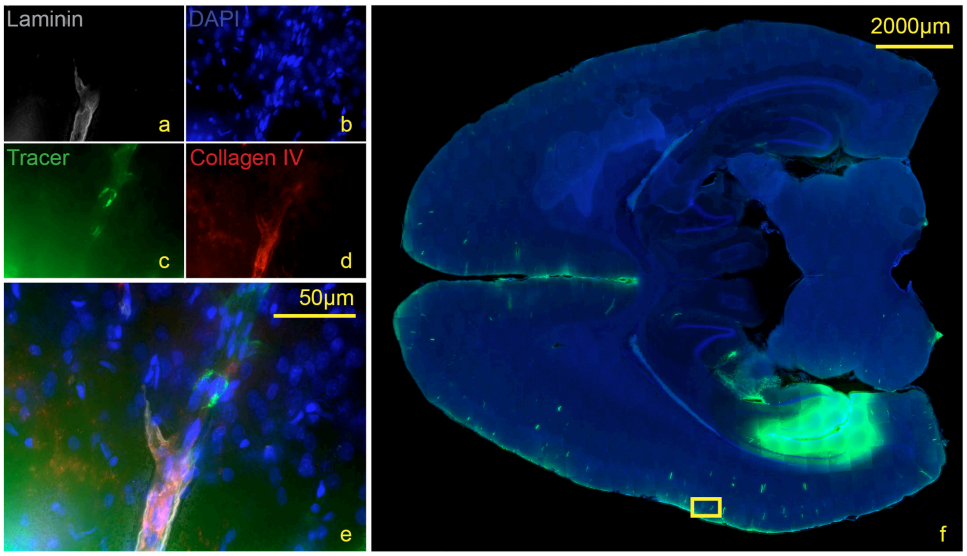

FIGURE 5 | Stained section of a living rat 90 min post injection with antibodies against collagen IV **(d)**, laminin **(a)**, DAPI **(b)**, tracer **(c)**, magnification 40× **(a–e)**. The corresponding scanned horizontal section at magnification 0.2× provides the exact location of the taken picture **(f)**. Tracer accumulates within the inner and outer basement membrane ipsilateral to the injection site.

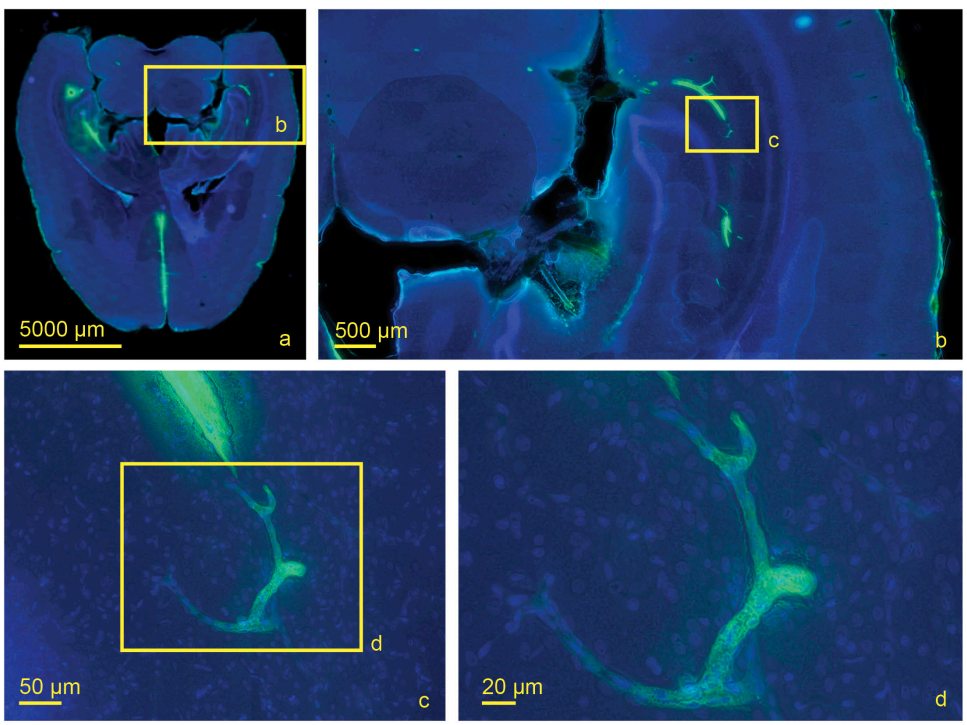

FIGURE 6 | Scanned horizontal section of a living rat 30 min post injection with DAPI and tracer with increasing magnifications **(a)** 0.2×, **(b)** 2.0×, **(c)** 20×, **(d)** 40×. Tracer accumulation in the contralateral hemisphere occurs at the level of capillaries which are identified by their size.

significantly higher tracer levels in living compared to sacrificed animals 90 min PI in right and left DCLN as well as SCLN (all $p \leq 0.001$) with no difference for ILN and all lymph nodes 30 min PI.

DISCUSSION

In this study, we aimed at visualizing the impact of vital functions on the spread of a hydrophilic tracer within the brain's neuropil.

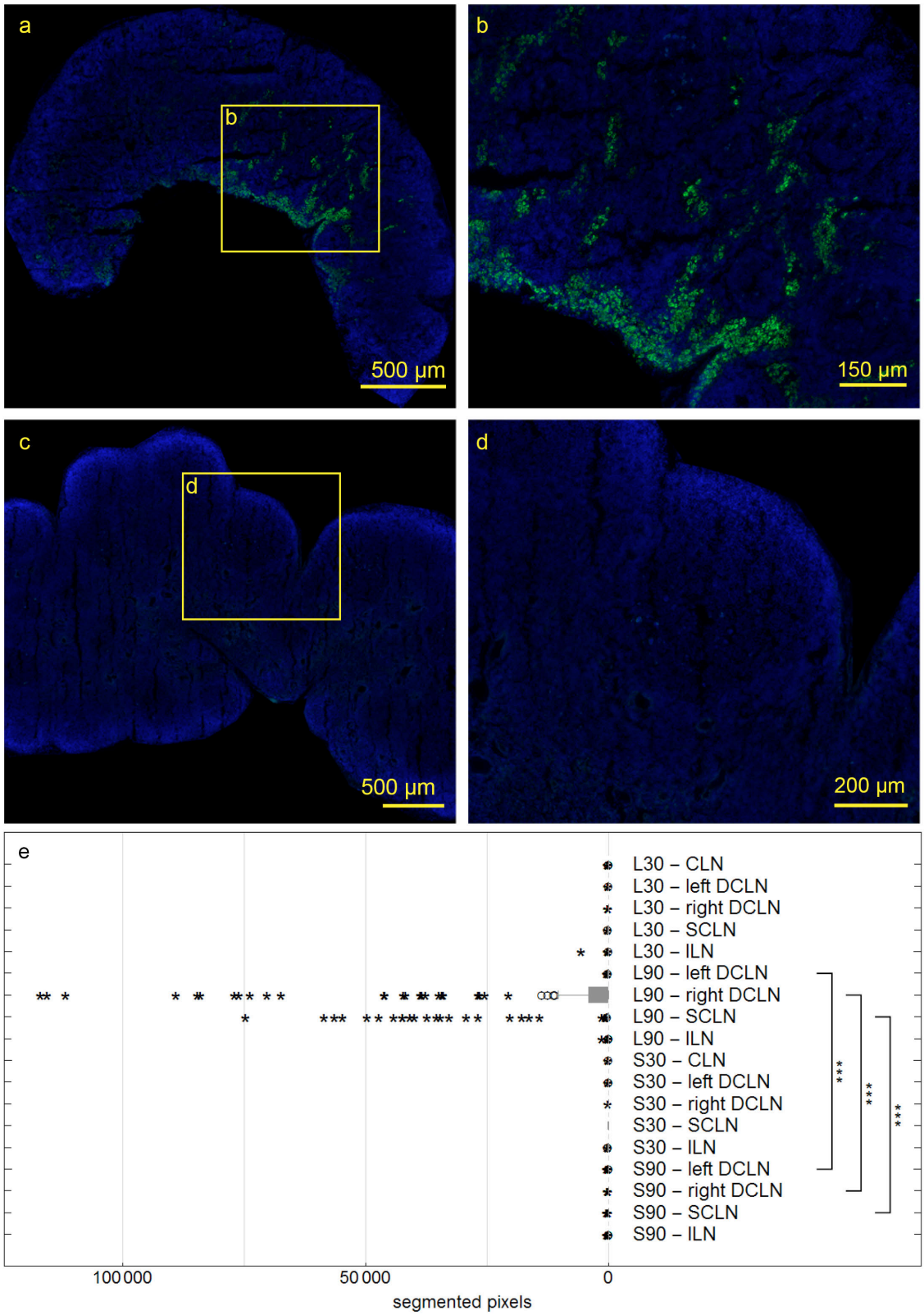

FIGURE 7 | Deep cervical lymph nodes (DCLN) of rats 90 min post injection. Autofluorescent material was eliminated by subtracting the red channel from the pictures. In DCLN **(a,b)** of a living rat tracer is found within cells along the medullary trabecula, while no tracer could be detected within any dissected lymph node of sacrificed rats **(c,d)**. Box plot shows numbers of segmented voxels depicting fluorescent tracer within LN groups **(e)**. Tracer amounts in living compared to sacrificed animals 90 min post injection are significantly higher in right and left DCLN as well as SCLN (all $^{***}p \leq 0.001$).

To this end, we compared maximum projections of three-dimensionally reconstructed brains from living and sacrificed rats 30 and 90 min after tracer injection into the entorhinal cortex. Our data show that the spread of extracellular fluids indeed is clearly enhanced in the presence of vital functions, suggesting that in living animals a fluid transport system contributes to tracer spread along the perivascular channel system. In contrast, in sacrificed animals diffusion mainly occurs either transparenchymal or across the vascular wall.

We found a highly significant increased tracer spread in living animals compared to sacrificed animals indicated by shorter distances between tracer positive and non-positive voxels in the volumetric reconstructions of the brain (**Figures 3A,C**). This includes perimortem changes which have been shown to play a crucial role in tracer spread (Ma et al., 2019). In the mentioned study tracer spread is detected in PVS of surface blood vessels after tracer injection into the lateral ventricle through the intact skull while life imaging, with an increase in perivascular tracer spread when the animal is sacrificed. The authors conclude that tracer spread to penetrating blood vessels only occurs under these conditions. We agree that perimortem changes/artifacts may contribute to the pattern of perivascular spread. With the shown top view and limited low resolution, it is not clear to us that penetrating blood vessels are excluded from tracer spread in living conditions. The infused tracer reaches the contralateral hemisphere and spreads along the vasculature and along fiber tracts in living animals, while it diffuses mostly along the ventricles and hippocampal fiber tracts in non-vital brains with less dissemination compared to living animals (**Figures 2**, **3B**). Tracer spread is significantly lower in living animals 90 min compared to 30 min post injection (**Figures 2**, **3B**). This could be explained by continues tracer clearance toward the cervical lymph nodes (**Figure 7**). At the moment it is unclear whether tracer penetrates into the ventricles or spreads along the subependymal space. Furthermore, the contribution of the changing perfusion pressure after death needs to be considered. In the sacrificed group it begins approximately 20 min before tracer injection. Since in both groups, the brains were immersion fixed, changing perfusion pressure before fixation occurs in both until the distribution of the PFA is complete. Tracer spread along fiber tracts has been described previously (Cserr et al., 1977; Rosenberg et al., 1980; Geer and Grossman, 1997). In contrast to the findings from Geer-Grossmann where frontal and temporal lobe injections were performed and the tracer remained within the same hemisphere, our study shows that dissemination of the tracer also occurs along the vasculature and fiber tracts in the contralateral hemisphere (**Figures 2–6**, **Supplementary Movies S1–S4**, and **Supplementary Figure S1**). Possible explanations could be faster needle removement after the injection, shorter infusion time, different injection sites, different tracers used or better tracer detection in our study. Cserr et al. (1977) used 0.5 μl whereas Geer-Grossmann infused 20 μl compared to 3 μl in our study. Thus, artifacts due to overflow must be considered but are difficult to predict and identify. Especially, as they would occur in both groups, living and sacrificed. In counterstained sections of living rats with laminin and collagen IV, the tracer is transported along the vascular wall of arterioles (**Figures 4a–l**, **5** and **Supplementary Figure S2**) and capillaries (**Figure 6**) as described previously (Carare et al., 2008; Morris et al., 2016) not spreading into the surrounding parenchyma, except for the immediate injection site where a degree of brain damage occurred. Possible leakage to the peripheral circulation cannot be excluded but seems to play a minor role since tracer spread has not occured in the shape of venous drainage. Contradicting, in sacrificed animals tracer is continuously detected after transparenchymal or transvascular diffusion. A limiting fact is that in the present study, vessels were only identified as arterioles by their size and the orientation of the two layers of nuclei. Similar studies using detailed characterization of the distribution of tracers demonstrate that they enter the parenchyma along arterial pial-glial basement membranes and tracers within the parenchyma enter the basement membranes surrounding smooth muscle cells, as IPD (Morris et al., 2016; Albargothy et al., 2018). In sacrificed rats the tracer was also observed to spread along fiber tracts and to accumulate within vessel walls, but the driving force is unclear at present. Non-physiological changes in vital processes concerning the cessation of the sacrificed group as well as postmortem changes need to be considered besides diffusion. It certainly would be interesting to perform further experiments comparing intracisternally applied tracer in living vs. sacrificed vs. sacrificed immediately after tracer injection to study the perimortem changes in greater detail. Furthermore, intraparenchymal injections in animals that were sacrificed after the stereotactic placement of the syringe right before tracer injection would help to reduce postmortem artifacts in the sacrificed group. To avoid blood clotting in the sacrificed group, transcardial perfusion with heparinized animals would minimize artifacts from the immersion fixation. Another possible limitation is the use of a saturated tracer solution, which might interfere with physiological processes differently than a more diluted tracer, as well as the intraparenchymal injected amount of 3 μl which may lead to localized pressure changes and therefore possibly affects tracer distribution in sacrificed and living animals differently. Corresponding with previous findings (Bradbury et al., 1981; Szentistványi et al., 1984; Ma et al., 2019) tracer is found within deep cervical and SCLN, specifically within cells along the medullary trabecular and not in ILN or sacrificed animals after intracerebral injection. The tracer could microscopically not be displayed in contralateral DCLN. This discrepancy could for one be explained with the shorter time points after intracerebral injection (90 min vs. 5–7 h), meaning that tracer did not yet reach the contralateral side in our study. Additionally, different animals were used (mice (Ma et al., 2019) vs. rabbit (Bradbury et al., 1981) vs. rat), different injections sites (intracisternal (Ma et al., 2019) vs. intraparenchymal (Bradbury et al., 1981) and our study), different tracer sizes 10kDa (our study) vs. 40 kDa (Ma et al., 2019) and different imaging techniques. Recognizing the previously described drainage via lymphatic vessels in dural sinuses (Louveau et al., 2015) in the present study we did not analyze the sagittal sinus for tracer spread. Statistical analysis of the highly sensitive image segmentation showed significantly higher tracer levels in living compared to sacrificed animals 90 min post injection in right and left DCLN as well as SCLN even though microscopically

no tracer could be seen contralaterally. The tracer may have begun to appear contralateral to the injection side but has not shown the same distribution pattern as in ipsilateral LN yet. In agreement with former findings (Bradbury et al., 1981; Koh et al., 2005; Ma et al., 2017, 2019), where intracisternally and intraventricular applied tracer first reached cervical lymph nodes and then concentration increased in the blood, we hypothesize that clearance from the brain and extracellular fluid occurred via ISF and CSF into cervical lymph nodes in living animals. We cannot exclude spillage into the CSF compartment of our tracer, although we took every precaution possible to prevent this.

Further studies are needed to characterize the tracer-fluorescent cells at the marginal and intermediate sinus to investigate if they phagocytosed the tracer after it reached the lymph nodes, if they internalized tracer before (e.g., intracranially and then drained to the lymph nodes) or if the tracer only adhered to the surface of these cells.

CONCLUSION

The spread of extracellular fluids depends on and increases in the presence of vital functions. In vital brains an intraparenchymal injected tracer is transported along the vasculature and fiber tracts to remote areas including the contralateral hemisphere. The tracer remained within the wall of the vasculature, almost solely found within the outer and inner basement membrane of the vessels, not spreading into the surrounding parenchyma. In contrast, in sacrificed animals, the tracer spread along ventricles and fiber tracts (predominantly the fornix), aligned with the outer vascular border close to the injection site. Thus, the presence of an active clearance system driven by vital functions is supported by the different patterns of distribution of the tracers in living and sacrificed animals. Furthermore, the intracerebrally injected tracer was only found in the cervical lymph nodes of living animals, suggesting that the drainage of ISF/CSF to the cervical lymph nodes is an active process.

DATA AVAILABILITY STATEMENT

The datasets used and analyzed during the current study are available from the corresponding author on reasonable request.

ETHICS STATEMENT

The animal study was reviewed and approved by the Landesdirektion Sachsen, Germany; TV03/13.

AUTHOR CONTRIBUTIONS

AP performed the experiment, tissue processing, histological examination of the slides and prepared the scanned sections for further processing, writing the manuscript. KW digitized all microscopic slides, performed all image processing (3D reconstructions, maximum projections, segmentation of 2D/3D image data, etc.) and statistical analysis. IB supervised the project, was involved in the conception and design. AP and IB were the major contributors in writing the manuscript. RC revised it critically for intellectual content. All authors read and approved the final manuscript.

FUNDING

This study was supported the collaborative research center DFG-1052. AP was a Scholar of the Studienstiftung des Deutschen Volkes.

ACKNOWLEDGMENTS

We thank PD Dr. Marcin Nowicki for assistance with the animal experiments, furthermore Angela Ehrlich, Jana Brendler and all medical laboratory assistants of the Institute of Anatomy, Leipzig who were involved in processing and staining of the tissue samples. We acknowledge support from the German Research Foundation (DFG) and Universität Leipzig within the program of Open Access Publishing.

SUPPLEMENTARY MATERIAL

The Supplementary Material for this article can be found online at: https://www.frontiersin.org/articles/10.3389/fnagi.2020.00015/full#supplementary-material

REFERENCES

Abbott, N., Joan Pizzo, M. E., Preston, J. E., Janigro, D., and Thorne, R. G. (2018). The role of brain barriers in fluid movement in the CNS: is there a 'glymphatic' system? *Acta Neuropathol.* 135, 387–407. doi: 10.1007/s00401-018-1812-4

Albargothy, N. J., Johnston, D. A., MacGregor-Sharp, M., Weller, R. O., and Verma, A. (2018). Convective influx/glymphatic system: tracers injected into the CSF enter and leave the brain along separate periarterial basement membrane pathways. *Acta Neuropathol.* 136, 139–152. doi: 10.1007/s00401-018-1862-7

Asgari, M., de Zélicourt, D., and Kurtcuoglu, V. (2016). Glymphatic solute transport does not require bulk flow. *Sci. Rep.* 6:38635. doi: 10.1038/srep38635

Bakker, E. N. T. P., Bacskai, B. J., Arbel-Ornath, M., and Aldea, R. (2016). Lymphatic clearance of the brain: perivascular, paravascular and significance for neurodegenerative diseases. *Cell. Mol. Neurobiol.* 36, 181–194. doi: 10.1007/s10571-015-0273-8

Bechmann, I., Galea, I., and Perry, V. H. (2007). What is the blood-brain barrier (not)? *Trends Immunol.* 28, 5–11. doi: 10.1016/j.it.2006.11.007

Bechmann, I., and Nitsch, R. (1997). Identification of phagocytic glial cells after lesion-induced anterograde degeneration using double-fluorescence labeling: combination of axonal tracing and lectin or immunostaining. *Histochem. Cell Biol.* 107, 391–397. doi: 10.1007/s004180050125

Bradbury, M. W., Cserr, H. F., and Westrop, R. J. (1981). Drainage of cerebral interstitial fluid into deep cervical lymph of the rabbit. *Am. J. Physiol.* 240, F329–F336. doi: 10.1152/ajprenal.1981.240.4.F329

Carare, R. O., Bernardes-Silva, M., Newman, T. A., Page, A. M., Nicoll, J. A. R., Perry, V. H., et al. (2008). Solutes, but not cells, drain from the brain parenchyma along basement membranes of capillaries and arteries: significance

for cerebral amyloid angiopathy and neuroimmunology. *Neuropathol. Appl. Neurobiol.* 34, 131–144. doi: 10.1111/j.1365-2990.2007.00926.x

Cserr, H. F., Cooper, D. N., and Milhorat, T. H. (1977). Flow of cerebral interstitial fluid as indicated by the removal of extracellular markers from rat caudate nucleus. *Exp. Eye Res.* 25(Suppl.), 461–473. doi: 10.1016/s0014-4835(77)80041-9

Cserr, H. F., and Knopf, P. M. (1992). Cervical lymphatics, the blood-brain barrier and the immunoreactivity of the brain: a new view. *Immunol. Today* 13, 507–512. doi: 10.1016/0167-5699(92)90027-5

Cserr, H. F., and Ostrach, L. H. (1974). Bulk flow of interstitial fluid after intracranial injection of Blue Dextran 2000. *Exp. Neurol.* 45, 50–60. doi: 10.1016/0014-4886(74)90099-5

de Vos, A. F., Meurs, M. V., Brok, H. P., Boven, L. A., Hintzen, R. Q., Valk, P. V. D., et al. (2002). Transfer of central nervous system autoantigens and presentation in secondary lymphoid organs. *J. Immunol.* 169, 5415–5423. doi: 10.4049/jimmunol.169.10.5415

Di Rocco, C., McLone, D. G., Shimoji, T., and Raimondi, A. J. (1975). Continuous intraventricular cerebrospinal fluid pressure recording in hydrocephalic children during wakefulness and sleep. *J. Neurosurg.* 42, 683–689. doi: 10.3171/jns.1975.42.6.0683

Dreha-Kulaczewski, S., Joseph, A. A., Merboldt, K.-D., Ludwig, H.-C., Gärtner, J., and Frahm, J. (2015). Inspiration is the major regulator of human CSF flow. *J. Neurosci.* 35, 2485–2491. doi: 10.1523/JNEUROSCI.3246-14.2015

el-Gindi, S., Salama, M., and el-Farag, S. (1973). Metastases of glioblastoma multiforme to cervical lymph nodes. Report of two cases. *J. Neurosurg.* 38, 631–634. doi: 10.3171/jns.1973.38.5.0631

Engelhardt, B., Carare, R. O., Bechmann, I., Flügel, A., Laman, J. D., and Weller, R. O. (2016). Vascular, glial, and lymphatic immune gateways of the central nervous system. *Acta Neuropathol.* 132, 317–338. doi: 10.1007/s00401-016-1606-5

Faghih, M. M., and Sharp, M. K. (2018). Is bulk flow plausible in perivascular, paravascular and paravenous channels? *Fluids Barriers CNS* 15:17. doi: 10.1186/s12987-018-0103-8

Gakuba, C., Gaberel, T., Goursaud, S., Bourges, J., Palma, C. D., Quenault, A., et al. (2018). General anesthesia inhibits the activity of the "glymphatic system.". *Theranostics* 8, 710–722. doi: 10.7150/thno.19154

Galea, I., Bernardes-Silva, M., Forse, P. A., Rooijen, N. V., Liblau, R. S., and Perry, V. H. (2007). An antigen-specific pathway for CD8 T cells across the blood-brain barrier. *J. Exp. Med.* 204, 2023–2030. doi: 10.1084/jem.20070064

Geer, C. P., and Grossman, S. A. (1997). Interstitial fluid flow along white matter tracts: a potentially important mechanism for the dissemination of primary brain tumors. *J. Neurooncol.* 32, 193–201.

Goldmann, J., Kwidzinski, E., Brandt, C., Mahlo, J., Richter, D., and Bechmann, I. (2006). T cells traffic from brain to cervical lymph nodes via the cribroid plate and the nasal mucosa. *J. Leukoc. Biol.* 80, 797–801. doi: 10.1189/jlb.0306176

Harrison, F., Siow, B., Akilo, A. B., Evans, P. G., Ismail, O., Ohene, Y., et al. (2018). Non-Invasive Imaging of CSF-mediated brain clearance pathways via assessment of perivascular fluid movement with diffusion tensor MRI. *eLife* 7:e34028. doi: 10.7554/eLife.34028

Hladky, S. B., and Barrand, M. A. (2014). Mechanisms of fluid movement into, through and out of the brain: evaluation of the evidence. *Fluids Barriers CNS* 11:26. doi: 10.1186/2045-8118-11-26

Holter, K. E., Kehlet, B., Devor, A., Sejnowski, T. J., Dale, A. M., Omholt, S. W., et al. (2017). Interstitial solute transport in 3D reconstructed neuropil occurs by diffusion rather than bulk flow. *Proc. Natl. Acad. Sci. U.S.A.* 114, 9894–9899. doi: 10.1073/pnas.1706942114

Iliff, J. J., and Nedergaard, M. (2013). Is there a cerebral lymphatic system? *Stroke* 44(6 Suppl. 1), S93–S95. doi: 10.1161/STROKEAHA.112.678698

Iliff, J. J., Wang, M., Liao, T., Plogg, B. A., Peng, W., Gundersen, G. A., et al. (2012). A paravascular pathway facilitates CSF flow through the brain parenchyma and the clearance of interstitial solutes, including amyloid β. *Sci. Transl. Med.* 4:147ra111. doi: 10.1126/scitranslmed.3003748

Iliff, J. J., Wang, M., Zeppenfeld, D. M., Venkataraman, A., Plog, B. A., Liao, Y., et al. (2013). Cerebral arterial pulsation drives paravascular CSF-interstitial fluid exchange in the murine brain. *J. Neurosci.* 33, 18190–18199. doi: 10.1523/JNEUROSCI.1592-13.2013

Ivens, S., Kaufer, D., Flores, L. P., Bechmann, I., Zumsteg, D., Tomkins, O., et al. (2007). TGF-beta receptor-mediated albumin uptake into astrocytes is involved in neocortical epileptogenesis. *Brain* 130(Pt 2), 535–547. doi: 10.1093/brain/awl317

Kaminski, M., Bechmann, I., Pohland, M., Kiwit, J., Nitsch, R., and Glumm, J. (2012). Migration of monocytes after intracerebral injection at entorhinal cortex lesion site. *J. Leukoc. Biol.* 92, 31–39. doi: 10.1189/jlb.0511241

Kida, S., Pantazis, A., and Weller, R. O. (1993). CSF drains directly from the subarachnoid space into nasal lymphatics in the rat. Anatomy, histology and immunological significance. *Neuropathol. Appl. Neurobiol.* 19, 480–488. doi: 10.1111/j.1365-2990.1993.tb00476.x

Koh, L., Zakharov, A., and Johnston, M. (2005). Integration of the subarachnoid space and lymphatics: is it time to embrace a new concept of cerebrospinal fluid absorption? *Cerebrospinal Fluid Res.* 2:6. doi: 10.1186/1743-8454-2-6

Locatelli, G., Wörtge, S., Buch, T., Ingold, B., Frommer, F., Sobottka, B., et al. (2012). Primary oligodendrocyte death does not elicit anti-CNS immunity. *Nat. Neurosci.* 15, 543–550. doi: 10.1038/nn.3062

Louveau, A., Smirnov, I., Keyes, T. J., Eccles, J. D., Rouhani, S. J., Peske, J. D., et al. (2015). Structural and functional features of central nervous system lymphatic vessels. *Nature* 523, 337–341. doi: 10.1038/nature14432

Ma, Q., Ineichen, B. V., Detmar, M., and Proulx, S. T. (2017). Outflow of cerebrospinal fluid is predominantly through lymphatic vessels and is reduced in aged mice. *Nat. Commun.* 8:1434. doi: 10.1038/s41467-017-01484-6

Ma, Q., Ries, M., Decker, Y., Müller, A., Riner, C., Bücker, A., et al. (2019). Rapid lymphatic efflux limits cerebrospinal fluid flow to the brain. *Acta Neuropathol.* 137, 151–165. doi: 10.1007/s00401-018-1916-x

McComb, J. G. (1983). Recent research into the nature of cerebrospinal fluid formation and absorption. *J. Neurosurg.* 59, 369–383. doi: 10.3171/jns.1983.59.3.0369

Morris, A. W. J., MacGregor Sharp, M., Albargothy, N. J., Fernandes, R., Hawkes, C. A., Verma, A., et al. (2016). Vascular basement membranes as pathways for the passage of fluid into and out of the brain. *Acta Neuropathol.* 131, 725–736. doi: 10.1007/s00401-016-1555-z

Murtha, L. A., Yang, Q., Parsons, M. W., Levi, C. R., and Beard, D. J. (2014). Cerebrospinal fluid is drained primarily via the spinal canal and olfactory route in young and aged spontaneously hypertensive rats. *Fluids Barriers CNS* 11:12. doi: 10.1186/2045-8118-11-12

Nedergaard, M. (2013). Neuroscience. Garbage truck of the brain. *Science* 340, 1529–1530. doi: 10.1126/science.1240514

Nilsson, C., Ståhlberg, F., Thomsen, C., Henriksen, O., Herning, M., and Owman, C. (1992). Circadian variation in human cerebrospinal fluid production measured by magnetic resonance imaging. *Am. J. Physiol.* 262(1 Pt 2), R20–R24. doi: 10.1152/ajpregu.1992.262.1.R20

Otsu, N. (1979). A threshold selection method from gray-level histograms. *IEEE Trans. Syst. Man Cybern.* 9, 62–66. doi: 10.1109/tsmc.1979.4310076

Pizzo, M. E., Wolak, D. J., Kumar, N. N., Brunette, E., Brunnquell, C. L., Hannocks, M.-J., et al. (2018). Intrathecal antibody distribution in the rat brain: surface diffusion, perivascular transport and osmotic enhancement of delivery. *J. Physiol.* 596, 445–475. doi: 10.1113/JP275105

Plog, B. A., and Nedergaard, M. (2018). The glymphatic system in central nervous system health and disease: past, present, and future. *Annu. Rev. Pathol.* 13, 379–394. doi: 10.1146/annurev-pathol-051217-111018

Rosenberg, G. A., Kyner, W. T., and Estrada, E. (1980). Bulk flow of brain interstitial fluid under normal and hyperosmolar conditions. *Am. J. Physiol.* 238, F42–F49. doi: 10.1152/ajprenal.1980.238.1.F42

Schwalbe, G. (1869). Der Arachnoidalraum Ein Lymphraum Und Sein Zusammenhang Mit Dem Perichorioidalraum. *Zentralbl. Med. Wiss.* 7, 465–467.

Sixt, M., Engelhardt, B., Pausch, F., Hallmann, R., Wendler, O., and Sorokin, L. M. (2001). Endothelial cell laminin isoforms, laminins 8 and 10, play decisive roles in T cell recruitment across the blood-brain barrier in experimental autoimmune encephalomyelitis. *J. Cell Biol.* 153, 933–946. doi: 10.1083/jcb.153.5.933

Szentistványi, I., Patlak, C. S., Ellis, R. A., and Cserr, H. F. (1984). Drainage of interstitial fluid from different regions of rat brain. *Am. J. Physiol.* 246(6 Pt 2), F835–F844. doi: 10.1152/ajprenal.1984.246.6.F835

Takahashi, S., and Patrick, G. (1987). Patterns of lymphatic drainage to individual thoracic and cervical lymph nodes in the rat. *Lab. Anim.* 21, 31–34. doi: 10.1258/002367787807406671

Xie, L., Kang, H., Xu, Q., Chen, M. J., Liao, Y., Thiyagarajan, M., et al. (2013). Sleep drives metabolite clearance from the adult brain. *Science* 342, 373–377. doi: 10.1126/science.1241224

Yang, L., Kress, B. T., Weber, H. J., Thiyagarajan, M., Wang, B., Deane, R., et al. (2013). Evaluating glymphatic pathway function utilizing clinically relevant intrathecal infusion of CSF tracer. *J. Transl. Med.* 11:107. doi: 10.1186/1479-5876-11-107

Conflict of Interest: The authors declare that the research was conducted in the absence of any commercial or financial relationships that could be construed as a potential conflict of interest.

frontiers in Aging Neuroscience

REVIEW
published: 14 April 2020
doi: 10.3389/fnagi.2020.00080

Brain Microvascular Pericytes in Vascular Cognitive Impairment and Dementia

Maiko T. Uemura[1,2], Takakuni Maki[3], Masafumi Ihara[4], Virginia M. Y. Lee[1] and John Q. Trojanowski[1]*

[1] Institute on Aging and Center for Neurodegenerative Disease Research, Department of Pathology and Laboratory Medicine, Perelman School of Medicine, University of Pennsylvania, Philadelphia, PA, United States, [2] JSPS Overseas Research Fellowship Program, Japan Society for the Promotion of Science, Tokyo, Japan, [3] Department of Neurology, Kyoto University Graduate School of Medicine, Kyoto, Japan, [4] Department of Neurology, National Cerebral and Cardiovascular Center, Osaka, Japan

Pericytes are unique, multi-functional mural cells localized at the abluminal side of the perivascular space in microvessels. Originally discovered in 19th century, pericytes had drawn less attention until decades ago mainly due to lack of specific markers. Recently, however, a growing body of evidence has revealed that pericytes play various important roles: development and maintenance of blood–brain barrier (BBB), regulation of the neurovascular system (e.g., vascular stability, vessel formation, cerebral blood flow, etc.), trafficking of inflammatory cells, clearance of toxic waste products from the brain, and acquisition of stem cell-like properties. In the neurovascular unit, pericytes perform these functions through coordinated crosstalk with neighboring cells including endothelial, glial, and neuronal cells. Dysfunction of pericytes contribute to a wide variety of diseases that lead to cognitive impairments such as cerebral small vessel disease (SVD), acute stroke, Alzheimer's disease (AD), and other neurological disorders. For instance, in SVDs, pericyte degeneration leads to microvessel instability and demyelination while in stroke, pericyte constriction after ischemia causes a no-reflow phenomenon in brain capillaries. In AD, which shares some common risk factors with vascular dementia, reduction in pericyte coverage and subsequent microvascular impairments are observed in association with white matter attenuation and contribute to impaired cognition. Pericyte loss causes BBB-breakdown, which stagnates amyloid β clearance and the leakage of neurotoxic molecules into the brain parenchyma. In this review, we first summarize the characteristics of brain microvessel pericytes, and their roles in the central nervous system. Then, we focus on how dysfunctional pericytes contribute to the pathogenesis of vascular cognitive impairment including cerebral 'small vessel' and 'large vessel' diseases, as well as AD. Finally, we discuss therapeutic implications for these disorders by targeting pericytes.

Keywords: pericytes, mural cells, small vessel disease, vascular cognitive impairment and dementia, Alzheimer's disease (AD), stroke, neurovascular coupling (NVC), blood–brain barrier (BBB)

OPEN ACCESS

Edited by:
Roxana Octavia Carare, University of Southampton, United Kingdom

Reviewed by:
David Attwell, University College London, United Kingdom
Kassandra Kisler, University of Southern California, United States

****Correspondence:***
Maiko T. Uemura
maikohs@kuhp.kyoto-u.ac.jp

Received: *02 December 2019*
Accepted: *04 March 2020*
Published: *14 April 2020*

Citation:
Uemura MT, Maki T, Ihara M, Lee VMY and Trojanowski JQ (2020) Brain Microvascular Pericytes in Vascular Cognitive Impairment and Dementia. Front. Aging Neurosci. 12:80. doi: 10.3389/fnagi.2020.00080

INTRODUCTION

Pericytes are mural cells, embedded within the basement membrane, and surrounding microvessels as illustrated in **Figures 1** and **2**. These cells were originally described in late 19th century (Eberth, 1871; Rouget, 1873) and initially named "pericytes" in 1923 by Zimmermann (Zimmermann, 1923) in accordance with their location enveloping the endothelium, and their being embedded in the basement membrane outside the microvessels (Zimmermann, 1923; Armulik et al., 2011; Geranmayeh et al., 2019). Although pericytes were considered to contribute to architectural maintenance and contraction of capillaries (Sandison, 1931; Zweifach, 1934; Clark and Clart, 1940), little had been known about their multifunctional characteristics and roles in neurological disorders until late 20th century (Brown et al., 2019). In the last 20 years, however, using a combination of markers and advancing technologies, a variety of functions of pericytes in health and disease have been revealed. Especially, microvascular pericytes in the central nervous system (CNS) have come into focus as they contribute to the maintenance of blood–brain barrier (BBB) (Armulik et al., 2010; Bell et al., 2010; Daneman et al., 2010; Quaegebeur et al., 2010), regulation of cerebral blood flow (CBF) (Peppiatt et al., 2006), and clearance of toxic waste products from the brain (Lendahl et al., 2019) as well as other multifunctional properties.

MURAL CELLS IN THE BRAIN SMALL VESSELS: VASCULAR SMOOTH MUSCLE CELLS AND PERICYTES

The brain constitutes ∼2% of the adult human body weight but receives ∼20% of the cardiac output through CNS vascular network (Xing et al., 2017). In the brain, small vessels can be largely classified as three different types by their size and constituent cell types: (1) arterioles, (2) capillaries, and (3) venules (Attwell et al., 2016). There are gradual transitions between these vessel types; the transitions between arterioles and capillaries are called as pre-capillary arterioles while those between capillaries and venules are called as post-capillary venules (Dalkara and Alarcon-Martinez, 2015).

The arterioles branch from large arteries and follow the outer rim of the brain via the meninges (Bevan et al., 1999; Onodera, 2011). They penetrate perpendicularly into the cortex (penetrating arterioles), and upon entering the white matter, they begin to coil, loop, and spiral (Nonaka et al., 2003). Running through the brain parenchyma, the arterioles further split into smaller arterioles (Yamazaki and Kanekiyo, 2017). As their diameters and constituent cell types are changed, the vessels make a transition to capillaries. The capillaries then increase their diameter again and transition into the post-capillary venules, which join to form collecting venules that collect into larger veins (Landau and Davis, 1957; Harnarine-Singh et al., 1972; Onodera, 2011; Itoh and Suzuki, 2012; El-Bouri and Payne, 2016). In the small vessels (from the arterioles to venules), there are two types of mural cells separately located outside of endothelial layer: (1) vascular smooth muscle cells (SMCs) and (2) pericytes (**Figure 1**).

Smooth muscle cells and pericytes express shared mural cell markers including neuron-glial antigen 2 (NG2, or transmembrane chondroitin sulfate proteoglycan; CSPG4) platelet derived growth factor receptor beta (PDGFRβ), alanyl aminopeptidase (ANPEP, or CD13), vimentin, regulator of G protein signaling 5 (RGS5) (Itoh and Suzuki, 2012; Yang et al., 2017; Smyth L. et al., 2018; Vanlandewijck et al., 2018). Other mural cell markers such as α-smooth muscle actin (αSMA, or actin alpha 2, smooth muscle; ACTA2), transgelin (or smooth muscle protein 22-α; SM22α), calponin1 (CNN1), desmin, and melanoma cell adhesion molecule (MCAM, or CD146) are expressed more in SMCs than pericytes (Smyth L. et al., 2018; Zeisel et al., 2018). On the other hand, pericytes, but not SMCs, express ATP binding cassette subfamily C member 9 (ABCC9) (Bondjers et al., 2006) and preferentially internalize or take up the fluoroNissl dye NeuroTrace 500/525 when applied to the brain surface (Damisah et al., 2017). Most of the gene expression of pericytes, however, overlaps between SMCs and a certain subtype of pericytes. Furthermore, the expression of all these markers changes during growth and development, and may be up- or down-regulated in pathological conditions (Hughes and Chan-Ling, 2004; Armulik et al., 2011). Therefore, cell morphology and anatomical position should be taken into consideration to distinguish SMCs and pericytes. **Table 1** provides anatomical differences in the cerebral small vessels and mural cell markers.

The classification of small vessels is sometimes complicated and controversial because of the definition of constituent mural cells. Although there is a consensus that SMCs are located in arterioles and venules as well as larger arteries and veins (Iadecola, 2017; Sweeney et al., 2018), the classification and nomenclature of pericyte-surrounding vessels have been greatly debated mainly due to the heterogeneity of pericytes (Cheng et al., 2018). Pericytes in the capillaries gradually transition to SMCs in the arterioles; drawing a clear line between those vessels is quite difficult (Zimmermann, 1923). Originally, Zimmermann defined pericytes including their transition form to SMCs, residing on the three consecutive vessels, namely, (1) pre-capillary arterioles, (2) capillaries, and (3) post-capillary venules (Zimmermann, 1923). Zimmermann therefore differently named the pericytes on each vessel: (1) pre-capillary pericytes, at the last arterial ends that merge into the capillary system; (2) capillary pericytes, at the capillaries in the narrowest sense; and (3) post-capillary pericytes, on post-capillary venules up to veins showing regular, fusiform smooth muscle fibers.

As techniques such as three-dimensional live imaging have been developed, the branching order coming off penetrating arterioles has also been taken into consideration to define the vessels in rodent brains. The definition of the vessels, however, has varied depending on the studies. While some studies have defined all vessels including proximal and distal branches coming off penetrating arterioles as capillaries (Peppiatt et al., 2006; Hall et al., 2014; Cai et al., 2018; Khennouf et al., 2018; Grubb et al., 2020), others have defined proximal branches as pre-capillary arterioles (Fernández-Klett et al., 2010; Hartmann et al., 2015; Hill et al., 2015). To make matters more complicated, Hill et al. (2015), have asserted that the mural cells on the proximal

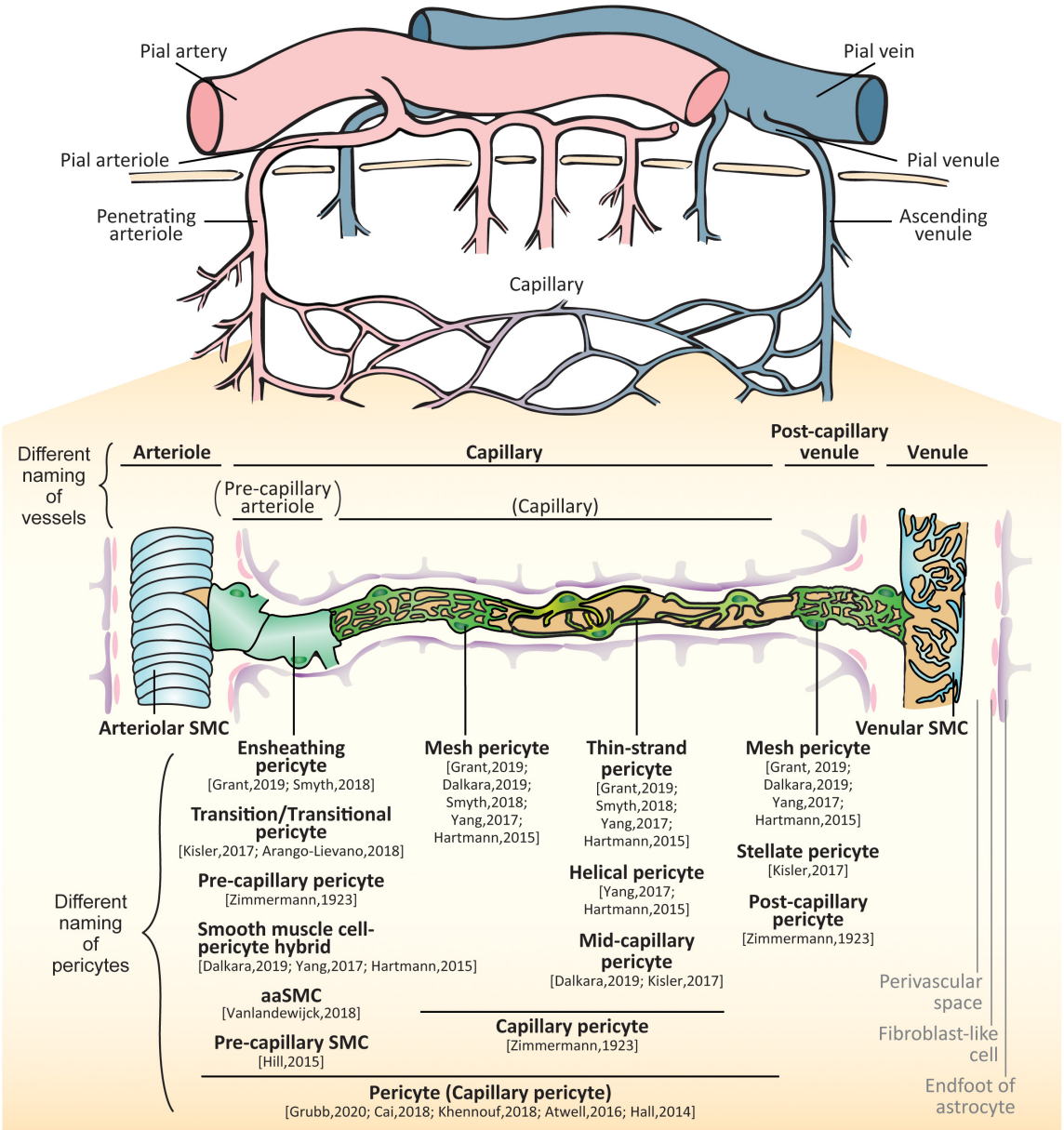

FIGURE 1 | Brain vessels and mural cells. The pial arterioles branch from pial arteries which follow the outer rim of the brain via the meninges. The arterioles penetrate perpendicularly into the brain parenchyma (penetrating arteries) and further split into smaller arterioles. As their diameters and constituent cell types are changed, the vessels make a transition to capillaries. The capillary join to form venules that collect into pial venules and further into pial veins. In the small vessels, there are two types of mural cells separately located outside of endothelial layer: vascular smooth muscle cells (SMCs) and pericytes. SMCs are localized at the arteries, arterioles, venules and veins whereas pericytes are localized at the capillaries and post-capillary venules. The proximal branches coming off penetrating arterioles are sometimes called as pre-capillary arterioles. The subtypes of pericytes are differently called: ensheathing pericytes, transitional pericytes, pre-capillary pericytes, smooth muscle cell-pericyte hybrids, arteriole SMC (aaSMCs), or pre-capillary SMCs in a few branches from arterioles; capillary pericytes, mesh pericytes, thin-strand pericytes, helical pericytes, or mid-capillary pericytes in the middle part of capillary; mesh pericytes, stellate/stellate-like pericytes, or post-capillary pericytes in the post-capillary venules.

branches coming off arterioles should be called as SMCs, which have provided confusion in the field with the result that different members of the field use different terminologies and definitions about pericytes and pericyte-residing vessels (Hartmann et al., 2015; He L. et al., 2016; Kisler et al., 2017a; Yang et al., 2017; Smyth L. et al., 2018; Dalkara, 2019; Grant et al., 2019). Nowadays, to avoid confusion, the researchers have claimed that the capillaries should include transition to the arterioles, and the mural cells on those capillaries should be called as "pericytes" (Attwell et al., 2016). In this review, we will describe the differences of mural cells in the small vessels, namely, (1) SMCs on the arterioles and venules and (2) pericytes on the capillaries and

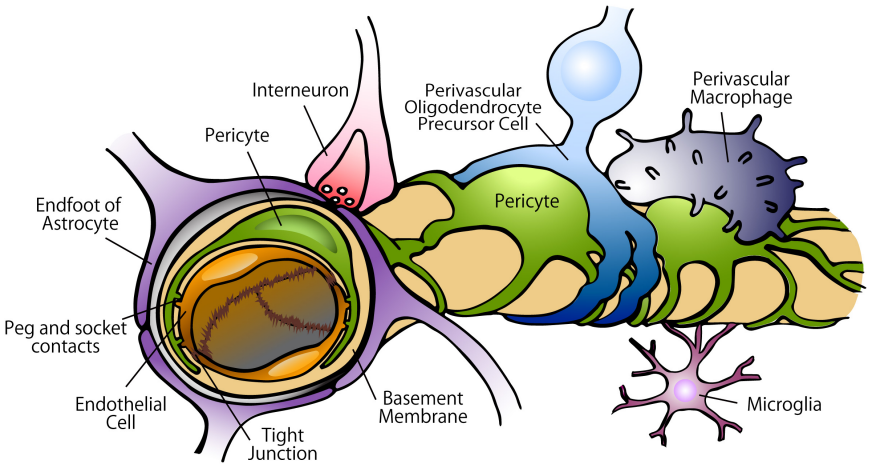

FIGURE 2 | Constituents of the BBB in the capillary. In the BBB, tight junctions created by endothelial cells strictly regulate the movement of ions, molecules, and cells between the blood and the brain. The tight junctions are controlled by the cells surrounding the endothelium, including pericytes, astrocytes, perivascular OPCs, interneurons, perivascular macrophages, and microglia. Pericytes are localized on the abluminal surface of the endothelial layers and embedded in the basement membrane. Astrocytes extend polarized cellular processes that almost completely ensheath the vessel tubes.

post-capillary venules, introducing the different terminology of pericytes. Thereafter, we will focus on the pericyte function and dysfunction in health and diseases.

Arteriolar SMCs

In the arterioles, SMCs continuously enwrap the abluminal side of endothelial cell layer and make myoendothelial gap junction (Aydin et al., 1991). The SMCs in the arterioles have an inconspicuous soma and extend broad processes (Attwell et al., 2016) that strongly express αSMA transgelin, desmin, CD146, and CNN1 as well as shared mural cell markers including NG2, PDGFRβ, CD13, vimentin, and RGS5. Outside of the SMCs is perivascular space with fibroblast-like cells, surrounded by collagen layer and endfeet of astrocytes (Mastorakos and McGavern, 2019).

Capillary Pericytes

In the capillaries, the vessel size further decreases, and the endothelial layer is intermittently surrounded by pericytes. Compared to the peripheral vascular beds, CNS capillaries have higher pericyte-to-endothelial cell ratios (1:1 to 1:3) and around 70–80% of the capillary surface area is covered with pericyte cell processes (Bell et al., 2010; Winkler et al., 2010, 2014). Capillary pericytes have a conspicuous protruding ovoid cell body with long thin processes that course along the capillary for longer distances and are embedded within the basement membrane.

The role of capillary pericytes in CBF control has long been debated. Using mouse models, some researchers have reported that arteriolar SMCs but not capillary pericytes regulate CBF in response to neuronal activities or ischemic stress (Fernández-Klett et al., 2010; Hill et al., 2015). Others, however, have shown that capillary pericytes also change the vessel diameter and CBF by stimuli, neuronal activation, or ischemia (Peppiatt et al., 2006; Yemisci et al., 2009; Hall et al., 2014; Pieper et al., 2014; Kisler et al., 2017b; Rungta et al., 2018), suggesting capillary pericytes also contribute to CBF regulation.

Because pericytes are morphologically and functionally heterogeneous, pericytes are sometimes subclassified according to their topology, morphology, and the protein expression levels.

Pericytes in the Proximal Capillaries

The studies of mouse brain cortices using two-photon microscopy have revealed the morphological and functional distinction of the pericytes on the proximal branches (mostly up to 2nd or 4th order) coming off penetrating arterioles from those on the higher branch-order capillaries or larger arterioles (Hartmann et al., 2015; Hill et al., 2015; Kisler et al., 2017a; Yang et al., 2017; Smyth L. et al., 2018; Grant et al., 2019). The pericytes located in this point of transition possess highly visible and protruding ovoid soma with thin and circumferential processes enveloping the vessels. These cells express more αSMA than pericytes in mid-capillaries, but not as much as SMCs in the penetrating arterioles (Alarcon-Martinez et al., 2018; Grant et al., 2019). Aside from αSMA, the cells also express desmin and transgelin, but hardly express CNN1 (Smyth L. et al., 2018; Vanlandewijck et al., 2018).

Because these pericytes are positioned at the transition between arterioles and capillaries, and have shared some characteristics with SMCs, the terminology and classification of these mural cells have been hotly debated. The cells have been variably called as ensheathing pericytes (Smyth L. et al., 2018; Grant et al., 2019), transition/transitional pericytes (Kisler et al., 2017a; Arango-Lievano et al., 2018), pre-capillary pericytes (Zimmermann, 1923), simply 'pericytes' or 'capillary pericytes' (Hall et al., 2014; Attwell et al., 2016; Cai et al., 2018; Khennouf et al., 2018; Grubb et al., 2020), smooth muscle-pericyte hybrids (Hartmann et al., 2015; Yang et al., 2017; Dalkara, 2019), arteriole SMC (aaSMC) (Vanlandewijck et al., 2018), or pre-capillary SMCs (Hill et al., 2015).

TABLE 1 | Anatomical differences in brain small vessels and mural cell markers.

	Arteriole	Proximal capillary	Mid-capillary	Post-capillary venule	Venule	References
Perivascular space	+[a]/+ (BG/WM)[b]/− (Cox)[c]	−	-	+	+	Zhang et al. (1990)[b], Pollock et al. (1997)[c], Salzman et al. (2005)[c], Onodera (2011)[a], Morris et al. (2016)[b]
Mural cell	SMC	Pericyte	Pericyte	Pericyte	SMC	Zimmermann (1923), Hall et al. (2014), Khennouf et al. (2018)
Different naming of mural cell		Ensheathing pericyte	Mesh pericyte / Thin-strand pericyte	Mesh pericyte	Stellate SMC	Dalkara (2019), Grant et al. (2019), Smyth L. et al. (2018), Yang et al. (2017)
		Transitional pericyte	Mid-capillary pericyte	Stellate pericytes		Kisler et al. (2017a), Arango-Lievano et al. (2018), Dalkara (2019)
		Pre-capillary pericyte	Capillary pericyte	Post-capillary pericyte		Zimmermann (1923)
		Smooth muscle-pericyte hybrid				Hartmann et al. (2015), Yang et al. (2017), Dalkara (2019)
		aaSMC				Vanlandewijck et al. (2018)
		Pre-capillary SMC				Hill et al. (2015)
SMCs and pericytes						
CSPG4 (NG2)	+	++	++	++	+	Hartmann et al. (2015), Hill et al. (2015), Yang et al. (2017), Smyth L.C.D. et al. (2018), Vanlandewijck et al. (2018)
PDGFRβ	+	++	++	++	+	Hartmann et al. (2015), Yang et al. (2017), Smyth L.C.D. et al. (2018), Vanlandewijck et al. (2018)
ANPEP (CD13)	+	+	+	+	+	Kunz et al. (1994), Yang et al. (2017), Smyth L.C.D. et al. (2018)
Vimentin	++	+	+	+	++	Nehls and Drenckhahn (1993), Itoh and Suzuki (2012)
RGS5	+	+	+	+	+	Bondjers et al. (2006), Özen et al. (2014), Yang et al. (2017)
SMCs preferential						
ACTA2 (αSMA)	+++	+	±	±	++	Boado and Pardridge (1994), Bandopadhyay et al. (2001), Itoh and Suzuki (2012), Damisah et al. (2017), Yang et al. (2017), Alarcon-Martinez et al. (2018), Smyth L.C.D. et al. (2018)
Transgelin	++	+	−	−	±	Smyth L.C.D. et al. (2018),
CNN1	++	±	−	−	−	Berthiaume et al. (2018), Vanlandewijck et al. (2018)
Desmin	++	− or ±	− or ±	− or ±	++	Nehls and Drenckhahn (1991), Itoh and Suzuki (2012), Smyth L.C.D. et al. (2018)
MCAM (CD146)	++	±	±	±	++	Smyth L.C.D. et al. (2018)
Pericytes preferential						
ABCC9	−	±	++	++	+	Bondjers et al. (2006), Berthiaume et al. (2018), Vanlandewijck et al. (2018)
Fluoro-Nissl dye	−	+	++	++	±	Damisah et al. (2017)

ABCC9, ATP binding cassette subfamily C member 9; ACTA2, actin alpha 2, smooth muscle; ANPEP, alanyl aminopeptidase, membrane; BG, basal ganglia; CNN1, calponin 1; Cox, cerebral cortex; CSPG4, chondroitin sulfate proteoglycan 4; MCAM, melanoma cell adhesion molecule; PDGFRβ, platelet derived growth factor receptor beta; RGS5, regulator of G protein signaling 5; WM, white matter.

At the same time, the vessels of proximal branches coming off penetrating arterioles are also differently defined as pre-capillary arterioles (Fernández-Klett et al., 2010; Hartmann et al., 2015; Hill et al., 2015; Berthiaume et al., 2018; Erdener and Dalkara, 2019; Grant et al., 2019), post-arteriole capillaries (Gould et al., 2016) or a part of capillaries (Hall et al., 2014; Attwell et al., 2016; Cai et al., 2018; Khennouf et al., 2018; Grubb et al., 2020).

The cells in this proximal branches (especially, 1st to 2nd branches) coming off arterioles has drawn attention as they highly contribute to neurovascular coupling (NVC) (Hall et al., 2014; Hill et al., 2015; Cai et al., 2018; Khennouf et al., 2018; Rungta et al., 2018; Grubb et al., 2020) and no-reflow phenomenon after acute ischemia (Hall et al., 2014; Hill et al., 2015). Although referring to these mural cells as a subtype of "pericytes" has become almost a consensus, the shifting nomenclature of these cells and vessels has been the root of recent controversies on pericyte roles as regulators of CBF (discussed below).

Pericytes in the Mid-Capillaries

In the mouse brain, pericytes in the mid-capillaries are divided into two subtypes according to the morphology of their processes, namely, (1) mesh pericyte and (2) thin-strand pericyte or helical pericyte (Hartmann et al., 2015; Yang et al., 2017; Smyth L. et al., 2018; Dalkara, 2019; Grant et al., 2019). The mesh pericytes adopt a mesh-like appearance and are located on the proximal side of a capillary with higher coverage area than thin-strand pericytes (Hartmann et al., 2015; Grant et al., 2019). The thin-strand pericytes or helical pericytes extend thin, meandering processes that run along the vessel lumen. These two types of pericytes express NG2, CD13, and PDGFRβ, and slightly express CD146 and αSMA, but hardly express desmin, transgelin, nor CNN1 (Alarcon-Martinez et al., 2018; Smyth L. et al., 2018; Vanlandewijck et al., 2018; Zeisel et al., 2018). Instead, pericytes express ABCC9 (Bondjers et al., 2006; Vanlandewijck et al., 2018) and preferentially take up the fluoroNissl dye NeuroTrace 500/525 (Damisah et al., 2017). The pericytes in these capillaries play vital roles for BBB maintenance and small molecule transport (Armulik et al., 2010; Bell et al., 2010; Liu et al., 2012).

Post-capillary Pericytes

In the post-capillary venules, different shaped mesh pericytes, also called stellate/stellate-shaped pericytes, surround the endothelial layer. These cells have many slender and shorter branching processes than capillary pericytes (Hashitani and Lang, 2016; Yang et al., 2017; Arango-Lievano et al., 2018). They express αSMA, ABCC9, cysteine sulfinic acid decarboxylase (P-selectin), and endomucin (Marín-Padilla, 2012). The expression level of αSMA is lower than the mural cells in the arterioles and proximal capillaries (Grant et al., 2019). The pericytes in the post-capillary venules are thought to regulate immune cell entry to the brain parenchyma like those in other tissues (Proebstl et al., 2012; Stark et al., 2013; Attwell et al., 2016; Dalkara, 2019; Rudziak et al., 2019). Outside of the pericytes are astroglial end-feet forming glia limitans. Between the endothelial basement membrane and astrocytic basement membrane is perivascular space, where antigen presenting cells reside (Engelhardt et al., 2017; Mastorakos and McGavern, 2019). Fibroblast-like cells are within the astrocytic basement membrane (Mastorakos and McGavern, 2019).

Venular SMCs

Post-capillary venules are collected to form ascending venules. In the venules, the endothelial cell layer is surrounded by stellate-shaped SMCs with broad leaf-like processes (Ushiwata and Ushiki, 1990; Armulik et al., 2011). Venous SMCs express NG2, CD13, PDGFRβ, αSMA, transgelin, ABCC9, but not CNN1 (Vanlandewijck et al., 2018). And the expression level of αSMA and transgelin in the venous SMCs is lower than the mural cells in the arterioles (Vanlandewijck et al., 2018; Grant et al., 2019). SMCs in brain venules express NG2, which is different from the venules of peripheral tissues (Murfee et al., 2005; Stark et al., 2013). Outside of SMCs are perivascular space and fibroblast-like cells (Mastorakos and McGavern, 2019).

FUNCTIONS OF PERICYTES

BBB Maintenance, Angiogenesis, and Vessel Stabilizing

The CNS vascular system possess a highly selective semipermeable border formed by the BBB wherein tight junctions and adherens junctions created by endothelial cells strictly regulate the movement of ions, molecules, and circulating cells between the blood and the brain (Luissint et al., 2012; Daneman and Prat, 2015). The tight and adherens junctions are controlled by various types of cells surrounding the endothelium, such as pericytes, astrocytes, perivascular oligodendrocyte precursor cells (OPCs), interneurons, perivascular macrophages, microglia, and other immune cells (Abbott et al., 2010; Seo et al., 2014; Faraco et al., 2017; Stebbins et al., 2019) (**Figure 2**).

Capillary pericytes play especially crucial roles in the function of the BBB. Pericyte ablation leads to breakdown of the BBB in the mouse brain (Nikolakopoulou et al., 2019). Pericytes control protein expression in the tight junctions, their alignment with endothelial cells, and the bulk-flow transcytosis of fluid-filled vesicles across the BBB (Armulik et al., 2010; Bell et al., 2010; Daneman et al., 2010; Quaegebeur et al., 2010).

Pericytes also play a key role in the generation of new blood vessels. During angiogenesis, a complex web of bidirectional signaling pathways between endothelial cells and pericytes is essential for forming and stabilizing new blood vessels (Gaengel et al., 2009; Stapor et al., 2014). The signaling molecules involved in these processes include platelet-derived growth factor B (PDGFB)/PDGF receptor beta (PDGFRβ), transforming growth factor beta (TGFβ), Notch, vascular endothelial growth factor (VEGF), sphingosine-1 phosphate (S1P)/S1P receptor 1 (S1PR1 or EDG), and angiopoietin 1 and 2 (ANGPT1, ANGPT2)/TEK receptor tyrosine kinase (TEK, or TIE2) all of which differentially contribute to these signaling activities (Liu et al., 2000; Winkler et al., 2011b; Zechariah et al., 2013; Eilken et al., 2017; Teichert et al., 2017; Cheng et al., 2018). During angiogenesis, pericytes are reported to be recruited from the bone marrow as well as brain parenchyma in response to the PDGF-BB secreted

from endothelial cells (Rajantie et al., 2004; Song et al., 2005; Kokovay et al., 2006; Gaengel et al., 2009). On the other hand, pericytes induce endothelial cell sprouting and stabilization via secreting TGFβ, VEGF, and ANGPT1 (Paik et al., 2004; Durham et al., 2014; Teichert et al., 2017; Blocki et al., 2018). Lack of pericytes leads to endothelial hyperplasia and abnormal vascular morphogenesis including microaneurysm (Lindahl et al., 1997; Hellström et al., 2001). When a single brain pericyte is ablated, the processes from neighboring pericytes are extended to contact uncovered regions of the endothelial cells and maintain the vessel diameter and vessel stability (Berthiaume et al., 2018).

Regulation of Capillary Diameter and Blood Flow

Cerebral blood flow is dynamically altered in response to changes of transient neuronal activity, which is referred to as NVC (Abbott et al., 2010; Attwell et al., 2010; Kisler et al., 2017a). It is controlled by the cells within the neurovascular unit (NVU) including endothelial cells, pericytes, SMCs, astrocytes, OPCs, and neurons (Peppiatt et al., 2006; Attwell et al., 2010; Hall et al., 2014; Mishra et al., 2016; Kisler et al., 2017a,b; Rungta et al., 2018). In response to the different neurotransmitters, pericytes dilate capillaries and increase local CBF (Hamilton et al., 2010). In pathological conditions such as ischemic stroke (Hall et al., 2014; Yemisci et al., 2009) and AD (Nortley et al., 2019), brain capillaries are constricted by pericytes. In ischemic stroke mouse brains, damaged and dead pericytes squeeze the capillaries and sustain the reduction of CBF even after recanalization of the larger vessels, causing the no-reflow phenomenon (Yemisci et al., 2009; Kloner et al., 2018). The burden of amyloid beta (Aβ) oligomer causes pericyte contraction and capillary stenosis, which decreases CBF in the AD brains (Nortley et al., 2019).

The role of pericytes in regulation of vessel diameter has been heatedly debated. When Rouget first describe the branched cells on the capillary wall, which is nowadays called as pericytes, he regarded them as contractile cells (Rouget, 1873). Thereafter, the studies which supported or objected to the pericyte contractility were successively reported (Krueger and Bechmann, 2010). In terms of CBF regulation, SMCs located at arterioles were traditionally thought to control CBF (Iadecola, 2004). This view of CBF dynamics was revolutionized by the findings that capillary diameter also changes with neural activity (Peppiatt et al., 2006; Hall et al., 2014; Kisler et al., 2017b; Khennouf et al., 2018; Rungta et al., 2018) and ischemia (Yemisci et al., 2009; Hall et al., 2014). Furthermore, the loss of pericytes has been reported to lead to diminishing CBF in response to functional hyperemia in pericytes-deficient mice (Bell et al., 2010; Kisler et al., 2017b, 2020). However, Hill et al. (2015) refuted that pericytes are involved in the regulation of CBF, and put forward the view that arteriolar SMCs may be the key players regulating CBF. Fernández-Klett et al. (2010) also showed pre-capillary and penetrating arterioles, but not pericyte in capillaries are responsible for the CBF increase induced by neural activity. These controversial reports most likely stem from the different definitions of pericytes in the proximal capillaries. Some of these reports concur that the mural cells in the proximal branches coming off penetrating arterioles respond to the stimulations outlined above and change vessel diameters accordingly (Fernández-Klett et al., 2010; Hall et al., 2014; Hill et al., 2015; Cai et al., 2018; Khennouf et al., 2018). Pericytes residing at the proximal capillaries possess both characteristics of pericytes and SMCs (Hartmann et al., 2015), which may lead to discrepant interpretations by different investigators. Some groups showed stimulation-evoked increases in synaptic activity and capillary dilation starting mostly at the first- or second-order capillary then propagating along arterioles and downstream capillaries (Cai et al., 2018; Khennouf et al., 2018), which may position the pericytes in the proximal capillaries as the major regulators of CBF. In addition, Grubb et al. (2020) reported that a pre-capillary sphincter, at the junction between the penetrating arteriole and first order branch, modulated capillary flow while protecting the downstream capillary bed from adverse pressure fluctuations. Taken together, the proximal branches coming off arterioles seem to be the gatekeeper that controls CBF in the capillary beds.

Clearance of Materials From the Brain

Pericytes internalize small molecules and neurotoxic blood-derived products which enter the breached BBB (i.e., immunoglobulins, fibrin and albumin) through receptor-mediated endocytosis or non-specific pinocytosis (Armulik et al., 2010; Bell et al., 2010; Schultz et al., 2017). Pericytes also internalize large solid substance through phagocytosis. Engulfed molecules are transported to lysosomes for enzymatic degradation (Diaz-Flores et al., 2009) or possibly transported to the blood circulation (Zhao et al., 2015). While tumor necrosis factor alpha (TNFα) and interferon-γ (IFNγ) enhance phagocytic uptake, TGFB1 attenuates phagocytic uptake in pericytes.

Pericytes may clear substances derived from the brain parenchyma as well as around vessels. Pericyte loss aggravates Aβ deposition in transgenic mice (Sagare et al., 2013). Aβ clearance by pericytes is mainly performed through receptor-mediated endocytic pathways, especially low-density lipoprotein receptor-related protein 1 (LRP-1) (Shibata et al., 2000; Zlokovic et al., 2010; Ma et al., 2018).

Another clearance system which might be related to pericytes is the CNS lymphatic drainage system. In the CNS, there are two major extracellular fluids, namely, (1) cerebrospinal fluid (CSF) and (2) interstitial fluid (ISF). CSF drains to cervical lymph nodes via the cribriform plate and nasal lymphatics (Kida et al., 1993; Spector et al., 2015), as well as via dural lymphatics (Aspelund et al., 2015; Louveau et al., 2015; Absinta et al., 2017; Ahn et al., 2019) and along cranial nerves (Hatterer et al., 2006; Aspelund et al., 2015). ISF containing metabolic products of the brain as well as Aβ and tau drains to lymph nodes by the shared or distinct pathways from CSF (Engelhardt et al., 2017; Cheng and Wang, 2020). Two different pathways for draining ISF to the periphery — the perivascular and paravascular pathways — are controversially proposed (Engelhardt et al., 2016). In the perivascular pathway, ISF and solutes from CNS parenchyma enter the basement membranes of capillaries, where pericytes are embedded, and drain directly via tunica media of arterioles and arteries out of the brain to cervical lymph nodes

(Carare et al., 2008, 2014; Engelhardt et al., 2016). Paravascular pathway, also known as glymphatic system, denotes the moving of CSF into the brain along arterial perivascular spaces and successively into the interstitium to mix with ISF, which then guides flow toward the venous perivascular spaces, removing metabolic waste of ISF to the CSF via convective bulk flow (Iliff et al., 2012). In the glymphatic system, astrocytes are important for ion buffering and fluid exchange between the CSF and ISF (Jessen et al., 2015). The exchange through the glymphatic system is suggested to be dependent on the water channel aquaporin-4 (AQP4) located in astrocytic endfeet (Iliff et al., 2012). However, it remains enigmatic whether or not AQP4 is solely responsible for this fluid transport or not (Lendahl et al., 2019). Recently, insufficient PDGFB signaling in the *Pdgfb*$^{ret/ret}$ mice has shown decreased pericyte coverage of the vessels with decreased AQP4 polarization to astrocyte endfeet, which impairs maturation of the glymphatic function (Munk et al., 2019). The focal absence of pericytes correlates with relocation of AQP4 from astrocytic endfeet to the soma of astrocytes (Armulik et al., 2010). Pericytes express laminin-α2 (LAMA2), laminin-β1, and laminin-γ1, which encode the subunits of laminin 211 (Vanlandewijck et al., 2018). Laminin 211 deposits in the vascular basement membrane and interacts with dystrophin in astrocytes, which acts as a molecular bridge to AQP4 to keep it in the astrocyte endfeet (Guadagno and Moukhles, 2004). Indeed, *Lama2* knockout in mice results in BBB abnormalities in association with loss of AQP4 polarization to astrocyte endfeet (Menezes et al., 2014). The above referenced reports suggest that pericytes might influence the development of the glymphatic system through deposition of laminin 211 in the vascular basement membrane, which maintains the polarization of AQP4 at astrocytic endfeet. However, there are critical assessments of the proposed glymphatic system (Hladky and Barrand, 2014, 2019; Abbott et al., 2018). Several observations or simulations do not support the glymphatic mechanism (Jin et al., 2016; Smith et al., 2017) nor convective fluid flow of CSF (Asgari et al., 2016; Holter et al., 2017). Hence, the existence of the paravascular pathway as a CNS drainage system is still under debate.

Inflammation and the Regulation of Immune Cells

Brain pericytes have many properties of immune regulating cells such as (1) responding to and expressing pro-inflammatory and anti-inflammatory molecules, (2) regulating leukocyte extravasation and trafficking, and (3) controlling immune cell activation including T cells, macrophages, and microglia (Rustenhoven et al., 2017; Thomas et al., 2017; Duan et al., 2018; Smyth L.C.D. et al., 2018). In the mouse brain, pericytes function as the initial sensor of systemic inflammation and relay the infection signal to neurons by secreting chemokine CC chemokine ligand 2 (CCL2, also known as monocyte chemotactic protein-1, MCP1) (Duan et al., 2018).

Pericytes express and release several mediator molecules that enhance leukocyte extravasation. Although the endothelial cells are well known to induce leukocyte crawling and extravasation (Muller, 2002), pericytes also contribute to leukocyte transmigration (Proebstl et al., 2012). *In vivo* observation of mouse skin vessels have demonstrated that leukocyte extravasation occur only post-capillary venular pericytes (Stark et al., 2013). After inflammation stimuli, neutrophils exhibited transendothelial migration (TEM) and sub-endothelial cell crawling along pericyte processes, which was supported by pericyte-derived intercellular adhesion molecule-1 (ICAM-1) and its leukocyte integrin ligands, macrophage-1 antigen (Mac-1) and lymphocyte function–associated antigen-1 (LFA-1). Then, the leukocytes transmigrated to the interstitium through the gaps between adjacent pericytes (Proebstl et al., 2012). After extravasation, the leukocytes interact with capillary pericytes as well. Pericyte-monocyte interaction is mediated mainly by macrophage migration-inhibitory factor (MIF) and CCL2, whereas neutrophil migration involves MIF and C-X3-C motif chemokine ligand 1 (CXCL8, also known as interleukin 8, IL8) (Stark et al., 2013).

Exposure of pericytes to cytokines such as interleukin 1 beta (IL1β) and TNFα triggers the release of inflammatory molecules and matrix metalloprotease 9 (MMP9), leading to BBB breakdown *in vitro* (Herland et al., 2016). The immunomodulatory factors secreted by pericytes including IL1β, TNFα, IFNγ, and interleukin 6 (IL6) induce a proinflammatory state in astrocytes, microglia, and endothelial cells, and cause apoptotic neuronal death (Kovac et al., 2011; Matsumoto et al., 2018).

Conversely, pericytes can also secrete several anti-inflammatory substances such as interleukin 33 (IL33) and C-X3-C motif chemokine ligand 1 (CX3CL1) (Rustenhoven et al., 2016, 2017; Yang et al., 2016), both of which are shown to promote anti-inflammatory microglial phenotype in mouse models (Cardona et al., 2006; Fu et al., 2016). Furthermore, depletion of pericytes induced inflammatory responses in endothelial cells and perivascular infiltration of macrophages in mouse retinal vessels, suggesting pericytes exerts an anti-inflammatory effect on endothelial cells under normal conditions (Ogura et al., 2017).

Phenotype Changes

Pericytes display some similarities to mesenchymal stem cells (Wong et al., 2015). Responding to the stimuli and environmental changes, pericytes may transform into multipotent stem cells and differentiate into various cells including neural, vascular, and glial cells (Dore-Duffy et al., 2006; Nakagomi et al., 2015b; Pombero et al., 2016). Pericytes extracted from ischemic mouse brain and human brain pericytes under oxygen-glucose deprivation states develop stem properties *in vitro* (Nakagomi et al., 2015a). Pericytes under ischemic condition *in vivo* and *in vitro* are also reported to acquire a microglial phenotype corresponding with increased phagocytic property (Özen et al., 2014; Sakuma et al., 2016).

These phenotype changes of pericytes under stimulation can be beneficial for the compensatory remodeling after brain injury and ischemia, rapid response to infection and inflammation, and clearing compromised cells or neurotoxic substances breaching an impaired BBB. However, no multipotency of pericytes in aging and injury *in vivo* has been reported, challenging the current

view of pericytes as tissue-resident multipotent progenitors (Guimaraes-Camboa et al., 2017).

Scar Formation

Central nervous system injury evokes the recruitment of astroglia and scar formation. Pericytes and OPCs as well as astrocytes are observed within glial scars. After spinal injury or ischemic stroke, pericytes proliferate and migrate to the injured region and form a glial scar (Göritz et al., 2011; Makihara et al., 2015; Dias et al., 2018; Hesp et al., 2018). Extracellular matrix proteins, such as periostin have shown to be expressed in the extracellular space of the injury region, which induces pericyte proliferation and leads to scar formation (Yokota et al., 2017). The glial scar around the injury site forms a barrier between the injured and the non-injured tissue to prevent further neuronal loss, which eventually hinders the axonal regeneration in the scarred area (Zhu et al., 2015; Anderson et al., 2016; Cheng et al., 2018; Dias et al., 2018). Recent evidence has demonstrated that the glial scar can also promote CNS regeneration after injury (Anderson et al., 2016), suggesting a dual function. The complexity and heterogeneity of the glial scar derived from different cell types (i.e., astrocytes, pericytes, and OPCs) at various phases in CNS diseases remains to be elucidated.

CROSS TALK OF PERICYTES WITH VASCULAR CELLS AND GLIA

Endothelial Cells and Pericytes

Pericytes and endothelial cells are connected to a shared basement membrane by several types of integrin molecules. In areas lacking the basement membrane, interdigitations of pericytes and endothelial cell membranes, called peg and socket contacts, form direct connections by N-cadherin and connexin 43 (Armulik et al., 2005; Winkler et al., 2011b). The crosstalk between pericytes and endothelial cells is indispensable for angiogenesis, vascular stability, and BBB formation. For CNS pericytes and endothelial cells, PDGFB/PDGFRβ, TGFβ, Notch, VEGF, and S1P/S1PR1 signaling events are well investigated (Darland et al., 2003; Paik et al., 2004; Gaengel et al., 2009; Walshe et al., 2009; Liu et al., 2010; Li et al., 2011). ANGPT signaling is investigated in the retinal endothelial cells and pericytes (Winkler et al., 2011b).

In the angiogenesis of the mouse brain, PDGF-BB secreted by endothelial cells recruits PDGFRβ-positive pericytes and progenitor cells (Tallquist et al., 2003; Gaengel et al., 2009). PDGFB signaling also stimulates pericyte proliferation (Geranmayeh et al., 2019), and sustained PDGF-BB–PDGFRβ signaling in the adult CNS is required for pericyte cell survival (Geraldes et al., 2009; Bell et al., 2010).

TGFβ signaling is vital for microvessel stability affecting both endothelial cells and pericytes. Endothelially secreted TGFβ regulates differentiation of pericyte progenitors (Ribatti et al., 2011) and induces pericyte contractile protein expression and extracellular matrix production and facilitates proper pericyte attachment in coordination with Notch signaling (Li et al., 2011; Winkler et al., 2011a). Pericyte-derived TGFβ contributes to endothelial maturation through SMAD signaling (Winkler et al., 2011b).

Vascular endothelial growth factor produced by pericytes and endothelial cells also shows reciprocal interaction (Sweeney et al., 2016). Pericyte-derived VEGF in the mouse brain promotes endothelial sprouting and cell survival (Franco et al., 2011; Eilken et al., 2017). VEGF treatment enhances pericyte coverage of brain endothelial cells with increased N-cadherin production (Zechariah et al., 2013). VEGF induces proliferation and migration of pericytes as well as endothelial cell stabilization (Darland et al., 2003).

S1P is originally described as secreted by endothelial cells. Its receptor, S1PR1 is expressed in mural cells including pericytes. S1P secreted by endothelial cells is essential for pericytes coverage in the mouse brain (Allende et al., 2003) and stabilizes endothelial/pericyte cell adhesion through N-cadherin (Paik et al., 2004; Gaengel et al., 2009) and maintains the BBB (Yanagida et al., 2017). Human pericytes secrete S1P, which induces the expression of adhesion proteins in human retinal endothelial cells *in vitro* (McGuire et al., 2011).

ANGPT1 and ANGPT2 differently contribute to angiogenesis. The ANGPT1 is mainly expressed in pericytes and ANGPT2 is mainly expressed in endothelial cells. The ligand of ANGPT, TEK is mainly expressed in endothelial cells (Sundberg et al., 2002). Pericyte-derived ANGPT1 activates endothelial TEK and promotes endothelial survival (Geevarghese and Herman, 2014). TEK is also expressed at lower levels by pericytes and its downstream signaling in pericytes is essential for angiogenesis (Teichert et al., 2017). In angiogenesis, ANGPT2 was thought to antagonize ANGPT1, but later was found to act as both agonist/antagonist of TEK signaling in the endothelium (Yuan et al., 2009; Akwii et al., 2019). ANGPT2 expressed by mouse endothelial cells leads to the dissociation of TEK expressing pericytes from vessels, which initiates endothelial cell sprouting (Armulik et al., 2005).

Crosstalk between pericytes and endothelial cells is also mediated by circular RNA. Diabetes-related stress up-regulates a circular RNA, *cPWWP2A* (PWWP domain containing 2A) expression in pericytes, which inhibit *microRNA-579* and regulate vascular integrity (Liu C. et al., 2019).

Astrocytes and Pericytes

The crosstalk between pericytes and astrocytes contributes to BBB maintenance, NVC, and white matter attenuation under chronic hypoperfusion (Bonkowski et al., 2011).

Pericytes facilitate the attachment of astrocyte endfeet to the BBB (Ihara and Yamamoto, 2016; Geranmayeh et al., 2019) and pericyte-deficient mice lose AQP4 in the endfeet of astrocytes (Armulik et al., 2010). On the other hand, astrocytes control pericyte migration, differentiation, and the juxtaposition of pericytes to endothelial cells (Nakagawa et al., 2009; Yao et al., 2014). Astrocyte-derived apolipoproteins differently regulate cyclophilin A (CypA) signaling in pericytes, which controls BBB integrity (Bell et al., 2012). In NVC, astrocytic calcium signaling mediates capillary dilation via pericytes (Mishra et al., 2016; Kisler et al., 2017a).

Oligodendrocyte Precursor Cells and Pericytes

Oligodendrocyte precursor cells (OPCs) have recently emerged as one of the contributors to BBB. According to their regional differences, OPCs can be divided into two subtypes, namely, perivascular OPCs and parenchymal OPCs (Maki, 2017; Kishida et al., 2019). In the human and mouse brain, perivascular OPCs are attached to cerebral endothelial cells and pericytes through basal lamina, and thereby are thought to become novel components of the BBB (Seo et al., 2013; Maki et al., 2015). OPC-specific TGFβ1 depleted mice exhibited cerebral hemorrhage and loss of BBB function, showing the role of OPCs for BBB maintenance through TGFβ1 signaling (Seo et al., 2014). *In vitro* experiments have shown that OPC-derived factors increase pericyte proliferation whereas pericyte-derived factors support OPC self-renewal and differentiation (Maki et al., 2015, 2018). In the developing mouse forebrain, pericyte-derived TGFβ family proteins contribute to the migration and distribution of OPCs in brain parenchyma (Choe et al., 2014), while perivascular OPC migration to the vessels in the developing CNS requires interaction with endothelium but not pericytes (Tsai et al., 2016).

In the adult mouse brain, pericytes respond to toxin-induced demyelination in the brain and stimulate OPC differentiation during remyelination through Lama2 (De La Fuente et al., 2017). Pericyte-derived Lama2 also instructs neuronal stem cells to an oligodendrocyte fate (Silva et al., 2019).

A recent report has shown that odor triggers rapid Ca^{2+} elevations in OPC processes before pericytes and SMCs dilate the vessels responding to synaptic activation, suggesting possible relationship between OPCs and pericytes in the NVC (Rungta et al., 2018).

Microglia and Pericytes

Microglia have been regarded as the main executor of inflammation after acute and chronic CNS disorders. The interaction between microglia and vascular cells – including pericytes – has important roles for vascular inflammation, angiogenesis, and BBB integrity (Ding et al., 2018; Thurgur and Pinteaux, 2019). Although endothelial cells are thought to be the main source of cytokines and chemokines which trigger microglial activation upon vascular inflammation, pericytes are also known to be key mediators in this process. In response to TNFα, rat brain pericytes *in vitro* produce IL6 and macrophage inflammatory protein 1 (MIP1), which trigger microglial activation (Matsumoto et al., 2014). Activated microglia disrupt the BBB, which triggers angiogenesis (Dudvarski Stankovic et al., 2016; Shigemoto-Mogami et al., 2018). In the mouse brain, pericytes initially respond to the systemic inflammation within 2 h and secrete CCL2 before the response of astrocytes or microglia (Duan et al., 2018). Given that CCL2 is also known to activate microglia (He M. et al., 2016; Zhang et al., 2017) and microglial process motility dynamics are altered 48 h after systemic infection (Gyoneva et al., 2014), pericytes might modulate microglial process motility and physical dynamics around the vessels in response to infection. Furthermore, pericytes themselves acquire a microglial phenotype after ischemic stroke as mentioned above (Özen et al., 2014; Sakuma et al., 2016). Conversely, pericytes also secrete several anti-inflammatory substances such as IL33 and CX3CL1 (Rustenhoven et al., 2016, 2017; Yang et al., 2016), both of which has shown promote anti-inflammatory microglial phenotype in mouse models (Cardona et al., 2006; Fu et al., 2016).

Perivascular Macrophages and Pericytes

In the human and mouse brain, perivascular macrophages lie under the basement membrane alongside pericytes (Fabriek et al., 2005; Goldmann et al., 2016). Perivascular macrophages maintain tight junctions between endothelial cells and limit vessel permeability, phagocytose potential pathogens before they enter tissues from the blood and restrict inappropriate inflammation (Zenker et al., 2003). Although pericytes and perivascular macrophages are localized close to each other and possess shared functions including regulation of vascular permeability and phagocytosis, little is known about how pericytes interact with perivascular macrophages in the vascular niche (Lapenna et al., 2018).

PATHOLOGICAL ROLES OF PERICYTES IN CEREBROVASCULAR DISEASES AND AD

Blood–brain barrier breakdown and microvessel dysfunction has been observed in various CNS disorders such as small vessel disease (SVD), ischemic acute stroke, intracerebral hemorrhage, Alzheimer's disease (AD), traumatic brain injury (TBI)/chronic traumatic encephalopathy (CTE), multiple sclerosis (MS), amyotrophic lateral sclerosis (ALS), Lewy body diseases (LBD), and epilepsy (Winkler et al., 2013; Coatti et al., 2019; Erdener and Dalkara, 2019; Geranmayeh et al., 2019). In particular, pericyte dysfunction is thought to be a critical factor for aggravating dementing diseases such as vascular cognitive impairment/dementia and AD (Sagare et al., 2013; Montagne et al., 2018; Nikolakopoulou et al., 2019).

Cognitive impairment/dementia related to vascular pathology is classified according to the causative vessel size, that is, 'small vessel' disease and 'large vessel' disease, although their crosstalk would be essential for the pathogenesis of both disorders (Ihara and Yamamoto, 2016). Cerebral SVD contributes to a wide range of pathological processes, which affect the small vessels including small arteries, arterioles, venules, and capillaries in the brain (Østergaard et al., 2016; Staszewski et al., 2017; Parkes et al., 2018). In contrast, large vessel disease in the brain may result in stroke and hemorrhage, which affect various type of arteries (Nomura et al., 2018). **Table 2** provides the roles of CNS pericytes in health and disease focusing on cerebrovascular diseases and AD.

Small Vessel Disease

SVD is characterized by pathological changes in the small vessels with a diameter < 100 μm, with concentric smooth

TABLE 2 | The roles of CNS pericytes in health and disease.

Pericyte functions	Pericyte roles under pathological conditions			References
	SVD	Stroke	AD	
BBB maintenance	BBB breakdown and white matter attenuation	BBB breakdown and causes hemorrhagic stroke	BBB breakdown and white matter attenuation	Armulik et al. (2010), Bell et al. (2010), Daneman et al. (2010), Seo et al. (2014), Nikolakopoulou et al. (2019), Stebbins et al. (2019)
Angiogenesis	Compensatory angiogenesis	Revascularization and blood vessel stabilization		Liu et al. (2000), Zechariah et al. (2013), Durham et al. (2014), Eilken et al. (2017), Teichert et al. (2017), Berthiaume et al. (2018), Blocki et al. (2018)
Regulation of CBF (neurovascular coupling)		Capillary constriction and no-reflow phenomenon after stroke	Capillary constriction and CBF reduction	Yemisci et al. (2009), Bell et al. (2010), Fernández-Klett et al. (2010), Hamilton et al. (2010), Hall et al. (2014), Hill et al. (2015), Kisler et al. (2017b), Cai et al. (2018), Khennouf et al. (2018)
Clearance of the brain	Trap toxic substances	Trap toxic substances	Aβ clearance	Armulik et al. (2010), Bell et al. (2010),Sagare et al. (2013), Schultz et al. (2017), Ma et al. (2018)
		Acquire microglial properties		Özen et al. (2014), Sakuma et al. (2016)
Immunological property	Release inflammatory substances	Release of pro- and anti-inflammatory substances	Release inflammatory substances	Kovac et al. (2011), Proebstl et al. (2012), Guijarro-Muñoz et al. (2014), Herland et al. (2016), Rustenhoven et al. (2016), Ogura et al. (2017), Duan et al. (2018), Matsumoto et al. (2018), Smyth L.C.D. et al. (2018)
Stem cell-like property		Change to microglia-like cells and stem cells		Özen et al. (2014), Nakagomi et al. (2015a), Sakuma et al. (2016)
Scar formation	Astrogliogenesis	Make barrier between infarcted and intact area		Göritz et al. (2011), Makihara et al. (2015), Dias et al. (2018), Hesp et al. (2018), Uemura et al. (2018)

Aβ, amyloid beta; BBB, blood–brain barrier; CBF, cerebral blood flow.

muscle thickening in arterioles, as well as pericyte degeneration, basal membrane thickening, endothelial, and astrocyte end-feet swelling in capillaries (Craggs et al., 2014; Bosetti et al., 2016; Østergaard et al., 2016). The slowly progressive worsening of microcirculatory structure and function results in white matter changes, which can be detected by magnetic resonance imaging (MRI).

Small vessel disease is commonly known to be co-morbid brain pathology in a wide range of neurodegenerative diseases including CTE, MS, LBD, and diverse tauopathies including AD (Erdener and Dalkara, 2019). In sporadic SVD, pericytes play pivotal roles as they reside in the small vessels and contribute to maintenance of the BBB, vascular integrity, inflammation, and angiogenesis. Chronic hypoperfusion in the rodent brain results in degeneration of pericytes and decreased pericyte coverage in brain blood vessels, and increased BBB permeability followed by white matter attenuation (Ueno et al., 2002; Liu Q. et al., 2019). Pericyte-deficient mice also cause circulatory failure in the brain which can trigger white matter functional deficits and neuronal loss (Bell et al., 2010; Montagne et al., 2018; Nikolakopoulou et al., 2019).

A leaky BBB allows for the extravasation of toxic-blood derived products such as fibrinogen, which accumulates around the vasculature as insoluble fibrin (Bell et al., 2010; Montagne et al., 2018; Nikolakopoulou et al., 2019). Fibrinogen/fibrin infiltration results in clustering and activation of macrophages and microglia as well as chemokine- and antigen presentation-mediated recruitment and activation of T cells, causing axonal degeneration (Davalos et al., 2012; Ryu et al., 2015). Pericytes produce numerous pro-inflammatory mediators including reactive oxygen/nitrogen species (ROS/RNS), which induces neurons to undergo stress-induced apoptosis (Rustenhoven et al., 2017). This pro-inflammatory status in the vessels induces leukocyte adhesion and microglial activation (Matsumoto et al., 2018; Erdener and Dalkara, 2019). Under chronic hypoperfusion, bone morphogenetic protein 4 (BMP4) expression is increased by pericytes, which induces astrogliogenesis and aggravates white matter attenuation (Uemura et al., 2018).

Chronic hypoperfusion induces compensatory angiogenesis by increasing the expression of angiogenetic factors such as VEGF, ANGPT1/2, and MMP9 (Jian et al., 2003; Ohtaki et al., 2006; Min-Soo et al., 2018). VEGF and ANGPT1 promote sprouting and proliferation of endothelial cells, and recruitment of pericytes (Shane and Didier, 2011). MMP9 regulates the detachment of pericytes from vessels thereby triggering angiogenesis (Joyce, 2005).

The importance of pericytes in SVD may be emphasized by the fact that one of the most common inherited cerebral SVD, cerebral autosomal dominant arteriopathy with subcortical infarcts and leukoencephalopathy (CADASIL), shows aggregation of mutant Notch3 protein around capillary pericytes as well as arteriolar SMCs (Ihara and Yamamoto, 2016). Pericytes express Notch3 and are first affected by Notch3 aggregation in *Notch3*^{R169C} mice, suggesting pericytes might be a main contributor in the pathogenesis of CADASIL (Ghosh et al., 2015). A recent study, however, has shown no change in pericyte

coverage in the white matter lesion of CADASIL patients nor *Notch3*^{R169C} mice, arguing against the prevailing hypothesis that pericyte loss is the primary driver of white matter lesions (Rajani et al., 2019). The jury is still out on the contribution of pericytes to the white matter damage.

Cerebral Ischemic Stroke

Residing in the microvessels, pericytes have a great influence on the condition of the brain following acute ischemic stroke caused by thrombosis or embolism affecting larger vessels. The biological roles of pericytes, such as regulation of CBF, BBB maintenance, inflammation and immunological properties, angiogenesis, and scar formation are all involved in the status of the ischemic brain (Gautam and Yao, 2018).

During arterial obstruction, pericytes positioned on the proximal capillaries constrict the vessels and impede capillary blood flow, which lasts even after arterial recanalization, developing a no-reflow phenomenon (Dalkara and Arsava, 2012; Gursoy-Ozdemir et al., 2012; Hall et al., 2014, Hill et al., 2015). The debate about whether these cells are pericytes or SMCs was discussed above.

During stroke, BBB permeability is increased, and sustained ischemia leads to increased BBB disruption (Simpkins et al., 2016). Severe BBB disruption during stroke increases the risk of hemorrhage in patients treated with intravenous tissue-type plasminogen activator (Deguchi et al., 2014). During ischemia, as in SVD, ROS production and MMP9 up-regulation in pericytes contribute to BBB breakdown. An enzymatic source of ROS production, nicotinamide adenine dinucleotide phosphate oxidase 4 (NOX4), is highly up-regulated by pericytes in the peri-infarct region of the mouse brain subjected to middle cerebral artery occlusion (MCAO), and overexpression of NOX4 in pericytes induces BBB breakdown by up-regulating MMP9 (Nishimura et al., 2016). Pericytes also directly release MMP9 during ischemia, which interrupts the tight junctions between endothelial cells and the binding of astrocyte endfeet to the vascular wall (Underly et al., 2017). VEGF up-regulation by pericytes under ischemic conditions has also been reported to disrupt the BBB *in vitro* and *in vivo* (Zheng Gang et al., 2000; Bai et al., 2015), and this triggers further angiogenesis. However, a report has shown that prolonged exposure to VEGF enhances post-ischemic BBB integrity and reduces infarct volume in mice subjected to transient MCAO (Zechariah et al., 2013). Thus, VEGF might have a pluripotent role in BBB integrity according to the dosage and timing of its release.

Pericytes might also play a role in regulating ischemia-induced leukocyte infiltration as pericytes express cell surface adhesion molecules and induce leukocyte transmigration in response to inflammatory mediators (Balabanov et al., 1999; Pieper et al., 2013; Stark et al., 2013). Pericytes express ICAM-1, which guide leukocyte migration through gaps between pericytes by interacting with the integrin ligands on leukocytes (Proebstl et al., 2012).

Aside from these detrimental roles, pericytes play a beneficial role in ischemic stroke via promoting angiogenesis and scar formation. During MCAO-inducing ischemia in the mouse brains, pericytes are recruited from the periphery as well as parenchyma, and are involved in angiogenesis and blood vessel stabilization (Renner et al., 2003; Kokovay et al., 2006). Pericyte migration to the infarcted area forming the core of the scar, which is distinct from the astroglial scar surrounding the core (Fernández-Klett et al., 2013). Consistent with that, *Pdgfrb*$^{+/-}$ mice demonstrated decreased fibrosis in the ischemic area and enlarged infarct volume (Makihara et al., 2015). Although glial scar formation is beneficial to prevent toxic substances from spreading, it should be noted that excessive or long-lasting glial scar formation inhibits axonal regeneration and stalls the recovery process (Dias et al., 2018). Furthermore, detachment of pericytes from capillaries allows them to migrate toward ischemic region thereby causing further leakage of the BBB. The same is true of angiogenesis. While angiogenesis increases the blood supply to the peri-infarct area, insufficient angiogenesis results in leaky blood vessels leading to brain hemorrhage (Kuhnert et al., 2010; Cullen et al., 2011).

Alzheimer's Disease

AD is the most prevailing dementia among the elderly and is defined pathologically by the presence of Aβ accumulation in brain parenchyma as Aβ plaque and aggregation of hyperphosphorylated tau as neurofibrillary tangles as well as neuritic plaques and neuropil threads. Aβ also accumulate in the vessels as cerebral amyloid angiopathy (CAA). Recently, it has been increasingly recognized that the decreased CBF and white matter attenuation associated with BBB breakdown correlates with the accumulation of AD pathology, and contributes to the onset and progression of dementia (Iturria-Medina et al., 2016; Leijenaar et al., 2017; Park et al., 2019). CBF reduction, BBB breakdown in the hippocampus, and an increase in PDGFRβ level in the CSF occur even in the very early stages of cognitive impairment (Iris et al., 2007; Montagne et al., 2015; Iturria-Medina et al., 2016; Nation et al., 2019) as well as later stages of AD (Miners et al., 2019). In AD patient brains, microvessels are frequently narrowed and irregular in diameter especially in the vicinity of the senile plaques, which is accompanied by decreased capillary bed densities (Kitaguchi et al., 2007). Some vessels in these area are collapsed with lacking endothelial cells, and do not carry blood flow, called string vessels (Hunter et al., 2012). In the mouse brain, infusion of Aβ caused endothelin-1 (ET1) upregulation in cerebral vasculature through receptor for advanced glycation end products (RAGE), which contributes to Aβ-induced CBF reduction (Deane et al., 2003). CBF reduction accompanied by increased vascular RAGE and ET1 is also observed in Tg2576 mice, which is ameliorated by blocking Aβ and RAGE binding (Deane et al., 2003). A recent study has shown that capillaries in the AD brains are constricted by pericytes, which causes a decrease in CBF (Nortley et al., 2019). In rat brains, Aβ oligomer-induced ROS triggers the release of ET1 to stimulate pericytes contraction and CBF reduction (Nortley et al., 2019). AD patients also show a decrease in pericyte coverage with an increase in extravascular immunoglobulin G and fibrin deposition (Sengillo et al., 2013). The apolipoprotein E4 genotype, which is a major genetic risk factor for late-onset AD, leads to pericyte loss and enhances CypA-MMP9 pathway of BBB degradation (Halliday et al., 2016). Pericytes

express LRP1 and other Aβ-binding receptors such as the low density lipoprotein receptor (LDLR), RAGE, and CD36 in brains with AD pathology including CAA (Zenaro et al., 2017). Aβ accumulation in pericytes is observed in human AD brains and in the brains of $APP^{sw/0}$ mice (Ma et al., 2018). At the ultrastructural level of AD brains, pericytes are disorganized and exhibit mitochondrial abnormalities, pinocytotic vesicles, and accumulation of osmophilic material (Farkas and Luiten, 2001; Baloyannis and Baloyannis, 2012).

Loss of BBB integrity caused by pericyte deterioration may induce an influx of immune cells into the brain, driving inflammation, and CBF stagnation and thereby impairing Aβ clearance, all of which aggravate AD pathology (Mazza et al., 2011; Kinney et al., 2018). Indeed, both the depletion of pericytes in the $APP^{sw/0}$ mice ($APP^{sw/0}$; $Pdfgfb^{+/-}$) (Sagare et al., 2013) and chronic cerebral hypoperfusion in the APP^{SwInd} Tg mice (Kitaguchi et al., 2009; Yamada et al., 2011) aggravate AD pathology such as increasing Aβ deposition and tau phosphorylation followed by neuronal loss. Notably, a high-fat diet, which leads to vascular related diseases, exacerbates AD pathology accompanied by pericyte dysfunction in the $APP^{sw/PS1}$ mice (Theriault et al., 2016).

Although Aβ is toxic to the pericytes, pericytes basically take an active part in the clearance of Aβ by phagocytosis and translocation through BBB (Winkler et al., 2014; Alla et al., 2019). Pericytes clear Aβ aggregates via an LRP1/ApoE isoform-specific mechanisms, suggesting a potential therapeutic target for controlling Aβ clearance in AD (Winkler et al., 2014; Ma et al., 2018).

THERAPEUTIC STRATEGIES FOCUSING ON PERICYTES

Since pericytes have multifunctional properties and contribute to the various neurological disorders, pericytes as a therapeutic target, can be approached from various aspects: (1) prevention of BBB dysfunction, (2) promoting angiogenesis and vascular stability, (3) reduction of pericyte constriction under pathological condition, (4) up-regulation of Aβ clearance, (5) control of inflammation, (6) implantation therapy through multipotential stem cell properties, and (7) regulation of proper scar formation.

As the BBB tightly restricts the passage of substances into the CNS, it is challenging to deliver drugs from blood circulation into the brain. Therefore, the delivery methods which enable the drugs to pass through BBB may be beneficial as exemplified by encapsulating drugs in liposomes or nanoparticles (Gaudin et al., 2014; Fullstone et al., 2016; Zhou et al., 2018).

Prevention of BBB Dysfunction, Promoting Angiogenesis, and Vascular Stability

Loss of pericytes and BBB dysfunction are common in a variety of neurological disorders including cerebrovascular diseases and AD. Thus, promoting the interaction of pericytes and endothelial cells by regulating PDGFB/PDGFRβ, TGFβ, Notch, ANGPT/TEK, and VEGF signaling could be therapeutic by preventing BBB dysfunction and facilitating proper angiogenesis and vascular stability. For instance, increasing PDGF-BB in the endothelial cells and/or PDGFRβ in the pericytes could boost pericyte proliferation and migration to microvessels while increasing TGFβ signaling could promote pericyte proliferation and attachment to the vessels (Winkler et al., 2011b). Indeed, administration of TGFβ showed increased BBB formation under ischemic condition *in vitro* and *in vivo* (Shen et al., 2019). VEGF treatment was also shown to enhance post-ischemic BBB integrity and reduce infarct volume in rodent models of MCAO (Zheng Gang et al., 2000; Zechariah et al., 2013). Recently, regulating RNA for maintaining the BBB has been investigated and overexpression of *cPWWP2A* or silencing *microRNA-579* expression promoted pericyte-endothelial cell crosstalk and microvascular stability (Liu C. et al., 2019). Administration of *microRNA-149-5p* attenuated BBB permeability and improved the outcomes of rat subjected with transient MCAO (Wan et al., 2018).

Reduction of ROS and MMP9 should also prevent pericyte-mediated BBB breakdown. A recent study observed that MMP9 inhibitors reduced pericyte-associated BBB leakage (Underly et al., 2017). A free radical scavenger edaravone has been sown to ameliorate brain damage after ischemia via pericyte-mediated angiogenesis and vessel stability (Deguchi et al., 2014). Further, cilostazol – a phosphodiesterase 3 inhibitor – promoted angiogenesis through pericyte proliferation with inhibition of the MMP9, which maintained vascular integrity in spontaneously hypertensive stroke prone (SHR-SP) rat (Omote et al., 2014) while cilostazol also ameliorated cerebral hemorrhage in mice by protecting the BBB (Takagi et al., 2017), suggesting cilostazol has additional effects of vascular stability aside from antithrombosis.

Reduction of Capillary Constriction by Pericytes Under Ischemia or Aβ Accumulation

Since the no-reflow phenomenon hampers the tissue recovery after recanalization in the arteries, researchers have tried to find clues to prevent capillary constriction by pericytes after ischemia. These ischemia-induced pericyte contraction have shown to be relieved by suppressing ROS/RNS (Yemisci et al., 2009; Deguchi et al., 2014; Hall et al., 2014), removal of external Ca^{2+} (Hall et al., 2014), or administration of adenosine and sodium nitroprusside (Neuhaus et al., 2017; O'Farrell et al., 2017). Capillary constriction by pericytes and CBF reduction are also observed in AD brains, which may aggravate cognitive decline. Aβ infusion into mouse brain causes RAGE-ET1 mediated CBF reduction, similar to the CBF reduction observed in aged Tg2576 mice (Deane et al., 2003). Furthermore, a RAGE-specific inhibitor recovered CBF and lowered the Aβ burden in $APP^{sw/0}$ mice (Deane et al., 2012). Aβ oligomers induce pericyte constriction by ROS mediated ET1 release (Nortley et al., 2019). This Aβ-evoked constriction was reversed by applying the vasodilator C-type natriuretic peptide and could be halted by blocking NOX4 or ET1 receptors, suggesting potential therapeutic target for CBF reduction in AD.

Up-Regulation of Aβ Clearance

Because pericytes take up Aβ, then degrade or excrete it into the circulation, boosting pericyte function could be therapeutic target for Aβ clearance in AD. Consistent with that, pericyte loss in the $APP^{sw/0}$ mice showed increased Aβ accumulation and tau phosphorylation (Sagare et al., 2013). Pericytes internalize and clear aggregated Aβ by LRP1-dependent ApoE isoform-specific mechanism (Ma et al., 2018), highlighting up-regulation of LRP1 as a therapeutic target for Aβ clearance.

Control of Inflammation

Neuroinflammation is present in almost all neurological diseases. Pericytes release both pro-inflammatory and anti-inflammatory mediators and regulate recruitment of immune cells from the blood to the brain parenchyma. Although inflammation may have some positive aspects such as immunoprotection against pathogens, clearance of toxic substances, and support of angiogenesis, excessive inflammation causes BBB leakage, tissue damages and neuronal loss.

Targeting ROS-mediated inflammation is a feasible therapeutic target in terms of suppressing release of pro-inflammatory cytokines by pericytes with preventing pericyte loss and BBB dysfunction. A free radical scavenger edaravone has been sown to ameliorate brain damage after ischemia (Deguchi et al., 2014). Targeting receptor or downstream signaling stimulated by pericyte-secreted cytokines may also be potential therapeutic target. Blocking pericyte-derived BMP4 by its receptor antagonist noggin treatment was shown to suppress astrogliogenesis and alleviate white matter damage resulting from chronic cerebral hypoperfusion (Uemura et al., 2018). Targeting transcription factors that regulate immune functions following inflammatory insults might be another option to suppress the detrimental effects of inflammation.

Implantation Therapy, Application of Multipotential Stem Cell Properties

Implantation of mesenchymal stem cell-derived pericytes in mice that model AD plaque pathology reduces the Aβ burden, demonstrating the possibility of cell-based therapy for AD treatment (Tachibana et al., 2018). Easy accessibility of pericytes for autologous transplantation highlights their capabilities for future therapeutic studies (Geranmayeh et al., 2019). Since pericyte-like cells derived from induced pluripotent stem cells (iPSC) acquire BBB properties and are incorporated with iPSC-derived endothelial cells, astrocytes and neurons (Faal et al., 2019; Stebbins et al., 2019), iPSC-derived pericytes might also be promising for implantation therapy of AD and other neurological disorders. Pericytes themselves have been shown to acquire stem cell-like and microglial properties after ischemia (Özen et al., 2014; Nakagomi et al., 2015a), which offers another potential therapeutic target for recovery form CNS diseases.

Regulation of Proper Scar Formation

As discussed above, scar formation in the ischemic brain and brain/spinal cord injury has pluripotent effects on diverse CNS conditions. While the scar formation by pericytes and glia play fundamental roles in promoting angiogenesis and tissue remodeling (Hesp et al., 2018), reducing pericyte-derived scar formation has been reported to promote axonal regeneration and recovery from spinal cord injury (Dias et al., 2018). Administration of periostin-neutralizing antibody, which suppresses pericyte-induced scar formation, ameliorates functional recovery after spinal cord injury (Yokota et al., 2017), but further studies are needed to demonstrate the therapeutic potential of these strategies including the appropriate timing and degree of intervention.

CONCLUSION

All CNS cells and tissues need a blood supply coming from outside the brain. Located at the interface between CNS tissue and blood circulation and having multi-functional properties, pericytes play a variety of fundamental roles in the healthy CNS. As a result, pericytes offer many opportunities for therapeutic intervention in a broad range of neurological disorders, including cerebrovascular disorders and AD. Vascular cognitive impairment/dementia and AD account for more than 3/4 of dementing diseases, and vascular pathology is often observed in a various neurodegenerative disease, especially in AD, where pericytes are thought to contribute. With increasing knowledge about the molecular mechanisms operating in pericytes and their crosstalk with neighboring cells, the targeting pericytes as a therapeutic strategy has become increasingly important and research on this topic is likely to accelerate more in the future.

AUTHOR CONTRIBUTIONS

MU conceptualized the study, designed and drafted the manuscript and figures, and handled the funding. TM supervised and critically revised the manuscript for important intellectual content. MI, VL, and JT handled the funding, supervising, and making critical revision of the manuscript for important intellectual content.

FUNDING

This work was funded by 201870008, JSPS overseas Research Fellowships (to MU), 19jm0210053h0003, Strategic International Collaborative Research Program (SICORP) from Japan Agency for Medical Research and Development (to MI), and also funded by P30 AG010124, U10 AG062418, the Jeff and Anne Keefer Fund and the Neurodegenerative Disease Research Fund (to VL and JT).

ACKNOWLEDGMENTS

The authors thank Mr. John Robinson for proofreading the manuscript.

REFERENCES

Abbott, J. N., Pizzo, M. E., Preston, J. E., Janigro, D., and Thorne, R. G. (2018). The role of brain barriers in fluid movement in the CNS: is there a 'glymphatic' system? *Acta Neuropathol.* 135, 387–407. doi: 10.1007/s00401-018-1812-4

Abbott, N. J., Patabendige, A. A., Dolman, D. E., Yusof, S. R., and Begley, D. J. (2010). Structure and function of the blood-brain barrier. *Neurobiol. Dis.* 37, 13–25. doi: 10.1016/j.nbd.2009.07.030

Absinta, M., Ha, S. K., Nair, G., Sati, P., Luciano, N. J., Palisoc, M., et al. (2017). Human and nonhuman primate meninges harbor lymphatic vessels that can be visualized noninvasively by MRI. *Elife* 6:29738. doi: 10.7554/eLife.29738

Ahn, J. H., Cho, H., Kim, J. H., Kim, S. H., Ham, J. S., Park, I., et al. (2019). Meningeal lymphatic vessels at the skull base drain cerebrospinal fluid. *Nature* 572, 62–66. doi: 10.1038/s41586-019-1419-5

Akwii, R. G., Sajib, M. S., Zahra, F. T., and Mikelis, C. M. (2019). Role of Angiopoietin-2 in vascular physiology and pathophysiology. *Cells.* 8:471. doi: 10.3390/cells8050471

Alarcon-Martinez, L., Yilmaz-Ozcan, S., Yemisci, M., Schallek, J., Kilic, K., Can, A., et al. (2018). Capillary pericytes express alpha-smooth muscle actin, which requires prevention of filamentous-actin depolymerization for detection. *Elife* 7:e34861. doi: 10.7554/eLife.34861

Alla, B. S., Yulia, K. K., Olga, L. L., and Alexander, B. (2019). Pericyte biology in disease. *Adv. Exp. Med. Biol.* 1147, 147–166. doi: 10.1007/978-3-030-16908-4_7

Allende, M. L., Yamashita, T., and Proia, R. L. (2003). G-protein-coupled receptor S1P1 acts within endothelial cells to regulate vascular maturation. *Blood* 102, 3665–3667. doi: 10.1182/blood-2003-02-0460

Anderson, M. A., Burda, J. E., Ren, Y., Ao, Y., O'Shea, T. M., Kawaguchi, R., et al. (2016). Astrocyte scar formation aids central nervous system axon regeneration. *Nature* 532, 195–200. doi: 10.1038/nature17623

Arango-Lievano, M., Boussadia, B., De Terdonck, L. D. T., Gault, C., Fontanaud, P., Lafont, C., et al. (2018). Topographic reorganization of cerebrovascular mural cells under seizure conditions. *Cell Rep.* 23, 1045–1059. doi: 10.1016/j.celrep.2018.03.110

Armulik, A., Abramsson, A., and Betsholtz, C. (2005). Endothelial/Pericyte interactions. *Circ. Res.* 97, 512–523. doi: 10.1161/01.res.0000182903.16652.d7

Armulik, A., Genové, G., and Betsholtz, C. (2011). Pericytes: developmental, physiological, and pathological perspectives, problems, and promises. *Dev. Cell* 21, 193–215. doi: 10.1016/j.devcel.2011.07.001

Armulik, A., Genové, G., Mäe, M., Nisancioglu, M. H., Wallgard, E., Niaudet, C., et al. (2010). Pericytes regulate the blood-brain barrier. *Nature* 468, 557–561. doi: 10.1038/nature09522

Asgari, M., de Zelicourt, D., and Kurtcuoglu, V. (2016). Glymphatic solute transport does not require bulk flow. *Sci. Rep.* 6:38635. doi: 10.1038/srep38635

Aspelund, A., Antila, S., Proulx, S. T., Karlsen, T. V., Karaman, S., Detmar, M., et al. (2015). A dural lymphatic vascular system that drains brain interstitial fluid and macromolecules. *J. Exp. Med.* 212, 991–999. doi: 10.1084/jem.20142290

Attwell, D., Buchan, A. M., Charpak, S., Lauritzen, M., Macvicar, B. A., and Newman, E. A. (2010). Glial and neuronal control of brain blood flow. *Nature* 468, 232–243. doi: 10.1038/nature09613

Attwell, D., Mishra, A., Hall, C. N., O'Farrell, F. M., and Dalkara, T. (2016). What is a pericyte? *J. Cereb. Blood Flow Metab.* 36, 451–455. doi: 10.1177/0271678x15610340

Aydin, F., Rosenblum, W. I., and Povlishock, J. T. (1991). Myoendothelial junctions in human brain arterioles. *Stroke* 22, 1592–1597. doi: 10.1161/01.Str.22.12.1592

Bai, Y., Zhu, X., Chao, J., Zhang, Y., Qian, C., Li, P., et al. (2015). Pericytes contribute to the disruption of the cerebral endothelial barrier via increasing VEGF expression: implications for stroke. *PLoS One* 10:e0124362. doi: 10.1371/journal.pone.0124362

Balabanov, R., Beaumont, T., and Dore-Duffy, P. (1999). Role of central nervous system microvascular pericytes in activation of antigen-primed splenic T-lymphocytes. *J. Neurosci. Res.* 55, 578–587. doi: 10.1002/(sici)1097-4547(19990301)55:5<578::Aid-jnr5<3.0.Co;2-e

Baloyannis, S. J., and Baloyannis, I. S. (2012). The vascular factor in Alzheimer's disease: a study in Golgi technique and electron microscopy. *J. Neurol. Sci.* 322, 117–121. doi: 10.1016/j.jns.2012.07.010

Bandopadhyay, R., Orte, C., Lawrenson, J. G., Reid, A. R., Silva, S. D., and Allt, G. (2001). Contractile proteins in pericytes at the blood-brain and blood-retinal barriers. *J. Neurocytol.* 30, 35–44.

Bell, R. D., Winkler, E. A., Sagare, A. P., Singh, I., LaRue, B., Deane, R., et al. (2010). Pericytes control key neurovascular functions and neuronal phenotype in the adult brain and during brain aging. *Neuron* 68, 409–427. doi: 10.1016/j.neuron.2010.09.043

Bell, R. D., Winkler, E. A., Singh, I., Sagare, A. P., Deane, R., Wu, Z., et al. (2012). Apolipoprotein E controls cerebrovascular integrity via cyclophilin A. *Nature* 485, 512–516. doi: 10.1038/nature11087

Berthiaume, A.-A., Hartmann, D. A., Majesky, M. W., Bhat, N. R., and Shih, A. Y. (2018). Pericyte structural remodeling in cerebrovascular health and homeostasis. *Front. Aging Neurosci.* 10:210. doi: 10.3389/fnagi.2018.00210

Bevan, J. A., Dodge, J., Walters, C. L., Wellman, T., and Bevan, R. D. (1999). As human pial arteries (internal diameter 200–1000 μm) get smaller, their wall thickness and capacity to develop tension relative to their diameter increase. *Life Sci.* 65, 1153–1161. doi: 10.1016/s0024-3205(99)00349-5

Blocki, A., Beyer, S., Jung, F., and Raghunath, M. (2018). The controversial origin of pericytes during angiogenesis – implications for cell-based therapeutic angiogenesis and cell-based therapies. *Clin. Hemorheol. Microcirc.* 69, 215–232. doi: 10.3233/ch-189132

Boado, R. J., and Pardridge, W. M. (1994). Differential expression of α—actin mRNA and immunoreactive protein in brain microvascular pericytes and smooth muscle cells. *J. Neurosci.* 39, 430–435.

Bondjers, C., He, L., Takemoto, M., Norlin, J., Asker, N., Hellstrom, M., et al. (2006). Microarray analysis of blood microvessels from PDGF-B and PDGF-Rbeta mutant mice identifies novel markers for brain pericytes. *FASEB J.* 20, 1703–1705. doi: 10.1096/fj.05-4944fje

Bonkowski, D., Katyshev, V., Balabanov, R. D., Borisov, A., and Dore-Duffy, P. (2011). The CNS microvascular pericyte: pericyte-astrocyte crosstalk in the regulation of tissue survival. *Fluids Barriers CNS* 8:8. doi: 10.1186/2045-8118-8-8

Bosetti, F., Galis, Z. S., Bynoe, M. S., Charette, M., Cipolla, M. J., Del Zoppo, G. J., et al. (2016). Small blood vessels: big health problems?" Scientific recommendations of the national institutes of health workshop. *J. Am. Heart Assoc.* 5:e004389. doi: 10.1161/jaha.116.004389

Brown, L. S., Foster, C. G., Courtney, J.-M., King, N. E., Howells, D. W., and Sutherland, B. A. (2019). Pericytes and neurovascular function in the healthy and diseased brain. *Front. Cell. Neurosci.* 13:282. doi: 10.3389/fncel.2019.00282

Cai, C., Fordsmann, J. C., Jensen, S. H., Gesslein, B., Lønstrup, M., Hald, B. O., et al. (2018). Stimulation-induced increases in cerebral blood flow and local capillary vasoconstriction depend on conducted vascular responses. *Proc. Natl. Acad. Sci.* 115, E5796–E5804. doi: 10.1073/pnas.1707702115

Carare, R. O., Bernardes-Silva, M., Newman, T. A., Page, A. M., Nicoll, J. A., Perry, V. H., et al. (2008). Solutes, but not cells, drain from the brain parenchyma along basement membranes of capillaries and arteries: significance for cerebral amyloid angiopathy and neuroimmunology. *Neuropathol. Appl. Neurobiol.* 34, 131–144. doi: 10.1111/j.1365-2990.2007.00926.x

Carare, R. O., Hawkes, C. A., and Weller, R. O. (2014). Afferent and efferent immunological pathways of the brain. Anatomy, function and failure. *Brain Behav. Immun.* 36, 9–14. doi: 10.1016/j.bbi.2013.10.012

Cardona, A. E., Pioro, E. P., Sasse, M. E., Kostenko, V., Cardona, S. M., Dijkstra, I. M., et al. (2006). Control of microglial neurotoxicity by the fractalkine receptor. *Nat. Neurosci.* 9, 917–924. doi: 10.1038/nn1715

Cheng, J., Korte, N., Nortley, R., Sethi, H., Tang, Y., and Attwell, D. (2018). Targeting pericytes for therapeutic approaches to neurological disorders. *Acta Neuropathol.* 136, 507–523. doi: 10.1007/s00401-018-1893-0

Cheng, Y., and Wang, Y. J. (2020). Meningeal lymphatic vessels: a drain of the brain involved in neurodegeneration? *Neurosci. Bull.* doi: 10.1007/s12264-019-00456-8 [Epub ahead of print].

Choe, Y., Huynh, T., and Pleasure, S. J. (2014). Migration of oligodendrocyte progenitor cells is controlled by transforming growth factor β family proteins during corticogenesis. *J. Neurosci.* 34, 14973–14983. doi: 10.1523/JNEUROSCI.1156-14.2014

Clark, E. R., and Clart, E. L. (1940). Microscopic observations on the extra-endothelial cells of living mammalian blood vessels. *Am. J. Anat.* 66, 39–49.

Coatti, G. C., Cavacana, N., and Zatz, M. (2019). Pericyte biology in disease. *Adv. Exp. Med. Biol.* 1147, 137–146. doi: 10.1007/978-3-030-16908-4_6

Craggs, L., Yamamoto, Y., Deramecourt, V., and Kalaria, R. N. (2014). Microvascular pathology and morphometrics of sporadic and hereditary small vessel diseases of the brain. *Brain Pathol.* 24, 495–509. doi: 10.1111/bpa.12177

Cullen, M., Elzarrad, M. K., Seaman, S., Zudaire, E., Stevens, J., Yang, M. Y., et al. (2011). GPR124, an orphan G protein-coupled receptor, is required for CNS-specific vascularization and establishment of the blood-brain barrier. *Proc. Natl. Acad. Sci. U.S.A.* 108, 5759–5764. doi: 10.1073/pnas.1017192108

Dalkara, T. (2019). Pericytes: a novel target to improve success of recanalization therapies. *Stroke* 50, 2985–2991. doi: 10.1161/strokeaha.118.023590

Dalkara, T., and Alarcon-Martinez, L. (2015). Cerebral microvascular pericytes and neurogliovascular signaling in health and disease. *Brain Res.* 1623, 3–17. doi: 10.1016/j.brainres.2015.03.047

Dalkara, T., and Arsava, E. (2012). Can restoring incomplete microcirculatory reperfusion improve stroke outcome after thrombolysis? *J. Cereb. Blood Flow Metab.* 32, 2091–2099. doi: 10.1038/jcbfm.2012.139

Damisah, E. C., Hill, R. A., Tong, L., Murray, K. N., and Grutzendler, J. (2017). A fluoro-Nissl dye identifies pericytes as distinct vascular mural cells during in vivo brain imaging. *Nat. Neurosci.* 20, 1023–1032. doi: 10.1038/nn.4564

Daneman, R., and Prat, A. (2015). The blood–brain barrier. *Cold Spring Harb. Perspect. Biol.* 7:a020412. doi: 10.1101/cshperspect.a020412

Daneman, R., Zhou, L., Kebede, A. A., and Barres, B. A. (2010). Pericytes are required for blood–brain barrier integrity during embryogenesis. *Nature* 468, 562–566. doi: 10.1038/nature09513

Darland, D. C., Massingham, L. J., Smith, S. R., Piek, E., Saint-Geniez, M., and D'Amore, P. A. (2003). Pericyte production of cell-associated VEGF is differentiation-dependent and is associated with endothelial survival. *Dev. Biol.* 264, 275–288. doi: 10.1016/j.ydbio.2003.08.015

Davalos, D., Ryu, J., Merlini, M., Baeten, K. M., Moan, N., Petersen, M. A., et al. (2012). Fibrinogen-induced perivascular microglial clustering is required for the development of axonal damage in neuroinflammation. *Nat. Commun.* 3:1227. doi: 10.1038/ncomms2230

De La Fuente, A. G., Lange, S., Silva, M. E., Gonzalez, G. A., Tempfer, H., van Wijngaarden, P., et al. (2017). Pericytes stimulate oligodendrocyte progenitor cell differentiation during CNS remyelination. *Cell Rep.* 20, 1755–1764. doi: 10.1016/j.celrep.2017.08.007

Deane, R., Du Yan, S., Submamaryan, R. K., LaRue, B., Jovanovic, S., Hogg, E., et al. (2003). RAGE mediates amyloid-beta peptide transport across the blood-brain barrier and accumulation in brain. *Nat. Med.* 9, 907–913. doi: 10.1038/nm890

Deane, R., Singh, I., Sagare, A. P., Bell, R. D., Ross, N. T., LaRue, B., et al. (2012). A multimodal RAGE-specific inhibitor reduces amyloid beta-mediated brain disorder in a mouse model of Alzheimer disease. *J Clin. Invest.* 122, 1377–1392. doi: 10.1172/jci58642

Deguchi, K., Liu, N., Liu, W., Omote, Y., Kono, S., Yunoki, T., et al. (2014). Pericyte protection by edaravone after tissue plasminogen activator treatment in rat cerebral ischemia. *J. Neurosci. Res.* 92, 1509–1519. doi: 10.1002/jnr.23420

Dias, D., Kim, H., Holl, D., Solnestam, B., Lundeberg, J., Carlén, M., et al. (2018). Reducing pericyte-derived scarring promotes recovery after spinal cord injury. *Cell* 173, 153–165.e22. doi: 10.1016/j.cell.2018.02.004

Diaz-Flores, L., Gutierrez, R., Madrid, J. F., Varela, H., Valladares, F., Acosta, E., et al. (2009). Pericytes, morphofunction, interactions and pathology in a quiescent and activated mesenchymal cell niche. *Histol. Histopathol.* 24, 909–969. doi: 10.14670/HH-24.909

Ding, X., Gu, R., Zhang, M., Ren, H., Shu, Q., Xu, G., et al. (2018). Microglia enhanced the angiogenesis, migration and proliferation of co-cultured RMECs. *BMC Ophthalmol.* 18:249. doi: 10.1186/s12886-018-0886-z

Dore-Duffy, P., Katychev, A., Wang, X., and Buren, E. (2006). CNS microvascular pericytes exhibit multipotential stem cell activity. *J. Cereb. Blood Flow Metab.* 26, 613–624. doi: 10.1038/sj.jcbfm.9600272

Duan, L., Zhang, X.-D., Miao, W.-Y., Sun, Y.-J., Xiong, G., Wu, Q., et al. (2018). PDGFRβ cells rapidly relay inflammatory signal from the circulatory system to neurons via chemokine CCL2. *Neuron.* 100, 183–200.e8. doi: 10.1016/j.neuron.2018.08.030

Dudvarski Stankovic, N., Teodorczyk, M., Ploen, R., Zipp, F., and Schmidt, M. H. H. (2016). Microglia-blood vessel interactions: a double-edged sword in brain pathologies. *Acta Neuropathol.* 131, 347–363. doi: 10.1007/s00401-015-1524-y

Durham, J. T., Surks, H. K., Dulmovits, B. M., and Herman, I. M. (2014). Pericyte contractility controls endothelial cell cycle progression and sprouting: insights into angiogenic switch mechanics. *Am. J. Physiol. Cell Physiol.* 307, C878–C892. doi: 10.1152/ajpcell.00185.2014

Eberth, C. G. (1871). *Handbuch der Lehre von der Gewegen des Menschen und der Tiere*, Vol. 1. Leipzig: Engelmann.

Eilken, H. M., Diéguez-Hurtado, R., Schmidt, I., Nakayama, M., Jeong, H.-W., Arf, H., et al. (2017). Pericytes regulate VEGF-induced endothelial sprouting through VEGFR1. *Nat. Commun.* 8:1574. doi: 10.1038/s41467-017-01738-3

El-Bouri, W. K., and Payne, S. J. (2016). A statistical model of the penetrating arterioles and venules in the human cerebral cortex. *Microcirculation* 23, 580–590. doi: 10.1111/micc.12318

Engelhardt, B., Carare, R. O., Bechmann, I., Flugel, A., Laman, J. D., and Weller, R. O. (2016). Vascular, glial, and lymphatic immune gateways of the central nervous system. *Acta Neuropathol.* 132, 317–338. doi: 10.1007/s00401-016-1606-5

Engelhardt, B., Vajkoczy, P., and Weller, R. O. (2017). The movers and shapers in immune privilege of the CNS. *Nat. Immunol.* 18, 123–131. doi: 10.1038/ni.3666

Erdener, Ş. E., and Dalkara, T. (2019). Small vessels are a big problem in neurodegeneration and neuroprotection. *Front. Neurol.* 10:889. doi: 10.3389/fneur.2019.00889

Faal, T., Phan, D., Davtyan, H., Scarfone, V. M., Varady, E., Blurton-Jones, M., et al. (2019). Induction of mesoderm and neural crest-derived pericytes from human pluripotent stem cells to study blood-brain barrier interactions. *Stem Cell Rep.* 12, 451–460. doi: 10.1016/j.stemcr.2019.01.005

Fabriek, B. O., Haastert, E. S., Galea, I., Polfliet, M., Döpp, E. D., Heuvel, M. M., et al. (2005). CD163−positive perivascular macrophages in the human CNS express molecules for antigen recognition and presentation. *Glia* 51, 297–305. doi: 10.1002/glia.20208

Faraco, G., Park, L., Anrather, J., and Iadecola, C. (2017). Brain perivascular macrophages: characterization and functional roles in health and disease. *J. Mol. Med.* 95, 1143–1152. doi: 10.1007/s00109-017-1573-x

Farkas, E., and Luiten, P. G. (2001). Cerebral microvascular pathology in aging and Alzheimer's disease. *Prog. Neurobiol.* 64, 575–611. doi: 10.1016/s0301-0082(00)00068-x

Fernández-Klett, F., Offenhauser, N., Dirnagl, U., Priller, J., and Lindauer, U. (2010). Pericytes in capillaries are contractile in vivo, but arterioles mediate functional hyperemia in the mouse brain. *Proc. Natl. Acad. Sci. U.S.A.* 107, 22290–22295. doi: 10.1073/pnas.1011321108

Fernández-Klett, F., Potas, J. R., Hilpert, D., Blazej, K., Radke, J., Huck, J., et al. (2013). Early loss of pericytes and perivascular stromal cell-induced scar formation after stroke. *J. Cereb. Blood Flow Metab.* 33, 428–439. doi: 10.1038/jcbfm.2012.187

Franco, M., Roswall, P., Cortez, E., Hanahan, D., and Pietras, K. (2011). Pericytes promote endothelial cell survival through induction of autocrine VEGF-A signaling and Bcl-w expression. *Blood* 118, 2906–2917. doi: 10.1182/blood-2011-01-331694

Fu, A. K., Hung, K. W., Yuen, M. Y., Zhou, X., Mak, D. S., Chan, I. C., et al. (2016). IL-33 ameliorates Alzheimer's disease-like pathology and cognitive decline. *Proc. Natl. Acad. Sci. U.S.A.* 113, E2705–E2713. doi: 10.1073/pnas.1604032113

Fullstone, G., Nyberg, S., Tian, X., and Battaglia, G. (2016). From the blood to the central nervous system: a Nanoparticle's journey through the blood-brain barrier by transcytosis. *Int. Rev. Neurobiol.* 130, 41–72. doi: 10.1016/bs.irn.2016.06.001

Gaengel, K., Genové, G., Armulik, A., and Betsholtz, C. (2009). Endothelial-mural cell signaling in vascular development and angiogenesis. *Arterioscler. Thromb. Vasc. Biol.* 29, 630–638. doi: 10.1161/atvbaha.107.161521

Gaudin, A., Yemisci, M., Eroglu, H., Lepetre-Mouelhi, S., Turkoglu, O. F., Donmez-Demir, B., et al. (2014). Squalenoyl adenosine nanoparticles provide neuroprotection after stroke and spinal cord injury. *Nat. Nanotechnol.* 9, 1054–1062. doi: 10.1038/nnano.2014.274

Gautam, J., and Yao, Y. (2018). Roles of pericytes in stroke pathogenesis. *Cell Transplant.* 27, 1798–1808. doi: 10.1177/0963689718768455

Geevarghese, A., and Herman, I. M. (2014). Pericyte-endothelial crosstalk: implications and opportunities for advanced cellular therapies. *Transl. Res.* 163, 296–306. doi: 10.1016/j.trsl.2014.01.011

Geraldes, P., Hiraoka-Yamamoto, J., Matsumoto, M., Clermont, A., Leitges, M., Marette, A., et al. (2009). Activation of PKC-delta and SHP-1 by hyperglycemia causes vascular cell apoptosis and diabetic retinopathy. *Nat. Med.* 15, 1298–1306. doi: 10.1038/nm.2052

Geranmayeh, M., Rahbarghazi, R., and Farhoudi, M. (2019). Targeting pericytes for neurovascular regeneration. *Cell Commun. Signal.* 17:26. doi: 10.1186/s12964-019-0340-8

Ghosh, M., Balbi, M., Hellal, F., Dichgans, M., Lindauer, U., and Plesnila, N. (2015). Pericytes are involved in the pathogenesis of cerebral autosomal dominant arteriopathy with subcortical infarcts and leukoencephalopathy. *Ann. Neurol.* 78, 887–900. doi: 10.1002/ana.24512

Goldmann, T., Wieghofer, P., Jordão, M., Prutek, F., Hagemeyer, N., Frenzel, K., et al. (2016). Origin, fate and dynamics of macrophages at central nervous system interfaces. *Nat. Immunol.* 17, 797–805. doi: 10.1038/ni.3423

Göritz, C., Dias, D. O., Tomilin, N., Barbacid, M., Shupliakov, O., and Frisén, J. (2011). A pericyte origin of spinal cord scar tissue. *Science* 333, 238–242. doi: 10.1126/science.1203165

Gould, I. G., Tsai, P., Kleinfeld, D., and Linninger, A. (2016). The capillary bed offers the largest hemodynamic resistance to the cortical blood supply. *J. Cereb. Blood Flow Metab.* 37, 52–68. doi: 10.1177/0271678X16671146

Grant, R. I., Hartmann, D. A., Underly, R. G., Berthiaume, A.-A., Bhat, N. R., and Shih, A. Y. (2019). Organizational hierarchy and structural diversity of microvascular pericytes in adult mouse cortex. *J. Cereb. Blood Flow Metab.* 39, 411–425. doi: 10.1177/0271678x17732229

Grubb, S., Cai, C., Hald, B. O., Khennouf, L., Murmu, R. P., Jensen, A. G. K., et al. (2020). Precapillary sphincters maintain perfusion in the cerebral cortex. *Nat. Commun.* 11:395. doi: 10.1038/s41467-020-14330-z

Guadagno, E., and Moukhles, H. (2004). Laminin—induced aggregation of the inwardly rectifying potassium channel, Kir4.1, and the water—permeable channel, AQP4, via a dystroglycan—containing complex in astrocytes. *Glia* 47, 138–149. doi: 10.1002/glia.20039

Guijarro-Muñoz, I., Compte, M., Álvarez-Cienfuegos, A., Álvarez-Vallina, L., and Sanz, L. (2014). Lipopolysaccharide activates toll-like receptor 4 (TLR4)-mediated NF-κB signaling pathway and proinflammatoryresponse in human pericytes. *J. Biol. Chem.* 4, 2457–2468.

Guimaraes-Camboa, N., Cattaneo, P., Sun, Y., Moore-Morris, T., Gu, Y., Dalton, N. D., et al. (2017). Pericytes of multiple organs do not behave as mesenchymal stem cells in vivo. *Cell Stem Cell* 20, 345–359.e5. doi: 10.1016/j.stem.2016.12.006

Gursoy-Ozdemir, Y., Yemisci, M., and Dalkara, T. (2012). Microvascular protection is essential for successful neuroprotection in stroke. *J. Neurochem.* 123(Suppl. 2), 2–11. doi: 10.1111/j.1471-4159.2012.07938.x

Gyoneva, S., Davalos, D., Biswas, D., Swanger, S. A., Garnier-Amblard, E., Loth, F., et al. (2014). Systemic inflammation regulates microglial responses to tissue damage in vivo. *Glia* 62, 1345–1360. doi: 10.1002/glia.22686

Hall, C. N., Reynell, C., Gesslein, B., Hamilton, N. B., Mishra, A., Sutherland, B. A., et al. (2014). Capillary pericytes regulate cerebral blood flow in health and disease. *Nature* 508, 55–60. doi: 10.1038/nature13165

Halliday, M. R., Rege, S. V., Ma, Q., Zhao, Z., Miller, C. A., Winkler, E. A., et al. (2016). Accelerated pericyte degeneration and blood–brain barrier breakdown in apolipoprotein E4 carriers with Alzheimer's disease. *J. Cereb. Blood Flow Metab.* 36, 216–227. doi: 10.1038/jcbfm.2015.44

Hamilton, N. B., Attwell, D., and Hall, C. N. (2010). Pericyte-mediated regulation of capillary diameter: a component of neurovascular coupling in health and disease. *Front. Neuroenergetics.* 2:5. doi: 10.3389/fnene.2010.00005

Harnarine-Singh, D., Geddes, G., and Hyde, J. B. (1972). Sizes and numbers of arteries and veins in normal human neopallium. *J. Anat.* 111, 171–179.

Hartmann, D. A., Underly, R. G., Grant, R. I., Watson, A. N., Lindner, V., and Shih, A. Y. (2015). Pericyte structure and distribution in the cerebral cortex revealed by high-resolution imaging of transgenic mice. *Neurophotonics* 2:041402. doi: 10.1117/1.nph.2.4.041402

Hashitani, H., and Lang, R. J. (2016). Spontaneous activity in the microvasculature of visceral organs: role of pericytes and voltage—dependent Ca2+ channels. *J. Physiol.* 594, 555–565. doi: 10.1113/jp271438

Hatterer, E., Davoust, N., Didier-Bazes, M., Vuaillat, C., Malcus, C., Belin, M. F., et al. (2006). How to drain without lymphatics? Dendritic cells migrate from the cerebrospinal fluid to the B-cell follicles of cervical lymph nodes. *Blood* 107, 806–812. doi: 10.1182/blood-2005-01-0154

He, L., Vanlandewijck, M., Raschperger, E., Mäe, M., Jung, B., Lebouvier, T., et al. (2016). Analysis of the brain mural cell transcriptome. *Sci. Rep.* 6:35108. doi: 10.1038/srep35108

He, M., Dong, H., Huang, Y., Lu, S., Zhang, S., Qian, Y., et al. (2016). Astrocyte-derived CCL2 is associated with M1 activation and recruitment of cultured microglial cells. *Cell. Physiol. Biochem.* 38, 859–870. doi: 10.1159/000443040

Hellström, M., Gerhardt, H., Kalén, M., Li, X., Eriksson, U., Wolburg, H., et al. (2001). Lack of pericytes leads to endothelial hyperplasia and abnormal vascular morphogenesis. *J. Cell Biol.* 153, 543–554. doi: 10.1083/jcb.153.3.543

Herland, A., van der Meer, A. D., FitzGerald, E. A., Park, T.-E., Sleeboom, J. J. F., and Ingber, D. E. (2016). Distinct contributions of astrocytes and pericytes to neuroinflammation identified in a 3D human blood-brain barrier on a chip. *PLoS One* 11:e0150360. doi: 10.1371/journal.pone.0150360

Hesp, Z. C., Yoseph, R. Y., Suzuki, R., Jukkola, P., Wilson, C., Nishiyama, A., et al. (2018). Proliferating NG2 cell-dependent angiogenesis and scar formation alter axon growth and functional recovery after spinal cord injury in mice. *J. Neurosci.* 38, 1366–1382. doi: 10.1523/jneurosci.3953-16.2017

Hill, R. A., Tong, L., Yuan, P., Murikinati, S., Gupta, S., and Grutzendler, J. (2015). Regional blood flow in the normal and ischemic brain is controlled by arteriolar smooth muscle cell contractility and not by capillary pericytes. *Neuron* 87, 95–110. doi: 10.1016/j.neuron.2015.06.001

Hladky, S. B., and Barrand, M. A. (2014). Mechanisms of fluid movement into, through and out of the brain: evaluation of the evidence. *Fluids Barriers CNS* 11:26. doi: 10.1186/2045-8118-11-26

Hladky, S. B., and Barrand, M. A. (2019). Is solute movement within the extracellular spaces of brain gray matter brought about primarily by diffusion or flow? A commentary on "Analysis of convective and diffusive transport in the brain interstitium" Fluids and Barriers of the CNS (2019) 16:6 by L. Ray, J.J. Iliff and J.J. Heys. *Fluids Barriers CNS* 16:24. doi: 10.1186/s12987-019-0141-x

Holter, K. E., Kehlet, B., Devor, A., Sejnowski, T. J., Dale, A. M., Omholt, S. W., et al. (2017). Interstitial solute transport in 3D reconstructed neuropil occurs by diffusion rather than bulk flow. *Proc. Natl. Acad. Sci. U.S.A.* 114, 9894–9899. doi: 10.1073/pnas.1706942114

Hughes, S., and Chan-Ling, T. (2004). Characterization of smooth muscle cell and pericyte differentiation in the rat retina in vivo. *Invest. Ophthalmol. Vis. Sci.* 45, 2795–2806. doi: 10.1167/iovs.03-1312

Hunter, J. M., Kwan, J., Malek-Ahmadi, M., Maarouf, C. L., Kokjohn, T. A., Belden, C., et al. (2012). Morphological and pathological evolution of the brain microcirculation in aging and Alzheimer's disease. *PLoS One.* 7:e36893. doi: 10.1371/journal.pone.0036893

Iadecola, C. (2004). Neurovascular regulation in the normal brain and in Alzheimer's disease. *Nat. Rev. Neurosci.* 5, 347–360. doi: 10.1038/nrn1387

Iadecola, C. (2017). The neurovascular unit coming of age: a journey through neurovascular coupling in health and disease. *Neuron* 96, 17–42. doi: 10.1016/j.neuron.2017.07.030

Ihara, M., and Yamamoto, Y. (2016). Emerging evidence for pathogenesis of sporadic cerebral small vessel disease. *Stroke* 47, 554–560. doi: 10.1161/STROKEAHA.115.009627

Iliff, J. J., Wang, M., Liao, Y., Plogg, B. A., Peng, W., Gundersen, G. A., et al. (2012). A paravascular pathway facilitates CSF flow through the brain parenchyma and the clearance of interstitial solutes, including amyloid beta. *Sci. Transl. Med.* 4:147ra111. doi: 10.1126/scitranslmed.3003748

Iris, A., Christian, H., Nikolaos, S., Ajna, B., Truman, R. B., and Yaakov, S. (2007). Multivariate and univariate analysis of continuous arterial spin labeling perfusion MRI in Alzheimer's disease. *J. Cereb. Blood Flow Metab.* 28, 725–736. doi: 10.1038/sj.jcbfm.9600570

Itoh, Y., and Suzuki, N. (2012). Control of brain capillary blood flow. *J. Cereb. Blood Flow Metab.* 32, 1167–1176. doi: 10.1038/jcbfm.2012.5

Iturria-Medina, Y., Sotero, R. C., Toussaint, P. J., Mateos-Perez, J. M., and Evans, A. C. (2016). Early role of vascular dysregulation on late-onset Alzheimer's disease based on multifactorial data-driven analysis. *Nat. Commun.* 7:11934. doi: 10.1038/ncomms11934

Jessen, N., Munk, A., Lundgaard, I., Nedergaard, M., and Nedergaard, N. (2015). The glymphatic system: a beginner's guide. *Neurochem. Res.* 40, 2583–2599. doi: 10.1007/s11064-015-1581-6

Jian, H., Shi-Ting, L., Qi, L., Qing-Gang, P., Fei, G., and Mei-Xiu, D. (2003). Vascular endothelial growth factor expression and angiogenesis induced by chronic cerebral hypoperfusion in rat brain. *Neurosurgery* 53, 963–972. doi: 10.1227/01.neu.0000083594.10117.7a

Jin, B. J., Smith, A. J., and Verkman, A. S. (2016). Spatial model of convective solute transport in brain extracellular space does not support a "glymphatic" mechanism. *J. Gen. Physiol.* 148, 489–501. doi: 10.1085/jgp.201611684

Joyce, E. R. (2005). Matrix metalloproteinases and angiogenesis. *J. Cell. Mol. Med.* 9, 267–285. doi: 10.1111/j.1582-4934.2005.tb00355.x

Khennouf, L., Gesslein, B., Brazhe, A., Octeau, J. C., Kutuzov, N., Khakh, B. S., et al. (2018). Active role of capillary pericytes during stimulation-induced activity and spreading depolarization. *Brain* 141, 2032–2046. doi: 10.1093/brain/awy143

Kida, S., Pantazis, A., and Weller, R. O. (1993). CSF drains directly from the subarachnoid space into nasal lymphatics in the rat. Anatomy, histology and immunological significance. *Neuropathol. Appl. Neurobiol.* 19, 480–488. doi: 10.1111/j.1365-2990.1993.tb00476.x

Kinney, J. W., Bemiller, S. M., Murtishaw, A. S., Leisgang, A. M., Salazar, A. M., and Lamb, B. T. (2018). Inflammation as a central mechanism in Alzheimer's disease. *Alzheimers Dement. Transl. Res. Clin. Interv.* 4, 575–590. doi: 10.1016/j.trci.2018.06.014

Kishida, N., Maki, T., Takagi, Y., Yasuda, K., Kinoshita, H., Ayaki, T., et al. (2019). Role of perivascular oligodendrocyte precursor cells in angiogenesis after brain ischemia. *J. Am. Heart Assoc.* 8:e011824. doi: 10.1161/JAHA.118.011824

Kisler, K., Nelson, A. R., Montagne, A., and Zlokovic, B. V. (2017a). Cerebral blood flow regulation and neurovascular dysfunction in Alzheimer disease. *Nat. Rev. Neurosci.* 18, 419–434. doi: 10.1038/nrn.2017.48

Kisler, K., Nelson, A. R., Rege, S. V., Ramanathan, A., Wang, Y., Ahuja, A., et al. (2017b). Pericyte degeneration leads to neurovascular uncoupling and limits oxygen supply to brain. *Nat. Neurosci.* 20, 406–416. doi: 10.1038/nn.4489

Kisler, K., Nikolakopoulou, A. M., Sweeney, M. D., Lazic, D., Zhao, Z., and Zlokovic, B. V. (2020). Acute ablation of cortical pericytes leads to rapid neurovascular uncoupling. *Front. Cell. Neurosci.* 14:27. doi: 10.3389/fncel.2020.00027

Kitaguchi, H., Ihara, M., Saiki, H., Takahashi, R., and Tomimoto, H. (2007). Capillary beds are decreased in Alzheimer's disease, but not in Binswanger's disease. *Neurosci. Lett.* 417, 128–131. doi: 10.1016/j.neulet.2007.02.021

Kitaguchi, H., Tomimoto, H., Ihara, M., Shibata, M., Uemura, K., Kalaria, R. N., et al. (2009). Chronic cerebral hypoperfusion accelerates amyloid beta deposition in APPSwInd transgenic mice. *Brain Res.* 1294, 202–210. doi: 10.1016/j.brainres.2009.07.078

Kloner, R. A., King, K. S., and Harrington, M. G. (2018). No-reflow phenomenon in the heart and brain. *Am. J. Physiol. Heart Circ. Physiol.* 315, H550–H562. doi: 10.1152/ajpheart.00183.2018

Kokovay, E., Li, L., and Cunningham, L. A. (2006). Angiogenic recruitment of pericytes from bone marrow after stroke. *J. Cereb. Blood Flow Metab.* 26, 545–555. doi: 10.1038/sj.jcbfm.9600214

Kovac, A., Erickson, M. A., and Banks, W. A. (2011). Brain microvascular pericytes are immunoactive in culture: cytokine, chemokine, nitric oxide, and LRP-1 expression in response to lipopolysaccharide. *J. Neuroinflamm.* 8:139. doi: 10.1186/1742-2094-8-139

Krueger, M., and Bechmann, I. (2010). CNS pericytes: concepts, misconceptions, and a way out. *Glia* 58, 1–10. doi: 10.1002/glia.20898

Kuhnert, F., Mancuso, M. R., Shamloo, A., Wang, H. T., Choksi, V., Florek, M., et al. (2010). Essential regulation of CNS angiogenesis by the orphan G protein-coupled receptor GPR124. *Science* 330, 985–989. doi: 10.1126/science.1196554

Kunz, J., Krause, D., Marian, K., and Dermietzel, R. (1994). The 140-kDa protein of blood-brain barrier-associated pericytes is identical to aminopeptidase. *N. J. Neurochem.* 62, 2375–2386. doi: 10.1046/j.1471-4159.1994.62062375.x

Landau, J., and Davis, E. (1957). Capillary thinning and high capillary blood-pressure in hypertension. *Lancet* 269, 1327–1330. doi: 10.1016/s0140-6736(57)91847-0

Lapenna, A., Palma, M., and Lewis, C. E. (2018). Perivascular macrophages in health and disease. *Nat. Rev. Immunol.* 18, 689–702. doi: 10.1038/s41577-018-0056-9

Leijenaar, J. F., van Maurik, I. S., Kuijer, J. P. A., van der Flier, W. M., Scheltens, P., Barkhof, F., et al. (2017). Lower cerebral blood flow in subjects with Alzheimer's dementia, mild cognitive impairment, and subjective cognitive decline using two-dimensional phase-contrast magnetic resonance imaging. *Alzheimers Dement. Transl. Res. Clin. Interv.* 9, 76–83. doi: 10.1016/j.dadm.2017.10.001

Lendahl, U., Nilsson, P., and Betsholtz, C. (2019). Emerging links between cerebrovascular and neurodegenerative diseases-a special role for pericytes. *EMBO Rep.* 20:e48070. doi: 10.15252/embr.201948070

Li, F., Lan, Y., Wang, Y., Wang, J., Yang, G., Meng, F., et al. (2011). Endothelial Smad4 maintains cerebrovascular integrity by activating N-cadherin through cooperation with notch. *Dev. Cell* 20, 291–302. doi: 10.1016/j.devcel.2011.01.011

Lindahl, P., Johansson, B. R., Levéen, P., and Betsholtz, C. (1997). Pericyte loss and microaneurysm formation in PDGF-B-deficient mice. *Science* 277, 242–245. doi: 10.1126/science.277.5323.242

Liu, C., Ge, H.-M., Liu, B.-H., Dong, R., Shan, K., Chen, X., et al. (2019). Targeting pericyte–endothelial cell crosstalk by circular RNA-cPWWP2A inhibition aggravates diabetes-induced microvascular dysfunction. *Proc. Natl. Acad. Sci. U.S.A.* 116, 7455–7464. doi: 10.1073/pnas.1814874116

Liu, H., Zhang, W., Kennard, S., Caldwell, R. B., and Lilly, B. (2010). Notch3 is critical for proper angiogenesis and mural cell investment. *Circ. Res.* 107, 860–870. doi: 10.1161/circresaha.110.218271

Liu, Q., Radwanski, R., Babadjouni, R., Patel, A., Hodis, D. M., Baumbacher, P., et al. (2019). Experimental chronic cerebral hypoperfusion results in decreased pericyte coverage and increased blood–brain barrier permeability in the corpus callosum. *J. Cereb. Blood Flow Metab.* 39, 240–250. doi: 10.1177/0271678x17743670

Liu, S., Agalliu, D., Yu, C., and Fisher, M. (2012). The role of pericytes in blood-brain barrier function and stroke. *Curr. Pharm. Des.* 18, 3653–3662. doi: 10.2174/138161212802002706

Liu, Y., Wada, R., Yamashita, T., Mi, Y., Deng, C. X., Hobson, J. P., et al. (2000). Edg-1, the G protein-coupled receptor for sphingosine-1-phosphate, is essential for vascular maturation. *J. Clin. Invest.* 106, 951–961. doi: 10.1172/jci10905

Louveau, A., Smirnov, I., Keyes, T. J., Eccles, J. D., Rouhani, S. J., Peske, J. D., et al. (2015). Structural and functional features of central nervous system lymphatic vessels. *Nature* 523, 337–341. doi: 10.1038/nature14432

Luissint, A.-C., Artus, C., Glacial, F., Ganeshamoorthy, K., and Couraud, P.-O. (2012). Tight junctions at the blood brain barrier: physiological architecture and disease-associated dysregulation. *Fluids Barriers CNS* 9:23. doi: 10.1186/2045-8118-9-23

Ma, Q., Zhao, Z., Sagare, A. P., Wu, Y., Wang, M., Owens, N., et al. (2018). Blood-brain barrier-associated pericytes internalize and clear aggregated amyloid-β42 by LRP1-dependent apolipoprotein E isoform-specific mechanism. *Mol. Neurodegener.* 13:57. doi: 10.1186/s13024-018-0286-0

Maki, T. (2017). Novel roles of oligodendrocyte precursor cells in the developing and damaged brain. *Clin. Exp. Neuroimmunol.* 8, 33–42. doi: 10.1111/cen3.12358

Maki, T., Choi, Y. K., Miyamoto, N., Shindo, A., Liang, A. C., Ahn, B. J., et al. (2018). A-kinase anchor protein 12 is required for oligodendrocyte differentiation in adult white matter. *Stem Cells* 36, 751–760. doi: 10.1002/stem.2771

Maki, T., Maeda, M., Uemura, M., Lo, E. K., Terasaki, Y., Liang, A. C., et al. (2015). Potential interactions between pericytes and oligodendrocyte precursor cells in perivascular regions of cerebral white matter. *Neurosci. Lett.* 597, 164–169. doi: 10.1016/j.neulet.2015.04.047

Makihara, N., Arimura, K., Ago, T., Tachibana, M., Nishimura, A., Nakamura, K., et al. (2015). Involvement of platelet-derived growth factor receptor β in fibrosis through extracellular matrix protein production after ischemic stroke. *Exp. Neurol.* 264, 127–134. doi: 10.1016/j.expneurol.2014.12.007

Marín-Padilla, M. (2012). The human brain intracerebral microvascular system: development and structure. *Front. Neuroanat.* 6:38. doi: 10.3389/fnana.2012.00038

Mastorakos, P., and McGavern, D. (2019). The anatomy and immunology of vasculature in the central nervous system. *Sci. Immunol.* 4:eaav0492. doi: 10.1126/sciimmunol.aav0492

Matsumoto, J., Dohgu, S., Takata, F., Machida, T., Hatip, F. F., Hatip-Al-Khatib, I., et al. (2018). TNF-α-sensitive brain pericytes activate microglia by releasing IL-6 through cooperation between IκB-NFκB and JAK-STAT3 pathways. *Brain Res.* 1692, 34–44. doi: 10.1016/j.brainres.2018.04.023

Matsumoto, J., Takata, F., Machida, T., Takahashi, H., Soejima, Y., Funakoshi, M., et al. (2014). Tumor necrosis factor-alpha-stimulated brain pericytes possess a unique cytokine and chemokine release profile and enhance microglial activation. *Neurosci. Lett.* 578, 133–138. doi: 10.1016/j.neulet.2014.06.052

Mazza, M., Marano, G., Traversi, G., Bria, P., and Mazza, S. (2011). Primary cerebral blood flow deficiency and Alzheimer's disease: shadows and lights. *J. Alzheimers Dis.* 23, 375–389. doi: 10.3233/jad-2010-090700

McGuire, P. G., Rangasamy, S., Maestas, J., and Das, A. (2011). Pericyte-derived sphingosine 1-phosphate induces the expression of adhesion proteins and modulates the retinal endothelial cell barrier. *Arterioscler. Thromb. Vasc. Biol.* 31, e107–e115. doi: 10.1161/atvbaha.111.235408

Menezes, M. J., McClenahan, F. K., Leiton, C. V., Aranmolate, A., Shan, X., and Colognato, H. (2014). The extracellular matrix protein laminin α2 regulates the maturation and function of the blood–brain barrier. *J. Neurosci.* 34, 15260–15280. doi: 10.1523/jneurosci.3678-13.2014

Miners, J. S., Kehoe, P. G., Love, S., Zetterberg, H., and Blennow, K. (2019). CSF evidence of pericyte damage in Alzheimer's disease is associated with markers of blood-brain barrier dysfunction and disease pathology. *Alzheimers Res. Ther.* 11:81. doi: 10.1186/s13195-019-0534-8

Min-Soo, K., Bo-Ryoung, C., Yong Woo, L., Dong-Hee, K., Ye Sun, H., Won Kyung, J., et al. (2018). Chronic cerebral hypoperfusion induces alterations of matrix metalloproteinase-9 and angiopoietin-2 levels in the rat hippocampus. *Exp. Neurobiol.* 27, 299–308. doi: 10.5607/en.2018.27.4.299

Mishra, A., Reynolds, J. P., Chen, Y., Gourine, A. V., Rusakov, D. A., and Attwell, D. (2016). Astrocytes mediate neurovascular signaling to capillary pericytes but not to arterioles. *Nat. Neurosci.* 19, 1619–1627. doi: 10.1038/nn.4428

Montagne, A., Barnes, S. R., Sweeney, M. D., Halliday, M. R., Sagare, A. P., Zhao, Z., et al. (2015). Blood-brain barrier breakdown in the aging human hippocampus. *Neuron* 85, 296–302. doi: 10.1016/j.neuron.2014.12.032

Montagne, A., Nikolakopoulou, A. M., Zhao, Z., Sagare, A. P., Si, G., Lazic, D., et al. (2018). Pericyte degeneration causes white matter dysfunction in the mouse central nervous system. *Nat. Med.* 24, 326–337. doi: 10.1038/nm.4482

Morris, A. W., Sharp, M. M., Albargothy, N. J., Fernandes, R., Hawkes, C. A., Verma, A., et al. (2016). Vascular basement membranes as pathways for the passage of fluid into and out of the brain. *Acta Neuropathol.* 131, 725–736. doi: 10.1007/s00401-016-1555-z

Muller, W. A. (2002). Leukocyte-endothelial cell interactions in the inflammatory response. *Lab. Invest.* 82, 521–534. doi: 10.1038/labinvest.3780446

Munk, A., Wang, W., Bèchet, N., Eltanahy, A. M., Cheng, A., Sigurdsson, B., et al. (2019). PDGF-B Is required for development of the glymphatic system. *Cell Rep.* 26, 2955–2969.e3. doi: 10.1016/j.celrep.2019.02.050

Murfee, W. L., Skalak, T. C., and Peirce, S. M. (2005). Differential arterial/venous expression of NG2 proteoglycan in perivascular cells along microvessels: identifying a venule−specific phenotype. *Microcirculation* 12, 151–160. doi: 10.1080/10739680590904955

Nakagawa, S., Deli, M. A., Kawaguchi, H., Shimizudani, T., Shimono, T., Kittel, A., et al. (2009). A new blood-brain barrier model using primary rat brain endothelial cells, pericytes and astrocytes. *Neurochem. Int.* 54, 253–263. doi: 10.1016/j.neuint.2008.12.002

Nakagomi, T., Kubo, S., Nakano-Doi, A., Sakuma, R., Lu, S., Narita, A., et al. (2015a). Brain vascular pericytes following ischemia have multipotential stem cell activity to differentiate into neural and vascular lineage cells. *Stem Cells (Dayton, Ohio)* 33, 1962–1974. doi: 10.1002/stem.1977

Nakagomi, T., Nakano-Doi, A., Kawamura, M., and Matsuyama, T. (2015b). Do vascular pericytes contribute to neurovasculogenesis in the central nervous system as multipotent vascular stem cells? *Stem Cells Dev.* 24, 1730–1739. doi: 10.1089/scd.2015.0039

Nation, D. A., Sweeney, M. D., Montagne, A., Sagare, A. P., D'Orazio, L. M., Pachicano, M., et al. (2019). Blood–brain barrier breakdown is an early biomarker of human cognitive dysfunction. *Nat. Med.* 25, 270–276. doi: 10.1038/s41591-018-0297-y

Nehls, V., and Drenckhahn, D. (1991). Heterogeneity of microvascularpericytes for smooth muscle type alpha-actin. *J. Cell Biol.* 113, 147–154.

Nehls, V., and Drenckhahn, D. (1993). The versatility of microvascular pericytes: from mesenchyme to smooth muscle ? *Histochemistry* 99, 1–12.

Neuhaus, A. A., Couch, Y., Sutherland, B. A., and Buchan, A. M. (2017). Novel method to study pericyte contractility and responses to ischaemia in vitro using electrical impedance. *J. Cereb. Blood Flow Metab.* 37, 2013–2024. doi: 10.1177/0271678X16659495

Nikolakopoulou, A. M., Montagne, A., Kisler, K., Dai, Z., Wang, Y., Huuskonen, M. T., et al. (2019). Pericyte loss leads to circulatory failure and pleiotrophin depletion causing neuron loss. *Nat. Neurosci.* 22, 1089–1098. doi: 10.1038/s41593-019-0434-z

Nishimura, A., Ago, T., Kuroda, J., Arimura, K., Tachibana, M., Nakamura, K., et al. (2016). Detrimental role of pericyte Nox4 in the acute phase of brain ischemia. *J. Cereb. Blood Flow Metab.* 36, 1143–1154. doi: 10.1177/0271678X15606456

Nomura, Y., Faegle, R., Hori, D., Al-Qamari, A., Nemeth, J. A., Gottesman, R., et al. (2018). Cerebral small vessel, but not large vessel disease, is associated with impaired cerebral autoregulation during cardiopulmonary bypass. *Anesth. Analg.* 127, 1314–1322. doi: 10.1213/ane.0000000000003384

Nonaka, H., Akima, M., Hatori, T., Nagayama, T., Zhang, Z., and Ihara, F. (2003). The microvasculature of the cerebral white matter: arteries of the subcortical white matter. *J. Neuropathol. Exp. Neurol.* 62, 154–161. doi: 10.1093/jnen/62.2.154

Nortley, R., Korte, N., Izquierdo, P., Hirunpattarasilp, C., Mishra, A., Jaunmuktane, Z., et al. (2019). Amyloid beta oligomers constrict human capillaries in Alzheimer's disease via signaling to pericytes. *Science* 365:eaav9518. doi: 10.1126/science.aav9518

O'Farrell, F. M., Mastitskaya, S., Hammond-Haley, M., Freitas, F., Wah, W. R., and Attwell, D. (2017). Capillary pericytes mediate coronary no-reflow after myocardial ischaemia. *eLife* 6:e29280. doi: 10.7554/elife.29280

Ogura, S., Kurata, K., Hattori, Y., Takase, H., Ishiguro-Oonuma, T., Hwang, Y., et al. (2017). Sustained inflammation after pericyte depletion induces irreversible blood-retina barrier breakdown. *JCI Insight* 2:e90905. doi: 10.1172/jci.insight.90905

Ohtaki, H., Fujimoto, T., Sato, T., Kishimoto, K., Fujimoto, M., Moriya, M., et al. (2006). "Progressive expression of vascular endothelial growth factor (VEGF) and angiogenesis after chronic ischemic hypoperfusion in rat," in *Brain Edema Acta Neurochirurgica Supplementum*, Vol. 96, eds J. T. Hoff, R. F. Keep, and Y. Hua (Vienna: Springer), 283–287. doi: 10.1007/3-211-30714-1_61

Omote, Y., Deguchi, K., Kono, S., Liu, N., Liu, W., Kurata, T., et al. (2014). Neurovascular protection of cilostazol in stroke-prone spontaneous hypertensive rats associated with angiogenesis and pericyte proliferation. *J. Neurosci. Res.* 92, 369–374. doi: 10.1002/jnr.23327

Onodera, O. (2011). What is cerebral small vessel disease? *Rinsho Shinkeigaku* 51, 399–405. doi: 10.5692/clinicalneurol.51.399

Østergaard, L., Engedal, T. S., Moreton, F., Hansen, M. B., Wardlaw, J. M., Dalkara, T., et al. (2016). Cerebral small vessel disease: capillary pathways to stroke and cognitive decline. *J. Cereb. Blood Flow Metab.* 36, 302–325. doi: 10.1177/0271678x15606723

Özen, I., Deierborg, T., Miharada, K., Padel, T., Englund, E., Genové, G., et al. (2014). Brain pericytes acquire a microglial phenotype after stroke. *Acta Neuropathol.* 128, 381–396. doi: 10.1007/s00401-014-1295-x

Paik, J.-H., Skoura, A., Chae, S.-S., Cowan, A. E., Han, D. K., Proia, R. L., et al. (2004). Sphingosine 1-phosphate receptor regulation of N-cadherin mediates vascular stabilization. *Genes Dev.* 18, 2392–2403. doi: 10.1101/gad.1227804

Park, J. H., Hong, J. H., Lee, S. W., Ji, H. D., Jung, J. A., Yoon, K. W., et al. (2019). The effect of chronic cerebral hypoperfusion on the pathology of Alzheimer's disease: a positron emission tomography study in rats. *Sci. Rep.* 9:14102. doi: 10.1038/s41598-019-50681-4

Parkes, I., Chintawar, S., and Cader, Z. M. (2018). Neurovascular dysfunction in dementia – human cellular models and molecular mechanisms. *Clin. Sci.* 132, 399–418. doi: 10.1042/cs20160720

Peppiatt, C. M., Howarth, C., Mobbs, P., and Attwell, D. (2006). Bidirectional control of CNS capillary diameter by pericytes. *Nature* 443, 700–704. doi: 10.1038/nature05193

Pieper, C., Marek, J., Unterberg, M., Schwerdtle, T., and Galla, H.-J. (2014). Brain capillary pericytes contribute to the immune defense in response to cytokines or LPS in vitro. *Brain Res.* 1550, 1–8. doi: 10.1016/j.brainres.2014.01.004

Pieper, C., Pieloch, P., and Galla, H. J. (2013). Pericytes support neutrophil transmigration via interleukin-8 across a porcine co-culture model of the blood-brain barrier. *Brain Res.* 1524, 1–11. doi: 10.1016/j.brainres.2013.05.047

Pollock, H., Jutchings, M., Weller, R. O., and Zhang, E.-T. (1997). Perivascular spaces in the basal ganglia of the human brain: their relationship to lacunes. *J. Anat.* 191, 337–346. doi: 10.1046/j.1469-7580.1997.19130337.x

Pombero, A., Garcia-Lopez, R., and Martinez, S. (2016). Brain mesenchymal stem cells: physiology and pathological implications. *Dev. Growth Differ.* 58, 469–480. doi: 10.1111/dgd.12296

Proebstl, D., Voisin, M.-B., Woodfin, A., Whiteford, J., D'Acquisto, F., Jones, G. E., et al. (2012). Pericytes support neutrophil subendothelial cell crawling and breaching of venular walls in vivo. *J. Exp. Med.* 209, 1219–1234. doi: 10.1084/jem.20111622

Quaegebeur, A., Segura, I., and Carmeliet, P. (2010). Pericytes: blood-brain barrier safeguards against neurodegeneration? *Neuron* 68, 321–323. doi: 10.1016/j.neuron.2010.10.024

Rajani, R. M., Ratelade, J., Domenga-Denier, V., Hase, Y., Kalimo, H., Kalaria, R. N., et al. (2019). Blood brain barrier leakage is not a consistent feature of white matter lesions in CADASIL. *Acta Neuropathol. Commun.* 7:187. doi: 10.1186/s40478-019-0844-x

Rajantie, I., Ilmonen, M., Alminaite, A., Ozerdem, U., Alitalo, K., and Salven, P. (2004). Adult bone marrow-derived cells recruited during angiogenesis comprise precursors for periendothelial vascular mural cells. *Blood* 104, 2084–2086. doi: 10.1182/blood-2004-01-0336

Renner, O., Tsimpas, A., Kostin, S., Valable, S., Petit, E., Schaper, W., et al. (2003). Time- and cell type-specific induction of platelet-derived growth factor receptor-β during cerebral ischemia. *Mol. Brain Res.* 113, 44–51. doi: 10.1016/S0169-328X(03)00085-8

Ribatti, D., Nico, B., and Crivellato, E. (2011). The role of pericytes in angiogenesis. *Int. J. Dev. Biol.* 55, 261–268. doi: 10.1387/ijdb.103167dr

Rouget, C. M. (1873). Memoire sur le developpement, de la structure et les proprietes physiologiques des capillaires sanguins et lympha-tiques. *Arch. Physiol. Norm. Path.* 5, 603–663.

Rudziak, P., Ellis, C. G., and Kowalewska, P. M. (2019). Role and molecular mechanisms of pericytes in regulation of leukocyte diapedesis in inflamed tissues. *Mediat. Inflamm.* 2019, 1–9. doi: 10.1155/2019/4123605

Rungta, R. L., Chaigneau, E., Osmanski, B.-F., and Charpak, S. (2018). Vascular compartmentalization of functional hyperemia from the synapse to the pia. *Neuron.* 99, 362–375.e4. doi: 10.1016/j.neuron.2018.06.012

Rustenhoven, J., Aalderink, M., Scotter, E. L., Oldfield, R. L., Bergin, P. S., Mee, E. W., et al. (2016). TGF-beta1 regulates human brain pericyte inflammatory processes involved in neurovasculature function. *J. Neuroinflamm.* 13:37. doi: 10.1186/s12974-016-0503-0

Rustenhoven, J., Jansson, D., Smyth, L. C., and Dragunow, M. (2017). Brain pericytes as mediators of neuroinflammation. *Trends Pharmacol. Sci.* 38, 291–304. doi: 10.1016/j.tips.2016.12.001

Ryu, J., Petersen, M. A., Murray, S. G., Baeten, K. M., Meyer-Franke, A., Chan, J. P., et al. (2015). Blood coagulation protein fibrinogen promotes autoimmunity and demyelination via chemokine release and antigen presentation. *Nat. Commun.* 6:8164. doi: 10.1038/ncomms9164

Sagare, A. P., Bell, R. D., Zhao, Z., Ma, Q., Winkler, E. A., Ramanathan, A., et al. (2013). Pericyte loss influences Alzheimer-like neurodegeneration in mice. *Nat. Commun.* 4:2932. doi: 10.1038/ncomms3932

Sakuma, R., Kawahara, M., Nakano-Doi, A., Takahashi, A., Tanaka, Y., Narita, A., et al. (2016). Brain pericytes serve as microglia-generating multipotent vascular stem cells following ischemic stroke. *J. Neuroinflamm.* 13:57. doi: 10.1186/s12974-016-0523-9

Salzman, K. L., Osborn, A. G., House, P., Jinkins, J. R., Ditchfield, A., Cooper, J. A., et al. (2005). Giant tumefactive perivascular spaces. *Am. J. Neuroradiol.* 26, 298–305.

Sandison, J. C. (1931). Observations of the circulating blood cells, adventitial (Rouget) cells and muscle cells, endothelium and macrophages in the transparent chamber of the rabbit's ear. *Anat. Rec.* 50, 355–379.

Schultz, N., Byman, E., Fex, M., and Wennström, M. (2017). Amylin alters human brain pericyte viability and NG2 expression. *J. Cereb. Blood Flow Metab.* 37, 1470–1482. doi: 10.1177/0271678x16657093

Sengillo, J. D., Winkler, E. A., Walker, C. T., Sullivan, J. S., Johnson, M., and Zlokovic, B. V. (2013). Deficiency in mural vascular cells coincides with blood–brain barrier disruption in Alzheimer's disease. *Brain Pathol.* 23, 303–310. doi: 10.1111/bpa.12004

Seo, J., Maki, T., Maeda, M., Miyamoto, N., Liang, A. C., Hayakawa, K., et al. (2014). Oligodendrocyte precursor cells support blood-brain barrier integrity via TGF-β signaling. *PLoS One* 9:e103174. doi: 10.1371/journal.pone.0103174

Seo, J., Miyamoto, N., Hayakawa, K., Pham, L.-D. D., Maki, T., Ayata, C., et al. (2013). Oligodendrocyte precursors induce early blood-brain barrier opening after white matter injury. *J. Clin. Invest.* 123, 782–786. doi: 10.1172/jci65863

Shane, P. H., and Didier, Y. R. S. (2011). Molecular control of endothelial cell behaviour during blood vessel morphogenesis. *Nat. Rev. Mol. Cell Biol.* 12, 551–564. doi: 10.1038/nrm3176

Shen, J., Xu, G., Zhu, R., Yuan, J., Ishii, Y., Hamashima, T., et al. (2019). PDGFR-β restores blood-brain barrier functions in a mouse model of focal cerebral ischemia. *J. Cereb. Blood Flow Metab.* 39, 1501–1515. doi: 10.1177/0271678x18769515

Shibata, M., Yamada, S., Kumar, R. S., Calero, M., Bading, J., Frangione, B., et al. (2000). Clearance of Alzheimer's amyloid-β1-40 peptide from brain by LDL receptor–related protein-1 at the blood-brain barrier. *J. Clin. Invest.* 106, 1489–1499. doi: 10.1172/jci10498

Shigemoto-Mogami, Y., Hoshikawa, K., and Sato, K. (2018). Activated microglia disrupt the blood-brain barrier and induce chemokines and cytokines in a rat in vitro model. *Front. Cell Neurosci.* 12:494. doi: 10.3389/fncel.2018.00494

Silva, M., Lange, S., Hinrichsen, B., Philp, A. R., Reyes, C. R., Halabi, D., et al. (2019). Pericytes favor oligodendrocyte fate choice in adult neural stem cells. *Front. Cell. Neurosci.* 13:85. doi: 10.3389/fncel.2019.00085

Simpkins, A. N., Dias, C., Leigh, R., Benson, R. T., Hsia, A. W., Latour, L. L., et al. (2016). Identification of reversible disruption of the human blood–brain barrier following acute ischemia. *Stroke* 47, 2405–2408. doi: 10.1161/strokeaha.116.013805

Smith, A. J., Yao, X., Dix, J. A., Jin, B. J., and Verkman, A. S. (2017). Test of the 'glymphatic' hypothesis demonstrates diffusive and aquaporin-4-independent solute transport in rodent brain parenchyma. *Elife* 6:e27679. doi: 10.7554/eLife.27679

Smyth, L., Rustenhoven, J., Scotter, E. L., Schweder, P., Faull, R., Park, T., et al. (2018). Markers for human brain pericytes and smooth muscle cells. *J. Chem. Neuroanat.* 92, 48–60. doi: 10.1016/j.jchemneu.2018.06.001

Smyth, L. C. D., Rustenhoven, J., Park, T., Schweder, P., Jansson, D., Heppner, P. A., et al. (2018). Unique and shared inflammatory profiles of human brain endothelia and pericytes. *J. Neuroinflamm.* 15:138. doi: 10.1186/s12974-018-1167-8

Song, S., Ewald, A. J., Stallcup, W., Werb, Z., and Bergers, G. (2005). PDGFRβ+ perivascular progenitor cells in tumours regulate pericyte differentiation and vascular survival. *Nat. Cell Biol.* 7, 870–879. doi: 10.1038/ncb1288

Spector, R., Robert Snodgrass, S., and Johanson, C. E. (2015). A balanced view of the cerebrospinal fluid composition and functions: focus on adult humans. *Exp. Neurol.* 273, 57–68. doi: 10.1016/j.expneurol.2015.07.027

Stapor, P. C., Sweat, R. S., Dashti, D. C., Betancourt, A. M., and Murfee, W. (2014). Pericyte dynamics during angiogenesis: new insights from new identities. *J. Vasc. Res.* 51, 163–174. doi: 10.1159/000362276

Stark, K., Eckart, A., Haidari, S., Tirniceriu, A., Lorenz, M., von Brühl, M.-L., et al. (2013). Capillary and arteriolar pericytes attract innate leukocytes exiting through venules and 'instruct' them with pattern-recognition and motility programs. *Nat. Immunol.* 14, 41–51. doi: 10.1038/ni.2477

Staszewski, J., Piusińska-Macoch, R., Brodacki, B., Skrobowska, E., Macek, K., and Stępień, A. (2017). Risk of vascular events in different manifestations of cerebral small vessel disease: a 2-year follow-up study with a control group. *Heliyon* 3:e00455. doi: 10.1016/j.heliyon.2017.e00455

Stebbins, M. J., Gastfriend, B. D., Canfield, S. G., Lee, M.-S., Richards, D., Faubion, M. G., et al. (2019). Human pluripotent stem cell–derived brain pericyte–like cells induce blood-brain barrier properties. *Sci. Adv.* 5:eaau7375. doi: 10.1126/sciadv.aau7375

Sundberg, C., Kowanetz, M., Brown, L. F., Detmar, M., and Dvorak, H. F. (2002). Stable expression of angiopoietin-1 and other markers by cultured pericytes: phenotypic similarities to a subpopulation of cells in maturing vessels during later stages of angiogenesis in vivo. *Lab. Invest.* 82, 387–401. doi: 10.1038/labinvest.3780433

Sweeney, M. D., Ayyadurai, S., and Zlokovic, B. V. (2016). Pericytes of the neurovascular unit'ey functions and signaling pathways. *Nat. Neurosci.* 19, 771–783. doi: 10.1038/nn.4288

Sweeney, M. D., Kisler, K., Montagne, A., Toga, A. W., and Zlokovic, B. V. (2018). The role of brain vasculature in neurodegenerative disorders. *Nat. Neurosci.* 21, 1318–1331. doi: 10.1038/s41593-018-0234-x

Tachibana, M., Yamazaki, Y., Liu, C.-C., Bu, G., and Kanekiyo, T. (2018). Pericyte implantation in the brain enhances cerebral blood flow and reduces amyloid-β pathology in amyloid model mice. *Exp. Neurol.* 300, 13–21. doi: 10.1016/j.expneurol.2017.10.023

Takagi, T., Imai, T., Mishiro, K., Ishisaka, M., Tsujimoto, M., Ito, H., et al. (2017). Cilostazol ameliorates collagenase-induced cerebral hemorrhage by protecting the blood-brain barrier. *J. Cereb. Blood Flow Metab.* 37, 123–139. doi: 10.1177/0271678X15621499

Tallquist, M. D., French, W. J., and Soriano, P. (2003). Additive effects of PDGF receptor beta signaling pathways in vascular smooth muscle cell development. *PLoS Biol.* 1:E52. doi: 10.1371/journal.pbio.0000052

Teichert, M., Milde, L., Holm, A., Stanicek, L., Gengenbacher, N., Savant, S., et al. (2017). Pericyte-expressed Tie2 controls angiogenesis and vessel maturation. *Nat. Commun.* 8:16106. doi: 10.1038/ncomms16106

Theriault, P., ElAli, A., and Rivest, S. (2016). High fat diet exacerbates Alzheimer's disease-related pathology in APPswe/PS1 mice. *Oncotarget* 7, 67808–67827. doi: 10.18632/oncotarget.12179

Thomas, H., Cowin, A. J., and Mills, S. J. (2017). The Importance of pericytes in healing: wounds and other pathologies. *Int. J. Mol. Sci.* 18:1129. doi: 10.3390/ijms18061129

Thurgur, H., and Pinteaux, E. (2019). Microglia in the neurovascular unit: blood-brain barrier-microglia interactions after central nervous system disorders. *Neuroscience* 405, 55–67. doi: 10.1016/j.neuroscience.2018.06.046

Tsai, H.-H., Niu, J., Munji, R., Davalos, D., Chang, J., Zhang, H., et al. (2016). Oligodendrocyte precursors migrate along vasculature in the developing nervous system. *Science* 351, 379–384. doi: 10.1126/science.aad3839

Uemura, M. T., Ihara, M., Maki, T., Nakagomi, T., Kaji, S., Uemura, K., et al. (2018). Pericyte-derived bone morphogenetic protein 4 underlies white matter damage after chronic hypoperfusion. *Brain Pathol.* 28, 521–535. doi: 10.1111/bpa.12523

Ueno, M., Tomimoto, H., Akiguchi, I., Wakita, H., and Sakamoto, H. (2002). Blood–brain barrier disruption in white matter lesions in a rat model of chronic cerebral hypoperfusion. *J. Cereb. Blood Flow Metab.* 22, 97–104. doi: 10.1097/00004647-200201000-00012

Underly, R. G., Levy, M., Hartmann, D. A., Grant, R. I., Watson, A. N., and Shih, A. Y. (2017). Pericytes as inducers of rapid, matrix metalloproteinase-9-dependent capillary damage during ischemia. *J. Neurosci.* 37, 129–140. doi: 10.1523/Jneurosci.2891-16.2016

Ushiwata, I., and Ushiki, T. (1990). Cytoarchitecture of the smooth muscles and pericytes of rat cerebral blood vessels. *J. Neurosurg.* 73, 82–90. doi: 10.3171/jns.1990.73.1.0082

Vanlandewijck, M., He, L., Mäe, M., Andrae, J., Ando, K., Gaudio, F., et al. (2018). A molecular atlas of cell types and zonation in the brain vasculature. *Nature* 554, 475–480. doi: 10.1038/nature25739

Walshe, T. E., Saint-Geniez, M., Maharaj, A. S., Sekiyama, E., Maldonado, A. E., and D'Amore, P. A. (2009). TGF-beta is required for vascular barrier function, endothelial survival and homeostasis of the adult microvasculature. *PLoS One* 4:e5149. doi: 10.1371/journal.pone.0005149

Wan, Y., Jin, H. J., Zhu, Y. Y., Fang, Z., Mao, L., He, Q., et al. (2018). MicroRNA-149-5p regulates blood–brain barrier permeability after transient middle cerebral artery occlusion in rats by targeting S1PR2 of pericytes. *FASEB J.* 32, 3133–3148.

Winkler, E. A., Bell, R. D., and Zlokovic, B. V. (2010). Pericyte-specific expression of PDGF beta receptor in mouse models with normal and deficient PDGF beta receptor signaling. *Mol. Neurodegener.* 5:32. doi: 10.1186/1750-1326-5-32

Winkler, E. A., Bell, R. D., and Zlokovic, B. V. (2011a). Lack of smad or notch leads to a fatal game of brain pericyte hopscotch. *Dev. Cell.* 20, 279–280. doi: 10.1016/j.devcel.2011.03.002

Winkler, E. A., Bell, R. D., and Zlokovic, B. V. (2011b). Central nervous system pericytes in health and disease. *Nat. Neurosci.* 14, 1398–1405. doi: 10.1038/nn.2946

Winkler, E. A., Sagare, A. P., and Zlokovic, B. V. (2014). The pericyte: a forgotten cell type with important implications for Alzheimer's disease? *Brain Pathol.* 24, 371–386. doi: 10.1111/bpa.12152

Winkler, E. A., Sengillo, J. D., Sullivan, J. S., Henkel, J. S., Appel, S. H., and Zlokovic, B. V. (2013). Blood–spinal cord barrier breakdown and pericyte reductions in amyotrophic lateral sclerosis. *Acta Neuropathol.* 125, 111–120. doi: 10.1007/s00401-012-1039-8

Wong, S.-P., Rowley, J. E., Redpath, A. N., Tilman, J. D., Fellous, T. G., and Johnson, J. R. (2015). Pericytes, mesenchymal stem cells and their contributions to tissue repair. *Pharmacol. Ther.* 151, 107–120. doi: 10.1016/j.pharmthera.2015.03.006

Xing, C.-Y., Tarumi, T., Liu, J., Zhang, Y., Turner, M., Riley, J., et al. (2017). Distribution of cardiac output to the brain across the adult lifespan. *J. Cereb. Blood Flow Metab.* 37, 2848–2856. doi: 10.1177/0271678x16676826

Yamada, M., Ihara, M., Okamoto, Y., Maki, T., Washida, K., Kitamura, A., et al. (2011). The influence of chronic cerebral hypoperfusion on cognitive function and amyloid β metabolism in APP overexpressing mice. *PLoS One* 6:e16567. doi: 10.1371/journal.pone.0016567

Yamazaki, Y., and Kanekiyo, T. (2017). Blood-brain barrier dysfunction and the pathogenesis of Alzheimer's disease. *Int. J. Mol. Sci.* 18:1965. doi: 10.3390/ijms18091965

Yanagida, K., Liu, C. H., Faraco, G., Galvani, S., Smith, H. K., Burg, N., et al. (2017). Size-selective opening of the blood-brain barrier by targeting endothelial sphingosine 1-phosphate receptor 1. *Proc. Natl. Acad. Sci. U.S.A.* 114, 4531–4536. doi: 10.1073/pnas.1618659114

Yang, S., Jin, H., Zhu, Y., Wan, Y., Opoku, E., Zhu, L., et al. (2017). Diverse functions and mechanisms of pericytes in ischemic stroke. *Curr. Neuropharmacol.* 15, 892–905. doi: 10.2174/1570159x15666170112170226

Yang, Y., Andersson, P., Hosaka, K., Zhang, Y., Cao, R., Iwamoto, H., et al. (2016). The PDGF-BB-SOX7 axis-modulated IL-33 in pericytes and stromal cells promotes metastasis through tumour-associated macrophages. *Nat. Commun.* 7:11385. doi: 10.1038/ncomms11385

Yao, Y., Chen, Z.-L., Norris, E. H., and Strickland, S. (2014). Astrocytic laminin regulates pericyte differentiation and maintains blood brain barrier integrity. *Nat. Commun.* 5:3413. doi: 10.1038/ncomms4413

Yemisci, M., Gursoy-Ozdemir, Y., Vural, A., Can, A., Topalkara, K., and Dalkara, T. (2009). Pericyte contraction induced by oxidative-nitrative stress impairs capillary reflow despite successful opening of an occluded cerebral artery. *Nat. Med.* 15, 1031–1037. doi: 10.1038/nm.2022

Yokota, K., Kobayakawa, K., Saito, T., Hara, M., Kijima, K., Ohkawa, Y., et al. (2017). Periostin promotes scar formation through the interaction between pericytes and infiltrating monocytes/macrophages after spinal cord injury. *Am. J. Pathol.* 187, 639–653. doi: 10.1016/j.ajpath.2016.11.010

Yuan, H., Khankin, E. V., Karumanchi, A. S., and Parikh, S. M. (2009). Angiopoietin 2 is a partial agonist/antagonist of Tie2 signaling in the endothelium. *Mol. Cell. Biol.* 29, 2011–2022. doi: 10.1128/mcb.01472-08

Zechariah, A., ElAli, A., Doeppner, T. R., Jin, F., Hasan, M. R., Helfrich, I., et al. (2013). Vascular endothelial growth factor promotes pericyte coverage of brain capillaries, improves cerebral blood flow during subsequent focal cerebral ischemia, and preserves the metabolic penumbra. *Stroke* 44, 1690–1697. doi: 10.1161/STROKEAHA.111.000240

Zeisel, A., Hochgerner, H., Lönnerberg, P., Johnsson, A., Memic, F., Zwan, J. V. D., et al. (2018). Molecular architecture of the mouse nervous system. *Cell* 174, 999–1014.e1022. doi: 10.1016/j.cell.2018.06.021

Zenaro, E., Piacentino, G., and Constantin, G. (2017). The blood-brain barrier in Alzheimer's disease. *Neurobiol. Dis.* 107, 41–56. doi: 10.1016/j.nbd.2016.07.007

Zenker, D., Begley, D., Bratzke, H., Rübsamen-Waigmann, H., and von Briesen, H. (2003). Human blood-derived macrophages enhance barrier function of cultured primary bovine and human brain capillary endothelial cells. *J. Physiol.* 551, 1023–1032. doi: 10.1113/jphysiol.2003.045880

Zhang, E.-T., Richards, H. K., Kida, S., and Weller, R. O. (1990). Interrelationships ofthe pia mater and the perivascular (Virchow-Robin) spaces in thehuman cerebrum. *J. Anat.* 170, 111–123.

Zhang, L., Tan, J., Jiang, X., Qian, W., Yang, T., Sun, X., et al. (2017). Neuron-derived CCL2 contributes to microglia activation and neurological decline in hepatic encephalopathy. *Biol. Res.* 50:26. doi: 10.1186/s40659-017-0130-y

Zhao, Z., Nelson, A. R., Betsholtz, C., and Zlokovic, B. V. (2015). Establishment and dysfunction of the blood-brain barrier. *Cell* 163, 1064–1078. doi: 10.1016/j.cell.2015.10.067

Zheng Gang, Z., Li, Z., Quan, J., Ruilan, Z., Kenneth, D., Cecylia, P., et al. (2000). VEGF enhances angiogenesis and promotes blood-brain barrier leakage in the ischemic brain. *J. Clin. Invest.* 106, 829–838. doi: 10.1172/jci9369

Zhou, Y., Peng, Z., Seven, E. S., and Leblanc, R. M. (2018). Crossing the blood-brain barrier with nanoparticles. *J Control. Release* 270, 290–303. doi: 10.1016/j.jconrel.2017.12.015

Zhu, Y., Soderblom, C., Krishnan, V., Ashbaugh, J., Bethea, J. R., and Lee, J. K. (2015). Hematogenous macrophage depletion reduces the fibrotic scar and increases axonal growth after spinal cord injury. *Neurobiol. Dis.* 74, 114–125. doi: 10.1016/j.nbd.2014.10.024

Zimmermann, K. W. (1923). Der feinere bau der blutcapillaren. *Z. Anat. Entwicklungsgesch.* 68, 29–109. doi: 10.1007/bf02593544

Zlokovic, B. V., Deane, R., Sagare, A. P., Bell, R. D., and Winkler, E. A. (2010). Low−density lipoprotein receptor−related protein−1: a serial clearance homeostatic mechanism controlling Alzheimer's amyloid β−peptide elimination from the brain. *J. Neurochem.* 115, 1077–1089. doi: 10.1111/j.1471-4159.2010.07002.x

Zweifach, B. W. (1934). A micro-manipulative study of blood capillaries. *Anat. Rec.* 59, 83–108.

Conflict of Interest: The authors declare that the research was conducted in the absence of any commercial or financial relationships that could be construed as a potential conflict of interest.

frontiers in Aging Neuroscience

ORIGINAL RESEARCH
published: 15 April 2020
doi: 10.3389/fnagi.2020.00082

Hypertension and Pathogenic hAPP Independently Induce White Matter Astrocytosis and Cognitive Impairment in the Rat

*Alexander Levit[1], Sonny Cheng[1], Olivia Hough[1], Qingfan Liu[1], Yuksel Agca[2], Cansu Agca[2], Vladimir Hachinski[3] and Shawn N. Whitehead[1,3]**

[1] Vulnerable Brain Lab, Department of Anatomy and Cell Biology, Schulich School of Medicine & Dentistry, Western University, London, ON, Canada, [2] Department of Veterinary Pathobiology, College of Veterinary Medicine, University of Missouri, Columbia, MO, United States, [3] Department of Clinical Neurological Sciences, University Hospital, Western University, London, ON, Canada

Hypertension is recognized as a risk factor for Alzheimer disease, but the causal link remains undetermined. Although astrocytes and microglia play an important role in maintaining the neurovascular unit, astrocytes and microglia have been understudied in comorbid models of hypertension and Alzheimer disease. In this study, male transgenic Fischer 344 rats (TgAPP21) overexpressing a pathogenic human amyloid precursor protein received 8 weeks of Angiotensin II infusion to increase blood pressure, and the rats were evaluated for astrocytosis, microgliosis, and cognitive function. A linear relationship between astrocytosis and blood pressure was observed in the corpus callosum and cingulum of wildtype rats, with hypertensive wildtype rats matching the elevated baseline astrocytosis seen in normotensive transgenic rats. In contrast, hypertensive transgenic rats did not demonstrate a further increase of astrocytosis, suggesting a deficient response. Angiotensin II infusion did not affect activation of microglia, which were elevated in the white matter and hippocampus of transgenic rats. Angiotensin II infusion did impair both wildtype and transgenic rats' executive functions in the Morris Water Maze. These results present important implications for the interaction between hypertension and pathogenic human amyloid precursor protein expression, as Angiotensin II infusion produced cognitive impairments in both genotypes, but transgenic rats were additionally impaired in developing a normal astrocytic response to elevated blood pressure.

Keywords: hypertension, amyloid, astrocytes, microglia, white matter, cognitive function, transgenic rat

OPEN ACCESS

Edited by:
JoAnne McLaurin, Sunnybrook Research Institute, Canada

Reviewed by:
Eric Thorin, Université de Montréal, Canada
Daniela Carnevale, Sapienza University of Rome, Italy

***Correspondence:**
Shawn N. Whitehead
Shawn.Whitehead@schulich.uwo.ca

Received: *25 November 2019*
Accepted: *10 March 2020*
Published: *15 April 2020*

Citation:
Levit A, Cheng S, Hough O, Liu Q, Agca Y, Agca C, Hachinski V and Whitehead SN (2020) Hypertension and Pathogenic hAPP Independently Induce White Matter Astrocytosis and Cognitive Impairment in the Rat. Front. Aging Neurosci. 12:82. doi: 10.3389/fnagi.2020.00082

INTRODUCTION

Cerebral vascular pathology is commonly observed in autopsy-confirmed cases of Alzheimer's disease (AD) at significantly greater rates than age-matched control cases (Toledo et al., 2013). The relationship between AD and vascular pathology has given rise to the neurovascular hypothesis of AD (Zlokovic, 2005, 2011; Kisler et al., 2017), which proposes that cerebrovascular dysregulation, including the effect of systemic hypertension on the brain, disrupts amyloid and tau protein

homeostasis, leading to neuronal injury and cognitive impairment. At the same time, amyloid- and tau-mediated injury can disrupt neurovascular coupling. Central to this bi-directional hypothesis is the neurovascular unit, maintained in part by astrocytes and microglia. Both of these glial cell types demonstrate important physiological responses to both hypertension and amyloid (Prokop et al., 2013; Dunn and Nelson, 2014; Shen et al., 2015; von Bernhardi et al., 2015; Frost and Li, 2017).

Hypertension is recognized as a leading vascular risk factor for AD (Oveisgharan and Hachinski, 2010; Iadecola, 2014; Livingston et al., 2017) but studies on whether anti-hypertensive therapy can offer cognitive protection have had mixed results (Lithell et al., 2004; Peters et al., 2008; McGuinness et al., 2009; Perrotta et al., 2016). A recent meta-analysis of prospective cohort studies showed a reduced risk of dementia with use of any antihypertensive medication (Ding et al., 2019), suggesting a benefit that was independent of drug class. The recent SPRINT-MIND trial demonstrated a reduced incidence of cognitive impairment in the intensive blood pressure control group when compared to standard treatment group (Williamson et al., 2019), further supporting a direct relationship between neurodegenerative disease and elevated blood pressure.

The importance of hypertension as a risk factor for AD is further supported by the strong link between hypertension and abnormal white matter changes presenting as leukoaraiosis, also known as white matter hyperintensities (van Dijk et al., 2004). Hypertension is the leading risk factor for leukoaraiosis, and in turn, leukoaraiosis is an important predictor for dementias, including AD (Debette and Markus, 2010). These white matter disruptions are associated with disruptions of white matter integrity (O'Sullivan et al., 2004; Altamura et al., 2016) and can cause impairments of executive functions such as working memory and behavioral flexibility (O'Sullivan et al., 2004). These changes are also observed in patients with hypertension (Raz et al., 2003; Vicario et al., 2005; Li et al., 2016). Hypertension disrupts astrocytic polarity (Yamagata et al., 1997; Vitaioli et al., 2004; Tomassoni et al., 2010; Wang et al., 2018), which may be an initiating factor in the development of leukoaraiosis (Huang et al., 2018). Thus, an experimental model that captures the effects of hypertension on white matter astrocytes will be crucial to investigating possible causal relationships between hypertension and AD.

Previous animal models of comorbid hypertension and AD have demonstrated that hypertension does exacerbate amyloidopathies and cognitive impairment (Díaz-Ruiz et al., 2009; Gentile et al., 2009; Carnevale et al., 2012, 2016; Csiszar et al., 2013; Cifuentes et al., 2015), but these studies did not present data on executive function and white matter gliosis. In the present study, we investigated the impact of hypertension on the transgenic Fischer 344 rat (TgAPP21) which overexpresses a pathogenic variant of the human amyloid precursor protein (hAPP; swe/ind mutations) (Agca et al., 2008), focusing on astrocytes, microglia, and executive function. Cerebral amyloid pathology does not occur spontaneously in TgAPP21 but can be induced (Agca et al., 2008; Rosen et al., 2012; Silverberg et al., 2015). Furthermore, TgAPP21 demonstrate a greater vulnerability to cerebrovascular injury than age-matched wildtype controls (Levit et al., 2017). Thus, TgAPP21 are ideal for modeling the roles of hypertension and glial cells in the early pre-plaque stages of AD. For 8 weeks, 8–10 month old male wildtype and transgenic rats were infused with either normal saline (Wt and Tg rats) or Angiotensin II (AngII; Wt-AngII and Tg-AngII rats) to elevate blood pressure and model the effects of hypertension (Crowley et al., 2006; Osborn et al., 2011; Lohmeier, 2012). We expected increased astrocytosis particularly in the white matter regions of Wt-AngII and Tg-AngII, accompanied by executive dysfunction, as both white matter and executive function are particularly vulnerable to hypertension (Raz et al., 2003; Vicario et al., 2005; Li et al., 2016). As both hypertension and high levels of amyloid activate both astrocytes and microglia (Vitaioli et al., 2004; Tomassoni et al., 2010; Prokop et al., 2013; Dunn and Nelson, 2014; Shen et al., 2015; von Bernhardi et al., 2015; Frost and Li, 2017; Wang et al., 2018), we expected the greatest amount of glial activity in the comorbid Tg-AngII rats.

Indeed, after 8 weeks of elevated blood pressure, we found greater astrocyte reactivity in the corpus callosum and cingulum of Wt-AngII rats than in Wt rats. The level of white matter astrocytosis in Wt-AngII rats was similar to Tg rats, which appeared to have an elevated baseline level of reactive astrocytes. However, Tg-AngII rats did not demonstrate a further increase of astrocytosis. AngII infusion did impair both Wt-AngII and Tg-AngII rats in the Morris Water Maze (MWM) adaptation of a delayed match-sample test, a spatial task that also tests working memory and behavioral flexibility. These results present important implications for the interactive effects of hypertension and genetic risk factors for AD, as AngII infusion produced cognitive impairments in both genotypes, but Tg-AngII were additionally impaired in developing a normal astrocytic response to elevated blood pressure.

MATERIALS AND METHODS

Animals

Animal ethics and procedures were approved by the Animal Care Committee at Western University (protocol 2014-016) and are in compliance with Canadian and National Institute of Health Guides for the Care and Use of Laboratory Animals (NIH Publication #80-23). Homozygous TgAPP21 rats were studied to model the effect of increased brain concentrations of pathogenic hAPP (Agca et al., 2008). Twenty-six male wildtype Fischer 344 rats and 29 male TgAPP21 rats were aged to 7.25 months (SD = 0.55 months), weighing an average of 367 g (SD = 38 g), before osmotic pumps were implanted to deliver saline or AngII for 8 weeks. Behavioral testing was performed during the last 2 weeks of saline or AngII infusion.

Blood Pressure Elevation and Measurement

With random allocation, 13 wildtype and 14 TgAPP21 rats were infused with normal saline (Wt, Tg); 13 Wt and 15 TgAPP21 rats were infused with AngII to elevate blood pressure (Wt-AngII, Tg-AngII) (Crowley et al., 2006; Osborn et al., 2011;

Lohmeier, 2012). Osmotic pumps (Alzet, model 2004; Cupertino, CA, United States) were filled with a saline-angiotensin II solution (Sigma Aldrich, A9525; Oakville, ON, Canada) or with normal saline. The angiotensin II solutions were diluted according to lot-specific osmotic pump flow rates and individual rat weight to deliver 10,000 ng/kg/h. The pumps were implanted subcutaneously on the medial dorsum at the level of the scapulae. The pump reservoir allowed for drug or saline delivery for only 4 weeks, so pumps were replaced once to allow delivery for a total of 8 weeks. Volume pressure reading tail cuffs were used to measure arterial tail blood pressure (Kent Scientific, CODA High Throughput) (Kurtz et al., 2005; Feng et al., 2008). In between pump implantation and behavioral tests, blood pressure was measured weekly, so that there were six measurements during the 8 week period of angiotensin II or normal saline infusion.

Morris Water Maze

On the 7th week of osmotic pump infusion of either normal saline or AngII, rats began behavioral testing. In a dimly lit room, a water tank (144 cm diameter) was filled with room temperature water, dyed with black non-toxic acrylic paint, and a target platform (12 cm diameter) was submerged below 3 cm of water. Rats were placed in a fixed start location and had to locate the hidden platform to be removed from the water tank (**Figure 5A**). The rats were given six 90 s learning trials (with 1 h inter-trial rest intervals) to learn the location of the submerged platform, aided by large distal visual cues; this learning schedule was adapted from Roof et al. (2001). Twenty-four hours after the last learning trial, the rats' memory for the platform location was evaluated on a test trial. Rats were also evaluated on a 5-day series of delayed match-sample testing, to test for performance in more challenging spatial shifts (**Figure 5B**; Vorhees and Williams, 2006; Bizon et al., 2009). Each day, during the "sample trial," a new start location and a new platform location was used. The rats are tested on these new spatial parameters 6 h later during the "match trial" and were assessed for improvement in their latency to find the platform. The 6 h delay was used to create a greater working memory challenge (Bizon et al., 2009). This was repeated with new start and platform locations each day over 5 days.

After MWM testing was complete, potentially confounding differences in visual perception or swim speed were evaluated on cued trials, wherein the location of the platform was visibly marked. All swim paths were tracked using ANYmaze tracking software, version 4.70 (Stoelting Company; Wood Dale, IL, United States), with a top-view webcam (C525, Logitech; Newark, CA, United States). The experimenter was not visible to the rats during testing.

Open Field

The day after MWM testing was complete, rat exploratory behavior and anxiety was evaluated in the open field. Rats were placed in a square 45 cm open field with 40 cm black walls and a black floor and permitted to explore freely for 20 min. A top-view webcam was used for behavioral tracking with ANYmaze software, version 4.70 (Stoelting Company; Wood Dale, IL, United States). The experimenter was not visible to the rats during testing.

Immunohistochemistry and Image Processing

Immediately after all behavioral testing was complete, before pump reservoirs were depleted, rats were euthanized, perfused with 200 ml of 0.01 PBS followed by 200 ml of 4% PFA, and brain tissue was collected and stored in 4% PFA for 24 h before transfer to 30% sucrose solution. 30 μm thick coronal sections were prepared from a subset of brains from each group (n = 8–10) using a cryostat (CryoStar NX50, Thermo Fischer Scientific; Ottawa, ON, Canada). DAB-mediated Immunohistochemistry (IHC) of free floating sections was performed with an ABC-HRP kit (Thermo Fischer Scientific #32020; Ottawa, ON, Canada), a 1:1,000 concentration of OX6 primary antibody for MHC-Class II to identify activated microglia (BD Biosciences #554926; Mississauga, ON, Canada) (Wong, 2013), a 1:2,000 concentration of GFAP primary antibody to identify reactive astrocytes (Sigma-Aldrich #G3893; Oakville, ON, Canada) (Sofroniew and Vinters, 2010), and a 1:500 concentration of 4G8 primary antibody for β-amyloid residues 18–23 (BioLegend, San Diego CA, United States) (Baghallab et al., 2018).

Stitched micrographs of slides were prepared using a 10× objective lens on an upright microscope (Nikon Eclipse Ni-E, Nikon DS Fi2 color camera, NIS Elements Imaging; Mississauga, ON, Canada). Anatomical regions of interest (cingulum, corpus callosum, internal capsule, and hippocampus) were captured at coronal sections: Bregma +2.00, +0.00, and -3.00 mm (Paxinos and Watson, 2007). Micrographs were processed and analyzed using ImageJ, version 1.50b; after regions of interest were outlined using the polygon tool, images were converted to 8-bit, processed using the subtract background command, and then thresholded with a fixed grayscale cutoff value of 237. Area coverage by DAB-positive cells (%) was recorded for each region of interest. The corpus callosum and cingulum were analyzed across three coronal planes and an average area coverage was calculated, weighted by cross-sectional area at each plane.

Data Analysis

Two-Way ANOVA and linear regressions were used to evaluate the effects of genotype and AngII infusion using GraphPad Prism 7.0 software (La Jolla, CA). ANCOVA models were used to evaluate the effect of blood pressure as a continuous predictor variable with IBM SPSS version 23 (Armonk, NY, United States). The conservative Sidak's *post hoc* analysis was used to compare outcome measures within genotype and infusate factors.

RESULTS

Blood Pressure Elevation and Measurement

Mean arterial pressure (MAP) increased over the 8 week AngII infusion period (**Figure 1A**). Averaged over the 8 week period, MAP was elevated by AngII infusion [**Figure 1B**; $p < 0.0001$, $F(1,51) = 31.52$; 2-Way ANOVA]. There were no genotype differences in response to AngII infusion and its effects on MAP, DBP, and SBP. *Post hoc* comparisons found a significant

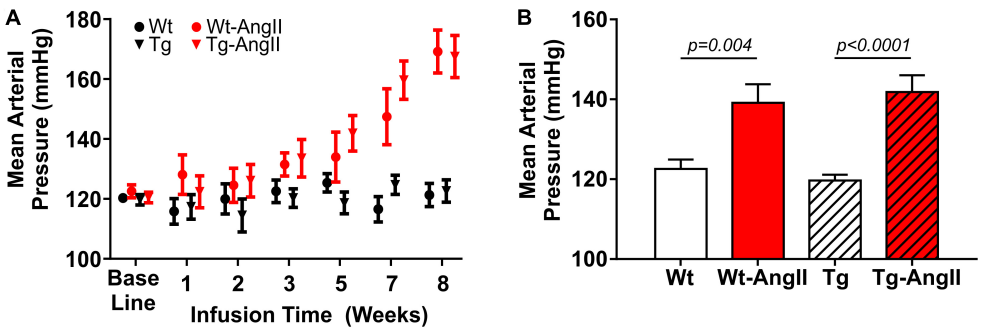

FIGURE 1 | Mean arterial pressure during 8 weeks of normal saline or AngII infusion. **(A)** Baseline blood pressure and a progressively increasing mean arterial pressure over the course of AngII infusion is shown; blood pressure was not measured around the time of osmotic pump reimplantation (week 4). **(B)** Averaged over the 8-week infusion period, AngII infusion had a significant effect on mean arterial pressure. There were no differences in the genotypes' response to AngII. n = 13–15; error bars indicate SEM.

average MAP increase of 17 ± 5 mmHg and 22 ± 6 mmHg in Wt-AngII and Tg-AngII rats, respectively (±SE of difference; Wt-AngII: p = 0.004, t = 3.307, df = 51, Tg-AngII: $p < 0.0001$, t = 4.673, df = 51; Sidak's test). DBP and SBP demonstrated the same pattern of significant changes; DBP respectively increased by 12 ± 5 mmHg and 21 ± 5 mmHg in Wt-AngII and Tg-AngII rats (Wt-AngII: p = 0.04, t = 2.446, df = 51; Tg-AngII: $p < 0.0001$, t = 4.547, df = 51), while SBP respectively increased by 19 ± 5 mmHg and 21 ± 5 mmHg Wt-AngII and Tg-AngII rats (Wt-AngII: p = 0.004, t = 4.039, df = 51; Tg-AngII: $p < 0.0001$, t = 4.604, df = 51; Sidak's test). There were no group differences in baseline blood pressures, measured prior to pump implantation.

Amyloid

Qualitative assessment revealed an absence of β-amyloid deposition in the hippocampal and cortical tissue of all experimental groups (**Figure 2**). This is in keeping with prior studies of naïve TgAPP21 rats and suggests that 8 weeks of blood pressure elevation by AngII infusion does not induce deposition of β-amyloid.

Reactive Astrocytes

Reactive astrocytes were found throughout white matter, cortical, subcortical, and hippocampal regions. However, qualitative observations identified more variable degrees of astrocytosis in major white matter tracts (corpus callosum, cingulum, internal capsule) and the hippocampus, so these regions were selected for closer investigation (**Figure 3**). AngII infusion was found to have a significant effect on astrocyte activity in the corpus callosum and cingulum [**Figure 3B**; corpus callosum: p = 0.05, $F(1,34)$ = 4.265; cingulum: p = 0.03, $F(1,34)$ = 4.973; 2-Way ANOVA]. This was driven by significant differences between Wt and Wt-AngII rats (corpus callosum: p = 0.03, t = 2.537, df = 34; cingulum: p = 0.04, t = 2.426, df = 34; Sidak's test). While area coverage by reactive astrocytes increased in the corpus callosum and cingulum of Wt-AngII rats, Tg rats also had elevated astrocytosis that did not increase further in Tg-AngII rats. Astrocytosis in the corpus callosum and cingulum was linearly correlated with MAP in wildtype rats (**Figure 3C**; R^2 = 0.52, p = 0.0007, df = 18), but not in transgenic rats (**Figure 3D**). Regardless of whether the corpus callosum and cingulum were pooled or analyzed separately, similar significant relationships were identified and the slopes of the regressions between astrocytosis and MAP were significantly different between wildtype and transgenic rats. Moreover, genotype, MAP, and their interaction were found to have significant effects on astrocytosis in the corpus callosum and cingulum in an ANCOVA model with MAP as a continuous predictor [genotype: p = 0.009, $F(1,34)$ = 7.568; MAP: p = 0.03, $F(1,34)$ = 4.893; genotype × MAP: p = 0.02, $F(1,34)$ = 6.407; ANCOVA). The same findings of significance were observed when the corpus callosum and cingulum were analyzed separately. Absolute MAP was found to be more informative than relative increases of MAP (as compared to baseline measurements prior to pump implantation), as relative change in MAP was not a significant predictor of astrocytosis. In Wt rats, blood pressure elevation increased white matter astrocyte reactivity to levels matching Tg and Tg-AngII rats. These findings suggest that white matter astrocyte reactivity was already saturated in Tg rats and could not increase further in response to elevated blood pressure.

In Wt-AngII rats, reactive astrocytes had extensive processes wrapping around blood vessels (**Figure 3A**). In contrast, Tg-AngII rats showed some increase of reactive astrocyte processes wrapping around blood vessels, but not as consistently as Wt-AngII. In comparison to Wt-AngII, astrocytic processes were qualitatively observed to be reduced in Tg-AngII around blood vessels ranging from 4 to 50 μm in diameter. This further supports the interpretation that astrocytes in Tg rats were already reactive at maximum capacity and could not respond to elevated blood pressure in Tg-AngII rats.

Activated Microglia

Activated microglia were found infrequently in Wt and Wt-AngII rats but they did appear consistently in major white matter tracts and the hippocampus of Tg and Tg-AngII rats (**Figure 4A**). Both Tg and Tg-AngII rats demonstrated a significant increase of microglia activation in the corpus callosum, cingulum, internal capsule, and hippocampus (**Figure 4B**; corpus callosum:

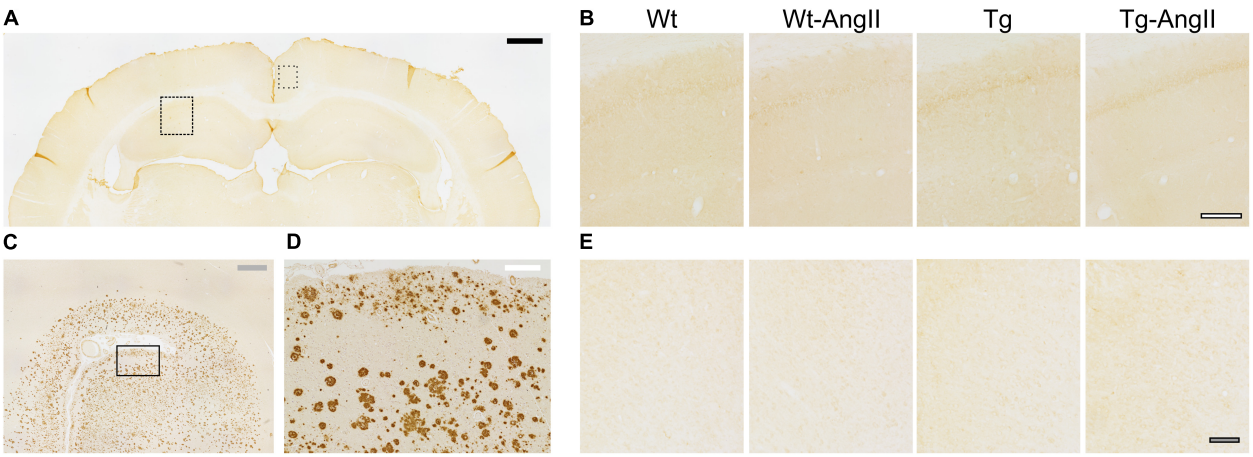

FIGURE 2 | No hippocampal or cortical amyloid deposits observed in wildtype or transgenic rats. **(A)** Representative coronal cross section stained with DAB-mediated IHC with the 4G8 antibody for β-amyloid amino acid residues 17–24. Dashed rectangle indicates area of dorsal hippocampal tissue shown in **(B)** and dotted rectangle indicates area of cortical tissue shown in **(E)**; black bar = 1,000 μm. **(B)** Representative Wt, Wt-AngII, Tg, and Tg-AngII hippocampal tissue stained with 4G8 demonstrated no amyloid deposits; white bar outlined in black = 200 μm. **(C,D)** Representative human autopsy cortical tissue with clinical history of AD was used as a positive control for the 4G8 antibody. Rectangle in **(C)** indicates area of tissue shown in **(D)**; gray and white bars represent 1,000 and 200 μm, respectively. **(E)** Representative Wt, Wt-AngII, Tg, and Tg-AngII cortical tissue stained with 4G8 demonstrated no deposits of amyloid; gray bar in black outline = 100 μm.

$p < 0.0001$, $F(1,33) = 22.02$; cingulum: $p = 0.006$, $F(1,33) = 14.26$; internal capsule: $p = 0.0005$, $F(1,33) = 15.33$; hippocampus: $p = 0.03$, $F(1,33) = 5.248$). Neither AngII infusion nor MAP had any significant relationship with microglia activation in these regions.

Open Field

Exploratory behavior was evaluated by measuring the total distance traveled in the open field test; a subanalysis also evaluated the first 5 min period, which is typically more anxiogenic and also a period of greater exploration (**Figure 5A**). Genotype was a significant factor, with Tg and Tg-AngII rats having demonstrated less exploration [first 5 min: $p = 0.006$, $F(1,51) = 8.342$; full 20 min: $p < 0.0001$, $F(1,51) = 22.39$; 2-Way ANOVA]. AngII infusion did not have an effect on exploratory behavior. Time spent in the center of the field is a proxy measure of anxiety, where increased avoidance of the center is considered to reflect increased levels of anxiety. There were no significant group differences in this measure during either the first 5 min period or the full 20 min test duration (**Figure 5B**). Thus, anxiety is unlikely to have confounded behavioral measures.

Morris Water Maze

No group differences were observed in spatial learning and memory (**Figure 6A**). However, AngII infusion appeared to impair performance on delayed match-sample testing (**Figure 6B**). Every day for 5 days, on the "sample" trial, rats began their swim from a new start location and had to find the new platform location. Swim time improvement was then evaluated on a 6 h delayed "match" trial. Averaged across the five test days, Wt and Tg rats demonstrated significant non-zero swim time improvements on the match trial (Wt: $p = 0.003$, $t = 4.482$, $df = 12$; Tg: $p = 0.03$, $t = 3.082$, $df = 13$; one-sample t-test with Bonferonni correction). In contrast, AngII infusion impaired rats of both genotypes, so that Wt-AngII and Tg-AngII did not demonstrate a significant swim time improvement. The frequently changing spatial parameters of delayed match-sample testing placed greater demands on spatial reference memory, working memory, and behavioral flexibility (Vorhees and Williams, 2006; Bizon et al., 2009). However, no group differences were observed in spatial reference memory (**Figure 6A**), so AngII infusion is more likely to have impaired working memory and/or behavioral flexibility. During cued trials, no differences were observed in swim time to platform nor swim speed, so visual acuity nor mobility were unlikely to have had any confounding effect.

DISCUSSION

Normotensive Tg rats had elevated baseline astrocyte reactivity in the corpus callosum and cingulum, while Tg-AngII rats did not show a further increase of astrocytosis. The increase of reactive astrocytes in Wt-AngII rats was accompanied with extensive astrocytic processes around blood vessels. The reactivity of astrocytes around blood vessels was less consistent and relatively incomplete in Tg-AngII. This suggested that astrocytes in AngII-infused transgenic rats did not develop a normal response to elevated blood pressure. Of note, these changes were observed in the absence of β-amyloid deposition. The role of transgenic hAPP in the insufficient response of TgAPP21 astrocytes is supported by previous findings of amyloid overwhelming astrocytes and inducing senescence in astrocytes (Bhat et al., 2012; Söllvander et al., 2016).

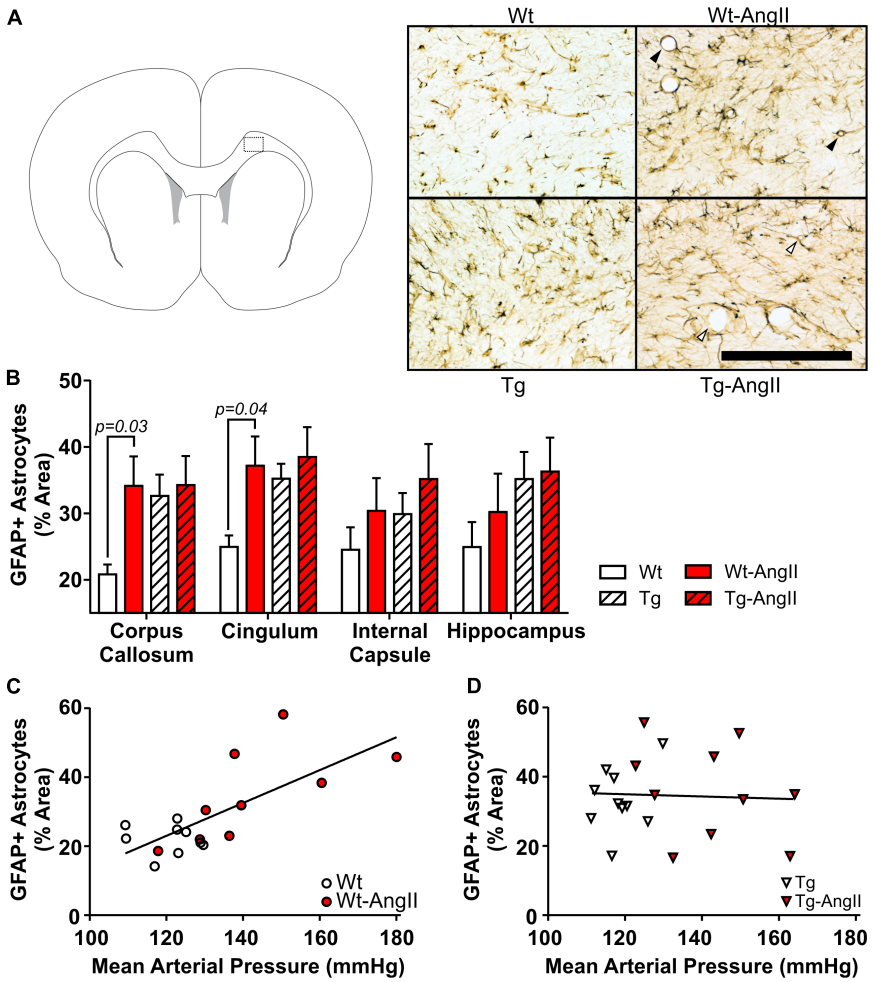

FIGURE 3 | White matter astrocytosis increases linearly with blood pressure elevation in wildtype rats but is elevated in transgenic rats irrespective of blood pressure. Reactive astrocytes were identified using DAB-mediated IHC with a primary antibody for GFAP. **(A)** The schematic shows one of the coronal planes on which the corpus callosum was analyzed (Bregma + 2.0 mm). Representative images of 30 μm thick sections were taken from the dotted outline; black bar = 200 μm. Black triangles identify representative blood vessels associated with extensive astrocyte processes, as commonly observed in Wt-AngII rats; in comparison, white triangles identify representative blood vessels with relatively incomplete astrocyte engagement, as observed in Tg-AngII rats. **(B)** AngII infusion was found to have a significant effect on astrocyte activity in the corpus callosum and cingulum in Wt and Wt-AngII rats only. **(C)** Elevated mean arterial pressure linearly increased astrocytosis in the cingulum and corpus callosum of wildtype rats (R^2 = 0.52, p = 0.0007), **(D)** but not transgenic rats. n = 9–10; error bars indicate SEM.

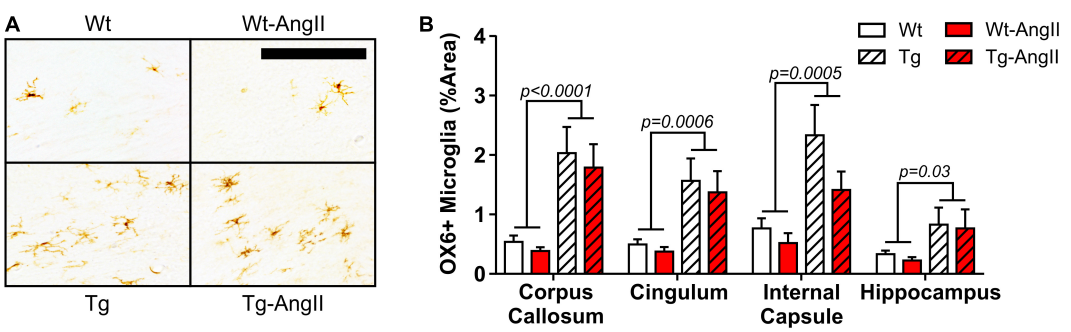

FIGURE 4 | Increased white matter and hippocampal microglia activation in transgenic rats. **(A)** Representative images show activated pro-inflammatory microglia in the corpus callosum and cingulum, identified using DAB mediated IHC with the OX6 primary antibody for MHC Class II. 30 μm thick coronal sections; 200 μm bar. **(B)** Genotype was a significant factor in microglial activation in all regions analyzed. n = 8–10; error bars indicate SEM.

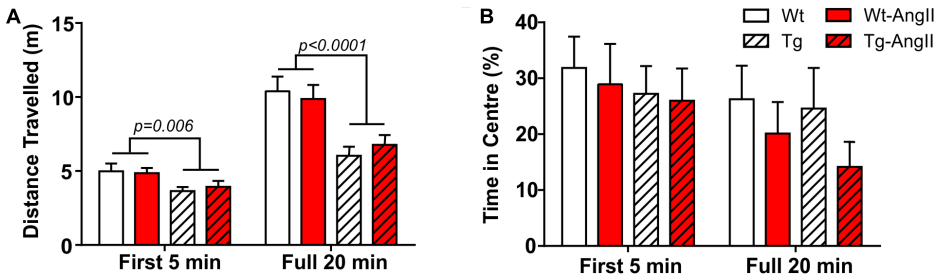

FIGURE 5 | Reduced exploratory behavior in transgenic rats. **(A)** Tg and Tg-AngII traveled significantly less during both the first 5 min period of the test and during the full 20 min test, while AngII had no significant effect on distance traveled. **(B)** No significant group differences were observed in avoidance of the anxiogenic center of the open field. *n* = 13–15; error bars indicate SEM.

AngII infusion impaired both Wt-AngII and Tg-AngII rats in the MWM adaptation of a delayed match-sample test, a spatial task that tests working memory and behavioral flexibility, consistent with the clinical studies on the cognitive effects of hypertension (Raz et al., 2003; Vicario et al., 2005; Li et al., 2016). Previous studies have found histological and cognitive effects of AngII infusion or AngII blockade to be independent of blood pressure, which has been attributed to the central effects of AngII (Tedesco et al., 2002; Iadecola and Gorelick, 2004; Takeda et al., 2009; Capone et al., 2011; Hajjar et al., 2012; Takane et al., 2017), though these studies did not explicitly assess for white matter changes. It remains a possibility that high blood pressure alone, independently of AII, induces astrocytosis in the WM. In support of this interpretation, we found a linear relationship between MAP and astrocytosis in wildtype rats. Altogether, this suggests that there may be distinct benefits of both blood pressure management and central AngII blockade. Our findings contribute to this literature by identifying the prevention of white matter astrocytosis as a potentially important process and a therapeutic target in the management of high blood pressure or AngII blockade.

While AngII infusion did not affect activation of microglia in either genotype, Tg and Tg-AngII rats demonstrated significantly more pro-inflammatory activation of microglia in the corpus callosum, cingulum, internal capsule, and hippocampus, consistent with previous findings (Levit et al., 2019). This further indicates dysregulation in the cerebral tissue of TgAPP21 rats and implicates pro-inflammatory microglia as an important factor in the early pre-plaque stages of AD (Prokop et al., 2013; von Bernhardi et al., 2015). White matter microgliosis has also been identified as an important early factor of neurodegeneration in recent animal and human studies (Raj et al., 2017; Hase et al., 2018).

Future studies to identify specific molecular targets in the astrocyte, such as cytokines and other cell signaling factors, may prove to be crucial to managing the intersection of hypertension and AD-related pathology. As AngII has been shown to have histological and cognitive effects independent of blood pressure, further work with TgAPP21 rat model should consider non-hypertensive doses of AngII, alternate means of inducing blood pressure elevation, and AngII blockade to discern the role of AngII and blood pressure on white matter changes. Future preclinical research on the cerebral and cognitive effects of hypertension should also evaluate for structural white matter damage, including myelin quantification, capillary density, and blood-brain-barrier integrity. Functional white matter changes could be assessed through electrophysiological studies as well as the responsiveness of cerebral blood flow in white matter. Investigating anterograde and retrograde neuronal integrity and density in comorbid animal models would offer additional important insight into mixed AD and vascular dementia.

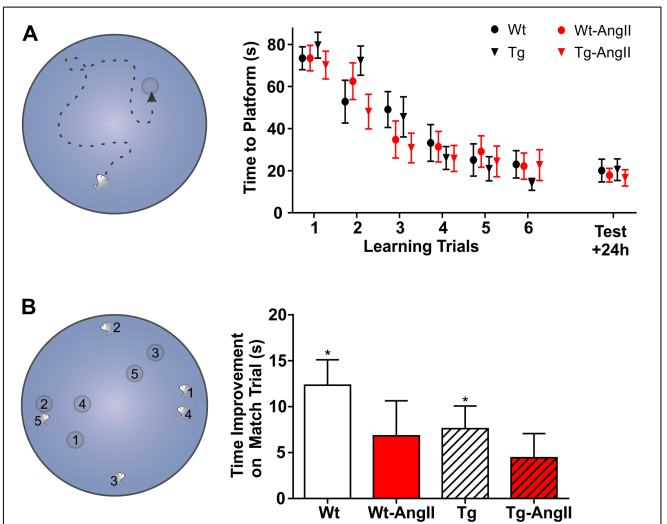

FIGURE 6 | AngII infusion impaired executive functions. **(A)** With a fixed start location, rats were given six trials to learn the platform location; 24 h later, a test trial evaluated spatial memory. No significant group differences were observed on the learning or test trials. **(B)** Every day for 5 days, rats were challenged to learn a new platform location from a new start location. The corresponding number pairs on the MWM schematic indicate the start location and platform location on each day. After the first exposure to a new platform location on a "sample" trial, swim time improvement was measured on a 6 h delayed "match" trial. *Averaged across the five test days, Wt and Tg rats demonstrated a significant swim time improvement on the match trial ($p < 0.03$) but Wt-AngII and Tg-AngII rats did not, suggesting that AngII infusion impaired working memory and/or behavioral flexibility. *n* = 13–15; error bars indicate SEM.

More comprehensive assessment of processing speed as well executive function, including the subdomain of inhibition control, should also be pursued.

In the present study we demonstrate that in rat model of AD that expresses a pathogenic variant of hAPP, white matter perivascular astrocytes do not react to elevated blood pressure in a normal fashion. This captures an important interaction that may present in the comorbid burden of hypertension and AD. The comorbidity of hypertension and pathogenic hAPP expression may have an overwhelming effect on astrocytes, which are central to the maintenance of the neurovascular unit. Regardless of genotype, we found that AngII-infused impaired the working memory and behavioral flexibility of rats with elevated blood pressure; further work will be needed to discern whether this effect was mediated by blood pressure elevation or by the central effects of AngII. Regardless of genotype, we found that AngII-infused impaired the working memory and behavioral flexibility of rats with elevated blood pressure; further work will be needed to discern whether this effect was mediated by blood pressure elevation or by the central effects of AngII. This will inform the ongoing study of the role of hypertension in white matter disease and executive dysfunction. Characterizing the potential dysregulations induced by hypertension and pathogenic hAPP will be crucial to refining ongoing research on the neuroprotective effects of antihypertensive treatment.

DATA AVAILABILITY STATEMENT

The datasets generated for this study are available on request to the corresponding author.

ETHICS STATEMENT

Animal ethics and procedures were approved by the Animal Care Committee at Western University (protocol 2014-016).

AUTHOR CONTRIBUTIONS

AL, VH, and SW made substantial contributions to the conception and design of the work. AL, SC, OH, QL, and SW made substantial contributions in the acquisition and analysis of the data. AL, YA, CA, and SW drafted the manuscript. All authors contributed to manuscript revision, read, and approved the submitted version.

FUNDING

This work was supported in part by research grants from the Natural Sciences and Engineering Research Council of Canada Discovery to SW (418489), the Canadian Consortium on Neurodegeneration in Aging, the Canadian Institutes of Health Research (126127), and the Canadian Foundation for Innovation (34213) to SW.

ACKNOWLEDGMENTS

We would like to thank Dr. Lynn Wang, Andrew Gibson, Murad Ahmad, Stella Iankov, and UWO's Animal Care and Veterinary Services staff for their technical assistance.

REFERENCES

Agca, C., Fritz, J. J., Walker, L. C., Levey, A. I., Chan, A. W. S., Lah, J. J., et al. (2008). Development of transgenic rats producing human β-amyloid precursor protein as a model for Alzheimer's disease: transgene and endogenous APP genes are regulated tissue-specifically. *BMC Neurosci.* 9:28. doi: 10.1186/1471-2202-9-28

Altamura, C., Scrascia, F., Quattrocchi, C. C., Errante, Y., Gangemi, E., Curcio, G., et al. (2016). Regional MRI diffusion, white-matter hyperintensities, and cognitive function in Alzheimer's disease and vascular dementia. *J. Clin. Neurol.* 12, 201–208. doi: 10.3988/jcn.2016.12.2.201

Baghallab, I., Reyes-Ruiz, J. M., Abulnaja, K., Huwait, E., and Glabe, C. (2018). Epitomic characterization of the specificity of the anti-amyloid Aβ monoclonal antibodies 6E10 and 4G8. *J. Alzheimer's Dis.* 66, 1235–1244. doi: 10.3233/JAD-180582

Bhat, R., Crowe, E. P., Bitto, A., Moh, M., Katsetos, C. D., Garcia, F. U., et al. (2012). Astrocyte senescence as a component of Alzheimer's disease. *PLoS ONE* 7:e45069. doi: 10.1371/journal.pone.0045069

Bizon, J. L., LaSarge, C. L., Montgomery, K. S., McDermott, A. N., Setlow, B., and Griffith, W. H. (2009). Spatial reference and working memory across the lifespan of male Fischer 344 rats. *Neurobiol. Aging* 30, 646–655. doi: 10.1016/j.neurobiolaging.2007.08.004

Capone, C., Faraco, G., Park, L., Cao, X., Davisson, R. L., and Iadecola, C. (2011). The cerebrovascular dysfunction induced by slow pressor doses of angiotensin II precedes the development of hypertension. *Am. J. Physiol. – Hear. Circ. Physiol.* 300:H397. doi: 10.1152/ajpheart.00679.2010

Carnevale, D., Mascio, G., D'Andrea, I., Fardella, V., Bell, R. D., Branchi, I., et al. (2012). Hypertension induces brain β-amyloid accumulation, cognitive impairment, and memory deterioration through activation of receptor for advanced glycation end products in brain vasculature. *Hypertension* 60, 188–197. doi: 10.1161/HYPERTENSIONAHA.112.195511

Carnevale, D., Perrotta, M., Lembo, G., and Trimarco, B. (2016). Pathophysiological links among hypertension and Alzheimer's disease. *High Blood Press. Cardiovasc. Prev.* 23, 3–7. doi: 10.1007/s40292-015-0108-1

Cifuentes, D., Poittevin, M., Dere, E., Broquères-You, D., Bonnin, P., Benessiano, J., et al. (2015). Hypertension accelerates the progression of Alzheimer-like pathology in a mouse model of the disease. *Hypertension* 65, 218–224. doi: 10.1161/HYPERTENSIONAHA.114.04139

Crowley, S. D., Gurley, S. B., Herrera, M. J., Ruiz, P., Griffiths, R., Kumar, A. P., et al. (2006). Angiotensin II causes hypertension and cardiac hypertrophy through its receptors in the kidney. *Proc. Natl. Acad. Sci. U.S.A.* 103, 17985–17990. doi: 10.1073/pnas.0605545103

Csiszar, A., Tucsek, Z., Toth, P., Sosnowska, D., Gautam, T., Koller, A., et al. (2013). Synergistic effects of hypertension and aging on cognitive function and hippocampal expression of genes involved in beta-amyloid generation and Alzheimer's disease. *Am. J. Physiol. Hear. Circ. Physiol.* 305, H1120–H1130. doi: 10.1152/ajpheart.00288.2013

Debette, S., and Markus, H. S. (2010). The clinical importance of white matter hyperintensities on brain magnetic resonance imaging: systematic review and meta-analysis. *BMJ* 341:c3666. doi: 10.1136/bmj.c3666

Díaz-Ruiz, C., Wang, J., Ksiezak-Reding, H., Ho, L., Qian, X., Humala, N., et al. (2009). Role of hypertension in aggravating Aβ neuropathology of AD type and tau-mediated motor impairment. *Cardiovasc. Psychiatry Neurol.* 2009, 1–9. doi: 10.1155/2009/107286

Ding, J., Meirelles, O., Launer, L. J., Ma, D.-P., Himali, J. J., Davis-Plourde, L., et al. (2019). Antihypertensive medications and risk for incident dementia and Alzheimer's disease: a meta-analysis of individual participant data from

prospective cohort studies. *Lancet Neurol.* 19, 61–70. doi: 10.1016/S1474-4422(19)30393-X

Dunn, K. M., and Nelson, M. T. (2014). Neurovascular signaling in the brain and the pathological consequences of hypertension. *AJP Hear. Circ. Physiol.* 306, H1–H14. doi: 10.1152/ajpheart.00364.2013

Feng, M., Whitesall, S., Zhang, Y., Beibel, M., D'Alecy, L., and DiPetrillo, K. (2008). Validation of volume-pressure recording tail-cuff blood pressure measurements. *Am. J. Hypertens.* 21, 1288–1291. doi: 10.1038/ajh.2008.301

Frost, G. R., and Li, Y.-M. (2017). The role of astrocytes in amyloid production and Alzheimer's disease. *Open Biol.* 7, 170228. doi: 10.1098/rsob.170228

Gentile, M. T., Poulet, R., Di Pardo, A., Cifelli, G., Maffei, A., Vecchione, C., et al. (2009). β-Amyloid deposition in brain is enhanced in mouse models of arterial hypertension. *Neurobiol. Aging* 30, 222–228. doi: 10.1016/j.neurobiolaging.2007.06.005

Hajjar, I., Brown, L., Mack, W. J., and Chui, H. (2012). Impact of angiotensin receptor blockers on Alzheimer disease neuropathology in a large brain autopsy series. *Arch. Neurol.* 69, 1632–1638. doi: 10.1001/archneurol.2012.1010

Hase, Y., Horsburgh, K., Ihara, M., and Kalaria, R. N. (2018). White matter degeneration in vascular and other ageing-related dementias. *J. Neurochem.* 144, 617–633. doi: 10.1111/jnc.14271

Huang, J., Li, J., Feng, C., Huang, X., Wong, L., Liu, X., et al. (2018). Blood-brain barrier damage as the starting point of leukoaraiosis caused by cerebral chronic hypoperfusion and its involved mechanisms: effect of agrin and aquaporin-4. *Biomed. Res. Int.* 2018, 1–10. doi: 10.1155/2018/2321797

Iadecola, C. (2014). Hypertension and dementia. *Hypertension* 64, 3–5. doi: 10.1161/HYPERTENSIONAHA.114.03040

Iadecola, C., and Gorelick, P. B. (2004). Hypertension, angiotensin, and stroke: beyond blood pressure. *Stroke* 35, 348–350. doi: 10.1161/01.STR.0000115162.16321.AA

Kisler, K., Nelson, A. R., Montagne, A., and Zlokovic, B. V. (2017). Cerebral blood flow regulation and neurovascular dysfunction in Alzheimer disease. *Nat. Rev. Neurosci.* 18, 419–434. doi: 10.1038/nrn.2017.48

Kurtz, T. W. T. W., Griffin, K. A., Bidani, A. K. A. K., Davisson, R. L. R. L., and Hall, J. E. J. E. (2005). Recommendations for blood pressure measurement in humans and experimental animals. Part 2: blood pressure measurement in experimental animals. *Hypertension* 45, 299–310. doi: 10.1161/01.HYP.0000150857.39919.cb

Levit, A., Regis, A. M., Garabon, J. R., Oh, S. H., Desai, S. J., Rajakumar, N., et al. (2017). Behavioural inflexibility in a comorbid rat model of striatal ischemic injury and mutant hAPP overexpression. *Behav. Brain Res.* 333, 267–275. doi: 10.1016/j.bbr.2017.07.006

Levit, A., Regis, A. M., Gibson, A., Hough, O. H., Maheshwari, S., Agca, Y., et al. (2019). Impaired behavioural flexibility related to white matter microgliosis in the TgAPP21 rat model of Alzheimer disease. *Brain. Behav. Immun.* 80, 25–34. doi: 10.1016/j.bbi.2019.02.013

Li, X., Ma, C., Sun, X., Zhang, J., Chen, Y., Chen, K., et al. (2016). Disrupted white matter structure underlies cognitive deficit in hypertensive patients. *Eur. Radiol.* 26, 2899–2907. doi: 10.1007/s00330-015-4116-2

Lithell, H., Hansson, L., Skoog, I., Elmfeldt, D., Hofman, A., Olofsson, B., et al. (2004). The study on COgnition and prognosis in the elderly (SCOPE); outcomes in patients not receiving add-on therapy after randomization. *J. Hypertens.* 22, 1605–1612.

Livingston, G., Sommerlad, A., Orgeta, V., Costafreda, S. G., Huntley, J., Ames, D., et al. (2017). Dementia prevention, intervention, and care. *Lancet* 390, 2673–2734.

Lohmeier, T. E. (2012). Angiotensin II infusion model of hypertension: is there an important sympathetic component? *Hypertension* 59, 539–541. doi: 10.1161/HYPERTENSIONAHA.111.188714

McGuinness, B., Todd, S., Passmore, P., Bullock, R., (2009). Blood pressure lowering in patients without prior cerebrovascular disease for prevention of cognitive impairment and dementia. *Cochrane Database Syst. Rev* 7:*CD*004034. doi: 10.1002/14651858.CD004034.pub3

Osborn, J. W., Fink, G. D., and Kuroki, M. T. (2011). Neural mechanisms of angiotensin II-salt hypertension: implications for therapies targeting neural control of the splanchnic circulation. *Curr. Hypertens. Rep.* 13, 221–228. doi: 10.1007/s11906-011-0188-9

O'Sullivan, M., Morris, R. G., Huckstep, B., Jones, D. K., Williams, S. C. R., and Markus, H. S. (2004). Diffusion tensor MRI correlates with executive dysfunction in patients with ischaemic leukoaraiosis. *J. Neurol. Neurosurg. Psychiatry* 75, 441–447. doi: 10.1136/jnnp.2003.014910.

Oveisgharan, S., and Hachinski, V. (2010). Hypertension, executive dysfunction, and progression to dementia: the Canadian study of health and aging. *Arch. Neurol.* 67, 187–192. doi: 10.1001/archneurol.2009.312.

Paxinos, G., and Watson, C. (2007). *The Rat Brain in Stereotaxic Coordinates*, 6th ed. Amsterdam?: ?Academic Press.

Perrotta, M., Lembo, G., and Carnevale, D. (2016). Hypertension and dementia: epidemiological and experimental evidence revealing a detrimental relationship. *Int. J. Mol. Sci.* 17: 347. doi: 10.3390/ijms17030347

Peters, R., Beckett, N., Forette, F., Tuomilehto, J., Clarke, R., Ritchie, C., et al. (2008). Incident dementia and blood pressure lowering in the hypertension in the very elderly trial cognitive function assessment (HYVET-COG): a double-blind, placebo controlled trial. *Lancet Neurol.* 7, 683–689. doi: 10.1016/s1474-4422(08)70143-1

Prokop, S., Miller, K. R., and Heppner, F. L. (2013). Microglia actions in Alzheimer's disease. *Acta Neuropathol.* 126, 461–77.

Raj, D., Yin, Z., Breur, M., Doorduin, J., Holtman, I. R., Olah, M., et al. (2017). Increased white matter inflammation in aging- and Alzheimer's disease brain. *Front. Mol. Neurosci.* 10:206. doi: 10.3389/fnmol.2017.00206

Raz, N., Rodrigue, K. M., and Acker, J. D. (2003). Hypertension and the brain: vulnerability of the prefrontal regions and executive functions. *Behav. Neurosci.* 117, 1169–1180. doi: 10.1037/0735-7044.117.6.1169

Roof, R. L., Schielke, G. P., Ren, X., and Hall, E. D. (2001). A comparison of long-term functional outcome after 2 middle cerebral artery occlusion models in rats. *Stroke* 32, 2648–2657. doi: 10.1161/hs1101.097397

Rosen, R. F., Fritz, J. J., Dooyema, J., Cintron, A. F., Hamaguchi, T., Lah, J. J., et al. (2012). Exogenous seeding of cerebral beta-amyloid deposition in betaAPP-transgenic rats. *J. Neurochem.* 120, 660–666. doi: 10.1111/j.1471-4159.2011.07551.x

Shen, X. Z., Li, Y., Li, L., Shah, K. H., Bernstein, K. E., Lyden, P., et al. (2015). Microglia participate in neurogenic regulation of hypertension. *Hypertension* 66, 309–316. doi: 10.1161/HYPERTENSIONAHA.115.05333

Silverberg, G. D., Miller, M. C., Pascale, C. L., Caralopoulos, I. N., Agca, Y., Agca, C., et al. (2015). Kaolin-induced chronic hydrocephalus accelerates amyloid deposition and vascular disease in transgenic rats expressing high levels of human APP. *Fluids Barriers CNS* 12:2.

Sofroniew, M. V., and Vinters, H. V. (2010). Astrocytes: biology and pathology. *Acta Neuropathol.* 119, 7–35. doi: 10.1007/s00401-009-0619-8

Söllvander, S., Nikitidou, E., Brolin, R., Söderberg, L., Sehlin, D., Lannfelt, L., et al. (2016). Accumulation of amyloid-β by astrocytes result in enlarged endosomes and microvesicle-induced apoptosis of neurons. *Mol. Neurodegener.* 11:38. doi: 10.1186/s13024-016-0098-z

Takane, K., Hasegawa, Y., Lin, B., Koibuchi, N., Cao, C., Yokoo, T., et al. (2017). Detrimental effects of centrally administered angiotensin II are enhanced in a mouse model of Alzheimer disease independently of blood pressure. *J. Am. Heart Assoc.* 6:e004897. doi: 10.1161/JAHA.116.004897

Takeda, S., Sato, N., Takeuchi, D., Kurinami, H., Shinohara, M., Niisato, K., et al. (2009). Angiotensin receptor blocker prevented β-amyloid-induced cognitive impairment associated with recovery of neurovascular coupling. *Hypertension* 54, 1345–1352. doi: 10.1161/HYPERTENSIONAHA.109.138586

Tedesco, M. A., Ratti, G., Di Salvo, G., and Natale, F. (2002). Does the angiotensin II receptor antagonist losartan improve cognitive function? *Drugs Aging* 19, 723–732. doi: 10.2165/00002512-200219100-00001

Toledo, J. B., Arnold, S. E., Raible, K., Brettschneider, J., Xie, S. X., Grossman, M., et al. (2013). Contribution of cerebrovascular disease in autopsy confirmed neurodegenerative disease cases in the national Alzheimer's coordinating centre. *Brain* 136, 2697–2706. doi: 10.1093/brain/awt188

Tomassoni, D., Bramanti, V., and Amenta, F. (2010). Expression of aquaporins 1 and 4 in the brain of spontaneously hypertensive rats. *Brain Res.* 1325, 155–163. doi: 10.1016/j.brainres.2010.02.023

van Dijk, E. J., Breteler, M. M. B., Schmidt, R., Berger, K., Nilsson, L.-G. G., Oudkerk, M., et al. (2004). The association between blood pressure, hypertension, and cerebral white matter lesions: cardiovascular determinants of dementia study. *Hypertension* 44, 625–630. doi: 10.1161/01.HYP.0000145857.98904.20

Vicario, A., Martinez, C. D., Baretto, D., Diaz Casale, A., and Nicolosi, L. (2005). Hypertension and cognitive decline: impact on executive function. *J. Clin. Hypertens. (Greenwich)* 7, 598–604. doi: 10.1111/j.1524-6175.2005.04498.x

Vitaioli, L., Avola, R., Tomassoni, D., Amenta, F., Di Tullio, M. A., and Sabbatini, M. (2004). Increased expression of glial fibrillary acidic protein in the brain of spontaneously hypertensive rats. *Clin. Exp. Hypertens.* 26, 335–350. doi: 10.1081/ceh-120034138

von Bernhardi, R., Eugenín-von Bernhardi, L., and Eugenín, J. (2015). Microglial cell dysregulation in brain aging and neurodegeneration. *Front. Aging Neurosci.* 7:124. doi: 10.3389/fnagi.2015.00124

Vorhees, C. V., and Williams, M. T. (2006). Morris water maze: procedures for assessing spatial and related forms of learning and memory. *Nat. Protoc.* 1, 848–858. doi: 10.1038/nprot.2006.116

Wang, Y., Zhang, R., Tao, C., Xu, Z., Chen, W., Wang, C., et al. (2018). Blood-brain barrier disruption and perivascular beta-amyloid accumulation in the brain of aged rats with spontaneous hypertension: evaluation with dynamic contrast-enhanced magnetic resonance imaging. *Korean J. Radiol.* 19, 498–507. doi: 10.3348/kjr.2018.19.3.498

Williamson, J. D., Pajewski, N. M., Auchus, A. P., Bryan, R. N., Chelune, G., Cheung, A. K., et al. (2019). Effect of intensive vs standard blood pressure control on probable dementia: a randomized clinical trial. *JAMA – J. Am. Med. Assoc.* 321:553. doi: 10.1001/jama.2018.21442

Wong, W. T. (2013). Microglial aging in the healthy CNS: phenotypes, drivers, and rejuvenation. *Front. Cell. Neurosci.* 7:22. doi: 10.3389/fncel.2013.00022

Yamagata, K., Tagami, M., Nara, Y., Fujino, H., Kuhota, A., Numano, F., et al. (1997). Faculty induction of blood-brain barrier functions by astrocytes isolated from stroke-prone spontaneously hypertensive rats. *Clin. Exp. Pharmacol. Physiol.* 24, 686–691. doi: 10.1111/j.1440-1681.1997.tb02113.x

Zlokovic, B. V. (2005). Neurovascular mechanisms of Alzheimer's neurodegeneration. *Trends Neurosci.* 28, 202–208. doi: 10.1016/j.tins.2005.02.001

Zlokovic, B. V. (2011). Neurovascular pathways to neurodegeneration in Alzheimer's disease and other disorders. *Nat. Rev. Neurosci.* 12, 723–738. doi: 10.1038/nrn3114

Conflict of Interest: The authors declare that the research was conducted in the absence of any commercial or financial relationships that could be construed as a potential conflict of interest.

frontiers in Aging Neuroscience

ORIGINAL RESEARCH
published: 21 April 2020
doi: 10.3389/fnagi.2020.00106

Cilostazol, a Phosphodiesterase 3 Inhibitor, Moderately Attenuates Behaviors Depending on Sex in the Ts65Dn Mouse Model of Down Syndrome

Masahiro Tsuji[1]†, Makiko Ohshima[1], Yumi Yamamoto[1], Satoshi Saito[1,2], Yorito Hattori[2], Emi Tanaka[1], Akihiko Taguchi[3], Masafumi Ihara[2] and Yuko Ogawa[1]*

[1]*Department of Regenerative Medicine and Tissue Engineering, National Cerebral and Cardiovascular Center, Osaka, Japan,* [2]*Department of Neurology, National Cerebral and Cardiovascular Center, Osaka, Japan,* [3]*Department of Regenerative Medicine Research, Institute of Biomedical Research and Innovation, Kobe, Japan*

OPEN ACCESS

Edited by:
Christian J. Pike, University of Southern California, United States

Reviewed by:
Carmen Martínez-Cué, University of Cantabria, Spain
Lydia Gimenez-Llort, Autonomous University of Barcelona, Spain

***Correspondence:**
Masahiro Tsuji
tsujima@kyoto-wu.ac.jp

†Present address:
Masahiro Tsuji, Department of Food and Nutrition, Kyoto Women's University, Kyoto, Japan

Received: *31 January 2020*
Accepted: *30 March 2020*
Published: *21 April 2020*

Citation:
Tsuji M, Ohshima M, Yamamoto Y, Saito S, Hattori Y, Tanaka E, Taguchi A, Ihara M and Ogawa Y (2020) Cilostazol, a Phosphodiesterase 3 Inhibitor, Moderately Attenuates Behaviors Depending on Sex in the Ts65Dn Mouse Model of Down Syndrome. Front. Aging Neurosci. 12:106. doi: 10.3389/fnagi.2020.00106

People with Down syndrome, which is a trisomy of chromosome 21, exhibit intellectual disability from infancy and neuropathology similar to Alzheimer's disease, such as amyloid plaques, from an early age. Recently, we showed that cilostazol, a selective inhibitor of phosphodiesterase (PDE) 3, promotes the clearance of amyloid β and rescues cognitive deficits in a mouse model of Alzheimer's disease. The objective of the present study was to examine whether cilostazol improves behaviors in the most widely used animal model of Down syndrome, i.e., Ts65Dn mice. Mice were supplemented with cilostazol from the fetal period until young adulthood. Supplementation significantly ameliorated novel-object recognition in Ts65Dn females and partially ameliorated sensorimotor function as determined by the rotarod test in Ts65Dn females and hyperactive locomotion in Ts65Dn males. Cilostazol supplementation significantly shortened swimming distance in Ts65Dn males in the Morris water maze test, suggesting that the drug improved cognitive function, although it did not shorten swimming duration, which was due to decreased swimming speed. Thus, this study suggests that early supplementation with cilostazol partially rescues behavioral abnormalities seen in Down syndrome and indicates that the effects are sex-dependent.

Keywords: down syndrome, cilostazol, Ts65Dn mouse, behavior, inhibitor of phosphodiesterase 3

INTRODUCTION

Down syndrome is characterized by a constellation of signs and symptoms caused by the presence of an extra copy of chromosome 21 (trisomy 21), which occurs in approximately 1 in 600 live births worldwide (Moorthie et al., 2018) and nearly 1 in 500 live births in Japan (Kajii, 2008), and is the most frequent cause of intellectual disability. Most adults with Down syndrome are not capable of living fully independently due to the burden of their intellectual impairments. There is currently no drug therapy to improve mental function, and the effects of education are not fully satisfactory. Hence, novel therapies for improvement of intellectual impairments are needed for individuals with Down syndrome, their families, and society.

Although the precise mechanisms underlying the intellectual disability of individuals with Down syndrome are not well understood, neuropathological changes characteristic of Alzheimer's disease is considered to be one of the main contributing factors to neurocognitive impairment. All people with Down syndrome over 35–40 years of age exhibit neuropathology similar to those observed in Alzheimer's disease, including β-amyloid (Aβ) plaques (Zigman and Lott, 2007). This phenomenon is presumably due to the triplication of genes on human chromosome 21 (Wiseman et al., 2018), in which increased levels of the amyloid precursor protein (*APP*) gene seem to play a major role. The accumulation of Aβ plaques appears as young as 8 years old (Leverenz and Raskind, 1998), and fetuses with Down syndrome may present amyloid protein as early as 21 weeks of gestation (Deutsch et al., 2003). Also, individuals with Down syndrome exhibit significant cerebral amyloid angiopathy (Wilcock et al., 2016). We hypothesized that prenatal therapy for neuropathology may alleviate the impairment. Recently, we and other groups showed that a vasoactive drug, cilostazol, which is a selective inhibitor of the cyclic nucleotide phosphodiesterase (PDE) 3, significantly ameliorates cognitive decline in senior citizens (Taguchi et al., 2013; Ihara et al., 2014; Tai et al., 2017). PDEs are crucial modulators of intracellular cyclic adenosine monophosphate (cAMP) and cyclic guanosine monophosphate (cGMP), which are important second messengers in intracellular signal transduction in numerous cell types. Cilostazol inhibits PDE3 activity and increases intracellular cAMP and cGMP (Kambayashi et al., 2003; Heckman et al., 2015). As PDE3 is abundant in vascular smooth muscle cells and platelets, cilostazol has potent vasodilative and antiplatelet effects (Kambayashi et al., 2003). The brain lacks conventional lymphatic vessels to drain interstitial fluid and solutes, i.e., waste products, from the brain parenchyma to cervical lymph nodes. Intramural periarterial drainage (IPAD) is hypothesized to be a major pathway by which waste products, such as Aβ, are drained from the brain (Bakker et al., 2016; Morris et al., 2016; Saito et al., 2019). Theoretical modeling studies suggested that the motive force for IPAD is derived from vascular smooth muscle contractions and biochemical interactions with basement membranes (Diem et al., 2017). We reported cilostazol promoted the IPAD and ameliorated cerebrovascular Aβ pathology by using Tg-SwDI mice, a mouse model of Alzheimer's disease (Maki et al., 2014). The effect of cilostazol on adult patients with mild cognitive impairment is being examined by a phase-II clinical trial (Saito et al., 2016).

The objective of this study was to examine whether cilostazol, a PDE3 inhibitor, improves behavioral function in the Ts65Dn mouse model, which is the most widely used mouse model of Down syndrome (Salehi et al., 2007). Ts65Dn mice have trisomy of a large region of chromosome 16 and the triplication of approximately 55% of the genes present on human chromosome 21 (Davisson et al., 1990). Higher maternal age is known to increase the probability of having offspring with Down syndrome exponentially, and Down syndrome can be diagnosed prenatally. Hence, if Down syndrome is diagnosed, therapies can start as early as before or during the pregnancy of the mother. To obtain the maximum therapeutic effects, dams were fed cilostazol during mating, pregnancy, and lactation periods. Of note, a rat study showed that the concentration of cilostazol in milk is 41–72% of that in the blood (Akiyama et al., 1985). The offspring were then continuously fed the drug. In the present study, we evaluated the effects of cilostazol up to young adulthood, which occurred at 16 weeks of age. In future studies, we plan to reevaluate the effects of continuous treatment in old age, i.e., older than 54 weeks of age, and to explore the mechanisms of action of cilostazol by using brain samples.

MATERIALS AND METHODS

Animals

The animal study was reviewed and approved by the Experimental Animal Care and Use Committee of the National Cerebral and Cardiovascular Center. The females were mated with diploid (2N) males. First, one-third of the mice in this study were bred by crossing Ts65Dn (B6EiC3Sn a/A-Ts (17 < 16 >) 65Dn/J) females and C57BL/6JEi × C3H/HeSnJ (B6EiC3Sn) F1 hybrid males, both of which were purchased from The Jackson Laboratory (Bar Harbor, ME, USA). As C3H/HeSnJ mice carry the retinal degeneration mutation *pde6b*^{rd1}, mice were screened by polymerase chain reaction (PCR) for the mutation, and animals homozygous for the mutation were excluded from this study. The last two-thirds of the mice in this study were bred by crossing mice with virtually identical genetic backgrounds without the *pde6b*^{rd1} mutation: B6EiC3Sn. BLiA a/A-Ts65Dn females and B6EiC3Sn. BLiA F1 males (Costa et al., 2010). A total of 164 pups were bred, excluding mice that died before genotyping, mice with retinal degeneration, and mice used for breeding. Mice were genotyped for genes in the trisomic segment: either trisomy (Ts65Dn) or disomy (2N) using the previously reported method with quantitative real-time PCR (Liu et al., 2003). Disomy littermates (2N) were used as control animals. Mice were housed in a conventional cage (40 cm × 25 cm × 20 cm) with same-sex littermates (three animals per cage) in a room with a 12-h light/dark cycle (lights on at 7 a.m.; room temperature 24°C, humidity 42%). All analyses were performed by investigators who were blinded to the experimental group.

Cilostazol (Phosphodiesterase 3 Inhibitor) Administration

Female breeding-stock Ts65Dn mice for the cilostazol-treated group were fed a 0.3% cilostazol-containing diet during the whole pregnancy and lactation period (**Figure 1**). The offspring were also fed a 0.3% cilostazol-containing diet for the entire study period. The serum concentration (Cmax) of cilostazol in human patients taking a regular medication dose is achieved in mice when mice are fed a 0.3% cilostazol-containing diet (communication from Otsuka Pharmaceutical Co., Limited). Our previous report demonstrated that 0.3% of cilostazol-treated mice showed beneficial effects on vascular function and behaviors (Maki et al., 2014). For the control group, female breeding-stock Ts65Dn mice were fed a regular diet (MF diet, Oriental Yeast Co. Limited, Tokyo, Japan) during the whole

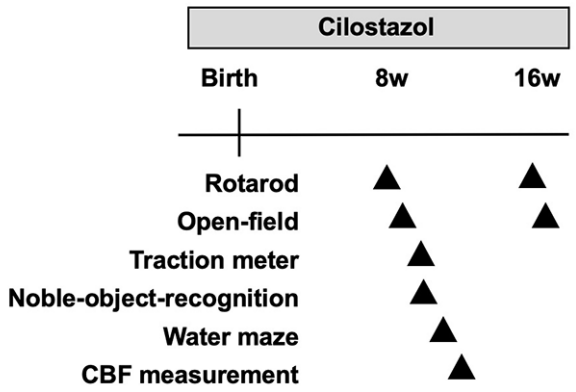

FIGURE 1 | Experimental schedule. CBF, cerebral blood flow; w, weeks.

pregnancy and lactation period. The offspring were also fed the same regular diet for the entire study period. Mice in both groups were given access to food and water *ad libitum*.

Behavioral Assessment

We performed a battery of behavioral tests starting at 8 weeks of age, which is considered young adulthood in mice after the pubertal and adolescent periods (**Figure 1**). The primary goal of this study was to assess cognitive function. Therefore, the Morris water maze test was used to evaluate learning and memory function as the crucial test in the battery of behavioral tests. As the water maze test causes great stress in mice, it was scheduled at the end of the battery at 11 weeks of age. The novel-object-recognition test was also an important test to evaluate learning and memory function and was scheduled a week before the water maze test at 10 weeks of age. In many animal studies, the open-field test is performed first among a battery of behavioral tests to assess general behavior so that the results are not influenced by other experiences. We, however, performed the rotarod test before the open-field test, as we thought that the rotarod test allowed mice to become familiar with the examiners and reduced stress. Hence, we performed it at 9 weeks of age before the novel-object-recognition test and water maze test and after the rotarod test. As individuals with Down syndrome present low-performance levels in motor activities and coordination as well as hypotonia, we assessed such performance levels in the rotarod test and traction meter test. Of note, each behavioral test was performed by a single examiner to avoid the influence of multiple examiners. Hence, some trials for some animals were not performed when the designated examiner was not available. This policy resulted in different sample sizes for each trial. All behavioral assessments were performed between 9 a.m. and 5 p.m.

Rotarod Test

Sensorimotor skills were evaluated in the rotarod test at 8 weeks and 16 weeks of age as described previously (Tsuji et al., 2013). The rotarod drum accelerated from 4 to 40 rpm over 5 min (Muromachi Kikai Co., Limited, Tokyo, Japan). The time until the mouse fell off the rotating drum was recorded. The average time to fall off the drum for five consecutive trials was used for statistical analyses.

Open-Field Test

Spontaneous activity was evaluated in the open-field test at 9 and 17 weeks of age as described previously (Tsuji et al., 2013). Animals were allowed to move freely in a box (30 cm × 30 cm × 30 cm) for 30 min in a light environment and the subsequent 30 min in a dark environment (Taiyo Electric Co., Limited, Osaka, Japan). Infrared beams were mounted horizontally and vertically at specific intervals on the X-, Y-, and Z-banks of the open field, and the total number of beam crossings by the animal was counted. The horizontal crossing was scored as "locomotion," and the vertical crossing was scored as "rearing." Of note, the box we used for the open-field test was smaller than conventional boxes, and the apparatus we used did not assess anxiety-like behavior.

Traction Meter

The muscle strength of the limbs was assessed by a traction meter with steel grids (Brain Science Idea, Co., Limited, Osaka, Japan) at 10 weeks of age as described previously with minor modifications (Ohshima et al., 2016). The four limbs of each mouse were placed on the steel grid of the apparatus, and an experimenter slowly pulled the tail backward and parallel to the surface of the grid at a constant speed. Five successful strength measurements were recorded, and the average peak strength was analyzed using BS-TM-SOF software (Brain Science Idea Co., Limited).

Novel-Object-Recognition Test

To evaluate learning and memory function, the novel-object-recognition test was performed at 10 weeks of age as described previously (Contestabile et al., 2013) with minor modifications (**Figure 1**). On the first day, a mouse was placed in a black acrylic chamber (40 cm × 55 cm) for 15 min with two identical objects. Twenty-four hours later, the mouse was placed in the same chamber for 15 min, but one of the two objects (the object on the right side) was replaced with a novel object. The exploratory behavior, i.e., the contact time with each object, was recorded using video analysis systems (EthoVision XT5; Noldus, Wageningen, Netherlands). Memory was measured as the proportion of time the animal spent exploring the novel object vs. the familiar object; the discriminatory index was calculated as follows: [right object (novel object on the second day) exploration time − left object (familiar object on the second day) exploration time]/total exploration time × 100%. The changes from the first day to the second day were analyzed.

Morris Water Maze Test

To evaluate learning and memory function, the Morris water maze test was performed at 11 weeks of age as previously described with some modifications (Tsuji et al., 2010; Hattori et al., 2014). A circular swimming pool (diameter, 120 cm; depth, 40 cm) was placed in a test room and filled with opaque white water. The swimming pool was filled with water 3 days before the trial to allow the water temperature to reach the same

TABLE 1 | The numbers of animals used in each group.

	Male				Female			
	2N		Ts65Dn		2N		Ts65Dn	
	Regular	Cilostazol	Regular	Cilostazol	Regular	Cilostazol	Regular	Cilostazol
survived	33	25	13	14	25	25	14	10
died	3	1	0	0	0	0	0	1

2N, diploid mice; Ts65Dn, trisomy mice.

temperature as the room temperature, which was kept at 24°C throughout the year. A circular platform (diameter, 8 cm) was submerged 1 cm below the water surface in the center of one quadrant of the pool. The pool was surrounded by several cues that were external to the maze and were visible from within the pool so that the mice could use the cues for spatial orientation. We performed four trials per day with a 15-min interval between attempts for five consecutive days. The mice were randomly placed into one quadrant of the water other than the one with the hidden platform. Each mouse was allowed to swim for 90 s to discover the hidden platform and climb onto it. The trial was terminated after the mouse climbed onto the platform or after 90 s had elapsed. Mice that failed to find the platform was placed on it for 10 s, which was the same length of time the successful animals were allowed to stay on the platform. Swimming duration, swimming distance required to reach the platform and the mean swimming speed were recorded using video analysis systems (EthoVision XT5).

Cerebral Blood Flow Measurements

The cortical surface cerebral blood flow (CBF) was measured by a laser speckle flowmetry imaging system (Omegazone, Omegawave Inc., Tokyo, Japan) at 12 weeks of age as described previously (Ohshima et al., 2012). We measured the CBF in regions perfused by the middle cerebral artery through the intact skull with an open scalp. Five consecutive raw speckle images were acquired every second. The average CBF data of the five images in the left and right hemispheres were used for analysis.

Statistics

All analyses were performed on males and females separately. At the beginning of the analyses in each test, we examined the difference between the 2N mice fed a regular diet and the Ts65Dn mice fed a regular diet; then, we examined the differences among the four groups. The mortality rate of the animals was analyzed using Fisher's exact test. The results of repeated evaluations for temporal changes in body weight, the rotarod test, water maze test, and open-field test were assessed using two-way repeated-measures analysis of variance (ANOVA) followed by the Bonferroni test. The averaged data from all trials during the 5-day experimental period for the water maze test, the averaged data for the 60 min experimental period in the open-field tests, and the data from the rotarod test for each age were then analyzed using two-way ANOVA. The results of the novel-object-recognition test and traction meter test were also assessed using two-way ANOVA followed by the Bonferroni test. Differences were considered significant at $P < 0.05$. The results are expressed as the mean ± the standard error of the mean (SEM). Differences are shown in figures only when there were significant differences between: (1) 2N mice fed a regular diet and Ts65Dn mice fed a regular diet; (2) 2N mice fed a regular diet and 2N mice fed cilostazol; (3) Ts65Dn mice fed a regular diet and Ts65Dn mice fed cilostazol; and (4) 2N mice fed a regular diet and Ts65Dn mice fed cilostazol.

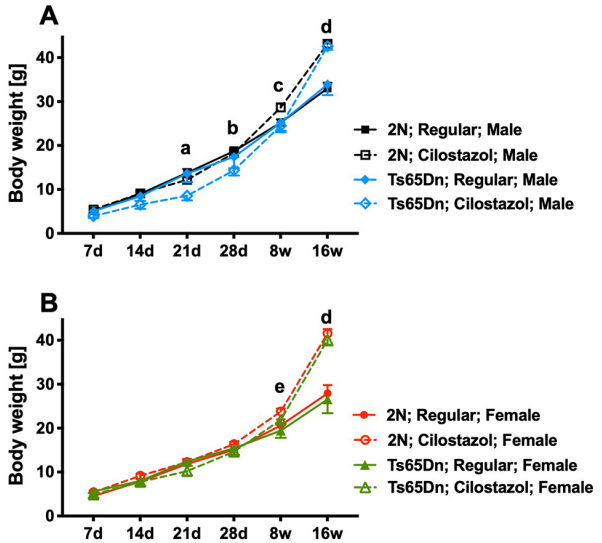

FIGURE 2 | Body weights. Temporal changes in body weights from 7 days of age to 16 weeks of age in males **(A)** and females **(B)**. Letters indicate significant differences in body weights between groups by *post hoc* tests of two-way repeated-measures analysis of variance (ANOVA). **(a)** Ts65Dn-Cilostazol vs. Ts65Dn- and 2N-Regular diet, **(b)** Ts65Dn-Cilostazol vs. 2N-Regular diet, **(c)** 2N-Cilostazol vs. 2N-Regular diet, **(d)** 2N-Cilostazol vs. 2N-Regular diet, Ts65Dn-Cilostazol vs. Ts65Dn- and 2N-Regular diet, **(e)** 2N-Cilostazol vs. 2N- and Ts65Dn-Regular diet groups. In male groups: 2N-Regular (n = 15), 2N-Cilostazol (n = 22), Ts65Dn-Regular (n = 6), Ts65Dn-Cilostazol (n = 10). In female groups: 2N-Regular (n = 22), 2N-Cilostazol (n = 17), Ts65Dn-Regular (n = 7), Ts65Dn-Cilostazol (n = 9). Mean ± SEM. 2N; diploid mice, Ts65Dn; trisomy mice.

RESULTS

Mortality and Body Weight

A total of 164 pups were prepared for this study. Five animals died before 17 weeks of age, which was the endpoint of this study. Mortality rates before 17 weeks of age did not differ among the four groups in each sex: 2N mice fed a regular diet, 2N mice fed a cilostazol-supplemented diet, Ts65Dn mice fed a regular diet, and Ts65Dn mice fed a cilostazol-supplemented diet (**Table 1**).

Ts65Dn mice had similar weights to 2N mice in both sexes throughout the observation period, from 7 days of age to 16 weeks of age, when fed a regular diet (**Figures 2A,B**). Ts65Dn

males fed cilostazol weighed significantly less than Ts65Dn males fed a regular diet at 21 days and 28 days of age (males, $F_{(3,51)} = 3.006$, $p = 0.0387$; **Figure 2A**). This bodyweight reduction by cilostazol supplementation was not observed in the other groups (2N males and females and Ts65Dn females). In contrast, upon aging, mice of all groups fed cilostazol, regardless of chromosome type and sex, became significantly heavier than the counterpart mice fed a regular diet (females, $F_{(3,49)} = 6.171$, $p = 0.0012$; **Figure 2B**). This weight increase caused by cilostazol was observed at 8 weeks of age (the human equivalent of adolescence) and later in all groups.

Recognition Memory

We evaluated recognition memory by the novel-object-recognition test at 10 weeks of age. The recognition and preference of a novel object over a familiar object was analyzed. In females, when fed a regular diet, 2N mice recognized and preferred the novel object, whereas Ts65Dn mice preferred the familiar object ($F_{(1,35)} = 5.635$, $p = 0.0232$; **Figure 3B**). Cilostazol supplementation reversed the abnormal preference of Ts65Dn females, i.e., Ts65Dn females fed cilostazol recognized and preferred the novel object, similar to 2N females ($F_{(1,35)} = 0.933$, *post hoc* $p = 0.0475$). In males, when fed a regular diet, 2N mice did not exhibit a preference for the novel object, i.e., mice spent almost equal amounts of time contacting the novel and familiar objects. Ts65Dn males tended to prefer the familiar object, but there was no significant difference compared with 2N males (**Figure 3A**). Cilostazol supplementation did not alter the recognition and preference in either Ts65Dn males or 2N males.

Spatial Learning and Memory

We examined spatial learning and memory by the Morris water maze test at 11 weeks of age. The swimming duration and the distance required to reach the platform became shorter each day, indicating that the mice learned to find the hidden platform more quickly (**Figures 4A,C,G,I**). Among males fed with a regular diet, as seen after we averaged the data from all trials during the 5-day experimental period, the duration and distance when finding the platform were significantly longer for Ts65Dn mice than 2N mice ($F_{(1,49)} = 3.701$, $p = 0.0406$; **Figures 4B,D**). The swimming speed did not differ between the two groups (**Figure 4F**). Cilostazol supplementation consistently decreased the swimming speed regardless of the chromosomal type and sex (males, $F_{(1,49)} = 6.093$, $p = 0.0171$; **Figures 4E,F**; females, $F_{(1,44)} = 13.50$, $p = 0.0006$; **Figures 4K,L**). Therefore, when interpreting the effects on cognitive function, the swimming distance would better reflect cognitive functioning than the swimming duration. For Ts65Dn males, cilostazol supplementation significantly shortened the swimming distance ($F_{(1,49)} = 1.285$, *post hoc* $p = 0.0341$), suggesting that cilostazol improved cognitive function. Cilostazol supplementation did not shorten the swimming duration, which was due to the decreased swimming speed. For 2N males, cilostazol supplementation did not alter the swimming distance, suggesting that cilostazol did not alter cognitive function. Among females fed a regular diet, 2N mice and Ts65Dn mice did not differ with respect to swimming duration, distance, or speed (**Figures 4H,J,L**).

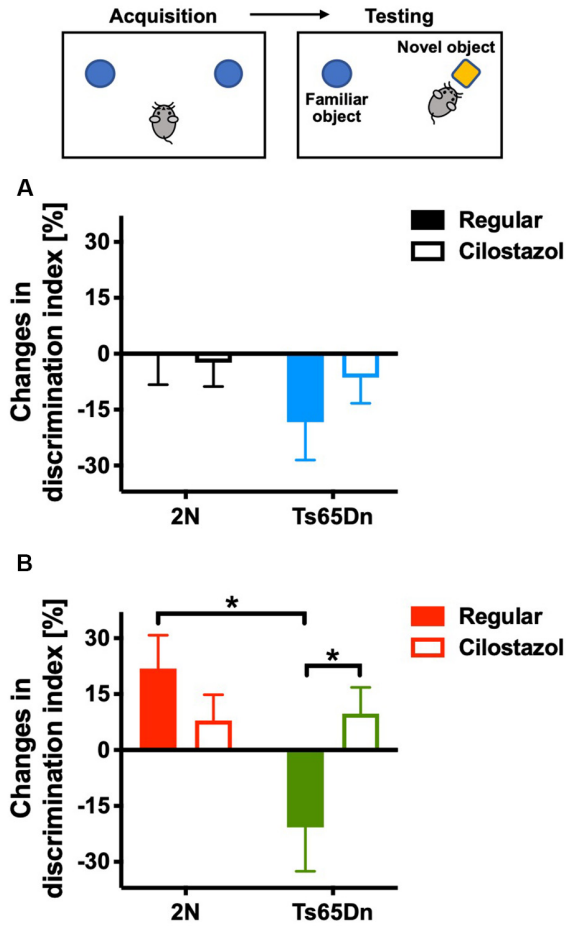

FIGURE 3 | Recognition memory. A novel-object-recognition test was performed at 10 weeks of age. Discrimination index = [time spent with the right object (novel object)] − [time spent with the left object (familiar object)]/(time spent with the right object) + (time spent with the left object) × 100%. As some animals exhibited a preference for contacting one of two identical objects on the first day, changes from the first day to the second day in males **(A)** and females **(B)** are shown. *$P < 0.05$. In male groups: 2N-Regular ($n = 17$), 2N-Cilostazol ($n = 18$), Ts65Dn-Regular ($n = 7$), Ts65Dn-Cilostazol ($n = 11$). In female groups: 2N-Regular ($n = 8$), 2N-Cilostazol ($n = 14$), Ts65Dn-Regular ($n = 6$), Ts65Dn-Cilostazol ($n = 11$). Mean ± SEM.

For Ts65Dn females, cilostazol supplementation did not change the swimming distance, suggesting that cilostazol did not alter cognitive function. For 2N females, cilostazol supplementation significantly shortened the swimming distance ($F_{(1,44)} = 4.792$, $p = 0.0339$), suggesting that cilostazol improved cognitive function, which was similar to the effect observed for Ts65Dn males. Taken together, the results showed that cilostazol treatment shortened the swimming distance in Ts65Dn males and 2N females, suggesting the improvement of cognitive functions.

Open-Field Activities

We performed the open-field test at 9 and 17 weeks of age to evaluate spontaneous activities. We initially analyzed the

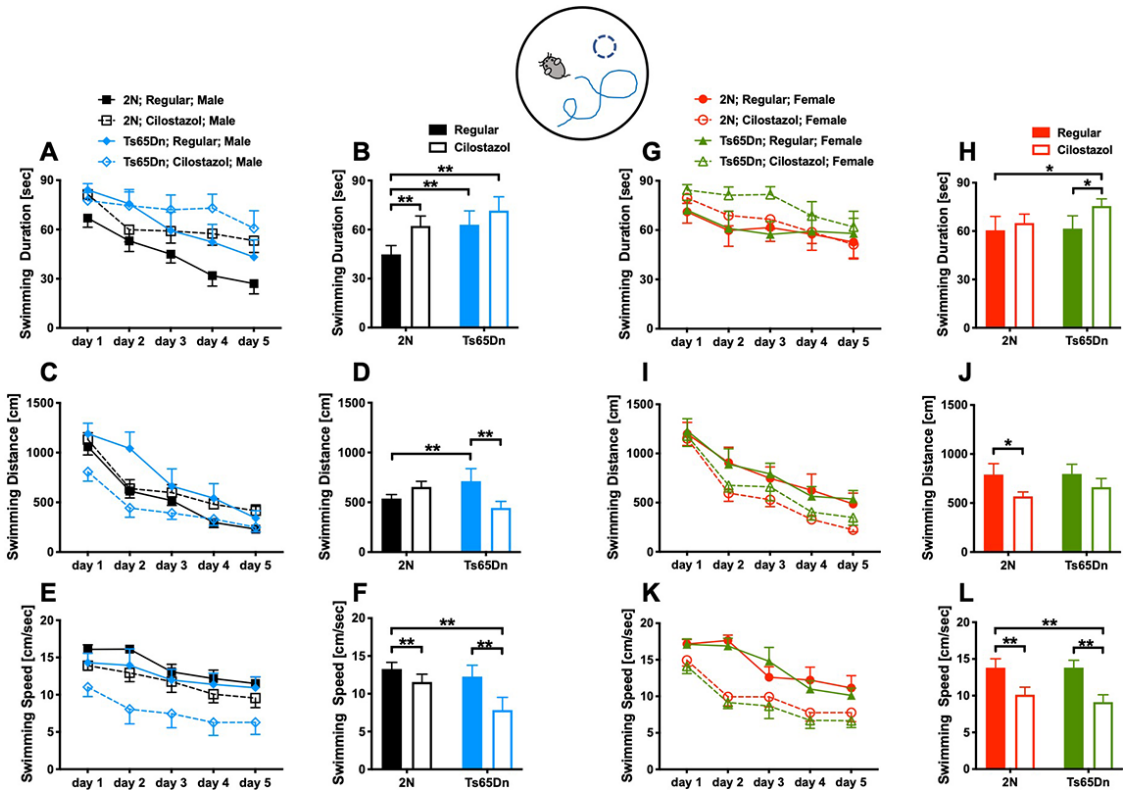

FIGURE 4 | Spatial learning and memory. The Morris water maze test was performed at 11 weeks of age. We measured swimming duration **(A,G)**, swimming distance **(C,I)** until mice reached the hidden platform, and swimming speed **(E,K)** for five consecutive days. We presented the average of the 5-day sessions for swimming duration **(B,H)**, swimming distance **(D,J)**, and swimming speed **(F,L)**. $^{*}P < 0.05$ and $^{**}P < 0.01$. The results in males **(A–F)** and females **(G–L)** are shown. In male groups: 2N-Regular (n = 20), 2N-Cilostazol (n = 15), Ts65Dn-Regular (n = 8), Ts65Dn-Cilostazol (n = 10). In female groups: 2N-Regular (n = 9), 2N-Cilostazol (n = 18), Ts65Dn-Regular (n = 11), Ts65Dn-Cilostazol (n = 10). Mean ± SEM.

overall activities during 60-min sessions at 9 and 17 weeks. In males, when fed a regular diet, Ts65Dn mice were significantly hyperactive compared to 2N mice concerning locomotion (horizontal movement; $F_{(1,23)} = 9.902$, $p = 0.0045$) but not rearing (vertical movement) at both time points (**Figures 5A,B**). Cilostazol supplementation partially ameliorated the hyperactivity in Ts65Dn males, and there was no significant difference between Ts65Dn males fed cilostazol and 2N males fed a regular diet at either point. In females, when fed a regular diet, Ts65Dn mice behaved similarly to 2N mice with respect to both locomotion and rearing at both time points (**Figures 5C,D**). Cilostazol supplementation did not alter the behaviors in Ts65Dn females, but it unexpectedly and significantly increased both locomotion ($F_{(3,44)} = 4.884$, *post hoc* $p = 0.0003$) and rearing ($F_{(3,44)} = 0.9577$, *post hoc* $p = 0.0416$) in 2N females at 9 weeks but not at 17 weeks of age.

We then analyzed temporal changes throughout the 60-min session in 5-min increments at 17 weeks of age. In males, when fed a regular diet, Ts65Dn mice were significantly more hyperactive than 2N mice concerning locomotion but not rearing during some of the 5-min increments in the dark environment ($F_{(3,52)} = 1.305$, *post hoc* 35 min $p = 0.0427$, 45 min $p = 0.0431$; **Figures 5E,F**). In contrast, Ts65Dn males fed cilostazol were not hyperactive compared with 2N males fed a regular diet during any of the 5-min increments. In females, when fed a regular diet, Ts65Dn mice did not exhibit altered activities compared with 2N mice with respect to either locomotion or rearing during any of the 5-min increments (**Figures 5G,H**). 2N females fed cilostazol were significantly more hyperactive than 2N females fed a regular diet with respect to locomotion during some of the 5-min increments in both light and dark environments ($F_{(3,44)} = 2.972$, *post hoc* 10 min $p = 0.0174$, 40 min $p = 0.0264$, 50 min $p = 0.0136$, 60 min $p = 0.0160$).

Rotarod Performance

We performed the rotarod test at 8 and 16 weeks of age to evaluate sensorimotor function. In males, rotarod performance did not differ between Ts65Dn and 2N mice fed a regular diet. Cilostazol supplementation did not change the performance in males of either chromosomal type (**Figure 6A**). In females, rotarod performance was worse in Ts65Dn mice than in 2N mice at 16 weeks of age when the mice were fed a regular diet ($F_{(3,48)} = 3.652$, *post hoc* $p = 0.0348$; **Figure 6B**). The performance in Ts65Dn females fed cilostazol was slightly better than that in Ts65Dn females fed a regular diet, and

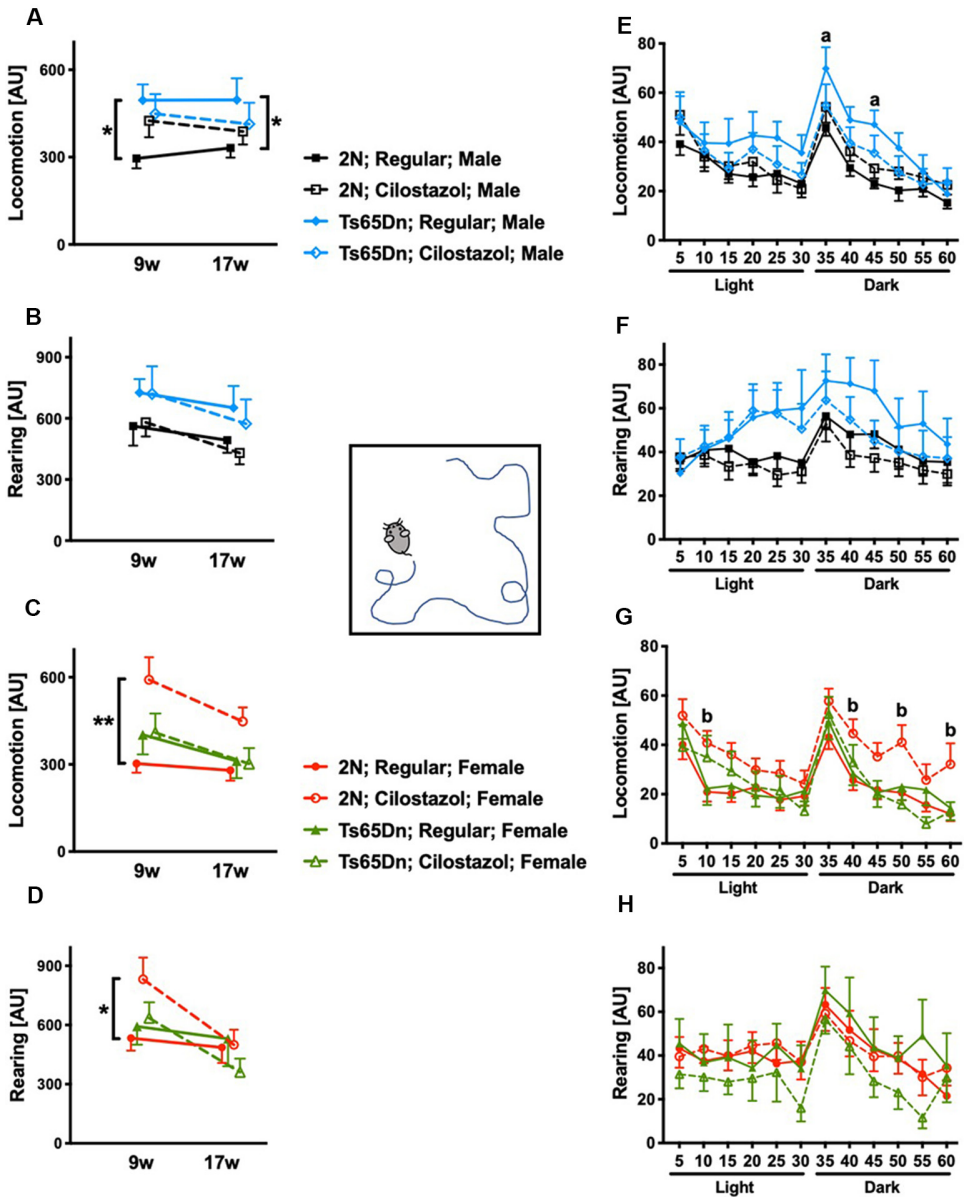

FIGURE 5 | Open-field activities. Spontaneous horizontal movement (locomotion) and vertical movement (rearing) were evaluated in the open-field test during 60-min sessions at 9 weeks and 17 weeks of age. The first 30 min was in a light environment, and the second 30 min was in a dark environment. Total activities during the 60-min session in males **(A,B)** and females **(C,D)** are shown. $^{*}P < 0.05$ and $^{**}P < 0.01$. Activities during 5-min increments throughout the 60-min session at 17 weeks of age are shown in males **(E,F)** and females **(G,H)**. **(a)** $P < 0.05$, Ts65Dn males fed a regular diet vs. 2N males fed a regular diet. **(b)** $P < 0.05$, 2N females fed cilostazol vs. 2N females fed a regular diet. In male groups: 2N-Regular (n = 14), 2N-Cilostazol (n = 17), Ts65Dn-Regular (n = 11), Ts65Dn-Cilostazol (n = 14). In female groups: 2N-Regular (n = 18), 2N-Cilostazol (n = 13), Ts65Dn-Regular (n = 8), Ts65Dn-Cilostazol (n = 9). Mean ± SEM. AU, arbitrary unit.

there were no significant differences between 2N females fed a regular diet and Ts65Dn females fed cilostazol at 16 weeks of age. Unexpectedly, the performance in 2N females was worse with cilostazol supplementation ($F_{(3,48)}$ = 3.652, *post hoc* p = 0.0089).

Muscle Strength

We measured the muscle strength of the four limbs using a traction meter at 10 weeks of age. Ts65Dn females (p = 0.0310) but not males exhibited significantly weaker peak muscle strength than 2N mice. Cilostazol supplementation did not change muscle strength significantly regardless of chromosomal type or sex (**Figures 7A,B**).

Cerebral Blood Flow

We measured CBF by laser speckle flowmetry at 12 weeks of age. CBF did not differ by chromosomal type or treatment in either males or females (**Figures 8A–C**).

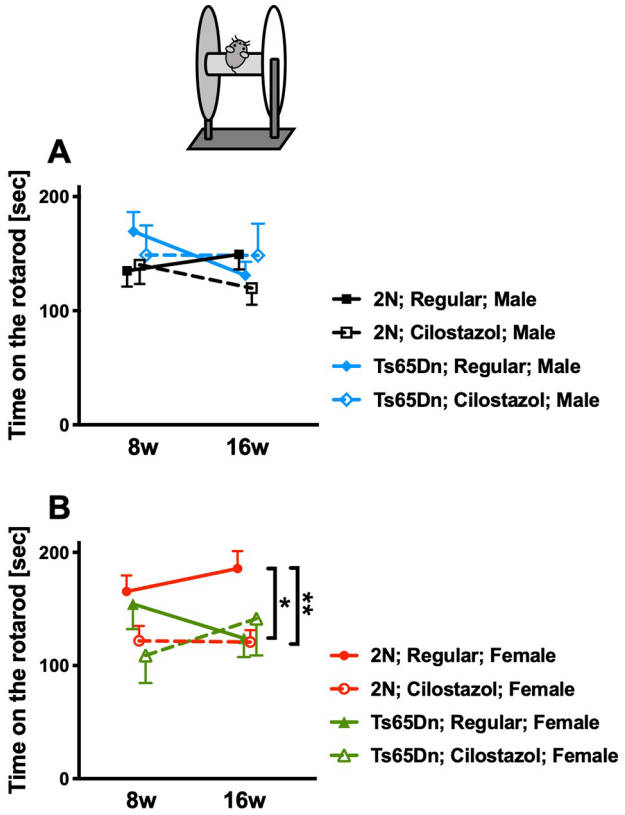

FIGURE 6 | Rotarod performance. Sensorimotor performance was evaluated by the rotarod test at 8 weeks and 16 weeks of age. Rotarod performance, i.e., time on the rotarod, in males **(A)** and in females **(B)** is shown. $^{*}P < 0.05$ and $^{**}P < 0.01$. In male groups: 2N-Regular (n = 19), 2N-Cilostazol (n = 14), Ts65Dn-Regular (n = 13), Ts65Dn-Cilostazol (n = 8). In female groups: 2N-Regular (n = 17), 2N-Cilostazol (n = 18), Ts65Dn-Regular (n = 12), Ts65Dn-Cilostazol (n = 5). Mean ± SEM.

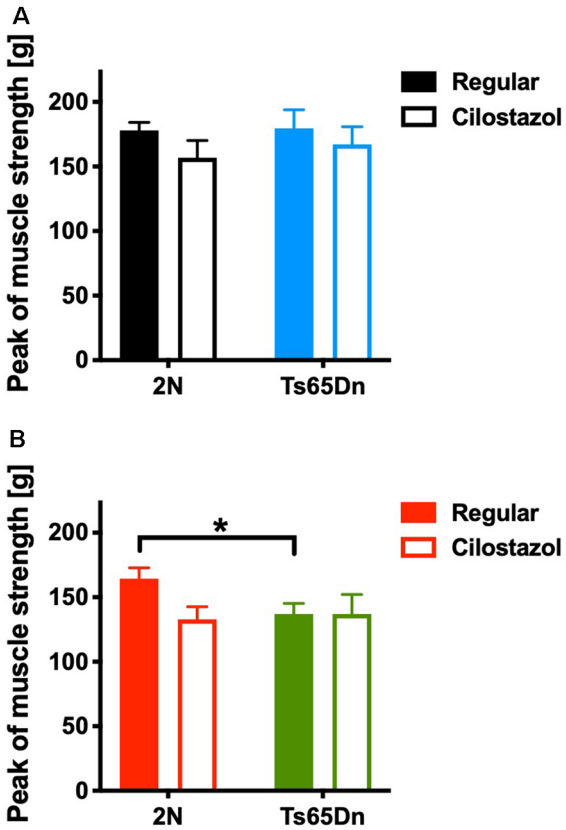

FIGURE 7 | Muscle strength in the four limbs was measured by a traction meter at 10 weeks of age. Peak muscle strength in males **(A)** and females **(B)** is shown. $^{*}P < 0.05$. In male groups: 2N-Regular (n = 20), 2N-Cilostazol (n = 8), Ts65Dn-Regular (n = 8), Ts65Dn-Cilostazol (n = 10). In female groups: 2N-Regular (n = 10), 2N-Cilostazol (n = 13), Ts65Dn-Regular (n = 11), Ts65Dn-Cilostazol (n = 6). Mean ± SEM.

DISCUSSION

This is the first study to examine the effects of cilostazol, a PDE3 inhibitor, on an animal model of Down syndrome. The supplementation of cilostazol began in the fetal period and continued until young adulthood. A battery of tests was used to discriminate different types of effects on different functions. Early and long-term supplementation with cilostazol altered behaviors; it ameliorated the low cognitive function and hyperactivity observed in the Ts65Dn mouse model of Down syndrome.

The Ts65Dn mouse is a well-established and widely used model of Down syndrome (Faizi et al., 2011) and has segmental trisomy of chromosome 16, which is highly (approximately 80%) homologous to human chromosome 21. The trisomy segment includes the *APP* gene (Salehi et al., 2007). Ts65Dn mice present an age-dependent increase in APP (Seo and Isacson, 2005) and Aβ (Hunter et al., 2004; Netzer et al., 2010) levels in the cortex and hippocampus. The Ts65Dn mouse exhibits several physical and functional abnormalities similar to those seen in people with Down syndrome (Faizi et al., 2011). People with Down syndrome have cognitive impairments, which usually range from mild to moderate, and behavioral problems, which include a short attention span and impulsive behavior (National Institute of Child Health and Human Development, in press; Bull, 2011). Attention-deficit/hyperactivity disorder (ADHD) is commonly found in people with Down syndrome (Capone et al., 2006), and both boys and girls with Down syndrome between the ages of 6 and 11 years are hyperactive (Pueschel et al., 1991). Other common symptoms include poor muscle tone (National Institute of Child Health and Human Development, in press; Bull, 2011). In the current study, Ts65Dn males that were fed a regular diet demonstrated poor learning and memory in the water maze test and increased locomotion activity in the open-field test compared with 2N males, and Ts65Dn females that were fed a regular diet demonstrated poor learning and memory in the novel-object-recognition test, poor sensorimotor performance in the rotarod test, and weaker muscle strength than 2N females. Previous studies using Ts65Dn mice have repeatedly demonstrated poor cognitive function (Faizi et al., 2011; Shichiri et al., 2011; Kleschevnikov et al., 2012; Vidal et al., 2012; Contestabile et al., 2013; Martínez-Cué et al., 2013;

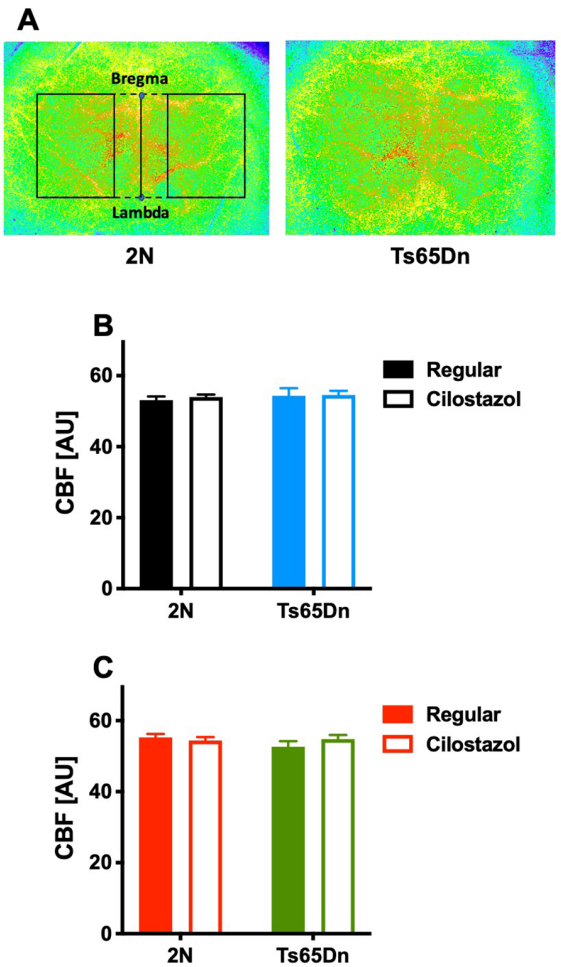

FIGURE 8 | Cerebral blood flow. Cerebral blood flow (CBF) was measured by laser speckle flowmetry at 12 weeks of age. A representative image of surface CBF in 2N and Ts65Dn male mice is shown **(A)**. The region of interest is indicated by the rectangle (solid lines), which was set to be square with bregma and lambda (dashed lines). The average CBF values in the bilateral hemispheres of males **(B)** and females **(C)** are shown. In male groups: 2N-Regular (n = 20), 2N-Cilostazol (n = 17), Ts65Dn-Regular (n = 6), Ts65Dn-Cilostazol (n = 14). In female groups: 2N-Regular (n = 8), 2N-Cilostazol (n = 16), Ts65Dn-Regular (n = 12), Ts65Dn-Cilostazol (n = 10). Mean ± SEM. AU, arbitrary unit.

Nakano-Kobayashi et al., 2017) and hyperactivity (Coussons-Read and Crnic, 1996; Stewart et al., 2007; Faizi et al., 2011; Kleschevnikov et al., 2012; Martínez-Cué et al., 2013). Studies reported in the literature have also frequently demonstrated that there were no behavioral deficits in Ts65Dn mice compared with those in 2N mice, e.g., in the novel-object-recognition test (Kleschevnikov et al., 2012), the rotarod test (Martínez-Cué et al., 2013), and the grip strength test (Vidal et al., 2012). Behavioral tests are sensitive to various factors, such as the conditions of the test room, examiners, and differences in the examination tools, and the animal performances change as they grow older. These factors may be the reasons for the contradictory reports. A vast majority of studies assessed behaviors only in males (Rueda et al., 2010; Park et al., 2011; Kleschevnikov et al., 2012; Vidal et al., 2012; Contestabile et al., 2013; Martínez-Cué et al., 2013; Nakano-Kobayashi et al., 2017). Fewer studies assessed behaviors only in females (Netzer et al., 2010; Kida et al., 2013) or in both sexes together (Begenisic et al., 2011), and even fewer studies assessed behaviors in males and females separately; Martínez-Cué et al. (2002) reported sex differences, while others did not (Stewart et al., 2007; Faizi et al., 2011).

Cilostazol significantly ameliorated hyperactivity in Ts65Dn males and novel-object-recognition in Ts65Dn females and partially ameliorated sensorimotor function, as determined by the rotarod test, in Ts65Dn females. Cilostazol was observed to improve learning and memory, as tested by the water maze in Ts65Dn males. The drug significantly shortened the swimming distance required to reach the hidden platform. Cilostazol significantly slowed the swimming speed in Ts65Dn males and females as well as in 2N males and females. Muscle strength, as measured by the traction meter, was not affected by cilostazol supplementation. The cause of slow swimming speed in the cilostazol-fed groups may be the heavier weight of the mice compared to that observed in the regular diet-fed groups. There was a significant negative correlation between body weight and swimming speed in Ts65Dn females fed cilostazol (R^2 = 0.573) and a trend toward a negative correlation in 2N males fed cilostazol (p = 0.070, R^2 = 0.268), but no such correlation was observed in Ts65Dn males fed cilostazol or 2N females fed cilostazol. Apart from the slowing of swimming speeds observed in both sexes and the longer swimming duration observed in females, long-term supplementation with cilostazol starting during the fetal period did not cause any adverse effects in Ts65Dn mice according to the battery of tests we performed. Taken together, the results indicated cilostazol supplementation in Ts65Dn mice is moderately beneficial to behavior and cognitive function.

Sex differences in the effects of cilostazol were evident in the present study. The blood and tissue concentrations of the drug are significantly higher in female rats than in male rats (Akiyama et al., 1985), and these differences in pharmacodynamics may cause the sex-dependent effects of the drug. To the best of our knowledge, sex-dichotomy-specific cilostazol effects have not been reported apart from the aforementioned report, as earlier studies have been performed only in male animals (Watanabe et al., 2006; Lee et al., 2007; Hiramatsu et al., 2010; Miyamoto et al., 2010; Chen et al., 2011; Hase et al., 2012; Kasahara et al., 2012; Kitamura et al., 2017).

Cilostazol is mainly used for the prevention of the recurrence of cerebrovascular accidents and the reduction of symptoms of peripheral arterial disease (intermittent claudication) as an antiplatelet vasoactive agent in the clinical setting. Therefore, the roles that cilostazol plays in the brain have been explored mostly in models of ischemia. Experimental studies have shown that cilostazol affects not only platelets but also blood vessel integrity and blood flow (Hase et al., 2012; Kasahara et al., 2012). In our present study, cilostazol did not increase baseline CBF, which is in line with previous reports in rodent models of chronic cerebral hypoperfusion (Watanabe et al., 2006; Miyamoto et al., 2010; Kitamura et al., 2017). Studies in rodent models of chronic cerebral hypoperfusion showed that cilostazol

reduces apoptotic cell death in association with decreased TNF-α; upregulates phosphorylated cAMP-responsive element-binding protein (CREB), leading to an increase in Bcl-2 and cyclooxygenase-2; increases mature oligodendrocytes, leading to the regeneration of white matter; and ameliorates increased endothelial adhesion molecules and gliosis (Lee et al., 2006; Watanabe et al., 2006; Miyamoto et al., 2010; Kitamura et al., 2017). An *in vitro* study with human umbilical vein endothelial cells showed that cilostazol reduces lipopolysaccharide-induced apoptotic cell death *via* cAMP-dependent protein kinase activation (Kim et al., 2006). A study showed that cilostazol promotes vascular smooth muscle cell differentiation both *in vivo* and *in vitro* (Chen et al., 2011). Taken together, *in vivo* studies demonstrated that cilostazol has pleiotropic effects on the brain and blood vessels, and *in vitro* studies demonstrated such effects on neurons, endothelial cells, and smooth muscle cells.

The mechanisms of the cilostazol-dependent behavioral alterations observed in a mouse model of Down syndrome were not explored in the present study. As this is the first study to examine the effects of cilostazol in a model of Down syndrome, the mechanisms underlying the behavioral alterations caused by this drug are not known. It is easily conceivable that cilostazol, a PDE3 inhibitor, exerts a variety of effects as it increases intracellular cAMP and cGMP (Kambayashi et al., 2003; Heckman et al., 2015). PDE3 is expressed at low levels in the human brain (Lakics et al., 2010; García-Osta et al., 2012). Our previous study in postmortem human brains showed that PDE3 is abnormally upregulated in cerebral blood vessels of patients with cerebral amyloid angiopathy and is closely correlated with the vascular amyloid burden (Maki et al., 2014). Our previous study in a transgenic mouse model of Alzheimer's disease showed that cilostazol supplementation does not increase resting CBF but restores vascular reactivity, promotes intramural periarterial drainage of Aβ, and rescues cognitive deficits (Maki et al., 2014). However, the efficacy of cilostazol does not thoroughly depend on its modulation of vascular functions; the same study also demonstrated that cilostazol decreases endogenous Aβ production in cultured neurons (Maki et al., 2014). Few studies have examined cilostazol's effects in models with cognitive impairment (Heckman et al., 2015). Oral administration of cilostazol attenuates learning and memory impairment caused by intracerebroventricular injections of $A\beta_{25–35}$ in mice (Hiramatsu et al., 2010; Park et al., 2011). Cilostazol prevents the increase in malondialdehyde, which is a marker for lipid peroxidation, in the brains of model mice (Hiramatsu et al., 2010) and decreases Aβ levels and ApoE expression in N2a cells expressing the human *APP* Swedish mutation (Park et al., 2011). Cilostazol reportedly improves cognitive function in wild-type mice by increasing the hippocampal production of insulin-like growth factor-1 (Zhao et al., 2010).

In conclusion, long-term treatment with cilostazol, a PDE3 inhibitor, from very early in life moderately attenuated cognitive deficits and hyperactivity in the Ts65Dn mouse model of Down syndrome. With proven safety of its long-term administration in practice and its low cost, cilostazol may be a useful drug to ameliorate cognitive deficits and behavioral problems in people with Down syndrome.

DATA AVAILABILITY STATEMENT

The datasets generated for this study are available on request to the corresponding author.

ETHICS STATEMENT

The animal study was reviewed and approved by the Experimental Animal Care and Use Committee of the National Cerebral and Cardiovascular Center.

AUTHOR CONTRIBUTIONS

All authors contributed substantially to this research study. MT, MO, YY, YH, ET, and YO performed the experiments. MT, AT, and MI designed the study. MT and YO analyzed the data and wrote the manuscript. SS and MI revised the manuscript critically for important intellectual content. MT supervised the project.

FUNDING

This research was supported by the Intramural Research Fund for Cardiovascular Diseases of the National Cerebral and Cardiovascular Center of Japan.

ACKNOWLEDGMENTS

We thank Mari Furuta, Mutsumi Sakamoto, and Ritsuko Maki for excellent technical assistance. We also thank Drs. Mariko Harada-Shiba, Kyoko Shioya, and Mototada Shichiri for helpful discussions.

REFERENCES

Akiyama, H., Kudo, S., and Shimizu, T. (1985). The absorption, distribution and excretion of a new antithrombotic and vasodilating agent, cilostazol, in rat, rabbit, dog and man. *Arzneimittelforschung* 35, 1124–1132.

Bakker, E. N., Bacskai, B. J., Arbel-Ornath, M., Aldea, R., Bedussi, B., Morris, A. W., et al. (2016). Lymphatic clearance of the brain: perivascular, paravascular and significance for neurodegenerative diseases. *Cell. Mol. Neurobiol.* 36, 181–194. doi: 10.1007/s10571-015-0273-8

Begenisic, T., Spolidoro, M., Braschi, C., Baroncelli, L., Milanese, M., Pietra, G., et al. (2011). Environmental enrichment decreases GABAergic inhibition and improves cognitive abilities, synaptic plasticity and visual functions in a mouse model of Down syndrome. *Front. Cell. Neurosci.* 5:29. doi: 10.3389/fncel.2011.00029

Bull, M. J., and Committee on Genetics. (2011). Health supervision for children with Down syndrome. *Pediatrics* 128, 393–406. doi: 10.1542/peds.2011-1605

Capone, G., Goyal, P., Ares, W., and Lannigan, E. (2006). Neurobehavioral disorders in children, adolescents, and young adults with Down syndrome. *Am. J. Med. Genet. C Semin. Med. Genet.* 142C, 158–172. doi: 10.1002/ajmg.c.30097

Chen, W. J., Chen, Y. H., Lin, K. H., Ting, C. H., and Yeh, Y. H. (2011). Cilostazol promotes vascular smooth muscles cell differentiation through the cAMP response element-binding protein-dependent pathway. *Arterioscler. Thromb. Vasc. Biol.* 31, 2106–2113. doi: 10.1161/atvbaha.111.230987

Contestabile, A., Greco, B., Ghezzi, D., Tucci, V., Benfenati, F., and Gasparini, L. (2013). Lithium rescues synaptic plasticity and memory in Down syndrome mice. *J. Clin. Invest.* 123, 348–361. doi: 10.1172/jci64650

Costa, A. C., Stasko, M. R., Schmidt, C., and Davisson, M. T. (2010). Behavioral validation of the Ts65Dn mouse model for Down syndrome of a genetic background free of the retinal degeneration mutation Pde6b(rd1). *Behav. Brain Res.* 206, 52–62. doi: 10.1016/j.bbr.2009.08.034

Coussons-Read, M. E., and Crnic, L. S. (1996). Behavioral assessment of the Ts65Dn mouse, a model for Down syndrome: altered behavior in the elevated plus maze and open field. *Behav. Genet.* 26, 7–13. doi: 10.1007/bf02361154

Davisson, M. T., Schmidt, C., and Akeson, E. C. (1990). Segmental trisomy of murine chromosome 16: a new model system for studying Down syndrome. *Prog. Clin. Biol. Res.* 360, 263–280.

Deutsch, S. I., Rosse, R. B., Mastropaolo, J., and Chilton, M. (2003). Progressive worsening of adaptive functions in Down syndrome may be mediated by the complexing of soluble Aβ peptides with the α 7 nicotinic acetylcholine receptor: therapeutic implications. *Clin. Neuropharmacol.* 26, 277–283. doi: 10.1097/00002826-200309000-00013

Diem, A. K., MacGregor Sharp, M., Gatherer, M., Bressloff, N. W., Carare, R. O., and Richardson, G. (2017). Arterial pulsations cannot drive intramural periarterial drainage: significance for Aβ drainage. *Front. Neurosci.* 11:475. doi: 10.3389/fnins.2017.00475

Faizi, M., Bader, P. L., Tun, C., Encarnacion, A., Kleschevnikov, A., Belichenko, P., et al. (2011). Comprehensive behavioral phenotyping of Ts65Dn mouse model of Down syndrome: activation of β1-adrenergic receptor by xamoterol as a potential cognitive enhancer. *Neurobiol. Dis.* 43, 397–413. doi: 10.1016/j.nbd.2011.04.011

García-Osta, A., Cuadrado-Tejedor, M., Garcia-Barroso, C., Oyarzábal, J., and Franco, R. (2012). Phosphodiesterases as therapeutic targets for Alzheimer's disease. *ACS Chem. Neurosci.* 3, 832–844. doi: 10.1021/cn3000907

Hase, Y., Okamoto, Y., Fujita, Y., Kitamura, A., Nakabayashi, H., Ito, H., et al. (2012). Cilostazol, a phosphodiesterase inhibitor, prevents no-reflow and hemorrhage in mice with focal cerebral ischemia. *Exp. Neurol.* 233, 523–533. doi: 10.1016/j.expneurol.2011.11.038

Hattori, Y., Kitamura, A., Tsuji, M., Nagatsuka, K., and Ihara, M. (2014). Motor and cognitive impairment in a mouse model of ischemic carotid artery disease. *Neurosci. Lett.* 581, 1–6. doi: 10.1016/j.neulet.2014.08.009

Heckman, P. R., Wouters, C., and Prickaerts, J. (2015). Phosphodiesterase inhibitors as a target for cognition enhancement in aging and Alzheimer's disease: a translational overview. *Curr. Pharm. Des.* 21, 317–331. doi: 10.2174/1381612820666140826114601

Hiramatsu, M., Takiguchi, O., Nishiyama, A., and Mori, H. (2010). Cilostazol prevents amyloid β peptide$_{25–35}$-induced memory impairment and oxidative stress in mice. *Br. J. Pharmacol.* 161, 1899–1912. doi: 10.1111/j.1476-5381.2010.01014.x

Hunter, C. L., Bimonte-Nelson, H. A., Nelson, M., Eckman, C. B., and Granholm, A. C. (2004). Behavioral and neurobiological markers of Alzheimer's disease in Ts65Dn mice: effects of estrogen. *Neurobiol. Aging* 25, 873–884. doi: 10.1016/j.neurobiolaging.2003.10.010

Ihara, M., Nishino, M., Taguchi, A., Yamamoto, Y., Hattori, Y., Saito, S., et al. (2014). Cilostazol add-on therapy in patients with mild dementia receiving donepezil: a retrospective study. *PLoS One* 9:e89516. doi: 10.1371/journal.pone.0089516

Kajii, T. (2008). Predicted prevalence of Down syndrome live births in Japan, 1970–2006. *Am. J. Med. Genet. A* 146A, 1387–1388. doi: 10.1002/ajmg.a.32323

Kambayashi, J., Liu, Y., Sun, B., Shakur, Y., Yoshitake, M., and Czerwiec, F. (2003). Cilostazol as a unique antithrombotic agent. *Curr. Pharm. Des.* 9, 2289–2302. doi: 10.2174/1381612033453910

Kasahara, Y., Nakagomi, T., Matsuyama, T., Stern, D., and Taguchi, A. (2012). Cilostazol reduces the risk of hemorrhagic infarction after administration of tissue-type plasminogen activator in a murine stroke model. *Stroke* 43, 499–506. doi: 10.1161/strokeaha.111.635417

Kida, E., Rabe, A., Walus, M., Albertini, G., and Golabek, A. A. (2013). Long-term running alleviates some behavioral and molecular abnormalities in Down syndrome mouse model Ts65Dn. *Exp. Neurol.* 240, 178–189. doi: 10.1016/j.expneurol.2012.11.022

Kim, M. J., Lee, J. H., Park, S. Y., Hong, K. W., Kim, C. D., Kim, K. Y., et al. (2006). Protection from apoptotic cell death by cilostazol, phosphodiesterase type III inhibitor, *via* cAMP-dependent protein kinase activation. *Pharmacol. Res.* 54, 261–267. doi: 10.1016/j.phrs.2006.05.006

Kitamura, A., Manso, Y., Duncombe, J., Searcy, J., Koudelka, J., Binnie, M., et al. (2017). Long-term cilostazol treatment reduces gliovascular damage and memory impairment in a mouse model of chronic cerebral hypoperfusion. *Sci. Rep.* 7:4299. doi: 10.1038/s41598-017-04082-0

Kleschevnikov, A. M., Belichenko, P. V., Faizi, M., Jacobs, L. F., Htun, K., Shamloo, M., et al. (2012). Deficits in cognition and synaptic plasticity in a mouse model of Down syndrome ameliorated by GABAB receptor antagonists. *J. Neurosci.* 32, 9217–9227. doi: 10.1523/JNEUROSCI.1673-12.2012

Lakics, V., Karran, E. H., and Boess, F. G. (2010). Quantitative comparison of phosphodiesterase mRNA distribution in human brain and peripheral tissues. *Neuropharmacology* 59, 367–374. doi: 10.1016/j.neuropharm.2010.05.004

Lee, J. H., Park, S. Y., Shin, Y. W., Hong, K. W., Kim, C. D., Sung, S. M., et al. (2006). Neuroprotection by cilostazol, a phosphodiesterase type 3 inhibitor, against apoptotic white matter changes in rat after chronic cerebral hypoperfusion. *Brain Res.* 1082, 182–191. doi: 10.1016/j.brainres.2006.01.088

Lee, J. H., Park, S. Y., Shin, Y. W., Kim, C. D., Lee, W. S., and Hong, K. W. (2007). Concurrent administration of cilostazol with donepezil effectively improves cognitive dysfunction with increased neuroprotection after chronic cerebral hypoperfusion in rats. *Brain Res.* 1185, 246–255. doi: 10.1016/j.brainres.2007.09.016

Leverenz, J. B., and Raskind, M. A. (1998). Early amyloid deposition in the medial temporal lobe of young Down syndrome patients: a regional quantitative analysis. *Exp. Neurol.* 150, 296–304. doi: 10.1006/exnr.1997.6777

Liu, D. P., Schmidt, C., Billings, T., and Davisson, M. T. (2003). Quantitative PCR genotyping assay for the Ts65Dn mouse model of Down syndrome. *BioTechniques* 35, 1170–1174, 1176, 1178 passim. doi: 10.2144/03356st02

Maki, T., Okamoto, Y., Carare, R. O., Hase, Y., Hattori, Y., Hawkes, C. A., et al. (2014). Phosphodiesterase III inhibitor promotes drainage of cerebrovascular β-amyloid. *Ann. Clin. Transl. Neurol.* 1, 519–533. doi: 10.1002/acn3.79

Martínez-Cué, C., Baamonde, C., Lumbreras, M., Paz, J., Davisson, M. T., Schmidt, C., et al. (2002). Differential effects of environmental enrichment on behavior and learning of male and female Ts65Dn mice, a model for Down syndrome. *Behav. Brain Res.* 134, 185–200. doi: 10.1016/s0166-4328(02)00026-8

Martínez-Cué, C., Martínez, P., Rueda, N., Vidal, R., García, S., Vidal, V., et al. (2013). Reducing GABAA α5 receptor-mediated inhibition rescues functional and neuromorphological deficits in a mouse model of down syndrome. *J. Neurosci.* 33, 3953–3966. doi: 10.1523/JNEUROSCI.1203-12.2013

Miyamoto, N., Tanaka, R., Shimura, H., Watanabe, T., Mori, H., Onodera, M., et al. (2010). Phosphodiesterase III inhibition promotes differentiation and survival of oligodendrocyte progenitors and enhances regeneration of ischemic white matter lesions in the adult mammalian brain. *J. Cereb. Blood Flow Metab.* 30, 299–310. doi: 10.1038/jcbfm.2009.210

Morris, A. W., Sharp, M. M., Albargothy, N. J., Fernandes, R., Hawkes, C. A., Verma, A., et al. (2016). Vascular basement membranes as pathways for the passage of fluid into and out of the brain. *Acta Neuropathol.* 131, 725–736. doi: 10.1007/s00401-016-1555-z

Moorthie, S., Blencowe, H., Darlison, M. W., Gibbson, S., Lawn, J. E., Mastroiacovo, P., et al. (2018). Chromosomal disorders: Estimating baseline birth prevalence and pregnancy outcomes worldwide. *J. Community Genet.* 9, 377–386. doi: 10.1007/s12687-017-0336-2

Nakano-Kobayashi, A., Awaya, T., Kii, I., Sumida, Y., Okuno, Y., Yoshida, S., et al. (2017). Prenatal neurogenesis induction therapy normalizes brain structure and function in Down syndrome mice. *Proc. Natl. Acad. Sci. U S A* 114, 10268–10273. doi: 10.1073/pnas.1704143114

National Institute of Child Health and Human Development. (in press). What are common symptoms of Down syndrome? Available online at: https://www.nichd.nih.gov/health/topics/down/conditioninfo/Pages/symptoms.aspx. Accessed 31 January 2017

Netzer, W. J., Powell, C., Nong, Y., Blundell, J., Wong, L., Duff, K., et al. (2010). Lowering β-amyloid levels rescues learning and memory in a Down syndrome mouse model. *PLoS One* 5:e10943. doi: 10.1371/journal.pone.0010943

Ohshima, M., Coq, J. O., Otani, K., Hattori, Y., Ogawa, Y., Sato, Y., et al. (2016). Mild intrauterine hypoperfusion reproduces neurodevelopmental disorders observed in prematurity. *Sci. Rep.* 6:39377. doi: 10.1038/srep39377

Ohshima, M., Tsuji, M., Taguchi, A., Kasahara, Y., and Ikeda, T. (2012). Cerebral blood flow during reperfusion predicts later brain damage in a mouse and a rat model of neonatal hypoxic-ischemic encephalopathy. *Exp. Neurol.* 233, 481–489. doi: 10.1016/j.expneurol.2011.11.025

Park, S. H., Kim, J. H., Bae, S. S., Hong, K. W., Lee, D. S., Leem, J. Y., et al. (2011). Protective effect of the phosphodiesterase III inhibitor cilostazol on amyloid β-induced cognitive deficits associated with decreased amyloid β accumulation. *Biochem. Biophys. Res. Commun.* 408, 602–608. doi: 10.1016/j.bbrc.2011.04.068

Pueschel, S. M., Bernier, J. C., and Pezzullo, J. C. (1991). Behavioural observations in children with Down's syndrome. *J. Ment. Defic. Res.* 35, 502–511. doi: 10.1111/j.1365-2788.1991.tb00447.x

Rueda, N., Llorens-Martín, M., Flórez, J., Valdizán, E., Banerjee, P., Trejo, J. L., et al. (2010). Memantine normalizes several phenotypic features in the Ts65Dn mouse model of Down syndrome. *J. Alzheimers Dis.* 21, 277–290. doi: 10.3233/jad-2010-100240

Saito, S., Kojima, S., Oishi, N., Kakuta, R., Maki, T., Yasuno, F., et al. (2016). A multicenter, randomized, placebo-controlled trial for cilostazol in patients with mild cognitive impairment: the COMCID study protocol. *Alzheimers. Dement.* 2, 250–257. doi: 10.1016/j.trci.2016.10.001

Saito, S., Yamamoto, Y., and Ihara, M. (2019). Development of a multicomponent intervention to prevent Alzheimer's disease. *Front. Neurol.* 10:490. doi: 10.3389/fneur.2019.00490

Salehi, A., Faizi, M., Belichenko, P. V., and Mobley, W. C. (2007). Using mouse models to explore genotype-phenotype relationship in Down syndrome. *Ment. Retard. Dev. Disabil. Res. Rev.* 13, 207–214. doi: 10.1002/mrdd.20164

Seo, H., and Isacson, O. (2005). Abnormal APP, cholinergic and cognitive function in Ts65Dn Down's model mice. *Exp. Neurol.* 193, 469–480. doi: 10.1016/j.expneurol.2004.11.017

Shichiri, M., Yoshida, Y., Ishida, N., Hagihara, Y., Iwahashi, H., Tamai, H., et al. (2011). α-tocopherol suppresses lipid peroxidation and behavioral and cognitive impairments in the Ts65Dn mouse model of Down syndrome. *Free Radic. Biol. Med.* 50, 1801–1811. doi: 10.1016/j.freeradbiomed.2011.03.023

Stewart, L. S., Persinger, M. A., Cortez, M. A., and Snead, O. C. III. (2007). Chronobiometry of behavioral activity in the Ts65Dn model of Down syndrome. *Behav. Genet.* 37, 388–398. doi: 10.1007/s10519-006-9119-y

Taguchi, A., Takata, Y., Ihara, M., Kasahara, Y., Tsuji, M., Nishino, M., et al. (2013). Cilostazol improves cognitive function in patients with mild cognitive impairment: a retrospective analysis. *Psychogeriatrics* 13, 164–169. doi: 10.1111/psyg.12021

Tai, S. Y., Chien, C. Y., Chang, Y. H., and Yang, Y. H. (2017). Cilostazol use is associated with reduced risk of dementia: a Nationwide Cohort Study. *Neurotherapeutics* 14, 784–791. doi: 10.1007/s13311-017-0512-4

Tsuji, M., Aoo, N., Harada, K., Sakamoto, Y., Akitake, Y., Irie, K., et al. (2010). Sex differences in the benefits of rehabilitative training during adolescence following neonatal hypoxia-ischemia in rats. *Exp. Neurol.* 226, 285–292. doi: 10.1016/j.expneurol.2010.09.002

Tsuji, M., Ohshima, M., Taguchi, A., Kasahara, Y., Ikeda, T., and Matsuyama, T. (2013). A novel reproducible model of neonatal stroke in mice: comparison with a hypoxia-ischemia model. *Exp. Neurol.* 247C, 218–225. doi: 10.1016/j.expneurol.2013.04.015

Vidal, V., García, S., Martínez, P., Corrales, A., Flórez, J., Rueda, N., et al. (2012). Lack of behavioral and cognitive effects of chronic ethosuximide and gabapentin treatment in the Ts65Dn mouse model of Down syndrome. *Neuroscience* 220, 158–168. doi: 10.1016/j.neuroscience.2012.06.031

Watanabe, T., Zhang, N., Liu, M., Tanaka, R., Mizuno, Y., and Urabe, T. (2006). Cilostazol protects against brain white matter damage and cognitive impairment in a rat model of chronic cerebral hypoperfusion. *Stroke* 37, 1539–1545. doi: 10.1161/01.str.0000221783.08037.a9

Wilcock, D. M., Schmitt, F. A., and Head, E. (2016). Cerebrovascular contributions to aging and Alzheimer's disease in Down syndrome. *Biochim. Biophys. Acta* 1862, 909–914. doi: 10.1016/j.bbadis.2015.11.007

Wiseman, F. K., Pulford, L. J., Barkus, C., Liao, F., Portelius, E., Webb, R., et al. (2018). Trisomy of human chromosome 21 enhances amyloid-β deposition independently of an extra copy of APP. *Brain* 141, 2457–2474. doi: 10.1093/brain/awy159

Zhao, J., Harada, N., Kurihara, H., Nakagata, N., and Okajima, K. (2010). Cilostazol improves cognitive function in mice by increasing the production of insulin-like growth factor-I in the hippocampus. *Neuropharmacology* 58, 774–783. doi: 10.1016/j.neuropharm.2009.12.008

Zigman, W. B., and Lott, I. T. (2007). Alzheimer's disease in Down syndrome: neurobiology and risk. *Ment. Retard. Dev. Disabil. Res. Rev.* 13, 237–246. doi: 10.1002/mrdd.20163

Conflict of Interest: The authors declare that the research was conducted in the absence of any commercial or financial relationships that could be construed as a potential conflict of interest.

The authors declare that this study received funding from Otsuka Pharmaceutical Co. Ltd. The funder was not involved in the study design, collection, analysis, interpretation of data, the writing of this article or the decision to submit it for publication.

frontiers in Aging Neuroscience

ORIGINAL RESEARCH
published: 29 April 2020
doi: 10.3389/fnagi.2020.00108

Channelrhodopsin Excitation Contracts Brain Pericytes and Reduces Blood Flow in the Aging Mouse Brain *in vivo*

Amy R. Nelson, Meghana A. Sagare, Yaoming Wang, Kassandra Kisler, Zhen Zhao and Berislav V. Zlokovic*

Department of Physiology and Neuroscience, Zilkha Neurogenetic Institute, University of Southern California, Los Angeles, CA, United States

Brains depend on blood flow for the delivery of oxygen and nutrients essential for proper neuronal and synaptic functioning. French physiologist Rouget was the first to describe pericytes in 1873 as regularly arranged longitudinal amoeboid cells on capillaries that have a muscular coat, implying that these are contractile cells that regulate blood flow. Although there have been >30 publications from different groups, including our group, demonstrating that pericytes are contractile cells that can regulate hemodynamic responses in the brain, the role of pericytes in controlling cerebral blood flow (CBF) has not been confirmed by all studies. Moreover, recent studies using different optogenetic models to express light-sensitive channelrhodopsin-2 (ChR2) cation channels in pericytes were not conclusive; one, suggesting that pericytes expressing ChR2 do not contract after light stimulus, and the other, demonstrating contraction of pericytes expressing ChR2 after light stimulus. Since two-photon optogenetics provides a powerful tool to study mechanisms of blood flow regulation at the level of brain capillaries, we re-examined the contractility of brain pericytes *in vivo* using a new optogenetic model developed by crossing our new inducible pericyte-specific CreER mouse line with ChR2 mice. We induced expression of ChR2 in pericytes with tamoxifen, excited ChR2 by 488 nm light, and monitored pericyte contractility, brain capillary diameter changes, and red blood cell (RBC) velocity in aged mice by *in vivo* two-photon microscopy. Excitation of ChR2 resulted in pericyte contraction followed by constriction of the underlying capillary leading to approximately an 8% decrease (p = 0.006) in capillary diameter. ChR2 excitation in pericytes substantially reduced capillary RBC flow by 42% (p = 0.03) during the stimulation period compared to the velocity before stimulation. Our data suggests that pericytes contract *in vivo* and regulate capillary blood flow in the aging mouse brain. By extension, this might have implications for neurological disorders of the aging human brain associated with neurovascular dysfunction and pericyte loss such as stroke and Alzheimer's disease.

Keywords: pericyte, optogenetics, channelrhodopsin, brain capillaries, red blood cell capillary flow

OPEN ACCESS

Edited by:
Roxana Octavia Carare, University of Southampton, United Kingdom

Reviewed by:
Andy Shih, Medical University of South Carolina, United States
Johannes Boltze, University of Warwick, United Kingdom
David Hartmann, Medical University of South Carolina, United States

***Correspondence:**
Berislav V. Zlokovic
zlokovic@usc.edu

Received: *10 December 2019*
Accepted: *30 March 2020*
Published: *29 April 2020*

Citation:
Nelson AR, Sagare MA, Wang Y, Kisler K, Zhao Z and Zlokovic BV (2020) Channelrhodopsin Excitation Contracts Brain Pericytes and Reduces Blood Flow in the Aging Mouse Brain in vivo. Front. Aging Neurosci. 12:108. doi: 10.3389/fnagi.2020.00108

INTRODUCTION

Brains depend on blood flow for the delivery of oxygen and nutrients essential for proper neuronal and synaptic functioning (Zlokovic, 2011; Iadecola, 2017; Kisler et al., 2017a; Sweeney et al., 2019). Cerebral blood flow (CBF) is regulated by different cell types within the neurovascular unit (Zlokovic, 2011; Iadecola, 2017; Kisler et al., 2017a; Sweeney et al., 2019). The mammalian brain has developed a unique mechanism to control regional CBF known as neurovascular coupling. This mechanism ensures a rapid increase in the rate of blood flow and oxygen delivery to activated brain regions (Kisler et al., 2017a). Several studies have shown that smooth muscle cells (SMCs) on small brain arteries and arterioles, and pericytes on brain capillaries, physically contract and dilate small arteries and arterioles, and capillaries, respectively, to regulate blood flow responses to neuronal stimulation and/or neurotransmitters (reviewed in Attwell et al., 2016; Kisler et al., 2017a; Sweeney et al., 2018). However, the role of pericytes in regulating CBF has not been confirmed by all studies (Fernández-Klett et al., 2010; Hill et al., 2015; Wei et al., 2016).

French physiologist Rouget was first to describe pericytes in 1873 as regularly arranged longitudinal amoeboid cells on capillaries that have a muscular coat, implying that these are contractile cells that regulate blood flow (Rouget, 1873). There have been >30 publications from different labs, many of which from recent years, demonstrating that pericytes are contractile cells. This has been shown by *in vitro* studies using isolated brain, retinal and cochlear pericytes from different species (see **Table 1** for details; Schor and Schor, 1986; Kelley et al., 1987, 1988; Das et al., 1988; Ferrari-Dileo et al., 1992; Haefliger et al., 1994, 1997, 2002; Murphy and Wagner, 1994; Chen and Anderson, 1997; Matsugi et al., 1997a,b,c; Dai et al., 2009, 2011; Neuhaus et al., 2017); *ex vivo* studies using cerebellar, cerebral and spinal cord slices and retinal microvessels or explants (see **Table 2** for details; Schönfelder et al., 1998; Kawamura et al., 2003, 2004; Wu et al., 2003; Peppiatt et al., 2006; Yamanishi et al., 2006; Hall et al., 2014; Fernández-Klett and Priller, 2015; Mishra et al., 2016; Ivanova et al., 2017; Li et al., 2017; Zong et al., 2017; Alarcon-Martinez et al., 2019; Nortley et al., 2019); and *in vivo* studies in rodents (see **Table 3** for details; Dai et al., 2009, 2011; Fernández-Klett et al., 2010; Hall et al., 2014; Hill et al., 2015; Biesecker et al., 2016; Mishra et al., 2016; Nelson et al., 2016; Wei et al., 2016; Bertlich et al., 2017; Kisler et al., 2017b; Hartmann et al., 2018; Khennouf et al., 2018; Alarcon-Martinez et al., 2019; Nortley et al., 2019). Recent optogenetic studies expressing light-sensitive channelrhodopsin-2 (ChR2) cation channels in mouse pericytes, however, were not conclusive. One using a chondroitin sulfate proteoglycan 4 (*Cspg4*) Cre-ChR2 mouse model did not show pericyte contractility after light stimulus (Hill et al., 2015), whereas the other one that used a platelet-derived growth factor receptor-β (*Pdgfrb*)-ChR2 mouse model demonstrated pericyte contractility (Hartmann et al., 2017, 2018). Another recent report suggested that capillaries do not dilate in response to neuronal stimulation, implying that pericytes do not control capillary diameter, although stimulation increased red blood cell (RBC) capillary flow (Wei et al., 2016).

Since two-photon optogenetics provides a powerful tool for studying the mechanisms of blood flow regulation at the level of brain capillaries, we re-examined the contractility of brain pericytes *in vivo* using a new optogenetic model developed by crossing our new inducible pericyte-specific CreER mouse line (Nikolakopoulou et al., 2019) with ChR2 mice (Madisen et al., 2012). We induced the expression of ChR2 in pericytes by tamoxifen, activated ChR2 by 488 nm excitation light, and monitored pericyte contractility, brain capillary diameter changes, and RBC flow velocity in aged mice by *in vivo* two-photon microscopy. Since many studies have shown that a rise in intracellular calcium causes pericytes to contract (Wu et al., 2003; Kawamura et al., 2004; Peppiatt et al., 2006; Yamanishi et al., 2006; Dai et al., 2009; Khennouf et al., 2018; Alarcon-Martinez et al., 2019), we hypothesized that light-induced excitation of ChR2 in pericytes *in vivo* will depolarize pericytes causing them to contract and constrict the underlying capillary, which in turn will reduce the capillary flow of RBCs.

MATERIALS AND METHODS

Mice

We utilized a recently developed and characterized pericyte-specific CreER mouse line generated by a double-promoter strategy using a combination of *Pdgfrb* and *Cspg4* promoters to drive CreER expression in pericytes (Nikolakopoulou et al., 2019). Briefly, *Pdgfrb* and *Cspg4* transgenic constructs were generated, one expressing Flippase recombinase (Flp) under the control of the *Pdgfrb* promoter, and the other carrying an Frt-Stop-Frt-CreER cassette (Frt: flippase recognition target; CreER: recombinant protein between Cre recombinase and a mutated ligand binding domain of the estrogen receptor) under the control of the *Cspg4* promoter (Nikolakopoulou et al., 2019). To test pericyte contractility, we utilized ChR2, a non-selective cation channel permeable to sodium, potassium and calcium that opens upon stimulation with 488 nm light and depolarizes the cell (**Figure 1A**). ChRs were initially used as tools to depolarize neuronal membranes (Zhang et al., 2006, 2007), but have also been used to study contractility of non-neuronal cells such as SMCs (Hill et al., 2015), cardiac myocytes (Johnston et al., 2017), and brain pericytes (Hill et al., 2015; Hartmann et al., 2017, 2018). We crossed pericyte-CreER mice (Nikolakopoulou et al., 2019) with mice that have a loxP-flanked STOP cassette that is excised in the presence of Cre to drive ChR2-EYFP fusion protein expression (Ai32, The Jackson Laboratory; **Figure 1B**). The progeny mice were termed pericyte-CreER; ChR2. Upon four consecutive daily injections of tamoxifen (40 mg/kg i.p.), approximately 40% of pericytes expressed Cre, as previously reported (Nikolakopoulou et al., 2019). ChR2 was expressed primarily in pericytes as shown by co-localization of ChR2-EYFP fusion protein with CD13+ pericytes on brain tissue sections 2 weeks after the last tamoxifen injection (**Figure 1C**), which was also visualized *in vivo* (**Figure 1D**, **Supplementary Video S1**).

Since neurovascular dysfunction is typically observed in neurological disorders associated with aging, such as stroke

TABLE 1 | *In vitro* pericyte contractility.

Model	Preparation	Stimulus	Contraction	Reference
Bovine	Retina	Collagen gel matrix	Yes	Schor and Schor (1986)
Bovine	Retina	Cytochalasin B	Yes	Kelley et al. (1987)
Bovine	Retina	Adenosine triphosphate	Yes	Das et al. (1988)
Bovine	Retina	Histamine, serotonin, cyclic adenosine monophosphate	Yes	Kelley et al. (1988)
Bovine	Retina	Cholinergic and adrenergic agonists	Yes	Ferrari-Dileo et al. (1992)
Bovine	Retina	Sodium nitroprusside	Yes	Haefliger et al. (1994)
Rat	Retina	Angiotensin II and histamine	Yes	Murphy and Wagner (1994)
Bovine	Retina	Angiotensin II	Yes	Matsugi et al. (1997b)
Bovine	Retina	Partial pressure of carbon dioxide, angiotensin II	Yes	Matsugi et al. (1997c)
Bovine	Retina	Adenosine	Yes	Matsugi et al. (1997a)
Bovine	Retina	Sodium nitroprusside	Yes	Haefliger et al. (1997)
Bovine	Retina	Partial pressure of carbon dioxide	Yes	Chen and Anderson (1997)
Bovine	Retina	Sodium nitroprusside	Yes	Haefliger et al. (2002)
Guinea pig	Cochlea	Potassium, calcium, norepinephrine	Yes	Dai et al. (2009)
Guinea pig	Cochlea	Extracellular lactate	Yes	Dai et al. (2011)
Human	Brain	Vasoactive peptide endothelin-1	Yes	Neuhaus et al. (2017)

TABLE 2 | *Ex vivo* pericyte contractility.

Model	Preparation	Stimulus	Contraction	Reference
Rat	Retina whole-mount	Angiotensin II, carbachol, bradykinin, histamine	Yes	Schönfelder et al. (1998)
Rat	Retina microvessels	Cholinergic agonists	Yes	Wu et al. (2003)
Rat	Retina microvessels	Adenosine triphosphate	Yes	Kawamura et al. (2003)
Rat	Retina microvessels	Angiotensin II	Yes	Kawamura et al. (2004)
Rat	Retina microvessels	Lactate	Yes	Yamanishi et al. (2006)
Rat	Retina whole-mount	Electrical stimulation or neurotransmitters	Yes	Peppiatt et al. (2006)
Rat	Cerebellar slices	Electrical stimulation or neurotransmitters	Yes	Hall et al. (2014)
Mouse	Brain slices	Thromboxane A2 agonist U46619	Yes	Fernández-Klett and Priller (2015)
Rat	Cortical slices	Thromboxane A2 agonist U46619	Yes	Mishra et al. (2016)
Rat	Retina whole-mount	Cannabinoid 2-arachidonoylglycerol and anandamide	Yes	Zong et al. (2017)
Rat	Spinal cord	Spinal cord injury	Yes	Li et al. (2017)
Mouse	Retina whole-mount	Electrical, P2Y-R agonist, nitric oxide donor, light	Yes	Ivanova et al. (2017)
Mouse	Retina whole-mount	Ischemia	Yes	Alarcon-Martinez et al. (2019)
Rat, Human	Cortical slices and surgically resected brain	Amyloid-beta$_{1-42}$ oligomers	Yes	Nortley et al. (2019)

TABLE 3 | *in vivo* pericyte contractility.

Model	Preparation	Stimulus	Contraction	Reference
Guinea pig	Cochlea	Potassium, calcium, norepinephrine	Yes	Dai et al. (2009)
Mouse	Cortex	Thromboxane A2 agonist U46619, cortical spreading depolarization	Yes	Fernández-Klett et al. (2010)
Guinea pig	Cochlea	Extracellular lactate	Yes	Dai et al. (2011)
Mouse	*in vivo*, cortex	Whisker stimulus	Yes	Hall et al. (2014)
Mouse	Cortex	Optogenic excitation of Channelrhodopsin-2	No	Hill et al. (2015)
Rat	Cortex	Forepaw stimulus	Yes	Mishra et al. (2016)
Mouse	Retina	Sensory stimulation	Yes	Biesecker et al. (2016)
Mouse	Cortex	Optogenic excitation of Channelrhodopsin-2	Yes	Hartmann et al. (2017, 2018)
Mouse	Cortex	Hind limb stimulus	No	Wei et al. (2016)
Guinea pig	Cochlea	Tumor necrosis factor	Yes	Bertlich et al. (2017)
Mouse	Somatosensory cortex	Hind limb stimulus	Yes	Kisler et al. (2017b)
Mouse	Cortex	Whisker pad stimulus or cortical spreading depolarization	Yes	Khennouf et al. (2018)
Mouse	Cortex	Amyloid-beta peptides	Yes	Nortley et al. (2019)
Mouse	Retina	Ischemia	Yes	Alarcon-Martinez et al. (2019)

and neurodegenerative diseases including Alzheimer's disease (Sweeney et al., 2018, 2019), we used 23–32-month-old mice in these studies. We also used 18 month old control mice that do not express ChR2. A 32-month-old mouse was only used to visualize ChR2YFP+ pericytes on lectin+ capillaries (**Figure 1D** and **Supplementary Video S1**) and was not used in any statistical analysis. All statistical analysis in pericyte-CreER; ChR2 mice in **Figures 2**, **3** was performed in 23-month-old mice. Both male and female animals were used for experiments. Mice were housed in plastic cages on a 12 h light cycle with *ad libitum*

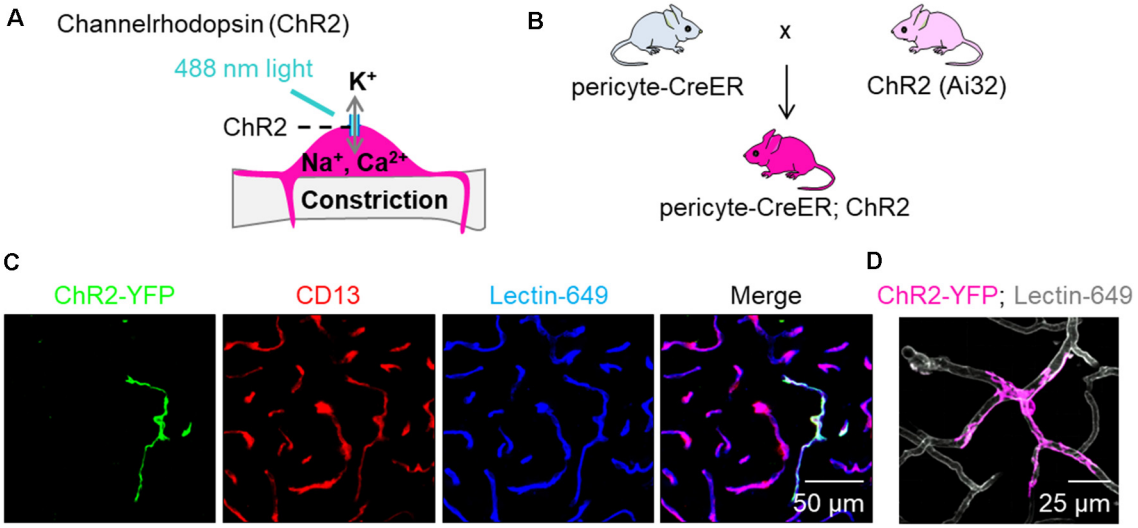

FIGURE 1 | Expression of channelrhodopsin (ChR2) in pericytes. **(A)** Schematic demonstrating our hypothesis that excitation of ChR2 expressing pericytes by 488 nm light will depolarize pericytes causing them to contract and constrict the underlying capillary. **(B)** Schematic showing the breeding scheme of recently characterized double promoter pericyte-CreER mice with tamoxifen inducible Cre-recombinase expression in pericytes, with mice that have a loxP-flanked STOP cassette that is excised in the presence of Cre to drive ChR2-EYFP fusion protein expression in pericytes (Ai32, Jackson Laboratory); the crossed mice were termed pericyte-CreER; ChR2. **(C)** Representative images of EYFP expression (green) showing co-localization of ChR2 cation channels with CD13+ pericytes (red) on Lectin-649+ capillary profiles (blue) in pericyte-CreER; ChR2 mice treated with tamoxifen (40 mg/kg i.p. daily for 4 days) and studied 2 weeks after the last tamoxifen injection. **(D)** *In vivo* z-stack maximum projection image demonstrating EYFP (pink) in a pericyte along lectin-649 + (gray) capillary profiles in a 32-month-old female pericyte-CreER; ChR2 mouse.

access to water and a standard laboratory diet. During *in vivo* surgery and experiments, body temperature was maintained with electric heating pads, with thermal feedback and respiration monitoring. Intraperitoneal injections of 5% glucose in isotonic saline (0.2 ml per 25 g) were administered every 2 h. Experiments were performed under isoflurane anesthesia (SomnoSuite, Kent Scientific), unless otherwise specified. For details, see specific experiments below.

Cranial Window Implantation

Mice were initially anesthetized with 100 mg/kg of ketamine and 50 mg/kg of xylazine and fixed in a stereotaxic frame (Kopf Instruments). A circular cranial window was drilled over the hindlimb region of the somatosensory cortex (center at AP = −0.94 mm, *L* = 1.5 mm) and the underlying dura was removed. To visualize pericytes in control mice that did not express ChR2 or YFP, 50–100 µl of NeuroTrace 500/525 dye [1:25 dilution in sterile artificial cerebrospinal fluid (aCSF)] was applied topically to the exposed cortical surface of the open cranial window for 5 min, then thoroughly washed with sterile aCSF (Damisah et al., 2017). The window was filled with sterile aCSF and covered with a 3-mm round coverslip. Mice were transitioned to isoflurane following cranial window implantation.

In vivo Multiphoton and Confocal Microscopy

In these studies, we used a Nikon A1R multiphoton and confocal microscopy system with NIS-Elements software control (25× objective, 1.1 numerical aperture, point spread function is 0.300 µm). For *in vivo* multiphoton imaging mice were anesthetized with 0.9% isoflurane. The vasculature was labeled *via* retro-orbital injection of 75 µl of 70 kDa Texas Red-dextran (0.1 ml of 10 mg/ml) or DyLight 649 labeled Lycopersicon Esculentum (Tomato) Lectin (1 mg/ml, DL-1178, Vector Labs) and imaged through the cranial window. In control mice not expressing ChR2, we utilized a previously described fluoro-Nissl dye that labels capillary pericyte somas that are alpha-smooth muscle cell actin (α-SMA)-negative (Damisah et al., 2017) to visualize and stimulate capillaries with a pericyte, including the soma. *In vivo* images were acquired at depths up to 200 µm below the pial surface using a mode-locked Ti:sapphire laser (Insight DS+; Spectra Physics) set to 950 nm (power ∼10 mW) for EYFP and Texas Red excitation. The image acquisition area (512 × 64 pixels) was restrained to maintain high spatial resolution (0.12 µm/pixel) and a fast frame rate (118.2 frames per second) to accurately measure RBC flow changes. Glucose in isotonic saline 5% weight/volume solution (200 µl/25 g mouse) was applied every 2 h i.p. for the duration of experiment, as we previously reported (Kisler et al., 2018).

Pericyte Stimulation

A region of interest was identified and set as the stimulation area by the NIS-Elements software to outline the pericytes on the capillary segment in the visible field. Concurrently with multiphoton imaging, 488 nm light excitation from the confocal microscope laser source (power ∼2.5 mW)

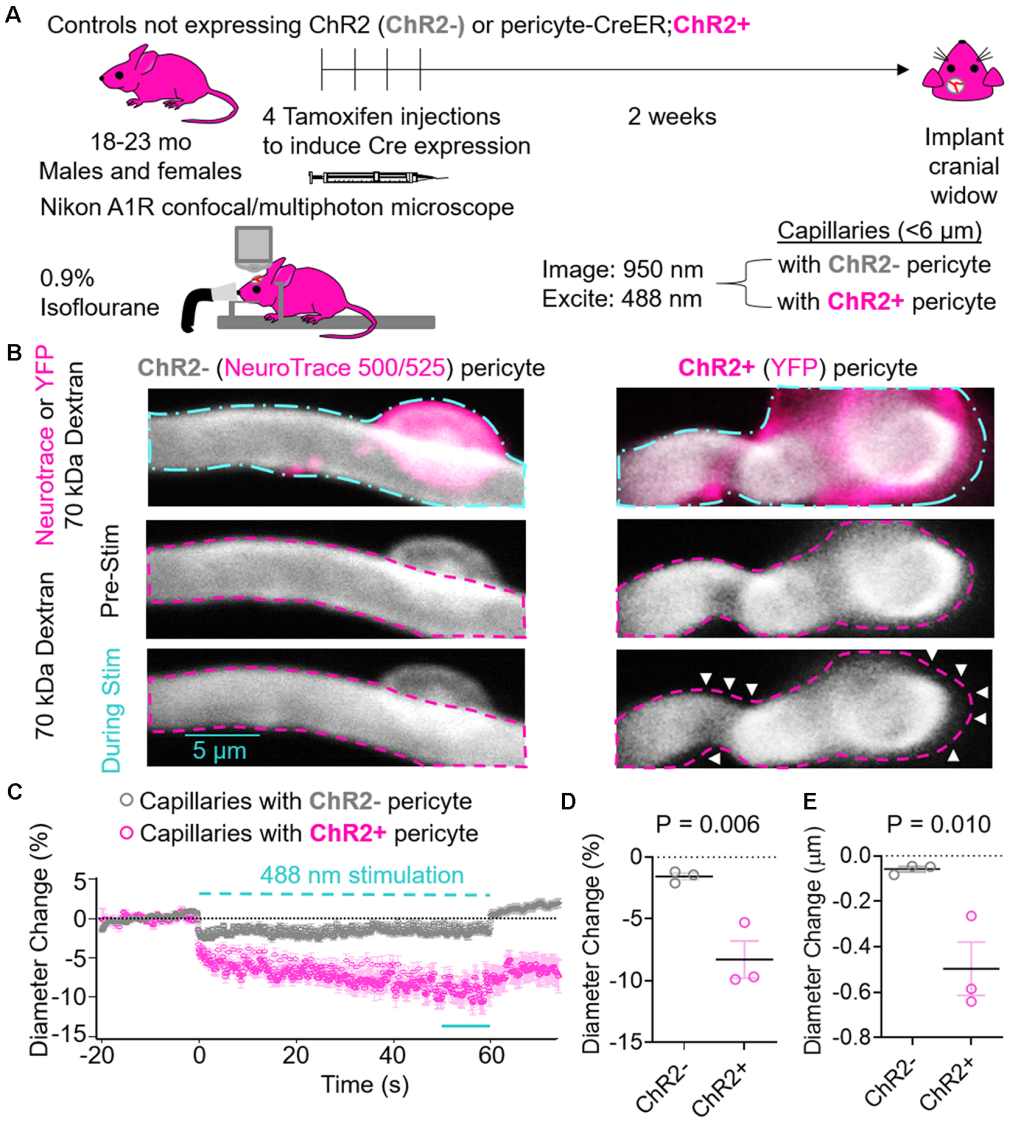

FIGURE 2 | Effects of ChR2 excitation in pericytes on the underlying capillary diameter. **(A)** Schematic of experimental paradigm. Control mice not expressing ChR2 (ChR2−; 18-month old, two males, one female, *n* = 3) or Pericyte-CreER; ChR2 (ChR2+; 23-month old, two males and one female, *n* = 3) mice received four consecutive tamoxifen injections (40 mg/kg i.p. daily), and 2 weeks later cranial windows were implanted and imaging was performed on a Nikon A1R confocal/multiphoton microscope under light anesthesia using 0.9% isofluorane. We used 950 nm light for imaging and 488 nm light for excitation of ChR2 cation channels. Capillaries (<6 µm) with ChR2− or ChR2+ pericytes were imaged before, during, and after light stimulus. **(B)** Representative images of capillaries with ChR2− pericytes visualized by NeuroTrace 500/525 (left) and ChR2+ pericytes visualized by YFP expression (right). The cyan dashed line (top panels) indicates regions of interest stimulated with 488 nm light, and the fuschia dashed lines indicate the capillary diameters before stimulation. White arrows indicate areas of capillary constriction. **(C)** Average time courses by mouse of capillary diameter changes of capillaries covered with ChR2− pericytes (gray circles) or ChR2+ pericytes (fuschia circles). Each single point along the time axis represents mean ± SEM, from *n* = 25 capillaries with ChR2+ pericytes from three pericyte-CreER; ChR2 mice and *n* = 29 capillaries with ChR2− pericytes from three control mice not expressing ChR2. Capillary diameter before stimulation was arbitrarily taken as zero (0). The dashed cyan line indicates the 60 s 488 nm stimulation period. The unbroken cyan line indicates the 10 s period quantified in panels **(D,E)**. **(D)** Quantification of relative mean capillary diameter change (%) by mouse for ChR2− (gray circles) vs. ChR2+ pericyte (fuschia circles) capillaries over the last 10 s period during stimulation indicated in **(C)**. **(E)** Quantification of absolute mean capillary diameter change (µm) by mouse for ChR2− (gray circles) vs. ChR2+ (fuschia circles) pericyte capillaries over the last 10 s period during stimulation indicated in **(C)**. In **(D,E)** mean ± SEM, individual values averaged per mouse derived from *n* = 25–29 pericyte-covered capillaries from three mice per group. *P* = 0.006 and 0.010, respectively by one-tailed student's *t*-test.

was triggered using a set protocol which consisted of a 20 s baseline (no 488 nm illumination), followed by 40 s of 488 nm stimulation (0.1 s duration, 1 s intervals). We did not collect topological information about where the stimulated capillaries were located, but since our pericyte-CreER line and the NeuroTrace dye labeled SMA-negative pericytes on capillaries (<6 µm), the stimulated cells were likely mid-capillary pericytes.

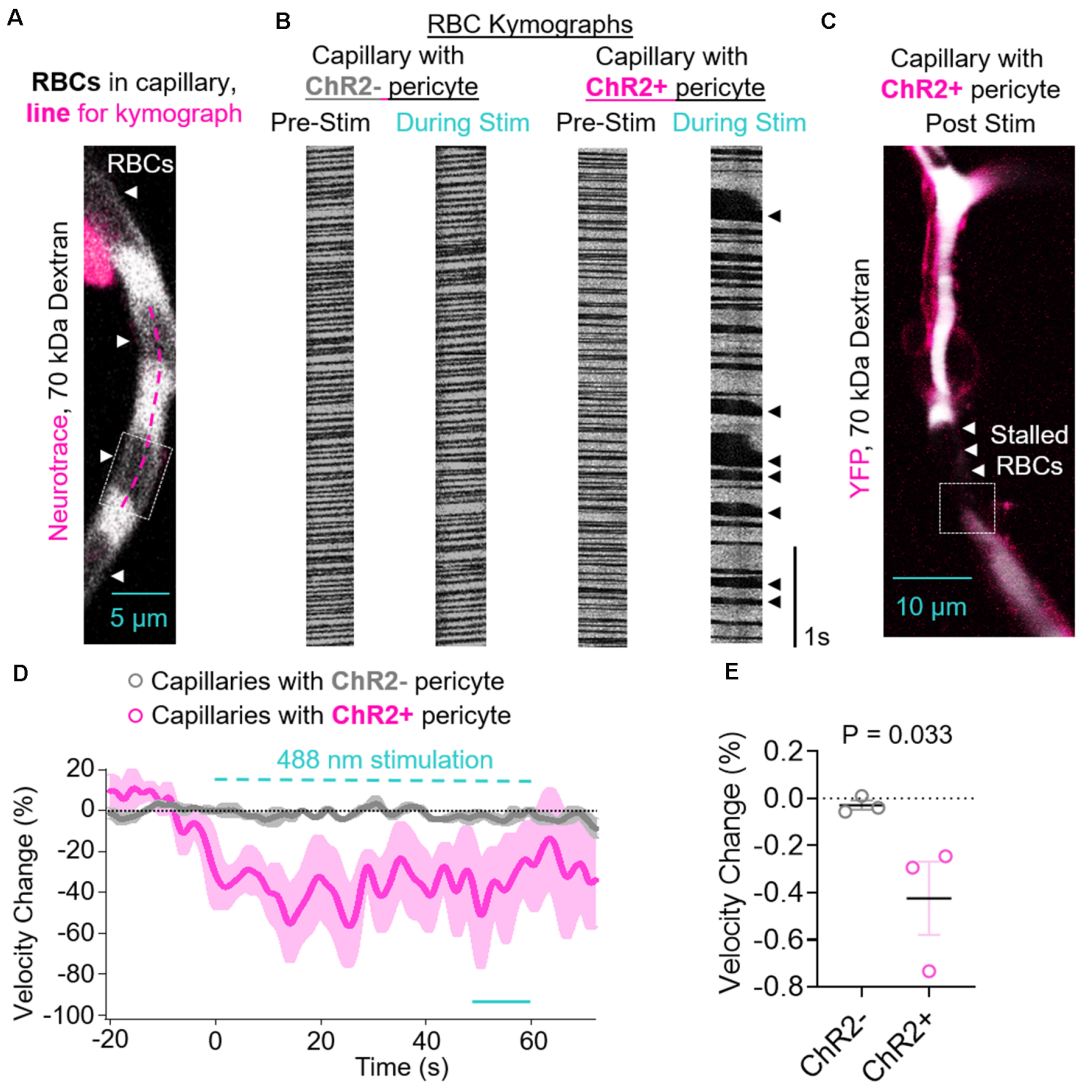

FIGURE 3 | Contraction of ChR2-positive pericytes leads to reduced capillary red blood cell (RBC) velocity. **(A)** Representative image of a capillary with a ChR2− pericyte demonstrating how RBCs are visualized in locations that are not 70 kDa dextran-positive, and an example line for a kymograph drawn along the length of the capillary (fuschia dashed line). The dashed box indicates the location shown in **Supplementary Video S2**. **(B)** Representative RBC kymographs acquired pre-stimulation and during light stimulation (488 nm) of capillaries with a ChR2− or ChR2+ pericyte. Black arrows indicate areas of slowed or stalled RBC flow. **(C)** Representative lower magnification image of the vessel segment with ChR2+ pericyte visualized in panel **(B)** showing stalled RBC in brain capillaries after stimulation of ChR2+ pericytes. The dashed box indicates the location shown in **Supplementary Video S3**. **(D)** Average time courses by mouse of capillary RBC velocity changes for capillaries covered with ChR2− pericytes (gray circles) or ChR2+ pericytes (fuschia circles). Each single point along the time axis represents the mean ± SEM, from n = 26 capillaries with ChR2− pericytes from three control mice that do not express ChR2 and n = 14 capillaries with ChR2+ pericytes from three pericyte-CreER; ChR2 mice. RBC velocity before stimulation was arbitrarily taken as zero (0). The dashed cyan line indicates the 60 s 488 nm stimulation period. The unbroken cyan line indicates the 10 s period during stimulation quantified in panel **(E)**. **(E)** Quantification of mean reduction in capillary RBC velocity (%) by mouse for ChR2− (gray circles) vs. ChR2+ pericyte (fuschia circles) capillaries over the last 10 s period during stimulation indicated in **(D)**. Mean ± SEM, individual values averaged per mouse derived from n = 14–26 pericyte-covered capillaries from three mice per group. P = 0.033, by one-tailed student's t-test.

Capillary Diameter Measurements

For diameter measurements, images of the 70 kDa Texas Red-dextran signal were taken using the resonance scanner at 60–120 frames per second, generating an image of the vessel over time. Using NIS-Element-Advanced Research software, 3–5 lines were drawn perpendicular to the capillary equidistant along the length of the vessel approximately 5–10 µm apart to generate a kymograph, where the vessel diameter was recorded as a line of pixels in one axis, and time in the other, as we previously reported (Kisler et al., 2018). We did not measure diameter directly under the soma of pericytes in either ChR2+ or ChR2− mouse capillaries due to NeuroTrace dye fluorescence bleed through of the pericyte soma signal in ChR2− mice. Each kymograph was thresholded and analyzed with custom protocols written in Igor Pro 6 (WaveMetrics), as we previously reported (Kisler et al., 2018): first, images were smoothed with a 3 × 3 pixel

Gaussian filter to remove noise and thresholded using the Igor Pro built-in "fuzzy entropy" threshold routine to generate a black-and-white (binary) image of the vessel diameter vs. time. The Igor Pro custom analysis protocol identified the transitions between black/white and white/black in each line of the image, indicating the edges of the vessel, and then calculated the width of the vessel for each line in the image. The resulting diameter data were low-pass filtered (1 Hz cut off) and notch filtered (0.5 Hz), then smoothed with a 1 s window box filter. Vessels with basal diameter <6 μm were considered capillaries. Basal diameters were calculated as an average over 20 s prior to stimulus, with basal diameters set to zero. For each capillary, 3–5 lines were averaged together to represent an individual capillary diameter. Diameter changes during stimulus were determined as a percent of basal diameter. For statistical comparisons, the percentage average diameter changes (**Figure 2D**) and absolute mean diameter changes (**Figure 2E**) over the last 10 s of stimulation (50–60 s after stimulation start) of individual values averaged per mouse from ChR2+ pericyte capillaries were calculated and statistically compared to ChR2− pericytes from $n = 25–29$ pericyte-covered capillaries from three mice per group.

Red Blood Cell (RBC) Velocity Measurements

For RBC velocity, only 70-kDa Texas Red-dextran was used for imaging. Kymographs were generated parallel to each capillary along the vessel midline. RBCs appear as dark spots in the dye-labeled blood plasma. Velocity data were analyzed using a MatLab algorithm as previously described (Kim et al., 2012; Kisler et al., 2018) and then low-pass filtered (1 Hz cut off) and notch filtered (0.5 Hz), then box filtered with a 1 s window to remove heartbeat and breathing artifacts using custom written protocols in Igor Pro to automate the filtering process, as we previously described (Kisler et al., 2018). Basal RBC velocities were calculated as an average over 20 s prior to stimulus, with individual basal capillary RBC velocities set to zero. RBC velocity changes during stimulus were determined as a percentage of basal velocity. For comparison in **Figure 3E**, individual values were averaged per mouse from ChR2+ and ChR2− pericyte capillary RBC velocities over the last 10 s of stimulation (averaging between 50 s and 60 s after stimulation start) were used to determine the average velocity change during stimulus and statistically compared.

Immunohistochemistry of ChR2-EYFP Protein Co-localization With Pericytes

Mice were anesthetized with 4% isoflurane and then transcardially perfused with 50 ml of phosphate buffered saline containing ethylenediaminetetraacetic acid. Brains were removed and embedded into O.C.T. compound (Tissue-Tek) on dry ice. They were cryosectioned at a thickness of 18 μm. The sections were cut sagittally and those from depths of 50–150 μm, to coincide with TPLSM imaging depths, were used for assessment. The sections were subsequently blocked with 5% normal donkey serum (Vector Laboratories) and Triton (0.05%) for 1 h and incubated in goat anti-CD13 (1:200) primary antibody (Kisler et al., 2017b) diluted in donkey serum blocking solution overnight at 4°C. To visualize CD13+ pericytes, donkey anti-goat IgG, Alexa 568 (1:500; Invitrogen, A-11057) secondary antibody was used for incubation for 1.5 h at room temperature. To visualize brain microvessels, sections were incubated with fluorescein-conjugated L. esculentum lectin (Vector Laboratories FL-1171, 1:200). In each animal five randomly selected fields from the cortex were analyzed in six nonadjacent sections (∼100 μm apart).

Statistics

Since ChR2-positive and ChR2-negative capillaries were assessed within the same animals, experiments were analyzed, but not performed, in a blinded fashion. Sample sizes were calculated using nQUERY assuming a two-sided α-level of 0.05, 80% power, and homogenous variances for the two samples to be compared, with the means and common s.d. for different parameters predicted from published data (Peppiatt et al., 2006; Hall et al., 2014; Mishra et al., 2016; Nortley et al., 2019) and our previous studies (Kisler et al., 2017b, 2018). Using nQUERY, we calculated that a sample size of three mice in each group will have 80% power to detect a difference in means of 6% diameter change (the difference between a Group 1 mean of 8% and a Group 2 mean of 2%) assuming that the common standard deviation is 2 using a two group *t*-test with a 5% one-sided significance level. Thus, we used three mice per group. Individual values in each mouse are averaged from $n = 14–29$ pericyte-covered capillaries. All data are expressed as mean ± SEM. Normality was determined with a Shapiro–Wilk test, and statistical significance was determined by a one-tailed student's *t*-test (GraphPad Prism 8.1). The accepted level of statistical significance was $P \leq 0.05$.

RESULTS

Excitation of ChR2-Positive Pericytes Contracts the Cell and Constricts the Underlying Capillary

Pericyte-CreER; ChR2 mice at 23 months of age and control mice not expressing ChR2 at 18 months of age were administered daily tamoxifen (40 mg/kg i.p.) for four consecutive days. Approximately 2 weeks later, cranial windows were implanted over the hindlimb somatosensory cortex. Mice were fixed in a stereotaxic frame under 0.9% isoflourane anesthesia and imaged with 950 nm light. Capillaries defined as vessels <6 μm in diameter with ChR2− or ChR2+ pericytes were imaged and stimulated on a Nikon A1R confocal and multiphoton microscope, and the diameter of the underlying capillary was measured (**Figure 2A**). Intermittent 60 s stimulation with 488 nm light caused ChR2+ pericytes to contract and constrict the underlying capillary resulting in a significant reduction in capillary diameter compared to capillaries with ChR2− pericytes (**Figures 2B,C**, **Supplementary Videos S2, S3**). The kinetics of the constriction during light stimulation had a rapid phase within the first few seconds in both capillaries with ChR2− and ChR2+ pericytes, though to a much greater degree in capillaries with ChR2+ pericytes. There was also a slower phase of contraction over tens of seconds occurring in capillaries with ChR2+

pericytes (**Figure 2C**). Previous studies have shown light-induced stimulation and contraction of neurovascular SMCs resulted in constriction of the underlying arteriole (Choi et al., 2010; Kimbrough et al., 2015). Therefore, it is possible that pericytes, or perhaps endothelial cells, have similar light-induced capabilities causing contraction possibly explaining why we observed a small diameter decrease in capillaries with ChR2− pericytes. Excitation of ChR2+ pericytes resulted in an 8.29 ± 1.51% and 0.50 ± 0.01 μm decrease in capillary diameter compared to baseline values, whereas ChR2− pericytes stimulated in a similar way showed only a small decrease in capillary diameter of 1.56 ± 0.47% and 0.06 ± 0.02 μm (**Figures 2D,E**; mean ± SEM; $p = 0.006$ and 0.010, respectively).

Pericyte Contraction Leads to Reduced RBC Velocity

Since, we found a significant decrease after light stimulation in the capillary diameter in capillaries covered with ChR2+ pericytes, we next studied if RBC flow was affected after pericyte stimulation. The contraction of ChR2+ pericytes upon 488 nm stimulation and constriction of the underlying capillary led to a reduction in RBC velocity compared to the velocity before stimulation (**Figures 3A–D**). This was visualized by irregular RBCs kymographs (**Figure 3B**) and stalled RBCs appeared as black gaps in the white pseudo colored 70 kDa Texas red-dextran in the capillary after ChR2 excitation (**Figure 3C**). RBC velocity was decreased during light stimulation in capillaries with ChR2+ pericytes, with minimal changes observed in ChR2− capillaries, averaged by mouse (**Figure 3D**). Compared to ChR2− pericytes, there is greater variability in RBC velocity change during stimulation of ChR2+ pericyte capillaries as in some capillaries the RBC flow not only slows down but also stalls and occasionally speeds up, possibly due to backlogged pressure in the stalled vessels (**Figure 3D**). Upon excitation of ChR2+ pericytes, RBC capillary velocity was reduced resulting in an average reduction of 42.44 ± 15.55% compared to the respective RBC velocity values before excitation, and significantly reduced compared to the excitation of ChR2− pericytes (**Figure 3E**, mean + SEM; $p = 0.03$).

DISCUSSION

Using two-photon optogenetics and our new pericyte-CreER; ChR2 mouse line (**Figure 1**), here we show that pericytes contract brain capillary diameter and regulate capillary blood flow in the aging mouse brain. Our findings are consistent with the majority of previous studies suggesting that pericytes are contractile cells that control CBF, including studies using isolated brain, retinal and cochlear pericytes (see fully referenced **Table 1**), *ex vivo* cerebellar, cerebral and spinal cord slices, and retinal microvessels or explants (see fully referenced **Table 2**), and *in vivo* studies in rodents (see fully referenced **Table 3**). The present study shows that light excitation of the ChR2 cation channel in pericytes directly leads to their contraction on brain capillaries <6 μm in diameter, which in turn leads to constriction of the underlying capillary and a significant 8% decrease in capillary diameter (**Figure 2**) accompanied by a 42% reduction in RBC flow during stimulation including some capillaries with stalled RBCs flow (**Figure 3**).

That pericytes are contractile cells is supported by single-cell RNAseq studies showing that mouse pericytes express several genes encoding for contractile proteins such as vimentin, desmin, titin, myosin heavy chains 9, 10 and 11, and myosin light chains 6, 9, 12a, and 12b, and other myosin genes (Myo1c, 1d, 5a, 6, 10 and 18a; He et al., 2018; Vanlandewijck et al., 2018). It has been debated whether or not pericytes can express low levels of α-SMA as this is typically considered as an SMC contractile protein (Hill et al., 2015; He et al., 2018; Vanlandewijck et al., 2018). Interestingly, it has been shown that the detection of α-SMA in capillary pericytes by immunostaining requires prevention of filamentous actin depolymerization, which when controlled, shows detectable levels of α-SMA protein in pericytes (Alarcon-Martinez et al., 2018). Nonetheless, a recent study suggested that optogenetic stimulation of pericytes lacking α-SMA produces a decrease in capillary diameter in the living mouse brain (Hartmann et al., 2018), supporting the concept that contractile proteins other than α-SMA can mediate pericyte contraction. Furthermore, our results provide evidence that α-SMA-negative pericytes likely use some alternative contractile mechanism to alter capillary tone. Altogether, these studies suggest that pericytes express contractile protein machinery that is different from SMCs. This, again, is consistent with their role in regulating blood flow in capillary vessels with a much narrower diameter compared to arterioles and small arteries, which might require a more robust contractile protein system. The exact role of proteins that mediate pericyte contraction remains, however, unclear at present. This could possibly be determined by future studies using our new pericyte-CreER model to delete specific pericyte genes encoding different contractile proteins from the brain.

A recent optogenetic study using *Cspg4*-driven ChR2 expression found that SMCs, but not pericytes, contract upon ChR2 stimulation (Hill et al., 2015). Although it is not entirely clear why this earlier study (Hill et al., 2015) was not able to show that pericytes contract after ChR2 excitation, there are several possibilities that could potentially account for the differences between the previous and the present study. It has been found that SMCs and pericytes express different contractile proteins and calcium channels (Kisler et al., 2017a; Vanlandewijck et al., 2018). This raises a possibility that a threshold for the optogenetic stimulation of ChR2 between SMCs and pericytes linked to contractility could also be different and might depend on the source and duration of the light stimulus. With regards to the potential differences in sensitivity to ChR2 stimulation between SMCs and pericytes, future studies should investigate the threshold of ChR2 stimulation between these two cell types with concurrently expressing genetically encoded calcium indicators, such as GCaMP6, to measure how much intracellular calcium rise is required to induce contractility in each of these two cell types vs. the duration and source of light stimulus.

Furthermore, we used 0.9% isoflurane, the minimum dose required to lightly anesthetize mice during our experiments to reduce potential off-target effects of anesthesia. Previous

studies have shown that inhaled anesthetics have neurovascular effects. For example, 1–3% sevoflurane, but not 1–3% isoflurane, increases BBB breakdown in aged rats (Acharya et al., 2015). Furthermore, 2% isoflurane has vasomotor effects that either constricts or dilates vessels depending on the tone of vessels at the time of administration (Park et al., 1998). Hill et al. (2015) used ketamine/xylazine anesthetic during ChR2 imaging experiments, which increases blood flow by vasodilation (Oren et al., 1987) and alters neuronal function impairing neurovascular coupling (Masamoto and Kanno, 2012). Future studies should evaluate the impact of ChR2 excitation of pericytes in awake mice.

Other factors such as the resolution of the microscope may also play a role in detecting pericyte contractility and diameter changes since the resting diameter of arteries and arterioles is quite large, and the contractility of SMCs and alteration of the underlying vessel diameter is much larger and easier to detect compared to the resting diameter of capillaries. Thus, observing significant changes in capillary diameter requires higher resolution and carefully considered experimental and statistical design, as previously discussed (Kisler et al., 2018). Recent *in vivo* studies reported that hindlimb or forepaw stimulation for 10 s (Mishra et al., 2016; Kisler et al., 2017b) and whisker pad stimulation for 15 s (Hall et al., 2014) both lead to capillary dilation ahead of arterioles, which resulted from isotonic pericyte relaxation and correlated with the degree of pericyte coverage. On the other hand, a reduced time of whisker pad stimulation of 2 s was not sufficient to produce changes in capillary diameter despite producing an increase in RBCs capillary flow (Wei et al., 2016); this could possibly result from an initial isometric relaxation of pericytes that with longer stimulation as used in other studies (Hall et al., 2014; Mishra et al., 2016; Kisler et al., 2017b) converts into isotonic relaxation causing a detectable change in capillary diameter. Because the present study was focused on constrictive responses of pericytes, it would be difficult to make any direct comparison with previous studies focused on dilation of capillaries and relaxation of pericyte tone. However, future optogenetic studies using hyperpolarization models of pericytes expressing, for example, halorhodopsin (e.q. eNpHR3.0) or archaerhodopsin-3 (e.q. ArchT) channels (Madisen et al., 2012), should be able to directly address the relationship between pericyte relaxation and dilation of the underlying capillary.

Recent studies found that Alzheimer's amyloid-β (Aβ) oligomers induced pericytes to contract and constrict the underlying capillary in acute cerebral slices from rats and humans, and that capillaries covered with pericytes were typically constricted in Alzheimer's disease brains post-mortem (Nortley et al., 2019). Since pericyte contractility may provide the force for intramural periarterial drainage at the capillary level (Aldea et al., 2019) this could potentially impact periarterial drainage of Aβ (Diem et al., 2016) and/or its trans-vascular clearance across the BBB (Shibata et al., 2000; Deane et al., 2004; Nelson et al., 2017), or *via* meningeal lymphatic vessels (Da Mesquita et al., 2018). Future studies should therefore investigate how Aβ directly interacts with a receptor on brain pericytes to trigger contractility, and how this could influence perivascular flow, BBB and meningeal lymphatic clearance, and BBB integrity, given that early pericyte injury is shown to be an early independent biomarker of human cognitive dysfunction (Montagne et al., 2015; Nation et al., 2019).

Altogether, our findings show that pericytes contract *in vivo* and regulate capillary blood flow in the aging mouse brain which might have broader implications for the understanding of CBF regulation in the aging human brain, particularly in neurological diseases associated with pericyte loss, degeneration and neurovascular dysfunction. This includes disorders such as stroke, Alzheimer's disease and possibly other neurodegenerative diseases (Sweeney et al., 2018, 2019). Future studies should compare young vs. old mice to determine if there is an effect of aging on pericyte contractility. Furthermore, prospective studies should also provide a better understanding of how age-dependent pericyte dysfunction occurs in different neurological diseases, and whether pericytes can be targeted therapeutically to correct for neurovascular and neuronal dysfunction associated with these neurological disorders.

DATA AVAILABILITY STATEMENT

The datasets generated for this study are available on request to the corresponding author.

ETHICS STATEMENT

The animal study was reviewed and approved by Institutional Animal Care and Use Committee at the University of Southern California.

AUTHOR CONTRIBUTIONS

AN planned and performed *in vivo* imaging experiments, data analysis and prepared the manuscript. MS assisted in data analyses. YW performed cranial window surgeries. KK developed protocols for capillary diameter and red blood cells (RBC) velocity analysis and discussed results. BZ and ZZ co-developed the pericyte-CreER mouse model. BZ planned experiments and wrote the manuscript.

FUNDING

The work of AN is supported by National Institute of Health (NIH) grant No. K99AG058780. The work of BZ is supported by NIH grants Nos. RF1AG039452, R01AG023084, R01NS090904, R01NS034467, R01AG039452, R01NS100459, P01AG052350, and P50AG005142 in addition to the Alzheimer's Association grant No. 509279, Cure Alzheimer's Fund, and the Foundation Leducq Transatlantic Network of Excellence for the Study of Perivascular Spaces in Small Vessel Disease reference No. 16 CVD 05.

SUPPLEMENTARY MATERIAL

The Supplementary Material for this article can be found online at: https://www.frontiersin.org/articles/10.3389/fnagi.2020.00108/full#supplementary-material.

REFERENCES

Acharya, N. K., Goldwaser, E. L., Forsberg, M. M., Godsey, G. A., Johnson, C. A., Sarkar, A., et al. (2015). Sevoflurane and Isoflurane induce structural changes in brain vascular endothelial cells and increase blood-brain barrier permeability: possible link to postoperative delirium and cognitive decline. *Brain Res.* 1620, 29–41. doi: 10.1016/j.brainres.2015.04.054

Alarcon-Martinez, L., Yilmaz-Ozcan, S., Yemisci, M., Schallek, J., Kılıç, K., Can, A., et al. (2018). Capillary pericytes express α-smooth muscle actin, which requires prevention of filamentous-actin depolymerization for detection. *Elife* 7:e34861. doi: 10.7554/eLife.34861.

Alarcon-Martinez, L., Yilmaz-Ozcan, S., Yemisci, M., Schallek, J., Kılıç, K., Villafranca-Baughman, D., et al. (2019). Retinal ischemia induces α-SMA-mediated capillary pericyte contraction coincident with perivascular glycogen depletion. *Acta Neuropathol. Commun.* 7:134. doi: 10.1186/s40478-019-0761-z

Aldea, R., Weller, R. O., Wilcock, D. M., Carare, R. O., and Richardson, G. (2019). Cerebrovascular smooth muscle cells as the drivers of intramural periarterial drainage of the brain. *Front. Aging Neurosci.* 11:1. doi: 10.3389/fnagi.2019.00001

Attwell, D., Mishra, A., Hall, C. N., O'Farrell, F. M., and Dalkara, T. (2016). What is a pericyte? *J. Cereb. Blood Flow Metab.* 36, 451–455. doi: 10.1177/0271678X15610340

Bertlich, M., Ihler, F., Weiss, B. G., Freytag, S., Strupp, M., and Canis, M. (2017). Cochlear pericytes are capable of reversibly decreasing capillary diameter *in vivo* after tumor necrosis factor exposure. *Otol. Neurotol.* 38, e545–e550. doi: 10.1097/mao.0000000000001523

Biesecker, K. R., Srienc, A. I., Shimoda, A. M., Agarwal, A., Bergles, D. E., Kofuji, P., et al. (2016). Glial cell calcium signaling mediates capillary regulation of blood flow in the retina. *J. Neurosci.* 36, 9435–9445. doi: 10.1523/JNEUROSCI.1782-16.2016

Chen, Q., and Anderson, D. R. (1997). Effect of CO_2 on intracellular pH and contraction of retinal capillary pericytes. *Invest. Ophthalmol. Vis. Sci.* 38, 643–651.

Choi, M., Yoon, J., and Choi, C. (2010). Label-free optical control of arterial contraction. *J. Biomed. Opt.* 15:015006. doi: 10.1117/1.3316404

Da Mesquita, S., Louveau, A., Vaccari, A., Smirnov, I., Cornelison, R. C., Kingsmore, K. M., et al. (2018). Functional aspects of meningeal lymphatics in aging and Alzheimer's disease. *Nature* 560, 185–191. doi: 10.1038/s41586-018-0368-8

Dai, M., Nuttall, A., Yang, Y., and Shi, X. (2009). Visualization and contractile activity of cochlear pericytes in the capillaries of the spiral ligament. *Hear. Res.* 254, 100–107. doi: 10.1016/j.heares.2009.04.018

Dai, M., Yang, Y., and Shi, X. (2011). Lactate dilates cochlear capillaries *via* type V fibrocyte-vessel coupling signaled by nNOS. *Am. J. Physiol. Heart Circ. Physiol.* 301, H1248–1254. doi: 10.1152/ajpheart.00315.2011

Damisah, E. C., Hill, R. A., Tong, L., Murray, K. N., and Grutzendler, J. (2017). A fluoro-Nissl dye identifies pericytes as distinct vascular mural cells during *in vivo* brain imaging. *Nat. Neurosci.* 20, 1023–1032. doi: 10.1038/nn.4564

Das, A., Frank, R. N., Weber, M. L., Kennedy, A., Reidy, C. A., and Mancini, M. A. (1988). ATP causes retinal pericytes to contract *in vitro*. *Exp. Eye Res.* 46, 349–362. doi: 10.1016/s0014-4835(88)80025-3

Deane, R., Wu, Z., Sagare, A., Davis, J., Du Yan, S., Hamm, K., et al. (2004). LRP/amyloid β-peptide interaction mediates differential brain efflux of Aβ isoforms. *Neuron* 43, 333–344. doi: 10.1016/j.neuron.2004.07.017

Diem, A. K., Tan, M., Bressloff, N. W., Hawkes, C., Morris, A. W. J., Weller, R. O., et al. (2016). A simulation model of periarterial clearance of amyloid-β from the brain. *Front. Aging Neurosci.* 8:18. doi: 10.3389/fnagi.2016.00018

Fernández-Klett, F., and Priller, J. (2015). Diverse functions of pericytes in cerebral blood flow regulation and ischemia. *J. Cereb. Blood Flow Metab.* 35, 883–887. doi: 10.1038/jcbfm.2015.60

Fernández-Klett, F., Offenhauser, N., Dirnagl, U., Priller, J., and Lindauer, U. (2010). Pericytes in capillaries are contractile *in vivo*, but arterioles mediate functional hyperemia in the mouse brain. *Proc. Natl. Acad. Sci. U S A* 107, 22290–22295. doi: 10.1073/pnas.1011321108

Ferrari-Dileo, G., Davis, E. B., and Anderson, D. R. (1992). Effects of cholinergic and adrenergic agonists on adenylate cyclase activity of retinal microvascular pericytes in culture. *Invest. Ophthalmol. Vis. Sci.* 33, 42–47.

Haefliger, I. O., Chen, Q., and Anderson, D. R. (1997). Effect of oxygen on relaxation of retinal pericytes by sodium nitroprusside. *Graefes Arch. Clin. Exp. Ophthalmol.* 235, 388–392. doi: 10.1007/bf00937289

Haefliger, I., Pedrini, M., and Anderson, D. R. (2002). Relaxing effect of CEDO 8956 and hydralazine HCl in cultured smooth muscle cells versus pericytes: a preliminary study. *Klin. Monbl. Augenheilkd.* 219, 277–280. doi: 10.1055/s-2002-30645

Haefliger, I. O., Zschauer, A., and Anderson, D. R. (1994). Relaxation of retinal pericyte contractile tone through the nitric oxide-cyclic guanosine monophosphate pathway. *Invest. Ophthalmol. Vis. Sci.* 35, 991–997.

Hall, C. N., Reynell, C., Gesslein, B., Hamilton, N. B., Mishra, A., Sutherland, B. A., et al. (2014). Capillary pericytes regulate cerebral blood flow in health and disease. *Nature* 508, 55–60. doi: 10.1038/nature13165

Hartmann, D. A., Grant, R. I., and Shih, A. Y. (2017). "*In vivo* optical imaging and manipulation of pericytes in the mouse brain," in *Optics in the Life Sciences Congress*. San Diego, CA: Optical Society of America. Available online at: https://www.osapublishing.org/abstract.cfm?uri=BRAIN-2017-BrW3B.1. Accessed April 13, 2020.

Hartmann, D., Grant, R. I., Harrill, S. A., Noonan, T., Lauer, A., and Shih, A. Y. (2018). Optogenetic stimulation of pericytes lacking α smooth muscle actin produces a decrease in capillary blood flow in the living mouse brain. *FASEB J.* 32:708. Available online at: https://www.fasebj.org/doi/abs/10.1096/fasebj.2018.32.1_supplement.708.1. Accessed April 13, 2020.

He, L., Vanlandewijck, M., Mäe, M. A., Andrae, J., Ando, K., Gaudio, F. D., et al. (2018). Single-cell RNA sequencing of mouse brain and lung vascular and vessel-associated cell types. *Sci. Data* 5:180160. doi: 10.1038/sdata.2018.160

Hill, R. A., Tong, L., Yuan, P., Murikinati, S., Gupta, S., and Grutzendler, J. (2015). Regional blood flow in the normal and ischemic brain is controlled by arteriolar smooth muscle cell contractility and not by capillary pericytes. *Neuron* 87, 95–110. doi: 10.1016/j.neuron.2015.06.001

Iadecola, C. (2017). The neurovascular unit coming of age: a journey through neurovascular coupling in health and disease. *Neuron* 96, 17–42. doi: 10.1016/j.neuron.2017.07.030

Ivanova, E., Kovacs-Oller, T., and Sagdullaev, B. T. (2017). Vascular pericyte impairment and connexin43 gap junction deficit contribute to vasomotor decline in diabetic retinopathy. *J. Neurosci.* 37, 7580–7594. doi: 10.1523/JNEUROSCI.0187-17.2017

Johnston, C. M., Rog-Zielinska, E. A., Wülfers, E. M., Houwaart, T., Siedlecka, U., Naumann, A., et al. (2017). Optogenetic targeting of cardiac myocytes and non-myocytes: tools, challenges and utility. *Prog. Biophys. Mol. Biol.* 130, 140–149. doi: 10.1016/j.pbiomolbio.2017.09.014

Kawamura, H., Kobayashi, M., Li, Q., Yamanishi, S., Katsumura, K., Minami, M., et al. (2004). Effects of angiotensin II on the pericyte-containing microvasculature of the rat retina. *J. Physiol.* 561, 671–683. doi: 10.1113/jphysiol.2004.073098

Kawamura, H., Sugiyama, T., Wu, D. M., Kobayashi, M., Yamanishi, S., Katsumura, K., et al. (2003). ATP: a vasoactive signal in the pericyte-containing microvasculature of the rat retina. *J. Physiol.* 551, 787–799. doi: 10.1113/jphysiol.2003.047977

Kelley, C., D'Amore, P., Hechtman, H. B., and Shepro, D. (1987). Microvascular pericyte contractility *in vitro*: comparison with other cells of the vascular wall. *J. Cell Biol.* 104, 483–490. doi: 10.1083/jcb.104.3.483

Kelley, C., D'Amore, P., Hechtman, H. B., and Shepro, D. (1988). Vasoactive hormones and cAMP affect pericyte contraction and stress fibres *in vitro*. *J. Muscle Res. Cell Motil.* 9, 184–194. doi: 10.1007/bf01773740

Khennouf, L., Gesslein, B., Brazhe, A., Octeau, J. C., Kutuzov, N., Khakh, B. S., et al. (2018). Active role of capillary pericytes during stimulation-induced activity and spreading depolarization. *Brain* 141, 2032–2046. doi: 10.1093/brain/awy143

Kim, T. N., Goodwill, P. W., Chen, Y., Conolly, S. M., Schaffer, C. B., Liepmann, D., et al. (2012). Line-scanning particle image velocimetry: an optical approach for quantifying a wide range of blood flow speeds in live animals. *PLoS One* 7:e38590. doi: 10.1371/journal.pone.0038590

Kimbrough, I. F., Robel, S., Roberson, E. D., and Sontheimer, H. (2015). Vascular amyloidosis impairs the gliovascular unit in a mouse model of Alzheimer's disease. *Brain J. Neurol.* 138, 3716–3733. doi: 10.1093/brain/awv327

Kisler, K., Lazic, D., Sweeney, M. D., Plunkett, S., El Khatib, M., Vinogradov, S. A., et al. (2018). *In vivo* imaging and analysis of cerebrovascular hemodynamic responses and tissue oxygenation in the mouse brain. *Nat. Protoc.* 13, 1377–1402. doi: 10.1038/nprot.2018.034

Kisler, K., Nelson, A. R., Montagne, A., and Zlokovic, B. V. (2017a). Cerebral blood flow regulation and neurovascular dysfunction in Alzheimer disease. *Nat. Rev. Neurosci.* 18, 419–434. doi: 10.1038/nrn.2017.48

Kisler, K., Nelson, A. R., Rege, S. V., Ramanathan, A., Wang, Y., Ahuja, A., et al. (2017b). Pericyte degeneration leads to neurovascular uncoupling and limits oxygen supply to brain. *Nat. Neurosci.* 20, 406–416. doi: 10.1038/nn.4489

Li, Y., Lucas-Osma, A. M., Black, S., Bandet, M. V., Stephens, M. J., Vavrek, R., et al. (2017). Pericytes impair capillary blood flow and motor function after chronic spinal cord injury. *Nat. Med.* 23, 733–741. doi: 10.1038/nm.4331

Madisen, L., Mao, T., Koch, H., Zhuo, J., Berenyi, A., Fujisawa, S., et al. (2012). A toolbox of Cre-dependent optogenetic transgenic mice for light-induced activation and silencing. *Nat. Neurosci.* 15, 793–802. doi: 10.1038/nn.3078

Masamoto, K., and Kanno, I. (2012). Anesthesia and the quantitative evaluation of neurovascular coupling. *J. Cereb. Blood Flow Metab.* 32, 1233–1247. doi: 10.1038/jcbfm.2012.50

Matsugi, T., Chen, Q., and Anderson, D. R. (1997a). Adenosine-induced relaxation of cultured bovine retinal pericytes. *Invest. Ophthalmol. Vis. Sci.* 38, 2695–2701.

Matsugi, T., Chen, Q., and Anderson, D. R. (1997b). Contractile responses of cultured bovine retinal pericytes to angiotensin II. *Arch. Ophthalmol.* 115, 1281–1285. doi: 10.1001/archopht.1997.01100160451011

Matsugi, T., Chen, Q., and Anderson, D. R. (1997c). Suppression of CO2-induced relaxation of bovine retinal pericytes by angiotensin II. *Invest. Ophthalmol. Vis. Sci.* 38, 652–657.

Mishra, A., Reynolds, J. P., Chen, Y., Gourine, A. V., Rusakov, D. A., and Attwell, D. (2016). Astrocytes mediate neurovascular signaling to capillary pericytes but not to arterioles. *Nat. Neurosci.* 19, 1619–1627. doi: 10.1038/nn.4428

Montagne, A., Barnes, S. R., Sweeney, M. D., Halliday, M. R., Sagare, A. P., Zhao, Z., et al. (2015). Blood-brain barrier breakdown in the aging human hippocampus. *Neuron* 85, 296–302. doi: 10.1016/j.neuron.2014.12.032

Murphy, D. D., and Wagner, R. C. (1994). Differential contractile response of cultured microvascular pericytes to vasoactive agents. *Microcirculation* 1, 121–128. doi: 10.3109/10739689409148267

Nation, D. A., Sweeney, M. D., Montagne, A., Sagare, A. P., D'Orazio, L. M., Pachicano, M., et al. (2019). Blood-brain barrier breakdown is an early biomarker of human cognitive dysfunction. *Nat. Med.* 25, 270–276. doi: 10.1038/s41591-018-0297-y

Nelson, A. R., Sagare, A. P., and Zlokovic, B. V. (2017). Role of clusterin in the brain vascular clearance of amyloid-β. *Proc. Natl. Acad. Sci. U S A* 114, 8681–8682. doi: 10.1073/pnas.1711357114

Nelson, A. R., Zhao, Z., and Zlokovic, B. V. (2016). *Optogenetic Regulation of Pericytes. Program No. 140.08.* San Diego, CA: Neuroscience Meeting Planner.

Neuhaus, A. A., Couch, Y., Sutherland, B. A., and Buchan, A. M. (2017). Novel method to study pericyte contractility and responses to ischaemia *in vitro* using electrical impedance. *J. Cereb. Blood Flow Metab.* 37, 2013–2024. doi: 10.1177/0271678X16659495

Nikolakopoulou, A. M., Montagne, A., Kisler, K., Dai, Z., Wang, Y., Huuskonen, M. T., et al. (2019). Pericyte loss leads to circulatory failure and pleiotrophin depletion causing neuron loss. *Nat. Neurosci.* 22, 1089–1098. doi: 10.1038/s41593-019-0434-z

Nortley, R., Korte, N., Izquierdo, P., Hirunpattarasilp, C., Mishra, A., Jaunmuktane, Z., et al. (2019). Amyloid β oligomers constrict human capillaries in Alzheimer's disease *via* signaling to pericytes. *Science* 365:eaav9518. doi: 10.1126/science.aav9518

Oren, R. E., Rasool, N. A., and Rubinstein, E. H. (1987). Effect of ketamine on cerebral cortical blood flow and metabolism in rabbits. *Stroke* 18, 441–444. doi: 10.1161/01.str.18.2.441

Park, K. W., Dai, H. B., Lowenstein, E., Stambler, A., and Sellke, F. W. (1998). Effect of isoflurane on the β-adrenergic and endothelium-dependent relaxation of pig cerebral microvessels after cardiopulmonary bypass. *J. Stroke Cerebrovasc. Dis.* 7, 168–178. doi: 10.1016/s1052-3057(98)80003-7

Peppiatt, C. M., Howarth, C., Mobbs, P., and Attwell, D. (2006). Bidirectional control of CNS capillary diameter by pericytes. *Nature* 443, 700–704. doi: 10.1038/nature05193

Rouget, C. (1873). Memoire sur le developpement, la structures et les proprietes des capillaries sanguins et lymphatiques. *Arch. Physiol. Norm. Pathol.* 5, 603–633.

Schönfelder, U., Hofer, A., Paul, M., and Funk, R. H. (1998). in situ observation of living pericytes in rat retinal capillaries. *Microvasc. Res.* 56, 22–29. doi: 10.1006/mvre.1998.2086

Schor, A. M., and Schor, S. L. (1986). The isolation and culture of endothelial cells and pericytes from the bovine retinal microvasculature: a comparative study with large vessel vascular cells. *Microvasc. Res.* 32, 21–38. doi: 10.1016/0026-2862(86)90041-5

Shibata, M., Yamada, S., Kumar, S. R., Calero, M., Bading, J., Frangione, B., et al. (2000). Clearance of Alzheimer's amyloid-β(1–40) peptide from brain by LDL receptor-related protein-1 at the blood-brain barrier. *J. Clin. Invest.* 106, 1489–1499. doi: 10.1172/JCI10498

Sweeney, M. D., Kisler, K., Montagne, A., Toga, A. W., and Zlokovic, B. V. (2018). The role of brain vasculature in neurodegenerative disorders. *Nat. Neurosci.* 21, 1318–1331. doi: 10.1038/s41593-018-0234-x

Sweeney, M. D., Zhao, Z., Montagne, A., Nelson, A. R., and Zlokovic, B. V. (2019). Blood-brain barrier: from physiology to disease and back. *Physiol. Rev.* 99, 21–78. doi: 10.1152/physrev.00050.2017

Vanlandewijck, M., He, L., Mäe, M. A., Andrae, J., Ando, K., Del Gaudio, F., et al. (2018). A molecular atlas of cell types and zonation in the brain vasculature. *Nature* 554, 475–480. doi: 10.1038/nature25739

Wei, H. S., Kang, H., Rasheed, I.-Y. D., Zhou, S., Lou, N., Gershteyn, A., et al. (2016). Erythrocytes are oxygen-sensing regulators of the cerebral microcirculation. *Neuron* 91, 851–862. doi: 10.1016/j.neuron.2016.07.016

Wu, D. M., Kawamura, H., Sakagami, K., Kobayashi, M., and Puro, D. G. (2003). Cholinergic regulation of pericyte-containing retinal microvessels. *Am. J. Physiol. Heart Circ. Physiol.* 284, H2083–2090. doi: 10.1152/ajpheart.01007.2002

Yamanishi, S., Katsumura, K., Kobayashi, T., and Puro, D. G. (2006). Extracellular lactate as a dynamic vasoactive signal in the rat retinal microvasculature. *Am. J. Physiol. Heart Circ. Physiol.* 290, H925–934. doi: 10.1152/ajpheart.01012.2005

Zhang, F., Aravanis, A. M., Adamantidis, A., de Lecea, L., and Deisseroth, K. (2007). Circuit-breakers: optical technologies for probing neural signals and systems. *Nat. Rev. Neurosci.* 8, 577–581. doi: 10.1038/nrn2192

Zhang, F., Wang, L.-P., Boyden, E. S., and Deisseroth, K. (2006). Channelrhodopsin-2 and optical control of excitable cells. *Nat. Methods* 3, 785–792. doi: 10.1038/nmeth936

Zlokovic, B. V. (2011). Neurovascular pathways to neurodegeneration in Alzheimer's disease and other disorders. *Nat. Rev. Neurosci.* 12, 723–738. doi: 10.1038/nrn3114

Zong, Y., Zhou, X., Cheng, J., Yu, J., Wu, J., and Jiang, C. (2017). Cannabinoids regulate the diameter of pericyte-containing retinal capillaries in rats. *Cell. Physiol. Biochem.* 43, 2088–2101. doi: 10.1159/000484193

Conflict of Interest: The authors declare that the research was conducted in the absence of any commercial or financial relationships that could be construed as a potential conflict of interest.

frontiers in Aging Neuroscience

MINI REVIEW
published: 05 May 2020
doi: 10.3389/fnagi.2020.00109

Clinical Features and Experimental Models of Cerebral Small Vessel Disease

Akihiro Shindo, Hidehiro Ishikawa, Yuichiro Ii, Atsushi Niwa and Hidekazu Tomimoto**

Department of Neurology, Mie University Graduate School of Medicine, Mie University, Tsu, Japan

Cerebral small vessel disease (SVD) refers to a group of disease conditions affecting the cerebral small vessels, which include the small arteries, arterioles, capillaries, and postcapillary venules in the brain. SVD is the primary cause of vascular cognitive impairment and gait disturbances in aged people. There are several types of SVD, though arteriolosclerosis, which is mainly associated with hypertension, aging, and diabetes mellitus, and cerebral amyloid angiopathy (CAA) comprise most SVD cases. The pathology of arteriolosclerosis-induced SVD is characterized by fibrinoid necrosis and lipohyalinosis, while CAA-associated SVD is characterized by progressive deposition of amyloid beta (Aβ) protein in the cerebral vessels. Brain magnetic resonance imaging (MRI) has been used for examination of SVD lesions; typical lesions are characterized by white matter hyperintensity, lacunar infarcts, enlargement of perivascular spaces (EPVS), microbleeds, cortical superficial siderosis (cSS), and cortical microinfarcts. The microvascular changes that occur in the small vessels are difficult to identify clearly; however, these consequent image findings can represent the SVD. There are two main strategies for prevention and treatment of SVD, i.e., pharmacotherapy and lifestyle modification. In this review, we discuss clinical features of SVD, experimental models replicating SVD, and treatments to further understand the pathological and clinical features of SVD.

Keywords: white matter, lacuna, Alzheimer's disease, blood-brain barrier, neurovascular unit

OPEN ACCESS

Edited by:
Satoshi Saito,
National Cerebral and Cardiovascular Center (Japan), Japan

Reviewed by:
Akihiro Kitamura,
Shiga University of Medical Science, Japan
Bogdan O. Popescu,
Carol Davila University of Medicine and Pharmacy, Romania

****Correspondence:***
Akihiro Shindo
a-shindo@clin.medic.mie-u.ac.jp
Hidekazu Tomimoto
tomimoto@clin.medic.mie-u.ac.jp

Received: *22 January 2020*
Accepted: *30 March 2020*
Published: *05 May 2020*

Citation:
Shindo A, Ishikawa H, Ii Y, Niwa A and Tomimoto H (2020) Clinical Features and Experimental Models of Cerebral Small Vessel Disease. Front. Aging Neurosci. 12:109. doi: 10.3389/fnagi.2020.00109

INTRODUCTION

Advances in neuroimaging technology have led to the recognition of the existence of various small vessel pathologies affecting the brain, including both ischemia and hemorrhages, called cerebral small vessel disease (SVD). The term SVD is an umbrella term used to describe several conditions that share common pathological, clinical, and neuroimaging features (Pantoni, 2010), and the two major types of SVD are arteriolosclerosis, which is mainly associated with hypertension, and cerebral amyloid angiopathy (CAA; Pantoni, 2010; Tomimoto, 2011). Brain magnetic resonance imaging (MRI) shows diverse vascular lesions in patients with SVD, such as white matter lesions, lacunar infarcts, hematomas, microbleeds (MBs), and cortical superficial siderosis (cSS; Pantoni, 2010; Wardlaw et al., 2019). Because MRI technology has allowed for improved visualization of SVD, not only can acute ischemic and hemorrhagic strokes be detected, but also chronic microvascular changes that lead to dementia, as SVD is not only associated with strokes but also with Alzheimer's disease (Tomimoto, 2011).

Since the underlying pathophysiological mechanisms of SVD are complicated, both *in vivo* and *in vitro* experiments are necessary to understand the disease etiology and the associated vascular changes induced by disease progression. Indeed, clinical features of SVD exhibit heterogeneity ranging from pure vascular disease to admixture with Alzheimer's disease, and thereby treatment strategy is now controversial. Moreover, recent MRI studies have shown that SVD lesions are detectable in clinical situations, allowing for early identification and treatment of patients with SVD.

Although SVD is associated with pathological and/or functional abnormalities of cerebral small vessels, as its name suggests, SVD shares many characteristics with atherosclerotic large vessel and cardiovascular diseases. Indeed, intracranial carotid arterial calcifications and internal carotid artery stenosis can be associated with changes in the imaging markers used to identify SVD (Chen et al., 2019; Shen et al., 2020), and lobar MBs are also seen in patients with atrial fibrillation (Horstmann et al., 2015). These findings suggest that upstream blood vessels can affect those downstream; this phenomenon is known as "large and small artery cross-talk."

In this mini review article, we will summarize the experimental models and clinical findings of SVD to further understand the pathological conditions in SVD.

TYPES OF CEREBRAL SMALL VESSEL DISEASE

SVD is the main cause of vascular cognitive impairment, mood disorders, and gait disturbances in aged people (Pantoni, 2010). Most SVD cases are related to hypertension, or other vascular risk factors, and CAA. Although few in number, some patients may develop SVD due to genetic variants that place them at higher risk, such as cerebral autosomal dominant arteriopathy with subcortical infarcts and leukoencephalopathy (CADASIL; Wardlaw et al., 2019) Neuroradiological findings of SVD vary depending on disease etiology. Representative images of SVD typically show white matter hyperintensities (WMH) in MRI, as well as lacunar infarcts, and cerebral MBs (Pantoni, 2010). Moreover, enlargement of perivascular spaces (EPVS), cSS, convexity subarachnoid hemorrhages, and cortical microinfarcts (CMIs) are also indicators of SVD (van Veluw et al., 2017; Wilson et al., 2017; Raposo et al., 2018; Ii et al., 2013, 2019; Wardlaw et al., 2019).

Because SVD can be caused by a number of different conditions, SVD classification was proposed by Pantoni (2010). The two most common types of SVD are arteriolosclerosis (type 1) and CAA (type 2). Type 1 SVD, caused by arteriolosclerosis, is related to aging and certain vascular factors, such as diabetes and, especially, hypertension (Furuta et al., 1991; Pantoni, 2010). The pathophysiology of type 1 SVD is characterized by fibrinoid necrosis, lipohyalinosis, fibrohyalinosis, microatheroma, and microaneurysm (Pantoni, 2010; Ogata et al., 2011). Type 2 SVD, caused by CAA, is characterized by the progressive deposition of amyloid beta (Aβ) protein in the cerebral vessels; the major peptide isoforms of Aβ mainly consisted of $A\beta_{1-40}$ and $A\beta_{1-42}$ (**Figure 1**; Thal et al., 2008; Pantoni, 2010). The deposition of Aβ in cerebral vessels appears mainly in leptomeningeal and cortical arteries, and capillary Aβ-deposition is not always confirmed (Thal et al., 2008). Positive immunostaining with Congo red dye and thioflavin S is a specific histopathological feature of CAA (Pantoni, 2010). The capillary type of CAA is associated with advanced stages of Alzheimer's disease-related pathology, the presence of the apolipoprotein E (APOE) ε4 allele, and complement immune system activation (Matsuo et al., 2018). Moreover, lobar MBs and CMIs are often observed in severe CAA cases, and these lesions are typically associated with cognitive impairments (van Veluw et al., 2016). Other types of SVD include inherited or genetic SVD (Type 3), inflammatory and immunologically mediated SVD (Type 4), SVD caused by venous collagenosis (Type 5), and SVD related to other causes (Type 6; Ii et al., 2019). CADASIL and Fabry disease are well-known causes of inherited or genetic SVD. Inflammatory and immunologically mediated SVD is usually a component of a systemic disease, including Wegener's granulomatosis, Churg-Strauss syndrome, and microscopic polyangiitis (Pantoni, 2010; Jennette and Falk, 1997). Type 5 SVD, caused by venous collagenosis, is observed in people of advanced age, and the pathological features include noninflammatory collagenosis of venous walls resulting in small vessel narrowing (Moody et al., 1995). Other types of SVD include postradiation angiopathy, as well as nonamyloid microvessel degeneration observed in Alzheimer's disease (Pantoni, 2010).

EXPERIMENT MODELS FOR EVALUATION OF SMALL VESSEL DISEASE

Several rodent models have been used to evaluate subcortical white matter changes caused by ischemia. Although animal models of chronic cerebral hypoperfusion cannot explain all features of SVD in humans, large vessel occlusion/stenosis models are widely accepted animal models of SVD for assessing large and small artery cross-talk. Two-vessel occlusion of the common carotid arteries is a common rat model of white matter ischemia (Wakita et al., 1994) in which a permanent occlusion causes pathophysiological changes in the corpus callosum, the internal capsule, and the optic nerve (Wakita et al., 2002; Farkas et al., 2004), and white matter demyelination similar to the white matter lesions in humans. Although this model results in analogous neuropathological changes, the visual pathway is damaged by the carotid artery occlusion, making it difficult to assess neuropsychological changes in behavioral testing paradigms (Farkas et al., 2004). To counteract these drawbacks, we have developed mice models which are subjected to bilateral carotid artery stenosis (BCAS) by attaching microcoils from outside of both carotid arteries (Shibata et al., 2004, 2007). This model exhibits white matter lesions and cognitive decline after chronic cerebral hypoperfusion for 1 month, and delayed hippocampal atrophy at 8 months after chronic cerebral hypoperfusion (Nishio et al., 2010), whereas there are little optic nerve damages and visual impairment. This BCAS mouse model has been most widely accepted as a model for vascular dementia with white matter pathologies, such as demyelination,

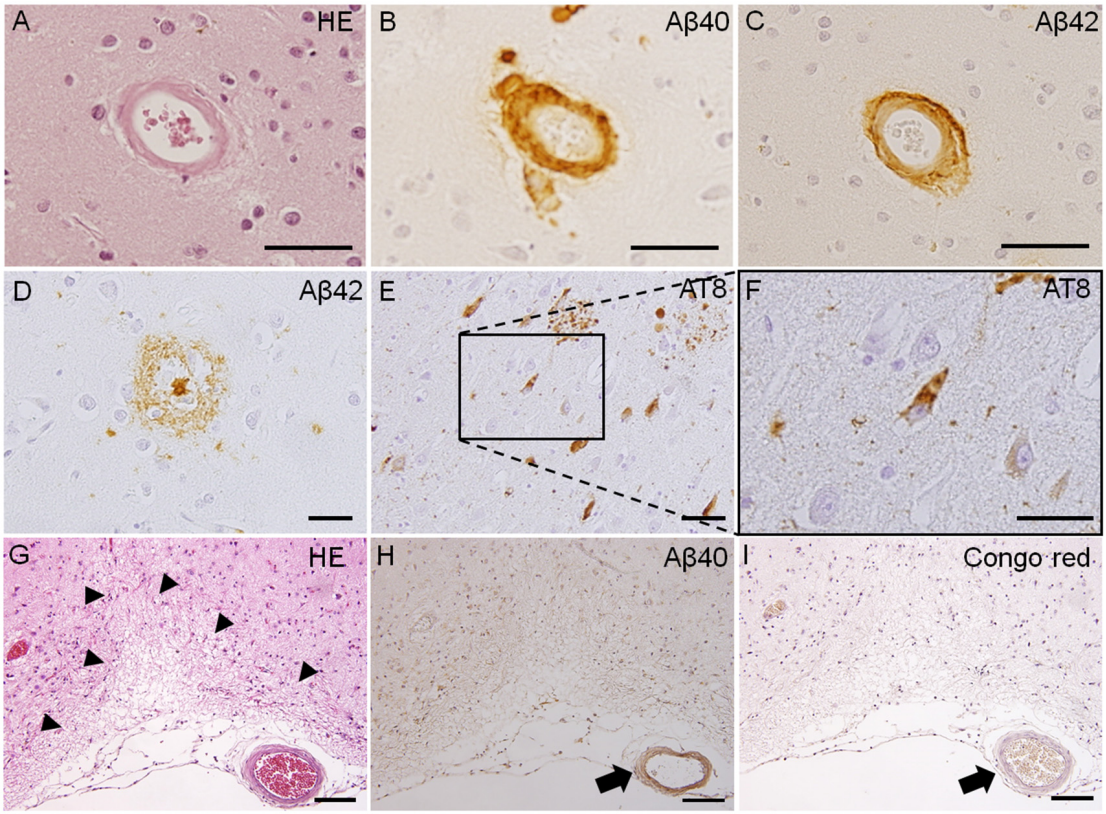

FIGURE 1 | Pathological features of Type 1 and Type 2 cerebral small vessel disease (SVD). Fibrinoid necrosis detected by hematoxylin & eosin (H&E) staining in the postmortem brain of a patient with arteriolosclerosis **(A)**. Immunohistochemistry of the postmortem brain affected by cerebral amyloid angiopathy (CAA) shows immunopositive-staining for beta-amyloid peptides $A\beta_{1-40}$ (Aβ40) and $A\beta_{1-42}$ (Aβ42) in arterioles **(B,C)**. Immunoreactive staining of senile plaque (Aβ40) and neurofibrillary tangles (phosphorylated tau; AT8) is also detected in CAA patients **(D–F)**. Cortical microinfarct stained with HE is observed in a CAA patient (arrowheads, **G**). Aβ40 and Congo red-positive vessels are observed close to the cortical microinfarct (arrows, **H,I**). Scale bars in **(A–F)**: 50 μm; in **(G–I)**: 200 μm.

axonal damage, oligodendrocyte loss, and blood-brain barrier (BBB) damage (Miyamoto et al., 2014). Because the two-vessel occlusion/stenosis model acutely decreases cerebral blood flow (CBF), a device that can narrow the arteries gradually has also been introduced. Ameroid constrictor devices applied to the bilateral common carotid arteries could replicate white matter pathologies, can reduce CBF gradually, and can induce changes resembling those associated with chronic cerebral hypoperfusion in humans (Kitamura et al., 2012; Hattori et al., 2016). The gradual common carotid artery stenosis (GCAS) model gradually and continuously reduces CBF (Hattori et al., 2016). A mouse asymmetric common carotid artery stenosis (ACAS) model is used to mimic white matter infarcts accompanied by motor deficits and dementia; the model is generated by the implantation of an ameroid constrictor and a microcoil in both carotid arteries (Hattori et al., 2015). The spontaneously hypertensive rat two-vessel gradual occlusion (SHR-2VGO) model is also generated using ameroid constrictors, and is used to model the evolution of white matter abnormalities and the associated impairments of spatial working memory (Kitamura et al., 2015). A nongenetic model of SVD is the stroke-prone spontaneously hypertensive rat (SHRSP), in which this rat strain has malignant hypertension, and reveals white matter loss and reductions in the levels of tight junction proteins (Yamori and Horie, 1977; Hainsworth and Markus, 2008; Bailey et al., 2011; Rajani and Williams, 2017).

Focal injection of vasoconstrictors has been used to model certain characteristics of human white matter stroke such as lacunar infarcts. For example, direct stereotaxic injection of vasoconstricting agents such as endothelin-1 (ET-1) and N5-(1-iminoethyl)-L-ornithine (L-NIO) into subcortical white matter can induce focal strokes in both rats and mice (Sozmen et al., 2009, 2012; Hinman et al., 2013). ET-1 can also reduce local blood flow, causing ischemic lesions, and injection into the white matter can induce a demyelinated and necrotic region in rats and a demyelinated area in mice (Silasi et al., 2015). Likewise, L-NIO injection can also cause focal white matter strokes in animals (Hinman et al., 2013).

Transgenic mouse lines for SVD are used to further understand the mechanisms of CAA and CADASIL. Although CAA is often seen sporadically, CAA can also be genetically inherited. Certain mutations in the amyloid precursor protein (APP) gene are a common cause of hereditary CAA. Dutch APP (E693Q) mice accumulate amyloid deposits in brain

vessels at ∼22–25 months, resulting in brain hemorrhages (Herzig et al., 2004). APP23 transgenic mice, which express mutant human APP_{751}, develop Aβ deposits in the neocortex and hippocampus (Sturchler-Pierrat et al., 1997), and develop similar Aβ deposits in cerebral vessels as those caused by CAA beginning at 9 months of age (Kuo et al., 2001). Another transgenic mouse line expressing human Swedish, Dutch, and Iowa triple-mutant APP (Tg-SwDI) has been used to model CAA as well (Davis et al., 2004). Tg-SwDI mice develop microvascular Aβ deposition in the thalamus and subiculum, and exhibit apoptotic vascular cells, and a loss of smooth muscle cells in vessel walls (Miao et al., 2005). Moreover, models combining chronic hypoperfusion models and transgenic mice have been reported, and chronic hypoperfusion could exacerbate BBB dysfunction in APP23 transgenic mice and increase the frequency of microinfarctions (Salvadores et al., 2017; Shang et al., 2019). On the other hand, CADASIL is linked to a mutation in the *NOTCH3* gene, with the pathological feature being the accumulation of granular osmiophilic material within the tunica media of vascular smooth muscle cell membranes (Ayata, 2010). *Notch3* knockout, knock-in, and transgenic mouse models, and *notch3* mutant zebrafish have been developed to better understand the pathological features of CADASIL (Ayata, 2010; Zaucker et al., 2013; Cognat et al., 2014). These models have demonstrated that white matter deficits are associated with oligodendrocyte death (Cognat et al., 2014), reduced expression of myelin basic protein, and a decreased number of oligodendrocyte progenitor cells (OPCs; Zaucker et al., 2013).

Several kinds of *in vitro* models are used for the evaluation of cellular changes associated with SVD, such as oxygen-glucose deprivation, hypoxia, growth factor deprivation, and glutathione depletion (Shindo et al., 2016). To mimic chronic mild hypoxic conditions, cobalt chloride was selected for use in some of these experiments (Miyamoto et al., 2013; Shimada et al., 2019). Recently, induced pluripotent stem (iPS) cell technology (Takahashi and Yamanaka, 2006) has been acknowledged as a useful cellular tool for the evaluation and treatment of various disease conditions, and iPS cell derived from the dermal fibroblasts of the patients with hereditary cerebral hemorrhage with amyloidosis-Dutch type (HCHWA-D) is considered to be a model for sporadic CAA (Daoutsali et al., 2019). Moreover, CADASIL and Fabry disease iPS cells have been used in several studies (Kawagoe et al., 2013; Ling et al., 2019). It is desired that these iPS cell-based SVD models can be used to help understand the pathogenic mechanisms of SVD and lead to the development of novel treatment strategies.

NEUROIMAGING OF CEREBRAL SMALL VESSEL DISEASE (FIGURE 2)

Brain MRI is typically used to examine SVD lesions, which are often characterized by WMH, lacunar infarcts, EPVS, MBs, cSS, and CMIs (Wardlaw et al., 2019).

WMH are often observed in both stroke patients and in nonstroke elderly people (Longstreth et al., 2002; Vermeer et al., 2002). In MRI, these hyperintensities are observed on T2-weighted images (WI) and fluid-attenuated inversion recovery (FLAIR), while hypointensities are observed on T1-WI, with no low intensity cavities in FLAIR images (Wardlaw et al., 2019). Although both hypertensive SVD and CAA show WMH in MRI on T2-WI and hypointensities on T1-WI, the distribution of these hyperintense regions differs; peri-basal ganglia WMH are strongly indicative of hypertensive arteriopathy, while multiple punctate FLAIR images are associated with CAA (Charidimou et al., 2016). Lacunar infarcts are round or ovoid, subcortical, fluid-filled cavities, 3–15 mm in diameter (Wardlaw et al., 2013). A common imaging feature of lacunar infarcts is a central hypointensity with a hyperintense rim in FLAIR images, but there are some cases without a central hypointensity lesion (Wardlaw et al., 2013). These WMH and silent lacunar infarcts can become important stroke risk factors, and might be associated with increased mortality rates (Bokura et al., 2006). EPVS are important markers of vascular dysfunction leading to brain damage (Wardlaw et al., 2019). MRI findings of EPVS are similar to cerebrospinal fluid on all sequences; they can be linear, round, or ovoid lesions with a diameter generally smaller than 3 mm (Wardlaw et al., 2013). The perivascular space is considered an important feature of glymphatic pathways as that is one of the main clearance pathways for the removal of amyloid-beta peptides, and changes in these areas are indicated in increased risk of Alzheimer's disease (Iliff et al., 2015).

Cerebral MBs are detected as small, hypointense, round lesions with a diameter of 5–10 mm on T2*-weighted gradient-echo (GRE) or susceptibility-weighted image (SWI) sequences (Fazekas et al., 1999; Charidimou et al., 2013). Two main types contribute to pathological features of cerebral MBs have been identified: hypertensive vasculopathy and CAA (Greenberg et al., 2009). Differential distribution patterns of these two types of MBs are observed; hypertensive vasculopathy is typically associated with deep MBs in the basal ganglia, thalamus, and brainstem, while advanced CAA is associated with lobar MBs (Greenberg et al., 2009). Moreover, there is a possibility of mixed types of MBs, which may indicate advanced hypertensive arteriopathy, or alternatively both hypertensive arteriopathy and CAA (Matsuyama et al., 2017; Pasi et al., 2018). On the other hand, based on the pathophysiological mechanisms producing these MBs, they can be classified as either primary or secondary (Fisher, 2014). Primary cerebral MBs are visualized as extravasated erythrocytes from cerebral small vessels upon histopathological examination (Fazekas et al., 1999); secondary MBs are caused by other mechanisms such as hemorrhagic transformation of cerebral infarction/microinfarction (Fisher, 2014; Ito et al., 2019; Ogawa Ito et al., 2019).

The MRI finding of cSS is a linear or curvilinear lesions at the gyral cortical surface, detected as a signal loss on T2*-weighted GRE and SWI sequences (Charidimou et al., 2015a). cSS is one of the key features of CAA and is associated with transient focal neurological episodes (Charidimou et al., 2012, 2015a). Moreover, cSS is a risk factor for intracerebral hemorrhage in CAA patients (Charidimou et al., 2015b), and multifocal cSS correlates with disease severity in patients with CAA (Charidimou et al., 2017). Although the neuropathological feature of cSS may be associated with complement immune

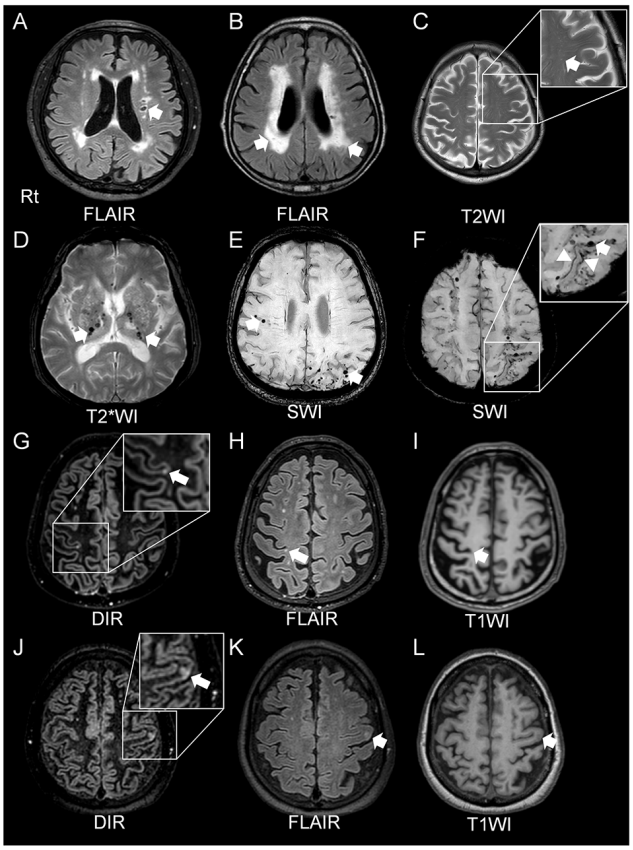

FIGURE 2 | Radiological features of cerebral SVD. A lacunar infarct in the left corona radiata **(A)** and white matter lesions, assessed by fluid attenuated inversion recovery (FLAIR) imaging, is detected in patients with hypertension (arrows, **A,B**). The arrow shows enlarged perivascular spaces in T2-weighted (T2WI) magnetic resonance imaging (MRI) in a patient with CAA **(C)**. Cerebral microbleeds (MBs) are classified as two types: deep MBs or lobar MBs. Deep MBs are detected in patients with hypertension on MRI T2*-weighted image (T2*WI; arrows, **D**). Both lobar MBs and cortical superficial siderosis (cSS) are seen in susceptibility-weighted imaging (SWI) sequences in CAA patients (arrows, **E,F**, and arrowheads, **F**). Both double inversion recovery (DIR; **G,J**) and FLAIR **(H,K)** imaging can clearly detect the cortical microinfarcts (CMIs). T1*-weighted imaging (T1WI) can also reveal CMIs but less obviously **(I,L)**. CAA and cerebral embolisms can cause CMIs. CMIs from patients with CAAs **(G–I)** showed that all lesions were localized within cortical structures, with a size of <5 mm (Ishikawa et al., 2020). CMIs caused by embolisms involved subcortical areas, and the size of the lesions was ≥5 mm (Ishikawa et al., 2020).

system activation (Matsuo et al., 2018), the details of this possible relationship remain unclear.

CMIs are frequently detected in autopsied brains of elderly people. Even though there is no visible macroscopic cerebral infarct, CMIs are frequently associated with cognitive impairment (Brundel et al., 2012; Kövari et al., 2017). CMIs are caused by various pathologies such as CAA, arteriolosclerosis, and microembolisms (Kövari et al., 2017). Although detection of CMIs has been difficult, historically, using MRI (Smith et al., 2012), recent reports have shown that *in vivo* visualization of MCIs is possible using higher resolution 7-Tesla (7T; van Veluw et al., 2013) and 3-Tesla (3T; Ii et al., 2013; van Veluw et al., 2015) MRI, and a combination method using three-dimensional double inversion recovery (3D-DIR) and three-dimensional FLAIR (3D-FLAIR) imaging with 3T-MRI has reportedly been able to detect CMIs (Ii et al., 2013; Umino et al., 2019). MRI features of CMIs show small, high-intensity intracortical lesions on 3D-DIR and 3D-FLAIR imaging, and hypointensities on T1-WI. Histopathological studies have demonstrated neuroradiological and pathological correlations (Niwa et al., 2017; Ishikawa et al., 2018). A recent study using 3T-MRI has shown that it may be possible to distinguish between CMIs due to CAA and those due to microembolism (Ishikawa et al., 2020). They say that CMIs in CAA patients are localized within the cortex, predominantly in the occipital lobe, smaller <5 mm in diameter, with fewer than three lesions (Ishikawa et al., 2020). On the other hand, CMIs resulting from microembolisms may involve the cortico-subcortical junction, are predominantly distributed in the frontal or parietal lobes, larger (≥5 mm) in diameter with multiple lesions, typically at least three (Ishikawa et al., 2020).

CLINICAL SYMPTOMS AND TREATMENT OF CEREBRAL SMALL VESSEL DISEASE

Symptoms of SVD vary depending on several factors, including the type and localization of vascular lesions. For lacunar infarcts, the symptoms include acute lacunar motor and/or sensory syndromes. Total number and volume of SVD lesions can be associated with cognitive impairment, gait disturbance, and mood disorders (Wardlaw et al., 2019). Even though MRI may show several SVD-related lesions, some patients may have symptoms that are clinically silent or may even be asymptomatic (Pantoni, 2010; Huijts et al., 2013). To determine the total MRI burden of SVD, calculation of a total SVD score has been described (Klarenbeek et al., 2013), based on four MRI features of SVD, including the presence of lacunae, the presence of MBs, the severity of the basal ganglia perivascular space, and the degree of WMH. This weighted score has been shown to be associated with age, sex, and vascular risk factors, including hypertension and smoking (Staals et al., 2014). Moreover, the total SVD score has been associated with cognitive impairment (Huijts et al., 2013), and may have predictive value for assessing risk of recurrent stroke after ischemic stroke (Lau et al., 2017), as well as mild parkinsonian signs (Hatate et al., 2016).

There are two main approaches of prevention and treatment strategies for SVD: pharmacotherapy and lifestyle modification. Pharmacotherapy includes anti-hypertensive drugs, statins, and antiplatelet treatments. Because hypertension is a risk factor for SVD, one of the most important treatments is anti-hypertensive therapy. The secondary prevention of small subcortical stroke (SPS3) trial enrolled patients with symptomatic lacunar infarctions, which were divided into two groups: those with a systolic blood pressure target of 130–149 mm Hg and those with a blood pressure less than 130 mm Hg (Benavente et al., 2013). Although there was no significant difference in the frequency of all strokes, the

rate of intracerebral hemorrhage was significantly lower in the group with lower blood pressure (Benavente et al., 2013). This SPS3 trial showed that a systolic blood pressure target of less than 130 mm Hg is beneficial in reducing risk in lacunar stroke patients. Moreover, a systematic review of SVD treatment showed that anti-hypertensive treatment has a protective role in limiting the progression of WMH, but does not affect the degree of brain atrophy (van Middelaar et al., 2018). Statins may have beneficial effects for SVD patients, as rosuvastatin has been shown to prevent WMH in patients expressing the APOEε4 allele (Ji et al., 2018). Diabetes mellitus is also associated with SVD, especially lacunar stroke and the low fractional anisotropy observed on MRI (Liu et al., 2018). Most patients with diabetes have another risk factor, such as hypertension, and blood pressure and lipid control is effective for stroke prevention (Chen et al., 2016).

In terms of antiplatelet treatment, the SPS3 trial also demonstrated that all-cause mortality was increased in dual antiplatelet therapy with aspirin and clopidogrel, and that there was no significant difference in recurrent stroke risk between single antiplatelet therapy and dual antiplatelet therapy in lacunar stroke patients (Benavente et al., 2012). A recent meta-analysis showed a significant risk reduction in recurrence of any type of stroke and ischemic stroke in patients with a lacunar stroke using any single antiplatelet medication (Kwok et al., 2015). Likewise, cilostazol, a phosphodiesterase 3 inhibitor, may have an advantage for treating lacunar stroke. A randomized double-blind, placebo-controlled trial in Japan, the Cilostazol Stroke Prevention Study (CSPS), showed that cilostazol reduced the risk of recurrent stroke compared with placebo (Matsumoto, 2005), and the Cilostazol for Prevention of Secondary Stroke study (CSPS2) demonstrated that there was no significant difference in stroke prevention measures between cilostazol and aspirin, but cilostazol resulted in fewer hemorrhagic events than aspirin alone (Shinohara et al., 2010). Moreover, dual antiplatelet therapy with cilostazol and aspirin or clopidogrel can reduce the incidence of ischemic stroke recurrence and bleeding compared with aspirin or clopidogrel alone (Toyoda et al., 2019). In addition, *in vivo* experiment data has shown that cilostazol had a protective effect against hypertension-induced endothelial dysfunction (Oyama et al., 2011), and may reduce the risk of developing dementia (Tai et al., 2017; Saito et al., 2019). These data may suggest that cilostazol can be a safe and effective treatment for SVD in certain cases.

Lifestyle modification is another important intervention for preventing and treating SVD. Smoking and high sodium diets exacerbate the risk of stroke, dementia, and WMH revealed in MRI (Staals et al., 2014; Karama et al., 2015; Hankey, 2017; Wardlaw et al., 2019). The Finnish Geriatric Intervention Study to Prevent Cognitive Impairment and Disability (FINGER) trial demonstrated that multidomain intervention, including diet, exercise, cognitive training, and vascular risk monitoring, improved cognitive function and reduced the risk of cognitive decline in elderly subjects (Ngandu et al., 2015). Although the number of patients enrolled was relatively small, another study showed that an aerobic exercise training program might have beneficial effects for patients with subcortical ischemic vascular cognitive impairments (Liu-Ambrose et al., 2016).

CONCLUSION

SVD is clinically important because it is not only associated with ischemic or hemorrhagic stroke but also with dementia. As SVD is an umbrella term for various conditions affecting cerebral vasculature, clinical characteristics of SVD can vary greatly depending on the etiology, which can affect optimization of treatment. In this mini review article, we have summarized the experimental models and the pathological and radiological features of SVD. Further elucidating the characteristics and pathophysiology of SVD may help identify novel therapeutic approaches and allow for earlier diagnoses to protect the human brain from disease progression.

ETHICS STATEMENT

The study was approved by the Ethics Committee of Mie University Hospital (number H2018-032).

AUTHOR CONTRIBUTIONS

AS: draft of manuscript, review concept and design, and acquisition of data. HI, YI, and AN: revision of manuscript and acquisition of data. HT: revision of the manuscript and review supervision.

FUNDING

This work was supported in part by Japan Society for the Promotion of Science (SPS KAKENHI) Grant Number JP 18K16557.

REFERENCES

Ayata, C. (2010). Cadasil: experimental insights from animal models. *Stroke* 41, S129–S134. doi: 10.1161/strokeaha.110.595207

Bailey, E. L., Smith, C., Sudlow, C. L., and Wardlaw, J. M. (2011). Is the spontaneously hypertensive stroke prone rat a pertinent model of sub cortical ischemic stroke? A systematic review. *Int. J. Stroke* 6, 434–444. doi: 10.1111/j.1747-4949.2011.00659.x

Benavente, O. R., Coffey, C. S., Conwit, R., Hart, R. G., McClure, L. A., Pearce, L. A., et al. (2013). Blood-pressure targets in patients with recent lacunar stroke: the SPS3 randomised trial. *Lancet* 382, 507–515. doi: 10.1016/s0140-6736(13)60852-1

Benavente, O. R., Hart, R. G., McClure, L. A., Szychowski, J. M., Coffey, C. S., and Pearce, L. A. (2012). Effects of clopidogrel added to aspirin in patients with recent lacunar stroke. *N. Engl. J. Med.* 367, 817–825. doi: 10.1056/NEJMoa1204133

Bokura, H., Kobayashi, S., Yamaguchi, S., Iijima, K., Nagai, A., Toyoda, G., et al. (2006). Silent brain infarction and subcortical white matter lesions increase the risk of stroke and mortality: a prospective cohort study. *J. Stroke Cerebrovasc. Dis.* 15, 57–63. doi: 10.1016/j.jstrokecerebrovasdis.2005.11.001

Brundel, M., de Bresser, J., van Dillen, J. J., Kappelle, L. J., and Biessels, G. J. (2012). Cerebral microinfarcts: a systematic review of neuropathological studies. *J. Cereb. Blood Flow Metab.* 32, 425–436. doi: 10.1038/jcbfm.2011.200

Charidimou, A., Boulouis, G., Haley, K., Auriel, E., van Etten, E. S., Fotiadis, P., et al. (2016). White matter hyperintensity patterns in cerebral amyloid angiopathy and hypertensive arteriopathy. *Neurology* 86, 505–511. doi: 10.1212/wnl.0000000000002362

Charidimou, A., Boulouis, G., Roongpiboonsopit, D., Auriel, E., Pasi, M., Haley, K., et al. (2017). Cortical superficial siderosis multifocality in cerebral amyloid angiopathy: a prospective study. *Neurology* 89, 2128–2135. doi: 10.1212/wnl.0000000000004665

Charidimou, A., Kakar, P., Fox, Z., and Werring, D. J. (2013). Cerebral microbleeds and recurrent stroke risk: systematic review and meta-analysis of prospective ischemic stroke and transient ischemic attack cohorts. *Stroke* 44, 995–1001. doi: 10.1161/strokeaha.111.000038

Charidimou, A., Linn, J., Vernooij, M. W., Opherk, C., Akoudad, S., Baron, J. C., et al. (2015a). Cortical superficial siderosis: detection and clinical significance in cerebral amyloid angiopathy and related conditions. *Brain* 138, 2126–2139. doi: 10.1093/brain/awv162

Charidimou, A., Martinez-Ramirez, S., Shoamanesh, A., Oliveira-Filho, J., Frosch, M., Vashkevich, A., et al. (2015b). Cerebral amyloid angiopathy with and without hemorrhage: evidence for different disease phenotypes. *Neurology* 84, 1206–1212. doi: 10.1212/wnl.0000000000001398

Charidimou, A., Peeters, A., Fox, Z., Gregoire, S. M., Vandermeeren, Y., Laloux, P., et al. (2012). Spectrum of transient focal neurological episodes in cerebral amyloid angiopathy: multicentre magnetic resonance imaging cohort study and meta-analysis. *Stroke* 43, 2324–2330. doi: 10.1161/strokeaha.112.657759

Chen, R., Ovbiagele, B., and Feng, W. (2016). Diabetes and stroke: epidemiology, pathophysiology, pharmaceuticals and outcomes. *Am. J. Med. Sci.* 351, 380–386. doi: 10.1016/j.amjms.2016.01.011

Chen, Y. C., Wei, X. E., Lu, J., Qiao, R. H., Shen, X. F., and Li, Y. H. (2019). Correlation between intracranial arterial calcification and imaging of cerebral small vessel disease. *Front. Neurol.* 10:426. doi: 10.3389/fneur.2019.00426

Cognat, E., Cleophax, S., Domenga-Denier, V., and Joutel, A. (2014). Early white matter changes in cadasil: evidence of segmental intramyelinic oedema in a pre-clinical mouse model. *Acta Neuropathol. Commun.* 2:49. doi: 10.1186/2051-5960-2-49

Daoutsali, E., Buijsen, R. A. M., van de Pas, S., Jong, A., Mikkers, H., Brands, T., et al. (2019). Generation of 3 human induced pluripotent stem cell lines LUMCi005-A, B and C from a hereditary cerebral hemorrhage with amyloidosis-dutch type patient. *Stem Cell Res.* 34:101359. doi: 10.1016/j.scr.2018.101359

Davis, J., Xu, F., Deane, R., Romanov, G., Previti, M. L., Zeigler, K., et al. (2004). Early-onset and robust cerebral microvascular accumulation of amyloid β-protein in transgenic mice expressing low levels of a vasculotropic dutch/iowa mutant form of amyloid β-protein precursor. *J. Biol. Chem.* 279, 20296–20306. doi: 10.1074/jbc.M312946200

Farkas, E., Donka, G., de Vos, R. A., Mihály, A., Bari, F., and Luiten, P. G. (2004). Experimental cerebral hypoperfusion induces white matter injury and microglial activation in the rat brain. *Acta Neuropathol.* 108, 57–64. doi: 10.1007/s00401-004-0864-9

Fazekas, F., Kleinert, R., Roob, G., Kleinert, G., Kapeller, P., Schmidt, R., et al. (1999). Histopathologic analysis of foci of signal loss on gradient-echo T2*-weighted MR images in patients with spontaneous intracerebral hemorrhage: evidence of microangiopathy-related microbleeds. *AJNR Am. J. Neuroradiol.* 20, 637–642.

Fisher, M. (2014). Cerebral microbleeds: where are we now? *Neurology* 83, 1304–1305. doi: 10.1212/wnl.0000000000000871

Furuta, A., Ishii, N., Nishihara, Y., and Horie, A. (1991). Medullary arteries in aging and dementia. *Stroke* 22, 442–446. doi: 10.1161/01.str.22.4.442

Greenberg, S. M., Vernooij, M. W., Cordonnier, C., Viswanathan, A., Al-Shahi Salman, R., Warach, S., et al. (2009). Cerebral microbleeds: a guide to detection and interpretation. *Lancet Neurol.* 8, 165–174. doi: 10.1016/S1474-4422(09)70013-4

Hainsworth, A. H., and Markus, H. S. (2008). Do *in vivo* experimental models reflect human cerebral small vessel disease? A systematic review. *J. Cereb. Blood Flow Metab.* 28, 1877–1891. doi: 10.1038/jcbfm.2008.91

Hankey, G. J. (2017). The role of nutrition in the risk and burden of stroke. *Stroke* 48, 3168–3174. doi: 10.1161/strokeaha.117.016993

Hatate, J., Miwa, K., Matsumoto, M., Sasaki, T., Yagita, Y., Sakaguchi, M., et al. (2016). Association between cerebral small vessel diseases and mild parkinsonian signs in the elderly with vascular risk factors. *Parkinsonism Relat. Disord.* 26, 29–34. doi: 10.1016/j.parkreldis.2016.02.011

Hattori, Y., Enmi, J.-I., Kitamura, A., Yamamoto, Y., Saito, S., Takahashi, Y., et al. (2015). A novel mouse model of subcortical infarcts with dementia. *J. Neurosci.* 35, 3915–3928. doi: 10.1523/JNEUROSCI.3970-14.2015

Hattori, Y., Enmi, J., Iguchi, S., Saito, S., Yamamoto, Y., Tsuji, M., et al. (2016). Gradual carotid artery stenosis in mice closely replicates hypoperfusive vascular dementia in humans. *J. Am. Heart Assoc.* 5:e002757. doi: 10.1161/JAHA.115.002757

Herzig, M. C., Winkler, D. T., Burgermeister, P., Pfeifer, M., Kohler, E., Schmidt, S. D., et al. (2004). Aβ is targeted to the vasculature in a mouse model of hereditary cerebral hemorrhage with amyloidosis. *Nat. Neurosci.* 7, 954–960. doi: 10.1038/nn1302

Hinman, J. D., Rasband, M. N., and Carmichael, S. T. (2013). Remodeling of the axon initial segment after focal cortical and white matter stroke. *Stroke* 44, 182–189. doi: 10.1161/strokeaha.112.668749

Horstmann, S., Mohlenbruch, M., Wegele, C., Rizos, T., Laible, M., Rauch, G., et al. (2015). Prevalence of atrial fibrillation and association of previous antithrombotic treatment in patients with cerebral microbleeds. *Eur. J. Neurol.* 22, 1355–1362. doi: 10.1111/ene.12608

Huijts, M., Duits, A., van Oostenbrugge, R. J., Kroon, A. A., de Leeuw, P. W., and Staals, J. (2013). Accumulation of mri markers of cerebral small vessel disease is associated with decreased cognitive function. A study in first-ever lacunar stroke and hypertensive patients. *Front. Aging Neurosci.* 5:72. doi: 10.3389/fnagi.2013.00072

Ii, Y., Maeda, M., Ishikawa, H., Ito, A., Matsuo, K., Umino, M., et al. (2019). Cortical microinfarcts in patients with multiple lobar microbleeds on 3 T MRI. *J. Neurol.* 266, 1887–1896. doi: 10.1007/s00415-019-09350-9

Ii, Y., Maeda, M., Kida, H., Matsuo, K., Shindo, A., Taniguchi, A., et al. (2013). *In vivo* detection of cortical microinfarcts on ultrahigh-field mri. *J. Neuroimaging* 23, 28–32. doi: 10.1111/j.1552-6569.2012.00722.x

Iliff, J. J., Goldman, S. A., and Nedergaard, M. (2015). Implications of the discovery of brain lymphatic pathways. *Lancet Neurol.* 14, 977–979. doi: 10.1016/s1474-4422(15)00221-5

Ishikawa, H., Ii, Y., Niwa, A., Shindo, A., Ito, A., Matsuura, K., et al. (2018). Comparison of premortem magnetic resonance imaging and postmortem autopsy findings of a cortical microinfarct. *J. Stroke Cerebrovasc. Dis.* 27, 2623–2626. doi: 10.1016/j.jstrokecerebrovasdis.2018.05.037

Ishikawa, H., Ii, Y., Shindo, A., Tabei, K.-I., Umino, M., Ito, A. O., et al. (2020). Cortical microinfarcts detected by 3-tesla magnetic resonance imaging. *Stroke* 51, 1010–1013. doi: 10.1161/strokeaha.119.028202

Ito, A. O., Shindo, A., Ii, Y., Ishikawa, H., Taniguchi, A., Shiba, M., et al. (2019). Small cortical infarcts transformed to lobar cerebral microbleeds: a case series. *J. Stroke Cerebrovasc. Dis.* 28, e30–e32. doi: 10.1016/j.jstrokecerebrovasdis.2018.12.050

Jennette, J. C., and Falk, R. J. (1997). Small-vessel vasculitis. *N. Engl. J. Med.* 337, 1512–1523. doi: 10.1056/NEJM199711203372106

Ji, T., Zhao, Y., Wang, J., Cui, Y., Duan, D., Chai, Q., et al. (2018). Effect of low-dose statins and apolipoprotein e genotype on cerebral small vessel disease in older hypertensive patients: a subgroup analysis of a randomized clinical trial. *J. Am. Med. Dir. Assoc.* 19, 995–1002.e1004 doi: 10.1016/j.jamda.2018.05.025

Kövari, E., Herrmann, F. R., Gold, G., Hof, P. R., and Charidimou, A. (2017). Association of cortical microinfarcts and cerebral small vessel pathology in the ageing brain. *Neuropathol. Appl. Neurobiol.* 43, 505–513. doi: 10.1111/nan.12366

Karama, S., Ducharme, S., Corley, J., Chouinard-Decorte, F., Starr, J. M., Wardlaw, J. M., et al. (2015). Cigarette smoking and thinning of the brain's cortex. *Mol. Psychiatry* 20, 778–785. doi: 10.1038/mp.2014.187

Kawagoe, S., Higuchi, T., Otaka, M., Shimada, Y., Kobayashi, H., Ida, H., et al. (2013). Morphological features of ips cells generated from fabry disease skin fibroblasts using sendai virus vector (SeVdp). *Mol. Genet. Metab.* 109, 386–389. doi: 10.1016/j.ymgme.2013.06.003

Kitamura, A., Fujita, Y., Oishi, N., Kalaria, R. N., Washida, K., Maki, T., et al. (2012). Selective white matter abnormalities in a novel rat model of

vascular dementia. *Neurobiol. Aging* 33, 1012.e25–1035.e25. doi: 10.1016/j.neurobiolaging.2011.10.033

Kitamura, A., Saito, S., Maki, T., Oishi, N., Ayaki, T., Hattori, Y., et al. (2015). Gradual cerebral hypoperfusion in spontaneously hypertensive rats induces slowly evolving white matter abnormalities and impairs working memory. *J. Cereb. Blood Flow Metab.* 36, 1592–1602. doi: 10.1177/0271678x15606717

Klarenbeek, P., van Oostenbrugge, R. J., Rouhl, R. P., Knottnerus, I. L., and Staals, J. (2013). Ambulatory blood pressure in patients with lacunar stroke: association with total MRI burden of cerebral small vessel disease. *Stroke* 44, 2995–2999. doi: 10.1161/strokeaha.113.002545

Kuo, Y. M., Beach, T. G., Sue, L. I., Scott, S., Layne, K. J., Kokjohn, T. A., et al. (2001). The evolution of a β peptide burden in the APP23 transgenic mice: implications for a β deposition in Alzheimer disease. *Mol. Med.* 7, 609–618. doi: 10.1007/bf03401867

Kwok, C. S., Shoamanesh, A., Copley, H. C., Myint, P. K., Loke, Y. K., and Benavente, O. R. (2015). Efficacy of antiplatelet therapy in secondary prevention following lacunar stroke: pooled analysis of randomized trials. *Stroke* 46, 1014–1023. doi: 10.1161/strokeaha.114.008422

Lau, K. K., Li, L., Schulz, U., Simoni, M., Chan, K. H., Ho, S. L., et al. (2017). Total small vessel disease score and risk of recurrent stroke: validation in 2 large cohorts. *Neurology* 88, 2260–2267. doi: 10.1212/wnl.0000000000004042

Ling, C., Liu, Z., Song, M., Zhang, W., Wang, S., Liu, X., et al. (2019). Modeling cadasil vascular pathologies with patient-derived induced pluripotent stem cells. *Protein Cell* 10, 249–271. doi: 10.1007/s13238-019-0608-1

Liu, J., Rutten-Jacobs, L., Liu, M., Markus Hugh, S., and Traylor, M. (2018). Causal impact of type 2 diabetes mellitus on cerebral small vessel disease. *Stroke* 49, 1325–1331. doi: 10.1161/strokeaha.117.020536

Liu-Ambrose, T., Best, J. R., Davis, J. C., Eng, J. J., Lee, P. E., Jacova, C., et al. (2016). Aerobic exercise and vascular cognitive impairment: a randomized controlled trial. *Neurology* 87, 2082–2090. doi: 10.1212/WNL.0000000000003332

Longstreth, W. T. Jr., Dulberg, C., Manolio, T. A., Lewis, M. R., Beauchamp, N. J. Jr., O'Leary, D., et al. (2002). Incidence, manifestations, and predictors of brain infarcts defined by serial cranial magnetic resonance imaging in the elderly: the cardiovascular health study. *Stroke* 33, 2376–2382. doi: 10.1161/01.str.0000032241.58727.49

Matsumoto, M. (2005). Cilostazol in secondary prevention of stroke: impact of the cilostazol stroke prevention study. *Atheroscler. Suppl.* 6, 33–40. doi: 10.1016/j.atherosclerosissup.2005.09.003

Matsuo, K., Shindo, A., Niwa, A., Tabei, K. I., Akatsu, H., Hashizume, Y., et al. (2018). Complement activation in capillary cerebral amyloid angiopathy. *Dement. Geriat. Cogn. Disord.* 44, 343–353. doi: 10.1159/000486091

Matsuyama, H., Ii, Y., Maeda, M., Umino, M., Ueda, Y., Tabei, K.-I., et al. (2017). Background and distribution of lobar microbleeds in cognitive dysfunction. *Brain Behav.* 7:e00856. doi: 10.1002/brb3.856

Miao, J., Xu, F., Davis, J., Otte-Holler, I., Verbeek, M. M., and Van Nostrand, W. E. (2005). Cerebral microvascular amyloid β protein deposition induces vascular degeneration and neuroinflammation in transgenic mice expressing human vasculotropic mutant amyloid β precursor protein. *Am. J. Pathol.* 167, 505–515. doi: 10.1016/s0002-9440(10)62993-8

Miyamoto, N., Pham, L. D., Hayakawa, K., Matsuzaki, T., Seo, J. H., Magnain, C., et al. (2013). Age-related decline in oligodendrogenesis retards white matter repair in mice. *Stroke* 44, 2573–2578. doi: 10.1161/strokeaha.113.001530

Miyamoto, N., Pham, L. D., Maki, T., Liang, A. C., and Arai, K. (2014). A radical scavenger edaravone inhibits matrix metalloproteinase-9 upregulation and blood-brain barrier breakdown in a mouse model of prolonged cerebral hypoperfusion. *Neurosci. Lett.* 573, 40–45. doi: 10.1016/j.neulet.2014.05.005

Moody, D. M., Brown, W. R., Challa, V. R., and Anderson, R. L. (1995). Periventricular venous collagenosis: association with leukoaraiosis. *Radiology* 194, 469–476. doi: 10.1097/00005072-199505000-00227

Ngandu, T., Lehtisalo, J., Solomon, A., Levalahti, E., Ahtiluoto, S., Antikainen, R., et al. (2015). A 2 year multidomain intervention of diet, exercise, cognitive training, and vascular risk monitoring versus control to prevent cognitive decline in at-risk elderly people (FINGER): a randomised controlled trial. *Lancet* 385, 2255–2263. doi: 10.1016/S0140-6736(15)60461-5

Nishio, K., Ihara, M., Yamasaki, N., Kalaria, R. N., Maki, T., Fujita, Y., et al. (2010). A mouse model characterizing features of vascular dementia with hippocampal atrophy. *Stroke* 41, 1278–1284. doi: 10.1161/strokeaha.110.581686

Niwa, A., Ii, Y., Shindo, A., Matsuo, K., Ishikawa, H., Taniguchi, A., et al. (2017). Comparative analysis of cortical microinfarcts and microbleeds using 3.0-tesla postmortem magnetic resonance images and histopathology. *J. Alzheimers Dis.* 59, 951–959. doi: 10.3233/jad-161242

Ogata, J., Yamanishi, H., and Ishibashi-Ueda, H. (2011). Review: role of cerebral vessels in ischaemic injury of the brain. *Neuropathol. Appl. Neurobiol.* 37, 40–55. doi: 10.1111/j.1365-2990.2010.01141.x

Ogawa Ito, A., Shindo, A., Ii, Y., Matsuura, K., Tabei, K. I., Maeda, M., et al. (2019). Microbleeds after carotid artery stenting: small embolism may induce cerebral microbleeds. *Cerebrovasc. Dis. Extra* 9, 57–65. doi: 10.1159/000500112

Oyama, N., Yagita, Y., Kawamura, M., Sugiyama, Y., Terasaki, Y., Omura-Matsuoka, E., et al. (2011). Cilostazol, not aspirin, reduces ischemic brain injury *via* endothelial protection in spontaneously hypertensive rats. *Stroke* 42, 2571–2577. doi: 10.1161/strokeaha.110.609834

Pantoni, L. (2010). Cerebral small vessel disease: from pathogenesis and clinical characteristics to therapeutic challenges. *Lancet Neurol.* 9, 689–701. doi: 10.1016/s1474-4422(10)70104-6

Pasi, M., Charidimou, A., Boulouis, G., Auriel, E., Ayres, A., Schwab, K. M., et al. (2018). Mixed-location cerebral hemorrhage/microbleeds: underlying microangiopathy and recurrence risk. *Neurology* 90, e119–e126. doi: 10.1212/wnl.0000000000004797

Rajani, R. M., and Williams, A. (2017). Endothelial cell-oligodendrocyte interactions in small vessel disease and aging. *Clin. Sci.* 131, 369–379. doi: 10.1042/cs20160618

Raposo, N., Calviere, L., Cazzola, V., Planton, M., Patsoura, S., Wargny, M., et al. (2018). Cortical superficial siderosis and acute convexity subarachnoid hemorrhage in cerebral amyloid angiopathy. *Eur. J. Neurol.* 25, 253–259. doi: 10.1111/ene.13484

Saito, S., Yamamoto, Y., and Ihara, M. (2019). Development of a multicomponent intervention to prevent Alzheimer's disease. *Front. Neurol.* 10:490. doi: 10.3389/fneur.2019.00490

Salvadores, N., Searcy, J. L., Holland, P. R., and Horsburgh, K. (2017). Chronic cerebral hypoperfusion alters amyloid-β peptide pools leading to cerebral amyloid angiopathy, microinfarcts and haemorrhages in Tg-SwDI mice. *Clin. Sci.* 131, 2109–2123. doi: 10.1042/cs20170962

Shang, J., Yamashita, T., Tian, F., Li, X., Liu, X., Shi, X., et al. (2019). Chronic cerebral hypoperfusion alters amyloid-β transport related proteins in the cortical blood vessels of Alzheimer's disease model mouse. *Brain Res.* 1723:146379. doi: 10.1016/j.brainres.2019.146379

Shen, M., Wei, G., Cheng, M., and Jiang, H. (2020). Association between enlarged perivascular spaces and internal carotid artery stenosis: a study in patients diagnosed by digital subtraction angiography. *J. Stroke Cerebrovasc. Dis.* 29:104635. doi: 10.1016/j.jstrokecerebrovasdis.2019.104635

Shibata, M., Ohtani, R., Ihara, M., and Tomimoto, H. (2004). White matter lesions and glial activation in a novel mouse model of chronic cerebral hypoperfusion. *Stroke* 35, 2598–2603. doi: 10.1161/01.str.0000143725.19053.60

Shibata, M., Yamasaki, N., Miyakawa, T., Kalaria, R. N., Fujita, Y., Ohtani, R., et al. (2007). Selective impairment of working memory in a mouse model of chronic cerebral hypoperfusion. *Stroke* 38, 2826–2832. doi: 10.1161/strokeaha.107.490151

Shimada, T., Shindo, A., Matsuyama, H., Yata, K., Niwa, A., Sasaki, R., et al. (2019). Chronic cerebral hypoperfusion upregulates leptin receptor expression in astrocytes and tau phosphorylation in tau transgenic mice. *Neurosci. Lett.* 704, 133–140. doi: 10.1016/j.neulet.2019.04.009

Shindo, A., Liang, A. C., Maki, T., Miyamoto, N., Tomimoto, H., Lo, E. H., et al. (2016). Subcortical ischemic vascular disease: roles of oligodendrocyte function in experimental models of subcortical white-matter injury. *J. Cereb. Blood Flow Metab.* 36, 187–198. doi: 10.1038/jcbfm.2015.80

Shinohara, Y., Katayama, Y., Uchiyama, S., Yamaguchi, T., Handa, S., Matsuoka, K., et al. (2010). Cilostazol for prevention of secondary stroke (csps 2): an aspirin-controlled, double-blind, randomised non-inferiority trial. *Lancet Neurol.* 9, 959–968. doi: 10.1016/s1474-4422(10)70198-8

Silasi, G., She, J., Boyd, J. D., Xue, S., and Murphy, T. H. (2015). A mouse model of small-vessel disease that produces brain-wide-identified microocclusions and regionally selective neuronal injury. *J. Cereb. Blood Flow Metab.* 35, 734–738. doi: 10.1038/jcbfm.2015.8

Smith, E. E., Schneider, J. A., Wardlaw, J. M., and Greenberg, S. M. (2012). Cerebral microinfarcts: the invisible lesions. *Lancet Neurol.* 11, 272–282. doi: 10.1016/s1474-4422(11)70307-6

Sozmen, E. G., Hinman, J. D., and Carmichael, S. T. (2012). Models that matter: white matter stroke models. *Neurotherapeutics* 9, 349–358. doi: 10.1007/s13311-012-0106-0

Sozmen, E. G., Kolekar, A., Havton, L. A., and Carmichael, S. T. (2009). A white matter stroke model in the mouse: axonal damage, progenitor responses and mri correlates. *J. Neurosci. Methods* 180, 261–272. doi: 10.1016/j.jneumeth.2009.03.017

Staals, J., Makin, S. D., Doubal, F. N., Dennis, M. S., and Wardlaw, J. M. (2014). Stroke subtype, vascular risk factors, and total mri brain small-vessel disease burden. *Neurology* 83, 1228–1234. doi: 10.1212/wnl.0000000000000837

Sturchler-Pierrat, C., Abramowski, D., Duke, M., Wiederhold, K. H., Mistl, C., Rothacher, S., et al. (1997). Two amyloid precursor protein transgenic mouse models with Alzheimer disease-like pathology. *Proc. Natl. Acad. Sci. U S A* 94, 13287–13292. doi: 10.1073/pnas.94.24.13287

Tai, S. Y., Chien, C. Y., Chang, Y. H., and Yang, Y. H. (2017). Cilostazol use is associated with reduced risk of dementia: a nationwide cohort study. *Neurotherapeutics* 14, 784–791. doi: 10.1007/s13311-017-0512-4

Takahashi, K., and Yamanaka, S. (2006). Induction of pluripotent stem cells from mouse embryonic and adult fibroblast cultures by defined factors. *Cell* 126, 663–676. doi: 10.1016/j.cell.2006.07.024

Thal, D. R., Griffin, W. S., de Vos, R. A., and Ghebremedhin, E. (2008). Cerebral amyloid angiopathy and its relationship to Alzheimer's disease. *Acta Neuropathol.* 115, 599–609. doi: 10.1007/s00401-008-0366-2

Tomimoto, H. (2011). Subcortical vascular dementia. *Neurosci. Res.* 71, 193–199. doi: 10.1016/j.neures.2011.07.1820

Toyoda, K., Uchiyama, S., Yamaguchi, T., Easton, J. D., Kimura, K., Hoshino, H., et al. (2019). Dual antiplatelet therapy using cilostazol for secondary prevention in patients with high-risk ischaemic stroke in japan: a multicentre, open-label, randomised controlled trial. *Lancet Neurol.* 18, 539–548. doi: 10.1016/s1474-4422(19)30148-6

Umino, M., Maeda, M., Ii, Y., Tomimoto, H., and Sakuma, H. (2019). 3D double inversion recovery MR imaging: clinical applications and usefulness in a wide spectrum of central nervous system diseases. *J. Neuroradiol.* 46, 107–116. doi: 10.1016/j.neurad.2018.06.002

van Middelaar, T., Argillander, T. E., Schreuder, F., Deinum, J., Richard, E., and Klijn, C. J. M. (2018). Effect of antihypertensive medication on cerebral small vessel disease: a systematic review and meta-analysis. *Stroke* 49, 1531–1533. doi: 10.1161/strokeaha.118.021160

van Veluw, S. J., Charidimou, A., van der Kouwe, A. J., Lauer, A., Reijmer, Y. D., Costantino, I., et al. (2016). Microbleed and microinfarct detection in amyloid angiopathy: a high-resolution mri-histopathology study. *Brain* 139, 3151–3162. doi: 10.1093/brain/aww229

van Veluw, S. J., Hilal, S., Kuijf, H. J., Ikram, M. K., Xin, X., Yeow, T. B., et al. (2015). Cortical microinfarcts on 3T MRI: clinical correlates in memory-clinic patients. *Alzheimers Dement.* 11, 1500–1509. doi: 10.1016/j.jalz.2014.12.010

van Veluw, S. J., Shih, A. Y., Smith, E. E., Chen, C., Schneider, J. A., Wardlaw, J. M., et al. (2017). Detection, risk factors, and functional consequences of cerebral microinfarcts. *Lancet Neurol.* 16, 730–740. doi: 10.1016/s1474-4422(17)30196-5

van Veluw, S. J., Zwanenburg, J. J., Engelen-Lee, J., Spliet, W. G., Hendrikse, J., Luijten, P. R., et al. (2013). *In vivo* detection of cerebral cortical microinfarcts with high-resolution 7T MRI. *J. Cereb. Blood Flow Metab.* 33, 322–329. doi: 10.1038/jcbfm.2012.196

Vermeer, S. E., Koudstaal, P. J., Oudkerk, M., Hofman, A., and Breteler, M. M. (2002). Prevalence and risk factors of silent brain infarcts in the population-based rotterdam scan study. *Stroke* 33, 21–25. doi: 10.1161/hs0102.101629

Wakita, H., Tomimoto, H., Akiguchi, I., and Kimura, J. (1994). Glial activation and white matter changes in the rat brain induced by chronic cerebral hypoperfusion: an immunohistochemical study. *Acta Neuropathol.* 87, 484–492. doi: 10.1007/s004010050114

Wakita, H., Tomimoto, H., Akiguchi, I., Matsuo, A., Lin, J. X., Ihara, M., et al. (2002). Axonal damage and demyelination in the white matter after chronic cerebral hypoperfusion in the rat. *Brain Res.* 924, 63–70. doi: 10.1016/s0006-8993(01)03223-1

Wardlaw, J. M., Smith, E. E., Biessels, G. J., Cordonnier, C., Fazekas, F., Frayne, R., et al. (2013). Neuroimaging standards for research into small vessel disease and its contribution to ageing and neurodegeneration. *Lancet Neurol.* 12, 822–838. doi: 10.1016/S1474-4422(13)70124-8

Wardlaw, J. M., Smith, C., and Dichgans, M. (2019). Small vessel disease: mechanisms and clinical implications. *Lancet Neurol.* 18, 684–696. doi: 10.1016/S1474-4422(19)30079-1

Wilson, D., Hostettler, I. C., Ambler, G., Banerjee, G., Jäger, H. R., and Werring, D. J. (2017). Convexity subarachnoid haemorrhage has a high risk of intracerebral haemorrhage in suspected cerebral amyloid angiopathy. *J. Neurol.* 264, 664–673. doi: 10.1007/s00415-017-8398-y

Yamori, Y., and Horie, R. (1977). Developmental course of hypertension and regional cerebral blood flow in stroke-prone spontaneously hypertensive rats. *Stroke* 8, 456–461. doi: 10.1161/01.str.8.4.456

Zaucker, A., Mercurio, S., Sternheim, N., Talbot, W. S., and Marlow, F. L. (2013). Notch3 is essential for oligodendrocyte development and vascular integrity in zebrafish. *Dis. Model. Mech.* 6, 1246–1259. doi: 10.1242/dmm.012005

Conflict of Interest: The authors declare that the research was conducted in the absence of any commercial or financial relationships that could be construed as a potential conflict of interest.

frontiers in Aging Neuroscience

REVIEW
published: 07 May 2020
doi: 10.3389/fnagi.2020.00091

Clinical and Genetic Aspects of CADASIL

Toshiki Mizuno, Ikuko Mizuta, Akiko Watanabe-Hosomi, Mao Mukai and Takashi Koizumi*

Department of Neurology, Graduate School of Medical Science, Kyoto Prefectural University of Medicine, Kyoto, Japan

Cerebral autosomal dominant arteriopathy with subcortical infarcts and leukoencephalopathy (CADASIL), a hereditary cerebral small vessel disease caused by mutations in *NOTCH3*, is characterized by recurrent stroke without vascular risk factors, mood disturbances, and dementia. MRI imaging shows cerebral white matter (WM) hyperintensity, particularly in the external capsule and temporal pole. Missense mutations related to a cysteine residue in the 34 EGFr on the NOTCH3 extracellular domain (N3ECD) are a typical mutation of CADASIL. On the other hand, atypical mutations including cysteine sparing mutation, null mutation, homozygous mutation, and other associate genes are also reported. From the viewpoint of gain of function apart from Notch signaling or loss of function of Notch signaling, we review the research article about CADASIL and summarized the pathogenesis of small vessel, stroke, and dementia in this disease.

OPEN ACCESS

Edited by:
Satoshi Saito, National Cerebral and Cardiovascular Center (Japan), Japan

Reviewed by:
Yumi Yamamoto, National Cerebral and Cardiovascular Center (Japan), Japan
Sabina-Capellari, University of Bologna, Italy

***Correspondence:**
Toshiki Mizuno
mizuno@koto.kpu-m.ac.jp

Received: *18 December 2019*
Accepted: *18 March 2020*
Published: *07 May 2020*

Citation:
Mizuno T, Mizuta I, Watanabe-Hosomi A, Mukai M and Koizumi T (2020) Clinical and Genetic Aspects of CADASIL. Front. Aging Neurosci. 12:91. doi: 10.3389/fnagi.2020.00091

Keywords: CADASIL, notch signaling, GOM, white matter lesion, vascular dementia

INTRODUCTION

Cerebral autosomal dominant arteriopathy with subcortical infarcts and leukoencephalopathy (CADASIL) is one of the most common hereditary cerebral small vessel diseases caused by mutations in *NOTCH3*. C was first recognized as a clinical and genetic hereditary small-vessel disease entity that induces cerebral infarction, white matter (WM) disease, microbleeds, and finally, vascular dementia. Understanding the impact of this disease is important for analyzing small-vessel diseases as well as vascular dementia. This review article is summarized in terms of whether CADASIL is caused by the gain of NOTCH3 function or by loss of NOTCH signaling function. Supporting data for a gain of function is pro-aggregatory property of cysteine related or cysteine-sparing *NOTCH3* mutations as well as homozygous *NOTCH3*

Abbreviations: ADAM10, A disintegrin and metalloprotease 10; ADC, apparent diffusion coefficient; BPF, brain parenchymal fraction; CADASIL, cerebral autosomal dominant arteriopathy with subcortical infarcts and leukoencephalopathy; CARASIL, cerebral autosomal recessive arteriopathy with subcortical infarcts and leukoencephalopathy; CM, cerebral microbleeds; CSL, CBF1-Su(H)-Lag1; DAD, Disability Assessment for Dementia; DSL, Delta/Serrate/LAG-2; ExAC, exome aggregation consortium; EGFrs, epidermal growth factor-like repeats; ICAS, intracranial arterial stenosis; Jag1, Jagged1; LTBP-1, latent TGF-β–binding protein 1; mean-ADC, mean apparent diffusion coefficient; NECD, Notch extracellular domain; NICD, Notch intracellular domain; N3ECD, Notch3 extracellular domain; N3ICD, Notch3 intracellular domain; Non-NOTCH3, NOTCH3-negative CADASIL–like patients; GOM, granular osmiophilic material; PVS, perivascular spaces; RNF213, ring finger protein 213; TGF-β, transforming growth factor-β; TIMP3, tissue inhibitor of metalloproteinases 3; VSMC, vascular smooth muscle cell; VTN, vitronectin; WM, white matter; WMH, white matter hyperintensity; WML, white matter lesion.

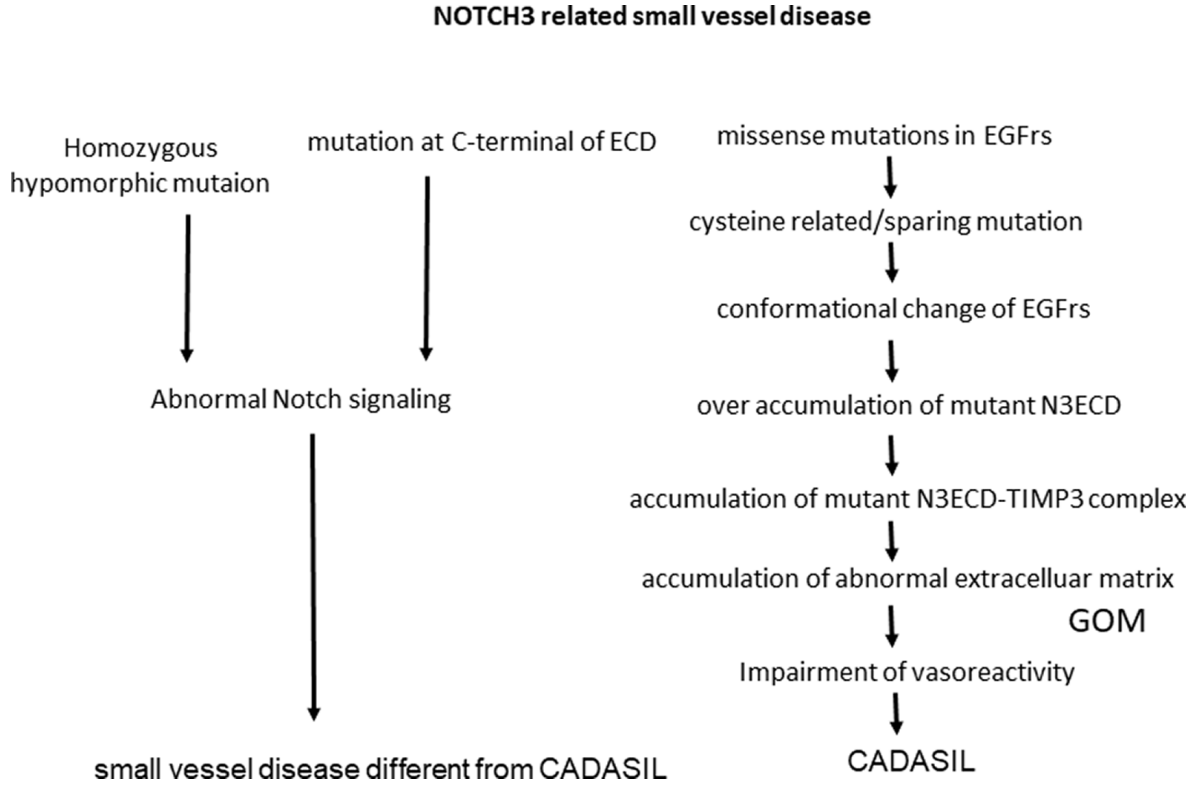

FIGURE 1 | NOTCH3 is related to small vessel disease. ECD, extracellular domain; N3ECD, Notch3 extracellular domain; EGFrs, Epidermal Growth Factor repeats; GOM, granular osmiophilic material; TIMP3, tissue inhibitor of metalloproteinases 3.

mutation. Also, pathological findings of the accumulation of extracellular matrix and granular osmiophilic material (GOM) supported the hypothesis that Notch extracellular domain (NECD) can be a core of aggregation. Looking from the other side, nonsense *NOTCH3* mutation or constitutive activation of NOTCH3 signaling can be related to the pathogenesis of different cerebral small vessel disease from CADASIL (**Figure 1**).

GENETICS

NOTCH3 Mutations

Notch signaling is evolutionarily conserved, and four members of the Notch receptor family: NOTCH1-4 exist in humans. *NOTCH3* encodes a single-pass transmembrane receptor, NOTCH3, which consists of a NECD including 34 epidermal growth factor-like repeats (EGFrs) and an Notch intracellular domain (NICD). The Notch protein is thought to undergo complex proteolytic processing events. The first cleavage, named as S1 cleavage of the receptor occurs on the Golgi for the maturation of the receptor (i.e., the formation of the NECD-NICD heterodimer). The second proteolysis, named as S2 cleavage by A disintegrin and metalloprotease 10 (ADAM10), occurs on the cell surface when the receptor interacts with NOTCH ligand, Jagged or Delta/Serrate/LAG-2 (DSL), on neighboring cells (Brou et al., 2000). The third cleavage, named as S3 cleavage: γ-secretase–dependent intra-membrane proteolysis, NICD is moved into the cytoplasm and shuttles to the nucleus. Finally, NICD activated target genes with transcriptional cofactors of the CBF1-Su(H)-Lag1 (CSL) family (Bray, 2006). While *NOTCH3* mainly expressed in the central nervous system in the fetus, *NOTCH3* is expressed predominantly in vascular smooth muscle cells (VSMCs) to maintain vascular contractility in adults (Joutel et al., 2000).

NOTCH3 MUTATIONS IN CADASIL PATIENTS

Cysteine-Related

To date, more than 200 cysteine-related mutations, most of which are single nucleotide changes, have been reported (**Supplementary Table S1**, Joutel et al., 1997; Rutten et al., 2014; Koizumi et al., 2019; Leiden Open Variation Database, or references therein). A few exceptions include in-frame insertion/deletion mutations and splicing-site mutations (Tikka et al., 2009). Also, a rare mutation of in-frame 15 bp duplication in exon 7 is reported (Lee et al., 2011). CADASIL-associated mutations are localized from exon2 to 24, which encode EGFrs. Each EGFr contains six cysteine residues that likely participate in forming three pairs of disulfide bonds to maintain the normal NOTCH3 protein conformation. Most of the mutations are of the

missense type, resulting in an even number to an odd number of cysteine residues (Joutel et al., 1997; Mizuta et al., 2017). The resulting unpaired cysteine is predicted to cause abnormal disulfide bridge formation that leads to aggregation of NECD (Duering et al., 2011).

The mutations accumulate in EGFrs 1–6, apart from the ligand-binding domain, EGFrs 10 and 11. Cellular experiments showed that most of the mutations do not affect Notch signaling, suggesting that CADASIL is not caused by signaling dysfunction. However, NOTCH3 harboring a p.Cys428Ser mutation in EGFr 10 and p.Cys455Arg in EGFr 11 exhibits attenuated ligand-binding activity, resulting in a significant reduction of NOTCH3 signaling (Joutel et al., 2004; Peters et al., 2004b). A previous report showed that mutations in EGFrs 10 and 11 are associated with milder cognitive deficits and a trend toward a lower volume of lacunar infarcts compared with the common mutations in EGFrs 2–5 (Monet-Leprêtre et al., 2009). This association remains to be elucidated, but it is possible that Notch signaling may affect the clinical symptoms.

Cases with duplication (Lee et al., 2011) or deletion of *NOTCH3* (Dichgans et al., 2000) are reported. These mutations also change the number of Cysteine residue as well as point mutation and GOM was detected in the cases with these mutations (Lee et al., 2011).

Biological Effect of CADASIL-Associated Mutations

A popular hypothesis holds that the *NOTCH3* mutations causing CADASIL are gain-of-function rather than loss-of-function mutations (Carare et al., 2013). One of the evidence supporting this hypothesis was the identification of hypomorphic mutations in individuals without the CADASIL phenotype. Rutten et al. (2013) reported two *NOTCH3* nonsense mutations, c.307C>T, p.Arg103*, in two brothers aged in their 50s; brain MRI and skin biopsy results showed incompatible with CADASIL. Also, they reported a CADASIL patient with compound heterozygous for a pathogenic *NOTCH3* mutation, p.Tyr710Cys, and an intragenic frameshift deletion. In that patient's family, p.Tyr710Cys segregated with the affected parent, whereas the intragenic frameshift deletion was also identified in the normal parent of the patient. They concluded that these hypomorphic NOTCH3 alleles do not cause CADASIL (Rutten et al., 2013). According to previous case reports, complete loss of, and also constitutive activation of NOTCH3 signaling are thought to cause arteriopathy. Pippucci et al. (2015) reported a 24 years-old man with childhood-onset arteriopathy and cavitating leukoencephalopathy. Exome analysis of the patient and his consanguineous parents identified homozygous NOTCH3 null mutation c.C2898A (p.C966*) in the patient. Fouillade et al. (2008) reported a 53-year-old woman with 35-years-onset stroke and MRI finding of WM hyperintensity. They identified *NOTCH3* c.4544T>C resulting in p.L1515P mutation which localizes in the C-terminal end of NOTCH3 extracellular domain (N3ECD). Although the precise mechanism remains unknown, cellular experiments suggested increased NOTCH3 signaling of this mutation in a ligand-independent manner (Pippucci et al., 2015). It is of note that the pathological hallmark of CADASIL, GOM, was not detected in either of these patients (Fouillade et al., 2008; Pippucci et al., 2015), suggesting that arteriopathy related to abnormal NOTCH3 signaling is different from CADASIL. In a study using a transgenic mouse model of CADASIL, Joutel described the toxic gain-of-function properties of mutant NOTCH3. Mice harboring human *NOTCH3* with p.Arg90Cys, p.Cys428Ser, or p.Arg169Cys mutations exhibited CADASIL-like pathologic changes, N3ECD accumulation, and deposition of GOM (see below). Notably, transgenic mice with p.Cys428Ser, which cannot mediate Notch signaling (see above), also showed GOM deposition, suggestive of toxic gain-of-function mutations leading to aggregation of mutated N3ECD (Joutel, 2011).

Cysteine-Sparing Mutations

Muino et al. (2017) recently reviewed cysteine-sparing *NOTCH3* missense mutations and proposed criteria for their pathogenicity: (a) typical clinical CADASIL syndrome; (b) diffuse white matter hyperintensity (WMH); (c) 33 NOTCH3 exons analyzed; (d) mutations that were not polymorphisms; and (e) GOM deposits noted in skin biopsy. Of the 25 mutations reviewed, they concluded that p.Arg61Trp, p.Arg75Pro, p.Asp80Gly, and p.Arg213Lys fulfilled these criteria. To uncover the pathogenicity of cysteine-sparing mutations, analysis of pro-aggregatory property may be important. Some cysteine-involving mutations (Duering et al., 2011) and also p.Arg75Pro and p.Asp80Gly (Wollenweber et al., 2015) was reported to be prone to aggregation by using a single-particle aggregation assay. In the very recent report of the patient with p.Gly73Ala, unfortunately, skin biopsy was declined, cellular and *in vitro* experiments showed pro-aggregatory property of the mutation (Huang et al., 2020).

Of the pathogenic cysteine-sparing mutations, p.Arg75Pro is probably the most frequent, and this mutation is primarily reported in eastern Asians (Kim et al., 2006; Mizuno et al., 2008; Ueda et al., 2015). In addition to positive skin biopsy findings, we also noted co-segregation in a p.Arg75Pro family and demonstrated the predicted conformational change in the EGFr harboring this mutation (Mizuno et al., 2008). Japanese CADASIL patients with p.Arg75Cys exhibit atypical and mild phenotypes, including a lower frequency of stroke/TIA and temporal pole lesions, with a tendency toward an older age at onset (Ueda et al., 2015; Koizumi et al., 2019).

Homozygous Mutations

Although CADASIL is generally caused by heterozygous mutations in *NOTCH3*, several CADASIL cases involving homozygous mutations have been reported (Mukai et al., 2018). Interestingly, some cases involving homozygous mutations showed a more-severe clinical phenotype than cases involving heterozygous mutations, but other cases were within the spectrum of the heterozygous phenotype.

The most frequent homozygous mutation is p.Arg544Cys. Mukai et al. (2018) reported a 63-year-old male case presenting first stroke attack with only mild weakness of the left leg and recovered well, involving a homozygous p.Arg544Cys mutation; GOM around the basement membrane of VSMCs on skin biopsy

were detected in this case. No other stroke patients were detected in his parents and siblings indicated the tendency toward a mild phenotype with the p.Arg544Cys mutation in agreement with previous reports (Liao et al., 2015; Lee et al., 2016). p.Arg544Cys locates not in EGFr, but between the 13th and 14th EGFrs. Therefore, we hypothesize that p.Arg544Cys may contribute to a milder effect to a conformational change of EGFr resulting in a milder phenotype. The p.Arg544Cys mutation is also notable because of its geographic accumulation. The frequency of this mutation in CADASIL patients is 93.6% in Jeju Island, Korea, and 70.5% in Taiwan (Liao et al., 2015; Lee et al., 2016).

DISEASE-MODIFYING GENES

Genome-Wide Association Study of CADASIL

Opherk et al. (2014) performed a genome-wide association study to identify genetic modifiers of WMH volume in CADASIL. They analyzed SNP array data for 466 patients and found no SNPs reaching genome-wide significance. However, polygenic score analyses which included SNPs with weak *p*-values, indicated significant association with WMH volume when 10,574 SNPs (each p-value < 0.1) or 52,125 SNPs (each p-value < 0.5) were included. They suggested that multiple variants exert small effects on the WMH burden in CADASIL.

RNF213

We recently reported ring finger protein 213 (RNF213)-related susceptibility to intracranial arterial stenosis (ICAS) in CADASIL patients (Yeung et al., 2018). The frequency of RNF213 variants was 23.5% in CADASIL patients with ICAS, compared with 1.9% in those without ICAS. CADASIL is recognized as a small-vessel disease, but intracranial major artery stenosis was reported in some CADASIL patients (Choi et al., 2005). The susceptibility variant rs112735431, c.14576G>A (p.R4859K) or c.14429G>A (p.R4110K) in RNF213, was originally identified as prominently associated with moyamoya disease, mainly reported in eastern Asia. Miyawaki et al. (2012) found the variant was linked to susceptibility to ICAS even in sporadic cases. These associated genes may contribute to the clinical phenotypes of CADASIL.

PATHOMECHANISM FROM THE PERSPECTIVE OF MUTATION AND PATHOLOGY

Pathology

CADASIL affects small vessels in the brain WM and deep gray matter, resulting in thickening of vascular walls and luminal stenosis. In the tunica media, degeneration of VSMCs, positive PAS staining, and granular deposits of N3ECD immunoreactivity are observed (Baudrimont et al., 1993; Joutel et al., 2000). In the tunica adventitia, accumulation of various fibrous extracellular matrices is observed, including collagen, laminin, and clusterin. However, vessel occlusion or thrombosis is rarely found (Ruchoux et al., 1995). Therefore, the direct pathogenic mechanism leading to lacunar infarction in CADASIL remains to be elucidated. A popular hypothetical pathomechanism involves hemodynamic disturbance of lesion-affected arterioles and loss of compliance and autoregulation (Tikka et al., 2014).

GOM

The first ultrastructural descriptions of perivascular deposits surrounding small, penetrating arteries in the brain, designated GOM, were reported by Baudrimont et al. (1993). This material has been examined mainly in the brain, but GOM is also found surrounding VSMCs in other tissues, including muscle and skin (Ruchoux et al., 1995). Tikka et al. (2009) investigated the GOM in CADASIL patients and concluded that COM is specific to CADASIL. Immunohistochemistry and immunogold electron microscopy studies revealed the distribution of GOM and N3ECD protein in the microvasculature of brain gray matter and WM. Immunogold electron microscopy using an antibody to N3ECD revealed abundant particles in the GOM within microvessels, VSMC membranes, and perivascular cells (Yamamoto et al., 2013). These results suggest that NOTCH3 fragments are major components of GOM deposits.

Transendocytosis of NOTCH3

Cisendocytosis of either the DSL ligands or the Notch receptor itself into the cytoplasm has been recognized as playing an important role in regulating Notch signaling (Bray, 2006; Fortini and Bilder, 2009; Pratt et al., 2011). Also, genetic and cellular biological studies have shown that Notch is endocytosed into neighboring ligand-expressing cells in *Drosophila* (Klueg and Muskavitch, 1999) and that endocytosis of NECD promotes Notch proteolysis and downstream signaling in mammals (Nichols et al., 2007). Therefore, endocytosis of NECD into ligand-expressing cells, known as trans-endocytosis, is believed to be more critical for Notch activation than proteolytic events (Nichols et al., 2007). Because CADASIL causing mutations localize in N3ECD, we hypothesized that impairment of N3ECD trans-endocytosis may be a pathological mechanism of CADASIL. We addressed this issue by using HEK293 cells harboring a single copy of mutant or wildtype human *NOTCH3* cDNA cocultured with Jagged1-expressing cells (Watanabe-Hosomi et al., 2012). In this co-culture system, Notch signaling quantified by HES1 expression was similar between mutant and wildtype N3ECD, in agreement with previous reports. However, we found that C185R mutant N3ECD on the cell surface is degraded significantly more slowly than wild-type N3ECD in NOTCH3 cells. While vesicles containing N3ECD were observed in Jag1-expressing cells co-cultured with wild-type NOTCH3, vesicles with mutant N3ECD within the Jag1-expressing cells were significantly fewer in number. These results indicate that the process of degradation of mutant N3ECD on the cell surface is disturbed due to the impairment of trans-endocytosis (Watanabe-Hosomi et al., 2012). It can also explain the abnormal accumulation of N3ECD in vascular walls without accumulation of the intracellular domain of Notch3 intracellular domain (N3ICD) or full-length protein, and signaling is activated normally. Further approach is necessary to uncover the process between impaired trans-endocytosis and abnormal accumulation of N3ECD and GOM deposit.

TIMPS3 and VTN

Using cultured cells, Monet-Leprêtre et al. (2013) provided evidence that excess levels of or multimerization of mutant Notch3 ECD facilitate interactions with key components of the vascular extracellular matrix, including tissue inhibitor of metalloproteinases 3 (TIMP3) and VTN. Brain vessels from transgenic mice and patients with CADASIL exhibit elevated levels of both insoluble cross-linked and soluble TIMP3 species (Monet-Leprêtre et al., 2013). Later, Capone et al. (2016) showed that reducing TIMP3 or VTN ameliorated CADASIL phenotype using transgenic mice, suggesting TIMP3 or VTN may be a novel therapeutic target of CADASIL.

Downstream Signaling Related to TGF-β

It is well known that transforming growth factor-β (TGF-β) signaling is important in the regulation of fibrotic events in vessels and other various tissues. Increased TGF-β signaling was reported as the pathophysiology of cerebral autosomal recessive arteriopathy with subcortical infarcts and leukoencephalopathy (CARASIL; Hara et al., 2009), suggesting TGF-β signaling as a key pathway to cerebral small vessel diseases. Kast et al. (2014) examined molecules involving in the regulation of TGF-β bioavailability, fibronectin, fibrillin-1, and latent TGF-β–binding protein 1 (LTBP-1), in post-mortem brain tissue from CADASIL patients. All the three molecules were enriched in the CADASIL vessel. However, fibronectin and fibrillin-1 did not colocalize with N3ECD deposits, whereas, LTBP-1 showed a striking co-localization with N3ECD deposits, suggesting specific recruitment of LTBP-1 into aggregates. Also, increased levels of the TGF-β prodomain indicate dysregulation of the TGF-β pathway in CADASIL development. *In vitro* co-aggregation assay showed a direct interaction between LTBP-1 and mutant N3-ECD but no interaction between LTBP-1 and wildtype N3-ECD. These suggested a specific co-aggregation of LTBP-1 with mutant NOTCH3 and possible TGF-β signaling impairment in CADASIL (Kast et al., 2014).

Reconstruction of Small Vessels

To examine the degree and extent of the pathologic changes, Okeda et al. (2002) analyzed the entire length of vessels by reconstructing 1,000 serial sections of the 11 cerebral medullary arteries in an autopsy of a CADASIL patient who was 75 years old. The predominant findings were loss of VSMCs in the tunica media and fibrosis in the tunica adventitia. Most arteries exhibited continuous complete loss of VSMCs in the WM. Severe adventitial fibrosis was found in all arteries but restricted to WM. However, no stenosis or occlusion was found in the arteries studied. Considering their results collectively, they used a "so-called earthen pipe state" to describe the state of lesioned arteries and proposed failure of autoregulation of cerebral blood flow due to the earthen pipe state as underlying the pathogenesis of CADASIL (Okeda et al., 2002).

Pericytes

As the receptor protein encoded by the *NOTCH3* gene is expressed not only on VSMCs but also on pericytes, pericytes and capillary vessels can be damaged by CADASIL (Dziewulska and Lewandowska, 2012). Degeneration and loss of pericytes in capillary vessels were detected in the microvessels in the autopsy of the brain and skin-muscle biopsy in CADASIL patients (Dziewulska and Lewandowska, 2012). GOM was usually seen near pericyte cell membranes or within infoldings (Dziewulska and Lewandowska, 2012). These findings suggested increased permeability of the capillary vessels and disturbances in cerebral microcirculation; this degeneration can also cause defective vasomotor reactivity in CADASIL (Okeda et al., 2002; Qin et al., 2019).

Why Clinical Symptoms Occur Only in the Brain

Because NOTCH3 is expressed ubiquitously in VSMCs, it is not surprising that pathological changes including GOM can be detected not only in the brain but also in other organs. It is reported that peripheral vascular function, as well as in the brain, was also impaired in patients with CADASIL and also a transgenic mice model of CADASIL (Fujiwara et al., 2012).

Clear phenotypes are restricted to the brain, but several studies suggested cardiovascular (van den Boom et al., 2003; Rufa et al., 2007) and renal (Kusaba et al., 2007; Guerrot et al., 2008; Ragno et al., 2012) involvement, though their causal relationship is still unclear. A recent article by Kelleher et al. (2019) showed that CADASIL iPSC-derived mural cells, including VSMCs and pericytes were susceptible to apoptotic stress. This may explain why major symptoms are restricted to the brain, because the blood-brain barrier, the crucial structure to maintain brain homeostasis, consists of astrocytes and pericytes (Ihara and Yamamoto, 2016).

CLINICAL FEATURES OF CADASIL

Incidence

To date, thousands of families with CADASIL have been diagnosed worldwide in many different ethnic groups. The disorder is often overlooked and misdiagnosed. Its minimum prevalence has been estimated at between 2 and 5 in 100,000 but may vary between populations (Razvi et al., 2005; Narayan et al., 2012; Moreton et al., 2014; Bianchi et al., 2015).

Genotype-Phenotype Correlation

There have been a limited number of studies involving genotype-phenotype analyses, some of which reported negative results (Adib-Samii et al., 2010). On the other hand, a German study including 371 CADASIL patients showed positive findings in genotype-phenotype analyses of eight of the most frequent genotypes: p.Arg90Cys, p.Cys117Phe, p.Arg133Cys, p.Arg14.

1Cys, p.Arg153Cys, p.Arg169Cys, p.Cys174Tyr, and p.Arg182Cys (Opherk et al., 2004). Both p.Cys174Tyr and p.Cys117Phe was significantly associated with a lower median age at death, and p.Cys117Phe alone was significantly associated with a lower median age at onset of stroke and immobilization (Opherk et al., 2004). Genotype-phenotype correlation analyses of each mutation should be carefully conducted due to the wide phenotype distribution, even in the same family harboring the same mutation.

EGF Repeats 1–6 vs. 7–34

Rutten et al. (2019) recently demonstrated the effect of mutation location on the severity of the disease. By comparing CADASIL patients with mutations in EGFr 1–6 and EGFr 7–34, those in the EGFr 1–6 group had a 12-year earlier onset of stroke, lower survival, and higher WMH volume than those in the EGFr 7–34 group. As described above, *NOTCH3* mutations in CADASIL patients accumulate in EGFr 1–6, at 71.8% in Europeans (Rutten et al., 2019). It is noteworthy that *NOTCH3* pathogenic variants were identified in a recent analysis of a large-scale genome variation database of a general population (Rutten et al., 2016). *NOTCH3* pathogenic variants in a general population accumulated in EGFr 7–34, at 97.5% in the general European population, based on the Genome Aggregation Database (Rutten et al., 2016). Taken together, the results of Rutten et al. (2019) suggest a predisposition toward EGFr 1–6 in the classical, more-severe CADASIL phenotype. They also suggest a broad disease spectrum involving EGFr 7–34, from a mild phenotype to possible non-penetrance, and these results highlight the significant role of *NOTCH3* pathogenic variants in general populations.

Environmental Factors

The difference between clinical symptoms and course in the same family harboring the same *NOTCH3* mutation indicates the importance of environmental factors. Of the two twin studies of CADASIL, the first reported one found apparent different phenotypes, including 14 years difference of the age at onset between the twins, suggesting an effect of environmental factors on the disease (Mykkänen et al., 2009). The second reported one found similar phenotypes, including the age at onset of 74–75 years old and parkinsonism in the twin (Ragno et al., 2016). A similar phenotype indicates similar lifestyle-related factors, and Ragno's cases did not contradict the possible effect of environmental factors on the CADASIL phenotype (Ragno et al., 2016). Conventional vascular risk factors may influence the severity of the disease. Adib-Samii et al. (2010) analyzed 200 symptomatic CADASIL patients in the UK; they found that hypertension (odds ratio 2.57) and pack-years of smoking (odds ratio 1.07) were associated with an increased risk of stroke. *Ciolli* also assessed the influence of vascular risk factors and revealed that hypertension was related to both disability assessment for dementia (DAD) score and disability (Ciolli et al., 2014). In our cohort, 62.9% of CADASIL patients had vascular risk factors, including hypertension, diabetes mellitus, hyperlipidemia, smoking, or alcohol consumption, and they were more prone to stroke (Mizuta et al., 2017). Management of these factors are essential in CADASIL as well as sporadic cases.

DIAGNOSIS

Criteria for CADASIL Diagnosis

Original criteria for CADASIL diagnosis were proposed by Davous in 1997 (Davous, 1998). This precious work contributed to the core concept of CADASIL when CADASIL was not well recognized by physicians yet. However, genetic tests of *NOTCH3* revealed atypical cases, and the clinical phenotype of CADASIL was diverse, ranging from asymptomatic to severe. The *Davous's* criteria cannot be applied to atypical CADASIL cases because the criteria are strict and have low sensitivity. In particular, cases involving elderly onset, no family history, or positive cardiovascular risk factors might be overlooked using these criteria. To avoid missing suspected CADASIL patients before genetic testing, we proposed more-sensitive criteria from Japanese CADASIL cases (Mizuta et al., 2017; **Supplementary Table S2**). The sensitivity of our new criteria is 97%, sufficient to screen candidates for CADASIL and to aid genetic testing (Mizuta et al., 2017).

CADASIL Scale and CADASIL Scale-J

To prioritize access to genetic testing for suspected CADASIL patients, a quantitative evaluation of CADASIL-specific features possessed by each patient is necessary. Markus proposed a diagnostic procedure based on skin biopsy and involvement of the anterior temporal lobe on MRI (Markus et al., 2002). As pre-genetic screening approaches are desirable, Pescini et al. (2012) developed the CADASIL scale, a screening tool applied in the clinical setting due to the high cost and time-consuming nature of genetic testing. The weighted scores to common disease features based on frequencies obtained in a pooled analysis of selected international CADASIL series. The cut-off score of the definitive CADASIL scale had a sensitivity of 96.7% and specificity of 74.2%. Unfortunately, the sensitivity of the CADASIL scale was 52.1% in our Japanese cohort because of some clinical differences about the CADASIL group as well as NOTCH3-negative CADASIL-like patients (non-NOTCH3) group between the European population and the Japanese population (Koizumi et al., 2019). Several studies revealed a low prevalence rate of migraine in Japanese CADASIL compared to European CADASIL patients (Uchino et al., 2002). Although WM lesion at the temporal pole is specific CADASIL patients in both cohort, WM lesion at the external capsule was different in the non-NOTCH3 group in each cohort. These differences decreased the sensitivity and specificity of the original CADASIL scale when applied to the Japanese cohort. Therefore, we modified the CADASIL scale based on the clinical features of 126 Japanese CADASIL patients and 53 Non-NOTCH3 to develop CADASIL scale-J (**Supplementary Table S3**; Koizumi et al., 2019). In CADASIL scale-J, the score ranged from 0 to 25 and a cut-off value of 16, using eight items. The sensitivity and specificity of the CADASIL scale-J were enough quality for prioritizing tool before genetic testing.

IMAGING

White Matter Lesions

MRI can visualize the characterization of WM lesions and lacunar infarction in stroke syndromes. In CADASIL, T2-weighted hyperintensity was noted in the deep WM, internal and external capsules, and the temporal pole. Temporal pole hyperintensity on T2-weighted and FLAIR MR sequences can be detected even in the early 20s of CADASIL patients (Chabriat et al., 1998; Mizuno, 2012). Dilated perivascular spaces

(PVS) in CADASIL patients are located in the lentiform nuclei (94%) and subcortical WM of the temporal lobes (66%; Chabriat et al., 1998). PVS around small perforating arteries are pial-lined, interstitial fluid-filled spaces, readily seen to be enlarged in the WM of elderly subjects. Yamamoto et al. (2009) performed a postmortem study to quantify the degree and extent of PVS and arteriopathic changes within the temporal pole WM of CADASIL subjects. They concluded that the MRI hyperintensity in the temporal pole of CADASIL patients could be explained by enlarged PVS and degeneration of myelin rather than lacunar infarcts.

Lacunar Infarction

Viswanathan analyzed clinical data from 147 consecutive patients and revealed a significant independent association between age, volume of lacunar lesions, and global cognitive function scales, although WMH and microbleeds had no independent influence on cognitive function. Disability was associated with the volume of lacunar lesions, microbleeds, systolic blood pressure, and age but not with WMH (Viswanathan et al., 2007). Liem et al. (2007) analyzed 62 symptomatic and 15 asymptomatic members of CADASIL and revealed that the severity of cognitive dysfunction in mutation carriers is independently associated with MRI infarct lesion load. In contrast, WMH lesion load and microbleeds were not associated with cognitive dysfunction after correcting for age. These data indicate the importance of lacunar infarction in the progression of CADASIL.

Viswanathan examined the relative impact of lesion burden and location of these MRI markers on cognitive impairment and disability combined with whole-brain mean apparent diffusion coefficient (mean-ADC) and brain parenchymal fraction (BPF). In multivariate models accounting for lesion burden and location, the volume of lacunar lesion, mean-ADC, and BPF each had an independent influence on global cognitive function and disability (Viswanathan et al., 2010). Particularly, brain atrophy was shown to have the strongest independent influence on clinical impairment in CADASIL when all MRI markers in the disease are considered together. These results suggest that the clinical impact of cerebral cortical loss is important for CADASIL dementia (Viswanathan et al., 2010).

7-T MRI Reveals Micro-cortical Infarction

Jouvent et al. (2011b) used high-resolution postmortem 7-T MRI to examine infarcts of the cerebral cortex in a CADASIL patient with pathology examination. These lesions were not visible on the *in vivo* MRI obtained at 1.5 T. They examined cortex morphology and clinical worsening in 190 CADASIL patients and showed that reduction of sulcal depth is independently associated with increased time to complete trail making test A and B and that of cortical thickness to increased disability. They also showed that the impact of volume of lacunar lesions on cortical changes is greater than that of the volume of WMH and that cortical changes related to lacunar lesions evolve parallel to clinical worsening. These results support the hypothesis that cortical changes in CADASIL play a role in disease pathophysiology (Jouvent et al., 2011a).

Natural History

Few prospective studies have examined the natural history of CADASIL. Davous summarized the natural history of 134 documented cases and showed a mean age at onset of 40.3 years. The mean duration of the disease was 13.6 years, and the mean age at death was 56.7 years (Davous, 1999). *Opherk* summarized the natural history of a larger CADASIL cohort and reported a median age at onset of stroke of 50.7 years in men and 52.5 years in women, the median age at death of 64.6 years in men and 70.7 years in women (Opherk et al., 2004). In our cohort including 200 CADASIL patients, the mean age at onset of stroke was 48.3 years in men and 52.2 years in women (Koizumi et al., 2019). These results indicated a similar clinical course in any ethics, but more studies need to clarify a difference in each ethics before starting a disease-modifying-therapy on CADASIL.

Peters et al. (2004a) reported that their cohort deteriorated for all clinical scales over 2 years. There were 18 strokes within 173 person-years, giving an average incidence rate of stroke of 10.4 per 100 person-years. Age at baseline was found to be a predictor of clinical progression (Peters et al., 2004a). These data indicate a younger age of onset of stroke and death compared with the general population. CADASIL researchers should thus develop new approaches to improve this natural history.

AUTHOR CONTRIBUTIONS

TM and IM conceived the original idea. TM wrote the manuscript with support from IM, AW-H, MM, and TK.

FUNDING

Grant-in-aid for Research on Intractable Disease from the Japanese Ministry of Health, Labour, and Welfare H28-Nanchitou(Nan)-Ippan-029, H30-Nanchitou(Nan)-Ippan-006.

SUPPLEMENTARY MATERIAL

The Supplementary Material for this article can be found online at: https://www.frontiersin.org/articles/10.3389/fnagi.2020.00091/full#supplementary-material.

REFERENCES

Adib-Samii, P., Brice, G., Martin, R. J., and Markus, H. S. (2010). Clinical spectrum of CADASIL and the effect of cardiovascular risk factors on phenotype: study in 200 consecutively recruited individuals. *Stroke* 41, 630–634. doi: 10.1161/strokeaha.109.568402

Baudrimont, M., Dubas, F., Joutel, A., Tournier-Lasserve, E., and Bousser, M. G. (1993). Autosomal dominant leukoencephalopathy and subcortical ischemic stroke. A clinicopathological study. *Stroke* 24, 122–125. doi: 10.1161/01.str.24.1.122

Bianchi, S., Zicari, E., Carluccio, A., Di Donato, I., Pescini, F., Nannucci, S., et al. (2015). CADASIL in central Italy: a retrospective clinical and genetic

study in 229 patients. *J. Neurol.* 1, 134–141. doi: 10.1007/s00415-014-7533-2

Bray, S. J. (2006). Notch signalling: a simple pathway becomes complex. *Nat. Rev. Mol. Cell Biol.* 7, 678–689. doi: 10.1038/nrm2009

Brou, C., Logeat, F., Gupta, N., Bessia, C., LeBail, O., Doedens, J. R., et al. (2000). A novel proteolytic cleavage involved in Notch signaling: the role of the disintegrin-metalloprotease TACE. *Mol. Cell* 2, 207–216. doi: 10.1016/s1097-2765(00)80417-7

Capone, C., Cognat, E., Ghezali, L., Baron-Menguy, C., Aubin, D., Mesnard, L., et al. (2016). Reducing Timp3 or vitronectin ameliorates disease manifestations in CADASIL mice. *Ann. Neurol.* 3, 387–403. doi: 10.1002/ana.24573

Carare, R. O., Hawkes, C. A., Jeffrey, M., Kalaria, R. N., and Weller, R. O. (2013). Review: cerebral amyloid angiopathy, prion angiopathy, CADASIL and the spectrum of protein elimination failure angiopathies (PEFA) in neurodegenerative disease with a focus on therapy. *Neuropathol. Appl. Neurobiol.* 39, 593–611. doi: 10.1111/nan.12042

Chabriat, H., Levy, C., Taillia, H., Iba-Zizen, M. T., Vahedi, K., Joutel, A., et al. (1998). Patterns of MRI lesions in CADASIL. *Neurology* 2, 452–457. doi: 10.1212/wnl.51.2.452

Choi, E. J., Choi, C. G., and Kim, J. S. (2005). Large cerebral artery involvement in CADASIL. *Neurology* 65, 1322–1324. doi: 10.1212/01.wnl.0000180965.79209.50

Ciolli, L., Pescini, F., Salvadori, E., Del Bene, A., Pracucci, G., Poggesi, A., et al. (2014). Influence of vascular risk factors and neuropsychological profile on functional performances in CADASIL: results from the MIcrovascular LEukoencephalopathy Study (MILES). *Eur. J. Neurol.* 1, 65–71. doi: 10.1111/ene.12241

Davous, P. (1998). CADASIL: a review with proposed diagnostic criteria. *Eur. J. Neurol.* 5, 219–233. doi: 10.1046/j.1468-1331.1998.530219.x

Davous, P. (1999). The natural history of CADASIL. *Stroke* 30:2247. doi: 10.1161/01.str.30.10.2238b

Dichgans, M., Ludwig, H., Müller-Höcker, J., Messerschmidt, A., and Gasser, T. (2000). Small in-frame deletions and missense mutations in CADASIL: 3D models predict misfolding of Notch3 EGF-like repeat domains. *Eur. J. Hum. Genet.* 8, 280–285. doi: 10.1038/sj.ejhg.5200460

Duering, M., Karpinska, A., Rosner, S., Hopfner, F., Zechmeister, M., Peters, N., et al. (2011). Co-aggregate formation of CADASIL-mutant NOTCH3: a single-particle analysis. *Hum. Mol. Genet.* 16, 3256–3265. doi: 10.1093/hmg/ddr237

Dziewulska, D., and Lewandowska, E. (2012). Pericytes as a new target for pathological processes in CADASIL. *Neuropathology* 32, 515–521. doi: 10.1111/j.1440-1789.2011.01290.x

Fortini, M. E., and Bilder, D. (2009). Endocytic regulation of Notch signaling. *Curr. Opin. Genet. Dev.* 19, 323–328. doi: 10.1016/j.gde.2009.04.005

Fouillade, C., Chabriat, H., Riant, F., Mine, M., Arnoud, M., Magy, L., et al. (2008). Activating NOTCH3 mutation in a patient with small-vessel-disease of the brain. *Hum. Mutat.* 3:452. doi: 10.1002/humu.9527

Fujiwara, Y., Mizuno, T., Okuyama, C., Nagakane, Y., Watanabe-Hosomi, A., Kondo, M., et al. (2012). Simultaneous impairment of intracranial and peripheral artery vasoreactivity in CADASIL patients. *Cerebrovasc. Dis.* 2, 128–134. doi: 10.1159/000334185

Guerrot, D., François, A., Boffa, J. J., Boulos, N., Hanoy, M., Legallicier, B., et al. (2008). Nephroangiosclerosis in cerebral autosomal dominant arteriopathy with subcortical infarcts and leukoencephalopathy: is NOTCH3 mutation the common culprit? *Am. J. Kidney Dis.* 52, 340–345. doi: 10.1053/j.ajkd.2008.04.017

Hara, K., Shiga, A., Fukutake, T., Nozaki, H., Miyashita, A., Yokoseki, A., et al. (2009). Association of HTRA1 mutations and familial ischemic cerebral small-vessel disease. *N. Engl. J. Med.* 17, 1729–1739. doi: 10.1056/NEJMoa0801560

Huang, L., Li, W., Li, Y., Song, C., Wang, P., Wang, H., et al. (2020). A novel cysteine-sparing G73A mutation of NOTCH3 in a Chinese CADASIL family. *Neurogenetics* 1, 39–49. doi: 10.1007/s10048-019-00592-3

Ihara, M., and Yamamoto, Y. (2016). Emerging evidence for pathogenesis of sporadic cerebral small vessel disease. *Stroke* 47, 554–560. doi: 10.1161/strokeaha.115.009627

Joutel, A. (2011). Pathogenesis of CADASIL: transgenic and knock-out mice to probe function and dysfunction of the mutated gene, Notch3, in the cerebrovasculature. *Bioessays* 33, 73–80. doi: 10.1002/bies.201000093

Joutel, A., Andreux, F., Gaulis, S., Domenga, V., Cecillon, M., Battail, N., et al. (2000). The ectodomain of the Notch3 receptor accumulates within the cerebrovasculature of CADASIL patients. *J. Clin. Invest.* 5, 597–605. doi: 10.1172/jci8047

Joutel, A., Monet, M., Domenga, V., Riant, F., and Tournier-Lasserve, E. (2004). Pathogenic mutations associated with cerebral autosomal dominant arteriopathy with subcortical infarcts and leukoencephalopathy differently affect Jagged1 binding and Notch3 activity *via* the RBP/JK signaling Pathway. *Am. J. Hum. Genet.* 74, 338–347. doi: 10.1086/381506

Joutel, A., Vahedi, K., Corpechot, C., Troesch, A., Chabriat, H., Vayssière, C., et al. (1997). Strong clustering and stereotyped nature of Notch3 mutations in CADASIL patients. *Lancet* 9090, 1511–1515. doi: 10.1016/s0140-6736(97)08083-5

Jouvent, E., Mangin, J. F., Duchesnay, E., Porcher, R., Düring, M., Mewald, Y., et al. (2011a). Longitudinal changes of cortical morphology in CADASIL. *Neurobiol. Aging* 33, 1002.e29–1002.e36. doi: 10.1016/j.neurobiolaging.2011.09.013

Jouvent, E., Poupon, C., Gray, F., Paquet, C., Mangin, J. F., Le Bihan, D., et al. (2011b). Intracortical infarcts in small vessel disease: a combined 7-T postmortem MRI and neuropathological case study in cerebral autosomal-dominant arteriopathy with subcortical infarcts and leukoencephalopathy. *Stroke* 42, e27–e30. doi: 10.1161/strokeaha.110.594218

Kast, J., Hanecker, P., Beaufort, N., Giese, A., Joutel, A., Dichgans, M., et al. (2014). Sequestration of latent TGF-β binding protein 1 into CADASIL-related Notch3-ECD deposits. *Acta neuropathol. Commun.* 1:96. doi: 10.1186/s40478-014-0096-8

Kelleher, J., Dickinson, A., Cain, S., Hu, Y., Bates, N., Harvey, A., et al. (2019). Patient-specific iPSC model of a genetic vascular dementia syndrome reveals failure of mural cells to stabilize capillary structures. *Stem Cell Reports* 5, 817–831. doi: 10.1016/j.stemcr.2019.10.004

Kim, Y., Choi, E. J., Choi, C. G., Kim, G., Choi, J. H., Yoo, H. W., et al. (2006). Characteristics of CADASIL in Korea: a novel cysteine-sparing Notch3 mutation. *Neurology* 10, 1511–1516. doi: 10.1212/01.wnl.0000216259.99811.50

Klueg, K. M., and Muskavitch, M. A. (1999). Ligand-receptor interactions and trans-endocytosis of Delta, Serrate and Notch: members of the Notch signalling pathway in Drosophila. *J. Cell Sci.* 112, 3289–3297.

Koizumi, T., Mizuta, I., Watanabe-Hosomi, A., Mukai, M., Hamano, A., Matsuura, J., et al. (2019). The CADASIL scale-J, a modified scale to prioritize access to genetic testing for japanese CADASIL-suspected patients. *J. Stroke Cerebrovasc. Dis.* 6, 1431–1439. doi: 10.1016/j.jstrokecerebrovasdis.2019.03.026

Kusaba, T., Hatta, T., Kimura, T., Sonomura, K., Tanda, S., Kishimoto, N., et al. (2007). Renal involvement in cerebral autosomal dominant arteriopathy with subcortical infarcts and leukoencephalopathy (CADASIL). *Clin. Nephrol.* 3, 182–187. doi: 10.5414/cnp67182

Lee, J. S., Ko, K., Oh, J. H., Park, J. H., and Lee, H. K. (2016). Phenotypic features of cerebral autosomal-dominant arteriopathy with subcortical infarcts and leukoencephalopathy subjects with R544C mutation. *Dement. Neurocogn. Disord.* 15, 15–19. doi: 10.12779/dnd.2016.15.1.15

Lee, S. J., Meng, H., Elmadhoun, O., Blaivas, M., and Wang, M. M. (2011). Cerebral autosomal dominant arteriopathy with subcortical infarcts and leukoencephalopathy affecting an African American man: identification of a novel 15-base pair NOTCH3 duplication. *Arch. Neurol.* 68, 1584–1586. doi: 10.1001/archneurol.2011.781

Liao, Y. C., Hsiao, C. T., Fuh, J. L., Chern, C. M., Lee, W. J., Guo, Y. C., et al. (2015). Characterization of CADASIL among the han chinese in taiwan: distinct genotypic and phenotypic profiles. *PLoS One* 10:e0136501. doi: 10.1371/journal.pone.0136501

Liem, M. K., van der Grond, J., Haan, J., van den Boom, R., Ferrari, M. D., Knaap, Y. M., et al. (2007). Lacunar infarcts are the main correlate with cognitive dysfunction in CADASIL. *Stroke* 3, 923–928. doi: 10.1161/01.str.0000257968.24015.bf

Markus, H. S., Martin, R. J., Simpson, M. A., Dong, Y. B., Ali, N., Crosby, A. H., et al. (2002). Diagnostic strategies in CADASIL. *Neurology* 8, 1134–1138. doi: 10.1212/wnl.59.8.1134

Miyawaki, S., Imai, H., Takayanagi, S., Mukasa, A., Nakatomi, H., and Saito, N. (2012). Identification of a genetic variant common to moyamoya disease and intracranial major artery stenosis/occlusion. *Stroke* 43, 3371–3374. doi: 10.1161/strokeaha.112.663864

Mizuno, T. (2012). Diagnosis, pathomechanism and treatment of CADASIL. *Rinsho Shinkeigaku* 52, 303–313. doi: 10.5692/clinicalneurol.52.303

Mizuno, T., Muranishi, M., Torugun, T., Tango, H., Nagakane, Y., Kudeken, T., et al. (2008). Two Japanese CADASIL families exhibiting Notch3 mutation R75P not involving cysteine residue. *Intern. Med.* 23, 2067–2072. doi: 10.2169/internalmedicine.47.1391

Mizuta, I., Watanabe-Hosomi, A., Koizumi, T., Mukai, M., Hamano, A., Tomii, Y., et al. (2017). New diagnostic criteria for cerebral autosomal dominant arteriopathy with subcortical infarcts and leukocencephalopathy in Japan. *J. Neurol. Sci.* 381, 62–67. doi: 10.1016/j.jns.2017.08.009

Monet-Leprêtre, M., Bardot, B., Lemaire, B., Domenga, V., Godin, O., Dichgans, M., et al. (2009). Distinct phenotypic and functional features of CADASIL mutations in the Notch3 ligand binding domain. *Brain* 132, 1601–1612. doi: 10.1093/brain/awp049

Monet-Leprêtre, M., Haddad, I., Baron-Menguy, C., Fouillot-Panchal, M., Riani, M., Domenga-Denier, V., et al. (2013). Abnormal recruitment of extracellular matrix proteins by excess Notch3ECD: a new pathomechanism in CADASIL. *Brain* 136, 1830–1845. doi: 10.1093/brain/awt092

Moreton, F. C., Razvi, S. S., Davidson, R., and Muir, K. W. (2014). Changing clinical patterns and increasing prevalence in CADASIL. *Acta Neurol. Scand.* 130, 197–203. doi: 10.1111/ane.12266

Muino, E., Gallego-Fabrega, C., Cullell, N., Carrera, C., Torres, N., Krupinski, J., et al. (2017). Systematic review of cysteine-sparing NOTCH3 missense mutations in patients with clinical suspicion of CADASIL. *Int. J. Mol. Sci.* 18:E1964. doi: 10.3390/ijms18091964

Mukai, M., Mizuta, I., Ueda, A., Nakashima, D., Kushimura, Y., Noto, Y. I., et al. (2018). A Japanese CADASIL patient with homozygous NOTCH3 p.Arg544Cys mutation confirmed pathologically. *J. Neurol. Sci.* 394, 38–40. doi: 10.1016/j.jns.2018.08.029

Mykkänen, K., Junna, M., Amberla, K., Bronge, L., Kääriäinen, H., Poyhonen, M., et al. (2009). Different clinical phenotypes in monozygotic CADASIL twins with a novel NOTCH3 mutation. *Stroke* 6, 2215–2218. doi: 10.1161/strokeaha.108.528661

Narayan, S. K., Gorman, G., Kalaria, R. N., Ford, G. A., and Chinnery, P. F. (2012). The minimum prevalence of CADASIL in northeast England. *Neurology* 78, 1025–1027. doi: 10.1212/wnl.0b013e31824d586c

Nichols, J. T., Miyamoto, A., Olsen, S. L., D'Souza, B., Yao, C., and Weinmaster, G. (2007). DSL ligand endocytosis physically dissociates Notch1 heterodimers before activating proteolysis can occur. *J. Cell Biol.* 176, 445–458. doi: 10.1083/jcb.200609014

Okeda, R., Arima, K., and Kawai, M. (2002). Arterial changes in cerebral autosomal dominant arteriopathy with subcortical infarcts and leukoencephalopathy (CADASIL) in relation to pathogenesis of diffuse myelin loss of cerebral white matter: examination of cerebral medullary arteries by reconstruction of serial sections of an autopsy case. *Stroke* 33, 2565–2569. doi: 10.1161/01.str.0000032620.91848.1c

Opherk, C., Gonik, M., Duering, M., Malik, R., Jouvent, E., Hervé, D., et al. (2014). Genome-wide genotyping demonstrates a polygenic risk score associated with white matter hyperintensity volume in CADASIL. *Stroke* 964, 968–972. doi: 10.1161/strokeaha.113.004461

Opherk, C., Peters, N., Herzog, J., Luedtke, R., and Dichgans, M. (2004). Long-term prognosis and causes of death in CADASIL: a retrospective study in 411 patients. *Brain* 127, 2533–2539. doi: 10.1093/brain/awh282

Pescini, F., Nannucci, S., Bertaccini, B., Salvadori, E., Bianchi, S., Ragno, M., et al. (2012). The cerebral autosomal-dominant arteriopathy with subcortical infarcts and leukoencephalopathy (CADASIL) Scale: a screening tool to select patients for NOTCH3 gene analysis. *Stroke* 11, 2871–2876. doi: 10.1161/STROKEAHA.112.665927

Peters, N., Herzog, J., Opherk, C., and Dichgans, M. (2004a). A two-year clinical follow-up study in 80 CADASIL subjects: progression patterns and implications for clinical trials. *Stroke* 35, 1603–1608. doi: 10.1161/01.str.0000131546.71733.f1

Peters, N., Opherk, C., Zacherle, S., Capell, A., Gempel, P., and Dichgans, M. (2004b). CADASIL-associated Notch3 mutations have differential effects both on ligand binding and ligand-induced Notch3 receptor signaling through RBP-Jk. *Exp. Cell Res.* 299, 454–464. doi: 10.1016/j.yexcr.2004.06.004

Pippucci, T., Maresca, A., Magini, P., Cenacchi, G., Donadio, V., Palombo, F., et al. (2015). Homozygous NOTCH3 null mutation and impaired NOTCH3 signaling in recessive early-onset arteriopathy and cavitating leukoencephalopathy. *EMBO Mol. Med.* 6, 848–858. doi: 10.15252/emmm.201404399

Pratt, E. B., Wentzell, J. S., Maxson, J. E., Courter, L., Hazelett, D., and Christian, J. L. (2011). The cell giveth and the cell taketh away: an overview of Notch pathway activation by endocytic trafficking of ligands and receptors. *Acta Histochem.* 113, 248–255. doi: 10.1016/j.acthis.2010.01.006

Qin, W., Li, J., Zhu, R., Gao, S., Fan, J., Xia, M., et al. (2019). Melatonin protects blood-brain barrier integrity and permeability by inhibiting matrix metalloproteinase-9 *via* the NOTCH3/NF-κB pathway. *Aging* 23, 11391–11415. doi: 10.18632/aging.102537

Ragno, M., Sanguigni, S., Manca, A., Pianese, L., Paci, C., Berbellini, A., et al. (2016). Parkinsonism in a pair of monozygotic CADASIL twins sharing the R1006C mutation: a transcranial sonography study. *Neurol. Sci.* 6, 875–881. doi: 10.1007/s10072-016-2497-x

Ragno, M., Trojano, L., Pianese, L., Boni, M. V., Silvestri, S., Mambelli, V., et al. (2012). Renal involvement in cerebral autosomal dominant arteriopathy with subcortical infarcts and leukoencephalopathy (CADASIL): report of a case with a six-year follow-up. *Histol. Histopathol.* 10, 1307–1314. doi: 10.14670/HH-27.1307

Razvi, S. S., Davidson, R., Bone, I., and Muir, K. W. (2005). The prevalence of cerebral autosomal dominant arteriopathy with subcortical infarcts and leucoencephalopathy (CADASIL) in the west of Scotland. *J. Neurol. Neurosurg. Psychiatry* 76, 739–741. doi: 10.1136/jnnp.2004.051847

Ruchoux, M. M., Guerouaou, D., Vandenhaute, B., Pruvo, J. P., Vermersch, P., and Leys, D. (1995). Systemic vascular smooth muscle cell impairment in cerebral autosomal dominant arteriopathy with subcortical infarcts and leukoencephalopathy. *Acta Neuropathol.* 89, 500–512. doi: 10.1007/bf00571504

Rufa, A., Guideri, F., Acampa, M., Cevenini, G., Bianchi, S., De Stefano, N., et al. (2007). Cardiac autonomic nervous system and risk of arrhythmias in cerebral autosomal dominant arteriopathy with subcortical infarcts and leukoencephalopathy (CADASIL). *Stroke* 2, 276–280. doi: 10.1161/01.STR.0000254530.38417.07

Rutten, J. W., Boon, E. M., Liem, M. K., Dauwerse, J. G., Pont, M. J., Vollebregt, E., et al. (2013). Hypomorphic NOTCH3 alleles do not cause CADASIL in humans. *Hum. Mutat.* 11, 1486–1489. doi: 10.1002/humu.22432

Rutten, J. W., Dauwerse, H. G., Gravesteijn, G., van Belzen, M. J., van der Grond, J., Polke, J. M., et al. (2016). Archetypal NOTCH3 mutations frequent in public exome: implications for CADASIL. *Ann. Clin. Transl. Neurol.* 11, 844–853. doi: 10.1002/acn3.344

Rutten, J. W., Haan, J., Terwindt, G. M., van Duinen, S. G., Boon, E. M., and Lesnik Oberstein, S. A. (2014). Interpretation of NOTCH3 mutations in the diagnosis of CADASIL. *Expert Rev. Mol. Diagn.* 14, 593–603. doi: 10.1586/14737159.2014.922880

Rutten, J. W., Van Eijsden, B. J., Duering, M., Jouvent, E., Opherk, C., Pantoni, L., et al. (2019). The effect of NOTCH3 pathogenic variant position on CADASIL disease severity: NOTCH3 EGFr 1-6 pathogenic variant are associated with a more severe phenotype and lower survival compared with EGFr 7–34 pathogenic variant. *Genet. Med.* 3, 676–682. doi: 10.1038/s41436-018-0088-3

Tikka, S., Baumann, M., Siitonen, M., Pasanen, P., Pöyhönen, M., Myllykangas, L., et al. (2014). CADASIL and CARASIL. *Brain Pathol.* 5, 525–544. doi: 10.1111/bpa.12181

Tikka, S., Mykkänen, K., Ruchoux, M. M., Bergholm, R., Junna, M., Pöyhönen, M., et al. (2009). Congruence between NOTCH3 mutations and GOM in 131 CADASIL patients. *Brain* 132, 933–939. doi: 10.1093/brain/awn364

Uchino, M., Hirano, T., Uyama, E., and Hashimoto, Y. (2002). Cerebral autosomal dominant arteriopathy with subcortical infarcts and leukoencephalopathy (CADASIL) and CADASIL-like disorders in Japan. *Ann. N Y Acad. Sci.* 977, 273–278. doi: 10.1111/j.1749-6632.2002.tb04826.x

Ueda, A., Ueda, M., Nagatoshi, A., Hirano, T., Ito, T., Arai, N., et al. (2015). Genotypic and phenotypic spectrum of CADASIL in Japan: the experience at a referral center in Kumamoto University from 1997 to 2014. *J. Neurol.* 8, 1828–1836. doi: 10.1007/s00415-015-7782-8

van den Boom, R., Lesnik Oberstein, S. A., Spilt, A., Behloul, F., Ferrari, M. D., Haan, J., et al. (2003). Cerebral hemodynamics and white matter hyperintensities in CADASIL. *J. Cereb. Blood Flow Metab.* 5, 599–604. doi: 10.1097/01.WCB.0000062341.61367.D3

Viswanathan, A., Godin, O., Jouvent, E., O'Sullivan, M., Gschwendtner, A., Peters, N., et al. (2010). Impact of MRI markers in subcortical vascular dementia: a multi-modal analysis in CADASIL. *Neurobiol. Aging* 9, 1629–1636. doi: 10.1016/j.neurobiolaging.2008.09.001

Viswanathan, A., Gschwendtner, A., Guichard, J. P., Buffon, F., Cumurciuc, R., O'Sullivan, M., et al. (2007). Lacunar lesions are independently associated with disability and cognitive impairment in CADASIL. *Neurology* 2, 172–179. doi: 10.1212/01.wnl.0000265221.05610.70

Watanabe-Hosomi, A., Watanabe, Y., Tanaka, M., Nakagawa, M., and Mizuno, T. (2012). Transendocytosis is impaired in CADASIL-mutant NOTCH3. *Exp. Neurol.* 233, 303–311. doi: 10.1016/j.expneurol.2011.10.020

Wollenweber, F. A., Hanecker, P., Bayer-Karpinska, A., Malik, R., Bäzner, H., Moreton, F., et al. (2015). Cysteine-sparing CADASIL mutations in NOTCH3 show proaggregatory properties *in vitro*. *Stroke* 3, 786–792. doi: 10.1161/STROKEAHA.114.007472

Yamamoto, Y., Craggs, L. J., Watanabe, A., Booth, T., Attems, J., Low, R. W., et al. (2013). Brain microvascular accumulation and distribution of the NOTCH3 ectodomain and granular osmiophilic material in CADASIL. *J. Neuropathol. Exp. Neurol.* 5, 416–431. doi: 10.1097/nen.0b013e31829020b5

Yamamoto, Y., Ihara, M., Tham, C., Low, R. W., Slade, J. Y., Moss, T., et al. (2009). Neuropathological correlates of temporal pole white matter hyperintensities in CADASIL. *Stroke* 6, 2004–2011. doi: 10.1161/strokeaha.108.528299

Yeung, W. T. E., Mizuta, I., Watanabe-Hosomi, A., Yokote, A., Koizumi, T., Mukai, M., et al. (2018). RNF213-related susceptibility of Japanese CADASIL patients to intracranial arterial stenosis. *J. Hum. Genet.* 5, 687–690. doi: 10.1038/s10038-018-0428-9

Conflict of Interest: The authors declare that the research was conducted in the absence of any commercial or financial relationships that could be construed as a potential conflict of interest.

frontiers in Aging Neuroscience

ORIGINAL RESEARCH
published: 14 May 2020
doi: 10.3389/fnagi.2020.00130

Prevalence and Atypical Clinical Characteristics of *NOTCH3* Mutations Among Patients Admitted for Acute Lacunar Infarctions

Takashi Okada[1], *Kazuo Washida*[1]*, *Kenichi Irie*[1], *Satoshi Saito*[1,2], *Michio Noguchi*[3], *Tsutomu Tomita*[3], *Masatoshi Koga*[4], *Kazunori Toyoda*[4], *Shuhei Okazaki*[5], *Takashi Koizumi*[6], *Ikuko Mizuta*[6], *Toshiki Mizuno*[6] and *Masafumi Ihara*[1]

[1] Department of Neurology, National Cerebral and Cardiovascular Center, Osaka, Japan, [2] Research Fellow of Japan Society for the Promotion of Science, Tokyo, Japan, [3] NCVC Biobank, National Cerebral and Cardiovascular Center, Osaka, Japan, [4] Department of Cerebrovascular Medicine, National Cerebral and Cardiovascular Center, Osaka, Japan, [5] Department of Neurology, Osaka University Graduate School of Medicine, Osaka, Japan, [6] Department of Neurology, Graduate School of Medical Science, Kyoto Prefectural University of Medicine, Kyoto, Japan

Objectives: Cerebral autosomal dominant arteriopathy with subcortical infarcts and leukoencephalopathy (CADASIL) is the most common hereditary small vessel disease, with reported frequencies of 2-5/100,000 individuals. Recently, it has been reported that some patients with *NOTCH3* gene mutations show atypical clinical symptoms of CADASIL. Assuming that CADASIL is underdiagnosed in some cases of lacunar infarction, this study was designed to examine the prevalence of *NOTCH3* gene mutations in the patients at highest risk who were admitted for lacunar infarctions.

Methods: From January 2011 to April 2018, 1,094 patients with lacunar infarctions were admitted to our hospital, of whom 31 patients without hypertension but with white matter disease (Fazekas scale 2 or 3) were selected and genetically analyzed for *NOTCH3* gene mutations (Phase 1). Furthermore, 54 patients, who were 60 years or younger, were analyzed for *NOTCH3* mutations (Phase 2). *NOTCH3* exons 2–24, which encode the epidermal growth factor-like repeat domain of the *NOTCH3* receptor, were analyzed for mutations by direct sequencing of genomic DNA.

Results: Three patients presented *NOTCH3* p.R75P mutations: two in the Phase 1 and one in the Phase 2 cohort. Among patients aged 60 years or younger and those without hypertension but with moderate-to-severe white matter lesions, the carrier frequency of p.R75P was 3.5% (3/85), which was significantly higher than that in the Japanese general population (4.7KJPN) (odds ratio [95% CI] = 58.2 [11.6–292.5]). All three patients with *NOTCH3* mutations had family histories of stroke, and the average patient age was 51.3 years. All three patients also showed white matter lesions in the external capsule but not in the temporal pole. The CADASIL and CADASIL scale-J scores of the three patients were 6, 17, 7 (mean, 10.0) and 13, 20, 10 (mean, 14.3), respectively.

Conclusion: Among patients hospitalized for lacunar infarctions, the p.R75P prevalence may be higher than previously estimated. The *NOTCH3* p.R75P mutation may be

OPEN ACCESS

Edited by:
Allison B. Reiss, Winthrop University Hospital, United States

Reviewed by:
Yi-Chung Lee, Taipei Veterans General Hospital, Taiwan
Raffaella Valenti, University of Florence, Italy

***Correspondence:**
Kazuo Washida
washida@ncvc.go.jp

Received: *02 December 2019*
Accepted: *20 April 2020*
Published: *14 May 2020*

Citation:
Okada T, Washida K, Irie K, Saito S, Noguchi M, Tomita T, Koga M, Toyoda K, Okazaki S, Koizumi T, Mizuta I, Mizuno T and Ihara M (2020) Prevalence and Atypical Clinical Characteristics of NOTCH3 Mutations Among Patients Admitted for Acute Lacunar Infarctions. Front. Aging Neurosci. 12:130. doi: 10.3389/fnagi.2020.00130

underdiagnosed in patients with early-onset lacunar infarctions due to the atypical clinical and neuroimaging features of CADASIL. Early-onset, presence of family history of stroke, external capsule lesions, and absence of hypertension may help predict underlying *NOTCH3* mutations despite no temporal white matter lesions.

Keywords: CADASIL, CADASIL scale-J, *NOTCH3*, R75P mutation, lacunar infarction

INTRODUCTION

Cerebral autosomal dominant arteriopathy with subcortical infarcts and leukoencephalopathy (CADASIL) is an autosomal dominant disorder caused by mutations in the *NOTCH3* gene in chromosome 19p13 (Tournier-Lasserve et al., 1993; Joutel et al., 1996) and is the most common hereditary small vessel disease, with clinical frequencies of 2-5/100,000 individuals (Joutel et al., 1997; Rutten et al., 2016). Patients with CADASIL have various clinical symptoms, such as lacunar infarction, migraines, progressive cognitive decline, and psychiatric problems (Chabriat et al., 2009), and the most specific imaging feature of patients with CADASIL are bilateral white matter hyperintensities (WMHs), especially WMHs of anterior temporal pole on magnetic resonance imaging (MRI) (Chabriat et al., 1995, 1998; Coulthard et al., 2000; Auer et al., 2001; Tomimoto et al., 2006; Bersano et al., 2018). However, some patients with *NOTCH3* mutations do not show the typical clinical and imaging features of CADASIL (Kim et al., 2006; Mizuno et al., 2008; Sari et al., 2019). Furthermore, it has been recently clarified that the potential prevalence of CADASIL may be higher than previously estimated (Rutten et al., 2016). Assuming that *NOTCH3* gene mutations may be involved in some cases of lacunar infarction, a representative small vessel disease, this study was designed to investigate the prevalence and clinical characteristics of *NOTCH3* gene mutations in the patients at highest risk who were admitted for lacunar infarction, using a whole sequence analysis of *NOTCH3* genes.

METHODS

Study Design and Participants

This single-center cross-sectional study was performed at the National Cerebral and Cardiovascular Center (NCVC) of Osaka, Japan, and conducted in accordance with Declaration of Helsinki standards and after approval by the local NCVC ethical committee (M29-117-3). All participants signed a comprehensive NCVC biobank consent form.

The subjects of this study were patients with lacunar infarction with hyperintense signal on MRI Diffusion-weighted imaging (DWI).

Lacunar infarction was divided into two types based on the diameter of the occluded vessels: lacunar infarction of 20 mm or less in diameter and penetrating artery occlusion stroke exceeding 20 mm in diameter. Lacunar infarction was defined as lesions of 20 mm or less in the brainstem or subcortex in the territory of a penetrating artery. In principle, there was no major artery stenosis and no embolic sources. Penetrating artery occlusion stroke was defined as lesions exceeding 20 mm in the brainstem or subcortex in the territory of a penetrating artery. In principle, there was no major artery stenosis and no embolic sources.

We defined the inclusion criteria for cohort 1 and 2 to evaluate the frequency of CADASIL in the patients with the highest risk because genetic testing of all 1,094 patients is impractical in terms of cost and time.

In this study, therefore, hypertension and aging were used as exclusion criteria for patient selection because these are the two strongest risk factors for lacunar infarction (Veglio et al., 2009; Regenhardt et al., 2018; Kalaria and Hase, 2019). In addition, white matter lesions were used as inclusion criteria for patient selection because white matter lesions were the most representative imaging finding of CADASIL (Chabriat et al., 1998; Koizumi et al., 2019).

Among patients with acute lacunar infarctions, patients without hypertension but with white matter disease (Fazekas scale 2 or 3) were selected and genetically analyzed for *NOTCH3* gene mutations, in order to strictly target patients with lacunar infarction of 20 mm or less in diameter (Phase 1). Furthermore, patients with acute lacunar infarctions or penetrating artery occlusion stroke aged 60 years old or younger were genetically analyzed for *NOTCH3* gene mutations in order to broadly target patients with lacunar infarctions or penetrating artery occlusion stroke (Phase 2).

Patients who satisfied the following criteria were included in this study:

- Phase 1 cohort: (1) patients who deposited samples in the NCVC biobank from January 2011 to April 2018, (2) patients with lacunar infarction (20 mm or less in diameter) without a past history of hypertension, and (3) patients with deep white matter hyperintensity (DWMH) or periventricular hyperintensity (PVH) of grade 2 or higher on the Fazekas scale (Fazekas et al., 1991).
- Phase 2 cohort: (1) patients who deposited samples in NCVC biobank from January 2011 to April 2018 and (2) patients with acute lacunar infarctions (20 mm or less in diameter) or penetrating artery occlusion stroke (exceeding 20 mm in diameter) who experienced their first stroke at the age of 60 years or younger.
- Lacunar infarction, penetrating artery occlusion stroke, and white matter lesions were diagnosed based on MRI. Patients who had already been diagnosed with CADASIL were excluded.
- A patient selection flow diagram is detailed in **Figures 1, 2**.

Clinical Assessment

We collected clinical information that included data on clinical background (age at onset, sex, family history, and vascular risk factors), neurological symptoms, and MRI

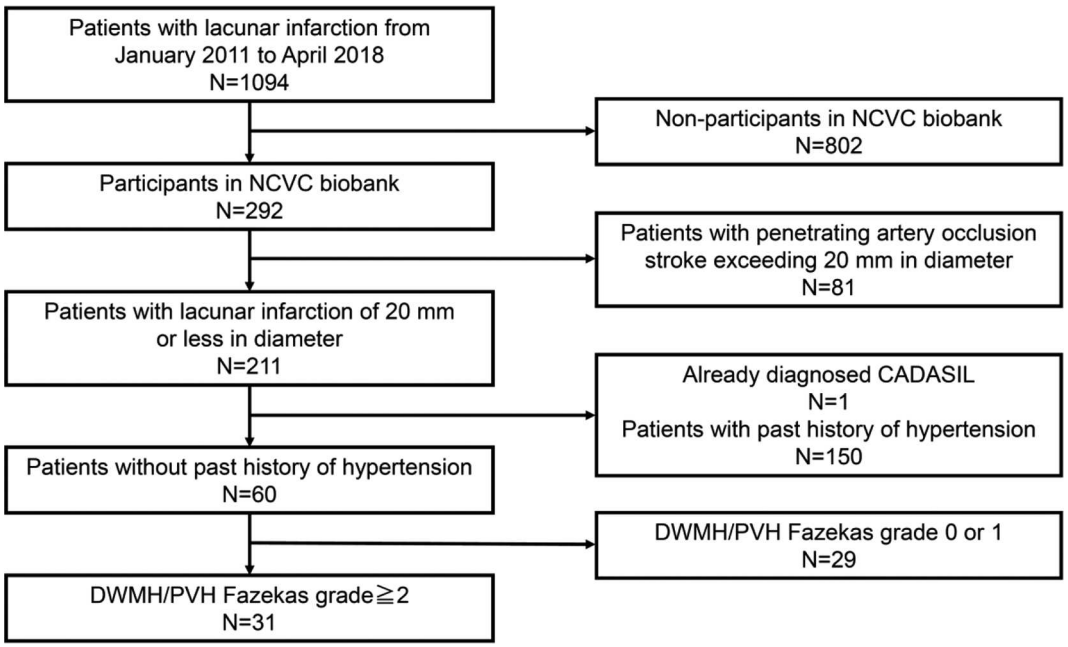

FIGURE 1 | Patient selection flow diagram for the phase 1 cohort. NCVC, National Cerebral and Cardiovascular Center; CADASIL, Cerebral autosomal dominant arteriopathy with subcortical infarcts and leukoencephalopathy; DWMH, deep white matter hyperintensity; PVH, periventricular hyperintensity.

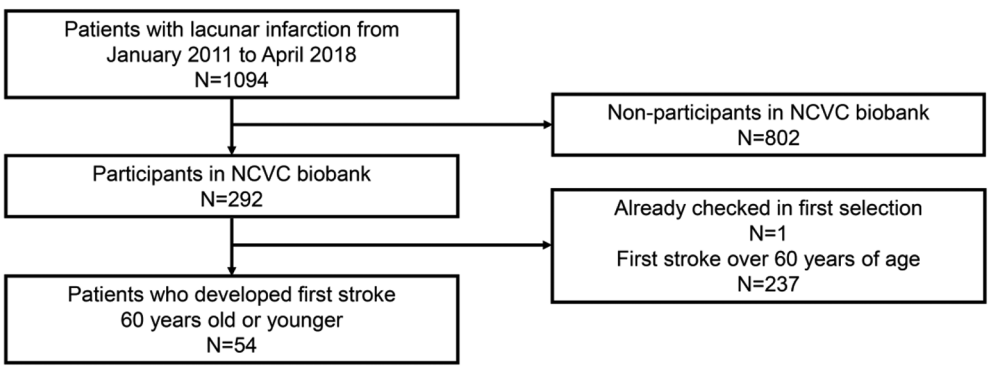

FIGURE 2 | Patient selection flow diagram for the phase 2 cohort. NCVC, National cerebral and cardiovascular center.

findings. The neurological symptoms that were evaluated included stroke, migraine, motor palsy, sensory disturbance, dizziness, pseudobulbar palsy, seizure, mood disturbance, and cognitive impairment.

Lacunar infarctions were diagnosed according to the Trial of Org 10172 Acute Stroke Treatment Criteria (Adams et al., 1993). Hypertension was defined as a blood pressure of at least 140/90 mmHg on two separate measurements or the use of antihypertensive drugs. Diabetes mellitus was defined as a fasting blood glucose level of at least 126 mg/dL, HbA1c 6.5% or higher, or the use of antidiabetic medications. Dyslipidemia was defined as a fasting serum low-density lipoprotein cholesterol level of at least 140 mg/dL or use of cholesterol-lowering therapy. Smoking status was determined by self-reporting as either a smoker (current or ex-smoker) or a nonsmoker. A family history of stroke was determined based on combined responses of the patient, sibling, and child to questions.

Magnetic Resonance Imaging Protocol

Participants underwent imaging of the brain with a 3.0 Tesla MRI (Magnetom Verio or Spectra; Siemens Medical Solutions, Erlangen, Germany) scanner. A standardized clinical protocol was employed that included DWI and apparent diffusion coefficient (ADC), fluid-attenuated inversion recovery (FLAIR), T2 star weighted imaging (T2*WI), and MR angiography.

Application of the CADASIL Scale and CADASIL Scale-J

The CADASIL scale of Pescini et al. (2012) is a simple scale that can be applied in a clinical setting as a screening tool for

predicting a genetic diagnosis of CADASIL. The scale involves the additive score of 12 items (ranging from 0 to 25), whose cut-off value is 15. Result categories of the CADASIL scale were determined as positive (≥15) or negative (<15).

The CADASIL scale-J of Koizumi et al. (2019) is a modified, Japanese version of the CADASIL scale, with a score range from 0 to 25 and cut-off value of 16. This version uses eight items: hypertension, diabetes, young onset (≤50 years old), pseudobulbar palsy, stroke/TIA, family history, subcortical infarction, and temporal pole lesion.

Genetic Examination

Genetic testing of *NOTCH3* was performed as described previously (Mizuta et al., 2017). In brief, *NOTCH3* exons 2–24, which encode the epidermal growth factor-like repeat (EGFr) domain of the NOTCH3 receptor, were analyzed for mutations by direct sequencing of genomic DNA that was extracted from the peripheral blood. The sequence data were analyzed with SEQUENCHER (Gene Codes, HITACHI) to screen for mutations. Nucleotide substitutions were confirmed by restriction fragment length polymorphism analysis. We concluded that the variation was pathogenic when it was previously reported as pathogenic and/or when it resulted in a cysteine-related missense mutation in one EGFr.

RESULTS

Baseline Demographics and Participants

During the study period, 1,094 patients with lacunar infarctions were admitted to the hospital (mean age ± standard deviation (*SD*), 72.0 ± 11.0; 61.0% men). In total, 292 of 1,094 patients participated in the NCVC biobank after providing written informed consent.

Of the overall cohort, 31 patients without hypertension but with white matter disease (Fazekas scale 2 or 3) were selected and genetically analyzed for *NOTCH3* gene mutations in the phase 1 cohort (mean age ± *SD*, 77.4 ± 9.6 11.0; 76.5% men) (**Figure 1**). The demographic data of the 31 patients in the phase 1 cohort are shown in **Table 1**.

Furthermore, 54 patients, who were 60 years old or younger, were genetically analyzed for *NOTCH3* gene mutations in the phase 2 cohort (mean age ± *SD*, 53.0 ± 5.7; 77.8% men) (**Figure 2**). The demographic data of the 54 patients in the phase 2 cohort are shown in **Table 2**.

Prevalence of *NOTCH3* Mutations Among Patients With Lacunar Infarctions

Three patients had *NOTCH3* p.R75P mutations (ClinVar accession number: VCV000632306.1): two in the Phase 1 cohort (cases 1 and 2) and one in the phase 2 cohort (case 3). Among patients aged 60 years or younger or patients without hypertension with moderate-to-severe white matter lesions, the carrier frequency of p.R75P was 3.5% (3/85), which was significantly higher than that in the Japanese general population (4.7KJPN) ($n = 4773$) (odds ratio [95% CI] = 58.2 [11.6–292.5]) (**Table 3**). The p.R75P carrier frequency in biobank patients with lacunar infarction (1.0%, 3/292) was also significantly higher than that in 4.7KJPN (odds ratio [95% CI] = 16.5 [3.3–82.1]).

The three patients with p.R75P mutations had no blood causality each.

Clinical Characteristics of Patients With p.R75P Mutations

The clinical characteristics of patients with p.R75P mutations are shown in **Table 4**. The average patient age was 51.3 years. All patients had dyslipidemia and family histories of stroke; however, only the patient in case 2 showed cognitive impairment while the patient in case 3 had hypertension. No history of diabetes mellitus or cigarette smoking was found. Furthermore, the patients in case 1 and 3 had symptoms of dysarthria and dysesthesia but did not show typical clinical characteristics of CADASIL such as migraine and temporal pole lesions. The patient in case 2 showed relatively typical clinical symptoms, such as migraines and cognitive impairment.

Brain MRI Characteristics of Patients With p.R75P Mutations

All three patients with p.R75P mutations had no temporal pole lesions (**Figures 3A,E,I**), while hyperintensity lesions were

TABLE 1 | Demographic data of the 31 patients in the Phase 1 cohort.

Demographics in 31 patients in Phase 1 cohort	
Age, years (*SD*)	77.4 (9.6)
Sex	
Men, *n* (%)	23 (76.5%)
Women, *n* (%)	8 (23.5%)
Median NIHSS at baseline	3 (IQR 2–4)
HTN, *n* (%)	0 (0%)
DL, *n* (%)	17 (82.4%)
DM, *n* (%)	12 (40%)
Smoking, *n* (%)	14 (55.3%)

SD, Standard deviation; NIHSS, national institute of health stroke scale; IQR, interquartile range; HTN, hypertension; DL, dyslipidemia; DM, diabetes mellitus.

TABLE 2 | Demographic data of the 54 patients in the Phase 2 cohort.

Demographics in 54 patients in Phase 2 cohort	
Age, years (*SD*)	53.0 (5.7)
Sex	
Men, *n* (%)	42 (77.8%)
Women, *n* (%)	12 (22.2%)
Median NIHSS at baseline	3 (IQR 2–4)
HTN, *n* (%)	45 (83.3%)
DL, *n* (%)	39 (72.2%)
DM, *n* (%)	22 (40.7%)
Smoking, *n* (%)	33 (61.1%)

SD, Standard deviation; NIHSS, national institute of health stroke scale; IQR, interquartile range; HTN, hypertension; DL, dyslipidemia; DM, diabetes mellitus.

TABLE 3 | Frequency of *NOTCH3* p.R75P mutations in patients and controls.

	This study	Japanese general population (4.7KJPN)**		Japanese CADASIL patients	
				Ueda et al. (2015)	Koizumi et al. (2019)
p.R75P carriers (*n*)	3		3	8	14
p.R75P non-carriers (*n*)	82		4770	62	139
Total (*n*)	85		4773	70	153
Frequency of p.R75P carrier (%)	3.5		0.06	11.4	9.2
		OR (95% CI)*			
		58.2 (11.6–292.5)			

**Internet calculator (http://www.hutchon.net/ConfidOR.htm) was used.*

***Number of p.R75P carriers among general Japanese population was estimated by its allele frequency (0.0003) and total number of participants (4773), because genotype frequency is not freely available on 4.7KJPN yet.*

OR, Odds ratio; CI, confidence interval.

noticeable at the external capsule (**Figures 3B,F,J**), and the white matter lesions that were evaluated by the Fazekas scale were of grades 2-3 (**Figures 3C,D,G,H,K,L**). The patients in cases 1 and 2 exhibited several cerebral microbleeds, while the patient in case 3 had no cerebral microbleeds on T2*WI. MR angiography showed no arterial stenoses in all three patients with CADASIL.

CADASIL Scale and CADASIL Scale-J Scores

The CADASIL and CADASIL scale-J scores of the three patients were 6, 17, 7 (mean, 10.0) and 13, 20, 10 (mean, 14.3), respectively (**Table 4**). The CADASIL scale-J score was higher than that of the CADASIL scale, although both scale scores were below their respective cut-off values (CADASIL scale: ≥15/25); CADASIL scale-J: ≥16/25).

DISCUSSION

In this study, the frequency of *NOTCH3* mutations was investigated for the first time in a Japanese lacunar stroke cohort; three patients had cysteine-sparing *NOTCH3* p.R75P mutations: two in the phase 1 cohort and one in the phase 2 cohort. The carrier frequency of p.R75P in this study was 3.5% (3/85), which was significantly higher than that in the Japanese general population (4.7KJPN) (odds ratio [95% CI] = 58.2 [11.6–292.5]). Furthermore, all three patients with *NOTCH3* mutations had family histories of stroke and showed hyperintensity lesions at external capsules and moderate-to-severe white matter lesions. However, these patients did not show typical CADASIL clinical and imaging features, such as temporal pole lesions. The CADASIL scale-J score was higher than that of the CADASIL scale.

CADASIL is the most common hereditary small vessel disease, and the estimated prevalence is 2-5/100,000 individuals in clinical practice (Joutel et al., 1997). The most frequent clinical symptoms are ischemic events (59%) and psychiatric disturbances (48%) (Bianchi et al., 2015). Migraine with aura and subcortical vascular cognitive impairment, which are associated with pseudobulbar palsy and urinary incontinence, are also characteristic symptoms of CADASIL (Chabriat et al., 2009). However, it has recently been reported that a subset of patients with *NOTCH3* gene mutations show atypical clinical symptoms of CADASIL, such as absence of temporal pole lesions (Ueda et al., 2015), elderly onset (Watanabe et al., 2012), and cerebellar atrophy (Sari et al., 2019). Furthermore, the exome aggregation consortium (ExAC) database study identified 206 EGFr cysteine-altering *NOTCH3* mutations in the ExAC, with an overall prevalence of 3.4/1,000 individuals (Rutten et al., 2016). The prevalence of CADASIL may be higher than previously thought; in fact, Dong Y et al. reported that one patient with a p.C697T mutation was found among 218 consecutive patients with lacunar infarction in the United Kingdom (Dong et al., 2003). Furthermore, Choi et al. reported that six patients with p.R544C mutations were found among 151 consecutive Korean patients with acute ischemic stroke (Choi et al., 2013), four of whom presented with large artery atherosclerosis and two with lacunar infarction. Our findings echo recent findings in Taiwan and the United Kingdom. Lee et al. reported that the *NOTCH3* p.R544C mutation was present in a significant number of individuals in Taiwan, including 60 of 7,038 healthy controls (0.9%), 17 of 800 patients with ischemic stroke (2.1%), and 16 of 245 patients with small vessel occlusion stroke (6.5%) from the Taiwan Biobank and that the other two cysteine-altering mutations (p.C853Y, and p.C884Y) were rarely detected (Lee et al., 2020). Furthermore, from the UK DNA Lacunar Stoke Study, Tan et al. identified single gene mutations in 14 patients (eight cysteine-altering *NOTCH3* variants in 11 patients, two *HTRA1* variants in two patients, and one missense *COL4A1* variant in one patient) among 950 patients with younger-onset apparently sporadic small vessel disease stroke using a targeted sequencing panel (14 of 950; 1.5%; Tan et al., 2019). These results strongly support our findings, which indicate that *NOTCH3* gene mutations may be involved in some cases of lacunar infarction, which is a representative small vessel disease. CADASIL is probably underdiagnosed in the wider stroke population.

In this study, all three patients with *NOTCH3* p.R75P mutations were relatively young and had family histories of stroke. Furthermore, all three patients showed hyperintensity lesions at external capsules and moderate-to-severe white matter lesions, but did not show temporal pole lesions. Temporal pole

TABLE 4 | Clinical characteristics of patients with R75P mutations.

Case	Age	Type of mutation	Stroke subtype	Symptoms	Migraine	Cognitive impairment	HTN	DL	DM	Smoking incidence	Family history of stroke	External capsule lesion	Temporal pole lesions	Cerebral microbleeds	Fazekas scale	CADASIL scale	CADASIL scale-J
1	60s	R75P	SVD	Dysarthria, Dysesthesia	–	–	–	+	–	–	+	+	–	+	2	6	13
2	40s	R75P	SVD	Cognitive decline	+	+	–	+	–	–	+	+	–	+	3	17	20
3	50s	R75P	SVD	Vertigo, Dysarthria,	–	–	+	+	–	–	+	+	–	–	2	7	10

Exact age is not shown for patient privacy.

HTN, Hypertension; DL, dyslipidemia; DM, diabetes mellitus; CADASIL, cerebral autosomal dominant arteriopathy with subcortical infarcts and leukoencephalopathy; SVD, small vessel disease.

white matter lesions on MRI is one of the most characteristic imaging features of patients with CADASIL (Singhal et al., 2005; Yamamoto et al., 2009); however, some patients with CADASIL do not show temporal pole lesions. Abnormal temporal pole white matter lesions are less common in Asian patients than among Caucasians (Wang et al., 2011), and the prevalence of temporal pole involvement is only between 33.8–71% in the Japanese population (Ueda et al., 2015). In particular, cysteine-sparing *NOTCH3* missense mutations, such as p.R75P (Kim et al., 2006), p.R61W (Brass et al., 2009), p.D80G (Wollenweber et al., 2015), and p.R213K (Santa et al., 2003) are associated with atypical MRI findings with less anterior temporal lobe involvement (Matsushima et al., 2017; Muino et al., 2017). In a prior study of patients with CADASIL, 91% of cysteine-sparing *NOTCH3* mutations did not have anterior temporal pole involvement (Muino et al., 2017). Furthermore, the cysteine at codon 76 could be related to fixation of the double hairpin in the NOTCH3 EGFr, and the substitution of the basic arginine for a proline at codon 75 could induce a partial three-dimensional conformational change in the EGFr that leads to less involvement of the anterior temporal lobe (Mizuno et al., 2008). The precise mechanisms by which cysteine-sparing *NOTCH3* missense mutations induce CADASIL remains to be elucidated. We previously showed that temporal pole changes partially reflect dilated perivascular spaces (Yamamoto et al., 2009). Therefore, the p.R75P mutation may be less likely to dilate perivascular spaces than the cysteine-substitution mutations of *NOTCH3*. Cysteine-sparing mutations should be further studied to confirm their pathological role in CADASIL (Rutten et al., 2014; Coupland et al., 2018). Interestingly, CADASIL patients with *NOTCH3* p.R75P were frequently found throughout Japan. The allele frequency of p.R75P in the general population is 0.0003, according to the largest Japanese whole genome reference panel 4.7KJPN (https://jmorp.megabank.tohoku.ac.jp/202001/variants [accessed 25 March 2020], in the Japanese Multi Omics Reference Panel [jMorp], Tohoku Medical Megabank Organization). It is of note that the carrier frequency of p.R75P in this study was 3.5% (3/85), which was significantly higher than that in 4.7KJPN (odds ratio [95% CI] = 58.2 [11.6–292.5]). The p.R75P carrier frequency in biobank patients with lacunar infarction (1.0%, 3/291) was also significantly higher than that in 4.7KJPN (odds ratio [95% CI] = 16.5 [3.3–82.1]). Our finding is compatible with the high frequency of p.R75P (9.2–11.4%) among Japanese CADASIL patients (Ueda et al., 2015; Koizumi et al., 2019). Mukai et al. analyzed the genotype–phenotype correlation based on the three most common mutations in Japanese CADASIL patients: the cysteine-sparing *NOTCH3* mutation p.R75P and cysteine-altering *NOTCH3* mutations p.R141C and p.R182C. p.R141C showed the most typical CADASIL phenotypes while p.R75P showed mild and atypical phenotypes, with a low frequency of temporal pole lesions, high frequency of hypertension, and low frequency of stroke/transient ischemic attack (TIA). Phenotypes of p.R182C were similar to those of p.R141C, except for a lower frequency of stroke/TIA. Initial symptoms of the 14 probands with p.R75P were none (four of 14; 28.6%), cognitive impairment (three of 14; 21.4%), depression (one of 14, 7.1%), and stroke/TIA (six

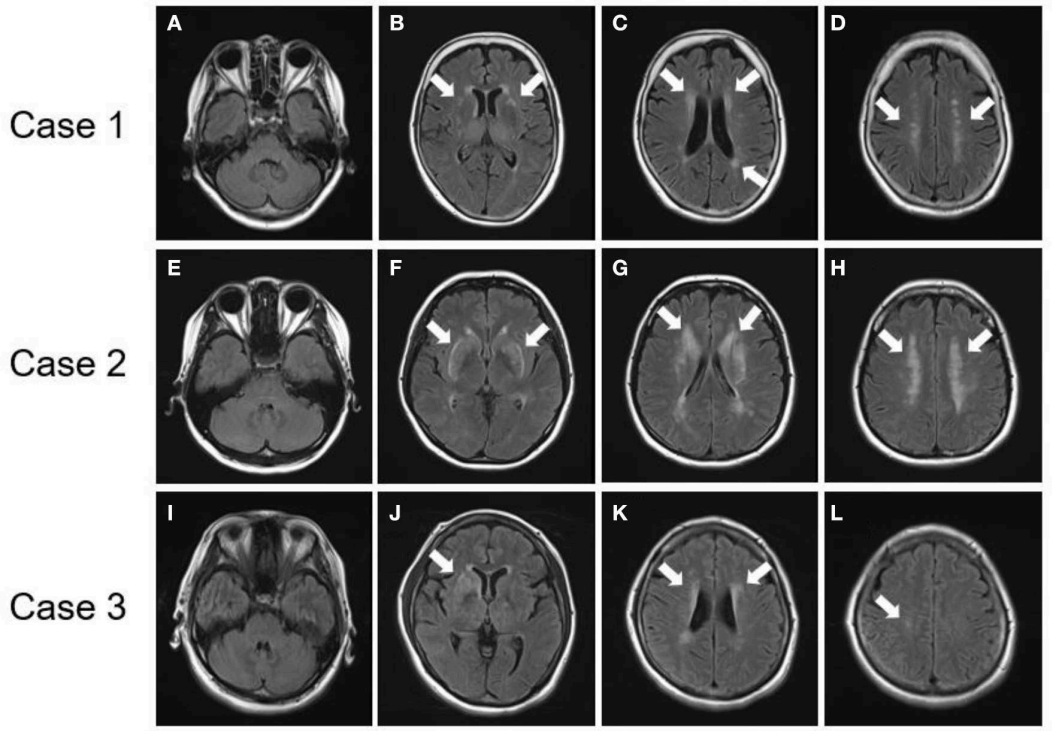

FIGURE 3 | Brain MRI findings of patients with *NOTCH3* mutation. **(A–D)** FLAIR images of a patient with a *NOTCH3* p.R75P mutation (Case 1). **(E–H)** FLAIR images of a patient with a *NOTCH3* p.R75P mutation (Case 2). **(I–L)** FLAIR images of a patient with a *NOTCH3* p.R75P mutation (Case 3). **(A,E,I)** No patients presented lesions on their temporal pole lobes. **(B,F,J)** Arrows indicate hyperintensity lesions at external capsules. **(C,D,G,H,K,L)** Arrows indicate periventricular hyperintensity.

of 14; 42.9%; Mukai et al., 2020). p.R75P presents as clinical symptoms that resemble sporadic lacunar infarcts, and head MRI often shows external capsule lesions and white matter lesions without temporal pole lesions (Kim et al., 2014; Ueda et al., 2015). Therefore, cysteine-sparing *NOTCH3* p.R75P mutation may be underdiagnosed in early-onset lacunar infarctions in daily clinical practice. Lacunar infarctions and white matter lesions of the external capsule, along with family history of stroke, can be prognostic factors that suggest the need for further genetic testing for possible underlying *NOTCH3* mutations.

NOTCH3 genetic testing remains the diagnostic gold standard, and a clinical screening tool is eagerly desired because genetic testing is costly and time-consuming. Pescini et al. proposed the CADASIL scale, a screening tool that can be used to select patients for *NOTCH3* gene analysis (Pescini et al., 2012). The CADASIL scale showed high sensitivity in European studies; however, low sensitivity was reported in Chinese patients, possibly due to ethnic differences in clinical manifestations (Liu et al., 2015). Recently, Koizumi et al. developed the CADASIL scale-J, which can effectively discriminate between patients with CADASIL and patients with *NOTCH3*-negative CADASIL-like symptoms, among Japanese patients. The CADASIL scale-J exhibited a higher diagnostic accuracy than that of the CADASIL scale (Koizumi et al., 2019). The CADASIL scale-J was also well validated in 69 consecutive patients who underwent genetic testing. As a result, the sensitivity and specificity of the CADASIL scale-J were 78.9 and 85.7%, respectively (Koizumi et al., 2019). Furthermore, the CADASIL scale and the CADASIL scale-J scores of the patients with p.R75P were 6, 7, 17, and 10, 13, 20, respectively, in this study. While the CADASIL scale-J score was higher than that of the CADASIL scale, both scores were below their respective cut-off values (CADASIL scale: $\geq$15/25, CADASIL scale-J: $\geq$16/25). The low average scores in patients with p.R75P mutations may be due to a lower frequency of temporal pole lesions and older age onset compared with other CADASIL subtypes, such as cysteine-altering *NOTCH3* mutations (Ueda et al., 2015). The p.R75P mutation, which involves an arginine residue rather than a cysteine, is related to less frequent involvement of the anterior temporal area, thus hampering the clinical utility of CADASIL screening tools. It has been also reported that there is no single pathogenomic clinical or neuroimaging finding that can distinguish patients with CADASIL from those with sporadic stroke (Pantoni et al., 2010). Therefore, the present study supports the notion that clinicians should exercise caution concerning the possibility that atypical patients with *NOTCH3* mutations, such as p.R75P, may be unrecognized among patients with lacunar infarctions due to the atypical clinical and neuroimaging features of CADASIL.

From management and therapeutic perspectives, no definitive treatment has been established for CADASIL progression (Bersano et al., 2017). However, the early diagnosis and treatment for CADASIL, including the strict management of modifiable vascular risk factors, can improve patient prognosis. There are several reports about management options for CADASIL, and

active smoking should be avoided, because it is independently associated with an earlier age of CADASIL onset and increased risk of stroke (Singhal et al., 2004; Chabriat et al., 2016). Additionally, the adequate control of homocysteine levels could decrease the risk of migraines (Singhal et al., 2004). Hypertension is also associated with an increased risk of stroke (Adib-Samii et al., 2010), cerebral microbleeds (Lee et al., 2017), intracerebral hemorrhage, and brain volume changes (Peters et al., 2006), as well as clinical progression. Other modifiable risk factors, such as diabetes mellitus (Viswanathan et al., 2006), alcohol abuse, and obesity, should also be controlled to prevent disease progression (Bersano et al., 2017). Furthermore, the administration of lomerizine, a diphenylmethylpiperazine Ca^{2+} channel blocker, could improve cognitive impairment and cerebral hypoperfusion in patients with CADASIL (Mizuno et al., 2009). Thus, the early detection of underdiagnosed CADASIL in patients who are initially admitted for lacunar infarctions should be carefully monitored to improve prognosis.

There are several limitations associated with the present study that warrant mentioning. First, this study is based on a relatively small number of patient because the genetic examination of all 1,094 patients was impractical in terms of cost and time. Patients aged 60–70 years and/or with white matter disease could be good targets for genetic testing (Tan et al., 2019; Lee et al., 2020). Age (60 years or younger), hypertension, and white matter lesions were used as criteria for patient selection in this study but these cohort selection criteria could be seen as arbitrary. Other characteristic findings of CADASIL, such as migraine, psychiatric symptoms, dementia, and family history of stroke could also be useful criteria for patient selection. More data are necessary to confirm the validity of our findings and their generalizability across other patient populations in the future. Second, this study was conducted at a single-center that was specialized for stroke and cardiovascular disease. Thus, selection biases may have led to an insufficient estimation of the frequency of *NOTCH3* gene mutations across more general populations. Further multi-center studies are needed to confirm the precise association of *NOTCH3* gene mutations with lacunar infarctions. Third, we only analyzed patients with lacunar infarctions in this study, and this could cause a bias in examining the exact prevalence of *NOTCH3* mutations among patients with overall subtypes of ischemic stroke, including large artery atherosclerosis, cardioembolism, and ischemic stroke of undetermined etiology. Further analyses including overall subtypes of ischemic stroke are necessary to confirm the exact prevalence of *NOTCH3* mutations in the future.

CONCLUSION

Among patients hospitalized for lacunar infarction, the carrier frequency of p.R75P may be higher than previously estimated. Furthermore, the *NOTCH3* p.R75P mutation may be underdiagnosed in early-onset lacunar infarctions due to the atypical clinical and neuroimaging features of CADASIL. Early-onset, non-hypertensive lacunar infarcts and white matter lesions of the external capsule, and a family history of stroke are candidate factors that suggest the need for further genetic testing for underlying *NOTCH3* mutations.

DATA AVAILABILITY STATEMENT

The genetic data generated in this study can be obtained on NCBI ClinVar, https://www.ncbi.nlm.nih.gov/clinvar/, under accession no: VCV000632306.1.

ETHICS STATEMENT

The studies involving human participants were reviewed and approved by Local ethics committee of NCVC. The patients/participants provided their written informed consent to participate in this study.

AUTHOR CONTRIBUTIONS

TO and KW: drafted the manuscript, designed the study, and acquired and analyzed the data. KI, SS, and MN: acquired and interpreted the data. SO, TT, MK, KT, and MI: revised the manuscript, interpreted the data, and supervised the study. TK, IM, and TM: performed the *NOTCH3* genetic examinations.

FUNDING

This work was supported by the Grant-in-Aid for Scientific Research of Japan on Priority Areas from the Japanese Ministry of Education, Science and Culture: 19K21321 (KW).

ACKNOWLEDGMENTS

We would like to thank patients and families who participated in this study. This research was performed using samples acquired from the National Center Biobank Network (NCBN)/ NCVC Biobank resource. For further details, please see http://www.ncbiobank.org/ and http://www.ncvc.go.jp/biobank/.

REFERENCES

Adams, H. P. Jr., Bendixen, B. H., Kappelle, L. J., Biller, J., Love, B. B., Gordon, D. L., et al. (1993). Classification of subtype of acute ischemic stroke. Definitions for use in a multicenter clinical trial. Toast. Trial of org 10172 in acute stroke treatment. *Stroke* 24, 35–41. doi: 10.1161/01.STR.24.1.35

Adib-Samii, P., Brice, G., Martin, R. J., and Markus, H. S. (2010). Clinical spectrum of cadasil and the effect of cardiovascular risk factors on phenotype: study in 200 consecutively recruited individuals. *Stroke* 41, 630–634. doi: 10.1161/STROKEAHA.109.568402

Auer, D. P., Putz, B., Gossl, C., Elbel, G., Gasser, T., and Dichgans, M. (2001). Differential lesion patterns in cadasil and sporadic subcortical arteriosclerotic encephalopathy: Mr imaging study with statistical parametric group comparison. *Radiology* 218, 443–451. doi: 10.1148/radiology.218.2.r01fe24443

Bersano, A., Bedini, G., Markus, H. S., Vitali, P., Colli-Tibaldi, E., Taroni, F., et al. (2018). The role of clinical and neuroimaging features in the diagnosis of cadasil. *J. Neurol.* 265, 2934–2943. doi: 10.1007/s00415-018-9072-8

Bersano, A., Bedini, G., Oskam, J., Mariotti, C., Taroni, F., Baratta, S., et al. (2017). Cadasil: Treatment and management options. *Curr. Treat. Options Neurol.* 19:31. doi: 10.1007/s11940-017-0468-z

Bianchi, S., Zicari, E., Carluccio, A., Di Donato, I., Pescini, F., Nannucci, S., et al. (2015). Cadasil in central italy: a retrospective clinical and genetic study in 229 patients. *J. Neurol.* 262, 134–141. doi: 10.1007/s00415-014-7533-2

Brass, S. D., Smith, E. E., Arboleda-Velasquez, J. F., Copen, W. A., and Frosch, M. P. (2009). Case records of the massachusetts general hospital. Case 12-2009. A 46-year-old man with migraine, aphasia, and hemiparesis and similarly affected family members. *N. Engl. J. Med.* 360, 1656–1665. doi: 10.1056/NEJMcpc0810839

Chabriat, H., Herve, D., Duering, M., Godin, O., Jouvent, E., Opherk, C., et al. (2016). Predictors of clinical worsening in cerebral autosomal dominant arteriopathy with subcortical infarcts and leukoencephalopathy: Prospective cohort study. *Stroke* 47, 4–11. doi: 10.1161/STROKEAHA.115.010696

Chabriat, H., Joutel, A., Dichgans, M., Tournier-Lasserve, E., and Bousser, M. G. (2009). The lancet. *Neurology* 8, 643–653. doi: 10.1016/S1474-4422(09)70127-9

Chabriat, H., Levy, C., Taillia, H., Iba-Zizen, M. T., Vahedi, K., Joutel, A., et al. (1998). Patterns of mri lesions in cadasil. *Neurology* 51, 452–457. doi: 10.1212/WNL.51.2.452

Chabriat, H., Vahedi, K., Iba-Zizen, M. T., Joutel, A., Nibbio, A., Nagy, T. G., et al. (1995). Clinical spectrum of cadasil: A study of 7 families. Cerebral autosomal dominant arteriopathy with subcortical infarcts and leukoencephalopathy. *Lancet* 346, 934–939. doi: 10.1016/S0140-6736(95)91557-5

Choi, J. C., Lee, K. H., Song, S. K., Lee, J. S., Kang, S. Y., and Kang, J. H. (2013). Screening for notch3 gene mutations among 151 consecutive korean patients with acute ischemic stroke. *J. Stroke Cerebrovasc. Dis.* 22, 608–614. doi: 10.1016/j.jstrokecerebrovasdis.2011.10.013

Coulthard, A., Blank, S. C., Bushby, K., Kalaria, R. N., and Burn, D. J. (2000). Distribution of cranial mri abnormalities in patients with symptomatic and subclinical ca.dasil. *Br. J. Radiol.* 73, 256–265. doi: 10.1259/bjr.73.867.10817040

Coupland, K., Lendahl, U., and Karlstrom, H. (2018). Role of notch3 mutations in the cerebral small vessel disease cerebral autosomal dominant arteriopathy with subcortical infarcts and leukoencephalopathy. *Stroke* 49, 2793–2800. doi: 10.1161/STROKEAHA.118.021560

Dong, Y., Hassan, A., Zhang, Z., Huber, D., Dalageorgou, C., and Markus, H. S. (2003). Yield of screening for cadasil mutations in lacunar stroke and leukoaraiosis. *Stroke* 34, 203–205. doi: 10.1161/01.STR.0000048162.16852.88

Fazekas, F., Kleinert, R., Offenbacher, H., Payer, F., Schmidt, R., Kleinert, G., et al. (1991). The morphologic correlate of incidental punctate white matter hyperintensities on mr images. AJNR. *Am. J. Neuroradiol.* 12, 915–921.

Joutel, A., Corpechot, C., Ducros, A., Vahedi, K., Chabriat, H., Mouton, P., et al. (1996). Notch3 mutations in cadasil, a hereditary adult-onset condition causing stroke and dementia. *Nature* 383, 707–710. doi: 10.1038/383707a0

Joutel, A., Vahedi, K., Corpechot, C., Troesch, A., Chabriat, H., Vayssiere, C., et al. (1997). Strong clustering and stereotyped nature of notch3 mutations in cadasil patients. *Lancet* 350, 1511–1515. doi: 10.1016/S0140-6736(97)08083-5

Kalaria, R. N., and Hase, Y. (2019). Neurovascular ageing and age-related diseases. *Sub-Cellular Biochem.* 91, 477–499. doi: 10.1007/978-981-13-3681-2_17

Kim, Y., Choi, E. J., Choi, C. G., Kim, G., Choi, J. H., Yoo, H. W., et al. (2006). Characteristics of cadasil in korea: a novel cysteine-sparing notch3 mutation. *Neurology* 66, 1511–1516. doi: 10.1212/01.wnl.0000216259.99811.50

Kim, Y. E., Yoon, C. W., Seo, S. W., Ki, C. S., Kim, Y. B., Kim, J. W., et al. (2014). Spectrum of notch3 mutations in korean patients with clinically suspicious cerebral autosomal dominant arteriopathy with subcortical infarcts and leukoencephalopathy. *Neurobiol. Aging* 35, 726.e721–726. doi: 10.1016/j.neurobiolaging.2013.09.004

Koizumi, T., Mizuta, I., Watanabe-Hosomi, A., Mukai, M., Hamano, A., Matsuura, J., et al. (2019). The cadasil scale-j, a modified scale to prioritize access to genetic testing for japanese cadasil-suspected patients. *J. Stroke Cerebrovasc. Dis.* 28, 1431–1439. doi: 10.1016/j.jstrokecerebrovasdis.2019.03.026

Lee, J. S., Ko, K., Oh, J. H., Park, J. H., Lee, H. K., Floriolli, D., et al. (2017). Cerebral microbleeds, hypertension, and intracerebral hemorrhage in cerebral autosomal-dominant arteriopathy with subcortical infarcts and leukoencephalopathy. *Front. Neurol.* 8:203. doi: 10.3389/fneur.2017.00203

Lee, Y. C., Chung, C. P., Chang, M. H., Wang, S. J., and Liao, Y. C. (2020). Notch3 cysteine-altering variant is an important risk factor for stroke in the taiwanese population. *Neurology* 94, e87–e96. doi: 10.1212/WNL.0000000000008700

Liu, X., Zuo, Y., Sun, W., Zhang, W., Lv, H., Huang, Y., et al. (2015). The genetic spectrum and the evaluation of cadasil screening scale in chinese patients with notch3 mutations. *J. Neurol. Sci.* 354, 63–69. doi: 10.1016/j.jns.2015.04.047

Matsushima, T., Conedera, S., Tanaka, R., Li, Y., Yoshino, H., Funayama, M., et al. (2017). Genotype-phenotype correlations of cysteine replacement in cadasil. *Neurobiol. Aging* 50, 169.e167–169.e114. doi: 10.1016/j.neurobiolaging.2016.10.026

Mizuno, T., Kondo, M., Ishigami, N., Tamura, A., Itsukage, M., Koizumi, H., et al. (2009). Cognitive impairment and cerebral hypoperfusion in a cadasil patient improved during administration of lomerizine. *Clin. Neuropharmacol.* 32, 113–116. doi: 10.1097/WNF.0b013e31816c82a6

Mizuno, T., Muranishi, M., Torugun, T., Tango, H., Nagakane, Y., Kudeken, T., et al. (2008). Two japanese cadasil families exhibiting notch3 mutation r75p not involving cysteine residue. *Internal Med.* 47, 2067–2072. doi: 10.2169/internalmedicine.47.1391

Mizuta, I., Watanabe-Hosomi, A., Koizumi, T., Mukai, M., Hamano, A., Tomii, Y., et al. (2017). New diagnostic criteria for cerebral autosomal dominant arteriopathy with subcortical infarcts and leukocencephalopathy in japan. *J. Neurol. Sci.* 381, 62–67. doi: 10.1016/j.jns.2017.08.009

Muino, E., Gallego-Fabrega, C., Cullell, N., Carrera, C., Torres, N., Krupinski, J., et al. (2017). Systematic review of cysteine-sparing notch3 missense mutations in patients with clinical suspicion of cadasil. *Int. J. Mol. Sci.* 18, pii:E1964. doi: 10.3390/ijms18091964

Mukai, M., Mizuta, I., Watanabe-Hosomi, A., Koizumi, T., Matsuura, J., Hamano, A., et al. (2020). Genotype-phenotype correlations and effect of mutation location in japanese cadasil patients. *J. Human Genetics*. doi: 10.1038/s10038-020-0751-9. [Epub ahead of print].

Pantoni, L., Pescini, F., Nannucci, S., Sarti, C., Bianchi, S., Dotti, M. T., et al. (2010). Comparison of clinical, familial, and mri features of cadasil and notch3-negative patients. *Neurology* 74, 57–63. doi: 10.1212/WNL.0b013e3181c7da7c

Pescini, F., Nannucci, S., Bertaccini, B., Salvadori, E., Bianchi, S., Ragno, M., et al. (2012). The cerebral autosomal-dominant arteriopathy with subcortical infarcts and leukoencephalopathy (cadasil) scale: a screening tool to select patients for notch3 gene analysis. *Stroke* 43, 2871–2876. doi: 10.1161/STROKEAHA.112.665927

Peters, N., Holtmannspotter, M., Opherk, C., Gschwendtner, A., Herzog, J., Samann, P., et al. (2006). Brain volume changes in cadasil: a serial mri study in pure subcortical ischemic vascular disease. *Neurology* 66, 1517–1522. doi: 10.1212/01.wnl.0000216271.96364.50

Regenhardt, R. W., Das, A. S., Lo, E. H., and Caplan, L. R. (2018). Advances in understanding the pathophysiology of lacunar stroke: a review. *JAMA Neurol.* 75, 1273–1281. doi: 10.1001/jamaneurol.2018.1073

Rutten, J. W., Dauwerse, H. G., Gravesteijn, G., van Belzen, M. J., van der Grond, J., Polke, J. M., et al. (2016). Archetypal notch3 mutations frequent in public exome: Implications for cadasil. *Ann. Clin. Transl. Neurol.* 3, 844–853. doi: 10.1002/acn3.344

Rutten, J. W., Haan, J., Terwindt, G. M., van Duinen, S. G., Boon, E. M., and Lesnik Oberstein, S. A. (2014). Interpretation of notch3 mutations in the diagnosis of cadasil. *Expert Rev. Mol. Diagnostics* 14, 593–603. doi: 10.1586/14737159.2014.922880

Santa, Y., Uyama, E., Chui, D. H., Arima, M., Kotorii, S., Takahashi, K., et al. (2003). Genetic, clinical and pathological studies of cadasil in japan: a partial contribution of notch3 mutations and implications of smooth muscle cell degeneration for the pathogenesis. *J. Neurol. Sci.* 212, 79–84. doi: 10.1016/S0022-510X(03)00109-6

Sari, U. S., Kisabay, A., Batum, M., Tarhan, S., Dogan, N., Coskunoglu, A., et al. (2019). Cadasil with atypical clinical symptoms, magnetic resonance imaging, and novel mutations: two case reports and a review of the literature. *J. Mol. Neurosci.* 68, 529–538. doi: 10.1007/s12031-019-01313-z

Singhal, S., Bevan, S., Barrick, T., Rich, P., and Markus, H. S. (2004). The influence of genetic and cardiovascular risk factors on the cadasil phenotype. *Brain* 127, 2031–2038. doi: 10.1093/brain/awh223

Singhal, S., Rich, P., and Markus, H. S. (2005). The spatial distribution of mr imaging abnormalities in cerebral autosomal dominant arteriopathy with subcortical infarcts and leukoencephalopathy and their relationship to age and clinical features. AJNR. *Am. J. Neuroradiol.* 26, 2481–2487.

Tan, R. Y. Y., Traylor, M., Megy, K., Duarte, D., Deevi, S. V. V., Shamardina, O., et al. (2019). How common are single gene mutations as a cause for

lacunar stroke? A targeted gene panel study. *Neurology* 93, e2007–e2020. doi: 10.1212/WNL.0000000000008544

Tomimoto, H., Ohtani, R., Wakita, H., Lin, J. X., Ihara, M., Miki, Y., et al. (2006). Small artery dementia in japan: radiological differences between cadasil, leukoaraiosis and binswanger's disease. *Dementia Geriatric Cognitive Disord.* 21, 162–169. doi: 10.1159/000090677

Tournier-Lasserve, E., Joutel, A., Melki, J., Weissenbach, J., Lathrop, G. M., Chabriat, H., et al. (1993). Cerebral autosomal dominant arteriopathy with subcortical infarcts and leukoencephalopathy maps to chromosome 19q12. *Nat. Genet.* 3, 256–259. doi: 10.1038/ng0393-256

Ueda, A., Ueda, M., Nagatoshi, A., Hirano, T., Ito, T., Arai, N., et al. (2015). Genotypic and phenotypic spectrum of cadasil in japan: the experience at a referral center in kumamoto university from 1997 to 2014. *J. Neurol.* 262, 1828–1836. doi: 10.1007/s00415-015-7782-8

Veglio, F., Paglieri, C., Rabbia, F., Bisbocci, D., Bergui, M., and Cerrato, P. (2009). Hypertension and cerebrovascular damage. *Atherosclerosis* 205, 331–341. doi: 10.1016/j.atherosclerosis.2008.10.028

Viswanathan, A., Guichard, J. P., Gschwendtner, A., Buffon, F., Cumurcuic, R., Boutron, C., et al. (2006). Blood pressure and haemoglobin a1c are associated with microhaemorrhage in cadasil: a two-centre cohort study. *Brain* 129, 2375–2383. doi: 10.1093/brain/awl177

Wang, Z., Yuan, Y., Zhang, W., Lv, H., Hong, D., Chen, B., et al. (2011). Notch3 mutations and clinical features in 33 mainland chinese families with cadasil. *J. Neurol. Neurosurgery Psychiatry* 82, 534–539. doi: 10.1136/jnnp.2010.209247

Watanabe, M., Adachi, Y., Jackson, M., Yamamoto-Watanabe, Y., Wakasaya, Y., Shirahama, I., et al. (2012). An unusual case of elderly-onset cerebral autosomal dominant arteriopathy with subcortical infarcts and leukoencephalopathy (cadasil) with multiple cerebrovascular risk factors. *J. Stroke Cerebrovasc. Dis.* 21, 143–145. doi: 10.1016/j.jstrokecerebrovasdis.2010.05.008

Wollenweber, F. A., Hanecker, P., Bayer-Karpinska, A., Malik, R., Bazner, H., Moreton, F., et al. (2015). Cysteine-sparing cadasil mutations in notch3 show proaggregatory properties *in vitro*. *Stroke* 46, 786–792. doi: 10.1161/STROKEAHA.114.007472

Yamamoto, Y., Ihara, M., Tham, C., Low, R. W., Slade, J. Y., Moss, T., et al. (2009). Neuropathological correlates of temporal pole white matter hyperintensities in cadasil. *Stroke* 40, 2004–2011. doi: 10.1161/STROKEAHA.108.528299

Conflict of Interest: The authors declare that the research was conducted in the absence of any commercial or financial relationships that could be construed as a potential conflict of interest.

frontiers in Aging Neuroscience

BRIEF RESEARCH REPORT
published: 03 June 2020
doi: 10.3389/fnagi.2020.00151

Excessive Production of Transforming Growth Factor β1 Causes Mural Cell Depletion From Cerebral Small Vessels

*Taisuke Kato[1], Yumi Sekine[2], Hiroaki Nozaki[2], Masahiro Uemura[2], Shoichiro Ando[2], Sachiko Hirokawa[2] and Osamu Onodera[2]**

[1]Department of System Pathology for Neurological Disorders, Brain Science Branch, Brain Research Institute, Niigata University, Niigata, Japan, [2]Department of Neurology, Clinical Neuroscience Branch, Brain Research Institute, Niigata University, Niigata, Japan

It is increasingly becoming apparent that cerebrovascular dysfunction contributes to the pathogenic processes involved in vascular dementia, Alzheimer's disease, and other neurodegenerative disorders. Under these pathologic conditions, the degeneration of cerebral blood vessels is frequently accompanied by a loss of mural cells from the vascular walls. Vascular mural cells play pivotal roles in cerebrovascular functions, such as regulation of cerebral blood flow and maintenance of the blood-brain barrier (BBB). Therefore, cerebrovascular mural cell impairment is involved in the pathophysiology of vascular-related encephalopathies, and protecting these cells is essential for maintaining brain health. However, our understanding of the molecular mechanism underlying mural cell abnormalities is incomplete. Several reports have indicated that dysregulated transforming growth factor β (TGFβ) signaling is involved in the development of cerebral arteriopathies. These studies have specifically suggested the involvement of TGFβ overproduction. Although cerebrovascular toxicity *via* vascular fibrosis by extracellular matrix accumulation or amyloid deposition is known to occur with enhanced TGFβ production, whether increased TGFβ results in the degeneration of vascular mural cells *in vivo* remains unknown. Here, we demonstrated that chronic TGFβ1 overproduction causes a dropout of mural cells and reduces their coverage on cerebral vessels in both smooth muscle cells and pericytes. Mural cell degeneration was also accompanied by vascular luminal dilation. TGFβ1 overproduction in astrocytes significantly increased TGFβ1 content in the cerebrospinal fluid (CSF) and increased TGFβ signaling-regulated gene expression in both pial arteries and brain capillaries. These results indicate that TGFβ is an important effector that mediates mural cell abnormalities under pathological conditions related to cerebral arteriopathies.

Keywords: TGFβ, mural cells, smooth muscle cells, pericytes, cerebral small vessel

OPEN ACCESS

Edited by:
Satoshi Saito, National Cerebral and Cardiovascular Center (Japan), Japan

Reviewed by:
Maiko T. Uemura, University of Pennsylvania, United States
Jaime Ramos-Cejudo, Langone Medical Center, New York University, United States

****Correspondence:***
Osamu Onodera
onodera@bri.niigata-u.ac.jp

Received: *07 December 2019*
Accepted: *05 May 2020*
Published: *03 June 2020*

Citation:
Kato T, Sekine Y, Nozaki H, Uemura M, Ando S, Hirokawa S and Onodera O (2020) Excessive Production of Transforming Growth Factor β1 Causes Mural Cell Depletion From Cerebral Small Vessels. Front. Aging Neurosci. 12:151. doi: 10.3389/fnagi.2020.00151

INTRODUCTION

The neurovascular unit is composed of endothelial cells, vascular mural cells, astrocytes, and neurons and plays a central role in rigorous brain functions. Vascular mural cells have been described as a heterogeneous cell population but are mainly divided into two types of cells, vascular smooth muscle cells (SMCs) and pericytes, which are distinguished by their cellular localization, structure, and gene expression profiling (Holm et al., 2018). Vascular SMCs surround brain pial arteries and arterioles, and pericytes envelope cerebral capillaries. These cells are involved in maintaining precise regulation of cerebral blood flow, blood-brain-barrier (BBB) integrity, and homeostasis of the central nervous system (Armulik et al., 2010; Hall et al., 2014; Hill et al., 2015). Therefore, maintaining the soundness of vascular mural cells is necessary to meet the high energy demand of the brain and BBB function. Impairment or deficiency of vascular mural cells has been reported in some neurodegenerative diseases, including Alzheimer's disease and amyotrophic lateral sclerosis, and in non-amyloid cerebral small vessel diseases (Ervin et al., 2004; Oide et al., 2008; Winkler et al., 2013). Vascular mural cell loss or dysfunction leads to BBB dysfunction, neuroinflammation, and disrupted coordination between cerebral blood flow and local neuronal activity, ultimately resulting in neuronal loss and dementia. However, the molecular mechanism underlying these impairments of vascular mural cells is unknown.

Transforming growth factor β (TGFβ) signaling promotes cell differentiation, maturation, proliferation, migration, and attachment of endothelial cells and mural cells (Holm et al., 2018). Canonical and normally controlled TGFβ signaling exerts beneficial functions in the vascular milieu. TGFβ signaling promotes the barrier function of the BBB through the upregulation of tight junction proteins (Ronaldson et al., 2009) and induces the differentiation of mural cells. On the other hand, disrupted TGFβ signaling is a common denominator in Alzheimer's disease and non-amyloid cerebral small vessel disease (Hara et al., 2009). In Alzheimer's disease, TGFβ protein and its mRNA levels have been reported to be upregulated (Chao et al., 1994; Wyss-Coray et al., 1997). Also, TGFβ protein and mRNA levels are positively correlated with the degree of angiopathy. Moreover, hypertension, which is the strongest risk factor for non-amyloid cerebral small vessel disease, upregulates TGFβ expression. Cerebrovascular accumulation of TGFβ is also observed in hereditary cerebral small vessel disease (Wyss-Coray et al., 1997; Hara et al., 2009; Müller et al., 2017). Although increased TGFβ levels and vascular mural cell abnormalities are important, common characteristics in several cerebral angiopathies, the direct relationships have not been fully investigated.

In this study, we investigated the alterations of vascular mural cells in an environment in which the cells are exposed to excess and long-term TGFβ signaling. To achieve this goal, we used transgenic mice expressing the bioactive form of TGFβ1 (TGFβ1 Tg mice) and assessed the effect on vascular mural cells.

MATERIALS AND METHODS

Animals

In this study, we used transgenic mice overexpressing bioactive porcine TGFβ1 under the control of a glial fibrillary acidic protein (GFAP) promoter (GFAP-TGFβ1 mice; line T64; Wyss-Coray et al., 1995). The animal study was approved by the Animal Use and Care Committee of Niigata University and followed the guidelines of the National Institutes of Health (USA). We maintained and used the Tg mice in the C57BL/6 genetic background as heterozygotes.

Tissue Preparation

Mice were deeply anesthetized with isoflurane, transcardially perfused with Hank's balanced salt solution (HBSS), and fixed with 4% paraformaldehyde. For paraffin sections, brains were processed for paraffin embedding. Coronal slices (4 μm) were sectioned from each paraffin-embedded brain block. For vibratome sections, fixed brains were embedded in 3% agarose. Coronal sections (50 μm) were cut on a vibratome.

Immunohistochemistry

Paraffinized brain sections were rehydrated and then boiled in a microwave oven in 0.01 M sodium citrate buffer (pH 6.0) for antigen retrieval. Brain slices were blocked in 5% fetal bovine serum in PBS + 0.1% Triton X-100 for 1 h at room temperature. Samples were incubated at 4°C with biotinylated anti-α-smooth muscle actin (αSMA) antibody (1:100, LS-C87562, LifeSpan BioScience Inc.), DyLight 594-labeled Lycopersicon esculentum (tomato) lectin (DL-1177, 1:100, Vector Lab.) for visualization of the endothelial cell layer, anti-porcine TGFβ1 antibody (CPT-001, 1:500, Cell Sciences), anti-GFAP antibody (MAB-360, 1:50, Merck Millipore) and anti-Nestin antibody (sc-23927, 1:100, Santa Cruz Biotech.) overnight. Excess antibody was removed by rinsing in PBS. Samples were then incubated at room temperature for 1 h with the secondary fluorescently labeled antibody. Excess antibody was removed by rinsing in PBS. Slides were mounted in Vectashield mounting medium with DAPI (Vector Labs, Burlingame, CA, USA) and imaged with an all-in-one microscope (Keyence; BioRevo BZ-9000). The vessel wall structure was visualized by detecting tissue autofluorescence along with the fluorescently labeled lectin signal.

Vibratome sections were blocked with 5% normal swine serum/1% BSA in PBS containing 0.5% Triton X-100 overnight at 4°C and incubated with rat anti-CD13 antibody (1:50, R3-63, AbD Serotec) with DyLight 594-labeled tomato lectin or rat anti-platelet endothelial cell adhesion molecule-1 (PECAM1) antibody (1:20, DIA-310, Optistain) for 48 h at 4°C. Then, the samples were incubated at 4°C for 24 h with the secondary fluorescently labeled antibody. Three-dimensional fluorescence microscopy images were captured by confocal laser microscopy (LSM710, Carl Zeiss).

Image Analysis

The occupancy of SMCs in the vascular wall was determined as the ratio of the αSMA-positive area to the vascular wall area. We analyzed micrographic images of cross-sections of the pial artery

(anterior cerebral artery) at equal intervals, avoiding arterial branching points. Four to five images were analyzed per mouse using Imaris software (ver. 6.2.0, Bitplane). The size of each SMC was measured using Imaris software. The luminal area of the pial arteries was analyzed using ImageJ software.

To measure pericyte coverage and capillary diameter, three to four three-dimensional fluorescence microscopy images obtained from the motor cortex or the hippocampus were analyzed per mouse. At the time of blood vessel imaging, the region including the parenchymal arterioles was excluded, and only capillaries (∼5 μm diameter) were imaged (Ma et al., 2018). Imaris software was used for three-dimensional volume rendering of pericytes and quantification of capillary diameter.

Quantification of TGFβ1 in Cerebrospinal Fluid (CSF)

Mouse CSF was sampled from the cisterna magna using a glass capillary tube. CSF TGFβ1 was quantified with a Mouse/Rat/Porcine/Canine TGFβ1 Quantikine ELISA Kit (R&D System) according to the manufacturer's guidelines.

Pial Artery Collection

Blood was removed by transcardial perfusion with HBSS. The segments of the middle and anterior cerebral arteries with medium-sized branches (referred to as the pial artery) were isolated from mouse brains under a dissecting microscope, immediately frozen on dry ice, and stored at −80°C.

Brain Capillary Purification

Brain capillaries were purified as previously described (Olson and Soriano, 2011). Cerebral cortexes with the leptomeninges and pial arteries removed were triturated and incubated in 5 mg/ml collagenase type 1 (GIBCO) for 30 min at 37°C. Capillaries were filtered through a 40-μm nylon mesh. The capillaries on the mesh were collected by washing with cold PBS containing 0.1% BSA and 2 mM EDTA and purified from the tissue slurries by affinity purification with anti-PECAM-1 antibody (550274, BD Biosciences) binding magnetic Dynabeads (Thermo Fisher Scientific) for 30 min at 4°C followed by RNA extraction.

RNA Isolation and cDNA Synthesis

RNA was isolated from the above-collected tissues using a Direct-zol RNA Kit (ZYMO Research). The quantitation and quality of RNA were determined using a Nanodrop 2000c spectrophotometer. Then, RNA from each sample was reverse transcribed to synthesize cDNA using SuperScript IV VILO MasterMix (ThermoFisher).

Quantitative RT-PCR

For quantitative RT-PCR analysis, reverse-transcribed cDNA was subjected to RT-PCR using the SYBR Green master mix and a Thermal Cycler Dice® Real Time System (Takara).

Cerebrovascular SMC Culture

Cerebrovascular SMCs isolated from human brains (ScienCell) were maintained in SMC medium (ScienCell) containing 5% FBS at 37°C with 5% CO_2-95% room air.

Proliferation Assay

The cell proliferation rate was measured by 5-ethynyl-2′-deoxyuridine (EdU), a thymidine analog, incorporation assay. Following starvation in 1% FBS for 24 h, EdU incorporation into cerebrovascular SMCs was assessed with or without recombinant human TGFβ1 (5 or 50 ng/ml) for 24 h. Recombinant TGFβ1 was dissolved in 4 mM HCl with 2% BSA. After EdU incorporation, cells were stained with a Click-iT EdU Imaging Kit (Thermo Fisher Scientific) according to the manufacturer's instructions.

Cell Death Assay

For the cell death assay, cerebrovascular SMCs were treated with recombinant human TGFβ1 (5 or 50 ng/ml) for 3 days. Dying cells were detected using an Apoptosis/Necrosis Assay Kit (Abcam) according to the manufacturer's instructions. As a positive control for this assay, cerebrovascular SMCs were also treated with camptothecin (6 μM).

Statistical Analysis

Statistical computation was performed using IBM SPSS 22. Data were first subjected to the Shapiro–Wilk test (for fit to the Gaussian distribution) and Levene's test (for equal variance). Either a one-way analysis of variance or a two-tailed unpaired *t*-test was adopted for data with a Gaussian distribution and equal variance. Subsequently, a Bonferroni test was applied to the data as a *post hoc* test. Alternatively, the Mann–Whitney *U*-test was applied to data with unequal variance. $P < 0.05$ was regarded as statistically significant.

Study Approval

All animal experiments described were approved by the Animal Use and Care Committee of Niigata University and followed the guidelines of the National Institutes of Health (USA).

RESULTS

First, we investigated pericytes on brain capillaries that were directly enveloped by the endfeet of astrocytes overexpressing TGFβ1 in Tg mice at 8 and 24 months of age. Indeed, TGFβ1 overexpression was confirmed in astrocytes in the brains of TGFβ1 Tg mice (**Figure 1A**). Also, overexpression of TGFβ1 was observed in Nestin-positive neural stem cells, which are a subpopulation of astrocytes that express GFAP and Nestin, around the lateral ventricle (**Figure 1B**; Gonzalez-Perez and Quiñones-Hinojosa, 2012). The pericyte coverage rate on the capillary walls was significantly lower in both the cerebral cortex and the hippocampus in TGFβ1 Tg mice than in wild-type (WT) mice at 24 months of age. The decrease in pericyte coverage in TGFβ1 Tg mice was not found at 8 months of age (**Figures 2A–C**). A decrease in pericyte coverage has been associated with the expansion of the capillary vessel diameter (Armulik et al., 2010). We examined capillary diameter by morphometric analysis of immunostained capillary endothelial cells and found that the capillary diameter in TGFβ1 Tg mice was significantly larger than that in WT mice only at 24 months of age but not at 8 months of age (**Figures 2D–F**).

Next, we investigated the effect of TGFβ1 overexpression on vascular SMCs in brain pial arteries by immunohistochemistry

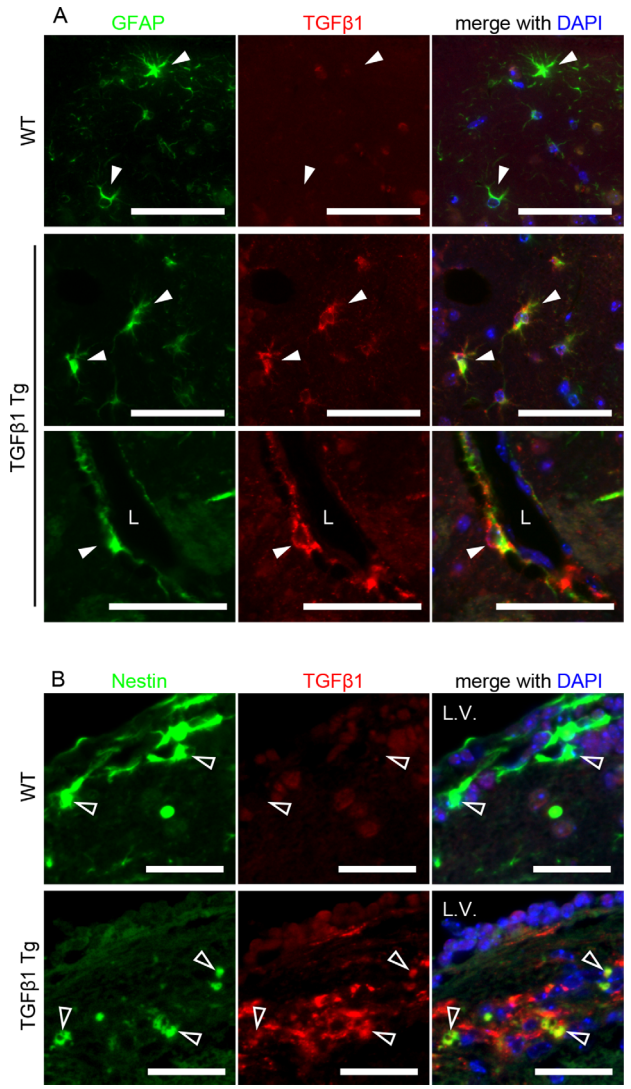

FIGURE 1 | Cellular distribution of porcine transforming growth factor β (TGFβ1) transgene expression. **(A)** Brain slices of 8-week-old TGFβ1 Tg mice were double-labeled with glial fibrillary acidic protein (GFAP) and porcine TGFβ1 antibodies. TGFβ1 immunoreactivity was specifically detected in astrocytes of TGFβ1 Tg mice but not wild-type (WT) mice. The overexpression of porcine TGFβ1 was also observed in perivascular astrocytes (lower images). Filled white arrowheads depict GFAP-positive astrocytes. L, vascular lumen. Scale bar = 50 μm. **(B)** Porcine TGFβ1 expression in Nestin-positive cells around the lateral ventricle was detected in the brains of 8-week-old TGFβ1 Tg mice. L.V., lateral ventricle. Empty arrowheads depict Nestin-positive cells. No detectable signal of TGFβ1 expression was found in the age-matched WT brain slices. Scale bar = 25 μm.

at 8 and 24 months of age. The entire circumference of the pial arteries in WT mice was covered by stratified SMCs, even at 24 months of age. In contrast, SMC loss from the vascular walls was frequently observed in TGFβ1 Tg mice at 24 months of age, resulting in a decreasing coverage rate of SMCs on the vascular walls (**Figures 3A,B**). At 24 months of age, the mean size of the remaining SMCs was also significantly smaller in TGFβ1 Tg mice than in age-matched WT mice (**Figures 3A,C**). Morphologically, the luminal area of the pial arteries was significantly larger in TGFβ1 Tg mice (**Figures 3A,D**). These abnormalities were not found in the pial arteries of 8-month-old TGFβ1 Tg mice (**Figures 3A–D**).

Vascular SMCs mainly lie on the pial arteries and the perforating arteries.

However, these types of brain vessels lack direct contact with astrocytes because the pial arteries or perforating arteries and astrocytes (astrocytic glia limitans) are separated by the subarachnoid space or the perivascular space, which contains CSF. Quantification of active TGFβ1 content in the CSF revealed that active TGFβ1 content was upregulated in TGFβ1 Tg mice compared with WT mice (**Figure 4A**). We also quantified the expression levels of mRNA regulated by TGFβ signaling using samples of dissected pial arteries and purified brain parenchymal small vessels. In both types of cerebral vessels, the expression levels of genes regulated by TGFβ signaling were significantly upregulated in TGFβ1 Tg mice compared with WT mice (**Figures 4B,C**).

The effects of TGFβ signaling on vascular mural cells have been reported in several studies. However, the response to signaling depends on the state of gene expression in cells receiving this signal (Grainger et al., 1994; Suwanabol et al., 2012). Because cerebral blood vessels have specialized gene expression profiling, we examined the direct response of cerebrovascular SMCs to TGFβ signaling (Jambusaria et al., 2020). EdU incorporation assay revealed that TGFβ1 exerts a dose-dependent inhibitory effect on cerebrovascular SMC proliferation (**Figure 4D**). On the other hand, even high concentrations of TGF did not induce cell death of vascular SMCs (**Figure 4E**).

DISCUSSION

We demonstrated that the constitutive overproduction of TGFβ1 from astrocytes results in the degeneration of vascular mural cells. While various cell types express TGFβ in the central nervous system, the main sources of increased TGFβ under pathological conditions are astrocytes and microglia (Finch et al., 1993; Buckwalter and Wyss-Coray, 2004; Yan et al., 2014). TGF production increases with aging as well as vascular injury (Yan et al., 2014). Astrocytes highly interact with cerebral blood vessels by enwrapping through their endfeet. Thus, the increased TGFβ production from astrocytes should more directly and strongly affect blood vessels than TGFβ production from other cell types. The adverse effect is extended not only to parenchymal pericytes surrounded by astrocyte endfeet but also to SMCs that were not in direct contact with astrocytes. Our analysis of mouse CSF revealed that TGFβ1 content was upregulated in TGFβ1 Tg mice. The entire subarachnoid space is sealed by the astrocytic glia limitans superficialis. We assume that TGFβ1 secreted from superficial glia limitans affects SMCs in pial arteries. Indeed, in concurrence with gene expression levels in the capillaries, gene expression levels regulated by TGFβ signaling were higher in the pial arteries of TGFβ1 Tg mice than in those of WT mice. The lowering of mural cell coverage was accompanied by dilation

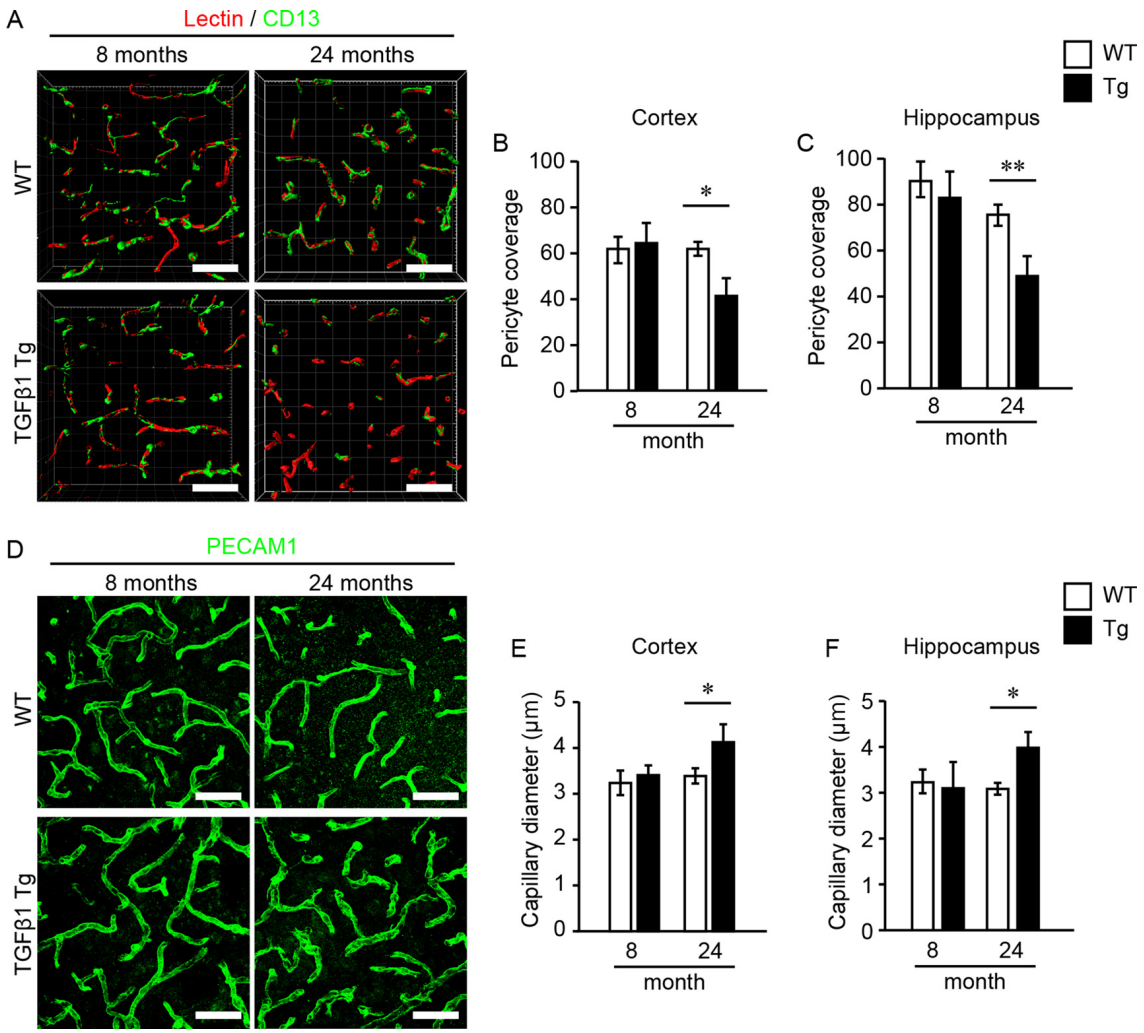

FIGURE 2 | Pericyte coverage analysis and quantification of brain capillary diameter. Pericyte coverage on brain capillaries and capillary diameter were quantified in 8- and 24-month-old mouse brain samples. **(A)** Representative 3D volume-rendered images of endothelial cells (red) and pericytes (green) in the cerebral cortex. The analysis was conducted using images obtained from the cerebral cortex **(B)** and the hippocampus **(C)**. Bar graphs show the results of quantifications of pericyte coverage in each brain region. Three images were analyzed in each brain region per mouse. **(D)** Representative images of endothelial cells depicted by PECAM1 immunostaining in the cerebral cortex. The bar graphs show the mean capillary diameter in the cerebral cortex **(E)** and the hippocampus **(F)** at 8 and 24 months of age. Two images were analyzed in each brain region per mouse. Data represent the mean ± SE, $^{*}P < 0.05$ and $^{**}P < 0.01$ according to a two-tailed unpaired *t*-test (n = 4–5 animals per group). Scale bar = 30 μm.

of brain vessels, which is compatible with reports of pericyte-deficient model mice (Armulik et al., 2010).

We speculate that the suppression of mural cell proliferation by TGFβ signaling is involved in the mechanism of the decrease in mural cell coverage rates of cerebral blood vessels in TGFβ1 Tg mice. It has been reported that the proliferation of vascular SMCs, which are derived from peripheral blood vessels, is suppressed by TGFβ treatment (Grainger et al., 1994; Martin-Garrido et al., 2013). In this study, we observed a similar inhibitory effect on the proliferation of brain-derived SMCs without cell death. Maintenance of medial SMC number involves the proliferation of resident vascular SMCs. Vascular SMC death induces cell proliferation of adjacent SMCs, and the portion that lost SMCs is repaired (Yu et al., 2011). The decreased mural cell coverage of cerebral blood vessels and the degenerative alteration may be due to impairment of cell proliferation-related tissue maintenance mechanisms. Our results that mural cell alterations manifest with age are compatible with this interpretation. Also, in an *in vitro* study of some progenitor or stem cells, TGFβ signaling has an inhibitory effect on the proliferation of these cells (Larsson et al., 2003). In this study, we found overexpression of TGFβ1 in Nestin-positive neural progenitor cells in TGFβ1 Tg mice. Indeed, reduced proliferation and fewer neural progenitor cells have been reported in TGFβ1 Tg mice (Buckwalter et al., 2006). As another source of vascular SMCs, local adventitial vascular SMC progenitors are known in peripheral blood vessels (Majesky et al., 2011). Whether these cells are present in cerebral blood vessels remains unknown, but the effect on the

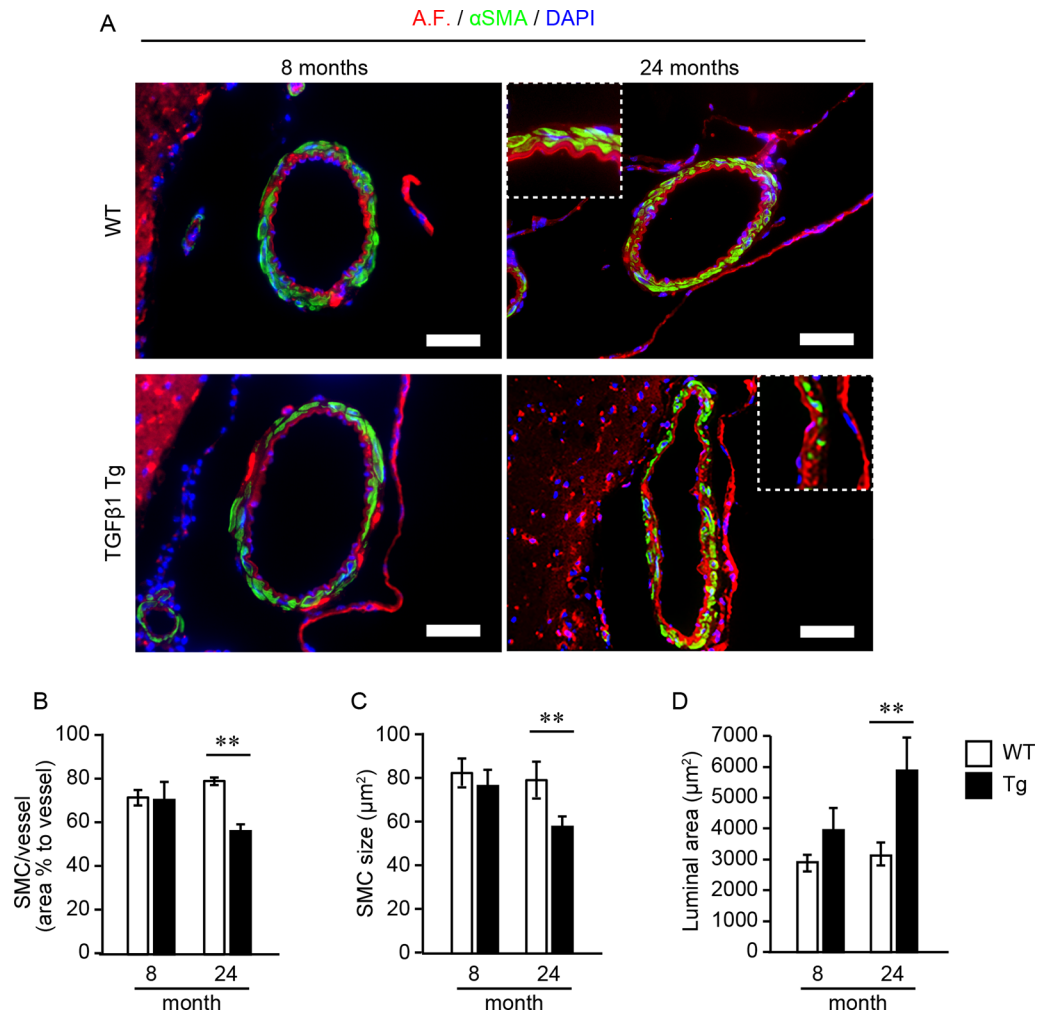

FIGURE 3 | Analysis of smooth muscle cell (SMC) occupancy in pial arteries and morphometric analysis. **(A)** Representative images of pial arteries depicted by anti-α-smooth muscle actin (αSMA) immunostaining (green) and tissue autofluorescence (A.F.). Each bar graph shows the SMC area occupancy to the area of the vascular wall **(B)**, the mean size of each SMC **(C)**, and the luminal area **(D)** in 8- and 24-month-old mice. Data represent the mean ± SE, $^{**}P < 0.01$ according to a two-tailed unpaired *t*-test (n = 4–5 animals per group).

self-proliferation of progenitor cells may also be related to the results obtained here.

Wyss-Coray et al. (1997) reported that astrocytic TGFβ1 overproduction in human β-amyloid precursor protein (hAPP) mice exacerbated cerebral amyloid angiopathy. Aβ exerts cell toxicity against vascular mural cells. In the monogenic TGFβ1 Tg mice used in this study, thioflavin S-positive amyloid is also deposited to the basement membrane of cerebral vessels (Wyss-Coray et al., 2000). Although the substances composing the amyloid deposition in monogenic TGFβ1 Tg mice are currently unknown, this amyloid deposition may be involved in mural cell degeneration. In addition to amyloid deposition, increases in basement membrane proteins, perlecan, and fibronectin have been observed in the cerebral vessels of TGFβ1 Tg mice (Wyss-Coray et al., 2000). The accumulation of extracellular matrix proteins precedes amyloid deposition. The brain drainage system flows from the brain parenchyma along the basement membrane to the lymph nodes. Therefore, altered basement membrane compositions may impede the elimination of toxic waste products and lead to harmful deposition of these products in cerebral vessels.

Notably, these accumulated extracellular matrix proteins identified in TGFβ1 Tg mice have been observed in both hereditary and sporadic non-amyloid cerebral small vessel disease (Nag and Kilty, 1997; Zellner et al., 2018). Conventionally, blood pressure overload, and high blood glucose levels have been noted to increase the expression of extracellular matrix proteins and cause vascular accumulation under these pathological conditions. In recent years, it has become clear that extracellular matrix abnormalities in hereditary non-amyloid cerebral small vessel disease also occur through sequestration of regulator protein or proteolytic dysregulation (Monet-Leprêtre et al., 2013; Zellner et al., 2018).

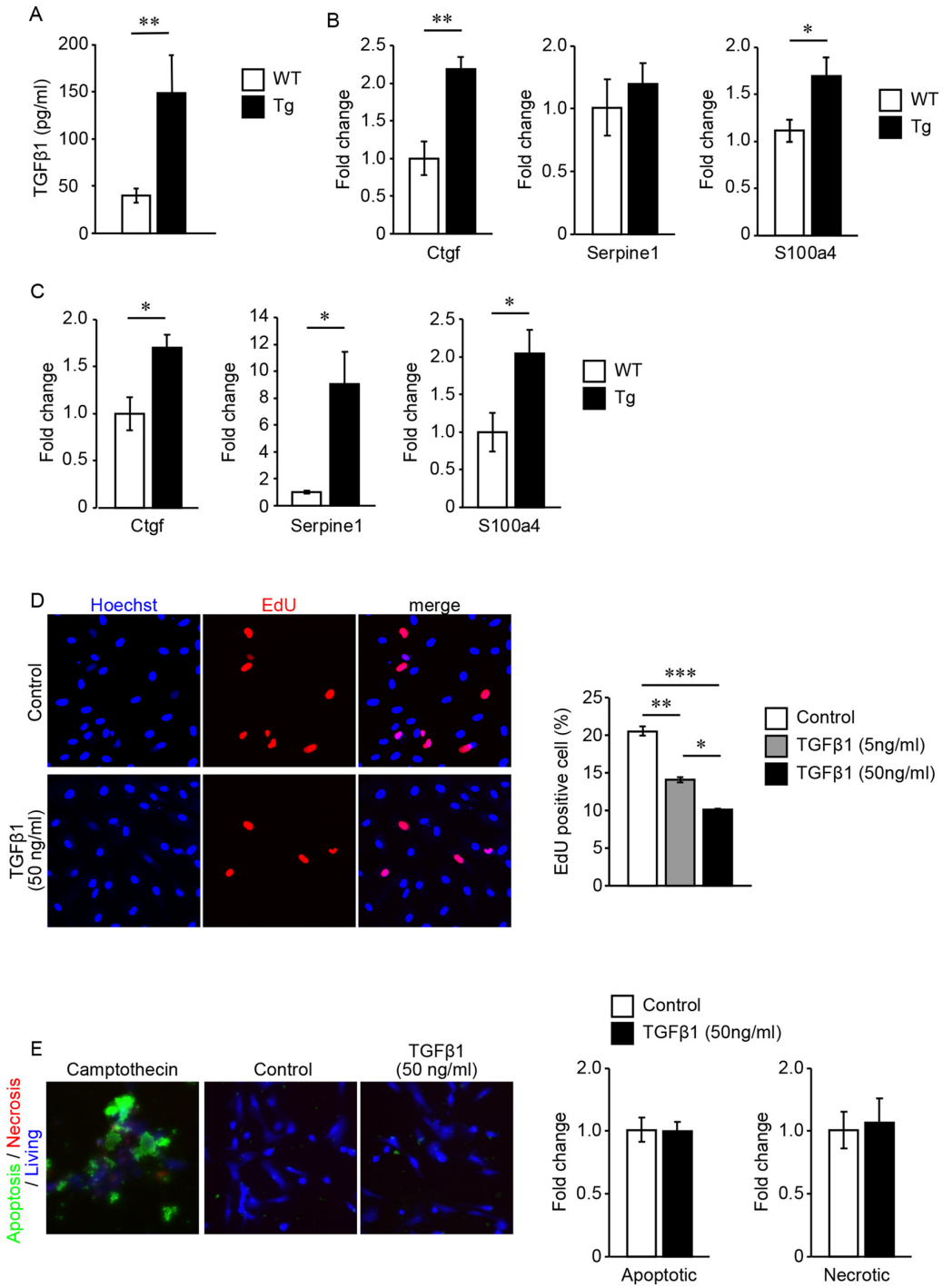

FIGURE 4 | (A–C) Quantification of TGFβ1 content in the cerebrospinal fluid (CSF) and gene expression levels regulated by TGFβ1 signaling. **(A)** TGFβ1 content in the CSF of 7-month-old TGFβ1 Tg mice and WT mice. $^{**}P < 0.01$ according to the Mann-Whitney *U*-test ($n = 3$ animals per group). **(B,C)** Gene expression levels regulated by TGFβ1 signaling in pial arteries **(B)** and brain capillaries **(C)** of 7-month-old TGFβ1 Tg mice and WT mice. $^{*}P < 0.05$ and $^{**}P < 0.01$ according to a two-tailed unpaired *t*-test ($n = 5$ animals per group). **(D)** Cell proliferation rate under treatment with vehicle or recombinant TGFβ1 was detected by an EdU incorporation assay. Representative images of vehicle- (4 mM HCl with 2% BSA) or 50 ng/ml recombinant TGFβ1-treated cells are shown. Recombinant TGFβ1 repressed the proliferation rate of cerebrovascular SMCs in a dose-dependent manner ($n = 5$ independent experiments). **(E)** Cerebrovascular SMCs treated with recombinant TGFβ1 or camptothecin (6 μM). Inducible apoptotic, necrotic, and living cells were detected by a phosphatidylserine sensor (green), 7-AAD (red), and cytocalcein violet 450 (blue), respectively. Apoptotic and necrotic cell signal areas were quantified and normalized by the area of the living cell signal. Data are represented as a relative value to non-treated control cells. $^{*}P < 0.05$, $^{**}P < 0.01$ and $^{***}P < 0.001$ according to Bonferroni's multiple comparison *post hoc* test ($n = 5$ independent experiments). Data represent the mean ± SE.

Extracellular matrix abnormalities have attracted attention as a major factor in the molecular pathogenesis of cerebral small vessel disease. In considering treatments, it is imperative to understand how TGFβ signaling participates in extracellular matrix abnormalities in various cerebral arteriopathies (Humphrey et al., 2014).

We demonstrated that TGFβ1 overproduction causes a dropout of mural cells from the vascular wall and decreases the coverage of small vessels. However, a long amount of time is needed for this phenotype to become apparent. The major limitation of this study is that it remains unclear whether the two phenomena are directly linked *in vivo*. Canonically, TGFβ signaling promotes the development of blood vessels and induces mural cells around blood vessels at the developmental stage. However, TGFβ signaling exerts context-dependent effects. In particular, the effect depends on the status of downstream signaling effectors, including their receptors (Armulik et al., 2005). TGFβ signaling also has pleiotropic effects on immune systems. For example, TGFβ signaling engages in crosstalk with interleukin-6 (IL-6) in orchestrating inflammatory responses. In vascular systems, IL-6 has the potential to increase pericyte coverage. Enhanced TGFβ signaling may inhibit the effect of IL-6 on promoting pericyte coverage by attenuating IL-6 signaling (Ricard et al., 2014; Wiegertjes et al., 2019). In addition to the immune system, TGFβ engages in crosstalk with various signal cascades that function in the vasculature, such as platelet-derived growth factor and vascular endothelial growth factor. We assume that not a single but multiple mechanisms are involved in the process of mural cell abnormalities in TGFβ1 Tg mice. Further research is required to clarify these issues.

In summary, our analysis using TGFβ1 Tg mice provides a link between the increased production of TGFβ and the degeneration of mural cells, both of which are observed in several cerebral arteriopathies. Mural cell degeneration has serious effects on brain functions that require high spatiotemporal regulation of blood flow. While further exploration is needed, our results indicate that TGFβ signaling may be a therapeutic target for protecting mural cell degeneration.

DATA AVAILABILITY STATEMENT

The datasets generated for this study are available on request to the corresponding author.

ETHICS STATEMENT

The animal study was reviewed and approved by the Animal Use and Care Committee of Niigata University.

AUTHOR CONTRIBUTIONS

The image analysis was performed by YS and TK. The biochemical analysis was performed by YS, SA, and TK. Animal care was provided by SH. MU, HN, and OO designed the project. TK and OO prepared the manuscript.

FUNDING

This work was supported by a grant-in-aid for Scientific Research (A) (JP16H02656), a grant-in-aid for Young Scientists (B) (JP26860208) from the Japan Society for the Promotion of Science, and a grant-in-aid for Scientific Research on Innovative Areas (Brain Protein Aging and Dementia Control; 26117006) from MEXT.

ACKNOWLEDGMENTS

We are grateful to Dr. Tony Wyss-Coray and Dr. Koji Yamanaka for providing the TGFβ1 Tg mice.

REFERENCES

Armulik, A., Abramsson, A., and Betsholtz, C. (2005). Endothelial/pericyte interactions. *Circ. Res.* 97, 512–523. doi: 10.1161/01.RES.0000182903.16652.d7

Armulik, A., Genove, G., Mae, M., Nisancioglu, M. H., Wallgard, E., Niaudet, C., et al. (2010). Pericytes regulate the blood-brain barrier. *Nature* 468, 557–561. doi: 10.1038/nature09522

Buckwalter, M. S., and Wyss-Coray, T. (2004). Modelling neuroinflammatory phenotypes *in vivo*. *J. Neuroinflammation* 1:10. doi: 10.1186/1742-2094-1-10

Buckwalter, M. S., Yamane, M., Coleman, B. S., Ormerod, B. K., Chin, J. T., Palmer, T., et al. (2006). Chronically increased transforming growth factor-β1 strongly inhibits hippocampal neurogenesis in aged mice. *Am. J. Pathol.* 169, 154–164. doi: 10.2353/ajpath.2006.051272

Chao, C. C., Ala, T. A., Hu, S., Crossley, K. B., Sherman, R. E., Peterson, P. K., et al. (1994). Serum cytokine levels in patients with Alzheimer's disease. *Clin. Diagn. Lab. Immunol.* 1, 433–436.

Ervin, J. F., Pannell, C., Szymanski, M., Welsh-Bohmer, K., Schmechel, D. E., and Hulette, C. M. (2004). Vascular smooth muscle actin is reduced in Alzheimer disease brain: a quantitative analysis. *J. Neuropathol. Exp. Neurol.* 63, 735–741. doi: 10.1093/jnen/63.7.735

Finch, C. E., Laping, N. J., Morgan, T. E., Nichols, N. R., and Pasinetti, G. M. (1993). TGF-β 1 is an organizer of responses to neurodegeneration. *J. Cell. Biochem.* 53, 314–322. doi: 10.1002/jcb.240530408

Gonzalez-Perez, O., and Quiñones-Hinojosa, A. (2012). Astrocytes as neural stem cells in the adult brain. *J. Stem Cells* 7, 181–188.

Grainger, D. J., Kemp, P. R., Witchell, C. M., Weissberg, P. L., and Metcalfe, J. C. (1994). Transforming growth factor β decreases the rate of proliferation of rat vascular smooth muscle cells by extending the G2 phase of the cell cycle and delays the rise in cyclic AMP before entry into M phase. *Biochem. J.* 299, 227–235. doi: 10.1042/bj2990227

Hall, C. N., Reynell, C., Gesslein, B., Hamilton, N. B., Mishra, A., Sutherland, B. A., et al. (2014). Capillary pericytes regulate cerebral blood flow in health and disease. *Nature* 508, 55–60. doi: 10.1038/nature13165

Hara, K., Shiga, A., Fukutake, T., Nozaki, H., Miyashita, A., Yokoseki, A., et al. (2009). Association of HTRA1 mutations and familial ischemic cerebral small-vessel disease. *N. Engl. J. Med.* 360, 1729–1739. doi: 10.1056/NEJMoa0801560

Hill, R. A., Tong, L., Yuan, P., Murikinati, S., Gupta, S., and Grutzendler, J. (2015). Regional blood flow in the normal and ischemic brain is controlled by arteriolar smooth muscle cell contractility and not by capillary pericytes. *Neuron* 87, 95–110. doi: 10.1016/j.neuron.2015.06.001

Holm, A., Heumann, T., and Augustin, H. G. (2018). Microvascular mural cell organotypic heterogeneity and functional plasticity. *Trends Cell Biol.* 28, 302–316. doi: 10.1016/j.tcb.2017.12.002

Humphrey, J. D., Dufresne, E. R., and Schwartz, M. A. (2014). Mechanotransduction and extracellular matrix homeostasis. *Nat. Rev. Mol. Cell Biol.* 15, 802–812. doi: 10.1038/nrm3896

Jambusaria, A., Hong, Z., Zhang, L., Srivastava, S., Jana, A., Toth, P. T., et al. (2020). Endothelial heterogeneity across distinct vascular beds during homeostasis and inflammation. *Elife* 9:e51413. doi: 10.7554/elife.51413

Larsson, J., Blank, U., Helgadottir, H., Björnsson, J. M., Ehinger, M., Goumans, M. J., et al. (2003). TGF-β signaling-deficient hematopoietic stem cells have normal self-renewal and regenerative ability *in vivo* despite increased proliferative capacity *in vitro*. *Blood* 102, 3129–3135. doi: 10.1182/blood-2003-04-1300

Ma, Q., Zhao, Z., Sagare, A. P., Wu, Y., Wang, M., Owens, N. C., et al. (2018). Blood-brain barrier-associated pericytes internalize and clear aggregated amyloid-β42 by LRP1-dependent apolipoprotein E isoform-specific mechanism. *Mol. Neurodegener.* 13:57. doi: 10.1186/s13024-018-0286-0

Majesky, M. W., Dong, X. R., Regan, J. N., and Hoglund, V. J. (2011). Vascular smooth muscle progenitor cells: building and repairing blood vessels. *Circ. Res.* 108, 365–377. doi: 10.1161/circresaha.110.223800

Martin-Garrido, A., Williams, H. C., Lee, M., Seidel-Rogol, B., Ci, X., Dong, J. T., et al. (2013). Transforming growth factor β inhibits platelet derived growth factor-induced vascular smooth muscle cell proliferation *via* Akt-independent, Smad-mediated cyclin D1 downregulation. *PLoS One* 8:e79657. doi: 10.1371/journal.pone.0079657

Monet-Leprêtre, M., Haddad, I., Baron-Menguy, C., Fouillot-Panchal, M., Riani, M., Domenga-Denier, V., et al. (2013). Abnormal recruitment of extracellular matrix proteins by excess Notch3 ECD: a new pathomechanism in CADASIL. *Brain* 136, 1830–1845. doi: 10.1093/brain/awt092

Müller, K., Courtois, G., Ursini, M. V., and Schwaninger, M. (2017). New insight into the pathogenesis of cerebral small-vessel diseases. *Stroke* 48, 520–527. doi: 10.1161/strokeaha.116.012888

Nag, S., and Kilty, D. W. (1997). Cerebrovascular changes in chronic hypertension. Protective effects of enalapril in rats. *Stroke* 28, 1028–1034. doi: 10.1161/01.str.28.5.1028

Oide, T., Nakayama, H., Yanagawa, S., Ito, N., Ikeda, S., and Arima, K. (2008). Extensive loss of arterial medial smooth muscle cells and mural extracellular matrix in cerebral autosomal recessive arteriopathy with subcortical infarcts and leukoencephalopathy (CARASIL). *Neuropathology* 28, 132–142. doi: 10.1111/j.1440-1789.2007.00864.x

Olson, L. E., and Soriano, P. (2011). PDGFRβ signaling regulates mural cell plasticity and inhibits fat development. *Dev. Cell* 20, 815–826. doi: 10.1016/j.devcel.2011.04.019

Ricard, N., Tu, L., Le Hiress, M., Huertas, A., Phan, C., Thuillet, R., et al. (2014). Increased pericyte coverage mediated by endothelial-derived fibroblast growth factor-2 and interleukin-6 is a source of smooth muscle-like cells in pulmonary hypertension. *Circulation* 129, 1586–1597. doi: 10.1161/circulationaha.113.007469

Ronaldson, P. T., Demarco, K. M., Sanchez-Covarrubias, L., Solinsky, C. M., and Davis, T. P. (2009). Transforming growth factor-β signaling alters substrate permeability and tight junction protein expression at the blood-brain barrier during inflammatory pain. *J. Cereb. Blood Flow Metab.* 29, 1084–1098. doi: 10.1038/jcbfm.2009.32

Suwanabol, P. A., Seedial, S. M., Shi, X., Zhang, F., Yamanouchi, D., Roenneburg, D., et al. (2012). Transforming growth factor-β increases vascular smooth muscle cell proliferation through the Smad3 and extracellular signal-regulated kinase mitogen-activated protein kinases pathways. *J. Vasc. Surg.* 56, 446–454. doi: 10.1016/j.jvs.2011.12.038

Wiegertjes, R., van Caam, A., van Beuningen, H., Koenders, M., van Lent, P., van der Kraan, P., et al. (2019). TGF-β dampens IL-6 signaling in articular chondrocytes by decreasing IL-6 receptor expression. *Osteoarthritis Cartilage* 27, 1197–1207. doi: 10.1016/j.joca.2019.04.014

Winkler, E. A., Sengillo, J. D., Sullivan, J. S., Henkel, J. S., Appel, S. H., and Zlokovic, B. V. (2013). Blood-spinal cord barrier breakdown and pericyte reductions in amyotrophic lateral sclerosis. *Acta Neuropathol.* 125, 111–120. doi: 10.1007/s00401-012-1039-8

Wyss-Coray, T., Feng, L., Masliah, E., Ruppe, M. D., Lee, H. S., Toggas, S. M., et al. (1995). Increased central nervous system production of extracellular matrix components and development of hydrocephalus in transgenic mice overexpressing transforming growth factor-β 1. *Am. J. Pathol.* 147, 53–67.

Wyss-Coray, T., Lin, C., Sanan, D. A., Mucke, L., and Masliah, E. (2000). Chronic overproduction of transforming growth factor-β1 by astrocytes promotes Alzheimer's disease-like microvascular degeneration in transgenic mice. *Am. J. Pathol.* 156, 139–150. doi: 10.1016/s0002-9440(10)64713-x

Wyss-Coray, T., Masliah, E., Mallory, M., McConlogue, L., Johnson-Wood, K., Lin, C., et al. (1997). Amyloidogenic role of cytokine TGF-β1 in transgenic mice and in Alzheimer's disease. *Nature* 389, 603–606. doi: 10.1038/39321

Yan, J., Zhang, H., Yin, Y., Li, J., Tang, Y., Purkayastha, S., et al. (2014). Obesity- and aging-induced excess of central transforming growth factor-β potentiates diabetic development *via* an RNA stress response. *Nat. Med.* 20, 1001–1008. doi: 10.1038/nm.3616

Yu, H., Clarke, M. C., Figg, N., Littlewood, T. D., and Bennett, M. R. (2011). Smooth muscle cell apoptosis promotes vessel remodeling and repair *via* activation of cell migration, proliferation, and collagen synthesis. *Arterioscler. Thromb. Vasc. Biol.* 31, 2402–2409. doi: 10.1161/ATVBAHA.111.235622

Zellner, A., Scharrer, E., Arzberger, T., Oka, C., Domenga-Denier, V., Joutel, A., et al. (2018). CADASIL brain vessels show a HTRA1 loss-of-function profile. *Acta Neuropathol.* 136, 111–125. doi: 10.1007/s00401-018-1853-8

Conflict of Interest: The authors declare that the research was conducted in the absence of any commercial or financial relationships that could be construed as a potential conflict of interest.

frontiers in Aging Neuroscience

ORIGINAL RESEARCH
published: 14 July 2020
doi: 10.3389/fnagi.2020.00216

A Nationwide Survey and Multicenter Registry-Based Database of Cerebral Autosomal Dominant Arteriopathy With Subcortical Infarcts and Leukoencephalopathy in Japan

Akihiro Shindo[1], Ken-ichi Tabei[2], Akira Taniguchi[1], Hiroaki Nozaki[3], Osamu Onodera[3], Akihiko Ueda[4], Yukio Ando[4,5], Takao Urabe[6], Kazumi Kimura[7], Kazuo Kitagawa[8], Haruo Hanyu[9], Teruyuki Hirano[10], Hideaki Wakita[11], Hidenao Fukuyama[12], Tatsuo Kagimura[13], Yoshihiro Miyamoto[14], Misa Takegami[15], Satoshi Saito[16], Akiko Watanabe-Hosomi[17], Ikuko Mizuta[17], Masafumi Ihara[16], Toshiki Mizuno[17] and Hidekazu Tomimoto[1]*

[1] Department of Neurology, Mie University Graduate School of Medicine, Tsu, Japan, [2] Department of Dementia Prevention and Therapeutics, Mie University Graduate School of Medicine, Tsu, Japan, [3] Department of Neurology, Clinical Neuroscience Branch, Brain Research Institute, Niigata University, Niigata, Japan, [4] Department of Neurology, Graduate School of Medical Sciences, Kumamoto University, Kumamoto, Japan, [5] Department of Amyloidosis Research, Nagasaki International University, Nagasaki, Japan, [6] Department of Neurology, Juntendo University Urayasu Hospital, Chiba, Japan, [7] Department of Neurology, Graduate School of Medicine, Nippon Medical School, Tokyo, Japan, [8] Department of Neurology, Tokyo Women's Medical University, Tokyo, Japan, [9] Department of Geriatric Medicine, Tokyo Medical University, Tokyo, Japan, [10] Department of Stroke and Cerebrovascular Medicine, Kyorin University, Tokyo, Japan, [11] Department of Internal Medicine, Nanakuri Memorial Hospital, Fujita Health University, Tsu, Japan, [12] Center for the Promotion of Interdisciplinary Education and Research, Kyoto University, Kyoto, Japan, [13] Translational Research Center for Medical Innovation, Foundation for Biomedical Research and Innovation at Kobe, Kobe, Japan, [14] Center for Cerebral and Cardiovascular Disease Information, National Cerebral and Cardiovascular Center, Osaka, Japan, [15] Department of Preventive Medicine and Epidemiologic Informatics, National Cerebral and Cardiovascular Center, Osaka, Japan, [16] Department of Neurology, National Cerebral and Cardiovascular Center, Suita, Japan, [17] Department of Neurology, Graduate School of Medical Science, Kyoto Prefectural University of Medicine, Kyoto, Japan

OPEN ACCESS

Edited by:
Ramesh Kandimalla, Texas Tech University Health Sciences Center, United States

Reviewed by:
Yi Li, Cornell University, United States
Hugues Chabriat, Université Paris Diderot, France

***Correspondence:**
Akihiro Shindo
a-shindo@clin.medic.mie-u.ac.jp

Received: *03 December 2019*
Accepted: *19 June 2020*
Published: *14 July 2020*

Citation:
Shindo A, Tabei K, Taniguchi A, Nozaki H, Onodera O, Ueda A, Ando Y, Urabe T, Kimura K, Kitagawa K, Hanyu H, Hirano T, Wakita H, Fukuyama H, Kagimura T, Miyamoto Y, Takegami M, Saito S, Watanabe-Hosomi A, Mizuta I, Ihara M, Mizuno T and Tomimoto H (2020) A Nationwide Survey and Multicenter Registry-Based Database of Cerebral Autosomal Dominant Arteriopathy With Subcortical Infarcts and Leukoencephalopathy in Japan. Front. Aging Neurosci. 12:216. doi: 10.3389/fnagi.2020.00216

Objectives: Clinical characteristics of cerebral autosomal dominant arteriopathy with subcortical infarcts and leukoencephalopathy (CADASIL) include migraine, recurrent stroke, white matter lesions, and vascular dementia. CADASIL is one of the most common hereditary cerebral small vessel diseases. Clinical presentation of CADASIL varies and a racial gap may exist between the Asian and Caucasian populations. This is the first nationwide epidemiological survey which aimed to elucidate the clinical features of CADASIL in Japan. Moreover, the registration database of CADASIL was constructed.

Methods: Subjects included CADASIL patients who visited the hospitals (totally 1,448 hospitals) certified by the Japanese Society of Neurology and/or Japan Stroke Society in 2016. This study consisted of a two-step survey; patients with CADASIL were identified genetically by the first questionnaire, and their clinical features were assessed by the second questionnaire. Selected 6 hospitals registered the data of all CADASIL patients using a Research Electronic Data Capture (REDCap) system for the second questionnaire.

Results: Based on the criteria, 88 patients (50 male and 38 female) with CADASIL were enrolled. The mean age of symptom onset was 49.5 years. Sixteen (18.2%) patients had an elderly onset (>60 years). Thirteen patients (13.6%) had history of migraine with aura and 33 patients (37.5%) had vascular risk factor(s). From among the 86 patients who were examined using magnetic resonance imaging, abnormal deep white matter lesions were detected in 85 patients (98.8%), WMLs extending to anterior temporal pole in 73 patients (84.9%), and cerebral microbleeds in 41 patients (47.7%). Anti-platelet therapy was received by 65 patients (73.9%). Thirty-eight patients (43.2%) underwent treatment with lomerizine hydrochloride. Thirty-four different mutations of *NOTCH3* were found in exons 2, 3, 4, 5, 6, 8, 11, 14, and 19. Most of the mutations existed in exon 4 (n = 44, 60.3%). The prevalence rate of CADASIL was 1.20 to 3.58 per 100,000 adults in Japan.

Conclusion: This questionnaire-based study revealed clinical features and treatment status in Japanese CADASIL patient, although it may not be an exhaustive search. We have constructed the REDCap database for these CADASIL patients.

Keywords: small vessel disease, CADASIL, NOTCH3, risk factors, migraine, microbleeds

INTRODUCTION

Cerebral autosomal dominant arteriopathy with subcortical infarcts and leukoencephalopathy (CADASIL) is an autosomal dominant disease and a common type of ischemic cerebral small artery disease and subcortical vascular dementia (Roman et al., 2002). First identified in 1996, mutations in the *NOTCH3* gene cause CADASIL and lead to small vessel arteriopathy in the central nervous system (Joutel et al., 1996). Patients with CADASIL commonly exhibit migraines with aura around at the age of 30 years, subcortical ischemic events at 50 years, and cognitive impairment between 50 and 60 years (Chabriat et al., 2009). Brain magnetic resonance imaging (MRI) displays extensive white matter hyperintensities including those in the anterior temporal lobe and external capsule. Although CADASIL is genetic small vessel disease, several reports have revealed the presence of vascular risk factors, such as hypertension, hyperlipidemia, and diabetes mellitus (Chabriat et al., 2009).

Although, Mizuta et al. (2017) found no significant difference in the clinical features of CADASIL between Japan and other countries, a nationwide survey in Japan was not conducted until 2019. The prevalence of migraines in Japanese CADASIL patients has been reported to be approximately 26.9–44.3% (Santa et al., 2003; Ueda et al., 2015; Mizuta et al., 2017; Koizumi et al., 2019), whereas a much lower prevalence of migraine has been reported in other Asian countries (Kim et al., 2006; Wang et al., 2011; Kang and Kim, 2015). While the clinical features of Asian CADASIL patients could be different from Caucasian patients (Kim et al., 2006; Wang et al., 2011; Choi et al., 2013; Kang and Kim, 2015), Japanese CADASIL patients might have other clinical characteristics.

Herein, this study aimed to elucidate the epidemiological and clinical features of Japanese CADASIL patients based on a Japanese nationwide survey. Moreover, we constructed a database for patients with CADASIL for future clinical studies.

MATERIALS AND METHODS

Study Design and Subjects (Figure 1)

We conducted a two-step postal survey in 1,448 hospitals in all 47 Japanese prefectures. This study was carried out in accordance with the Declaration of Helsinki and approved by the Ethics Committee of the Mie University Graduate School of Medicine (permit number 2918).

The Two-Step Postal Survey

First-Step Postal Survey

Target subjects were CADASIL patients who visited the hospitals between April 1st, 2011 and June 30th, 2016. The hospitals surveyed were certified by the Japanese Society of Neurology and/or Japan Stroke Society in 2016 (in total 1,448 hospitals) and covered all 47 prefectures in Japan. In the first survey, a simple questionnaire asked whether there were any patients with CADASIL, and if so, how many.

Second-Step Survey

We obtained a response to the first questionnaires from 687 hospitals (47.4%). Of those, 78 hospitals had one or more patients with CADASIL and agreed to the next step. We sent a second questionnaire to the 78 hospitals to obtain further details. Detailed clinical information including age, sex, age at the onset (excluding migraine), height, weight, blood pressure (BP), birthplace, clinical presentations (stroke-like episodes, dementia, pyramidal sign, pseudobulbar palsy), migraine (with or without aura), ischemic stroke, hemorrhagic stroke, past medical history (hypertension, hyperlipidemia, diabetes mellitus, renal dysfunction, ischemic heart disease, and atrial fibrillation), type of the mutation of *NOTCH3* gene, family history, treatment, modified Rankin Scale (Japanese version) (Shinohara et al., 2006), findings of magnetic resonance imaging (MRI) including Fazekas scale (Fazekas et al., 1987), findings of single photon

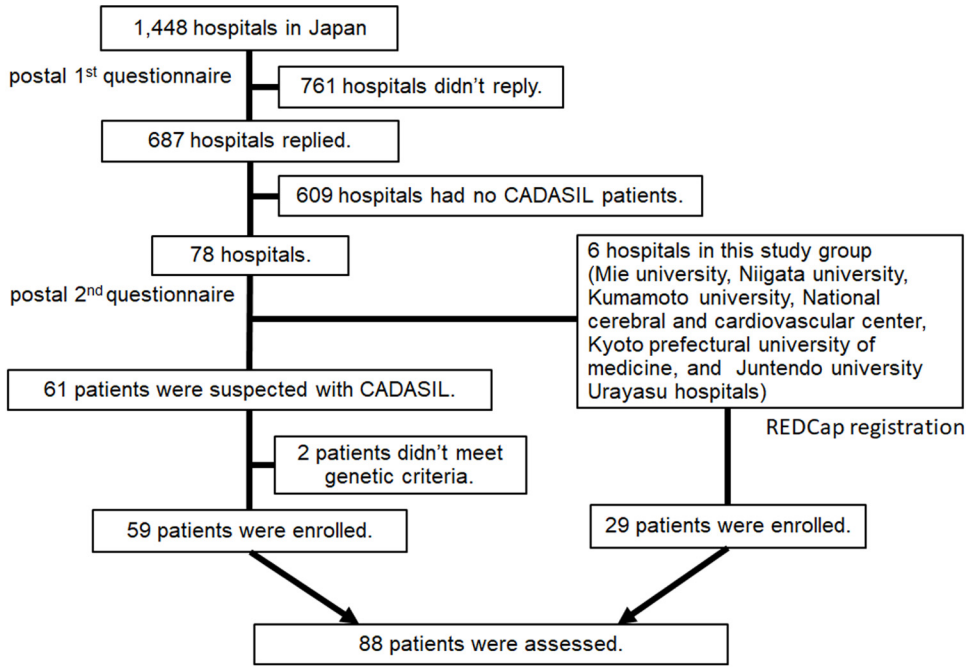

FIGURE 1 | Flow diagram of study enrollment.

emission computed tomography (SPECT), and skin biopsy were requested. We received a response to the second questionnaire from 38 hospitals (48.7%) and 61 patients with cases defined as CADASIL were enrolled.

REDCap Survey

We sent out a simple second-step questionnaire to six core hospitals, including Mie University Hospital, Niigata University Hospital, Kumamoto University Hospital, National Cerebral and Cardiovascular Center, Kyoto Prefectural University of Medicine Hospital, and Juntendo University Urayasu Hospital with questions regarding age, sex, age at onset, birthplace, and type of *NOTCH3* mutation. After the two-step postal survey, data for core hospitals were also collected using a Research Electronic Data Capture (REDCap) system (Harris et al., 2009). The REDCap database was built to elucidate the natural history, clinical features, and clinical studies for patients with CADASIL in Japan. After obtaining the consent and approval of the Local Institutional Review Board (IRB) Committee to participate, the physician sent a registration form to the secretariat at National Cerebral and Cardiovascular Center of Japan. Detailed data same as the second postal survey was obtained from REDCap. A written consent form was obtained from each patient. REDCap survey enrolled a total 29 patients with CADASIL and all data remained anonymous without any patients' identifying clinical information.

Diagnosis of CADASIL

The diagnosis of CADASIL was based on the genetic criteria that either the patient or a third-degree relative had *NOTCH3* mutations. Seventy-nine patients were identified to have *NOTCH3* mutations, and the other nine patients had the gene mutations present in their relatives.

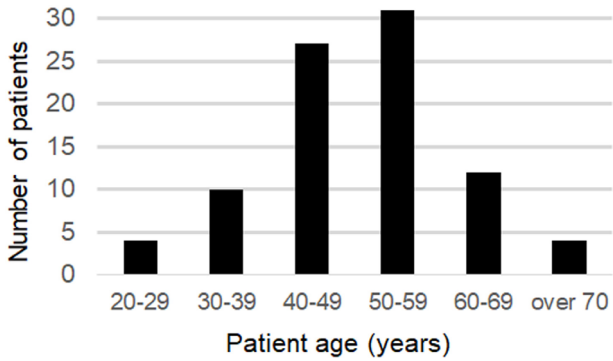

FIGURE 2 | Distribution of ages at the onset.

Statistical Analysis

Three types of prevalence rates of CADASIL: the most conservative estimate, the moderate estimate, and the most aggressive estimate, were estimated from the questionnaire sampling process and the Japanese population in 2017, i.e., 106,367,000 adults (over 18 years old) data from the Ministry of Internal Affairs and Communications.

The most conservative estimate was based on the assumption that there were no patients in the not answered site in the first survey, and that the number of patients of the not answered site

	Present	Birth place
Hokkaido:	1	1
Tohoku:	2	2
Kanto :	19	15
Chubu :	14	12
Kansai :	35	23
Chugoku/Shikoku :	2	2
Kyusyu/Okinawa :	15	12
Outside of Japan :	0	2

FIGURE 3 | Current residence region and birthplace of CADASIL patients in Japan.

in the second survey was at least one. The moderate estimate was based on the assumption that there were no patients in the not answered site in the first survey, and that the percentage of patients in the not answered site in the secondary survey was same that in the answered site. The most aggressive estimate was based on the assumption that the percentage of patients in the not answered site in the first survey was same that in the answered site, and that the percentage of patients in the not answered site in the secondary survey was same that in the answered site.

RESULTS

Study Patients

A total of 90 patients with CADASIL were registered from 44 hospitals (38 hospitals by questionnaires and 6 hospitals using the REDCap system). Of those, we excluded 2 patients as they had no family history nor they filled the genetic diagnostic criteria. Data from 88 CADASIL patients were collected and analyzed (**Figure 1**).

Age at the Onset and Geographic Data

The mean age at onset was 49.5 years old (20–76) for all patients and for the 58 patients (65.9%), the age of onset was between 40 and 59 years old. Sixteen of the patients had an onset over 60 years of age (18.2%), and 4 patients had an onset over 70 years of age (**Figure 2**).

The current residence region and place of birth are shown in **Figure 3**. Kansai region has the highest number of CADASIL patients, followed by the Kanto and Kyusyu/Okinawa region. Birthplace tends to be the same as the current residence. Only a few patients with CADASIL were found in Hokkaido, Tohoku, and Chugoku/Shikoku regions. Two patients were born in out of Japan, and their birthplace was Taiwan.

Demographic and Clinical Data in Japanese CADASIL Patients (Table 1)

Body mass index (BMI) was calculated using the patients' height and weight, and the mean BMI was 22.8 kg/m^2. Mean systolic BP was 120.0 mmHg, and mean diastolic BP was 74.2 mmHg. *NOTCH3* mutations were detected in 79 patients (89.7%) and 28 patients (31.8%) had a close family member with *NOTCH3* mutations. Nineteen patients were identified to have *NOTCH3* mutations in both the patients and their relatives. Skin biopsy was performed in 15 patients (17.0%), and granular osmiophilic material (GOM) was detected in 8 patients (9.1%). The detection rate of GOM was 53.3%.

From past history, migraine was noted in 25 patients (28.4%) and migraine with aura in 12 patients (13.6%). Vascular risk factors including hypertension, dyslipidemia, and diabetes mellitus were detected in 13 (14.8%), 31 (35.2%), and 1 (1.1%) patients, respectively. There were 33 patients (37.5%) who possessed one or more of these vascular risk factors. None of the patients had any ischemic heart disease.

Stroke and the stroke-like episode was the most common symptom in 59 patients (67.0%) and dementia was reported in 31 patients (35.2%). Pyramidal sign and pseudobulbar palsy were detected in 41 (46.6%) and 20 (22.7%) patients, respectively. Two patients (2.3%) did not show these before mentioned symptoms. Modified Rankin scale outcome at the time of this investigation was excellent [0–2] in 59 (67.0%), moderate [3, 4] in 21 (23.9%), poor [5] in 5 (5.7%), and death [6] in 2 patients (2.3%).

Regarding the neuroimaging findings, brain MRI was performed in 86 patients (97.7%), from among whom, white matter lesions were detected in 85 patients (98.8%) and anterior temporal lobe lesions were detected in 73 patients (84.9%). Fazekas score 2 was reported in 23 patients (26.7%) and score 3 for 56 patients (65.1%). Cerebral microbleeds were detected in 41 patients (47.7%). Although, SPECT was performed in 53 patients (60.2%), findings suggestive of CADASIL were reported in only 40 patients (45.4%). Decreased in cerebral blood flow was detected 25 patients in frontal lobe (62.5%, out of 40 patients), in 22 patients in temporal lobe (55.0%), in 26 patients in parietal lobe (65.0%), and in seven patients in occipital lobe (17.5%).

Sixty-five patients (73.9%) underwent an antiplatelet therapy, 16 (18.2%) had aspirin, 42 (47.7%) had cilostazol, and 16 patients had (18.2%) clopidogrel. Dual antiplatelet therapy was given to 6 patients (6.8%). Thirty-eight patients were treated with lomerizine hydrochloride (43.2%).

NOTCH3 Mutations

Of the total 88 CADASIL patients, we confirmed *NOTCH3* gene mutations in 73 patients (83.0%) (**Table 2**). There was no

TABLE 1 | Demographic data in 88 Japanese CADASIL patients.

Demographics in 88 patients with CADASIL		
Mean age at onset (years)	49.5 ± 11.2	(20–76)
Male sex, (*n*, %)	50	62.5%
Body mass index (kg/m^2)	22.8 ± 2.8	
Blood pressure		
Systolic (mmHg)	120.0 ± 13.6	
Diastolic (mmHg)	74.2 ± 9.8	
***NOTCH3* mutations**		
Patient (*n*, %)	79	89.7%
Close family (*n*, %)	28	31.8%
Skin biopsy		
Performed (*n*, %)	15	17.0%
Detected granular osmiophilic material (*n*, %)	8	9.1%
Past history		
Migraine (*n*, %)	25	28.4%
Migraine with aura (*n*, %)	12	13.6%
Hypertension (*n*, %)	13	14.8%
Dyslipidemia (*n*, %)	31	35.2%
Diabetes mellitus (*n*, %)	1	1.1%
One or more of above 3 vascular risk factors (*n*, %)	33	37.5%
Ischemic heart disease (*n*, %)	0	0%
Clinical presentation		
Stroke-like episode/Stroke (*n*, %)	59	67.0%
Dementia (*n*, %)	31	35.2%
Pyramidal sign (*n*, %)	41	46.6%
Pseudobulbar palsy (*n*, %)	20	22.7%
None of above (*n*, %)	2	2.3%
Modified Rankin Scale		
Excellent (0–2) (*n*, %)	59	67.0%
Moderate (3, 4) (*n*, %)	21	23.9%
Poor (5) (*n*, %)	5	5.7%
Death (6) (*n*, %)	2	2.3%
Image findings		
Magnetic resonance imaging (*n*, %)	86	97.7%
MRI findings (out of 86 patients)		
White matter lesion (*n*, %)	85	98.8%
Anterior temporal pole lesion (*n*, %)	73	84.9%
Fazekas grade 2 (*n*, %)	23	26.7%
Fazekas grade 3 (*n*, %)	56	65.1%
Microbleeds (*n*, %s)	41	47.7%
Single photon emission computed tomography (*n*, %)	40	45.5%
Cerebral blood flow reduction (% out of 40 patients)		
Frontal lobe (*n*, %)	25	28.4%
Temporal lobe (*n*, %)	22	25.0%
Parietal lobe (*n*, %)	26	29.5%
Occipital lobe (*n*, %)	7	8.0%
Treatment		
Anti-platelet therapy (*n*, %)	65	73.9%
Aspirin (*n*, %)	16	18.2%
Cilostazol (*n*, %)	42	47.7%
Clopidogrel (*n*, %)	16	18.2%
Dual anti-platelet therapy (*n*, %)	6	6.8%
Lomerizine hydrochloride (*n*, %)	38	43.2%

description on the type of gene mutation in 15 patients. Thirty-four different mutations of *NOTCH3* were found in exons 2, 3, 4, 5, 6, 8, 11, 14, and 19. Most of the mutations existed in exon 4 (*n* = 44, 60.3%), and the most common mutations were p.R141C, p.R182C, p.R133C, and p.R153C. A novel mutation (p.C318Y) was found in one case.

Prevalence Rate of CADASIL in Japan

In terms of the most conservative estimate, 128 CADASIL patients were estimated and the prevalence rate was 1.20 per 100,000 adults. In terms of the moderate estimate, 180.6 CADASIL patients were estimated and the prevalence rate was 1.70 per 100,000 adults. In terms of the most aggressive estimate, 380.7 CADASIL patients were estimated and the prevalence rate was 3.58 per 100,000 adults. The prevalence rate of CADASIL in Japan was estimated to between 1.20 to 3.58 per 100,000 adults.

DISCUSSION

This is the first nationwide study for Japanese CADASIL patients. We show that the prevalence rate of migraines in Japanese CADASIL patients to be lower than European populations. The presence of vascular risk factors with hypertension and/or diabetes mellitus had a lower tendency than other European and Asian populations. The prevalence rate of CADASIL was 1.20 to 3.58 per 100,000 adults, and Kansai, Kanto, and Kyusyu/Okinawa regions had the largest distribution of CADASIL patients in Japan.

We also described a tendency of a low prevalence rate of migraine with aura in Japanese patients (13.6%) compared to the European counterparts. **Table 3** shows the difference in CADASIL patients between Japan and other countries (Peters et al., 2004; Singhal et al., 2004; Kim et al., 2006; Herve et al., 2009; Adib-Samii et al., 2010; Wang et al., 2011; Pescini et al., 2012; Ciolli et al., 2014; Bianchi et al., 2015; Kang and Kim, 2015; Ueda et al., 2015; Nannucci et al., 2018; Koizumi et al., 2019). This table reveals a trend: a higher prevalence rate of migraine in European countries (34–75.3%) (Peters et al., 2004; Adib-Samii et al., 2010; Pescini et al., 2012; Ciolli et al., 2014; Bianchi et al., 2015; Nannucci et al., 2018), but a much lower prevalence in other Asian countries such as China and South Korea (4–8.7%) (Kim et al., 2006; Wang et al., 2011; Kang and Kim, 2015). Similarly, the nationwide survey showed that prevalence rate of migraine in the general population was reported to be lower in Japan than other European countries (Rasmussen et al., 1991; Gobel et al., 1994; Sakai and Igarashi, 1997); Japan appears midway in the prevalence rate scale of migraines between European and other Asian countries. In terms of past histories, the presence of vascular risk factors with hypertension and/or diabetes mellitus had a lower tendency than other European and Asian populations (Peters et al., 2004; Singhal et al., 2004; Herve et al., 2009; Ciolli et al., 2014; Bianchi et al., 2015; Kang and Kim, 2015; Nannucci et al., 2018). The prevalence rate of dyslipidemia was in the range of previous reports (Peters et al., 2004; Herve et al., 2009; Adib-Samii et al., 2010; Ciolli et al., 2014; Kang and Kim, 2015; Nannucci et al., 2018; Koizumi et al., 2019). The prevalence rate of hypertension and diabetes mellitus in Japan (14.8 and 1.1%) seems to be much lower than the other countries (20–35.6% and 3–12.7%) (Peters et al., 2004;

TABLE 2 | Summary of *NOTCH3* mutations in Japanese CADASIL patients.

Nucleotide change	Amino acid change	Exon	EGF-like repeat	Number of cases
c.163T>G	p.C55G	2	1	1
c.194G>C	p.C65S	2	1	2
c.224G>C	p.R75P	3	1	1
c.277T>G	p.C93G	3	2	1
c.316T>C	p.C106R	3	2	2
c.328C>T	p.R110C	3	2	1
c.397C>T	p.R133C	4	3	7
c.421C>T	p.R141C	4	3	10
c.431G>T	p.R144F	4	3	1
c.457C>T	p.R153C	4	3	5
c.505C>T	p.R169C	4	4	3
c.521_522delinsTG	p.C174L	4	4	2
c.544C>T	p.R182C	4	4	8
c.554G>A	p.C185Y	4	4	3
c.634T>C	p.C212R	4	5	1
c.635G>A	p.C212Y	4	5	1
c.665G>C	p.C222S	4	5	1
c.665G>A	p.C222Y	4	5	1
c.598_610delinsAGAACCC	p.Pro200_Ser204delinsArgThrPro	4	5	1
c.734G>A	p.C245Y	5	6	1
*c.953G>A	p.C318Y	6	8	1
c.969C>G	p.C323W	6	8	2
c.994C>T	p.R332C	6	8	2
c.1255T>C	p.C419R	8	10	2
c.1304G>A	p.C435Y	8	11	1
c.1370G>C	p.C457S	8	11	1
c.1630C>T	p.R544C	11	13–14	1
c.1703G>A	p.C568Y	11	14	1
c.1819C>T	p.R607C	11	15	1
c.2185T>G	p.C729G	14	18	1
c.3010T>G	p.C1004G	19	26	3
c.3045C>G	p.C1015W	19	26	1
c.3062A>G	p.Y1021C	19	26	2
c.3064T>G	p.C1022G	19	26	1
			Total	73

** c.953G>A (p.C318Y) identified as a novel mutation.*

Singhal et al., 2004; Herve et al., 2009; Adib-Samii et al., 2010; Ciolli et al., 2014; Bianchi et al., 2015; Kang and Kim, 2015; Nannucci et al., 2018) similar to the previous report (Mizuta et al., 2017). The mean age of onset in Japanese CADASIL patients is within the range of other countries (42.7–52 years old) (Peters et al., 2004; Kim et al., 2006; Herve et al., 2009; Wang et al., 2011; Pescini et al., 2012; Ciolli et al., 2014; Kang and Kim, 2015).

The prevalence rate of CADASIL was slightly lower than in other countries. Razvi et al. (2005) showed that the prevalence of CADASIL was 1.98 per 100,000 adults in Scotland, and Bianchi et al. (2015) described the prevalence at 4.1 per 100,000 adults in Italy. Uchino et al. (2002) reported that CADASIL was found in one of 2,030 stroke patients. It had been estimated that the incidence of new stroke was 220,000 per year in Japan (Takashima et al., 2017). Although, the number of patients with CADASIL expected to increase by approximately 108 per year from previous reports, we could identify only 88 patients in this study. There is a high possibility that the recognition of CADASIL varies depending on the facility, and there might be many undetected cases. Moreover, our study indicates that there is a regional difference in prevalence in Japanese CADASIL patients. Kansai, Kanto, and Kyusyu/Okinawa region have the three largest areas of the distribution of CADASIL patients. Note that we sent the questionnaire to all regions of Japan, and moreover, got replies from them all. Kanto region has the largest population, followed by Kansai, Chubu, and the Kyusyu/Okinawa region according to the 2015 data of Statistic Bureau, Ministry of Internal Affairs and Communications. Our study showed that Kansai region was the largest area in terms of distribution of CADASIL, indicating a predominance in the western part of Japan. In accordance with this observation, Ueda et al. (2015) reported a similar distribution

TABLE 3 | Comparison between Japanese CADASIL patients and other worldwide populations.

		Patient number and sex			Past History				Clinical presentation		MRI findings		Treatment
References	**Countries**	***n***	**Onset (mean age)**	**Male sex (%)**	**Migraine (%)**	**HTN (%)**	**DL (%)**	**DM (%)**	**Stroke like episodes/Stroke (%)**	**Dementia (%)**	**Anterior temporal lobe lesion (%)**	**Microbleeds (%)**	**Anti-thrombotic medication (%)**
Peters et al., 2004	Germany	80	45.7	46.3	34	25	23	3	78	44	NA	NA	75
Singhal et al., 2004	United Kingdom	127	NA	39.6	NA	20	9	4	NA	NA	NA	NA	NA
Herve et al., 2009	Germany and France	113	52	40.7	NA	19.5	41.9	3.6	NA	NA	NA	NA	NA
Adib-Samii et al., 2010	United Kingdom	200	33.6*	43	75.3	23.9	68.6	NA	NA	NA	NA	NA	NA
Pescini et al., 2012	Italy	61	50.7	49	49	NA	NA	NA	80	57	77	NA	NA
Ciolli et al., 2014	Italy	51	50.3	47.1	47.1	35.3	36	7.8	41.2	41.3	NA	NA	NA
Bianchi et al., 2015	Italy	229	NA	51	42	35.6	15.8	12.7	59	38	NA	NA	NA
Nannucci et al., 2018	Italy and United Kingdom	125	NA	45	67	30	58	6	NA	NA	88	34	70
Wang et al., 2011	China	33	42.7	51.5	5	NA	NA	NA	82	60	46	NA	NA
Kim et al., 2006	South Korea	40	47.7	55.6	4	NA	NA	NA	NA	NA	NA	NA	33.3
Kang and Kim, 2015	South Korea	49	52.7	43.5	8.7	21.7	60.9	6.3	NA	NA	NA	34.8	NA
Ueda et al., 2015	Japan	51	44.2–53.6	52.9	33	NA	NA	NA	69	31	70.6	NA	NA
Koizumi et al., 2019	Japan	126	NA	47.6	44.3	16.1	26.2	4.9	70.6	46.8	79.2	54.3	NA
Present study	Japan	88	49.5	62.5	13.6**	14.8	35.2	1.1	67	35.2	84.9	47.7	73.9

*HTN, hypertension; DL, dyslipidemia; DM, diabetes mellitus. *migraine age at onset. **migraine with and without aura was 28.4%.*

of CADASIL patients in Japan and reported fewer numbers of CADASIL patients in the Hokkaido and Tohoku region. These results might depend on recognizing CADASIL itself in some hospitals in Japan.

The majority of *NOTCH3* gene mutations existed in exon 4 in Japan. This result is similar to the previous Japanese reports (Ueda et al., 2015; Mizuta et al., 2017; Koizumi et al., 2019). Previous studies showed a high frequency of *NOTCH3* gene mutation in exon 4 in Asian and European populations except Italy (Markus et al., 2002; Peters et al., 2004; Adib-Samii et al., 2010; Wang et al., 2011; Bianchi et al., 2015). Our study showed a lower prevalence of *NOTCH3* mutations in exon 3, especially the R75P, than previous reports in Japan (Ueda et al., 2015; Mizuta et al., 2017; Koizumi et al., 2019).

Although we conducted the first nationwide survey of CADASIL patients in Japan and constructed a registration database of CADASIL, we acknowledge that there are several limitations to our study. First, the number of the patients included in this study were small. Second, the prevalence rate of CADASIL might be lower than expected. However, this limitation may be related to the approach used by our survey study: we sent questionnaires to the departments of neurology of certificated hospitals. Thus, we might have missed patients treated by other departments or clinics. Moreover, there is a possibility that asymptomatic patients or those with only minor symptoms could not be identified. Therefore, the number of individuals with *NOTCH3* mutations might be underestimated. An alternative strategy involves asking genetic testing facilities for the number of *NOTCH3* mutation-positive individuals, which would ensure the inclusion of all the possible cases of *NOTCH3* mutation and thus, guarantee a larger study population. However, genetic testing for CADASIL is performed at several independent institutions, which might make it difficult to include all the positives in a single study. Therefore, we sent the questionnaire survey to hospitals for this study. This study sought the characteristics of CADASIL using a simple, two-step questionnaire, and therefore, detailed information may be lacking. However, through this study, we conducted a large survey involving more than one thousand certificated hospitals and created a novel registration database for future studies. We hope this study enables the increased recognition of CADASIL in Japan.

CONCLUSION

This is the first nationwide survey of CADASIL in Japan. We have constructed the REDCap database for CADASIL patients in Japan. This database could be expanded and used for future clinical trials.

DATA AVAILABILITY STATEMENT

The raw data supporting the conclusions of this article will be made available by the authors, without undue reservation, to any qualified researcher.

ETHICS STATEMENT

The studies involving human participants were reviewed and approved by the Ethics Committee of the Mie University Graduate School of Medicine (permit number 2918). Written consent was obtained from the patients who were registered in REDCap survey.

AUTHOR CONTRIBUTIONS

AS: draft of the manuscript, study concept and design, and acquisition of the data and analysis. KT, AT, TK, IM, MI, and TM: revision of the manuscript, interpretation of the data, and study supervision. TH, HW, MT, and SS: revision of the manuscript and interpretation of the data. HN, OO, AU, YA, TU, KKim, KKit, HH, HF, YM, and AW-H: acquisition of the data and interpretation of the data. HT: revision of the manuscript, study concept and design, and study supervision. All authors contributed to the article and approved the submitted version.

FUNDING

This research was supported by AMED under Grant Number JP17ek010913h0003.

ACKNOWLEDGMENTS

We would like to thank Dr. Yumi Yamamoto, Dr. Fumiyuki Otsuka, and Dr. Kazuyuki Nagatsuka (National Cerebral and Cardiovascular Center), Dr. Soichiro Shimizu (Tokyo Medical University), Dr. Toshihiko Aso and Dr. Takakuni Maki (Kyoto University), Dr. Takashi Koizumi, Dr. Mao Mukai, and Dr. Jun Matsuura (Kyoto Prefectural University of Medicine), Dr. Masahiro Uemura, (Niigata University), Dr. Makoto Nakajima and Dr. Yihong Ma (Kumamoto University), and Dr. Eiji Nakatani and Dr. Shinsuke Kojima (Foundation for Biomedical Research and Innovation at Kobe), for their kind contribution. We would also like to thank all the patients and families with CADASIL and express our gratitude to all the neurologists, neurosurgeons, and strokologists for answering the questionnaire.

REFERENCES

Adib-Samii, P., Brice, G., Martin, R. J., and Markus, H. S. (2010). Clinical spectrum of CADASIL and the effect of cardiovascular risk factors on phenotype: study in 200 consecutively recruited individuals. *Stroke* 41, 630–634. doi: 10.1161/strokeaha.109.568402

Bianchi, S., Zicari, E., Carluccio, A., Di Donato, I., Pescini, F., Nannucci, S., et al. (2015). CADASIL in central Italy: a retrospective clinical and genetic study in 229 patients. *J. Neurol.* 262, 134–141. doi: 10.1007/s00415-014-7533-2

Chabriat, H., Joutel, A., Dichgans, M., Tournier-Lasserve, E., and Bousser, M. G. (2009). Cadasil. *Lancet Neurol.* 8, 643–653.

Choi, J. C., Lee, K. H., Song, S. K., Lee, J. S., Kang, S. Y., and Kang, J. H. (2013). Screening for NOTCH3 gene mutations among 151 consecutive Korean patients with acute ischemic stroke. *J. Stroke Cerebrovasc. Dis.* 22, 608–614. doi: 10.1016/j.jstrokecerebrovasdis.2011.10.013

Ciolli, L., Pescini, F., Salvadori, E., Del Bene, A., Pracucci, G., Poggesi, A., et al. (2014). Influence of vascular risk factors and neuropsychological profile on functional performances in CADASIL: results from the MIcrovascular LEukoencephalopathy Study (MILES). *Eur. J. Neurol.* 21, 65–71. doi: 10.1111/ene.12241

Fazekas, F., Chawluk, J. B., Alavi, A., Hurtig, H. I., and Zimmerman, R. A. (1987). MR signal abnormalities at 1.5 T in Alzheimer's dementia and normal aging. *AJR Am. J. Roentgenol.* 149, 351–356. doi: 10.2214/ajr.149.2.351

Gobel, H., Petersen-Braun, M., and Soyka, D. (1994). The epidemiology of headache in Germany: a nationwide survey of a representative sample on the basis of the headache classification of the International Headache Society. *Cephalalgia* 14, 97–106. doi: 10.1046/j.1468-2982.1994.1402097.x

Harris, P. A., Taylor, R., Thielke, R., Payne, J., Gonzalez, N., and Conde, J. G. (2009). Research electronic data capture (REDCap)–a metadata-driven methodology and workflow process for providing translational research informatics support. *J. Biomed. Inform.* 42, 377–381. doi: 10.1016/j.jbi.2008.08.010

Herve, D., Godin, O., Dufouil, C., Viswanathan, A., Jouvent, E., Pachai, C., et al. (2009). Three-dimensional MRI analysis of individual volume of Lacunes in CADASIL. *Stroke* 40, 124–128. doi: 10.1161/strokeaha.108.520825

Joutel, A., Corpechot, C., Ducros, A., Vahedi, K., Chabriat, H., Mouton, P., et al. (1996). Notch3 mutations in CADASIL, a hereditary adult-onset condition causing stroke and dementia. *Nature* 383, 707–710. doi: 10.1038/383707a0

Kang, H. G., and Kim, J. S. (2015). Intracranial arterial disease in CADASIL patients. *J. Neurol. Sci.* 359, 347–350. doi: 10.1016/j.jns.2015.11.029

Kim, Y., Choi, E. J., Choi, C. G., Kim, G., Choi, J. H., Yoo, H. W., et al. (2006). Characteristics of CADASIL in Korea: a novel cysteine-sparing Notch3 mutation. *Neurology* 66, 1511–1516. doi: 10.1212/01.wnl.0000216259.99811.50

Koizumi, T., Mizuta, I., Watanabe-Hosomi, A., Mukai, M., Hamano, A., Matsuura, J., et al. (2019). The CADASIL scale-J, a modified scale to prioritize access to genetic testing for Japanese CADASIL-suspected patients. *J. Stroke Cerebrovasc. Dis.* 28, 1431–1439. doi: 10.1016/j.jstrokecerebrovasdis.2019.03.026

Markus, H. S., Martin, R. J., Simpson, M. A., Dong, Y. B., Ali, N., Crosby, A. H., et al. (2002). Diagnostic strategies in CADASIL. *Neurology* 59, 1134–1138. doi: 10.1212/wnl.59.8.1134

Mizuta, I., Watanabe-Hosomi, A., Koizumi, T., Mukai, M., Hamano, A., Tomii, Y., et al. (2017). New diagnostic criteria for cerebral autosomal dominant arteriopathy with subcortical infarcts and leukocencephalopathy in Japan. *J. Neurol. Sci.* 381, 62–67. doi: 10.1016/j.jns.2017.08.009

Nannucci, S., Rinnoci, V., Pracucci, G., MacKinnon, A. D., Pescini, F., Adib-Samii, P., et al. (2018). Location, number and factors associated with cerebral microbleeds in an Italian-British cohort of CADASIL patients. *PLoS One* 13:e0190878. doi: 10.1371/journal.pone.0190878

Pescini, F., Nannucci, S., Bertaccini, B., Salvadori, E., Bianchi, S., Ragno, M., et al. (2012). The cerebral autosomal-dominant arteriopathy with subcortical infarcts and leukoencephalopathy (CADASIL) scale: a screening tool to select patients for NOTCH3 gene analysis. *Stroke* 43, 2871–2876.

Peters, N., Herzog, J., Opherk, C., and Dichgans, M. (2004). A two-year clinical follow-up study in 80 CADASIL subjects: progression patterns and implications for clinical trials. *Stroke* 35, 1603–1608. doi: 10.1161/01.str.0000131546.71733.f1

Rasmussen, B. K., Jensen, R., and Olesen, J. (1991). A population-based analysis of the diagnostic criteria of the International Headache Society. *Cephalalgia* 11, 129–134. doi: 10.1046/j.1468-2982.1991.1103129.x

Razvi, S. S., Davidson, R., Bone, I., and Muir, K. W. (2005). The prevalence of cerebral autosomal dominant arteriopathy with subcortical infarcts and leucoencephalopathy (CADASIL) in the west of Scotland. *J. Neurol. Neurosurg. Psychiatry* 76, 739–741. doi: 10.1136/jnnp.2004.051847

Roman, G. C., Erkinjuntti, T., Wallin, A., Pantoni, L., and Chui, H. C. (2002). Subcortical ischaemic vascular dementia. *Lancet Neurol.* 1, 426–436. doi: 10.1016/s1474-4422(02)00190-4

Sakai, F., and Igarashi, H. (1997). Prevalence of migraine in Japan: a nationwide survey. *Cephalalgia* 17, 15–22. doi: 10.1046/j.1468-2982.1997.1701015.x

Santa, Y., Uyama, E., Chui, D. H., Arima, M., Kotorii, S., Takahashi, K., et al. (2003). Genetic, clinical and pathological studies of CADASIL in Japan: a partial contribution of Notch3 mutations and implications of smooth muscle cell degeneration for the pathogenesis. *J. Neurol. Sci.* 212, 79–84. doi: 10.1016/s0022-510x(03)00109-6

Shinohara, Y., Minematsu, K., Amano, T., and Ohashi, Y. (2006). Modified Rankin scale with expanded guidance scheme and interview questionnaire: interrater agreement and reproducibility of assessment. *Cerebrovasc. Dis.* 21, 271–278. doi: 10.1159/000091226

Singhal, S., Bevan, S., Barrick, T., Rich, P., and Markus, H. S. (2004). The influence of genetic and cardiovascular risk factors on the CADASIL phenotype. *Brain* 127(Pt 9), 2031–2038. doi: 10.1093/brain/awh223

Takashima, N., Arima, H., Kita, Y., Fujii, T., Miyamatsu, N., Komori, M., et al. (2017). Incidence, management and short-term outcome of stroke in a general population of 1.4 million Japanese- shiga stroke registry. *Circ. J.* 81, 1636–1646. doi: 10.1253/circj.cj-17-0177

Uchino, M., Hirano, T., Uyama, E., and Hashimoto, Y. (2002). Cerebral autosomal dominant arteriopathy with subcortical infarcts and leukoencephalopathy (CADASIL) and CADASIL-like disorders in Japan. *Ann. N. Y. Acad. Sci.* 977, 273–278.

Ueda, A., Ueda, M., Nagatoshi, A., Hirano, T., Ito, T., Arai, N., et al. (2015). Genotypic and phenotypic spectrum of CADASIL in Japan: the experience at a referral center in Kumamoto University from 1997 to 2014. *J. Neurol.* 262, 1828–1836. doi: 10.1007/s00415-015-7782-8

Wang, Z., Yuan, Y., Zhang, W., Lv, H., Hong, D., Chen, B., et al. (2011). NOTCH3 mutations and clinical features in 33 mainland Chinese families with CADASIL. *J. Neurol. Neurosurg. Psychiatry* 82, 534–539. doi: 10.1136/jnnp.2010.209247

Conflict of Interest: The authors declare that the research was conducted in the absence of any commercial or financial relationships that could be construed as a potential conflict of interest.

frontiers in Aging Neuroscience

ORIGINAL RESEARCH
published: 31 August 2020
doi: 10.3389/fnagi.2020.00234

Altered Brain Function in Cerebral Small Vessel Disease Patients With Gait Disorders: A Resting-State Functional MRI Study

*Xia Zhou[1], Chao Zhang[2], Linlin Li[1], Yimei Zhang[1], Wei Zhang[1], Wenwen Yin[1], Xianfeng Yu[1], Xiaoqun Zhu[1], Yinfeng Qian[3] and Zhongwu Sun[1]**

[1] Department of Neurology, The First Affiliated Hospital of Anhui Medical University, Hefei, China, [2] Department of Neurology, The First Affiliated Hospital of University of Science and Technology of China, Hefei, China, [3] Department of Radiology, The First Affiliated Hospital of Anhui Medical University, Hefei, China

Gait disturbances are important clinical features of cerebral small vessel disease (CSVD) that increase the risk of falls and disability. Brain structural alterations and gait disturbances in CSVD patients have been well demonstrated. However, intrinsic resting cerebral function patterns in CSVD patients with gait disorders remain largely unknown. Fifty-eight CSVD patients were enrolled in our studies and categorized into the gait disorder group (CSVD-GD, $n = 29$) and no-gait disorder group (CSVD-NGD, $n = 29$) based on a gait examination. Gait was quantitatively assessed with the Timed Up and Go test and the intelligent device for energy expenditure and activity (IDEEA). Functional MRI and fractional amplitude of low-frequency fluctuation (fALFF) analyses were employed to explore local intrinsic neural oscillation alterations. Functional connectivity based on fALFF results was calculated to detect the potential changes in remote connectivity. Compared with the CSVD-NGD group, the CSVD-GD group showed decreased fALFF in regions mainly located in the sensorimotor network and frontoparietal network, such as the left supplementary motor area (SMA.L) and the left superior parietal gyrus, and increased fALFF in the right inferior frontal gyrus (orbital part), the left caudate, and the left precuneus. Moreover, the CSVD-GD patients exhibited lower connectivity between the SMA.L and temporal lobe, which was related to gait speed. The fALFF value of the SMA.L was associated with cadence. This study highlights the regional and network interaction abnormalities of the SMA in CSVD patients with gait disturbances. These findings could provide further insight into the neural mechanisms of gait disturbances in CSVD.

Keywords: cerebral small vessel disease, gait disorder, ALFF/fALFF, functional connectivity, supplementary motor area (SMA)

OPEN ACCESS

Edited by:
JoAnne McLaurin, Sunnybrook Research Institute, Toronto, Canada

Reviewed by:
Paolo Bazzigaluppi, Sunnybrook Research Institute (SRI), Canada
Xiuqin Jia, Capital Medical University, China

***Correspondence:**
Zhongwu Sun
sunzhwu@hotmail.com

Received: *29 January 2020*
Accepted: *06 July 2020*
Published: *31 August 2020*

Citation:
Zhou X, Zhang C, Li L, Zhang Y, Zhang W, Yin W, Yu X, Zhu X, Qian Y and Sun Z (2020) Altered Brain Function in Cerebral Small Vessel Disease Patients With Gait Disorders: A Resting-State Functional MRI Study. Front. Aging Neurosci. 12:234. doi: 10.3389/fnagi.2020.00234

INTRODUCTION

Gait disturbances are quite common in elderly adults and are associated with an increased risk of falls, disability, and mortality (van der Holst et al., 2016). Normal gait control involves both the motor system and cognition control system (Rosano et al., 2012). The effect of peripheral nervous system factors, such as sarcopenia or plantar cutaneous sensory on gait stability, has received ample

attention in recent years (Kwon et al., 2019; Navarro-Peternella et al., 2019); however, research on the influence of central nervous system factors is still limited. Recently, an extensive body of evidence has focused on the contributing role of cerebral small vessel disease (CSVD) on gait impairments in elderly individuals (Pinter et al., 2017; Loos et al., 2018; van der Holst et al., 2018). White matter hyperintensities (WMHs) and lacunar infarcts (LAs), two major imaging markers of CSVD, have been suggested to be correlated with motor impairments in balance and gait function, even after adjusting for a range of confounding covariates (Smith et al., 2015). Cognition impairment is the most striking symptom of CSVD that attracts much attention from patients. However, subcortical syndromes, such as gait disorders, tend to be neglected because of their insidious onset. Certainly, not all individuals with CSVD eventually experience gait disturbances, although CSVD has been recognized as a possible cause of gait impairment (Su et al., 2018). In other words, the motor impairments associated with CSVD cannot be fully interpreted by WMHs or LAs on MRI. Therefore, a better understanding of the characteristics of gait disturbances and exploring the potential pathophysiological mechanisms of gait disorders in CSVD are critical scientific endeavors that will eventually help to achieve further advances in the therapy of gait disorders.

In recent years, a number of studies have tried to identify structural changes in CSVD patients with gait disorders (de Laat et al., 2011). These studies have shown that widespread structural alterations were exhibited in CSVD patients with gait disturbances, including white matter integrity loss, gray matter atrophy, and cortical thinning. Moreover, loss of microstructural integrity not only within the WMH area but also within the normal-appearing white matter (NAWM) contributes to gait impairments (Rosario et al., 2016). However, very few studies have directly examined functional alteration patterns. Resting-state functional MRI (rs-fMRI) is a potentially powerful approach to investigate brain functional alterations with its unique advantage of not requiring ongoing activity (Fox and Raichle, 2007). The assessment of amplitude of low-frequency fluctuation (ALFF), one of the methods based on rs-fMRI, has been widely applied to probe regional spontaneous brain activity by measuring the square root of the power spectrum in the low-frequency range (Zuo et al., 2010). However, as it is difficult to eliminate physiological noise, the fractional amplitude of low-frequency fluctuation (fALFF) technique has been recommended and calculates the ratio of the low-frequency power spectrum to that of the entire frequency range (Zou et al., 2008), and this method has been used to explore regional spontaneous brain activity in several diseases, such as Parkinson's disease (PD) (Shen et al., 2018) and Alzheimer's disease (AD) (Yang et al., 2018). Functional connectivity (FC) provides additional information by measuring levels of integrated local activity across distant regions and can have utility for advancing our understanding of dysfunctions in integrated brain networks involved in gait disorders associated with CSVD.

Therefore, the aim of the present study was to identify patterns of functional alterations in CSVD patients with gait disturbances using both fALFF and seed-based FC analyses. We hypothesized that altered resting function would not be limited to regional brain areas, but also observed in remote areas or networks that have also been implicated in gait problems in CSVD patients.

MATERIALS AND METHODS

Subjects

Sixty-five right-handed consecutive CSVD patients were enrolled in our study from the First Affiliated Hospital of Anhui Medical University. CSVD was defined as subcortical white matter hyperintensity with a Fazekas scale score $\geq$2 (at least 2 on the Fazekas scale for either deep or periventricular WMH) or LAs on T2-weighted images and/or fluid-attenuated inversion recovery (FLAIR) images, without any acute stroke appearances in diffusion-weighted imaging, according to the commonly applied criterion (Takakusaki, 2017). WMHs were assessed using the Fazekas scale on the FLAIR sequence (Fazekas et al., 1987). LAs were defined as focal lesions from 3 to 15 mm with cerebral spinal fluid-like signal on FLAIR or T2-weighted images. We also assessed the WMH volume semi-automatically using volumetric measurements and calculated the number of LAs. In brief, lesion load of white matter measurements was performed on FLAIR images by a trained operator (L.L.). All lesion areas were outlined on the computer image and automatically computed by the MRIcro and ITK-SNAP software (Chen et al., 2018).

The exclusion criteria for the CSVD patients included the following: WMH resulting from non-vascular diseases, such as poisoning, multiple sclerosis, encephalitis, and infection; a history of known stroke, head injury, Parkinson's disease, epilepsy, major depression, or other neurological or psychiatric illness; severe visuospatial deficits, hearing impairments, or language disorders; *in vivo* dentures or metallic stents; serious orthopedic diseases, such as osteoarthritis, fracture, congenital malformation, amputation, and arthroplasty of the lower limbs.

The institutional review board of the First Affiliated Hospital of Anhui Medical University Subcommittee on Human Studies approved the study, and informed written consent was obtained from the participants.

Cognitive and Neuropsychological Assessments

A series of neuropsychological assessments was performed by a trained neuropsychological technician within 1 week after the MRI scan, including the Mini-Mental State Examination (MMSE), Cambridge Cognitive Examination–Chinese version (CAMCOG-C), Geriatric Depression Scale (GDS), Activities of Daily Living Scale (ADL), and Stroop test (Stroop-1: dot; Stroop-2: characters; Stroop-3: color) to evaluate global cognition and functions of episodic memory, attention, psychomotor speed, executive function, visuospatial skills, and emotion. The administration of the battery took between 1.5 and 2.0 h.

Gait Analysis and Patient Classification

Timed Up and Go (TUG) Test and Berg Balance Scale (BBS)

The TUG test (Mathias et al., 1986) is a classic and simple test to assess mobility and walking by measuring the time a person takes to rise from a standard chair without using armrests, walk 3 m at a usual pace, turn around, walk back to the chair, and finally sit down again, and has been used in the assessment of patients with several diseases, such as PD (Sato et al., 2019). The TUG test identified the fall risk among the elderly population at high sensitivity (87%) and specificity (87%) with 15 s as the threshold (Shumway-Cook et al., 2000). In our study, all participants were instructed to take the TUG test twice, and the mean time of the two trials was calculated as the result. In the present study, the CSVD patients were divided into the gait disturbance group (CSVD-GD; TUG test $\geq$15 s) and no-gait disturbance group (CSVD-NGD; TUG test $<$15 s).

To obtain more information, the TUG dual task (TUG-2) and BBS test were also performed. The former was executed by extracting all the numbers containing 7 from 1 to 100 (such as 7, 17, 27…) during the walking process and calculating the time and the number of errors. The BBS test was used to measure balance function and included 14 balance tests ranging from simple tasks (such as transfer, unsupported standing, sitting to standing) to complex tasks (such as turning 360°, standing on one leg). Each item was graded on a 5-point scale (0–4), in which grade 0 indicated that the motion could not be performed, and grade 4 indicated that the individual completed the specified task, for a total of 56 points (14 × 4).

Intelligent Device for Energy Expenditure and Activity (IDEEA)

The IDEEA (MiniSun, LLC, Fresno, CA, USA), a portable and useful instrument for recording and analyzing physical activities and gait, was used to capture gait parameters (sampling frequency 64 Hz). The IDEEA has been shown to have excellent test–retest reliability and validity (Gorelick et al., 2009). It was performed with seven tiny accelerometers/inclinometers (1.4 × 1.1 × 0.3 cm^3) fixed to the skin by medical tape. Each participant was asked to walk for 30 m at a comfortable walking speed with IDEEA, and the gait parameters were collected by the device at the same time, which were subsequently transferred to a personal computer for data analysis. To measure steady-state walking, spatiotemporal parameters from only the middle 20 strides, including gait speed, cadence, and stride length, single support duration, and double support duration, were analyzed using IDEEA software.

MRI Acquisition

MRI data were obtained using a 3.0 Tesla GE Signa HDxt MRI scanner (GE, Milwaukee, WI, USA) equipped with an eight-channel head coil. All participants were instructed to keep their eyes closed without falling asleep and to think as little as possible during the scan. To minimize head movement and eliminate scanner noise, foam padding and ear plugs were used. The resting-state data were obtained using echo-planar imaging (EPI) at 2-s intervals for a total of 8 min, which comprised 240 contiguous EPI whole-brain functional volumes with the following parameters: repetition time (TR) = 2 s; echo time (TE) = 30 ms; field of view (FOV) = 240 × 240 mm^2; flip angle (FA) = 80; matrix size = 64 × 64; slice thickness = 4 mm; gap = 0.6 mm. Three-dimensional (3D) T1-weighted images were acquired using a spoiled gradient recalled echo sequence with the following parameters: TR = 9.5 ms; TE = 3.9 ms; FA = 20; FOV = 256 × 256 mm^2; matrix size = 512 × 512. The following structural brain sequences were also acquired: T2-weighted spin echo (TR = 3,500 ms; TE = 85 ms; echo train length = 15; FA = 90; 22 contiguous, 5-mm-thick, axial slices; matrix size = 512 × 512; and FOV = 230 × 184 mm^2); FLAIR (TR = 11 s; TE = 120 ms; FA = 90; 22 contiguous, 5-mm-thick, axial slices; matrix size = 512 × 512; and FOV = 230 × 230 mm^2).

Image Processing and Analysis

The rs-fMRI data were preprocessed using Data Processing and Analysis for (Resting-State) Brain Imaging (DPABI) software (Yan et al., 2016) (http://www.restfmri.net) running in MATLAB (Mathworks, Natick, MA, USA). The process comprised removal of the first 10 EPI time points to ensure steady state and allow the participant to acclimate to the scanning environment, slice timing to correct for differences in image acquisition time between slices, image realignment for head motion correction, nuisance covariates regression (the estimated motion parameters based on the Friston-24 model, the cerebrospinal fluid signal, and the white matter signal), spatial normalization to the Montreal Neurological Institute (MNI) by diffeomorphic anatomical registration through exponentiated lie algebra (DARTEL) and resampled at a resolution of 3 × 3 × 3 mm^3, spatial smoothing with 6-mm full-width at half-maximum Gaussian kernel, detrending to remove the linear trends, and band-pass filtering (0.01–0.08 Hz). During the processing, head motion of more than 2.5 mm maximum translation in any direction of x, y, or z or 2.5° of maximal rotation throughout the course of scanning were excluded (three CSVD-GD patients and four CSVD-NGD patients). We also calculated framewise displacement (FD Jenkinson), which indexes the volume-to-volume changes in head position. No significant group differences were found in FD Jenkinson between the CSVD-GD patients and CSVD-NGD patients ($t = -0.383$, $p = 0.703$).

ALFF analysis was also carried out using DPABI software. A fast-Fourier transform (FFT) algorithm was used to transform the time series for each voxel into frequency domain data. ALFF was calculated by obtaining the square root of the power spectrum from 0.01 to 0.08 Hz, and then the ratio low-frequency fluctuation amplitude (fALFF) was obtained by dividing the ALFF of each voxel by the average over the entire frequency range. fALFF values were converted to Z score.

To explore whether brain regions with fALFF alterations also exhibited FC changes, the peak points of the regions with significant group differences in fALFF were selected as seeds for FC analyses. The time courses of the seed regions and all other brain voxels were extracted for estimating alterations in connectivity. Pearson's correlation coefficients were computed between the mean signal change in the seed and all other voxels

across the brain. In addition, Fisher's r to Z-transformation was applied to improve the normality of the correlation coefficients.

Voxel-Based Morphometry (VBM)

To clarify whether there were structural differences between the two groups, VBM (http://dbm.neuro.uni-jena.de/vbm8/) and Computational Anatomy Toolbox (CAT12; http://www.neuro.uni-jena.de/cat12/CAT12-Manual.pdf) with SPM12 were used for gray matter analyses. First, 3D T1-weighted images were segmented into gray matter, white matter, and cerebrospinal fluid. Then, high-dimensional DARTEL was used to normalize the gray matter maps to the MNI standard space. The modulated spatial normalized gray matter image was smoothed with an 8-mm FWHM kernel. In addition, to evaluate whether functional alterations were contributed to gray matter atrophy, we extracted the regional gray matter volume (GMV) for the regions of interest based on the results of the fALFF and FC analyses by REST (http://www.restfmri.net/forum/REST_V1.8) software.

Statistical Analysis

The Statistical Package of Social Science (IBM SPSS Statistics 22, SPSS Inc., Chicago, IL, USA) was used for *t*-tests, χ^2-tests, nonparametric analyses, and correlation analyses. The continuous data are presented as the mean ± SD for normally distributed variables and as the median (P_{25}, P_{75}) for the skew-distributed continuous variables. We also used SPM 8 and DPABI software for statistical analyses for fALFF and FC.

A general linear model–based approach was used to detect significant between-group differences in fALFF using SPM 8. Age, sex, and education were included as covariates. For the FC analysis, a one-sample *t*-test was performed on each z-value map to examine functional connectivity in the two groups. Two-sample *t*-tests were used to compare the z values in each voxel of the above groups. Multiple comparisons were corrected using the cluster-level false discovery rate (FDR) method, resulting in a cluster defining threshold of $p = 0.001$ and a corrected cluster significance of $p < 0.05$. To determine the relationship between z values and clinical measures, Pearson's correlation analyses were performed in all CSVD patients ($p < 0.05$). The results are presented using xjview and BrainNet viewer.

TABLE 1 | Demographic, clinical, and neuropsychological test data.

	CSVD-GD	CSVD-NGD	*P*-value
N	29	29	
Age (years)	68.66 ± 6.46	65.45 ± 9.79	0.147
Sex (male/female)	15/14	13/16	0.599
Years of education	9.13 ± 3.90	11.35 ± 4.60	0.053
BMI	24.17 ± 3.35	24.18 ± 3.10	0.995
MMSE	25.14 ± 3.24	25.69 ± 3.32	0.525
CAMCOG-C	77.58 ± 12.55	82.48 ± 11.97	0.134
Orientation	9(8,10)	9(9,10)	0.530
Languages	24(22,27)	27(23,28)	0.064
Memory	16.10 ± 4.79	17.03 ± 5.12	0.525
Attention	7(5,7)	6(5,7)	0.868
Praxis	10(8,12)	11(9,12)	0.148
Calculation	2(2,2)	2(2,2)	0.643
Abstraction	5.76 ± 1.94	5.83 ± 1.93	0.892
Perception	7.24 ± 1.43	7.34 ± 1.49	0.789
ADL	20(20,22.25)	20(20,21)	0.993
GDS	7(3.5,12)	5(3,10)	0.374
Stroop-1	30.65 ± 9.61	23.62 ± 7.35	**0.003**
Stroop-2	35.32 ± 10.70	29.94 ± 10.47	0.058
Stroop-3	48.74 ± 19.64	44.01 ± 14.58	0.302
Enlarged perivascular spaces, no. (%)	5 (17.24%)	6 (20.69%)	0.738
LAs (no.)	7.45 ± 4.01	5.62 ± 3.35	0.065
WMHs (mm^3)	6.13(2.21,6.13)	3.53(1.46,8.74)	0.266
TUG(s)	17.51(15.48,18.73)	11.18(10.42,11.68)	**<0.001**
TUG-2(s)	17.14 ± 3.94	12.19 ± 2.28	**<0.001**
BBS	53(51.75,56)	55(53,56)	0.483
Step length (m)	0.50 ± 0.08	0.55 ± 0.08	**0.007**
Gait speed (m/s)	0.85 ± 0.18	1.02 ± 0.18	**0.001**
Cadence (steps/min)	101.71 ± 10.41	108.68 ± 10.14	**0.012**
Step duration (s)	1.17 ± 0.10	1.10 ± 0.087	**0.004**
Cycle duration (s)	1.17(1.11,1.21)	1.1(1.05,1.17)	**0.006**
Single support time (%)	38.61(37.51,39.98)	37.42(36.63,38.81)	**0.014**
Double support time (%)	25.64(24.18,26.71)	25.24(23.86,26.12)	0.423

BMI, body mass index; MMSE, Mini-Mental State Examination; CAMCOG-C, Cambridge Cognitive Examination–Chinese version; ADL, Activities of Daily Living Scale; GDS, Geriatric Depression Scale; LA, lacunar infarct; WMH, white matter hyperintensity; TUG, Timed Up and Go; TUG-2, TUG dual task; BBS, Berg Balance Scale.

RESULTS

Demographic, Clinical, and Neuropsychological Results

The socio-demographic and clinical data for each group are shown in **Table 1**. No significant differences in age, sex, educational levels, or body mass index (BMI) were found between the CSVD-GD group and CSVD-NGD group. Lower levels of gait speed, cadence, and step length were observed in the CSVD-GD group. Moreover, the CSVD-GD group exhibited longer cycle duration and single support time, but no significant differences in double support time were found.

Furthermore, the CSVD-GD group exhibited significantly lower executive function scores, as indicated by the Stroop test. No significant differences were found in the CAMCOG-C, MMSE, GDS, and ADL scores. In addition, the differences between the two groups in the number of LAs and the volume of WMHs did not reach statistical significance.

fALFF Analysis

After adjusting for age, sex, and education level, the CSVD-GD group, compared with the CSVD-NGD group, showed a significant fALFF decrease in the left supplementary motor area (SMA.L) (−0.028 ± 0.583 vs. 0.663 ± 0.602, respectively; $t = -4.438$, $p < 0.001$), the left superior parietal lobe (SPL.L) (−0.248 ± 0.509 vs. 0.498 ± 0.481; $t = -5.735$, $p < 0.001$), and the right postcentral gyrus (PoCG.R) (−0.098 ± 0.626 vs. 0.816 ± 0.853; $t = -3.650$, $p = 0.001$) (**Figure 1**), while the fALFF value increased in the right orbital inferior frontal gyrus (IFG.R, orbital part) (0.146 ± 0.707 vs. −0.656 ± 0.651; $t = 4.491$, $p < 0.001$), the left caudate (CAU.L) (0.165 ± 0.781 vs. −0.557 ± 0.677; $t = 3.828$, $p < 0.001$), and the left precuneus (Pcu.L) (0.336 ± 0.779 vs.

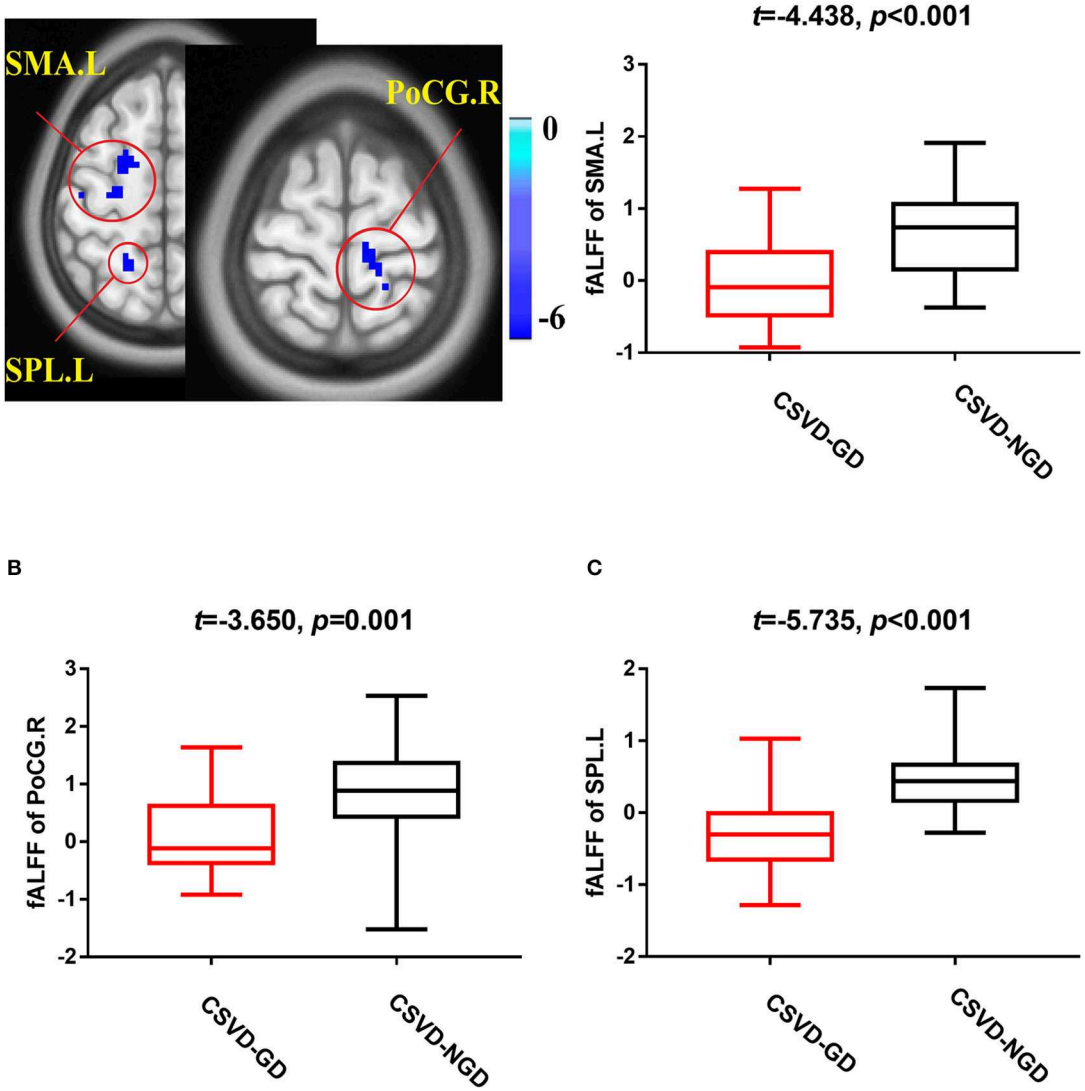

FIGURE 1 | Brain views showing decreased fractional amplitude of low-frequency fluctuations (fALFF) in the SMA.L **(A)**, PoCG.R **(B)**, and SPL.L **(C)** in the CSVD-GD patients compared with the CSVD-NGD patients ($p < 0.05$, cluster-level FDR corrected). The color bar indicates the T score. SMA.L, left supplementary motor area; PoCG.R, right postcentral gyrus; SPL.L, left superior parietal lobe; fALFF, fractional amplitude of low-frequency fluctuations.

-0.463 ± 0.505; $t = 4.633$, $p < 0.001$) (**Figure 2**). These results are summarized in **Table 2**.

Seed-Based Functional Connectivity Analysis

Brain regions with significant group differences in fALFF (i.e., the SMA.L, SPL.L, PoCG.R, IFG.R, orbital part, CAU.L, and Pcu.L) were selected as seeds in the voxel-based FC analysis. The CSVD-GD group, compared with the CSVD-NGD group, showed significantly decreased FC between the left SMA and the right lateral temporal cortex (LTC.R) (-0.072 ± 0.161 vs. 0.142 ± 0.179, respectively, $t = -4.789$, $p < 0.001$), including the right middle temporal gyrus, the supramarginal gyrus and the superior temporal gyrus ($p < 0.05$, cluster-level FDR corrected; minimum cluster size = 213 voxels). The peak voxel coordinates on MNI were $x = 60$, $y = -63$, $z = 21$ and the T-value was -5.262 (**Figure 3**). No significant difference in FC was found in other regions.

VBM Analysis

There was no significant difference of total GMV between the CSVD-GD and CSVD-NGD patients (540.76 ± 54.37 cm^3 vs. 550.00 ± 44.09 cm^3, respectively; $t = -0.711$, $p = 0.480$). In addition, further analysis of regional GMV based on the results of the fALFF and FC analyses did not reveal any differences in

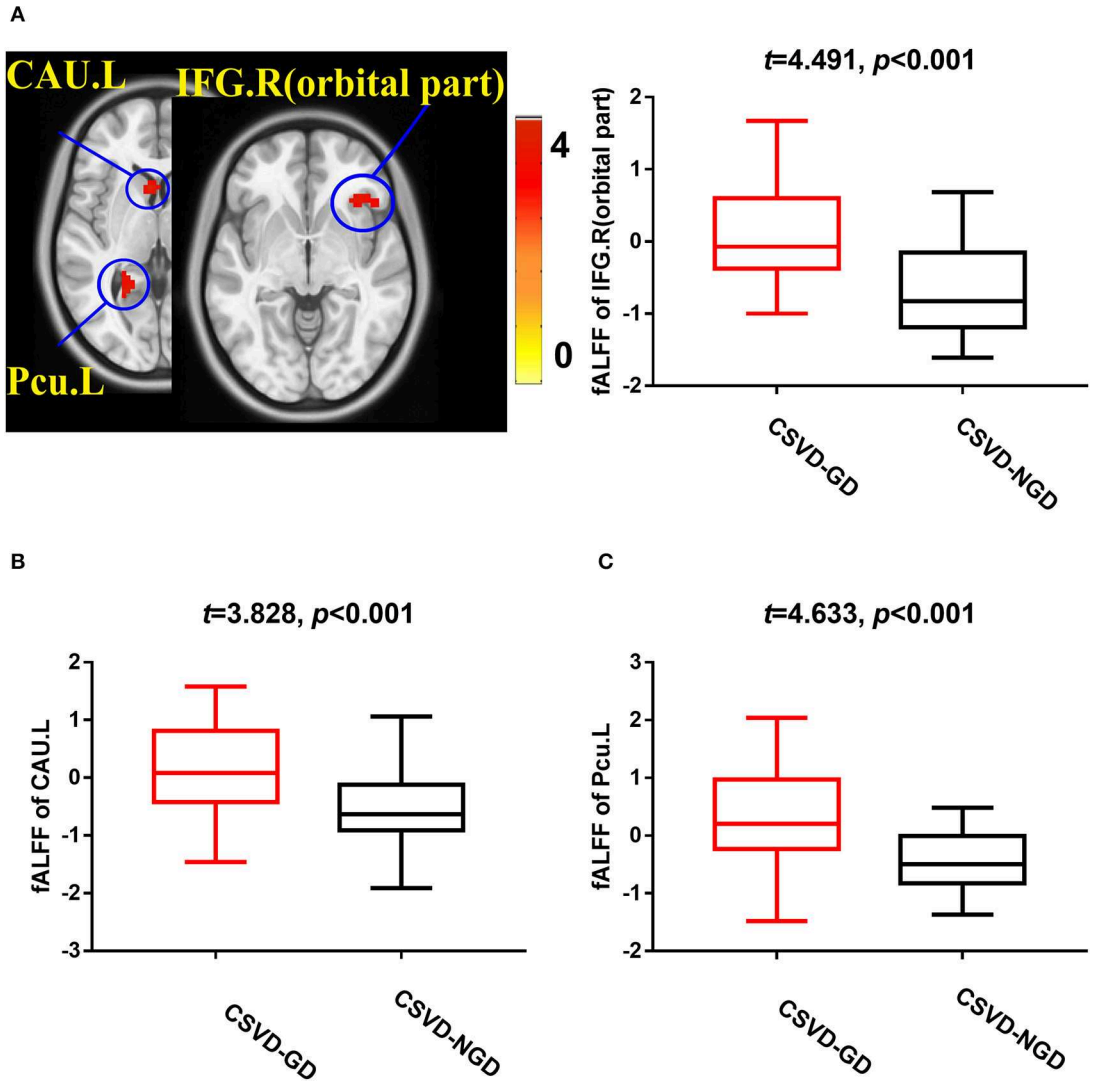

FIGURE 2 | Brain views showing increased fALFF in the IFG.R, orbital part **(A)**, CAU.L **(B)**, and Pcu.L **(C)** in the CSVD-GD patients compared with the CSVD-NGD patients ($p < 0.05$, cluster-level FDR corrected). The color bar indicates the T score. IFG.R, orbital part., right orbital inferior frontal gyrus; CAU.L, left caudate; Pcu.L, left precuneus; fALFF, fractional amplitude of low-frequency fluctuations.

local GMV between the two groups, using a significance level of $p < 0.05$, FDR corrected for multiple comparisons ($p > 0.05$).

Correlation Analysis Results

The significant correlations between altered brain function value and clinical variables are illustrated graphically in **Figures 4**, **5** ($p < 0.05$, cluster-level FDR corrected). The strength of FC (SMA.L-LTC.R) was negatively correlated with TUG ($r = -0.400$, $p = 0.002$) (**Figure 4B**) and positively correlated with gait speed ($r = 0.266$, $p = 0.043$) (**Figure 4C**). There was negative correlation between the fALFF of SMA.L and TUG ($r = -0.460$, $p < 0.001$) (**Figure 5A**), and positive correlation between the fALFF of SMA.L and cadence ($r = 0.308$, $p = 0.019$) (**Figure 5B**). The fALFF of SPL.L was negatively correlated with TUG ($r = -0.504$, $p < 0.001$) (**Figure 5C**), positively associated with both gait speed ($r = 0.361$, $p = 0.005$) (**Figure 5D**) and cadence ($r = 0.474$, $p < 0.001$) (**Figure 5E**). The altered fALFF value in other regions was also negatively correlated with TUG [PoCG.R ($r = -0.414$, $p = 0.001$); IFG.R, orbital part ($r = -0.333$, $p = 0.011$), Pcu.L ($r = -0.522$, $p < 0.001$), CAU.L ($r = -0.276$, $p = 0.036$)] ($p < 0.05$, cluster-level FDR corrected). However, no significant correlations were observed between altered brain function value and neuropsychological test scores ($p > 0.05$).

DISCUSSION

The present study used both fALFF and seed-based FC measures to examine regional and large network brain alterations in a cohort of CSVD patients with gait disorders. Decreased and increased low-frequency oscillation amplitudes were found in

TABLE 2 | Brain clusters showing significant differences in the fractional amplitude of low-frequency fluctuations (fALFF) ($p < 0.05$, FDR corrected).

Brain regions (AAL)	Cluster size (voxels)	Peak voxel coordinate—MNI coordinates			*T*-value
		x	y	z	
Decreased regions					
SMA.L	108	−18	−3	63	−6.125
PoCG.R	22	18	−42	72	−4.305
SPL.L	22	−24	−54	48	−4.179
Increased regions					
IFG.R(Orbital part)	57	45	27	−3	4.443
CAU.L	28	−6	15	3	4.595
Pcu.L	21	−24	−54	0	4.615

AAL, anatomical automatic labeling; MNI, Montreal Neurological Institute; SMA.L, left supplementary motor area; PoCG.R, right postcentral gyrus; SPL.L, left superior parietal lobe; IFG.R(Orbital part), right orbital inferior frontal gyrus; CAU.L, left caudate; Pcu.L, left precuneus.

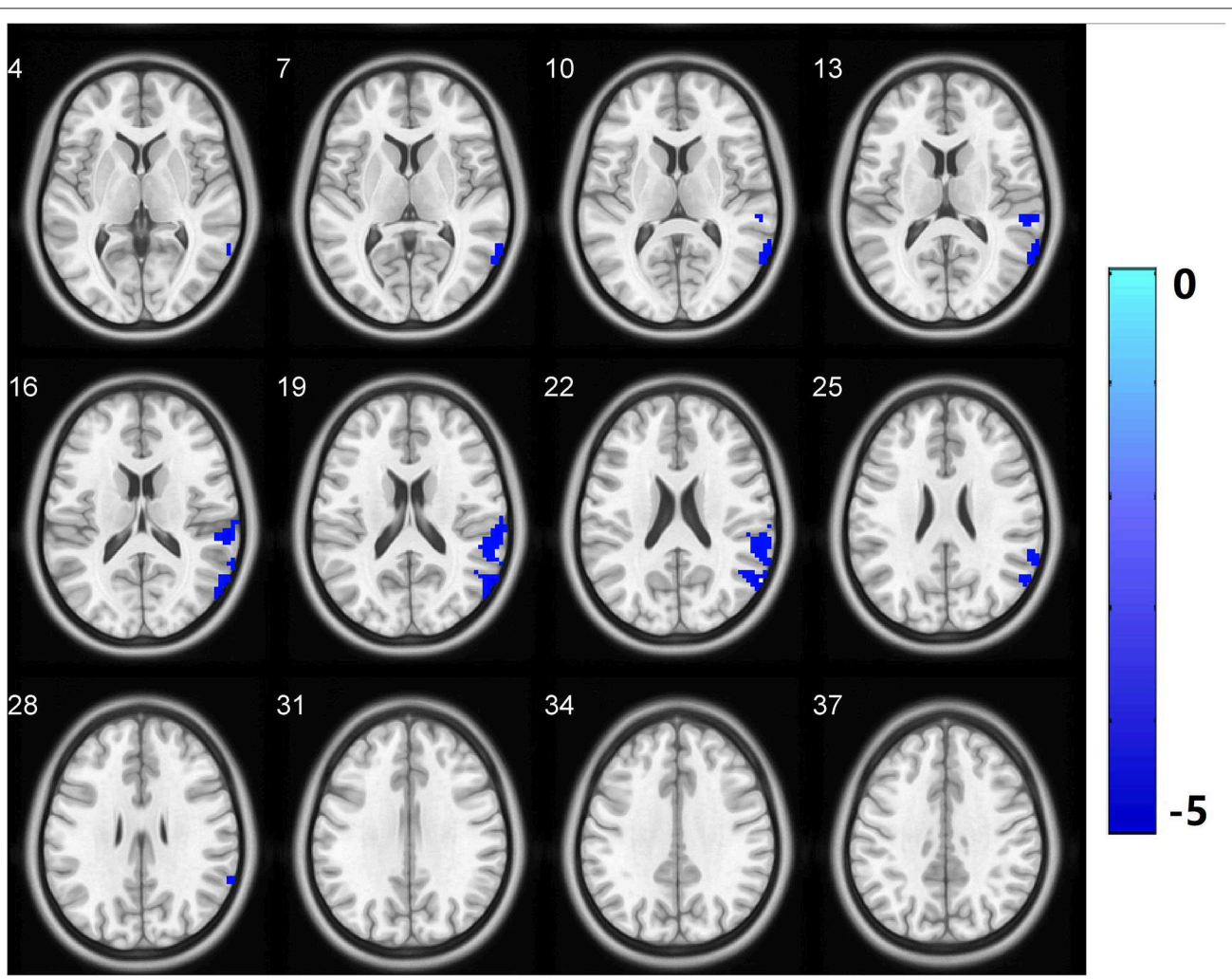

FIGURE 3 | Functional connectivity analysis based on fALFF differences revealed significantly decreased functional connectivity in the LTC.R with the left supplementary motor area as the region of interest in the CSVD-GD patients relative to the controls. All comparisons were performed using two-sample *t*-tests ($p < 0.05$, cluster-level FDR corrected). LTC.R, right lateral temporal cortex. The color bar indicates the T score. fALFF, fractional amplitude of low-frequency fluctuations.

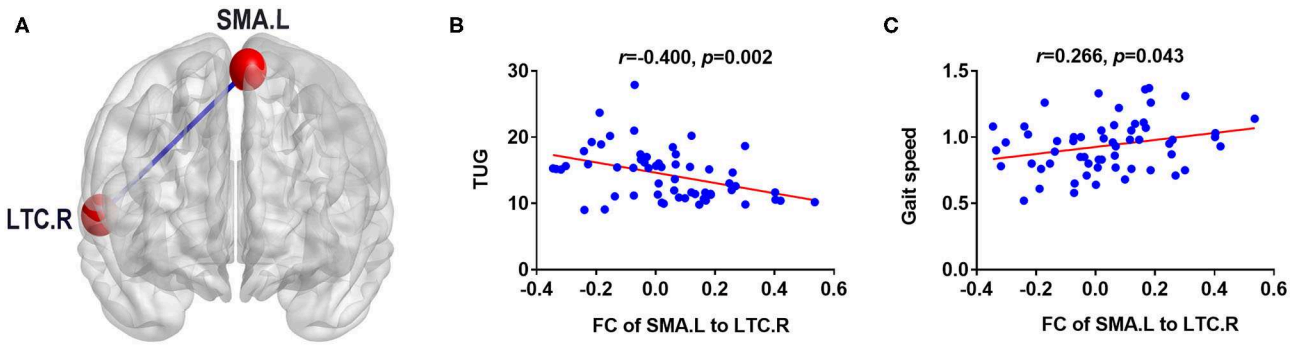

FIGURE 4 | Correlation results between FC (SMA.L-LTC.R) and clinical variables ($p < 0.05$, cluster-level FDR corrected). **(A)** FC analysis with the left supplementary motor area as the seed. **(B)** Negative correlation between FC (SMA.L-LTC.R) and TUG. **(C)** Positive correlation between FC (SMA.L-LTC.R) and gait speed. FC, functional connectivity; LTC.R, right lateral temporal cortex; SMA.L, left supplementary motor area; TUG, Timed Up and Go test.

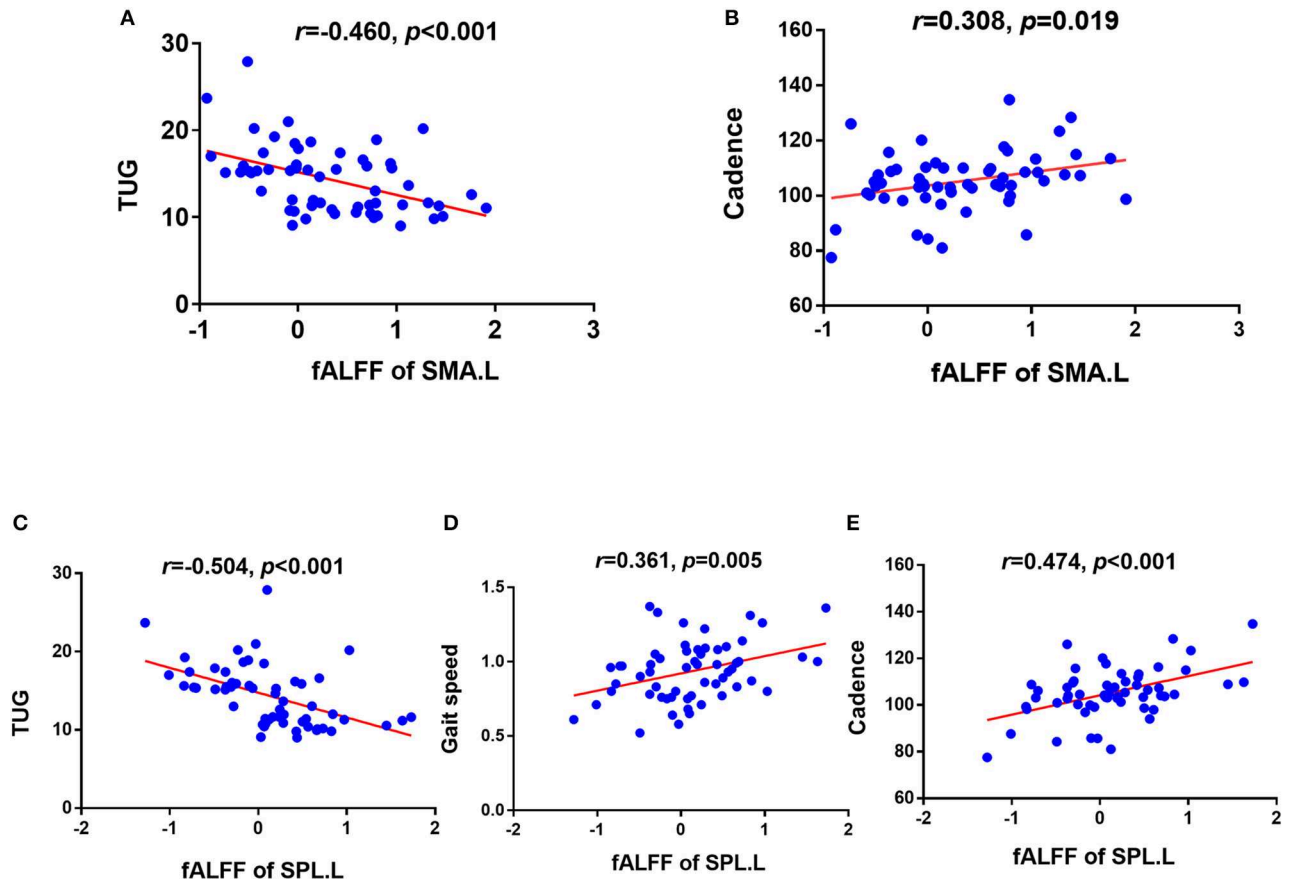

FIGURE 5 | Correlation results between altered fALFF and clinical variables ($p < 0.05$, cluster-level FDR corrected). **(A)** Negative correlation between fALFF of SMA.L and TUG. **(B)** Positive correlation between fALFF of SMA.L and cadence. **(C)** Negative correlation between fALFF of SPL.L and TUG. **(D)** Positive correlation between fALFF of SPL.L and gait speed. **(E)** Positive correlation between fALFF of SPL.L and cadence. TUG, timed up and go test; SMA.L, left supplementary motor area; SPL.L, left superior parietal lobe.

multiple brain regions distributed over cortical and subcortical regions in the CSVD-GD patients. Abnormal local neural function in the SMA and its remote connectivity with the temporal lobe were observed in our study, which were associated with cadence and gait speed, respectively. The altered brain function and its significant relationship with gait may be helpful for understanding the pathophysiology and underlying neural mechanisms of gait disturbances in CSVD patients.

ALFF is a sensitive tool to detect spontaneous function in the brain. In the present study, a notable finding was that CSVD-GD patients showed significantly decreased fALFF values in the SMA region. Neuropsychological studies have suggested that the SMA is an important part of the sensorimotor network, contributing to motor processes and mediating action initiation by directly or indirectly linking to the prefrontal cortex, motor cortex, and spinal cord (Bonini et al., 2014). During movement, the SMA serves in several processes, including action preparation, action initiation and selection of actions, motor learning, inhibition, control, and monitoring roles (Lima et al., 2016). It is reasonable that the reduced local neural function in the SMA may lead to deficits in motor processes and subsequent gait disorders. A recent study exhibited significant improvements by stimulating the SMA, rather than other motor cortex or dorsal lateral prefrontal cortex, using repetitive transcranial magnetic stimulation in PD patients with freezing gait (Kim et al., 2018), which indicated the important role of SMA in the pathophysiologic processes of gait disorders.

Further FC analysis also exhibited decreased connectivity between the SMA and widespread temporal areas, such as the middle temporal lobe, the superior temporal lobe, and supramarginal gyrus. Previous studies have demonstrated that visuospatial function and vestibular information processing are related to the temporal cortex (Li et al., 2019). It is accepted that both visuospatial and vestibular function are essential for gait and balance maintenance. Structural abnormalities in the temporal lobe and supramarginal gyrus were also reported in previous studies. For instance, gray matter alterations in the superior and middle temporal gyri and supramarginal gyrus (Smith et al., 2015) and FC reductions in the medial temporal gyrus were reported in VBM and rs-fMRI studies (Wang et al., 2016). On the basis of the hypothesis that a connection exists between the temporal gyrus and SMA and that the SMA receives input from the temporal lobe, our finding of decreased FC between the SMA and widespread temporal regions sheds light on the involvement of the temporal lobe via the SMA in the neuropathology of CSVD-GD. The SMA, a pivotal motor-related hub region, was altered at both the regional and network levels in CSVD patients with gait disorders.

Compared with CSVD patients without gait disturbance, GD patients also displayed significant fALFF reductions in the PoCG and the SPL regions. The PoCG served as the hub region in somatosensory network, engaging in daily activities (Fu et al., 2019). According to previous studies, the somatosensory inputs are of great importance in regulating the ongoing movements by feed-forward adjustments (Brooks and Stoney, 1971), which is helpful for posture and gait adjudgment (Takakusaki, 2017). It was also reported that the somatosensory system dominates learning in the early stages of motor skill acquisition (Bernardi et al., 2015). Thus, the decreased integrity of somatosensory networks may suggest the reduced abilities of gait adjudgment and motor learning in patients with CSVD-GD. The SPL is a vital component of the frontoparietal network, a network closely linked to executive function (Jor'dan et al., 2017; Lo et al., 2017), which is implicated in initiating and modulating cognitive control. In previous studies, the SPL has consistently been suggested to be involved in motor coordination and control, especially when speed is decreased and variability is large (Bürki et al., 2017). Thus, the hypofunction of the SPL may be related to ineffective motor control and slow gait speed. This observation is in keeping with the findings of previous fMRI clinical studies, which found that the FC strength within the frontoparietal network was closely correlated with gait speed (Lo et al., 2017). Taken together, the altered patterns of spontaneous low-frequency oscillations in multiple regions implied that the changes in function were not confined to motor areas and that additional widespread somatosensory and frontoparietal network regions were also involved, indicating the important roles of both somatosensory inputs and control roles of cognition on motor function, which was in accordance with a previous study (Takakusaki, 2017).

A further noteworthy finding of the present study is that there were also several regions showing increased fALFF, such as the orbital part of the inferior frontal gyrus, caudate, and precuneus. The inferior frontal gyrus, orbital part, part of the orbitofrontal cortex in the prefrontal cortex, is specifically associated with cognitive processes and involved in processing the motivational or emotional value of incoming information (Rosso et al., 2017), which is suggested to be especially essential for the initiation of motor activities. The precuneus is one of the highest metabolically active brain regions in the default mode network (DMN) during the resting state that directly interacts with other nodes in the default network and participates in monitoring the external environment. Previous studies have confirmed the vital roles of the precuneus in the regulation of body movement by connecting with the precentral gyrus and SMA. The caudate nucleus also receives inputs from various prefrontal regions and plays a major part in task-switching behavior, which can be understood in terms of activating different modules for specialized function (Jarbo and Verstynen, 2015). In the current study, increased local functional connections may serve to compensate adjustments in posture and movement by enhancing the motivation process and interaction with the motor areas. Higher local brain function may act to buffer the detrimental effects of ischemic changes on slower gait.

In addition, we found that the brain FC between the SMA and temporal lobe in CSVD patients was positively related to the gait speed, whereas the fALFF in the left SMA was positively associated with cadence. Gait speed has been consistently treated as the most important factor regarding gait disorders in previous studies, which may be directly associated with incident disability, mortality, and hospitalizations (Studenski et al., 2011; Jung et al., 2018). The correlation of FC and gait speed may imply the important predication role of brain function alteration in slower gait of CSVD. Apart from the gait speed, the cadence is another essential gait parameter, which was associated with the fALFF alteration in the SMA. This was in accordance with a cortical thickness study that found that the cortical area in the SMA was positively related to cadence (de Laat et al., 2012). Based on the aforementioned findings, we suspected that the SMA may be a key region for regulating cadence. Of note, the fALFF of the left SPL was related to both the

velocity and cadence in our study. These results may further emphasize the important roles of frontoparietal network on gait adjustment. In addition, we found that all the altered brain function indicators were correlated with longer time consumption of TUG, suggesting that both the local brain function alteration and network interaction abnormalities may contribute to gait disorder. To further clarify the relationship between structural and functional alterations, both total and regional GMV in the CSVD patients were examined. Relative to controls, CSVD-GD patients exhibited no significant difference in either the total GMV or local GMV based on fALFF and FC alterations. This finding of preserved structure also suggested that functional alterations may precede structural changes. However, further longitudinal studies will be helpful to examine this speculation.

Several limitations involved in this study should be considered. First, although ALFF and FC are promising tools for detecting spontaneous functional activity in the brain, several factors may influence the interpretation of our results, for example, low signal-to-noise ratio of the acquired neuroimaging data, poor temporal resolution, and potential confounding effects on neurovascular coupling (such as concomitant vascular diseases). Thus, we should take caution when interpreting our findings. Second, the sample size was relatively small, which limits the statistical power; thus, the findings of the present study should be considered preliminary. Further study should be carried out to verify the results in the future. Third, the present study was a cross-sectional design, and whether these abnormalities in local brain function and remote connectivity dynamically change should be explored with a follow-up study. In addition, all patients included in the study had no severe muscle power or ankle problems, but we did not explicitly evaluate these factors. Finally, the healthy elderly were not included in the present study, and the differences in mechanism of gait disorder were not further explored in CSVD with different levels of cognitive impairment; classifying and stratifying patients in future studies are needed to extend the understanding of the pathogenesis of gait disorders in CSVD.

CONCLUSION

In the current study, we investigated the possible pathogenesis of CSVD-GD by analyzing resting-state local brain function and large distance connectivity patterns in CSVD patients. The results suggested that abnormal changes in spontaneous function and remote connectivity in the sensorimotor network, frontoparietal network, and DMN may explain gait disorders, instability, and aggravating factors in CSVD patients. These findings might provide novel insights into pathophysiological mechanisms in gait disturbances.

DATA AVAILABILITY STATEMENT

All datasets generated for this study are included in the article/supplementary material.

ETHICS STATEMENT

The studies involving human participants were reviewed and approved by the Institutional Review Board of the first affiliated hospital of Anhui Medical University Subcommittee on Human Studies. The patients/participants provided their written informed consent to participate in this study.

AUTHOR CONTRIBUTIONS

XZho, CZ, and ZS conceived and designed the experiments. LL, YZ, XY, WY, WZ, XZhu, and YQ performed the experiments. XZho, CZ, and YQ analyzed the data and created the figures. XZho and ZS wrote the article and provided the funding. All authors approved the final version of the manuscript.

ACKNOWLEDGMENTS

We thank all the patients for their participation in our study. This work was supported by grants from the National Natural Science Foundation of China (81771154), National Key R & D Program of China (2016YFC1305900), and the Natural Science Foundation of Anhui province (1908085QH322).

REFERENCES

Bernardi, N. F., Darainy, M., Ostry, D. J. (2015). Somatosensory contribution to the initial stages of human motor learning. *J. Neurosci.* 35, 14316–14326. doi: 10.1523/JNEUROSCI.1344-15.2015

Bonini, F., Burle, B., Liégeois-Chauvel, C., Régis, J., Chauvel, P., Vidal, F. (2014). Action monitoring and medial frontal cortex: leading role of supplementary motor area. *Science* 343, 888–891. doi: 10.1126/science.1247412

Brooks, V. B., Stoney, S. D. Jr. (1971). Motor mechanisms: the role of the pyramidal system in motor control. *Annu. Rev. Physiol.* 33, 337–392. doi: 10.1146/annurev.ph.33.030171.002005

Bürki, C. N., Bridenbaugh, S. A., Reinhardt, J., Stippich, C., Kressig, R. W., Blatow, M. (2017). Imaging gait analysis: an fMRI dual task study. *Brain Behav.* 7:e00724. doi: 10.1002/brb3.724

Chen, X., Jin, Y., Chen, J., Chen, X., Cao, X., Yu, L., et al. (2018). Relationship between white matter hyperintensities and hematoma volume in patients with intracerebral hematoma. *Aging Dis.* 9, 999–1009. doi: 10.14336/AD.2018.0108

de Laat, K. F., Reid, A. T., Grim, D. C., Evans, A. C., Kötter, R., van Norden, A. G., et al. (2012). Cortical thickness is associated with gait disturbances in cerebral small vessel disease. *Neuroimage* 59, 1478–1484. doi: 10.1016/j.neuroimage.2011.08.005

de Laat, K. F., Tuladhar, A. M., van Norden, A. G., Norris, D. G., Zwiers, M. P., de Leeuw, F. E. (2011). Loss of white matter integrity is associated with gait disorders in cerebral small vessel disease. *Brain* 134, 73–83. doi: 10.1093/brain/awq343

Fazekas, F., Chawluk, J. B., Alavi, A., Hurtig, H. I., Zimmerman, R. A. (1987). MR signal abnormalities at 1.5 T in Alzheimer's dementia and normal aging. *Am. J. Roentgenol.* 149, 351–356. doi: 10.2214/ajr.149.2.351

Fox, M. D., Raichle, M. E. (2007). Spontaneous fluctuations in brain activity observed with functional magnetic resonance imaging. *Nat. Rev. Neurosci.* 8, 700–711. doi: 10.1038/nrn2201

Fu, J., Chen, X., Gu, Y., Xie, M., Zheng, Q., Wang, J., et al. (2019). Functional connectivity impairment of postcentral gyrus in relapsing-remitting multiple sclerosis with somatosensory disorder. *Eur. J. Radiol.* 118, 200–206. doi: 10.1016/j.ejrad.2019.07.029

Gorelick, M. L., Bizzini, M., Maffiuletti, N. A., Munzinger, J. P., Munzinger, U. (2009). Test-retest reliability of the IDEEA system in the quantification of step parameters during walking and stair climbing. *Clin. Physiol. Funct. Imaging* 29, 271–276. doi: 10.1111/j.1475-097X.2009.00864.x

Jarbo, K., Verstynen, T. D. (2015). Converging structural and functional connectivity of orbitofrontal, dorsolateral prefrontal, and posterior parietal cortex in the human striatum. *J. Neurosci.* 35, 3865–3878. doi: 10.1523/JNEUROSCI.2636-14.2015

Jor'dan, A. J., Poole, V. N., Iloputaife, I., Milberg, W., Manor, B., Esterman, M., et al. (2017). Executive network activation is linked to walking speed in older adults: functional MRI and TCD ultrasound evidence from the MOBILIZE boston study. *J. Gerontol. A Biol. Sci. Med. Sci.* 72, 1669–1675. doi: 10.1093/gerona/glx063

Jung, H. W., Jang, I. Y., Lee, C. K., Yu, S. S., Hwang, J. K., Jeon, C., et al. (2018). Usual gait speed is associated with frailty status, institutionalization, and mortality in community-dwelling rural older adults: a longitudinal analysis of the Aging Study of Pyeongchang Rural Area. *Clin. Interv. Aging*, 13, 1079–1089. doi: 10.2147/CIA.S166863

Kim, S. J., Paeng, S. H., Kang, S. Y. (2018). Stimulation in supplementary motor area versus motor cortex for freezing of gait in parkinson's disease. *J. Clin. Neurol.* 14, 320–326. doi: 10.3988/jcn.2018.14.3.320

Kwon, I., Kim, J. S., Shin, C. H., Park, Y., Kim, J. H. (2019). Associations between skeletal muscle mass, grip strength, and physical and cognitive functions in elderly women: effect of exercise with resistive theraband. *J. Exerc. Nutrition Biochem*. 23, 50–55. doi: 10.20463/jenb.2019.0023

Li, K., Si, L., Cui, B., Ling, X., Shen, B., Yang, X. (2019). Altered spontaneous functional activity of the right precuneus and cuneus in patients with persistent postural-perceptual dizziness. *Brain Imaging Behav*. doi: 10.1007/s11682-019-00168-7

Lima, C. F., Krishnan, S., Scott, S. K. (2016). Roles of supplementary motor areas in auditory processing and auditory imagery. *Trends Neurosci*. 39, 527–542. doi: 10.1016/j.tins.2016.06.003

Lo, O. Y., Halko, M. A., Zhou, J., Harrison, R., Lipsitz, L. A., Manor, B. (2017). Gait speed and gait variability are associated with different functional brain networks. *Front. Aging Neurosci*. 9:390. doi: 10.3389/fnagi.2017.00390

Loos, C. M., McHutchison, C., Cvoro, V., Makin, S. D., Staals, J., Chappell, F., et al. (2018). The relation between total cerebral small vessel disease burden and gait impairment in patients with minor stroke. *Int. J. Stroke* 13, 518–524. doi: 10.1177/1747493017730780

Mathias, S., Nayak, U. S., Isaacs, B. (1986). Balance in elderly patients: the "get-up and go" test. *Arch. Phys. Med. Rehabil.* 67, 387–379.

Navarro-Peternella, F. M., Teston, E. F., Dos Santos Santiago Ribeiro, B. M., Marcon, S. S. (2019). Plantar cutaneous sensory stimulation improves foot sensibility and gait speed in older adults with diabetes: a clinical trial. *Adv. Skin Wound Care* 32, 568–573. doi: 10.1097/01.ASW.0000604196.79133.68

Pinter, D., Ritchie, S. J., Doubal, F., Gattringer, T., Morris, Z., Bastin, M. E., et al. (2017). Impact of small vessel disease in the brain on gait and balance. *Sci. Rep*. 7:41637. doi: 10.1038/srep41637

Rosano, C., Studenski, S. A., Aizenstein, H. J., Boudreau, R. M., Longstreth W. T., Jr., Newman, A. B. (2012). Slower gait, slower information processing and smaller prefrontal area in older adults. *Age Ageing* 41, 58–64. doi: 10.1093/ageing/afr113

Rosario, B. L., Rosso, A. L., Aizenstein, H. J., Harris, T., Newman, A. B., Satterfield, S., et al. (2016). Cerebral white matter and slow gait: contribution of hyperintensities and normal-appearing parenchyma. *J. Gerontol. A Biol. Sci. Med. Sci*. 71, 968–973. doi: 10.1093/gerona/glv224

Rosso, A. L., Verghese, J., Metti, A. L., Boudreau, R. M., Aizenstein, H. J., Kritchevsky, S., et al. (2017). Slowing gait and risk for cognitive impairment: the hippocampus as a shared neural substrate. *Neurology* 89, 336–342. doi: 10.1212/WNL.0000000000004153

Sato, K., Aita, N., Hokari, Y., Kitahara, E., Tani, M., Izawa, N., et al. (2019). Balance and gait improvements of postoperative rehabilitation in patients with parkinson's disease treated with subthalamic nucleus deep brain stimulation (STN-DBS). *Parkinsons Dis*. 2019:7104071. doi: 10.1155/2019/7104071

Shen, Y. T., Li, J. Y., Yuan, Y. S., Wang, X. X., Wang, M., Wang, J. W., et al. (2018). Disrupted amplitude of low-frequency fluctuations and causal connectivity in Parkinson's disease with apathy. *Neurosci. Lett*. 683:75–81. doi: 10.1016/j.neulet.2018.06.043

Shumway-Cook, A., Brauer, S., Woollacott, M. (2000). Predicting the probability for falls in community-dwelling older adults using the Timed Up & Go Test. *Phys. Ther*. 80, 896–903. doi: 10.1093/ptj/80.9.896

Smith, E. E., O'Donnell, M., Dagenais, G., Lear, S. A., Wielgosz, A., Sharma, M., et al. (2015). Early cerebral small vessel disease and brain volume, cognition, and gait. *Ann. Neurol*. 77, 251–261. doi: 10.1002/ana.24320

Studenski, S., Perera, S., Patel, K., Rosano, C., Faulkner, K., Inzitari, M., et al. (2011). Gait speed and survival in older adults. *JAMA* 305, 50–58. doi: 10.1001/jama.2010.1923

Su, N., Liang, X., Zhai, F. F., Zhou, L. X, Ni, J., Yao, M., et al. (2018). The consequence of cerebral small vessel disease: linking brain atrophy to motor impairment in the elderly. *Hum. Brain Mapp*. 39, 4452–4461. doi: 10.1002/hbm.24284

Takakusaki, K. (2017). Functional neuroanatomy for posture and gait control. *J. Mov. Disord*. 10, 1–17. doi: 10.14802/jmd.16062

van der Holst, H. M., Tuladhar, A. M., Zerbi, V., van Uden, I., de Laat, K. F., van Leijsen, E., et al. (2018). White matter changes and gait decline in cerebral small vessel disease. *Neuroimage Clin.* 17, 731–738. doi: 10.1016/j.nicl.2017.12.007

van der Holst, H. M., van Uden, I. W., Tuladhar, A. M., de Laat, K. F., van Norden, A. G., Norris, D. G., et al. (2016). Factors associated with 8-year mortality in older patients with cerebral small vessel disease: the radboud university nijmegen diffusion tensor and magnetic resonance cohort (RUN DMC) study. *JAMA Neurol.* 73, 402–409. doi: 10.1001/jamaneurol.2015.4560

Wang, M., Jiang, S., Yuan, Y., Zhang, L., Ding, J., Wang, J., et al. (2016). Alterations of functional and structural connectivity of freezing of gait in Parkinson's disease. *J. Neurol.* 263, 1583–1592. doi: 10.1007/s00415-016-8174-4

Yan, C. G., Wang, X. D., Zuo, X. N., Zang, Y. F. (2016). DPABI: data processing & analysis for (Resting-State) brain imaging. *Neuroinformatics* 14, 339–351. doi: 10.1007/s12021-016-9299-4

Yang, L., Yan, Y., Wang, Y., Hu, X., Lu, J., Chan, P., et al. (2018). Gradual disturbances of the amplitude of low-frequency fluctuations (ALFF) and fractional ALFF in Alzheimer spectrum. *Front. Neurosci*. 12:975. doi: 10.3389/fnins.2018.00975

Zou, Q. H., Zhu, C. Z., Yang, Y., Zuo, X. N., Long, X. Y., Cao, Q. J., et al. (2008). An improved approach to detection of amplitude of low-frequency fluctuation (ALFF) for resting-state fMRI: fractional ALFF. *J. Neurosci. Methods* 172, 137–141. doi: 10.1016/j.jneumeth.2008.04.012

Zuo, X. N., Di Martino, A., Kelly, C., Shehzad, Z. E., Gee, D. G., Klein, D. F., et al. (2010). The oscillating brain: complex and reliable. *Neuroimage* 49, 1432–1445. doi: 10.1016/j.neuroimage.2009.09.037

Conflict of Interest: The authors declare that the research was conducted in the absence of any commercial or financial relationships that could be construed as a potential conflict of interest.

frontiers in Genetics

ORIGINAL RESEARCH
published: 15 September 2020
doi: 10.3389/fgene.2020.01022

Insulin-Independent and Dependent Glucose Transporters in Brain Mural Cells in CADASIL

Mahmod Panahi[1], Patricia Rodriguez Rodriguez[1], Seyed-Mohammad Fereshtehnejad[2,3], Donia Arafa[1], Nenad Bogdanovic[2,4], Bengt Winblad[1], Angel Cedazo-Minguez[1], Juha Rinne[5], Taher Darreh-Shori[2], Yoshiki Hase[6], Raj N. Kalaria[6†], Matti Viitanen[2,7†] and Homira Behbahani[1*†]*

[1] Department of Neurobiology, Care Sciences and Society, Center for Alzheimer Research, Division of Neurogeriatrics, Karolinska Institutet, Stockholm, Sweden, [2] Department of Neurobiology, Care Sciences and Society, Division of Clinical Geriatrics, Karolinska Institutet, Huddinge, Sweden, [3] Department of Neurology and Neurosurgery, McGill University, Montreal, QC, Canada, [4] Neurogeriatric Clinic, Karolinska University Hospital, Huddinge, Sweden, [5] University of Turku, Turku University Hospital Kiinanmyllynkatu, Turku, Finland, [6] Translational and Clinical Research Institute, Newcastle University, Newcastle upon Tyne, United Kingdom, [7] Department of Geriatrics, Turun Kaupunginsairaala, University Hospital of Turku, University of Turku, Turku, Finland

Typical cerebral autosomal-dominant arteriopathy with subcortical infarcts and leukoencephalopathy (CADASIL) is caused by mutations in the human NOTCH3 gene. Cerebral autosomal-dominant arteriopathy with subcortical infarcts and leukoencephalopathy is characterized by subcortical ischemic strokes due to severe arteriopathy and fibrotic thickening of small vessels. Blood regulating vascular smooth muscle cells (VSMCs) appear as the key target in CADASIL but the pathogenic mechanisms remain unclear. With the hypothesis that brain glucose metabolism is disrupted in VSMCs in CADASIL, we investigated post-mortem tissues and VSMCs derived from CADASIL patients to explore gene expression and protein immunoreactivity of glucose transporters (GLUTs), particularly GLUT4 and GLUT2 using quantitative RT-PCR and immunohistochemical techniques. *In vitro* cell model analysis indicated that both GLUT4 and -2 gene expression levels were down-regulated in VSMCs derived from CADASIL patients, compared to controls. *In vitro* studies further indicated that the down regulation of GLUT4 coincided with impaired glucose uptake in VSMCs, which could be partially rescued by insulin treatment. Our observations on reduction in GLUTs in VSMCs are consistent with previous findings of decreased cerebral blood flow and glucose uptake in CADASIL patients. That impaired ability of glucose uptake is rescued by insulin is also consistent with previously reported lower proliferation rates of VSMCs derived from CADASIL subjects. Overall, these observations are consistent with the development of severe cerebral arteriopathy in CADASIL, in which VSMCs are replaced by widespread fibrosis.

Keywords: CADASIL, GLUT4, GLUT2, VSMCs, stroke

OPEN ACCESS

Edited by:
Satoshi Saito,
National Cerebral and Cardiovascular Center (Japan), Japan

Reviewed by:
Toshiki Mizuno,
Kyoto Prefectural University of Medicine, Japan
Yun Yuan,
Peking University First Hospital, China

***Correspondence:**
Raj N. Kalaria
raj.kalaria@newcastle.ac.uk;
r.n.kalaria@ncl.ac.uk
Homira Behbahani
homira.behbahani@ki.se

† These authors share senior authorship

Specialty section:
This article was submitted to Genetics of Aging, a section of the journal Frontiers in Genetics

Received: *24 April 2020*
Accepted: *10 August 2020*
Published: *15 September 2020*

Citation:
Panahi M, Rodriguez PR, Fereshtehnejad S-M, Arafa D, Bogdanovic N, Winblad B, Cedazo-Minguez A, Rinne J, Darreh-Shori T, Hase Y, Kalaria RN, Viitanen M and Behbahani H (2020) Insulin-Independent and Dependent Glucose Transporters in Brain Mural Cells in CADASIL. Front. Genet. 11:1022. doi: 10.3389/fgene.2020.01022

INTRODUCTION

Cerebral autosomal-dominant arteriopathy with subcortical infarcts and leukoencephalopathy (CADASIL) is a hereditary disease resulting from mutations of the NOTCH3 gene (Joutel et al., 1996). The initial clinical manifestation often presents as migraine with aura or minor cerebral attacks (Burkett and Dougherty, 2017) (which usually occurs during the third decade of life) and progresses to subcortical ischemic attacks, mood disturbance, cognitive decline, encephalopathy and white matter (WM) changes (Choi, 2015; Di Donato et al., 2017).

The pathological hallmarks of CADASIL are (i) a finding of granular osmiophilic material (GOM) in close proximity to vascular smooth muscle cells (VSMCs) and (ii) fibrotic thickening of small penetrating arteries. GOM can be observed under electron microscopy from skin biopsy samples, making it a suitable primary diagnostic indicator for CADASIL. Additionally, the fibrotic thickening of small vessels results in stenosis, thereby reducing blood flow and causing the ischemic attacks characteristic of CADASIL (Wang, 2018). Histopathological findings show there is severe degeneration of brain VSMCs surrounding the thickened arteries, with the cause being investigated under various hypotheses (Tikka et al., 2014). Some studies suggest that the reduced number of VSMCs is a consequence of increased apoptosis (Wang et al., 2002; Formichi et al., 2009). Other studies have reported that a reduced quantity of VSMCs may reflect a lower proliferation rate (Takahashi et al., 2010) rather than a higher apoptotic rate (Wang et al., 2002; Ihalainen et al., 2007; Viitanen et al., 2013).

In contrast to the ongoing investigations on proliferation and apoptotic rates in VSMCs (Takahashi et al., 2010), no study to-date is available that investigates the metabolic requirements and possible metabolic deficiencies in VSMCs of patients with CADASIL. Another unexplored issue concerns the lack of investigation of a possible association between glucose transport and CADASIL, particularly in VSMCs, although numerous studies have reported association between NOTCH3 and glucose transporters (GLUT) in other disease models (Santio et al., 2016; Altalhi et al., 2017; Chang et al., 2017).

Glucose is the main energy source in mammalian cells and its movement across the plasma membrane is facilitated by transporters, mainly GLUTs (Szablewski, 2017). Although several GLUTs have been identified in VSMCs, we decided to focus on GLUT2 and -4 as they have previously been implicated in other disease models (Pyla et al., 2013). GLUT4 is an insulin-dependent GLUT (Brosius et al., 1992; Cooper et al., 1993; Standley and Rose, 1994; Kahn et al., 1995; Banz et al., 1996) whereas GLUT2 is, in contrast, an insulin-independent transporter (Pyla et al., 2013). In non-stimulated cells, GLUT4 exists predominately perinuclear, but upon insulin stimulation it is translocated to the cell membrane for active transport of glucose into the cell (Park et al., 2005). In hypertension animal models, both aortic and carotid artery VSMCs show a several-fold decrease in GLUT4 gene expression, followed by reduced glucose uptake ability (Atkins et al., 2001). Interestingly, these animal models show GLUT4 insulin insensitivity with regard to VSMCs, but this phenomenon is not observed in other vessels suggesting that these VSMCs are key pressure regulators and more prone to insulin insensitivity than other VSMCs (Atkins et al., 2001). In other diseases, such as diabetes, GLUT4 seems to have been down regulated (Marcus et al., 1994), thereby indicating a lowered glucose uptake capacity in VSMCs with a possible consequence in contractibility of the blood vessels.

The most common technique for studying the role of glucose metabolism in CADASIL patients is positron emission tomography (PET) scan with 18-fluorodeoxyglucose (FDG; Tuominen et al., 2001, 2004; Tatsch et al., 2003). Early studies have implicated low cerebral blood flow as the cause of low glucose uptake in the central nervous system (Tuominen et al., 2004). It is reasonable to extrapolate from those findings that CADASIL patients would exhibit lower cerebral blood flow due to small vessel stenosis, which in turn would result in a reduced cerebral glucose metabolic rate estimated by FDG-PET (Tuominen et al., 2004; Yoon et al., 2015). In fact, a correlation has been demonstrated between low cerebral blood flow and hypo-metabolism of glucose assessed by FDG-PET (Tuominen et al., 2001). However, impaired glucose metabolism assessed by 2-deoxy-D-glucose (2DG-) or FDG-PET could also be caused by reduced total glucose transport into the brain rather than only neuronal hypometabolism *per se* since FDG-PET measures the amount of the phosphorylated tracer (and, hence, trapped glucose analogs in the brain cells) as opposed to actual cellular metabolism (Southworth et al., 2003). Moreover, other studies have confirmed that CADASIL patients have glucose hypo-metabolism, but the cause of this has not been completely elucidated (Tatsch et al., 2003).

Reduced glucose uptake could also explain both atrophy of VSMCs via either an altered proliferation or apoptosis rate (Takahashi et al., 2010; Viitanen et al., 2013; Panahi et al., 2018). We hypothesized that cerebral VSMCs have defective glucose uptake, which may be partially responsible for the previously described glucose hypometabolism assessed by PET in brains of CADASIL patients. In the present study, we used cerebral VSMCs-models derived from CADASIL patients and relevant controls and post-mortem brain tissues to investigate the expression level of key GLUTs. We focused on the insulin-insensitive GLUT2 and the insulin-sensitive GLUT4 in particular since GLUT4 has been implicated in other vascular diseases, such as diabetes-related cerebral small vessel disease (SVD; Vermeer et al., 2007; Palacio et al., 2014; Umemura et al., 2017).

MATERIALS AND METHODS

Cell Lines and Culture

Cerebral VSMCs were established from genetically verified CADASIL patients with C133R mutation and control subjects as previously described (Panahi et al., 2018). Patient-derived cerebral arterial VSMC ($VSMC^{R133C}$) as well as control VSMC ($VSMC^{WT}$) cell lines were established from *post mortem* subarachnoidal branches of cerebral arteries (human cerebral arterial VSMC) by collagenase digestion as described previously (Gimbrone et al., 1974; Ihalainen et al., 2007; Tikka et al., 2012). Briefly, post-mortem brain samples were collected within 24 h

of death and all cell cultures were planned and established immediately after obtaining the samples. Small blocks of brain tissue (1-2 cm × 1-2 cm) were cut, fragmented with razor blades and the tissues surrounding the vessels (diameter approximately 0.4–1 mm) were removed with sterile scalpels. The fragments were then transferred to tubes with ice-cold 20 mM HEPES in Dulbecco's modified Eagle's medium (DMEM; Life Technologies, United States), centrifuged for 5 min at 500 × *g* at RT. After discarding the supernatant, tissues were resuspended in 0.05% collagenase/dispase mixture (100 μg/mL, Roche) in 20 mM HEPES in DMEM, and incubated for 5 min at RT. The tissues were homogenized usinga10 mL pipette for every 5 min and the undigested material was removed by centrifugation at 1000 × *g* for 10 min at RT. The pellets were washed with 10 mL of PBS (with calcium and magnesium) four times following resuspension in 10 mL complete culture medium containing 10% FBS 2 mM L-glutamine, 100 U/mL penicillin and 100 μg/mL streptomycin at RT. Approximately, 1.5 mL aliquots of the free vessels in solution were transferred into sterile 12-well cell culture plates and incubated at 37°C and 5% CO_2 in a humidified environment. The media were changed every 2^{nd} day and once the vessels had settled down at the bottom of the wells (∼3 days) observing out-crawling cells from the tissues and their confluency, the smooth muscle cells were harvested using 0.25% trypsin for further culturing into 35-mm cell culture dishes (1:1.23 surface ratio) (Gauthier et al., 2012). For partial immortalization, the cells were infected with a human papilloma virus construct E6/E7 at early passage (p1 to p3). The infection was verified by culturing the cells in the presence of G418 (Invitrogen, Auckland, NZ, United States) (400 μg/mL) for a 10-day period. Primary cells (passage 1) were confirmed to be VSMC using the marker α-smooth muscle actin (α-SMA). After the viral infection (passage 2–5), all VSMC lines were screened negative for mycoplasma using the VenorGeM mycoplasma detection kit (Minerva Biolabs GmbH, Berlin, Germany) and with DAPI staining.

Vascular smooth muscle cells (CADASIL and control) were routinely cultured in DMEM]/F-12, GlutaMAX medium (Life Technologies, United States) supplemented with 10% heat inactivated fetal bovine serum (FBS), 1% Penicillin-Streptomycin and 1% L-glutamine. The cell lines were kept in an incubator with 5% CO_2 at 37°C. Passages of cells were matched for each experiment and were between 18 and 28. Umbilical artery smooth muscle cells (UASMC, Lonza) were cultured in smooth muscle cell medium BulletKit according to the manufacturer's instructions or cultured in M 231 medium with smooth muscle growth supplement (Life Technologies) (Panahi et al., 2018).

Real Time Quantitative PCR

Vascular smooth muscle cells (CADASIL and control) were grown overnight in a six-well plate chamber with confluence of 100,000 cells. The following day, the cells were lysed with RIPA buffer (Thermo Fisher Scientific, United States) and the quality of RNA was determined with RIN (RNA Integrity Number) of 10. cDNA was prepared using Taqman gene expression master mix (Applied Biosystem) and SuperScript VILO cDNA Synthesis kit (Thermo Fisher Scientific, United States) according to the manufacturer's protocol. Quantitative (q)RT-PCR was performed using costume format TaqMan fast plate (Applied Biosystems; No. 4427562, Rev C)[1]. The gene designations for control and *GLUTs* were: *HPRT1*-Hs99999909_m1 (endogenous control), *GAPDH*-Hs99999905_m1 (endogenous control), 18S-Hs99999901_s1, *SLC2A2*-Hs01096908_m1; *SLC2A3*-Hs00359840_m1, and *SLC2A4*-Hs00168966_m1. All probes were used in duplicates with 30 ng of cDNA. Quantitative RT-PCR was performed on a 7500 Fast Real-Time PCR System (Life Technologies, United States). The expressions of genes were normalized to internal control HPRT gene and analysis was used comparing the normalized value of control cell line to the normalized values of CADASIL cell line. All the quantitative data were from three independent biological replicates for each experiment and the control value was normalized to 1.

Immunofluorescent Staining of GLUT4 in VSMC Cells

For VSMCs staining, 3.0 × 10^4 cells were seeded onto 8-well chamber slides (Lab-Tek) for 48 h. The cells were grown until 80% confluency, harvested, washed twice with PBS and fixed with paraformaldehyde (PFA; 4% v/v, Sigma-Aldrich) for 10 min. Following blocking with the Bovine Serum Albumin (BSA; 1% w/v) for 30 min, the cells were permeabilized with Triton X-100 (0.1% v/v, Sigma-Aldrich) for 30 min at RT. Later, cells were incubated with goat anti-GLUT4 (C-20m Santa Cruz) primary antibody overnight at 4°C. Subsequently, the cells were washed and incubated with conjugated secondary Alexa Fluor 488 antibody for 1 h at RT. The slides were mounted with DAPI. Vascular smooth muscle cells were examined using a laser scanning confocal microscope (LSM 510 META, ZEISS).

Immunoblotting of VSMCs

Vascular smooth muscle cells (CADASIL and control) grown to 80% confluence were harvested by scraping from the plate after washing twice with PBS. Cells were collected by 5 min centrifugation at 300 *g*, and lysed in lysis buffer (0.65% NP40, 10 mM Tris pH 8.0, 1 mM EDTA, 150 mM NaCl) containing protease inhibitor (100×, ProteaseArrest G-Biosciences). The total protein content was measured using the Pierce bicinchoninic acid (BCA) protein assay kit (Thermo Fisher Scientific). Laemmli sample buffer (2× LDS, Sigma-Aldrich) was added to the samples. 2× LDS sample buffer (Invitrogen) was used for SDS-PAGE and immunoblotting as previously described (Behbahani et al., 2010). For GLUT4, a rabbit polyclonal antibody (H-43: sc-7903, Santa Cruz Biotechnology), and rabbit polyclonal Cpt1C (carnitine palmitoyltransferase I) antibody (**Supplementary Figure S1**) was purchased from abcam (ab87498, United States).

Functional Glucose Uptake Assay Using NBDG-Flow Cytometry

First, the cells were incubated and grown in DMEM (Life Technologies, United States) without the additional FBS

[1]https://www.thermofisher.com/order/taqman-files

and glucose for 24 h to a monolayer confluence. Later, the medium was removed and cells were washed 3× with PBS Krebs ringer phosphate buffer with 50 mM glucose and 200 μM 2-NBDG (2-(*N*-(7-Nitrobenz-2-oxa-1,3-diazol-4-yl)Amino)-2-Deoxyglucose) (Thermo Fisher Scientific, United States) was added to the cell layer. Cells were incubated with and without 50 mM insulin for 30 min. The cells were harvested and the 2-NBDG uptake was measured by flow cytometry using a FACSCalibur™ Cytometry (BD Biosciences, United States). Approximately, 10,000 events were collected for each analysis. Data from the experiments were analyzed using the CellQuest software (BD Biosciences, United States).

Human Brain Tissues

Table 1 provides demographic details and diagnoses in the subjects used in immunohistochemical studies (Craggs et al., 2014). The mean age of CADASIL subjects were not different from mean ages of controls. Available case notes and radiological reports indicated that CADASIL subjects showed extensive WM changes consistent with SVD of the brain and met the minimum criteria for cognitive impairment (Allan et al., 2011; Skrobot et al., 2018). Majority of the CADASIL subjects had no known vascular disease risk (Craggs et al., 2014). However, one patient each had exhibited cardiac arrythmias, obesity and >10 year smoking history. The diagnosis of CADASIL was confirmed by the presence of *NOTCH3* gene mutations or the presence of GOM in arteries within skin biopsies (Yamamoto et al., 2009). None of the controls had neurological or pathological evidence for cerebrovascular disease or neurodegenerative disorder.

For immunohistochemical analyses, the brain tissues from CADASIL subjects (frontal and occipital lobes) and aged-matched controls were from the Newcastle Brain Tissue Resource (NBTR), Newcastle University, Campus for Ageing and Vitality, and the Swedish Brain Bank (Stockholm, KI). All studies involving human subjects have been approved by the local research ethics committee of the Newcastle; the NBTR committee, and the Regional Ethical Review Board in Stockholm or the Research Ethics Committee of the South Huddinge University Hospital.

Immunofluorescence Staining and Confocal Microscopy

Immunofluorescence staining was performed on 5 μm sections of formalin-fixed paraffin-embedded (FFPE) frontal cortex of post-mortem brains. The sections were de-paraffinzed and hydrated through xylene and graded alcohol series. The sections were autoclaved with antigen retrieval buffer (DV2004, DIVA Decloaker, Biocare Medical) for 30 min at 110°C (Decloaking Chamber NxGen, Biocare Medical). After the temperature decreased to room temperature (RT), sections were washed with water for 5 min and then in Tris-Buffered Saline (TBS) + 0.05% Tween 20 (TBS-T) (91414, Sigma-Aldrich). The sections were blocked with Background Punisher (BP974, Biocare Medical) for 10 min at RT followed by washing and incubation with primary antibodies; α-SMA antibody (Abcam, SMA, 1:500, Clone 1A4, Abcam, United States), as an indicator for VSMC, and GLUT4 (ab48547, 1:500, Abcam, United States) and GLUT2 antibodies (ab54460, 1:500, Abcam, United States), in TBS-T (overnight 4°C, humid chamber).

After washing in TBS-T, sections were incubated (1 h at RT) with appropriate secondary antibodies [anti-mouse and anti-rabbit IgG (H + L)] conjugated to Alexa Fluor 546 or Alexa Fluor 488 (Invitrogen) at a concentration of 1:500 in TBS-T. To reduce auto-fluorescence, the slides were further washed in TBS-T (3 × 10 min) and incubated with or without Sudan Black B (199664, Sigma-Aldrich), 5 min at RT. Sections were then washed in TBS-T and were mounted with DAPI Vectashield Hard Set (H-1200, Vector Laboratories) and the slides were stored at 4°C. Sections from controls and patients were also incubated without primary antibody and used as negative control. Quantification of cerebral vessels was undertaken essentially as described previously (Craggs et al., 2015). We focused on vessels of size 50-300 μm in diameter consisting largely of arterioles. The appropriate gray and while matter boundaries were delineated by the DAPI background staining within tissue sections.

Imaging Analysis

Sections were examined using a laser scanning confocal microscope (LSM 510 META, ZEISS, or core Facility Bionut Microscopy), and images were acquired using the same settings (laser intensity, detector gain and amplifier offset). Also,

TABLE 1 | Demographic details of CADASIL subjects and controls.

Group (*n*)[#]	Age (year) (Range)	Gender distribution	*NOTCH3* Mutation Type (no)	Duration (year)	Notable clinical features and risk factors
CADASIL* (14)	59.0 ± 8.0 (33–74)	9M/5F	Arg133Cys (6); Arg141Cys (2); Arg153Cys (2); Arg169Cys (2); Arg558Cys (1); Arg985Cys (1)	6–28	Majority of cases did not have preexisting vascular risk factors. Cardiac arrhythmias (1); Brief history of gout (1); obesity (1); prostate tumor (1); smoking history (3)
Controls (13)	65.7 ± 8.1 (49–78)	5M/8F	–		No significant cerebrovascular or neurodegenerative disorder. No pathological diagnosis

*Cases and controls used for the various experiments. *The MMSE scores for the patients ranged from 12 to 24 (not available for all cases). Controls, mean age was not significantly different from that of CADASIL group ($p > 0.05$). [#]There are three samples each from the Swedish Brain Bank.*

the tissues fluorescence staining was recorded sequentially in separate channels with Plan-Apochromate 20× (NA, 0.8), 40× (NA, 1.2) oil and 100× (NA, 1.45) oil objectives. Image processing was performed with the included ZEN software. Cell quantifications were performed with Neurolucida. Fluorescence intensity was measured with the ImageJ 1.383 software (NIH, MA, United States).

Statistical Analyses

Statistical comparison of values between groups was measured by one-way ANOVA followed by Bonferroni's *post hoc* test. Student *t*-test was used for two-group comparisons. p-values < 0.05 were considered significant. The results are representative of three independent biological replicates expressed as mean ± SEM. All univariate and multivariate analyses were performed using *IBM SPSS Statistics* software (version 23.0). A two-tailed p-value of <0.05 was considered as the threshold for statistically significant differences or associations in all analyses.

RESULTS

GLUT4 Is Down-Regulated in CADASIL VSMCs

To shed light on the mechanism of previously observed lower FDG-PET value in the CADASIL subjects (Tuominen et al., 2004), we investigated gene expression levels of GLUT isoforms [*SLC2A2* (GLUT2), *SLC2A3* (GLUT3), and *SLC2A4* (GLUT4)] in VSMC models of CADASIL and control subjects.

Quantitative RT-PCR revealed significantly decreased *SLC2A2* and *SLC2A4* gene expressions in CADASIL VSMCs compared to controls ($p < 0.001$, and $p < 0.01$, respectively) (**Figure 1**). *SLC2A3* gene expression tended to be lower but was only different from *SLC2A2* and *SLC2A4*. Since the insulin-dependent transporter GLUT4 was previously assessed in hypertension models and in diabetes as a model of small vessel disease, we focused on this specific transporter for the gene product studies in relation to the insulin-independent GLUT2. In view of the findings on *SLC2A3* gene expression we did not perform further protein studies on GLUT3.

Using confocal microscopy analysis, we also observed reduced GLUT4 and GLUT2 expressions in CADASIL VSMCs. Quantification of GLUT4 and GLUT2 distribution in these cells showed significant lower expression of GLUTs in CADASIL VSMCs compared to controls (**Figures 2A,B,E,F**). Furthermore, immunoblotting analysis showed reduced GLUT4 protein levels in CADASIL VSMCs compared to control (**Figures 2C,D,G,H**). These data together suggest that the glucose uptake receptors are impaired in these arterial cells.

Glucose Uptake Is Not Affected by Insulin in CADASIL VSMCs

Low GLUT expression in CADASIL VSMCs suggests that these cells have potentially lower glucose uptake ability. VSMCs derived from CADASIL also exhibited a lower proliferation rate compared to VSMCs from control (Panahi et al., 2018).

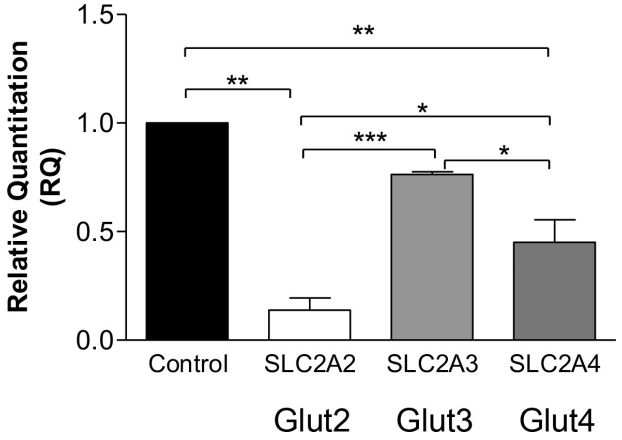

FIGURE 1 | Glucose transporters gene expression in CADASIL compared to control VSMCs. qRT-PCR analysis of GLUT2 (*SLC2A2*), GLUT3 (*SLC2A3*), and GLUT4 (*SLC2A4*), genes in CADASIL and control VSMCs. The expression of GLUT2, GLUT3, and GLUT4 genes were normalized to the endogenous control gene; HPRT1, and the RQ (Relative Quantitation) was calculated using control VSMC normalized to 1. $*p < 0.05$, $**p < 0.01$ and $***p < 0.001$. The results are representative of three independent replicates ($n = 3$). One-way ANOVA followed by Bonferroni's *post hoc* test was used for statistical analysis.

Therefore, we hypothesized that lower proliferation rate might be due to the lower glucose uptake ability of VSMCs in CADASIL.

An experimental procedure was set up to measure the uptake of glucose in both CADASIL and control VSMCs. Validation of glucose uptake was carried out using 2-NDBG, a fluorescent indicator for monitoring glucose uptake into living cells, which could be assessed by flow cytometry. Flow cytometry analyses showed that CADASIL VSMCs had a significantly lower glucose uptake capability ($p < 0.05$), most likely reflecting the lower gene expression of GLUT in CADASIL VSMCs (**Figure 3**). These analyses indicated that the reduced gene expression was in line with an overall functional effect.

To further confirm the above findings, we assessed the extent to which insulin could rescue the deficit in glucose uptake in the cellular model of CADASIL. The results indicated that insulin rescued glucose uptake by ∼10% in both CADASIL and control VSMCs. Since GLUT4 is an insulin-sensitive transporter, the findings suggest that GLUT4 is functional in CADASIL VSMCs and, hence, the observed differences are mainly related to an altered GLUT-4 gene expression in CADASIL VSMCs (**Figure 3**). Considering that gene expression analyses indicated that reduced gene expression of GLUTs occurs in the following order GLUT2 > GLUT4 > GLUT3 in CADASIL VSMCs (see **Figure 1**) and that GLUT2 is an insulin-independent transporter, the functional result here, further suggested that overall altered glucose uptake in CADASIL VSMCs is caused by both insulin-dependent and insulin-independent transport mechanisms. We also found that carnitine palmitoyltransferase I (Cpt1), specifically the Cpt1c isoform, highly expressed in brain (Schreurs et al., 2010), did not differ between the control VSMCs and CADASIL VSMCs (**Supplementary Figure S1**). This indicated that the reduced glucose uptake in VSMCs was not

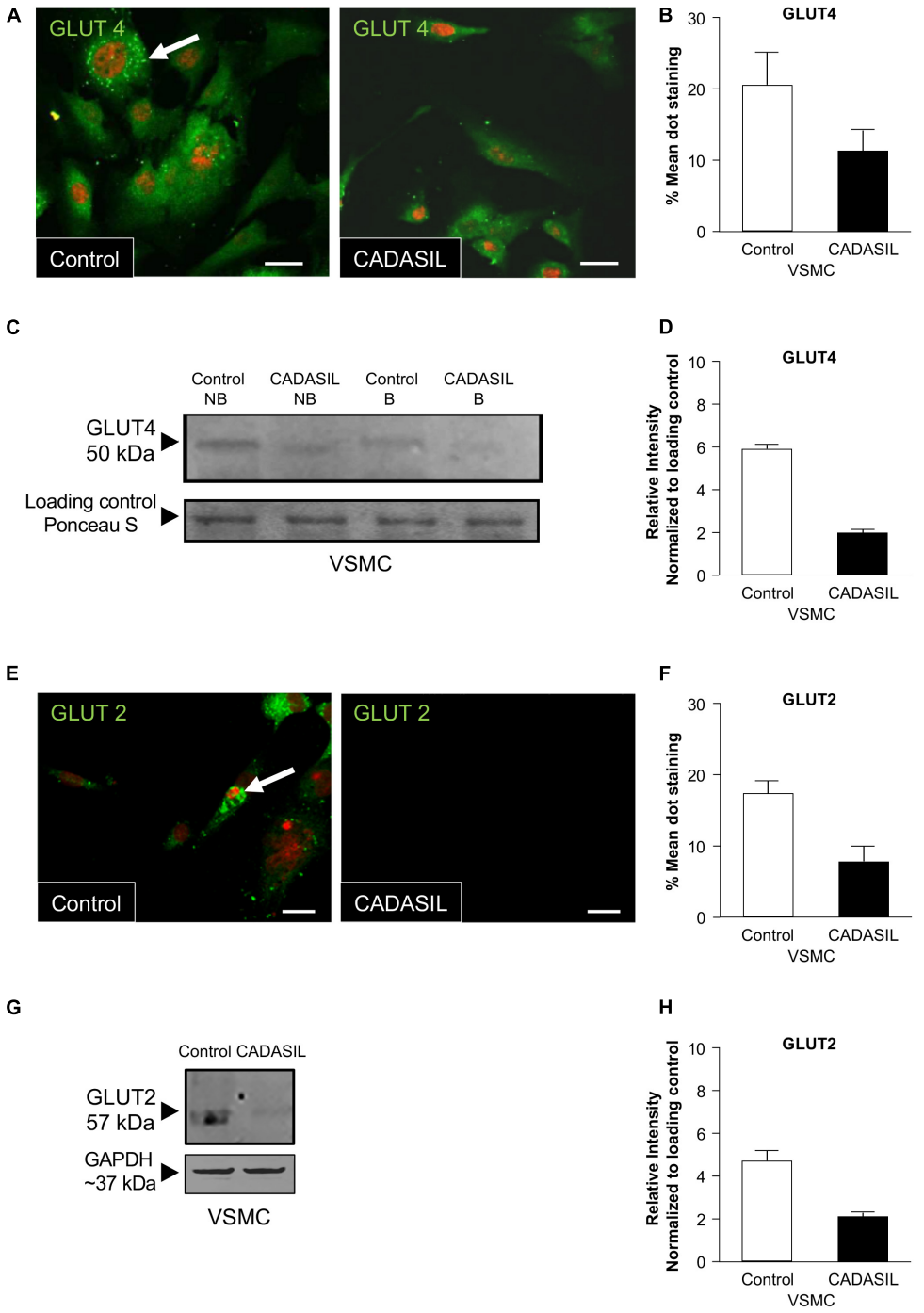

FIGURE 2 | GLUT4 expression in CADASIL compared to control VSMCs. PFA-fixed VSMCs were immunostained with goat anti-GLUT4 and GLUT2 antibodies, visualized using confocal microscopy and assessed for expression of the GLUTs. **(A,E)** Images of VSMCs stained for GLUT4 and GLUT 2 using an Alexa Fluor-conjugated 488 secondary antibody. GLUT dot-staining is shown in green (arrows) and Nuclei are stained with DAPI (here showed in fluoresces red). Representative images were taken from one experiment ($n = 3$), Scale bar, 10 μm. **(B,F)** Mean values of GLUT4 and GLUT2 dot-staining in control and CADASIL VSMCs. Each data point represents mean of intensely fluorescent GLUT-positive dots per cell in 12 cells from 3 independent experiments ($n = 3$) (*$p < 0.05$). **(C,G)** Immunoblotting analyses, non-boiled (NB) and boiled samples (B) were conducted to assess the expression of GLUT4 in VSMCs. The samples were visualized using the Odyssey CLx Imager. 15 μg of protein was loaded into the gel and ponceau S staining was used as loading control. The intensity of the GLUT4 and GLUT2 band was lower than in both CADASIL boiled and non-boiled samples as compared to control VSMC lysates **(D,H)** Densitometry data from CADASIL and control protein bands normalized to Ponceau S total protein stain showed lower expression of GLUT4 and GLUT2 in CADASIL VSMCs than in controls. The immunoblot is representative of one experiment.

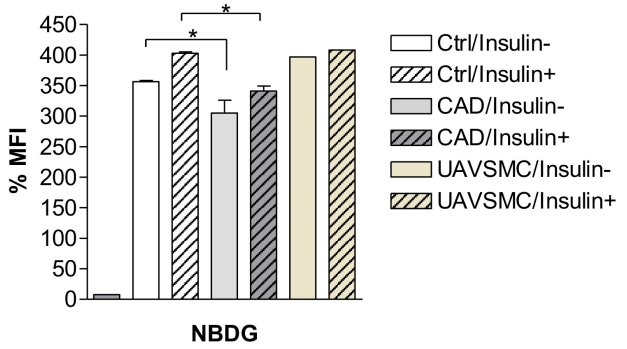

FIGURE 3 | Effects of Insulin on Glucose uptake in CADASIL VSMCs. The VSMCs (CADASIL, control and UAVSMCs) were cultured and 200 μM 2-NBDG; a fluorescent indicator for monitoring glucose uptake, was added to the cells (M&M), incubated with and without 50 mM insulin. The 2-NBDG uptake was measured by flow cytometry. Flow cytometry analysis showed a reduced glucose uptake before addition of insulin in CADASIL VSMCs (*$p < 0.05$), however, lower glucose uptake was not affected by insulin in CADASIL VSMCs. Ctrl: control VSMC, CAD: CADASIL, MFI: mean fluorescence intensity, UAVSMC: Umbilical artery smooth muscle cells.

associated with changes in beta-oxidation of fatty acids and insulin sensitivity in the VSMCs.

GLUT4 and GLUT2 Expression Level in Brain Tissues From CADASIL Subjects

Our observations were based on cellular experiments derived from patients with the *NOTCH3* C133R mutation. However, to validate our findings, and to test if there was any association between GLUTs and other mutations, we assessed the expression level of GLUT2 and GLUT4 in post-mortem brain tissues from CADASIL and controls using immunohistochemical techniques and analyzed the results using confocal microscopy. Confocal analysis of multiple brain tissues revealed increased GLUT4 immunoreactivity in control samples compared to CADASIL samples (**Figure 4**). Furthermore, an association of GLUT4 expression with different *NOTCH3* mutations was observed in CADASIL subjects compared to controls (**Figures 4A–D**). We also found that there were no clear differences in GLUT expression in the 3 CADASIL subjects who exhibited previous vascular disease risk compared to those who did not. Preliminary observations indicated that there was also a correlation between vessel diameter and GLUT4 expression (data not shown), but further investigation is needed to confirm this finding.

We observed that the smaller the vessel in CADASIL, the less GLUT4 is expressed compared to controls. Overall, quantitative analysis demonstrated lower GLUT4 protein expression in small vessels in CADASIL compared to control subjects ($p < 0.001$, **Figure 4E**). Similarly, quantitative immunostaining of GLUT2 in small vessels (**Figures 5A,B**) indicated significantly lower levels of GLUT2 in CADASIL compared to controls ($p < 0.01$, **Figure 5C**). In accord with our previous work (Craggs et al., 2014), we concentrated on the WM but we found that invariably arteriolosclerotic vessels in the gray matter also exhibited GLUT reduction (data not shown).

Nonetheless, based on the dual immunofluorescence labeling of GLUT2 and GLUT4 in relation to α-SMA (**Figures 4**, **5**), the altered levels of GLUT2 and GLUT4 may reflect an altered gene expression in GLUTs in smooth muscle component of the small blood vessels. This is because the dual immuno-staining analysis indicated co-localized staining between GLUT2/4 positive cells and α-SMA. Thus, these findings were consistent with the relative changes observed in the GLUT2 and GLUT4 gene expression analyses in the cellular models of CADASIL versus control (compare **Figure 1** and **Figures 4E**, **5C**). Remarkably, the relative changes in GLUT2 immunoreactivity were lower than the corresponding GLUT4 immunoreactivity in these small vessels. There was ∼ 67% decrease in GLUT2 compared to ∼50% inGLUT4 relative to controls (cf. **Figures 4E**, **5C**).

DISCUSSION

We showed here for the first time that the gene and protein expression of the main GLUTs, GLUT2 and GLUT4 are altered in both cellular models as well as post-mortem brain of CADASIL patients compared to controls. It is difficult to set specific thresholds on what degree of reduction in GLUTs would alter physiological conditions. However, we were careful to compare like VSMCs from controls and patients that were isolated, maintained and cultured in parallel in a similar manner. Irrespective of how the previously reported reduction in glucose metabolism using FDG-PET analyses (Southworth et al., 2003; Tatsch et al., 2003; Tuominen et al., 2004) is interpreted or whether there is true reduction in cellular metabolism or in glucose uptake, we found GLUTs were reduced in the CADASIL VSMCs models and brain microvessels or arterioles of CADASIL patients in the order: GLUT2 > GLUT4 > GLUT3. These findings suggest the possibility that to some degree the profoundly reduced FDG-PET coupled with low cerebral blood flow (CBF) values in CADASIL patients reflect reduced glucose uptake rather than only cellular hypo-metabolism. This suggestion is not inconsistent with the previous findings, albeit in normal aging and Alzheimer's disease subjects that deficits in CBF and cerebral metabolic rate for glucose determined by FDG-PET as in CADASIL could more significantly reflect degradation of the K_1* parameter (transport of glucose) rather than the k_3* (phosphorylation) step (Jagust et al., 1991; Fukuyama et al., 1994).

GLUT4 has also previously been shown to exhibit an altered expression level in arterial myocytes in different disease models (Marcus et al., 1994; Zhang et al., 1999; Atkins et al., 2001). Here, we showed that CADASIL VSMCs expressed lower levels of GLUT4 and GLUT2 both in post-mortem brain tissues and VSMCs derived from CADASIL patients. It is unclear whether NOTCH3 may regulate GLUT4 and GLUT2 directly or via a non-covalent binding mechanism. In preliminary experiments, we were unable to detect co-immunoprecipitates of purified NOTCH3 and either GLUT4 or GLUT2. However, NOTCH3 could alter their expression via another protein that is currently elusive or the expression is related to the reduced glucose metabolism during lower proliferation rates of VSMCs with *NOTCH3* mutants (Takahashi et al., 2010).

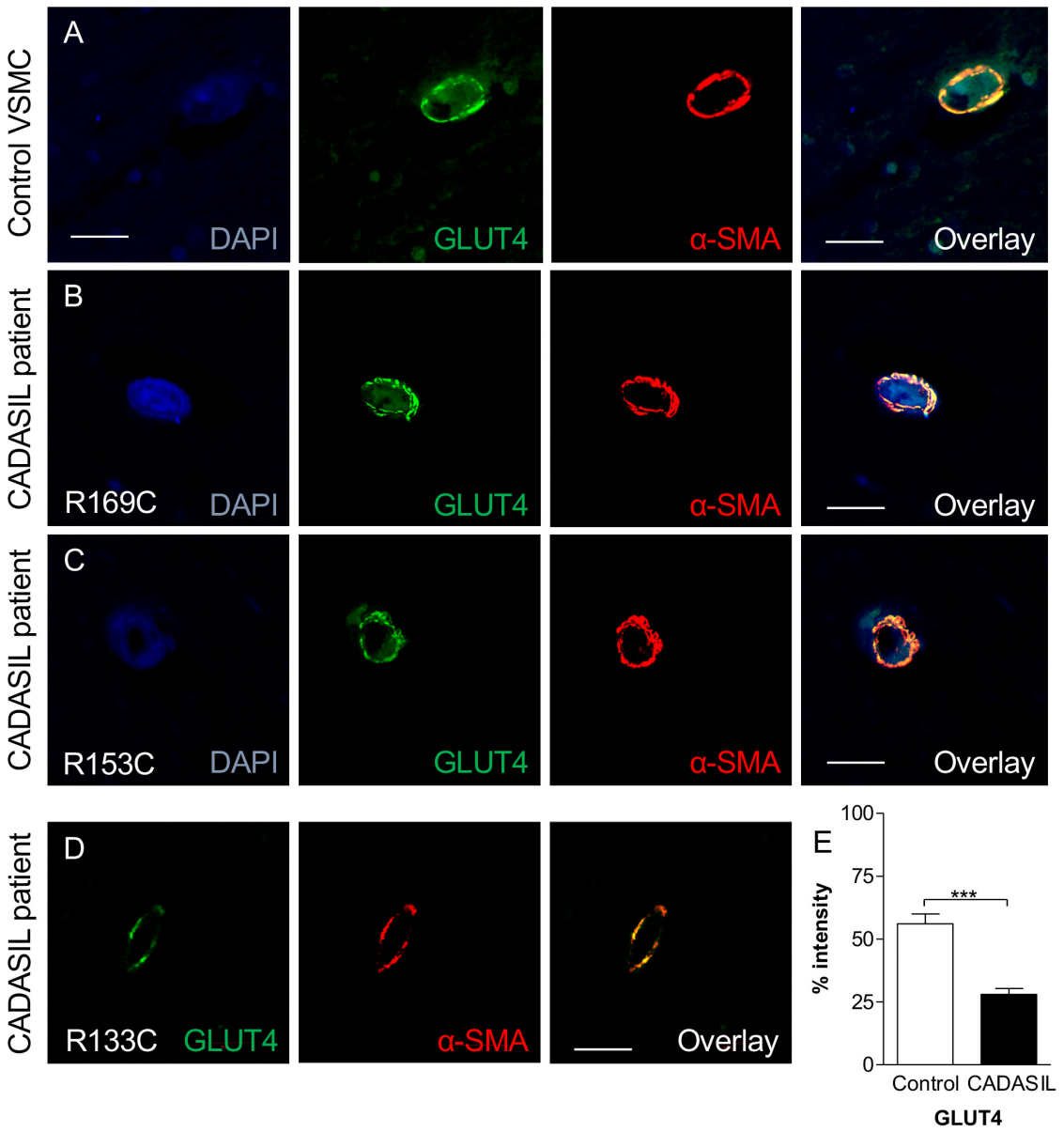

FIGURE 4 | GLUT4 immunoreactivity in VSMC in frontal white matter in CADASIL. **(A)** Immunofluorescent labeling with GLUT4 (green) and α-SMA (red) antibodies (Nuclear, DAPI, blue) is shown. A strong GLUT4-immunostaining in control within the cortex was observed. GLUT4 staining in CADASIL patient carrying **(B)** p.Arg169Cys mutation, **(C)** p.Arg153Cys, and **(D)** p.ArgR133Cys mutation is shown. Magnification bar = 20 μm in panels **(A,B,D)**, and 50 μm in panels **(C)**. **(E)** Quantification of GLUT4 expression demonstrated significantly lower GLUT4 expression in CADASIL brain tissues as compared to controls (***$p < 0.001$). CADASIL, cerebral autosomal dominant arteriopathy with subcortical infarcts and leukoencephalopathy. α-SMA: anti-smooth muscle alpha-actin.

It is plausible that reductions in arteriolar GLUT4 and other GLUTs including capillary GLUT1 could impact on WM integrity. Our previous observations showed there is severe WM arteriopathy and capillary degeneration in CADASIL (Craggs et al., 2014; Hase et al., 2019). Thus, if the vascular entry routes for glucose are impaired or that arterial muscle cells exhibit reduced GLUTs arteriosclerosis may ensue to affect perfusion and flow affecting the WM. This is consistent with previous observations of reduced WM CBF (Tuominen et al., 2004) and frontal WM pathology and axonal disconnectivity in CADASIL (Craggs et al., 2014). However, NOTCH3 mutations could also have a direct effect on WM cells not necessarily involving the microvasculature (Rajani et al., 2019).

Among the known GLUTs, GLUT4 is the main insulin-dependent transporter, which makes it a suitable candidate for developing a potential medical intervention. Nonetheless, our results indicated that GLUT2 had the most reduced levels in both cellular models and the brain VSMCs of the patients. Indeed, our functional glucose uptake experiment indicated that a significant proportion of glucose uptake was through non-insulin dependent

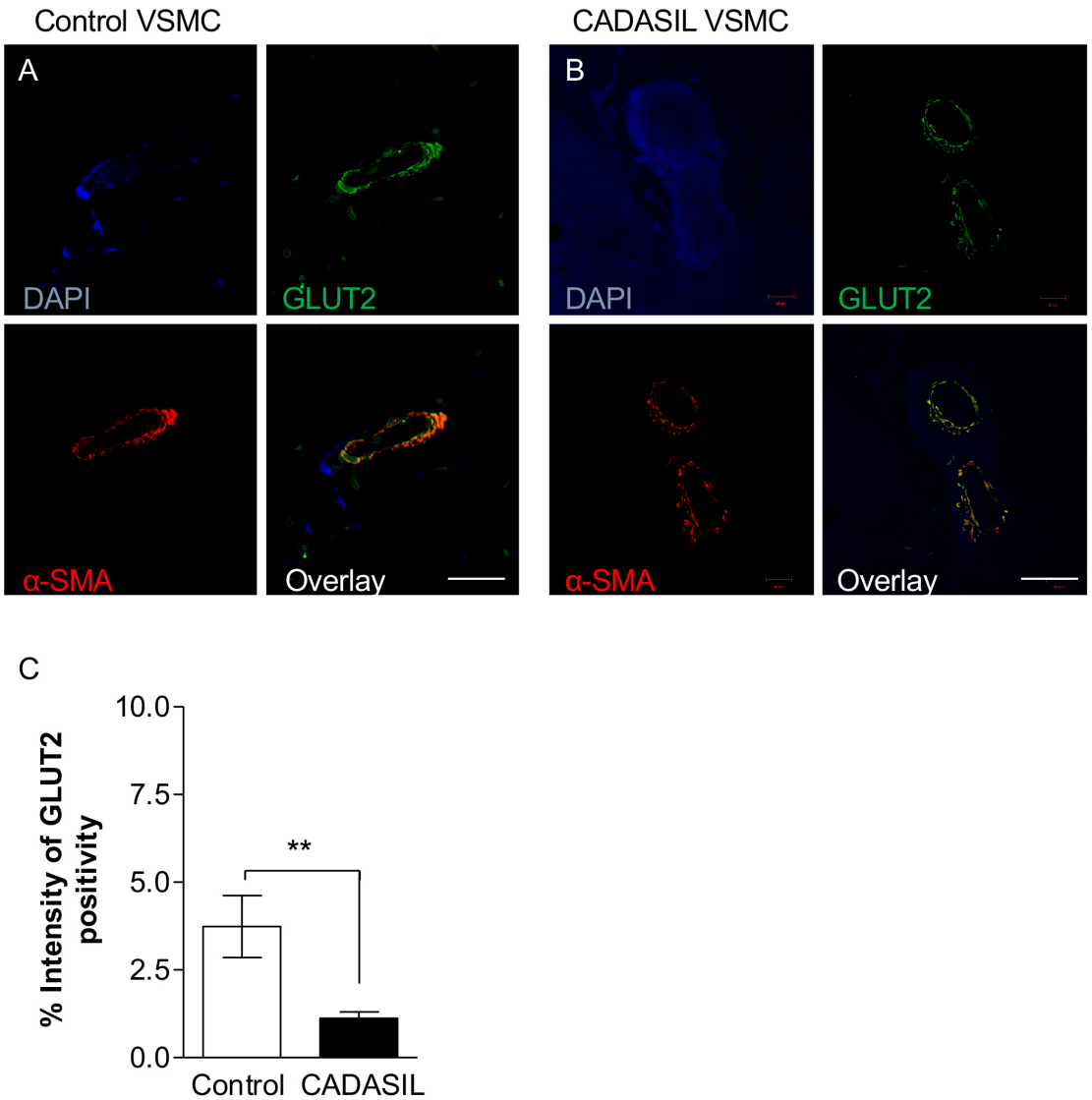

FIGURE 5 | GLUT2 immunoreactivity in cerebral microvessels in CADASIL. Immunofluorescent labeling of GLUT2 (green), smooth muscle α-actin (SMA; red) and arteries and arterioles in the frontal white matter, counterstained with DAPI **(A,B)**. Sections from panel **(A)** a 94-year-old non-demented female control and **(B)** 68-year-old female CADASIL case with p.Arg133Cys mutation. Severe capillary degeneration was observed in CADASIL **(B)**, with low GLUT2 expression observed in VSMCs compared to control subject. There was minimal SMA immunoreactivity in capillaries in CADASIL. Scale bar = 20 μm in panels **(A,B)**. **(C)** Quantification of GLUT2 expression demonstrated significantly lower GLUT2 expression in CADASIL brain tissues as compared to controls (**$p < 0.01$). CADASIL: cerebral autosomal dominant arteriopathy with subcortical infarcts and leukoencephalopathy.

transporters. A previous work based on CADASIL endothelial cells (ECs) showed abnormalities in GLUTs in ECs (Mann et al., 2003). GLUT1 is the major glucose transporter in ECs, and its expression level is decreased in CADASIL as shown in brain biopsy studies (Giwa et al., 2012; Craggs et al., 2013; Craggs et al., 2015). Since GLUTs are expressed in VSMC of systemic organs, and there are few studies that indicate that the VSMC of other organs are bear GOM deposits in CADASIL subjects (Lorenzi et al., 2017) and that endothelium-dependent vasodilation is impaired in forearm resistance arteries (Stenborg et al., 2007) it is not unlikely that GLUT4 and -2 are affected in other organs of CADASIL patients. We were not able to analyze GLUTs in other organs VSMC due the unavailability of systemic tissues. Since CADASIL is largely characterized as a cerebral small vessel disease with consequent brain pathology and dysfunction we focused on the brain. Furthermore, the brain microvasculature is more of interest because it is endowed with the blood-brain barrier unlike systemic the vessels. Further research is needed to clarify the disruption of glucose metabolism in VSMCs derived from other organs and ascertain whether this phenomenon is only seen in VSMCs derived from brain vessels.

We found that the expression of GLUT varied based on blood vessel size, which is in accord with the variable densities of VSMCs in different size vessels (Craggs et al., 2015). Another

recent report indicates that GLUT4 may act as one of the regulators of the tonic capacity of VSMCs (Atkins et al., 2015), suggesting that in CADASIL the blood flow restriction might be, in part, due to reduced GLUT4 (and GLUT2).

Cerebral autosomal-dominant arteriopathy with subcortical infarcts and leukoencephalopathy causes degeneration in the walls of small vessels of the brain leading to lacunar infarcts and leukoencephalopathy. Like in other diseases, vascular risk factors such as hypertension and diabetes, and lifestyle modifications including obesity and smoking can also exacerbate disease progression. This may create chronic hypoxia altering GLUT4 expression and impair proliferation of VSMCs (Zhang et al., 1999; Chou et al., 2004; Takahashi et al., 2010; Szablewski, 2017; Zhao et al., 2017). The same factors might also affect expression of GLUT2, as evident in the current study. Acknowledging these factors play a role in GLUT4 and GLUT2 expressions, we attempted to normalize our data. However, given that in this study we used CADASIL brain tissue collected post-mortem, it is impossible for us to definitively control for such variables. We gathered tissue sections from different Brain Bank sources and some of these tissues are from different individuals that have the same mutation on the *NOTCH3* gene.

Another limitation in this study is that the *in vitro* data was based on a few available cerebral VSMCs cell lines models. However, we should emphasize the difficulties and limitations of preparing cerebral VSMCs derived from CADASIL patients. It was too small to address the effect of various mutations known to cause this disease. Multi-center studies with a larger number of CADASIL patients are required to address such effects.

Whether *NOTCH3* directly affects GLUT4 expression or there are other mechanisms at play remains to be clarified. Using insulin, we were able to increase glucose uptake in CADASIL VSMCs; however, this did not restore glucose uptake to the control level. These data together with lower GLUT2 expression in CADASIL subjects suggest that *NOTCH3* mutations affect the spectrum of GLUTs. Animal models would be of interest in following up the findings in this study. Since all of our experimental material is obtained from human subjects with varying genetic backgrounds, it would be most interesting to study the same phenotype using animals with the same genetic background. It would also be noteworthy to study glucose metabolism in VSMCs in animals that have both copies of *NOTCH3* mutated, considering that in our experiments the mutations are heterozygous.

CONCLUSION

Our observations suggest both the insulin independent and dependent GLUT2 and GLUT4, respectively are impaired in VSMCs and WM arteries of CADASIL subjects. These findings are consistent with decreased cerebral blood flow and glucose uptake demonstrated by FDG-PET in CADASIL patients. The impaired ability of glucose uptake being rescued by insulin is further consistent with lower proliferation rates of VSMCs in CADASIL subjects. Our findings are consistent with the development of severe arteriopathy in CADASIL, in which VSMCs are replaced by widespread fibrosis.

DATA AVAILABILITY STATEMENT

All datasets presented in this study are included in the article/**Supplementary Material**.

ETHICS STATEMENT

The studies involving human participants were reviewed and approved by LEC of the Newcastle Health Trust, Newcastle Brain Resource Centre the NBTR committee, and the Regional Ethical Review Board in Stockholm or the Research Ethics Committee of the South Huddinge University Hospital. The patients/participants provided their written informed consent to participate in this study.

AUTHOR CONTRIBUTIONS

MP, PR, and HB conceived and designed the experiments. MP, DA, NB, and PR performed the experiments. MP, PR, DA, S-MF, JR, and HB analyzed the data. MP, PR, BW, AC-M, MV, YH, RK, TD-S, and HB wrote and edited drafts of the manuscript. All authors contributed to the article and approved the submitted version.

FUNDING

This research was funded by grants from Gun and Bertil Stohne's Foundation, Olle Engkvist Byggmästare Foundation, and Foundation for Gamla Tjärnarinor. RK's work was supported by grants from the UK Medical Research Council (MRC, G0500247), Newcastle Centre for Brain Ageing and Vitality (BBSRC, EPSRC, ESRC and MRC, LLHW), and Alzheimer's Research (ARUK). The NBTR is funded by a grant from the UK MRC (G0400074) with further support from the Newcastle NIHR Biomedical Research Centre in Ageing and Age Related Diseases award to the Newcastle upon Tyne Hospitals NHS Foundation Trust, and a grant from the Alzheimer's Society and ART as part of the Brains for Dementia Research Project.

SUPPLEMENTARY MATERIAL

The Supplementary Material for this article can be found online at: https://www.frontiersin.org/articles/10.3389/fgene.2020.01022/full#supplementary-material

FIGURE S1 | Immunoblotting analyses were conducted to assess the expression of Cpt1c in VSMCs. The samples were visualized using the Odyssey CLx Imager. Fifteen μg of protein was loaded into the gel and GAPDH was used as loading control. Band intensity of Cpt1c immunoreactivity was similar between CADASIL and control VSMC lysates. Abbreviation: CAD: CADASIL VSMC, Crtl: Control VSMC, GAPDH, Glyceraldehyde-3-phosphate dehydrogenase.

REFERENCES

Allan, L. M., Rowan, E. N., Firbank, M. J., Thomas, A. J., Parry, S. W., Polvikoski, T. M., et al. (2011). Long term incidence of dementia, predictors of mortality and pathological diagnosis in older stroke survivors. *Brain* 134(Pt 12), 3716–3727. doi: 10.1093/brain/awr273

Altalhi, W., Sun, X., Sivak, J. M., Husain, M., and Nunes, S. S. (2017). Diabetes impairs arterio-venous specification in engineered vascular tissues in a perivascular cell recruitment-dependent manner. *Biomaterials* 119, 23–32. doi: 10.1016/j.biomaterials.2016.12.003

Atkins, K. B., Johns, D., Watts, S., and Clinton Webb, R. (2001). Decreased vascular glucose transporter expression and glucose uptake in DOCA-salt hypertension. *J. Hypertens.* 19, 1581–1587.

Atkins, K. B., Seki, Y., Saha, J., Eichinger, F., Charron, M. J., and Brosius, F. C. (2015). Maintenance of GLUT4 expression in smooth muscle prevents hypertension-induced changes in vascular reactivity. *Physiol. Rep.* 3:12299. doi: 10.14814/phy2.12299

Banz, W. J., Abel, M. A., and Zemel, M. B. (1996). Insulin regulation of vascular smooth muscle glucose transport in insulin-sensitive and resistant rats. *Horm. Metab. Res.* 28, 271–275. doi: 10.1055/s-2007-979790

Behbahani, H., Pavlov, P. F., Wiehager, B., Nishimura, T., Winblad, B., and Ankarcrona, M. (2010). Association of Omi/HtrA2 with gamma-secretase in mitochondria. *Neurochem. Int.* 57, 668–675. doi: 10.1016/j.neuint.2010.08.004

Brosius, F. C. III, Briggs, J. P., Marcus, R. G., Barac-Nieto, M., and Charron, M. J. (1992). Insulin-responsive glucose transporter expression in renal microvessels and glomeruli. *Kidney Int.* 42, 1086–1092. doi: 10.1038/ki.1992.391

Burkett, J. G., and Dougherty, C. (2017). Recognizing CADASIL: a secondary cause of migraine with aura. *Curr. Pain Headac. Rep.* 21:21. doi: 10.1007/s11916-017-0621-620

Chang, Y. C., Chi, L. H., Chang, W. M., Su, C. Y., Lin, Y. F., Chen, C. L., et al. (2017). Glucose transporter 4 promotes head and neck squamous cell carcinoma metastasis through the TRIM24-DDX58 axis. *J. Hematol. Oncol.* 10:11. doi: 10.1186/s13045-016-0372-370

Choi, J. C. (2015). Genetics of cerebral small vessel disease. *J. Stroke* 17, 7–16. doi: 10.5853/jos.2015.17.1.7

Chou, S. W., Chiu, L. L., Cho, Y. M., Ho, H. Y., Ivy, J. L., Ho, C. F., et al. (2004). Effect of systemic hypoxia on GLUT4 protein expression in exercised rat heart. *Jpn. J. Physiol.* 54, 357–363.

Cooper, D. R., Khalakdina, A., and Watson, J. E. (1993). Chronic effects of glucose on insulin signaling in A-10 vascular smooth muscle cells. *Arch. Biochem. Biophys.* 302, 490–498. doi: 10.1006/abbi.1993.1244

Craggs, L. J., Fenwick, R., Oakley, A. E., Ihara, M., and Kalaria, R. N. (2015). Immunolocalization of platelet-derived growth factor receptor-beta (PDGFR-beta) and pericytes in cerebral autosomal dominant arteriopathy with subcortical infarcts and leukoencephalopathy (CADASIL). *Neuropathol. Appl. Neurobiol.* 41, 557–570. doi: 10.1111/nan.12188

Craggs, L. J., Hagel, C., Kuhlenbaeumer, G., Borjesson-Hanson, A., Andersen, O., Viitanen, M., et al. (2013). Quantitative vascular pathology and phenotyping familial and sporadic cerebral small vessel diseases. *Brain Pathol.* 23, 547–557. doi: 10.1111/bpa.12041

Craggs, L. J., Yamamoto, Y., Ihara, M., Fenwick, R., Burke, M., Oakley, A. E., et al. (2014). White matter pathology and disconnection in the frontal lobe in cerebral autosomal dominant arteriopathy with subcortical infarcts and leukoencephalopathy (CADASIL). *Neuropathol. Appl. Neurobiol.* 40, 591–602. doi: 10.1111/nan.12073

Di Donato, I., Bianchi, S., De Stefano, N., Dichgans, M., Dotti, M. T., Duering, M., et al. (2017). Cerebral autosomal dominant arteriopathy with subcortical infarcts and leukoencephalopathy (CADASIL) as a model of small vessel disease: update on clinical, diagnostic, and management aspects. *BMC Med.* 15:41. doi: 10.1186/s12916-017-0778-8

Formichi, P., Radi, E., Battisti, C., Di Maio, G., Tarquini, E., Leonini, A., et al. (2009). Apoptosis in CADASIL: an in vitro study of lymphocytes and fibroblasts from a cohort of Italian patients. *J. Cell. Physiol.* 219, 494–502. doi: 10.1002/jcp.21695

Fukuyama, H., Ogawa, M., Yamauchi, H., Yamaguchi, S., Kimura, J., Yonekura, Y., et al. (1994). Altered cerebral energy metabolism in Alzheimer's disease: a PET study. *J. Nucl. Med.* 35, 1–6.

Gauthier, S. A., Sahoo, S., Jung, S. S., and Levy, E. (2012). Murine cerebrovascular cells as a cell culture model for cerebral amyloid angiopathy: isolation of smooth muscle and endothelial cells from mouse brain. *Methods Mol. Biol.* 849, 261–274. doi: 10.1007/978-1-61779-551-0_18

Gimbrone, M. A. Jr., Cotran, R. S., and Folkman, J. (1974). Human vascular endothelial cells in culture. Growth and DNA synthesis. *J. Cell Biol.* 60, 673–684. doi: 10.1083/jcb.60.3.673

Giwa, M. O., Williams, J., Elderfield, K., Jiwa, N. S., Bridges, L. R., Kalaria, R. N., et al. (2012). Neuropathologic evidence of endothelial changes in cerebral small vessel disease. *Neurology* 78, 167–174. doi: 10.1212/WNL.0b013e3182407968

Hase, Y., Ding, R., Harrison, G., Hawthorne, E., King, A., Gettings, S., et al. (2019). White matter capillaries in vascular and neurodegenerative dementias. *Acta Neuropathol. Commun.* 7:16. doi: 10.1186/s40478-019-0666-x

Ihalainen, S., Soliymani, R., Iivanainen, E., Mykkanen, K., Sainio, A., Poyhonen, M., et al. (2007). Proteome analysis of cultivated vascular smooth muscle cells from a CADASIL patient. *Mol. Med.* 13, 305–314. doi: 10.2119/2006-00069.Ihalainen

Jagust, W. J., Seab, J. P., Huesman, R. H., Valk, P. E., Mathis, C. A., Reed, B. R., et al. (1991). Diminished glucose transport in Alzheimer's disease: dynamic PET studies. *J. Cereb. Blood Flow Metab.* 11, 323–330. doi: 10.1038/jcbfm.1991.65

Joutel, A., Corpechot, C., Ducros, A., Vahedi, K., Chabriat, H., Mouton, P., et al. (1996). Notch3 mutations in CADASIL, a hereditary adult-onset condition causing stroke and dementia. *Nature* 383, 707–710. doi: 10.1038/383707a0

Kahn, A. M., Lichtenberg, R. A., Allen, J. C., Seidel, C. L., and Song, T. (1995). Insulin-stimulated glucose transport inhibits Ca2+ influx and contraction in vascular smooth muscle. *Circulation* 92, 1597–1603. doi: 10.1161/01.cir.92.6.1597

Lorenzi, T., Ragno, M., Paolinelli, F., Castellucci, C., Scarpelli, M., and Morroni, M. (2017). CADASIL: ultrastructural insights into the morphology of granular osmiophilic material. *Brain Behav.* 7:e00624. doi: 10.1002/brb3.624

Mann, G. E., Yudilevich, D. L., and Sobrevia, L. (2003). Regulation of amino acid and glucose transporters in endothelial and smooth muscle cells. *Physiol. Rev.* 83, 183–252. doi: 10.1152/physrev.00022.2002

Marcus, R. G., England, R., Nguyen, K., Charron, M. J., and Briggs, J. P. (1994). Altered renal expression of the insulin-responsive glucose transporter GLUT4 in experimental diabetes mellitus. *Am. J. Physiol.* 267(5 Pt 2), F816–F824.

Palacio, S., McClure, L. A., Benavente, O. R., Bazan, C. III, Pergola, P., and Hart, R. G. (2014). Lacunar strokes in patients with diabetes mellitus: risk factors, infarct location, and prognosis: the secondary prevention of small subcortical strokes study. *Stroke* 45, 2689–2694. doi: 10.1161/STROKEAHA.114.005018

Panahi, M., Yousefi Mesri, N., Samuelsson, E. B., Coupland, K. G., Forsell, C., Graff, C., et al. (2018). Differences in proliferation rate between CADASIL and control vascular smooth muscle cells are related to increased TGFbeta expression. *J. Cell Mol. Med.* 22, 3016–3024. doi: 10.1111/jcmm.13534

Park, J. L., Loberg, R. D., Duquaine, D., Zhang, H., Deo, B. K., Ardanaz, N., et al. (2005). GLUT4 facilitative glucose transporter specifically and differentially contributes to agonist-induced vascular reactivity in mouse aorta. *Arterioscler. Thromb. Vasc. Biol.* 25, 1596–1602. doi: 10.1161/01.ATV.0000170137.41079.ab

Pyla, R., Poulose, N., Jun, J. Y., and Segar, L. (2013). Expression of conventional and novel glucose transporters, GLUT1, -9, -10, and -12, in vascular smooth muscle cells. *Am. J. Physiol. Cell Physiol.* 304, C574–C589. doi: 10.1152/ajpcell.00275.2012

Rajani, R. M., Ratelade, J., Domenga-Denier, V., Hase, Y., Kalimo, H., Kalaria, R. N., et al. (2019). Blood brain barrier leakage is not a consistent feature of white matter lesions in CADASIL. *Acta Neuropathol. Commun.* 7:187. doi: 10.1186/s40478-019-0844-x

Santio, N. M., Landor, S. K., Vahtera, L., Yla-Pelto, J., Paloniemi, E., Imanishi, S. Y., et al. (2016). Phosphorylation of Notch1 by Pim kinases promotes oncogenic signaling in breast and prostate cancer cells. *Oncotarget* 7, 43220–43238. doi: 10.18632/oncotarget.9215

Schreurs, M., Kuipers, F., and van der Leij, F. R. (2010). Regulatory enzymes of mitochondrial beta-oxidation as targets for treatment of the metabolic syndrome. *Obes. Rev.* 11, 380–388. doi: 10.1111/j.1467-789X.2009.00642.x

Skrobot, O. A., Black, S. E., Chen, C., DeCarli, C., Erkinjuntti, T., Ford, G. A., et al. (2018). Progress toward standardized diagnosis of vascular cognitive impairment: guidelines from the vascular impairment of cognition classification consensus study. *Alzheimers Dement.* 14, 280–292. doi: 10.1016/j.jalz.2017.09.007

Southworth, R., Parry, C. R., Parkes, H. G., Medina, R. A., and Garlick, P. B. (2003). Tissue-specific differences in 2-fluoro-2-deoxyglucose metabolism beyond FDG-6-P: a 19F NMR spectroscopy study in the rat. *NMR Biomed.* 16, 494–502. doi: 10.1002/nbm.856

Standley, P. R., and Rose, K. A. (1994). Insulin and insulin-like growth factor-1 modulation of glucose transport in arterial smooth muscle cells: implication of GLUT-4 in the vasculature. *Am. J. Hypertens.* 7(4 Pt 1), 357–362. doi: 10.1093/ajh/7.4.357

Stenborg, A., Kalimo, H., Viitanen, M., Terent, A., and Lind, L. (2007). Impaired endothelial function of forearm resistance arteries in CADASIL patients. *Stroke* 38, 2692–2697. doi: 10.1161/STROKEAHA.107.490029

Szablewski, L. (2017). Glucose transporters in healthy heart and in cardiac disease. *Int. J. Cardiol.* 230, 70–75. doi: 10.1016/j.ijcard.2016.12.083

Takahashi, K., Adachi, K., Yoshizaki, K., Kunimoto, S., Kalaria, R. N., and Watanabe, A. (2010). Mutations in NOTCH3 cause the formation and retention of aggregates in the endoplasmic reticulum, leading to impaired cell proliferation. *Hum. Mol. Genet.* 19, 79–89. doi: 10.1093/hmg/ddp468

Tatsch, K., Koch, W., Linke, R., Poepperl, G., Peters, N., Holtmannspoetter, M., et al. (2003). Cortical hypometabolism and crossed cerebellar diaschisis suggest subcortically induced disconnection in CADASIL: an 18F-FDG PET study. *J. Nucl. Med.* 44, 862–869.

Tikka, S., Baumann, M., Siitonen, M., Pasanen, P., Poyhonen, M., Myllykangas, L., et al. (2014). CADASIL and CARASIL. *Brain Pathol.* 24, 525–544. doi: 10.1111/bpa.12181

Tikka, S., Ng, Y. P., Di Maio, G., Mykkanen, K., Siitonen, M., Lepikhova, T., et al. (2012). CADASIL mutations and shRNA silencing of NOTCH3 affect actin organization in cultured vascular smooth muscle cells. *J. Cereb. Blood Flow Metab.* 32, 2171–2180. doi: 10.1038/jcbfm.2012.123

Tuominen, S., Juvonen, V., Amberla, K., Jolma, T., Rinne, J. O., Tuisku, S., et al. (2001). Phenotype of a homozygous CADASIL patient in comparison to 9 age-matched heterozygous patients with the same R133C Notch3 mutation. *Stroke* 32, 1767–1774.

Tuominen, S., Miao, Q., Kurki, T., Tuisku, S., Poyhonen, M., Kalimo, H., et al. (2004). Positron emission tomography examination of cerebral blood flow and glucose metabolism in young CADASIL patients. *Stroke* 35, 1063–1067. doi: 10.1161/01.STR.0000124124.69842.2d

Umemura, T., Kawamura, T., and Hotta, N. (2017). Pathogenesis and neuroimaging of cerebral large and small vessel disease in type 2 diabetes: a possible link between cerebral and retinal microvascular abnormalities. *J. Diabetes Investig.* 8, 134–148. doi: 10.1111/jdi.12545

Vermeer, S. E., Longstreth, W. T. Jr., and Koudstaal, P. J. (2007). Silent brain infarcts: a systematic review. *Lancet Neurol.* 6, 611–619. doi: 10.1016/S1474-4422(07)70170-70179

Viitanen, M., Sundstrom, E., Baumann, M., Poyhonen, M., Tikka, S., and Behbahani, H. (2013). Experimental studies of mitochondrial function in CADASIL vascular smooth muscle cells. *Exp. Cell Res.* 319, 134–143. doi: 10.1016/j.yexcr.2012.09.015

Wang, M. M. (2018). CADASIL. *Handb. Clin. Neurol.* 148, 733–743. doi: 10.1016/B978-0-444-64076-5.00047-8

Wang, W., Prince, C. Z., Mou, Y., and Pollman, M. J. (2002). Notch3 signaling in vascular smooth muscle cells induces c-FLIP expression via ERK/MAPK activation. Resistance to Fas ligand-induced apoptosis. *J. Biol. Chem.* 277, 21723–21729. doi: 10.1074/jbc.M202224200

Yamamoto, Y., Ihara, M., Tham, C., Low, R. W., Slade, J. Y., Moss, T., et al. (2009). Neuropathological correlates of temporal pole white matter hyperintensities in CADASIL. *Stroke* 40, 2004–2011. doi: 10.1161/STROKEAHA.108.528299

Yoon, C. W., Kim, Y. E., Seo, S. W., Ki, C. S., Choi, S. H., Kim, J. W., et al. (2015). NOTCH3 variants in patients with subcortical vascular cognitive impairment: a comparison with typical CADASIL patients. *Neurobiol. Aging* 36, e2441–e2447. doi: 10.1016/j.neurobiolaging.2015.04.009

Zhang, J. Z., Behrooz, A., and Ismail-Beigi, F. (1999). Regulation of glucose transport by hypoxia. *Am. J. Kidney Dis.* 34, 189–202. doi: 10.1053/AJKD03400189

Zhao, L. L., Zhang, F., Chen, P., Xie, X. L., Dou, Y. Q., Lin, Y. L., et al. (2017). Insulin-independent GLUT4 translocation in proliferative vascular smooth muscle cells involves SM22alpha. *J. Mol. Med.* 95, 181–192. doi: 10.1007/s00109-016-1468-1462

Conflict of Interest: The authors declare that the research was conducted in the absence of any commercial or financial relationships that could be construed as a potential conflict of interest.

frontiers in Aging Neuroscience

CASE REPORT
published: 10 November 2020
doi: 10.3389/fnagi.2020.538456

Cerebral Amyloid Angiopathy Presenting as Massive Subarachnoid Haemorrhage: A Case Study and Review of Literature

Satoshi Saito[1,2,3,4]*, *Yoshihiko Ikeda*[5], *Daisuke Ando*[2], *Roxana Octavia Carare*[1], *Hatsue Ishibashi-Ueda*[5] *and Masafumi Ihara*[2]*

[1]Clinical Neurosciences, Faculty of Medicine, University of Southampton, Southampton, United Kingdom, [2]Department of Neurology, National Cerebral and Cardiovascular Center, Suita, Japan, [3]Department of Pediatric Dentistry, Graduate School of Dentistry, Osaka University, Suita, Japan, [4]Research Fellow of Japan Society for the Promotion of Science, Tokyo, Japan, [5]Department of Pathology, National Cerebral and Cardiovascular Center, Suita, Japan

Cerebral amyloid angiopathy (CAA) is characterised by the progressive accumulation of β-amyloid (Aβ) in the walls of cerebral capillaries and arteries representing a major cause of haemorrhagic stroke including lobar intracerebral haemorrhage (ICH) and convexity subarachnoid haemorrhage (SAH). Haemorrhaging from CAA predominantly involves smaller arteries rather than arterial aneurysm. Restricted bleeding into the subarachnoid space in CAA results in asymptomatic or mild symptomatic SAH. Herein, we present an autopsied case of massive SAH related to CAA. An 89-year-old male with a history of mild Alzheimer's disease (AD) and advanced pancreatic cancer with liver metastasis developed sudden onset of coma. Head CT illustrated ICH located in the right frontal lobe and right insula, as well as SAH bilaterally spreading from the basal cistern to the Sylvian fissure, with hydrocephalus and brain herniation. He died about 24 h after onset and the post-mortem examination showed no evidence of arterial aneurysm. The substantial accumulation of Aβ in the vessels around the haemorrhagic lesions led to the diagnosis of ICH related to CAA and secondary SAH, which may have been aggravated by old age and malignancy. This case suggests that CAA can cause severe SAH resembling aneurysmal origin and thus may be overlooked when complicated by atypical cerebral haemorrhage.

Keywords: case report, intracerebral haemorrhage, subarachnoid haemorrhage, cerebral amyloid angiopathy, pathology

OPEN ACCESS

Edited by:
Changiz Geula, Northwestern University, United States

Reviewed by:
Mark Stecker, Independent Practitioner, Fresno, United States
Ashkan Shoamanesh, McMaster University, Canada
Alain Viguier, Hôpital Purpan, France

***Correspondence:**
Satoshi Saito
saitou.satoshi.43m@kyoto-u.jp
Masafumi Ihara
ihara@ncvc.go.jp

Received: *27 February 2020*
Accepted: *25 September 2020*
Published: *10 November 2020*

Citation:
Saito S, Ikeda Y, Ando D, Carare RO, Ishibashi-Ueda H and Ihara M (2020) Cerebral Amyloid Angiopathy Presenting as Massive Subarachnoid Haemorrhage: A Case Study and Review of Literature. Front. Aging Neurosci. 12:538456. doi: 10.3389/fnagi.2020.538456

INTRODUCTION

Cerebral amyloid angiopathy (CAA) is a cerebrovascular amyloidosis and a known cause of haemorrhagic stroke. Seven amyloid proteins have so far been reported in CAA including β-amyloid (Aβ), cystatin C, transthyretin, gelsolin, prion protein, ABri/ADan, and immunoglobulin light-chain amyloid (Yamada, 2015). The most common form is Aβ-type CAA, which is frequently concomitant with Alzheimer's disease (AD; Love et al., 2014).

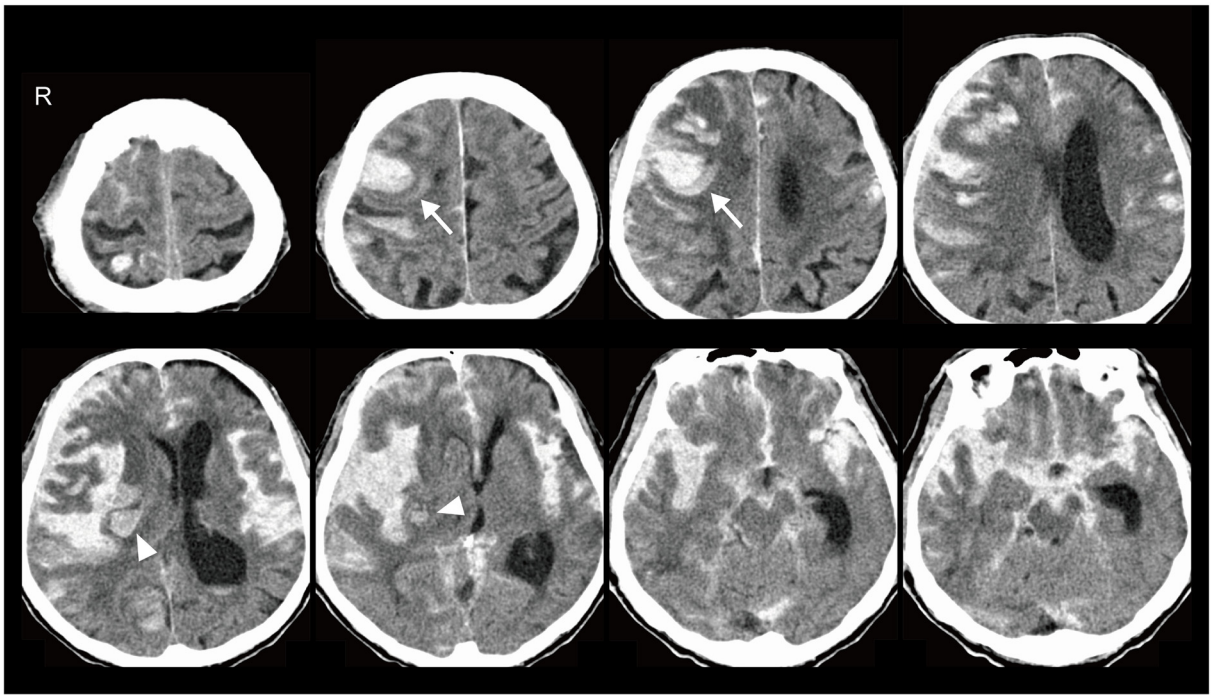

FIGURE 1 | Head CT showed right frontal lobe (arrows) and insula (arrowheads) intracerebral haemorrhage (ICH) adjacent to the brain surface. Blood was also noted in the subarachnoid space, spreading from the basal cistern to the bilateral Sylvian fissure with hydrocephalus and brain herniation.

Cerebrovascular Aβ accumulation induces smooth muscle cell degeneration and vessel wall thickening, resulting in variable degrees of intracerebral haemorrhage (ICH; Love et al., 2014). Bleeding into the subarachnoid space is also common in CAA, presenting as convexity subarachnoid haemorrhage (SAH) in acute and superficial siderosis in the chronic phase. However, CAA is seldom described as a cause of massive SAH resembling aneurysmal rupture (Ohshima et al., 1990; Charidimou et al., 2015; Ni et al., 2015; Raposo et al., 2018). Here, we report an autopsied case of widespread SAH related to CAA.

CASE DESCRIPTION

An 89-year-old male was admitted to our hospital due to sudden onset of coma. Pancreatic cancer with liver metastasis was diagnosed 8 months before admission, and palliative care had been performed. He had a history of mild AD at the age of 88 and brainstem haemorrhage at 82. He was able to look after his own affairs without assistance just before the admission. Amlodipine besilate, sitagliptin phosphate hydrate and febuxostat were administered for hypertension, diabetes mellitus and hyperuricemia. Heavy drinking and smoking in middle age was reported by the family of the patient. Blood pressure and pulse rate were 135/78 mmHg and 92/min. Glasgow Coma Scale score was 6/15 (E4V1M1). Conjugate gaze deviation to the right, anisocoria, facial nerve palsy on the left side and urinary retention were noted. National Institutes of Health Stroke Scale was 37/42. Head CT showed right frontal lobe and insula ICH adjacent to the brain surface (**Figure 1**). Haematoma volume was estimated as 14.9 and 5.9 cm^3, respectively (manual segmentation using OsiriX software: Pixmeo, Bernex, Switzerland). Blood was also noted in the subarachnoid space, spreading from the basal cistern to the bilateral Sylvian fissure with hydrocephalus and brain herniation. MR/CT angiography and digital subtraction angiogram were not performed based on the living will. Complete blood count showed decreased haemoglobin (11.0 g/dl) and haematocrit concentration (33.4%), elevated white blood cells (14,100/μl) and normal level of platelets (183,000/μl). Coagulation assays were normal except for elevated d-dimer (193.6 μl/ml). Slightly decreased renal function (estimated glomerular filtration rate: 67.4 ml/min/1.73 m^2) and elevated level of blood glucose (281 mg/dl) were observed. Hepatic function was normal. He was diagnosed as ICH with secondary SAH and subsequently died approximately 24 h after onset.

At autopsy, the total brain weight, including intracranial haematoma, was 1,285 g. Acute ICH was observed in the right frontal lobe and insula. Bleeding into the subarachnoid space widely spread to the sulcus of the frontotemporal cortex in the right hemisphere, accompanied by an uncal and subfalcine hernia (**Figure 2A**). We did not find any aneurysm in the cerebral vasculature (**Figure 2B**). Histologically, abundant Aβ deposits were observed within the leptomeningeal and cortical arteries around the parenchymal haemorrhagic lesions (**Figure 2C**),

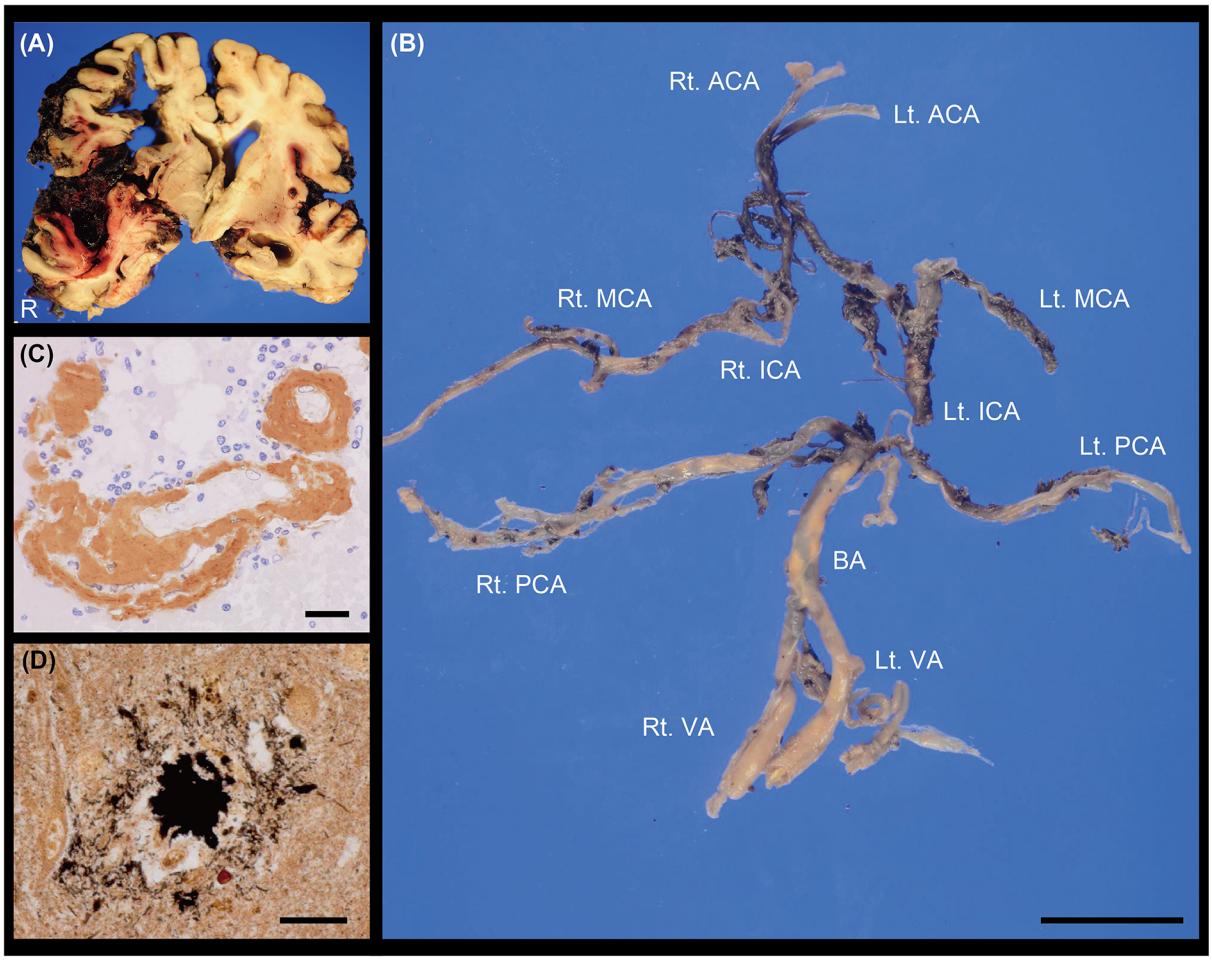

FIGURE 2 | (A) Coronal section of the brain. ICH with subarachnoid haemorrhage (SAH) extension was observed in the right hemisphere. **(B)** Macroscopic image showing the cerebral vasculature. We did not find any evidence of saccular aneurysm in these vessels. The posterior communicating arteries were not identified. **(C)** Cerebrovascular immunostaining of Aβ (brown; M0872, DAKO, 1:50) with nuclear counterstain (blue). **(D)** Senile plaque with modified Bielschowsky staining. Scale bars indicate 2 cm **(B)** and 20 μm **(C,D)**. ACA, anterior cerebral artery; BA, basilar artery; ICA, internal carotid artery; Lt, left; MCA, middle cerebral artery; PCA, posterior cerebral artery; Rt, right; VA, vertebral artery.

which led to the pathological diagnoses of ICH related to CAA with SAH extension. Periarterial spaces were enlarged around the ICH. There were no other lesions contributing to the bleeding, including brain metastasis. Modified Bielschowsky staining uncovered senile plaques and neurofibrillary tangles (**Figure 2D**), which was compatible with the diagnosis of AD (Hyman et al., 2012); Aβ plaque score, A1 (Thal et al., 2002), neurofibrillary tangle stage, B2 (Braak and Braak, 1991), neuritic plaque score, C3 (Mirra et al., 1991).

Written informed consent for autopsy and the publication was obtained from his legal representatives.

DISCUSSION

The presented case was CAA-related ICH accompanied by massive SAH, although the volume of parenchymal haematoma was relatively small (Patel et al., 2009). Severe SAH resembling that of aneurysmal origin is rare in CAA (Ohshima et al., 1990; Charidimou et al., 2015; Ni et al., 2015; Raposo et al., 2018). Old age and pancreatic cancer may have exacerbated the bleeding from the Aβ-positive vessels into the subarachnoid space.

SAH is a life-threatening cerebrovascular disease with a high mortality rate. It accounts for only 3% of all strokes, but for 5% of stroke deaths and more than one-quarter of potential life years lost through stroke (van Gijn and Rinkel, 2001). More than 80% of SAH arise from the rupture of saccular aneurysms. The findings of digital subtraction angiogram are well correlated with the pathology (Smith, 1963; Smith et al., 1983). The angiogram is therefore regarded as the gold standard for aneurysm detection. Approximately 30% of aneurysmal SAH induce ICH (van Gijn and Rinkel, 2001). SAH is also caused by a variety of conditions including perimesencephalic haemorrhage, arterial dissection, cerebral arteriovenous malformation, dural arteriovenous fistula, vascular lesions around the spinal cord,

septic aneurysm, pituitary apoplexy, cocaine abuse and trauma (van Gijn and Rinkel, 2001). CAA occasionally induce convexity SAH, which are usually asymptomatic or mild symptomatic, although the risk of future intracranial haemorrhage and death of patients with CAA-convexity SAH is very high (Calviere et al., 2019). Convexity SAH is excluded if the involvement of the adjoining brain parenchyma is observed (Kumar et al., 2010).

Approximately 40% of ICH cases are associated with moderate or severe CAA in the UK (Rodrigues et al., 2018). Lobar, but not deep, ICH is especially related to CAA (Rodrigues et al., 2018). The extension of SAH is a frequent finding and recognized in about 80% of CAA-ICH cases (Rodrigues et al., 2018; Renard et al., 2019), which could be attributed to CAA predominantly affecting leptomeningeal and cortical arteries compared to intracortical arteries and capillaries (Takeda et al., 2003; Thal et al., 2008). Both the Boston MRI and Edinburgh CT-based diagnostic criteria are now available for the diagnosis of CAA-ICH (Greenberg and Charidimou, 2018; Rodrigues et al., 2018). However, CAA is likely to be clinically underdiagnosed due to multiple clinical phenotypes, especially in the elderly (Sakai et al., 2019; Fakan et al., 2020). Early diagnosis of CAA is important for guiding prognosis and treatment decisions. A recent prospective study (a median follow-up time of 2.5 years) showed progression to dementia was found in more than a quarter of patients with CAA-ICH, even if no dementia was recognized after the acute phase of ICH (Xiong et al., 2019). High ICH recurrence rate was also reported in patients with CAA-ICH, compared to other forms of ICH (Pasi et al., 2018).

In conclusion, this case demonstrates that CAA-ICH can mimic severe SAH resembling that of aneurysmal origin, suggesting that CAA induces a wider spectrum of cerebrovascular disorders than previously expected.

DATA AVAILABILITY STATEMENT

All datasets generated for this study are included in the article.

ETHICS STATEMENT

Written informed consent for autopsy and the publication of this case report was obtained from his legal representatives.

AUTHOR CONTRIBUTIONS

SS and MI contributed to the conceptualisation and writing of the first draft. YI and HI-U performed pathological evaluation. YI, DA, RC, and HI-U critically reviewed and edited this manuscript. All authors contributed to the article and approved the submitted version.

FUNDING

This work was supported in part by a Grant-in-Aid for Japan Society for the Promotion of Science Fellows to SS (19J00106).

ACKNOWLEDGMENTS

We wish to thank Prof. Roy Weller and Mr. MacGregor Sharp at the University of Southampton for insightful discussions and Dr. Ahmad Khundakar at Newcastle University for editorial assistance.

REFERENCES

Braak, H., and Braak, E. (1991). Neuropathological stageing of Alzheimer-related changes. *Acta Neuropathol.* 82, 239–259. doi: 10.1007/bf00308809

Calviere, L., Viguier, A., Patsoura, S., Rousseau, V., Albucher, J. F., Planton, M., et al. (2019). Risk of intracerebral hemorrhage and mortality after convexity subarachnoid hemorrhage in cerebral amyloid angiopathy. *Stroke* 50, 2562–2564. doi: 10.1161/STROKEAHA.119.026244

Charidimou, A., Linn, J., Vernooij, M. W., Opherk, C., Akoudad, S., Baron, J. C., et al. (2015). Cortical superficial siderosis: detection and clinical significance in cerebral amyloid angiopathy and related conditions. *Brain* 138, 2126–2139. doi: 10.1093/brain/awv162

Fakan, B., Reisz, Z., Zadori, D., Vecsei, L., Klivenyi, P., and Szalardy, L. (2020). Predictors of localization, outcome and etiology of spontaneous intracerebral hemorrhages: focus on cerebral amyloid angiopathy. *J. Neural Transm.* 127, 963–972. doi: 10.1007/s00702-020-02174-2

Greenberg, S. M., and Charidimou, A. (2018). Diagnosis of cerebral amyloid angiopathy: evolution of the boston criteria. *Stroke* 49, 491–497. doi: 10.1161/STROKEAHA.117.016990

Hyman, B. T., Phelps, C. H., Beach, T. G., Bigio, E. H., Cairns, N. J., Carrillo, M. C., et al. (2012). National institute on aging-Alzheimer's association guidelines for the neuropathologic assessment of Alzheimer's disease. *Alzheimers Dement.* 8, 1–13. doi: 10.1016/j.jalz.2011.10.007

Kumar, S., Goddeau, R. P., Jr., Selim, M. H., Thomas, A., Schlaug, G., Alhazzani, A., et al. (2010). A traumatic convexal subarachnoid hemorrhage: clinical presentation, imaging patterns and etiologies. *Neurology* 74, 893–899. doi: 10.1212/WNL.0b013e3181d55efa

Love, S., Chalmers, K., Ince, P., Esiri, M., Attems, J., Jellinger, K., et al. (2014). Development, appraisal, validation and implementation of a consensus protocol for the assessment of cerebral amyloid angiopathy in post-mortem brain tissue. *Am. J. Neurodegener. Dis.* 3, 19–32.

Mirra, S. S., Heyman, A., McKeel, D., Sumi, S. M., Crain, B. J., Brownlee, L. M., et al. (1991). The consortium to establish a registry for Alzheimer's disease (CERAD). Part II: Standardization of the neuropathologic assessment of Alzheimer's disease. *Neurology* 41, 479–486. doi: 10.1212/wnl.41.4.479

Ni, J., Auriel, E., Jindal, J., Ayres, A., Schwab, K. M., Martinez-Ramirez, S., et al. (2015). The characteristics of superficial siderosis and convexity subarachnoid hemorrhage and clinical relevance in suspected cerebral amyloid angiopathy. *Cerebrovasc. Dis.* 39, 278–286. doi: 10.1159/000381223

Ohshima, T., Endo, T., Nukui, H., Ikeda, S., Allsop, D., and Onaya, T. (1990). Cerebral amyloid angiopathy as a cause of subarachnoid hemorrhage. *Stroke* 21, 480–483. doi: 10.1161/01.str.21.3.480

Pasi, M., Charidimou, A., Boulouis, G., Auriel, E., Ayres, A., Schwab, K. M., et al. (2018). Mixed-location cerebral hemorrhage/microbleeds: underlying microangiopathy and recurrence risk. *Neurology* 90, e119–e126. doi: 10.1212/WNL.0000000000004797

Patel, P. V., FitzMaurice, E., Nandigam, R. N., Auluck, P., Viswanathan, A., Goldstein, J. N., et al. (2009). Association of subdural hematoma with increased mortality in lobar intracerebral hemorrhage. *Arch. Neurol.* 66, 79–84. doi: 10.1001/archneur.66.1.79

Raposo, N., Calviere, L., Cazzola, V., Planton, M., Patsoura, S., Wargny, M., et al. (2018). Cortical superficial siderosis and acute convexity subarachnoid hemorrhage in cerebral amyloid angiopathy. *Eur. J. Neurol.* 25, 253–259. doi: 10.1111/ene.13484

Renard, D., Parvu, T., and Thouvenot, E. (2019). Finger-like projections in lobar haemorrhage on early magnetic resonance imaging is associated

with probable cerebral amyloid angiopathy. *Cerebrovasc. Dis.* 47, 121–126. doi: 10.1159/000499032

Rodrigues, M. A., Samarasekera, N., Lerpiniere, C., Humphreys, C., McCarron, M. O., White, P. M., et al. (2018). The edinburgh CT and genetic diagnostic criteria for lobar intracerebral haemorrhage associated with cerebral amyloid angiopathy: model development and diagnostic test accuracy study. *Lancet Neurol.* 17, 232–240. doi: 10.1016/S1474-4422(18)30006-1

Sakai, K., Ueda, M., Fukushima, W., Tamaoka, A., Shoji, M., Ando, Y., et al. (2019). Nationwide survey on cerebral amyloid angiopathy in Japan. *Eur. J. Neurol.* 26, 1487–1493. doi: 10.1111/ene.14031

Smith, B. (1963). Cerebral pathology in subarachnoid haemorrhage. *J. Neurol. Neurosurg. Psychiatry* 26, 535–539. doi: 10.1136/jnnp.26.6.535

Smith, R. R., Clower, B. R., Peeler, D. F., Jr., and Yoshioka, J. (1983). The angiopathy of subarachnoid hemorrhage: angiographic and morphologic correlates. *Stroke* 14, 240–245. doi: 10.1161/01.str.14.2.240

Takeda, S., Yamazaki, K., Miyakawa, T., Onda, K., Hinokuma, K., Ikuta, F., et al. (2003). Subcortical hematoma caused by cerebral amyloid angiopathy: Does the first evidence of hemorrhage occur in the subarachnoid space? *Neuropathology* 23, 254–261. doi: 10.1046/j.1440-1789.2003.00506.x

Thal, D. R., Griffin, W. S., de Vos, R. A., and Ghebremedhin, E. (2008). Cerebral amyloid angiopathy and its relationship to Alzheimer's disease. *Acta Neuropathol.* 115, 599–609. doi: 10.1007/s00401-008-0366-2

Thal, D. R., Rub, U., Orantes, M., and Braak, H. (2002). Phases of Aβ-deposition in the human brain and its relevance for the development of AD. *Neurology* 58, 1791–1800. doi: 10.1212/wnl.58.12.1791

van Gijn, J., and Rinkel, G. J. (2001). Subarachnoid haemorrhage: diagnosis, causes and management. *Brain* 124, 249–278. doi: 10.1093/brain/124.2.249

Xiong, L., Charidimou, A., Pasi, M., Boulouis, G., Pongpitakmetha, T., Schirmer, M. D., et al. (2019). Predictors for late post-intracerebral hemorrhage dementia in patients with probable cerebral amyloid angiopathy. *J. Alzheimers Dis.* 71, 435–442. doi: 10.3233/JAD-190346

Yamada, M. (2015). Cerebral amyloid angiopathy: emerging concepts. *J. Stroke* 17, 17–30. doi: 10.5853/jos.2015.17.1.17

Conflict of Interest: The authors declare that the research was conducted in the absence of any commercial or financial relationships that could be construed as a potential conflict of interest.

Advantages of publishing in Frontiers

OPEN ACCESS
Articles are free to read for greatest visibility and readership

FAST PUBLICATION
Around 90 days from submission to decision

HIGH QUALITY PEER-REVIEW
Rigorous, collaborative, and constructive peer-review

TRANSPARENT PEER-REVIEW
Editors and reviewers acknowledged by name on published articles

Frontiers
Avenue du Tribunal-Fédéral 34
1005 Lausanne | Switzerland

Visit us: www.frontiersin.org
Contact us: info@frontiersin.org | +41 21 510 17 00

REPRODUCIBILITY OF RESEARCH
Support open data and methods to enhance research reproducibility

DIGITAL PUBLISHING
Articles designed for optimal readership across devices

FOLLOW US
@frontiersin

IMPACT METRICS
Advanced article metrics track visibility across digital media

EXTENSIVE PROMOTION
Marketing and promotion of impactful research

LOOP RESEARCH NETWORK
Our network increases your article's readership